Diagenesis and provenance of the Middle Jurassic sandstones and carbonates of the Mohican Formation in Mic Mac H-86, Mohican I-100, and Wyandot E-53 wells, offshore Scotian Basin

By

Catherine Sedge

A Thesis Submitted to

Saint Mary's University, Halifax, Nova Scotia

in Partial Fulfillment of the Requirements for a

Bachelor of Science Honours Degree in Geology

April 2015, Halifax, Nova Scotia

Approved: Dr. Georgia Pe-Piper

Supervisor

Certification

I certify that this thesis was submitted by Catherine Sedge in fulfillment of the honours degree requirement for the Bachelor of Science Honours degree in Geology at Saint Mary's University, Halifax, Nova Scotia. This thesis represents the original work carried out by Ms. Sedge under my supervision.

_____

Dr. Georgia Pe-Piper

Professor of Geology

Diagenesis and provenance of the Middle Jurassic sandstones and carbonates of the Mohican Formation in Mic Mac H-86, Mohican I-100, and Wyandot E-53 wells, offshore Scotian Basin

By Catherine E. Sedge

Abstract

Diagenetic processes can be studied to determine the oil and gas reservoir potential within a sedimentary basin. The majority of focus within the Scotian Basin has been on Lower Cretaceous sandstones, with minimal studies done on the Middle Jurassic sandstones that appear in the Mohican Formation of the Scotian Basin. To increase potential oil and gas exploration in the future, it is important that other areas of the Scotian Basin be studied, such as the Middle Jurassic sandstones.

To understand the diagenetic processes that occur in the Mohican Formation wells, petrographic data, lithofacies descriptions, X-Ray diffraction data, chemical mineralogy, and porosity and permeability data were combined and analyzed to determine reservoir potential in this part of the Scotian Basin. To determine provenance of these sandstones, petrographic data was used to observe minerals and textures of lithic clasts and compared to samples from known potential sources from elsewhere in the onshore area.

Petrographic data shows that diagenesis in the Middle Jurassic Mohican Formation is similar to that of the Lower Cretaceous sandstones previously studied. However, main differences occur in the chemical mineralogy of minerals, particularly chlorite. Chlorite within studied wells contains high MgO wt% and low FeO^t wt%, whereas in the Lower Cretaceous sandstones there is low MgO wt% and high FeO^t wt%. This suggests that chlorite diagenesis is variable throughout the basin.

Provenance studies show that most detrital minerals, within the studied samples, likely come from the Meguma Supergroup slates and meta-sandstones, and the Meguma Terrane granites, which also provide detrital minerals throughout other parts of the Scotian Basin, either as first or second cycle detritus.

Acknowledgements

I would like to thank Dr. Georgia Pe-Piper for giving me the wonderful opportunity to undertake an honours thesis. Thank you for guiding me through this project. Thank you to Dr. David J.W. Piper for your assistance with lithofacies and XRD. Thank you both for the wealth of knowledge you have imparted on me, and the countless hours of editing my drafts.

Thank you to Xiang Yang, at Saint Mary's University, for educating me on the SEM and for helping me whenever needed. Thank you to Dan MacDonald, at Dalhousie University, for teaching me how to use the electron microprobe. Thank you to Yuanyuan Zhang, at Saint Mary's University for helping me with any questions I had. Thank you to Randy Corney, at Saint Mary's University, for teaching me point counting.

Thank you to Owen Brown at the Geological Survey of Canada for showing me how to prepare samples for XRD and sharing stories during the process. Thank you to Lori Campbell, at the GSC, for running my XRD samples.

Thank you to the staff at the Canada-Nova Scotia Offshore for allowing me access to conventional core, and to Kris Kendall at CNOSPB for being the external examiner of this thesis.

Thank you to my parents, Lynn and James Sedge, who have supported me and always encouraged me to follow my dreams. I could not have done any of this without you.

This project was funded by a Collaborate Research and Development (CRD) Grant from NSERC-Encana to G. Pe-Piper. Thank you very much for this funding that has allowed me this opportunity.

TABLE OF CONTENTS

List of figures

List of tables

List of appendices

Chapter 1: Introduction

Oil and gas reservoir potential can be determined by studying the diagenetic processes that occur within a basin. The Scotian Basin, located offshore Eastern Canada, is a passive margin basin initially formed during rifting in the Late Triassic to Early Jurassic. This basin is strongly affected by salt tectonics and contains hydrocarbon resources in Mesozoic sandstones (Wade and MacLean, 1990). Most of the oil and gas discoveries within the Scotian Basin have been from sandstones of the uppermost Jurassic and Lower Cretaceous from the Sable Project (CNSOPB, 2000) and currently there is gas production from the Jurassic carbonate reservoirs in the Deep Panuke Field (Encana). Differences between the diagenesis of the Middle Jurassic and the younger, more well-known, Cretaceous sandstones, will be investigated. Also, the provenance of the Middle Jurassic sandstones will be studied. These two results taken together may give insight into the reservoir potential of the Mohican Formation regionally.

1.1 Geological Setting

The Scotian Basin is a Mesozoic-Cenozoic passive-margin sedimentary basin offshore Nova Scotia, Canada (Fig. 1.1). Formation of the basin occurred during Late Triassic rifting followed by Early Jurassic separation of the African and North American plates (Wade & MacLean, 1990). The rift subbasins are characterized by clastic fluvial-deltaic strata interbedded with Late Triassic carbonate and evaporitic strata. The Middle Jurassic Mohican Formation is a mix of carbonate and clastic rocks that unconformably lies atop rift basalt, salt, and terrigenous red beds. This event is thought to have happened in the Late Triassic to the Early Jurassic. The Mohican Formation transitions

laterally into the Iroquois Formation (Fig. 1.2) and underlies the Scatarie Formation. Seismic profiles show that the maximum thickness of the Mohican Formation is found in the Laurentian subbasin, where it is 5.5 km thick (MacLean & Wade, 1992). Seismic profiles also show that below the drill depth of the Mic Mac H-86 well there is a regional unconformity in the Mohican Formation (Wade & MacLean, 1990).

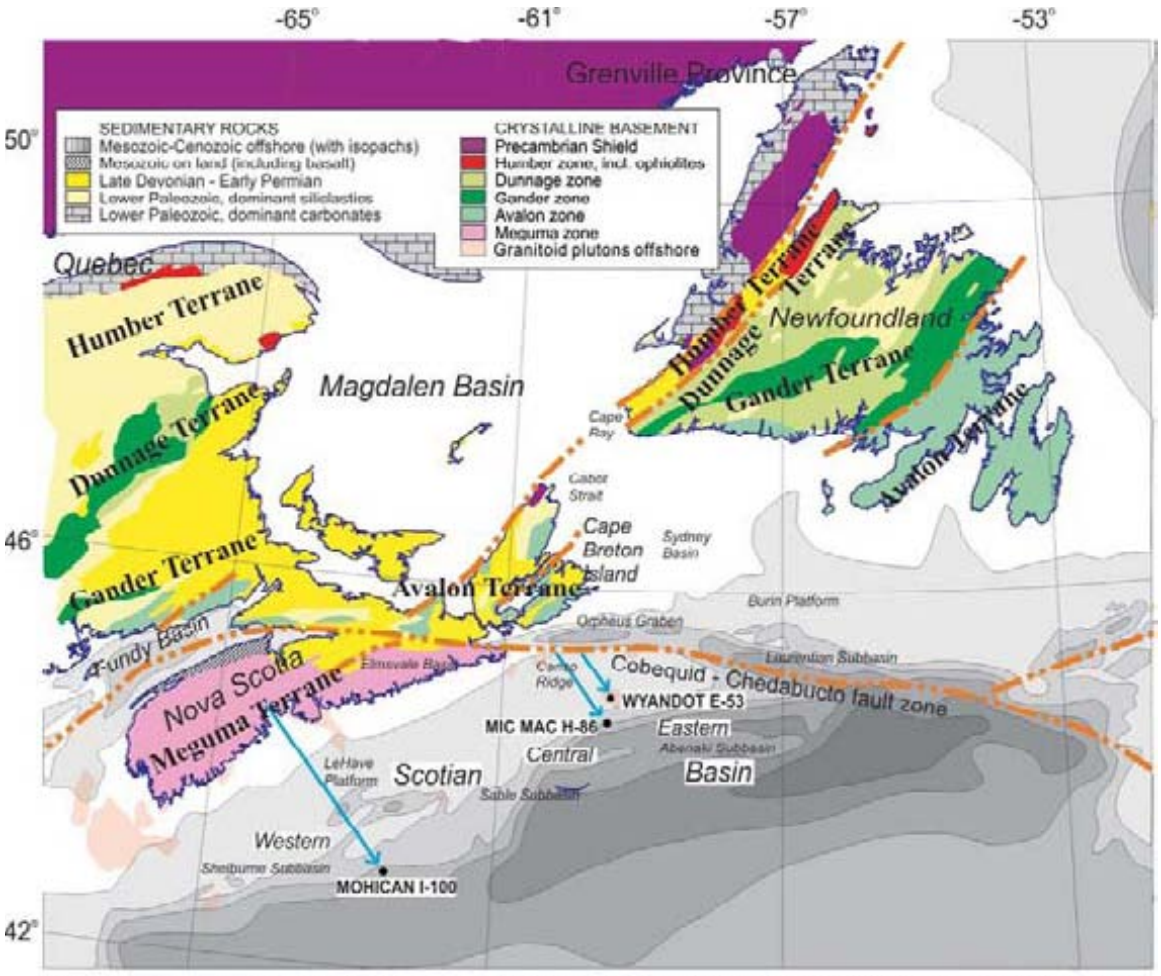

Figure 1.1: Map of the Scotian Basin showing well locations. Terrane also shown for potential source rock for lithic clasts and framework grains. Map modified from Li et al. (2012).

1.2 Well Locations

The three wells of this study are located in the Scotian Basin of the Scotian Shelf, and were all drilled by Shell Canada Resources Ltd. Mic Mac H-86 well was drilled to a

depth of 4785.42 m between August 30, 1970 and December 2, 1970. It is located within the Abenaki Subbasin at 44° 35' 29.0688"N, 59° 26' 59.6688"W. Mohican I-100 well was drilled to a depth of 4393.4 m between December 28, 1971 and March 10, 1972. It is located within the LaHave Platform at 42° 59' 39.3108"N, 62° 28' 48.759"W. Wyandot E-53 was drilled to a depth of 3049.5 m between November 7, 1970 and December 14, 1970. It is located within the Canso Ridge at 44° 52' 19.9698"N, 59° 23' 52.929"W.

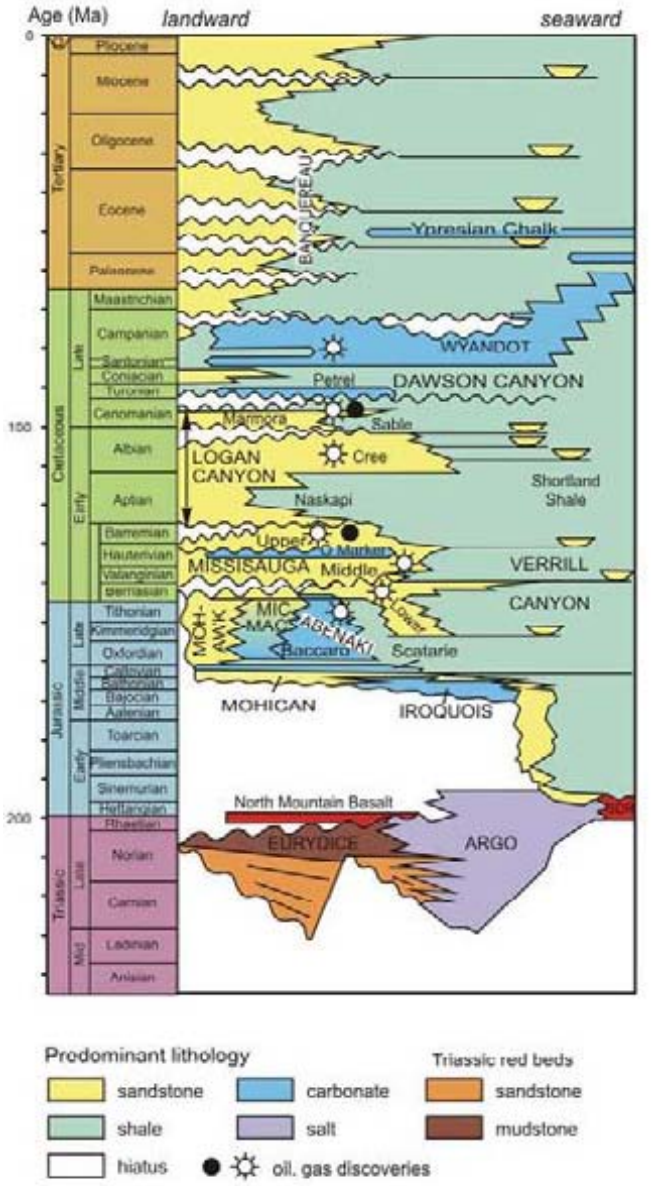

Figure 1.2 Stratigraphic Column of the Scotian Basin, modified from Weston et al. 2012.

1.3 Previous Studies

The Middle Jurassic sandstones of the Mohican Formation have only been studied to date by two groups of researchers: Wade & MacLean (1990), and Li et al. (2012). The diagenesis and reservoir quality of the Upper Jurassic to Lower Cretaceous sandstones, which serves as a comparison for the sandstones of this study, have been studied by Karim et al. (2010), Gould et al. (2010), and Pe-Piper et al. (2011, 2014). The results of four of these studies will be summarized here.

In part of a larger study to describe the characteristics of the Scotian Basin, Wade and MacLean (1990) have discussed the Mohican Formation, its formation, composition, and setting. The Mohican Formation is a clastic unit, lying above the Iroquois Formation and below the Abenaki Formation. It consists of dolomitic siltstone, sandstones, and shale. After the breakup along the margin, the sediments of the Mohican Formation filled in the rift grabens, depositing themselves atop the breakup unconformity, and overlapped basement highs. Where the Mohican Formation is thin on basement highs, there are increased contents of limestone or siltstone. On the outer edge of the LaHave Platform, in the Mohican I-100 well location, this formation is partly a dolomitized oolitic and pelletoid grainstone that indicates deposition occurred in a warm, shallow, agitated marine environment. Landward, the Mohican Formation contains microcrystalline dolomitic mudstone with nodular anhydrite, characteristic of a sabhka environment. Further landward, the formation comprises poorly sorted, white to red thinly bedded sandstones interbedded with red siltstone and shale, and occasional dolostone laminations. Seaward the Mohican Formation increases in thickness, showing a prograding, mainly clastic molasse-type sequence. The thickness of the Mohican

Formation is interpreted to be 1600 m, however within the Abenaki Subbasin it varies from 500 m thick in the west, to more than 4000 m thick in the east.

Middle Jurassic sandstones from the Mohican Formation were studied by Li et al. (2012) for the purpose of determining provenance, which helps in understanding deposition, tectonics, and hydrocarbon reservoir distribution. This was undertaken on three wells (Mic Mac H-86, Mohican I-100, and Wyandot E-53), and was conducted by doing heavy mineral separation on rock samples from conventional core, then analyzing these heavy minerals using the scanning electron microscope (SEM). These thin sections were studied for modal abundance and chemical composition of the minerals. Modal abundance analysis found that the main heavy minerals are garnet, tourmaline, zircon, monazite, magnetite, rutile and ilmenite. Mic Mac H-86 well was found to have >85% magnetite, and the high abundance is attributed there being a local source, which was suggested might be the North Mountain Basalt of Triassic age, as it has abundant magnetite within it. Altered ilmenite was found to be abundant only in the Mohican I-100 well. The Mic Mac H-86 and Wyandot E-53 wells had more zircon compared to ilmenite and rutile which in the overlying Cretaceous rocks of the Scotian Basin is characteristic of polycyclic reworking. Chemical composition of minerals can be used to determine source rocks for sediments of sedimentary basins. This study showed that garnet is present as spessartine with almandine substitution, as well as almandine with spessartine substitution. Spessartine-rich garnets are present in Meguma Group metasedimentary rocks, and almandine-rich garnets are found in both metasedimentary rocks and in peraluminous granites. It was concluded that within the Mohican Formation, the Mohican I-100 well received first-cycle sediments from Meguma terrane;

Mic Mac H-86 and Wyandot E-53 wells received polycyclic sediments from Lower Carboniferous sandstones that were also sourced originally from the Meguma terrane rocks.

One of the studies that serve as a comparison for the diagenetic minerals of the Mohican Formation is the study of Lower Cretaceous sandstones of the Scotian Basin by Karim et al. (2010), to determine the distribution and chemistry of diagenetic minerals in nine wells of the Sable Subbasin within the Scotian Basin. In this study, samples representing various lithofacies were selected, from a range of burial depth and temperature, and were analyzed with petrographic microscope and electron microprobe for minerals and textures. Diagenetic minerals observed were carbonate cements (Mg-calcite, calcite, Fe-calcite ankerite, siderite), silicate cements (clay minerals, quartz, albite) and other cements (pyrite, francolite, titania), and coated grains. Mg-calcite occurred as microcrystalline cement, filling pores before compaction, and was common in marine progradational fine sandstones. Calcite (Mg- and Fe- poor), present as microcrystalline and pore-filling cement, was common in fine to coarse grained fluvial and river mouth sandstones. This form of calcite postdates kaolinite and chlorite cements, but predates quartz overgrowths. Fe-calcite is present in two generations, one predating and one postdating quartz overgrowths. The first generation Fe-calcite is present in transgressive and marine progradational sandstones, and the second generation is present in all sandstone lithofacies. Ankerite forms as a sparry, coarse-crystalline cement that partly to fully fills intergranular pores, postdating quartz overgrowths and other cements. Ankerite is only present in samples from fluvial and river mouth sandstones. Nine varieties of siderite were observed, occurring at different times during

diagenesis, and varying in abundance with varying stratigraphy. The main siderite cements were found in sandstones from prodeltaic mudstones and in marine progradational fine sandstone-mudstone. Clay minerals that form part of silicate cements, include kaolinite, illite, chlorite and an undetermined Fe-clay. Kaolinite is found in intergranular pores between framework grains, predating quartz overgrowths, as well as along cleavage planes of mica grains. Kaolinite is found mainly in samples from fluvial and prodeltaic sandstones. Illite is found as fibrous pore-lining crystals in sandstones from fluvial and estuarine settings. Diagenetic chlorite was mainly found as chlorite rims in fluvial and estuarine sandstones. The presence of chlorite rims prevents quartz overgrowths. Quartz forms cement mainly as quartz overgrowths. They grow over kaolinite cement, but are engulfed by late carbonate cements. These are mostly found in coarse-grained fluvial and deltaic sandstones. Pyrite occurred as framboidal pyrite, found in all lithofacies, and coarsely crystalline pyrite filling intergranular pores. Francolite was found in transgressive sandstones, occurring as layers with illite and chlorite in coated grains. Albite and titania (rutile) occur as patches in fluvial and prodeltaic sandstones. Finally, coated grains, found as concentric layers in transgressive sediments, were noted in several wells. Some have layers of mainly Fe-calcite and others are mainly chlorite + illite. These coated grains, as well as pyrite, are evidence that sea floor diagenesis occurred. It was concluded that seafloor diagenesis occurred producing siderite, early Fe-calcite, Mg-calcite, francolite, pyrite and Fe-rich clay; eogenesis produced kaolinite, siderite, calcite, and corrosion of pyrite; mesogenesis produced chlorite, both pore-filling and as rims, and later calcite, later Fe-calcite, ankerite, illite and

fibrous chlorite. It was also found that the lithofacies play a major role on which diagenetic minerals will be present.

Diagenetic chlorite rims in sandstones of the Lower Cretaceous Mississauga Formation and their relationship to depositional facies, as well as ability to produce gas reservoirs, were studied by Gould et al. (2010). Six types of sandstones were identified based on diagenetic minerals: with chlorite rims, with rims and pore-filling clays, carbonate cement, with rims and patchy carbonate cement, silica cement, and fine-grained and muddy. Chlorite rims were found on framework grains and are thought to form from Fe-rich clay minerals during burial diagenesis, and prevented the formation of quartz overgrowths. Samples were studied using an electron microprobe. It was found that chlorite is present in five forms: pore-rimming, pore-filling (rare), replacement of framework grains, concentric layers on coated grains, and mixed with illite in muddy matrix. Overall, it was found that chlorite rims are best developed in delta front sandstones that are well-sorted, as well as in muddy bioturbated sandstones that lie below transgressive ravinements. They are less developed in those delta front sandstones with muddy laminae or bioturbation. They are absent in fluvial-estuarine sandstones. The chlorite rim occurrence correlates with whole rock P and Ti abundance. P and Ti probably determine Fe availability, mainly supplied by alteration of ilmenite during the sea floor diagenesis.

Chapter 2: Methods

2.1 Conventional Core

Conventional core from three wells (Table 2.1), Mic Mac H-86, Mohican I-100, and Wyandot E-53, all from the Scotian Basin, were described and sampled at the Geoscience Research Centre of the Canada-Nova Scotia Offshore Petroleum Board (CNSOPB) in Dartmouth, Nova Scotia. Samples collected at CNSOPB were combined with those of a previous study, from Gould et al. (2011), and used for a variety of analyses. The software LogPlot 7 was used to build stratigraphic columns for each well showing lithology and lithofacies.

Wells	Core	Depth Range (m)	Location in Scotian Basin	Stratigraphic Unit
Mic Mac H-86	1	4717.75-4725.37	Abenaki	Mohican Fm
Mohican I-100	6	3691.17-3700.32	LaHave Platform	Mohican Fm
Wyandot E-53	2	2872.47-2881.61	Canso Ridge	Mohican Fm

Table 2.1: Summary of well data

2.2 Lithofacies Definition

Lithofacies are representative of the depositional environment where they occurred. Lithofacies of the studied wells were previously described by Gould et al. (2011), and will be expanded on in this study in chapter 3. This process was done by describing, in more detail than previous, the conventional core (see section 2.1) at the CNSOPB. Lithofacies names used were those modified by Gould et al. (2010).

2.3 Sample Preparation

Samples were washed and brushed to remove contaminants such as dust, drilling mud, and other contaminants. These were then made into polished thin sections (PTS),

Well	Depth (m)	Activities					
		PTS	SEM	Probe	Point Counting	XRD	Porosity & Permeability
Mic Mac H-86	4717.78	●	●	●	●	●	●
Mic Mac H-86	4718.97	●	●	●	●		●
Mic Mac H-86	4719.78	●	●	●	●	●	●
Mic Mac H-86	4719.83	●					
Mic Mac H-86	4721.04	●					
Mic Mac H-86	4721.13	●	●	●			●
Mohican I-100	3691.23A	●	●		●		
Mohican I-100	3691.23B	●					
Mohican I-100	3692.06	●					
Mohican I-100	3692.42	●	●		●	●	
Mohican I-100	3693.04	●					
Mohican I-100	3694.38	●	●				
Mohican I-100	3694.73	●					
Mohican I-100	3696.55					●	
Mohican I-100	3696.69	●	●				
Mohican I-100	3697.36A	●					
Mohican I-100	3697.36B	●	●				
Mohican I-100	3697.95					●	
Mohican I-100	3697.86	●	●		●		
Mohican I-100	3699.15	●					
Wyandot E-53	2873.10	●	●		●		●
Wyandot E-53	2873.79	●					
Wyandot E-53	2874.33	●					
Wyandot E-53	2875.02	●					
Wyandot E-53	2876.35	●				●	
Wyandot E-53	2876.81	●	●		●	●	●
Wyandot E-53	2877.03					●	
Wyandot E-53	2878.66	●	●		●		●
Wyandot E-53	2879.42	●					
Wyandot E-53	2879.77	●					
Wyandot E-53	2879.98	●					
Wyandot E-53	2880.22	●	●		●		●

Table 2.2: Summary of samples and activities

impregnated with blue epoxy that fills porosity, and were further studied using a variety of analytical methods. From the 29 available thin sections (Table 2.2), 14 were selected for further analysis. Selection of these was based primarily on grain size, in order to

obtain a set of samples that are representative of the cored section, and secondarily on interesting features such as nodules, visible clasts, and variations in bedding. This representative set of polished thin sections was carbon coated and was studied using a variety of analytical methods.

2.4 Scanning Electron Microscope

A transmitting and reflected light petrographic microscope was used to obtain microphotos of interesting minerals, lithic clasts, textures, and other significant features. A LEO 1450 VP scanning electron microscope (SEM) at the Regional Analytical Centre at Saint Mary's University in Halifax, Nova Scotia was used to analyze for diagenetic and detrital minerals. The SEM uses a tungsten filament to send electrons to the sample to produce a back-scattered electron (BSE) image of the grains in the polished thin section. The SEM also uses energy dispersive spectrometry (EDS) to identify minerals by giving a chemical analysis of each spot selected. The SEM has a maximum resolution of up to 3.5 nm at 30kV and is equipped with an INCA X-max 80 mm^2 silicon-drift detector (SDD) EDS system that has a detection limit of >0.1%. The average beam diameter is 10 microns, which leads to analysis mixing in grains smaller than the beam.

2.5 Electron Microprobe

Of these 14 samples, the four samples from Mic Mac H-86 well were also analyzed at the Regional Electron Microprobe Centre at Dalhousie University, in Halifax, NS. This was done by a JOEL-8200 electron microprobe (EMP) composed of a Noran 133 eV energy dispersive spectrometer and five wavelength spectrometers. It was used

to determine the proper classification of iron oxides and micas, as the microprobe gives a higher quality and more accurate chemical analysis by using wavelength dispersive spectroscopy (WDS). The beam used on the EMP had an average diameter of 1 micron, and the working conditions were set at 20nA and 15kV for micas, and 20nA and 20kV for iron oxides. For mica analyses the elements analyzed for were Si, Ti, Al, Fe, Mn, Mg, Ca, Na, K and Cr, and the standards used were garnet, sanidine, and KK. For iron oxide analyses the elements analyzed for were Si, Ti, Al, Fe, Mn, Mg, Ca, Cr, and V, and the standards used were magnetite and chromite.

2.6 Rock Classification

Classification of sedimentary rock types was determined by point counting. The point counting data was collected using a Nikon Eclipse E 400 Pol polarizing microscope equipped with a Coolpix digital camera, an automated stepping stage, and the Petrog software from Conwy Valley Systems. 10 of the 14 samples were point counted. Four samples were omitted, three because they were carbonate rocks (Mohican I-100 3694.38, 3696.69, and 3697.36B) and one because it was mainly composed of two large detrital lithic clasts (Mic Mac H-86 4721.13). Data collected was plotted, using the software MinPet, into 3 ternary diagrams to determine rock classification and probable provenance type.

The MinPet software was also utilized to plot binary and ternary diagrams of chemical variations and classifications of a variety of minerals, such as chlorite, muscovite, illite, biotite, carbonates, as well as the above mentioned modal rock classifications.

2.7 Mineral Identification and Selection

Iron oxide classification was determined based on the weight percent of FeO^t as analyzed by the electron microprobe. If FeO^t was >89% then it was classified as magnetite; between 81-88% as hematite; between 73-80% as goethite, and <72% as limonite. Any iron oxide that was not analyzed using the electron microprobe is classified as iron oxide because analysis on the SEM is not precise enough to classify otherwise. If there are other minerals present in the analysis it is a mixture, and so the specific iron oxide is not normally named.

Chlorites were classified as detrital or diagenetic based on appearance in BSE images. They were classified as detrital if they were well formed crystals. They were classified as diagenetic if they appeared to be pseudomorphs (i.e. if they appeared altered or if they appear as small grains within the matrix or within areas of dissolution).

Illite and muscovite grains were petrographically distinguished from each other based on two components. First, using SEM chemical analysis, illite was determined to have an Al_2O_3 concentration ≤25%, if >25wt% it was classified as muscovite. Second, using BSE image analysis, grains of ≤30 microns in size, and the right Al_2O_3 content, were classified as illite, >30 microns it was classified as muscovite.

Muscovite and K-feldspar were distinguished from each other by looking at the ratio of Al_2O_3 to K_2O. If Al_2O_3 was approximately 3 or more times the amount of K_2O the mineral was classified as muscovite. If Al_2O_3 was approximately 1.5 times the amount of K_2O then the mineral was classified as K-feldspar. This method is especially useful when analyses are mixtures of two or more minerals.

In producing diagrams from the program MinPet, only minerals that were not part of mixtures, and were within certain limits for contaminants were used. For muscovite, only analyses with contaminant levels of <1wt% CaO and TiO_2, and <2% MgO and FeO were used. For chlorite only analyses with contaminant levels of <1wt% of CaO, Na_2O, TiO_2 and K_2O were used. For carbonates (including calcite, dolomite and ankerite) only analyses with <1 wt% of SiO_2, K_2O, Al_2O_3, P_2O_5, and SO_3 were used. These standards were applied to studied samples, as well as those of previous studies that were plotted for comparison.

2.8 X-ray Diffraction

Eight powdered samples from the studied wells were studied using X-ray diffraction (XRD) at the Geological Survey of Canada Atlantic Division at the Bedford Institute of Oceanography. The first method used incorporated the sediments, which had been crushed into a powder in a previous study, without grain size separation. Small amounts of each sample was mixed with methanol and the paste was pipetted onto a 1" x 1" slide, in order to create a randomly oriented mount as the methanol evaporated.

The second method involved separation of sediment, of less than 2 microns, which was then used to make an oriented clay mount. The grain size separation enhances the proportion of clay minerals in the XRD sample, and the use of an oriented mount enhances the diagnostic '001' diffractions of the clay minerals. Larger minerals, such as silt-sized quartz grains, in the random bulk XRD analysis masked the presence of smaller clay grains of interest, particularly illite and muscovite. The first step involved adding 40 mL of sodium hexametaphosphate to a 1000 mL-graduated cylinder. Sodium

hexametaphosphate is used as a deflocculating agent to prevent grains from flocculating. Next, the powdered samples were weighed and then added to the cylinder, and then water was added until 1000 mL volume. The solution was then shaken until adequately mixed and then left undisturbed for 16 hours allowing for all sediment larger than 2 microns to settle, while keeping suspended as much sediment of less than 2 microns as possible. At the 16-hour mark, the contents of the cylinders more than 20 cm above the base, were decanted into 800 mL centrifuge bottles, which already contained 2 mL of magnesium chloride which flocculated the particles. The eight samples were then centrifuged for 90 minutes, and decanted. After decanting, samples were each added to a 500 mL-graduated cylinder, and topped up with water. From this 500 mL, 20 mL were extracted and added to small aluminum dishes, and then placed in an oven to dry. Each of these dishes was weighed before sample was added, and then again after, to determine the total sample. This weight was added to a spreadsheet, which was set up to determine the mass of zinc oxide needed. Zinc oxide is used as a standard against which to compare XRD results. Zinc oxide, or zincite, was added to each sample as a standard, the sample was mixed, and again it was centrifuged and decanted. The sediment that accumulated was then transferred into 50 mL tubes. From here sample was pipetted onto 1" x 1" glass slides, and then oriented by running a strip of stiff plastic, or 35 mm film, over the top. Using the plastic strip allows the clay minerals to become oriented as compared with the first method where this was not done and so the samples were considered random mounts.

Next, four of the oriented less than 2 micron mounts (E-53 2877.03, H-86 4719.78, H-86 4717.78, and I-100 3697.95), were run glycolated. These samples (excluding I-100 3697.95) were then made into less than 2 micron random mounts. To

do this, the remaining greater than 2 micron powders were separated again to get the maximum amount of less than 2 micron fraction separated to combine with the existing amount. These samples were then made random mounts as side packs. These side packs were run on a scan from 2 to 40 degrees 2θ at half the normal clay run scan speed. Once satisfactory diffractograms results were obtained the random mounts were cannibalized in order to make less than 2 micron oriented mounts on heat resistant slides to be analyzed at various heat stages.

Diffractograms were produced using Siemens Evaluation Software (diffractplus EVA). Diffractograms were produced for all samples with both the methanol random mounts and the less than 2 micron oriented mounts. In addition diffractograms at heat stages of 150°C and 300°C for four of the samples (E-53 2877.03, H-86 4719.78, H-86 4717.78, and I-100 3697.95) were produced.

Chapter 3: Lithofacies

3.1 Description

Lithofacies description used for the purposes of this study is that of Gould et al. (2010). These authors have identified 11 types of facies, which will be described here, and which serve to describe the general environment of deposition of the sediment. Each facies is then subdivided into subfacies, which are used to distinguish different rock types within each type of depositional environment.

Facies 0: thin bedded sandstones and mudstones, generally fine grains, with absent to sparse bioturbation. Deposition in river mouth to shoreface and prodelta turbidites. *Subfacies: 0g* (fine sandstone no mudstone)*, 0b* (dominated by fine sandstone, lesser mudstone and siltstone)*, 0m* (dominated by mudstone, lesser siltstone and very fine sandstone) *,* and *0a* (mudstone with fine to coarse sandstone).

Facies 1: mudstone, with <5% fine sandstone or siltstone, abundant bioturbation. Deposition on the open shelf. No subfacies.

Facies 2: sandstone and mudstone, sparse to common bioturbation. Deposition on the shoreface. *Subfacies: 2b* (mudstone, with 10-60% fine sandstone, common bioturbation)*, 2c* (60-95% fine sandstone, with lesser mudstone, common bioturbation)*, 2o* (fine sandstone, no mud drapes, sparse to moderate bioturbation), and *2x* (fine to medium sandstone, cross-bedding, sparse bioturbation).

Facies 3: sandstone, mudstone, limestone and conglomerate, bioturbation present often with shells. Deposition on the open shelf, in a transgressive environment. *Subfacies: 3x* (sandy mudstone, 10-50% sand)*, 3y* (muddy sandstone, 50-90% sand)*, 3i*

(intraclast conglomerate), *3c* (lithic conglomerate), *3f* (firm ground – rare), *3l* (bioclastic limestone), and *3o* (oolitic limestone and sandstone).

Facies 4: sandstone, absent to sparse bioturbation. Deposition in tidal estuary to fluvial environments. *Subfacies: 4o* (fine sandstone, mud drapes), *4a* (medium to coarse sandstone, mudstone, coal laminations, intraclasts), *4g* (medium to coarse sandstone, coarse grained lag), *4x* (medium to coarse sandstone, mudstone intraclasts, coarse grained lag, coal), and *4n* (mudstone, siltstone, very fine sandstone – sandstone more abundant than mudstone).

Facies 5: sandy to muddy mix (sand dominates), absent to complete bioturbation. Depositional environment variable between subfacies. *Subfacies: 5m* (>75% sandstone, sparse to moderate bioturbation, deposition in mixed flat-intertidal environment), *5s* (>95% sandstone, sparse to moderate bioturbation, shells, deposition in intertidal to subtidal sand flats), *5b* (20-75% sandstone, sedimentary structures destroyed, complete bioturbation, deposition in intertidal mixed flats), and *5c* (medium sandstone, absent bioturbation, thin beds, deposition in subtidal channel).

Facies 6: muddy to sandy mix (mud dominates), absent to complete bioturbation. Depositional environment variable between subfacies. *Subfacies: 6s* (60-75% mudstone, burrows and bioturbation, current ripples, deposition in intertidal mixed flats), *6b* (>80% mudstone, fine to very fine sandstone, complete bioturbation, oyster shells common, deposition in intertidal mudflats), and *6m* (>95% mudstone, minor medium-coarse sandstone, absent to common bioturbation, deposition in intertidal mudflats).

Facies 7: lignite, or carbon-rich mud, often with rootlets. Deposition in tidal marsh environments. No subfacies.

Facies 8: mudstone with rare siltstone, bioturbation absent to sparse, but can be locally intense. Deposition in a lagoon environment. No subfacies.

Facies 9: thick bedded sandstones, absent to moderate bioturbation. Deposition in river mouth to prodelta turbidite settings. *Subfacies: 9g* (coarse to fine sandstone, some grading) and *9s* (fine sandstone with minor mudstone).

Facies 10: destroyed by deformation, original facies unidentifiable. *Subfacies: 10f* (mudstone to muddy sandstone, massive texture and horizontal foliation), *10g* (sandstone, liquefied beds), and *10s* (sandstone, siltstone, mudstone, sheared and folded beds).

3.2 Mic Mac H-86 Facies

The Mic Mac H-86 core extends from 4717.69 m depth to 4725.37m depth (Fig. 3.1) (CNSOPB), however the recovered core extends only to 4721.23 m depth, the remainder has been classified as lost core. This core has been divided into two facies classification as in Gould et al. (2011):

Interval 4717.69 m – 4718.16 m: This interval has been classified as 2b (Gould et al., 2011), with a depositional environment that was on the shoreface. This section is primarily a red sandy mudstone. Grain size is predominately fine to medium grained sands, with some coarse grains throughout. Bedding is shallowly dipping, and alternates in places between muddy and sandy layers. Mud patches occur in places, up to 25 mm in width, suggesting tidal conditions of primary deposits. At 4717.88 m there is a sharp contact between medium grained sands on top of very fine grained sands, representing a period where there was an increase in energy in the water flow to allow the coarse grains

to be entrained and deposited. Lithic clasts occur throughout, however not in abundance. There is some minimal bioturbation.

Interval 4718.16 m – 4721.23 m: This interval has been classified as 9s/9g (Gould et al., 2011), with a depositional environment that was in the river mouth to a prodelta turbidite. The top of the core begins at a sharp contact that separates the above red mudstone from this section of grey muddy sandstone, which then transitions into a medium grained red-grey sandstone throughout. Grain size for this section is fine to medium grained. There is an alternation between sandier and muddier sections. Laminations are subparallel when visible, although they are very faint. Sub-vertical burrows, 2 to 6 cm length, cut through some laminations, leaving the laminations intact to either side of the track. These burrows are Skolithos as they are simple tubes, in-filled with sediment. It is possible that these structures appearing in the muddier layers may be from escaping water. A few laminae of non-penetrative phytodetritus occur in a section with more visible laminations, in the 4719.24-4719.87 m interval. Near the bottom of this section there are very coarse sand to gravel sized sub-angular lithic clasts, surrounded by a muddy matrix, possibly from grading or lag.

Interval 4721.23 m – 4725.37 m: Missing core.

3.3 Mohican I-100 Facies

The Mohican Formation core in the Mohican I-100 well extends from 3691.10 m depth to 3700.30 m depth (Fig. 3.1) (CNSOPB). The lithofacies in this core was described by Gould et al. (2011) using depositional environment instead of lithofacies designation because this core does not fit the lithofacies scheme developed for

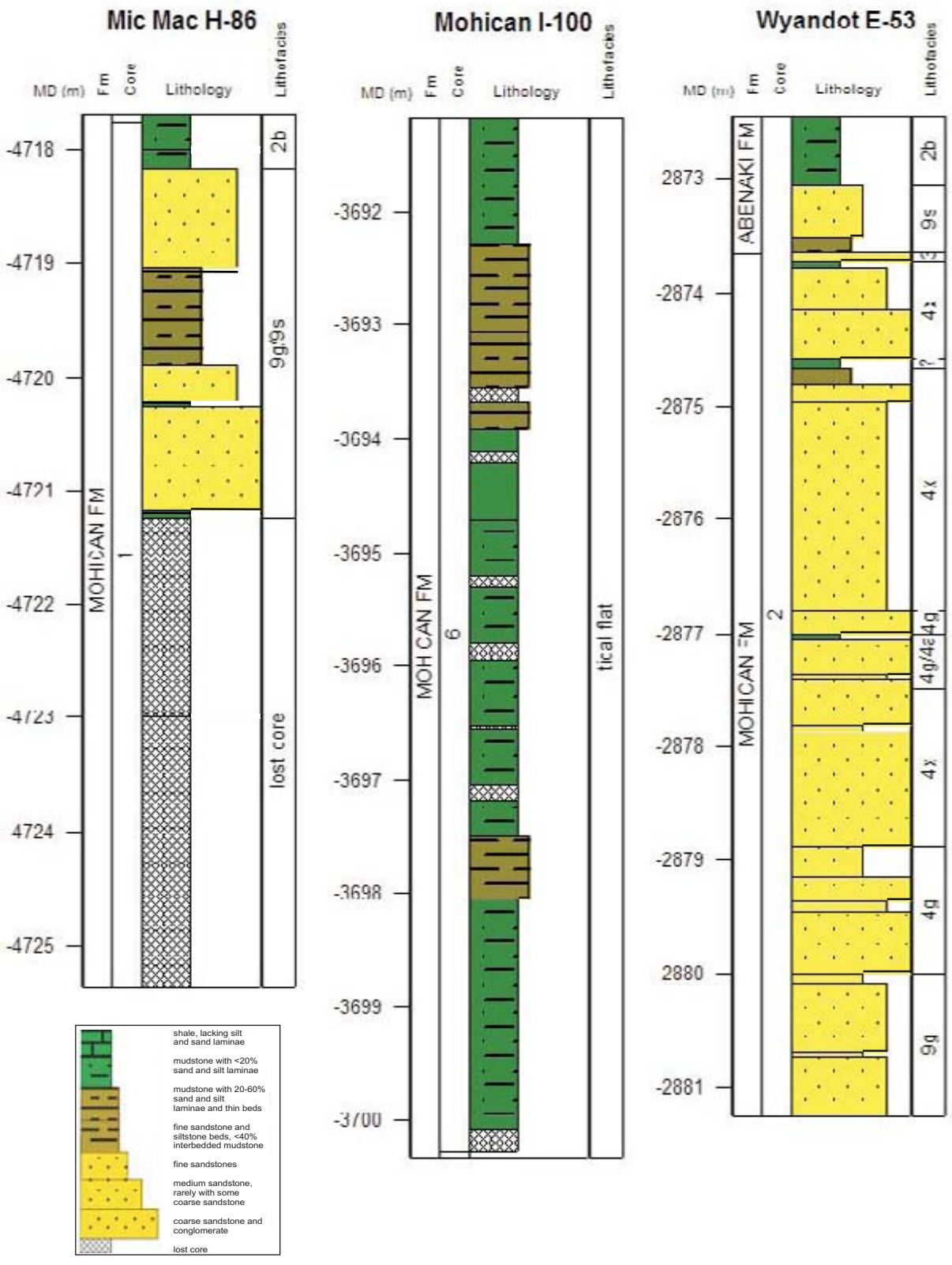

Fig. 3.1 Core logs for Mic Mac H-86, Mohican I-100 and Wyandot E-53, showing formation, core, lithology and lithofacies

Late Cretaceous rocks (Gould et al., 2011). There are 8 small sections (totaling 0.89 m) throughout this core that have been identified as lost core. This core is divided into 4 depositional environments (Gould et al., 2011): transgression, tidal, coastal, and shelf. The characteristics of each environment within this core is described below:

Interval 3691.10 m to ~ 3692.32 m: This interval of core is from a depositional environment that was in transgression (Gould et al., 2011). The top of this section may represent a soil horizon. It is a dark red fine grained sandy mudstone with green patches throughout. It is highly bioturbated and contains nodules of carbonate. This transitions into a section containing laminations, and anhydrite nodules. Grain size becomes slightly more coarse below a lamination which is bordered by tan coloured sediment below which is a 5 cm reduction zone. Then there is an erosion surface overlying a bed of muddy sandstone. Next there is a section of fine grained sandstone with thin horizontal laminations, which contain spots of reduction throughout, as well as tan coloured nodules of anhydrite. Laminations transition to green laminations, with alternations of red laminations. Near the base of this section the laminations are grey-green, there is a short section of bioturbation, and some cross-stratification.

Interval ~ 3692.32 m to ~ 3693.91 m: This interval of core was from a depositional environment that was in the tidal zone (Gould et al., 2011). The top of this section is at a sharp contact with the above section, and is composed of shale, however part of it has crumbled away. Then there is another sharp contact into a section of mudstone with silty laminae. Laminations are grey-green and are horizontal, with some doming (wavy laminations). There is another sharp contact, below the laminations, where the core becomes a more brown sand or siltstone, which contains tan fragments

and nodules, as well as some larger whitish-clear fragments, likely quartz. There is a burrow track present in a section which contains no visible laminations. Then there is a thicker section (~41 cm) of silty sandstone with pink anhydrite nodules throughout, and some shell fragments towards the base. This section is underlain by a grey shale. This contains very fine laminations, alternating light and dark grey, with sporadic burrows. Bioturbation is present, increasing with depth. Laminae become black-dark grey, with some wavy laminations. Burrows are present as well as large anhydrite nodules. Near the base of this section there is an angular contact with layers that lack bioturbation, and show minimal appearance of laminae. Dark grey flecks appear throughout. There is an irregular wavy contact at the base into a more clay rich sandstone that transitions to a silty sandstone.

Interval ~ 3693.91 m to ~ 3695.96 m: This interval of core is from a coastal depositional environment (Gould et al., 2011), however it seems that it is actually from a tidal flat, that was close to river input. At the top of this section is a silty sandstone, tan-grey in colour. Laminations are very faint, and bioturbation is minimal. There is a shallowly dipping contact and then laminations are more apparent, and bioturbation becomes more abundant. Burrows are present, as well as anhydrite nodules. Layers of laminae have been bioturbated. There is another contact into a zone lacking bioturbation and visible laminae, with indistinguishable grain size, classified as a mudstone. As above, this section becomes bioturbated again passing downwards with more anhydrite nodules, along with fragments of phytodetritus, and probably shell fragments. It is followed again by a section with laminations that have been bioturbated. There is a section missing here, including a contact zone. Below, grain sizes become visible again,

laminations are slightly wavy, and there is some bioturbation. Grey coloured laminations transition to become almost horizontal, and darken with depth. Below a section of missing core, there is a muddy sandstone, containing rare shells, but it should contain some carbonate as it reacts to 10% HCl. This transitions to become more muddy, highly bioturbated, with shell and burrows both present.

Interval ~ 3695.96 m to 3700.30 m: This interval of core was originally classified as being from a shelf environment (Gould et al., 2011), however it seems that it is actually a tidal flat. It begins with a section containing small flecks of phytodetritus, shell fragments up to 2 cm in length, with rare laminae, a few anhydrite nodules, some bioturbation, and muddy layers. This section passes down into a tan sandstone, with some wavy mud layers throughout. Grain size is fine and then coarsens slightly with depth. Burrows are present in much of this section. Brown sandstone passes down into grey sandstone with black laminations. There is a contact and then a transition to a greenish sandstone, appearing mottled in places with black flecks of phytodetritus. A 1.5 cm thick coal seam at 3697.84 m is in contact with quartz, or quartzite clasts, ~3 mm in length. The dark green sandstone continues below the coal seam, and contains burrows and mud drapes, some of which are bioturbated. Laminations become more faint and there is a transition into red mudstone, also containing burrows which are green. Laminations are shallowly dipping. The red mudstone passes down into red sandstone with mud laminations. The core appears to have been dewatered, where muds have pushed up into coarser sands. Below this the core looks like a bioturbated paleosol as it did at the top of the core. There are mud drapes, prominent green patches, and anhydrite nodules. The remainder of the core is a mudstone. It has cross laminations, mud drapes,

bioturbation, burrows, mud pockets, and anhydrite nodules throughout, and possibly very small shell fragments.

3.4 Wyandot E-53 Facies

The Wyandot E-53 core extends from 2872.44 m depth to 2881.25 m depth (Fig. 3.1)(CNSOPB). This section of core spans two formations. From 2872.44 m to 2873.06 m the core is part of the Abenaki Formation. From 2873.06 m to 2881.25 m the core is part of the Mohican Formation. This core was divided into eleven facies by Gould et al. (2011):

Interval 2872.44 m – 2873.06 m: This interval of core is the base of the Abenaki Formation, and has been classified as facies 2b (Gould et al., 2011), with a depositional environment that was on the shoreface. This section of the core is tan to blue-grey coloured limestone with mud drapes and flaser bedding present. Grain size is fine to medium sand sized, with a 3 cm clast rich section consisting of sizes up to very coarse sand. This section of core is limy, reacting with 10% HCl. It contains abundant shell fragments, with some places more concentrated than others. There are also black fragments throughout, possibly coal pieces, or phytodetritus. There are burrows present and bioturbation has occurred. This section appears to become less carbonate rich towards the base of the section (with depth) where it is only slightly reactive to 10% HCl.

Interval 2873.06 m – 2873.65 m: This interval of core is the top of the Mohican Formation, and has been classified as facies 9s (Gould et al., 2011), with a depositional environment that was river mouth to prodelta turbidite. This section is a grey sandstone, beginning at a contact with the upper carbonate core. There are darker, shallowly dipping

laminations, some truncating those below it. Grain size is about fine sand sized. Bioturbation is present, but not abundant. Burrows are seen cutting through a layer of mud at about 2873.45 m. At the base of this section there is a layer ~1cm thick of phytodetritus.

Interval 2873.65 m – 2873.72 m: This interval of core has been classified as facies 3c (Gould et al., 2011), with a depositional environment that was transgressive shelf. The top of the core is coarse grained sandstone that contains lithic clasts up to 3cm in length. Grains coarsen with depth. It is probable that a piece of core is missing in this section as the contact with the above interval is very sharp and different in lithology.

Interval 2873.72 m – 2874.58 m: This interval of core has been classified as facies 4x (Gould et al., 2011), with a depositional environment that was a tidal estuary to fluvial setting. This section is mostly a coarse grained grey sandstone, with grains up to gravel sized. The top of this section is muddy sandstone, before transitioning into cleaner sandstone. There are interbedded finer grained layers alternating with coarser grained layers. There is rare phytodetritus present in this interval.

Interval 2874.58 m – 2874.68 m: This interval of core was classified as an unknown facies (Gould et al., 2011). It is composed of green-grey sandstone, with grains hard to distinguish with the naked eye. Alternating light and dark grey laminations are observed, with minor amounts of mud. No bioturbation is present. Based on core observations, this interval may be classified as facies 4o with a depositional environment that was tidal estuary to fluvial, or as facies 0b with a depositional environment that was river mouth to shoreface.

Interval 2874.68 m – 2876.81 m: This interval of core has been classified as facies 4x (Gould et al., 2011), with a depositional environment that was a tidal estuary to fluvial setting. This section is primarily a sandstone, ranging from fine to coarse grained. Bedding is subparallel, and alternates between fine and coarser layers. Phytodetritus is present, easily viewed looking at the end section of the core, however, bioturbation and shells are both absent. Fine grained cross planar beds are present, sitting atop parallel beds at about 2875.23 m. This suggests a probable strong event eroded the parallel beds, and when it settled the fine grained cross beds were deposited. Mud laminations are present, but sporadic. There is a 1 mm thick layer of phytodetritus, or possibly coal, present at 2875.80 m, parallel with layers of fine muds and sands. There is a burrow track at 2876.21 m that is bordered by small coal fragments, ~1 cm length at most. Towards the base of this section there is a layer of phytodetritus (~1mm), and then it transitions into coarser sandstone.

Interval 2876.81 m – 2877.00 m: This interval of core has been classified as facies 4g (Gould et al., 2011), with a depositional environment that was tidal estuary to fluvial. This section is mostly a poorly sorted, coarse grained sandstone, with some layers of fine grains. Mud and sand laminae alternate, with mud layers being very thin (<1mm thick).

Interval 2877.00 m – 2877.50 m: This section of core has been classified as facies 4g/4a (Gould et al., 2011), with a depositional environment that was tidal estuary to fluvial. This section begins with a dark coloured shale, and grades into a lighter sandstone. Phytodetritus is present, bioturbation is absent. Wavy laminations are present, beginning as fine grained and coarsening with depth. Below the wavy

laminations, there are parallel layers of a brown sandstone, alternating with green layers and blue-grey layers until the base of the section.

Interval 2877.50 m – 2878.88 m: This interval of core has been classified as facies 4x (Gould et al., 2011), with a depositional environment that was tidal estuary to fluvial. This section begins with lenticular bedding, alternating yellow-tan sandstone with mud laminations. Grains are overall coarsening with depth, layers become subparallel. There is a mud layer at 2877.83 m serving as a contact with a section of finer grained sandstone. Grains coarsen again with depth and sandstone layers alternate with mud layers. Phytodetritus fragments are present throughout. Some larger angular lithic clasts are present in some poorly sorted sandstone layers. The base of this interval consists of a layer of larger lithic clasts (up to 1.5 cm length), showing this must have had a higher energy environment to deposit this portion.

Interval 2878.88 m – 2880.00 m: This interval of core has been classified as facies 4g (Gould et al., 2011), with a depositional environment of tidal estuary to fluvial. The top of this section of core is a very fine sandstone, sharply underlain by a section of medium sands. The majority of the rest of this section is composed of rubble. The rubble appears to be mostly fine grained to coarse grained green sandstone, and containing phytodetritus and mud drapes. The rubble becomes a darker green with depth, and this section ends in a 5 cm piece of core that alternates the dark green layers with clastic layers and abundant phytodetritus.

Interval 2880.00 m – 2881.25 m: This interval of core has been classified as facies 9g (Gould et al., 2011), with a depositional environment of river mouth to prodelta turbidite. This section is a grey sandstone, it contains some larger clasts but these are

sparse. Burrows are present, and there are phytodetritus fragments, but less than the previous section. Subparallel bedding is present with alternating coarse and fine grained layers. The layers become slightly green tinted with depth, and there are mud laminations present underneath a layer of very coarse sands. At 2880.49 m there is a sharp contact of green mud, and then parallel layers of mud and sands. Towards the base of this section the green sandstone transitions to a more grey sandstone with parallel to subparallel laminae, and then back to light green subparallel fine grained sands.

Chapter 4: Data Presentation

The data presented in this section is based on analytical methods outlined in Chapter 2. Mineral analyses from both the SEM and the EMP, along with accompanying BSE images, were collected (Appendices 1-3) and analyzed. Important minerals, textures, and clasts from the three wells and from potential source rocks have also been documented with microphotos (Appendices 4 & 5), and all these describe the petrography of the cores from these wells. Chemical analyses obtained from SEM and EMP were utilized, along with diagrams, to determine the chemical mineralogy of these wells. X-ray diffraction was used to determine minerals present, particularly the presence of illite versus muscovite, and if there are mixed layers present.

4.1 Petrography

From the selection of 14 thin sections that were analyzed in this study, 10 of them were chosen to determine sandstone classification and their paleotectonic origin, and four as previously mentioned were left out. The ten samples were analyzed with a polarizing transmitted light microscope and their detrital minerals were divided into six categories. These categories were monocrystalline quartz, polycrystalline quartz, feldspars (includes both K-feldspar and plagioclase), lithic clasts (includes igneous, metamorphic, and sedimentary rock fragments), heavy minerals (such as garnet, apatite, TiO_2 minerals, and ilmenite), and unstable minerals (muscovite, chlorite, and biotite) (Table 4.1). For sandstone classification and paleotectonic origin, only monocrystalline quartz, polycrystalline quartz, feldspars, and lithic clasts were used.

	% of total rock					
Sample	**Monocrystalline Quartz**	**Polycrystalline Quartz**	**Feldspar**	**Lithic Clasts**	**Heavy Minerals**	**Unstable Minerals**
H-86 4717.78	60.75	0	14.75	15.75	3	5.75
H-86 4718.98	68.25	9	12	7.25	2.5	1
H-86 4719.78	63.5	7	11.5	10.5	2.5	5
I-100 3691.23	74	17.5	0.5	0.5	5.25	2.25
I-100 3692.42	69.75	0.25	12.5	7.75	8.75	1
I-100 3697.86	70	0.5	15.75	3.75	7	3
E-53 2873.10	68	1.5	27	1.75	1.75	0
E-53 2876.81	73.5	19.75	5.5	0.25	0.5	0.5
E-53 2878.66	60.75	26.25	7.5	4	1.5	0
E-53 2880.22	67.75	9.5	19	2.25	0.75	0.75

Table 4.1: Data from point counting, shown in percentage.

4.1.1 Modal Composition

4.1.1.1 Sandstone Classification

Sandstone classification was determined for the ten samples by using percentages of total quartz (monocrystalline plus polycrystalline), feldspars, and lithic clasts. These were plotted on the QFL sandstone classification diagram of Folk (1968) (Fig. 4.1). This diagram contains seven fields dependent upon variations in the percentages of each total quartz (Q) including both monocrystalline and polycrystalline, feldspar (F) including K-feldspar and plagioclase, and lithics (L) including igneous, metamorphic and sedimentary rock fragments. These fields, as shown in Fig. 4.1, are arkose, lithic arkose, feldspathic litharenite, litharenite, subarkose, sublitharenite, and quartzarenite.

There are three sandstone samples from Mic Mac H-86. Of the three, two are classified as subarkose (4718.97 and 4719.78) and one is a feldspathic litharenite (4717.78). Mohican I-100 well has three sandstone samples, and two of these are subarkose (3692.42 and 3697.86) and one is a quartzarenite (3691.23). Wyandot E-53 well contains four samples, and three of these plot as subarkose (2876.81, 2878.66, and

2880.22) and one is an arkose (2873.10). In summary, most of the studied samples are subarkose (Fig. 4.2).

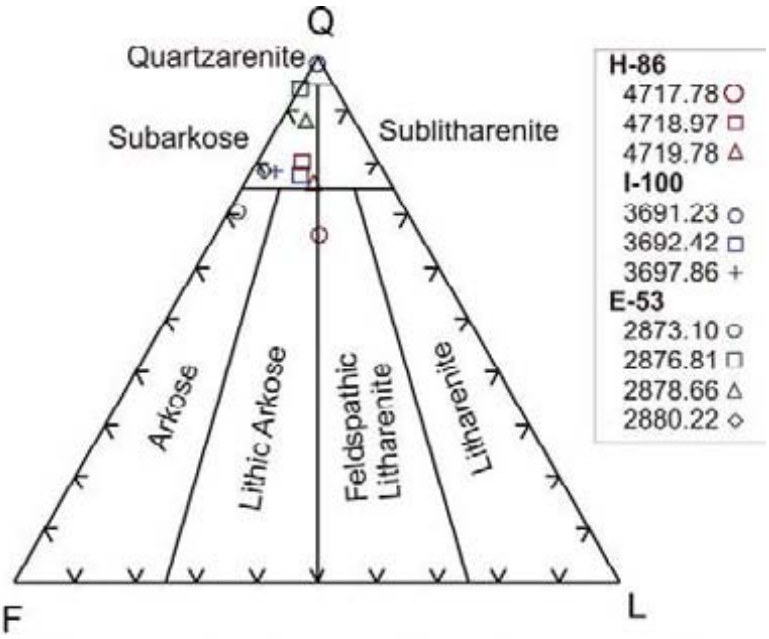

Figure 4.1: QFL plot showing composition of sandstone using nomenclature and fields from Folk (1968).

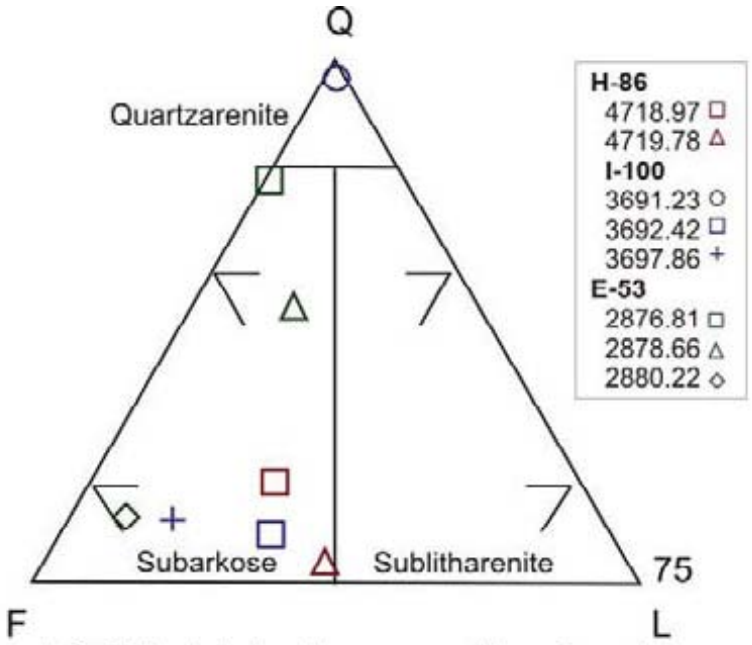

Figure 4.2: QFL plot showing composition of sandstone above 75% quartz, using nomenclature and fields from Folk (1968).

4.1.1.2 Paleotectonic Classification

Paleotectonic origin of sandstones can be determined by using two diagrams, the QFL and the QmFLt diagrams, developed by Dickinson et al. (1983). They are divided into three main categories of provenance, which are continental block, magmatic arc, and recycled orogen. The first diagram (Fig. 4.3), the QFL plot, is from Folk (1968), in that it uses total quartz grains (Q) including both monocrystalline and polycrystalline quartz, versus feldspar (F) including both K-feldspar and plagioclase, and lithics (L) including rock fragments of igneous, metamorphic or sedimentary origin. The second diagram (Fig. 4.4) is the QmFLt plot, beneficial when much of the quartz fraction of the QFL plot is composed of polycrystalline quartz or siliceous quartz (chert). This ternary plot uses the percentages of monocrystalline quartz (Qm), feldspars (F), and total lithics (Lt) including polycrystalline quartz.

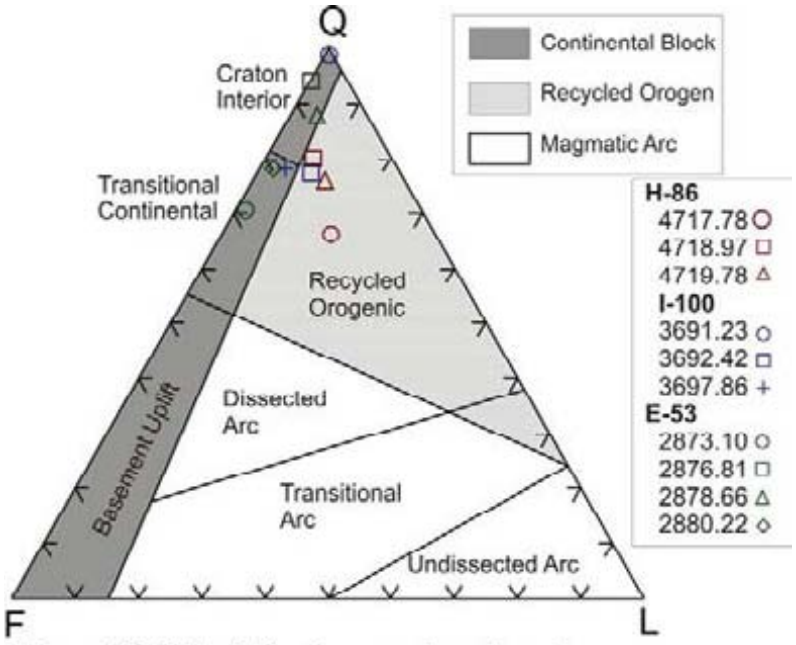

Figure 4.3: QFL plot for framework modes using paleotectonic fields from Dickinson et al (1983).

All three samples from Mic Mac H-86 plotted in the recycled orogen field in both QFL and QmFLt plots. The QmFLt plot (Fig. 4.4) further classifies these three samples as quartzose recycled orogen. The three samples within Mohican I-100 plot differently within each diagram. Using the QFL diagram, one sample plots as recycled orogen (3692.42); two samples plot as continental block: with one plotting as craton interior (3691.23), and the other as transitional continental (3697.86). Using the QmFLt diagram, one plots as recycled orogen within the subdivision of quartzose recycled orogen (3691.23); two samples plot as continental block and in the craton interior subdivision (3692.42 and 3697.86). From Wyandot E-53, two samples plots in both diagrams as continental block in the transitional continental subdivision (2873.10 and 2880.22). The other two samples (2876.81 and 2878.66) plot in the QFL diagram within the craton interior subdivision of continental block; and they plot in the QmFLt diagram as a quartzose recycled orogen.

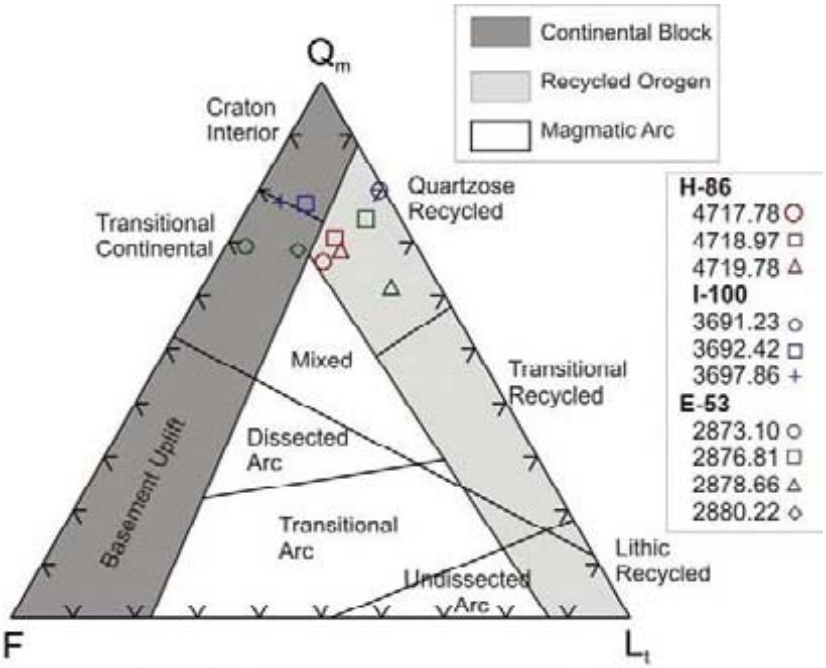

Figure 4.4: Q_mFL_t (Q_m = monocrystalline quartz. L_t = lithic clasts plus polycrystalline quartz) for framework modes using paleotectonic fields from Dickinson et al (1983).

Three samples, varied significantly between the QFL and the QmFLt diagrams of Dickinson (1983). They are Mohican I-100 3691.23 and Wyandot E-53 2867.81 and 2878.66. These all plot on the QFL (Fig. 4.3) as craton interior of the continental block division. However, on the QmFLt (Fig. 4.4) they plot as quartzose recycled orogen showing that there is a higher portion of polycrystalline quartz in these samples causing the bigger shift in classification.

4.1.2 Petrographic Textures

4.1.2.1 Mic Mac H-86

Sample 4717.78: Based on drill core observation this sample is a red sandy mudstone. It contains thin laminations and small mud pockets throughout the sand sized grains. In polished thin section, the modal composition is that of feldspathic litharenite (Fig. 4.1), based on point counts of detrital minerals. It contains detrital grains of biotite, quartz, K-feldspar, albite, muscovite, altered ilmenite, chlorite (in the matrix), and lithic clasts. Biotite is present as a large grain, with possibly diagenetic iron oxides along its cleavage planes. Lithic clasts are common in this sample. Some of them are with abundant diagenetic iron oxides (Fig. 4.5A, position A), whereas others are quartz and muscovite-rich clasts situated within the muddy matrix (Fig. 4.5B, position A). Dissolution voids are present in some framework grains (e.g. albite), however they are not abundant. Diagenetic minerals include illite, TiO_2 minerals, chlorite, and iron oxides. Illite and chlorite form along grain boundaries. Although some illite may be detrital, most of it comes from detrital muscovite altered to diagenetic illite upon burial. TiO_2 minerals form as products of alteration of ilmenite. Iron oxides, goethite/hematite and

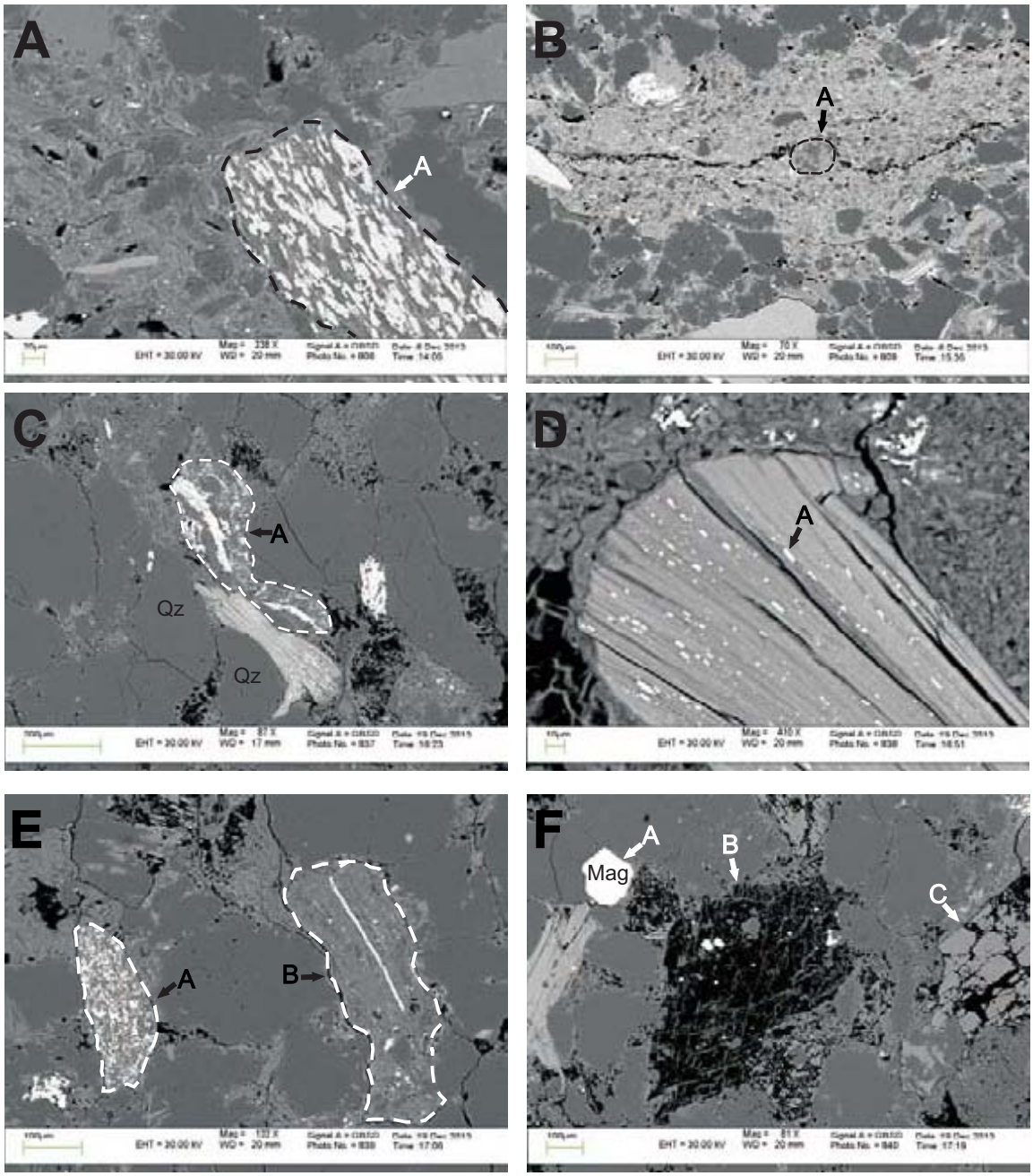

Figure 4.5: Representative backscattered electron images of minerals and textures from Mic Mac H-86 well. **A:** 4717.78 (App. 1A, Fig. 2). Lithic clast (A) with abundant iron oxides. **B:** 4717.78 (from App. 1A, Fig.5). Quartz and muscovite-rich lithic clast (A) within muddy matrix **C:** 4718.97 (App 1B, Fig 3). Plastically deformed lithic clast (A) containing iron oxides. **D:** 4718.97 (App. 1B, Fig. 4). Plastically deformed biotite with iron oxides along cleavage planes (A) (App. 1B, Fig. 4 and see App 4A, Fig 7 for microphoto of whole grain showing deformation). **E:** 4718.97 (App. 1B, Fig. 5). Plastically deformed lithic clasts (A & B) containing iron oxides. **F:** 4718.97 (App. 1B, Fig. 6). Diagenetic magnetite (A) cutting fractures. Highly dissolved mineral (B) creating secondary porosity. Partially dissolved K-feldspar (C).

limonite, in this sample likely formed from the oxidation of pyrrhotite during diagenesis. Iron oxides are mostly found in lithic clasts (Fig. 4.5A, position A), although in places they also form along intergranular boundaries. The matrix of this sample is largely composed of chlorite, muscovite, and illite; many of these grains are partially plastically deformed enclosing framework grains.

Summary: The detrital minerals present in this sample are quartz, K-feldspar, albite, biotite, muscovite, ilmenite, chlorite, and lithic clasts. The diagenetic minerals are illite, TiO_2 minerals, chlorite, and iron oxides. The paragenetic sequence appears to be alteration of ilmenite to TiO_2 minerals, oxidation of pyrrhotite to iron oxides, formation of illite from muscovite, and chlorite precipitation with illite along grain boundaries.

Sample 4718.97: Based on drill core observation, this sample is a fine grained red sandstone; it contains shallowly dipping laminations and sparse amounts of mud pockets. The modal composition of this sample is that of subarkose (Fig. 4.1). In thin section, detrital grains include quartz, K-feldspar, biotite, muscovite, altered ilmenite, and lithic clasts. Diagenetic minerals include illite, chlorite, and iron oxides (including magnetite and hematite). Dissolution voids occur in quartz, K-feldspar, and muscovite, leaving areas of secondary porosity that are partly filled with diagenetic illite and chlorite (Fig. 4.5F). Lithic clasts are abundant, some of which are composed of iron oxides (Figs. 4.5C, position A & Fig. 4.5E, positions A & B) which may have been a product of pyrrhotite oxidation during diagenesis. Lithic clasts also show partial plastic deformation (Fig. 4.5C, position A, and Fig. 4.5E, position A & B) being squeezed between bending

around more resistant detrital grains such as quartz. Magnetite present as a solitary grain (Fig. 4.5F, position A) is diagenetic as it cuts fractures. Iron oxides also form along cleavage planes of detrital biotite grains (Fig. 4.5D, position A). Secondary porosity is present from mineral dissolution. In some places dissolution is so extensive it eliminates the majority of the original mineral (Fig. 4.5F, position B). K-feldspar has undergone much dissolution as well, leaving large voids (Fig. 4.5F, position C). Ilmenite present in the sample is a detrital mineral; however, during diagenesis it undergoes alteration, producing TiO_2 minerals in some places throughout this well.

Summary: The detrital minerals present in this sample include quartz, K-feldspar, biotite, muscovite, altered ilmenite, and lithic clasts. There was plastic deformation of both detrital phyllosilicate minerals and pelitic lithic clasts during compaction. Diagenetic minerals include illite, chlorite, and iron oxides. The paragenetic sequence appears to be iron oxide formation from pyrrhotite oxidation, dissolution of K-feldspar and quartz, and formation of illite and chlorite within dissolution voids.

Sample 4719.78: Based on drill core observation, this sample is a sandstone containing thin, closely spaced laminations. The modal composition of this sample is that of subarkose (Fig. 4.1), as determined by point counting. Detrital minerals, in this sample include zircon, albite, chlorite, quartz, biotite, K-feldspar, muscovite, and lithic clasts. Diagenetic minerals include illite, TiO_2 minerals, chlorite (some within matrix), and iron oxides. There is high secondary porosity in this sample, seen in the dissolution of detrital grains such as quartz and K-feldspar (Fig. 4.6B, position B). Quartz grains appear fractured in places (Fig. 4.6C, position A), leaving open spaces. Muscovite, along

with chlorite and illite, is seen as a pseudomatrix of grains that have been squeezed between framework grains of quartz and K-feldspar (Fig. 4.6B, position D). Muscovite is also present as larger grains, such as where it has been squeezed between a grain of K-feldspar and a lithic clast (Fig. 4.6A, position A). Large detrital grains of biotite are often partially plastically deformed in intergranular space between framework grains (Fig. 4.6A, position B, & Fig. 4.6B, position A). Some biotite grains have been partly chloritized (Fig. 4.6A, position B). Lithic clasts present in this sample have been plastically deformed, wrapping around stronger framework grains such as quartz (Fig. 4.6C, position B). TiO_2 minerals formed as a product of ilmenite alteration. Iron oxides are present in this sample (such as hematite), occurring within lithic clasts (Fig. 4.6B, position C).

Summary: The detrital minerals present in this sample include quartz, albite, chlorite, zircon, K-feldspar, muscovite, biotite, and lithic clasts. The lithic clasts and detrital phyllosilicate minerals underwent plastic deformation during compaction. Diagenetic minerals include illite, TiO_2 minerals, chlorite, and iron oxides. The paragenetic sequence is chloritization of biotite, alteration of ilmenite producing TiO_2 minerals, oxidation of pyrrhotite forming iron oxides and dissolution of framework grains. The position of illite formation within the paragenetic sequence is uncertain.

Sample 4721.13: Based on drill core observation, this sample is a fine grained sandy mudstone, with large rounded matrix-supported lithic clasts. This samples lies near a contact between matrix-supported mudstone and clast-supported conglomerate.

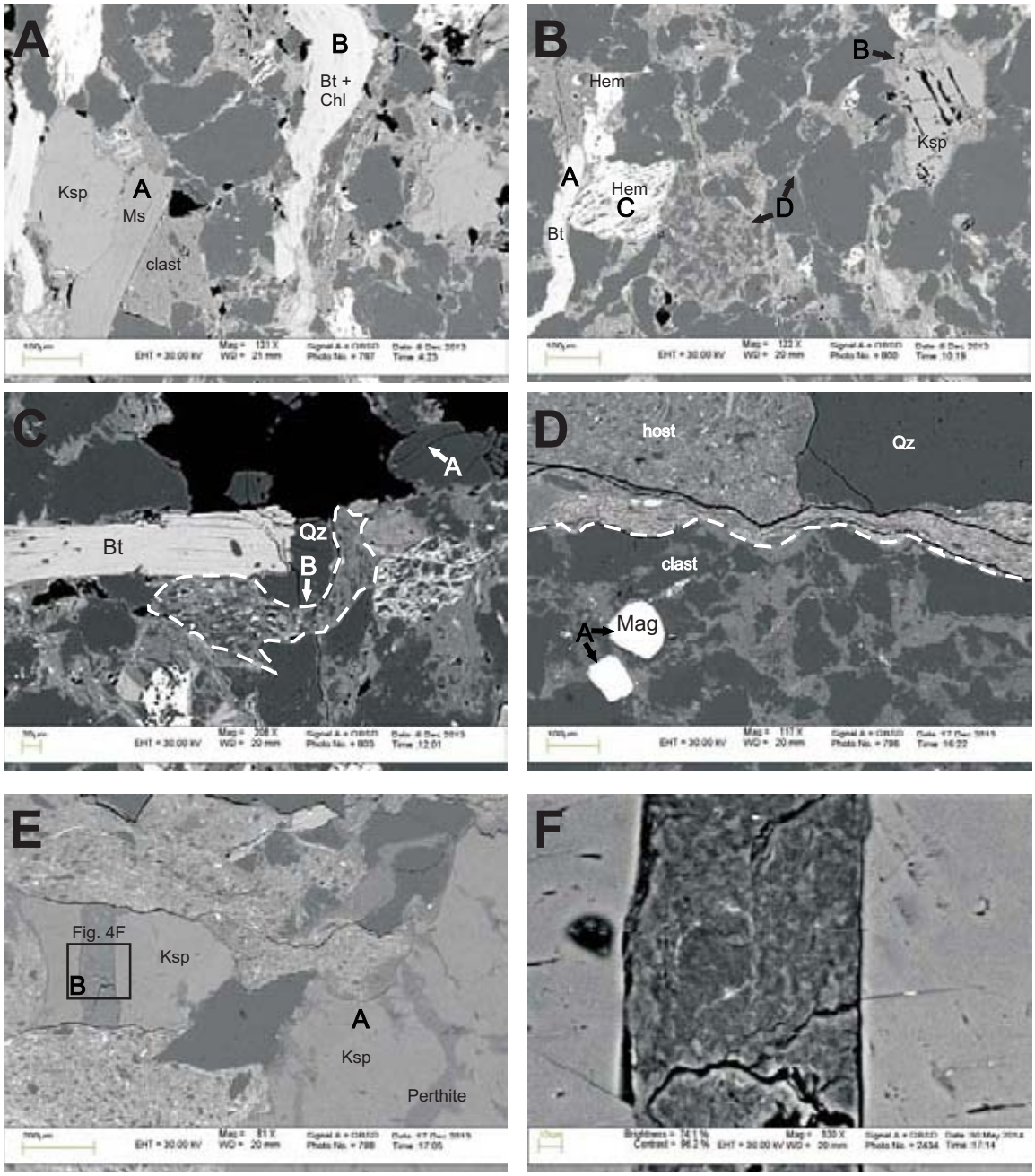

Figure 4.6: Representative backscattered electron images of minerals and textures from Mic Mac H-86 well. **A:** 4719.78 (App. 1C, Fig. 2). Detrital muscovite (A) fills intergranular boundary between K-feldspar and quartz-muscovite-rich clast. Plastically deformed chloritized biotite (B). **B:** 4719.78 (App. 1C, Fig. 5). Plastically deformed detrital biotite (A) fills intergranular boundary. Partially dissolved K-feldspar (B). Hematite within a clast (C). Muscovite, chlorite and illite filling intergranular boudaries (D). **C:** 4719.78 (App. 1C, Fig. 8). Quartz showing fracturing (A). Plastically deformed muscovite-rich lithic clast bending around quartz (B). **D:** 4721.13 (App. 1D, Fig. 1). Contact between lithic clast and mudstone host. Magnetite within detrital clast (A). **E:** 4721.13 (App. 1D, Fig. 3). Large K-feldspar grain of microcline with exsolution of perthite (see App. 4A, Fig. 12 for microphoto). Muscovite and chlorite fills fracture in detrital K-feldspar (B) (Fig. 4F). **F:** 4721.13 (App. 1D, Fig. 8). Fracture in K-feldspar filled with fine-grained muscovite and chlorite.

The modal composition of this sample was not calculated because the polished thin section is made up 2 lithic clasts that fill the majority of the thin section. In thin section, the detrital minerals are quartz, magnetite, biotite, muscovite, chlorite, K-feldspar, albite, and lithic clasts. The lithic clasts are surrounding by large detrital minerals, and a host of fine grained sandy mud (Fig. 4.6D). These lithic clasts contain framework grains, such as quartz and biotite, within a matrix of fine grain muscovite and chlorite, making these clasts similar to other samples within the Mic Mac well. Magnetite in this sample is within the lithic clast (Fig. 4.6D, position A), so it may be detrital, or it may have formed from pyrrhotite oxidation during diagenesis. K-feldspar is found in one location as microcline with perthitic texture from albite exsolution (Fig. 4.6E, position A, and see App. 4A, Fig. 12 for microphoto). Thin fractures can be seen within the muddy matrix, as well as a larger fracture (or wide dissolution zone) in a detrital K-feldspar grain (Fig. 4.6E, position A, and Fig. 4.6F). The fracture has been infilled by a muscovite and chlorite-rich matrix, along with a thin line of dissolution on the contact between the matrix and the surrounding K-feldspar grain.

Summary: The detrital minerals present are quartz, K-feldspar, albite, biotite, magnetite, muscovite, K-feldspar, and lithic clasts. Diagenetic mineral is chlorite. The paragenetic sequence dissolution (or fracturing) of K-feldspar, breakdown of muscovite for matrix, and chlorite precipitation in matrix.

4.1.2.2 Mohican I-100

Sample 3691.23A: Based on drill core observation, this sample is a red muddy sandstone with green muddy laminations, and pockets of carbonate. This section of core

has been partly bioturbated. In polished thin section, the modal abundance of this sample is that of subarkose (Fig. 4.1), based on point counts of detrital minerals. Detrital grains include quartz, muscovite, chlorite, biotite, K-feldspar, ilmenite and albite. Larger framework grains of mainly quartz, with minor amounts of K-feldspar and albite, are surrounded by muscovite rich muddy matrix or pseudomatrix. Other minerals in the matrix include chlorite. The diagenetic minerals include dolomite, chlorite, illite, iron oxides, and barite. Chlorite thus is found both as a detrital mineral and as a diagenetic mineral. Detrital chlorite is found as larger lath shaped grains, as well as within matrix, and diagenetic chlorite is often found as an alteration on muscovite grains. Detrital biotite is also present in large lath shaped grains. Detrital ilmenite is present, and has been partly altered. Iron oxides precipitated along intergranular boundaries. There are a few patches of dolomite, including one patch surrounding a barite grain. This barite appears of diagenetic origin because it forms well-defined grain boundaries with dolomite. The dolomite patches seen are those pockets visible in the drill core. An unmineralized thin fracture runs through part of the sample and the matrix.

Summary: The detrital minerals present in this sample include quartz, K-feldspar, albite, chlorite, biotite, muscovite, and ilmenite. Diagenetic minerals include illite, chlorite, dolomite, iron oxides, and barite. The paragenetic sequence is alteration of ilmenite, iron oxide precipitation, barite precipitation, and dolomite precipitation. The precipitation of chlorite and illite in this sequence is uncertain.

Sample 3692.42: Based on drill core observation, this sample lies along a contact zone between a red muddy sandstone and a grey anhydrite nodule. It also contains

smaller patches of anhydrite. In polished thin section, the modal composition is that of arkose (Fig. 4.1), based on point counts of detrital minerals. The detrital grains include quartz, albite, K-feldspar, biotite, ilmenite, chlorite, and lithic clasts. There is a muddy matrix, and the main cement mineral is anhydrite. Other diagenetic minerals include quartz overgrowths, TiO_2 minerals, fluorapatite, illite, and an Al-phosphate mineral. Secondary porosity is present from the dissolution of framework grains, such as quartz. Framework grains, such as quartz, K-feldspar, and albite are hosted within a muddy matrix and in places cemented by anhydrite. This serves as a transition from matrix-supported sandstone to anhydrite cemented sandstone (Fig 4.7A, position A). In places anhydrite is replacing albitized K-feldspar (Fig. 4.7A, position B). The albite occurred earlier than the final mobility of anhydrite. Ilmenite has been altered (Fig. 4.7A & B), to TiO_2 minerals. Muscovite is present as large detrital grains (Fig. 4.7B) as well as within the matrix along with chlorite and illite. Illite is also present filling in secondary porosity in places. Quartz overgrowths (Fig. 4.7B, position A) are present, however they are not well expressed in this sample; likely because the anhydrite cement is early and mostly appeared before quartz overgrowths had a chance to precipitate in abundance. A single grain of fluorapatite was located, as well as an unknown Al-phosphate minerals, both diagenetic. Lithic clasts are not abundant in this sample, but where present they are quartzite clasts and do not show plastic deformation, as is commonly seen in other wells.

Summary: The detrital minerals present in this sample include quartz, albite, K-feldspar, muscovite, chlorite, biotite, ilmenite, and lithic clasts. Diagenetic minerals include illite, anhydrite (as cement), quartz overgrowths, apatite, Al-phosphate mineral, and TiO_2 minerals. The paragenetic sequence is anhydrite (seafloor diagenesis as

nodules), formation of TiO_2 minerals, dissolution of albitized K-feldspar, formation of quartz overgrowths, quickly followed by later anhydrite (thus halting the overgrowths) , and illite precipitation in secondary porosity. and formation of apatite and Al-phosphate.

Sample 3694.38: Based on drill core observation, this sample is a carbonate rock, mostly dolostone. There are sparse shell fragments present and minimal bioturbation. Grain size is very fine. Being a carbonate rock, the modal abundance of this sample was not calculated as there is a low abundance of framework grains to point count. Detrital grains in this sample include quartz, muscovite, chlorite, albite, and a bone fragment (phosphorite). Quartz and albite are very low in abundance in this sample. Minor muscovite, possibly with hydromuscovite, formed during diagenesis, and chlorite can be found in dissolution voids and in intergranular boundaries of dolomite, forming a minimal matrix component in this sample. The bone fragment, or phosphorite, will be discussed further in section 4.1.3 on coated grains. Diagenetic minerals include calcite, dolomite, pyrite, and chlorite. Dolomite precipitated in two phases: first there was early diagenetic dolomite, then it was followed by later diagenetic dolomite overgrowths (Fig. 4.7C, position A) on the existing dolomite grains (only those exposed to porosity or matrix), giving a zone appearance. Pyrite formed mainly in early diagenesis. It forms mostly as framboidal pyrite within intergranular spaces between dolomite grains (Fig. 4.7C, position B), as well as along edges of calcite, and along lines of dissolution. Calcite cement forms between dolomite phases. In places where calcite forms boundaries with dolomite, there is an absence of later diagenetic dolomite, thus calcite prevented dolomite overgrowths in these places.

Summary: The detrital minerals in this sample include quartz, muscovite, chlorite, albite, and bioclasts. Diagenetic minerals include dolomite, chlorite, calcite, and pyrite. The paragenetic sequence appears to be early diagenetic dolomite, followed by early diagenetic pyrite, followed by calcite, then later diagenetic dolomite overgrowths in places best exposed in matrix or porosity, but absent when in contact with calcite or other dolomite grains, and chlorite precipitation in porosity and between intergranular boundaries.

Sample 3696.69: Based on drill core observation, this sample is a carbonate rock. It appears homogeneous except for some large nodules, and sparse shell fragments. This section of the core transitions into muddy sandstone. The modal abundance of this sample was not calculated as this is a carbonate rock with minimal framework grains. The detrital minerals present are quartz, chlorite, zircon, and apatite as a bone fragment (phosphorite). The detrital grains present are mostly surrounded by diagenetic dolomite; this includes small grains of quartz, and laths of chlorite. Apatite is present as a bone fragment, or phosphorite, and will be discussed further in section 4.1.3 on coated grains. A single grain of zircon was found also surrounded by dolomite. Diagenetic minerals, in addition to dolomite, include calcite, ankerite, anhydrite, and pyrite. Dolomite has replaced aragonitic lime mud and bioclasts. Dolomite is both early and late as later diagenetic dolomite forms overgrowths on earlier precipitated dolomite. Pyrite forms along lines of dissolution, as well as in spherical zones between grains of dolomite (Fig. 4.7F). Where pyrite fills in void spaces, it is likely to be later diagenetic. Calcite

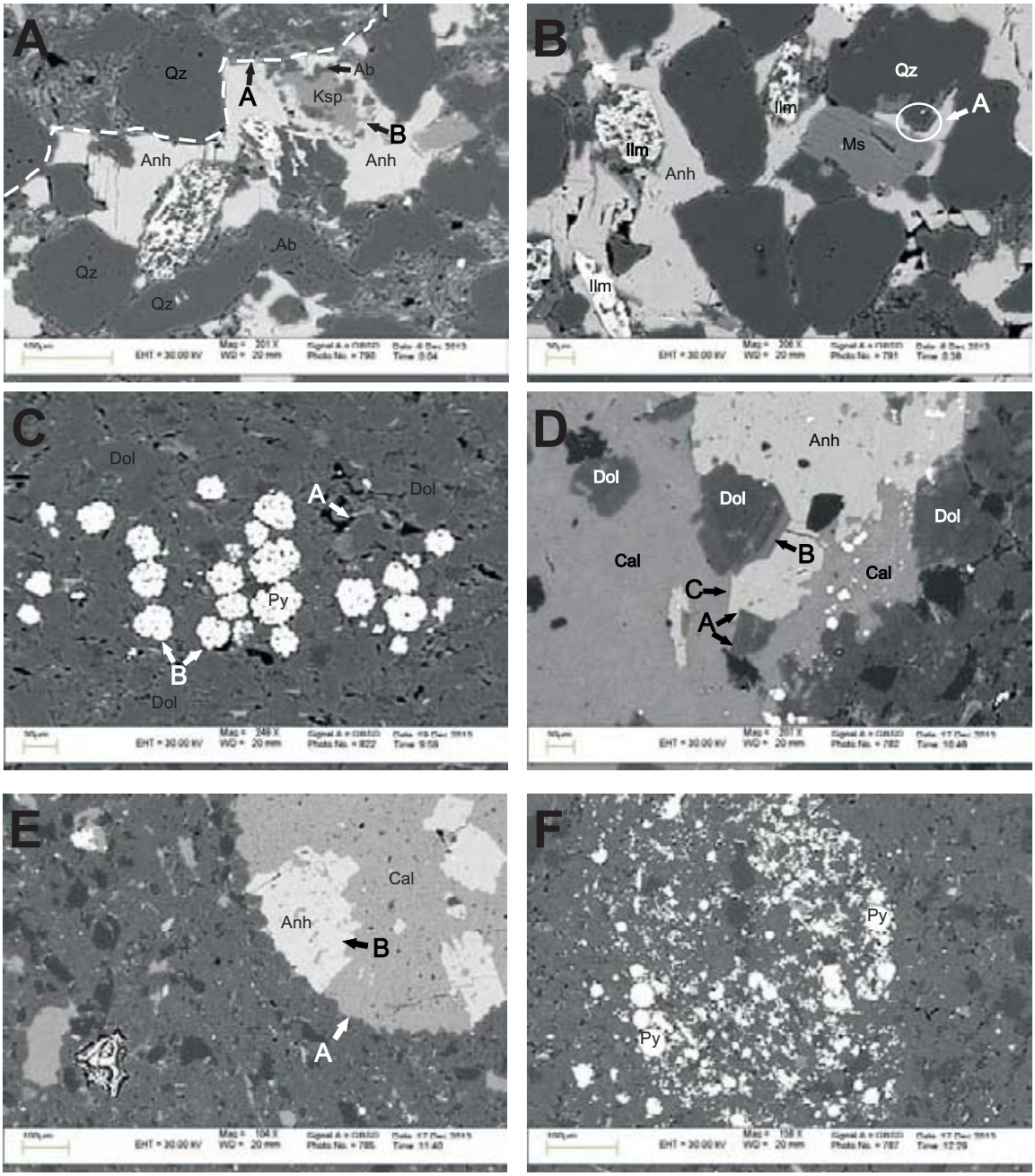

Figure 4.7: Representative backscattered electron images of minerals and textures from Mohican I-100 well. **A:** 3692.42 (App. 2B, Fig. 4). Transition zone (A) between framework grains supported by muddy matrix, and those cemented by anhydrite. Anhydrite replaces albitized K-feldspar (B). **B:** 3692.42 (App. 2B, Fig. 5). Quartz overgrowths (A) formed before anhydrite cementation. Abundant altered ilmenite. Anhydrite engulfs TiO_2 minerals. **C:** 3694.38 (App. 2C, Fig. 3). Dolomite overgrowths (A). Intergranular framboidal pyrite (B). **D:** 3696.69 (App. 2D, Fig. 3). 2 phases of dolomite precipitation: initial replacement of aragonitic lime mud, and second phase of dolomite overgrowths (A). Ankerite rimming dolomite in places (B). Calcite replaced by anhydrite (C). **E:** 3696.69 (App. 2D, Fig. 5). Zone of dolomitization (A) around calcite concretion which hosts later anhydrite that converted during diagenesis from gypsum. Dolomite also within calcite and anhydrite that formed later evidenced by straight grain boundary. **F:** 3696.69 (App. 2D, Fig. 7). Spherical zone of diagenetic pyrite fills intergranular spaces between early dolomite.

precipitated, filling in porosity along lineations, where pyrite previously formed, and forming calcite nodules as well between intergranular boundaries of dolomite. There is a zone of dolomitization (Fig. 4.7E, position A) surrounding a calcite nodule. Late anhydrite (Fig. 4.7E, position B), which probably converted from gypsum during diagenesis, is replacing the calcite nodule. Dolomite overgrowths formed after calcite and anhydrite as evidenced by straight grain boundaries between the two (Fig. 4.7D, position A), and because dolomite cross cuts both the calcite and the anhydrite. Ankerite is not abundant but is found rimming dolomite in places (Fig. 4.7D, position B). Anhydrite is found within the phosphorite showing diagenesis had an effect on the bone fragment. Anhydrite is also found in places to be replacing calcite (Fig. 4.7D, position C) evidence by straight grain boundaries.

Summary: The detrital minerals present are quartz, bioclasts, zircon, and chlorite. Diagenetic minerals are dolomite, calcite, ankerite, anhydrite, and pyrite. The paragenetic sequence is early dolomite replacing aragonitic lime mud and bioclasts, early pyrite formation, calcite precipitation, ankerite precipitation, anhydrite precipitation and replacement of calcite, and late diagenetic dolomite overgrowths, and with potential late pyrite.

Sample 3697.36B: Based on drill core observation, this sample is a carbonate rock. It contains burrows, and a large anhydrite nodule (which forms much of the polished thin section). The nodule is surrounded by fine grained grey dolomite. Being a carbonate rock, this sample was not point counted for modal composition. The detrital minerals include quartz, K-feldspar, muscovite, albite, and chlorite. Quartz, K-feldspar,

and albite are not abundant in this sample. Chlorite is also sparse, and is found as small laths bordering dolomite grains. Diagenetic minerals include dolomite, calcite, coated grains, anhydrite, barite, illite and pyrite. Dolomite is present in two stages, as early dolomite (Fig. 4.8D, position A, and as later dolomite overgrowths (Fig. 4.8D, position B). Dolomite overgrowths only form where exposed to matrix or porosity, and not when in contact with other grains of dolomite or other diagenetic minerals. There was a fracturing event during diagenesis, sub-parallel to bedding, which shows a relationship with dolomite diagenesis. Fracturing occurred within early diagenetic dolomite grains, where the dolomite crystal outline is seen across the fracture (Fig. 4.8A, position A). After fracturing, late diagenetic dolomite has precipitated along the edges of the dolomite, including the portion that was fractured (Figs. 4.8A & C). Calcite forms small nodules in places (Fig. 4.8C, position A) and is partly replaced by anhydrite. Anhydrite forms not only as a replacement to calcite, but as large nodules (Fig. 4.8B), and is visible in the drill core. Along the boundary of the nodule there is a zone of dolomitization. Pyrite fills microporosity forming a cement along with muscovite and illite (Fig. 4.8D). There is a coated grain present in this sample which will be further discussed in section 4.1.3 on coated grains. Barite was found within a calcite nodule, showing that it may be diagenetic, however, it is difficult to determine as barite does not appear elsewhere as a diagenetic mineral, only as drilling mud. In places where dolomite contained >3% of FeO^t it was classified as Fe-dolomite.

Summary: The detrital minerals in this sample include quartz, K-feldspar, muscovite, albite, and chlorite. Diagenetic minerals include dolomite, calcite, chlorite, pyrite, anhydrite, barite, illite, and coated grains. The paragenetic sequence is coated

grains, early diagenetic dolomite, pyrite precipitation filling microporosity, fracturing, barite precipitation, calcite precipitation, anhydrite precipitation with replacement of calcite, illite precipitation filling microporosity, and later diagenetic dolomite.

Sample 3697.86: Based on drill core observation, this sample is a very fine grained sandstone, with silty mud layers. It is sparsely bioturbated and contains mud drapes and pockets of anhydrite. In polished thin section, the modal composition of this sample is that of subarkose (Fig. 4.1), based on detrital mineral point counts. It contains detrital minerals of quartz, albite, K-feldspar, muscovite, zircon, fluorapatite, ilmenite, chlorite, biotite, monazite, perthite, and lithic clasts. Secondary porosity is found within framework grains, mainly albite, but also quartz and K-feldspar (some with perthite texture). There are sporadic grains of zircon, fluorapatite, and monazite throughout. There are laths of biotite and chlorite present as larger grains, and chlorite is also present as fine grains within the matrix. Lithic clasts present in this sample are not abundant, but there is one clast that contains K-feldspar, albite, and chalcopyrite (Fig. 4.8F, position A), whereas another clast forms a pseudomatrix between detrital quartz and albite (see App. 2F, Fig. 8). Diagenetic minerals include anhydrite, quartz overgrowths, illite, TiO_2 minerals, and dolomite. TiO_2 minerals formed from the alteration of ilmenite. Dolomite is sparse, but in places can be found replacing K-feldspar after dissolution. Illite forms within the matrix supporting framework grains. Quartz overgrowths form bordering anhydrite, showing that the overgrowths formed before anhydrite precipitated. Quartz overgrowths are also found forming an apparent triple point showing that overgrowths

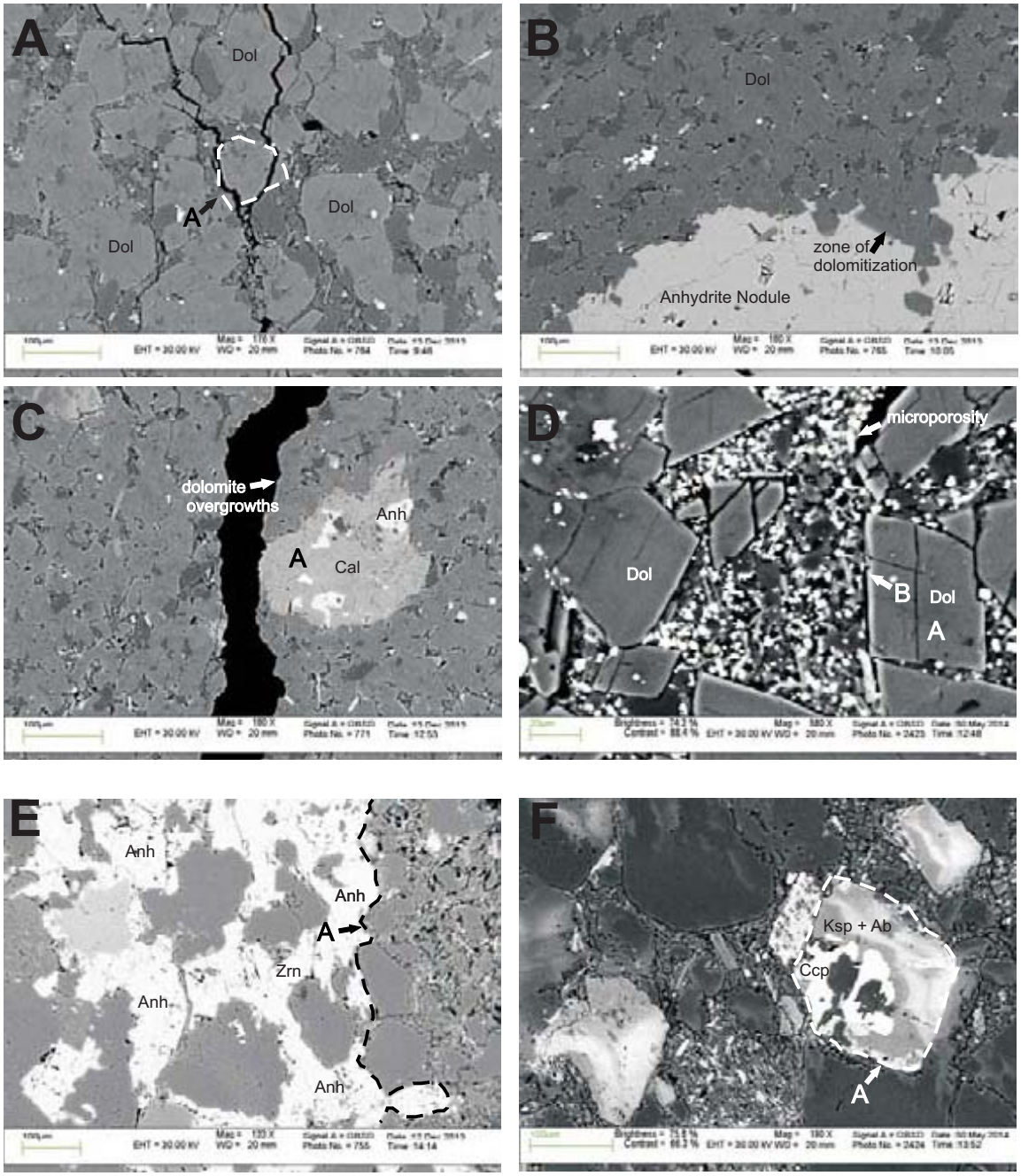

Figure 4.8: Representative backscattered electron images of minerals and textures from Mohican I-100 well. **A:** 3697.36B (App. 2E, Fig. 1). Fracturing event (A) occured after precipitation of early dolomite, and before that of late dolomite overgrowth. **B:** 3697.36B (App. 2E, Fig. 2). Anhydrite nodule surrounded by zone of dolomitization. **C:** 3697.36B (App. 2E, Fig. 5). Calcite nodule (A) partly replaced by anhydrite. Dolomite overgrowths visible bordering porosity from fracture. **D:** 3697.36B (App. 2E, Fig. 10). Early dolomite (A) rimmed by later diagenetic overgrowths (B); microporosity of pyrite, dolomite, muscovite and illite. **E:** 3697.86 (App. 2F. Fig. 1). Contact (A) between matrix-supported zone and an anhydrite cemented zone. Detrital euhedral zircon grain cemented by anhydrite. **F:** 3697.86 (App. 2F, Fig. 2). Lithic clast (A) composed of chalcopyrite, K-feldspar, and albite.

formed after compaction. Anhydrite forms cement, and can be seen in contact with the matrix-supported zone of this thin section (Fig. 4.8E, position A).

Summary: The detrital minerals in this sample include quartz, albite, K-feldspar, muscovite, zircon, fluorapatite, ilmenite, chlorite, biotite, monazite, perthite, and lithic clasts. Diagenetic minerals include dolomite, anhydrite, illite, TiO_2 minerals, and quartz overgrowths. Compaction created a pseudomatrix with lithic clasts. The paragenetic sequence is diagenetic dolomite, alteration of ilmenite to produce TiO_2 minerals, illite precipitation, quartz overgrowth formation, and late anhydrite precipitation.

4.1.2.3 Wyandot E-53

Sample 2873.10: Based on drill core observation, this sample is a carbonate rock that contains visible shell fragments and burrow tracks in the drill core. This section of core is overlying sandstone interbedded with mud drapes. In polished thin section, the modal composition of this sample is that of arkose (Fig. 4.1), based on point counts of detrital minerals, which do not include the carbonate portion. It contains detrital grains of quartz, K-feldspar, albite, and bioclasts. The main cement is calcite. The detrital minerals, mainly quartz and K-feldspar, suffered both dissolution and replacement by diagenetic minerals throughout the sample. A large bioclast (Fig. 4.9A, position A), which contains sparry calcite in places, obviously underwent dissolution followed by partial replacement by ankerite that fills dissolution voids. The smaller bioclast (Fig. 4.9A, position B) is composed of calcite and is only partially dissolved. In Figure 4.9B, there is slight dissolution of quartz, and a more advanced dissolution of K-feldspar. The K-feldspar (Fig. 4.9B, position A) has been partly replaced by ankerite, with only K-

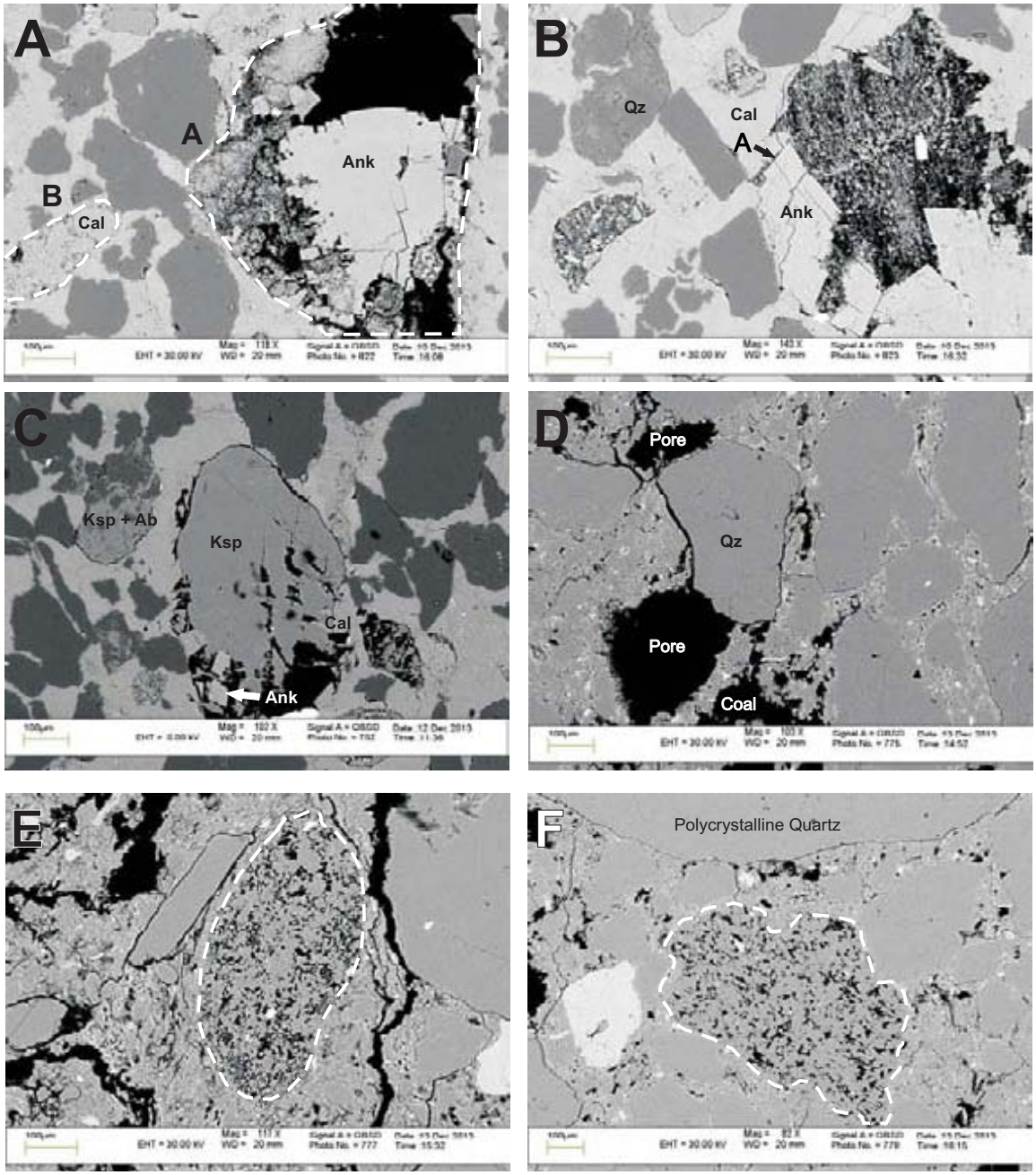

Figure 4.9: Representative backscattered electon images of minerals and textures from Wyandot E-53 well. **A:** 2873.10 (App 3A, Fig. 3). Large bioclast (position A) dissolved with replacement by ankerite, and smaller bioclast (position B) of calcite. **B:** 2873.10 (App 3A, Fig. 4) Early dissolution of quartz. Advanced dissolution of K-feldspar with partial replacement by ankerite. **C:** 2873.10 (App 3A, Fig. 8). Partial dissolution of K-feldspar with minimal replacement by ankerite and calcite. Quartz overgrowths. **D:** 2876.81 (App 3B, Fig. 2). Coal. Fractured quartz. **E:** 2876.81 (App 3B, Fig. 4). Quartzite lithic clast with secondary porosity. **F:** 2876.81 (App 3B, Fig. 6). Quartzite lithic clast with secondary porosity. Diagenetic rutile and detrital polycrystalline quartz present.

feldspar relics left. However, K-feldspar is not always highly dissolved. As seen in Figure 4.9C, K-feldspar has undergone only partial dissolution with minimal replacement by ankerite and some calcite. In some locations, illite fills pores left by K-feldspar dissolution. Calcite present in this sample is a Fe-calcite. Quartz overgrowths are also present (Fig. 4.9C), with a narrow zone of dissolution separating the overgrowths from the calcite cement. Diagenetic dolomite is present, but not abundant, and when present it is in conjunction with partially dissolved bioclasts. Minimal amounts of diagenetic chlorite is present within dissolution voids. Pyrite is present in minimal amounts. Coated grains are also present in this sample and are further discussed later (in section 4.1.3). Barite is present within voids, but textural evidence suggests that it is not diagenetic. It fills voids but it does not exhibit sharp crystal outlines.

Summary: The detrital minerals present in this sample are K-feldspar, quartz, albite, and bioclasts. The diagenetic minerals are calcite, Fe-calcite, ankerite, dolomite, pyrite, illite, chlorite, quartz overgrowths, and coated grains. The paragenetic sequence appears to be coated grain formation, pyrite precipitation, K-feldspar and quartz dissolution, bioclast dissolution, quartz overgrowths, calcite precipitation, illite precipitation, chlorite precipitation, Fe-calcite precipitation, ankerite precipitation, and dolomite precipitation.

Sample 2876.81: Based on drill core observation, this sample is a coarse grained sandstone containing a slightly green matrix. The grain size is overall coarse grained, but it varies from fine to coarse. The core also contains a coal seam and coal fragments. The modal composition of this sample is that of subarkose (Fig. 4.1). In thin section it

contains high porosity, both within grains (secondary porosity) and within intergranular spaces between framework grains. The detrital minerals include K-feldspar (some with perthite texture), quartz, albite, zircon, muscovite, monazite, and lithic clasts. Lithic clasts in this sample are mostly quartzite (Fig. 4.9E and F), and have undergone some dissolution. Most quartz grains are highly fractured (Fig. 4.9D). Diagenetic minerals include kaolinite, TiO_2 minerals, and coal. Coal is present in this sample (Fig. 4.9D), which is misleading in the BSE images as both pores and coal appear as black in BSE images. Determination of coal versus porosity had to be made using a petrographic microscope in plane polarized light where the coal appears clear and porosity appears blue from the epoxy used for the impregnation of the polished thin section. TiO_2 minerals formed as diagenetic minerals, appearing within secondary porosity of a lithic clast (Fig. 4.9E), and within matrix and cement in other places. Kaolinite is not abundant, but is present in the matrix as well as filling in dissolution voids in lithic clasts. Apatite is present in a lithic clast, though it is difficult to distinguish if it is a detrital mineral within the clast, or if it is diagenetic and formed after the clast was partially dissolved.

Summary: The detrital minerals in this sample include K-feldspar, quartz, albite, zircon, muscovite, monazite, and lithic clasts. The diagenetic minerals include TiO_2 minerals, coal, kaolinite, and possibly apatite. Fracturing and secondary porosity are high in this sample. The paragenetic sequence is coal formation, dissolution of lithic clasts, kaolinite and possibly apatite, and TiO_2 precipitation.

Sample 2878.66: Based on drill core observation, this sample is a coarse grained, poorly sorted, sandstone, which contains clasts up to 1.5cm in length. The modal

composition of this sample is that of subarkose (Fig. 4.1). Detrital minerals include quartz, K-feldspar, albite, and muscovite. K-feldspar in this sample has not undergone much dissolution, however, albitized K-feldspar and albite grains, have undergone much dissolution, contributing to the high secondary porosity seen (Fig. 4.10A). Diagenetic minerals are pyrite, illite, kaolinite, and TiO_2. Kaolinite appears to have been in the early stages of forming cement where framework grains have undergone dissolution leaving high intergranular porosity between more stable framework grains (Fig 4.10A). Kaolinite also precipitates within spaces between expanding cleavage planes of detrital muscovite (Fig. 4.10B). Pyrite fills both primary and secondary porosity. It is thus found within intergranular spaces between framework grains, as well as within secondary porosity in lithic clasts (Fig. 4.10C). TiO_2 minerals precipitated, in small amounts, within secondary porosity. Illite also fills dissolution voids. Barite is present in this sample, but it appears only as a drilling mud.

Summary: Detrital minerals present are K-feldspar, quartz, albite, and muscovite. Diagenetic minerals are pyrite, illite, kaolinite, and TiO_2. Important textures in this sample is the high secondary porosity created by albite and albitized K-feldspar dissolution and their partial replacement by kaolinite. The paragenetic sequence is dissolution of feldspars, kaolinite precipitation, pyrite, illite and TiO_2 precipitation.

Sample 2880.22: Based on drill core observation, this sample is a carbonate rock. It lies near a sharp contact with a section of coarser sandstone. The modal composition of this sample is that of subarkose (Fig. 4.1). Detrital minerals include quartz, K-feldspar, albite, muscovite, garnet-spessartine, zircon, and lithic clasts. Diagenetic

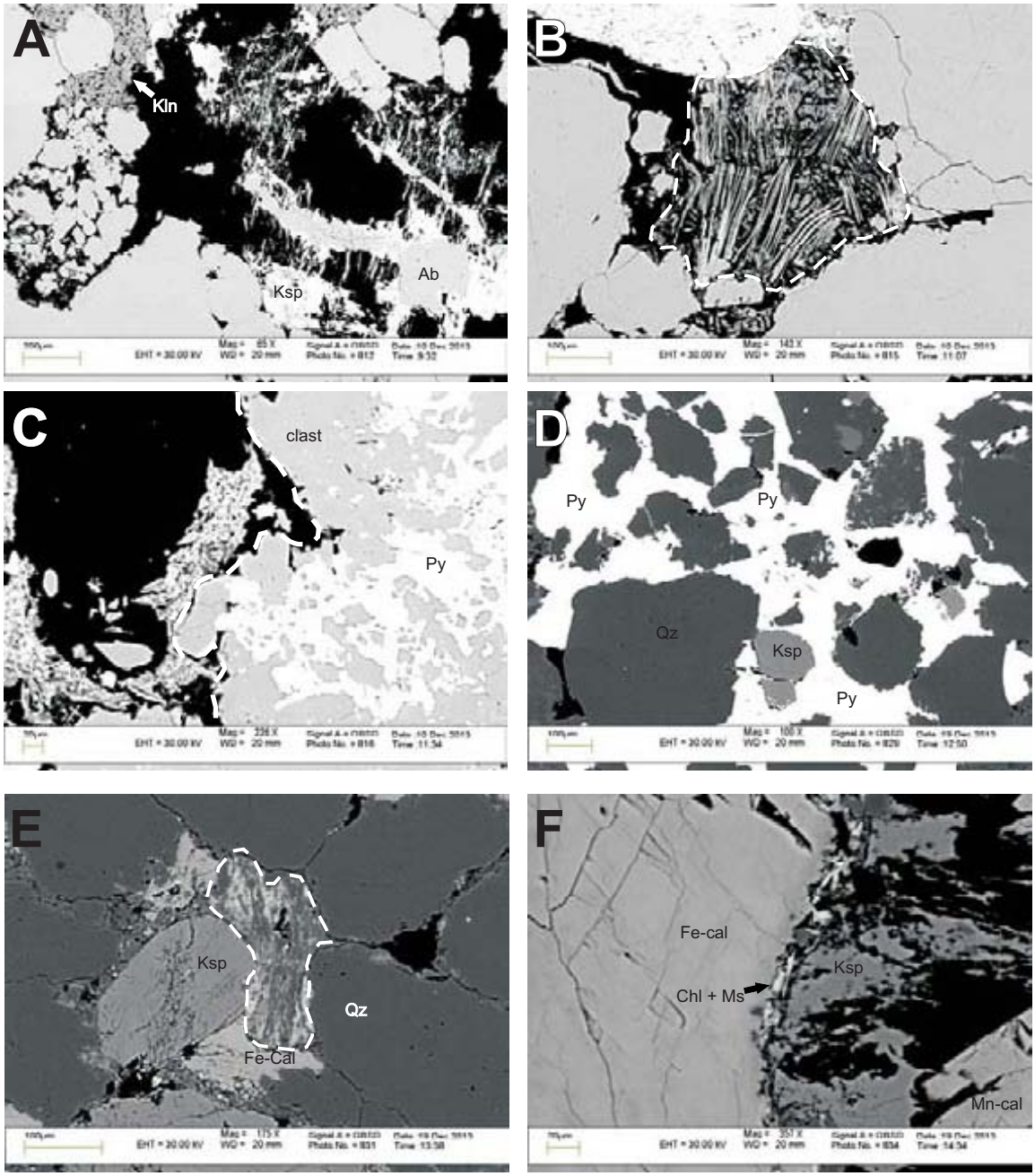

Figure 4.10: Representative backscattered electron images of minerals and textures from Wyandot E-53 well. **A:** 2878.66 (App. 3C, Fig. 2). High secondary porosity from mostly dissolution of K-feldspar and albite, partly filled in by kaolinite. **B:** 2878.66 (App. 3C, Fig. 5). Precipitation of kaolinite between expanding cleavage planes of detrital muscovite. **C:** 2878.66 (App. 3C, Fig. 6). Diagenetic pyrite forms in porosity in quartz-rich lithic clast. **D:** 2880.22 (App. 3D, Fig. 2) Diagenetic pyrite forming a cemented concretion around detrital grains. **E:** 2880.22 (App. 3D, Fig. 4). Lithic clast, composed of quartz, muscovite, and illite, plastically deformed around detrital minerals, and cemented by Fe-calcite. **F:** 2880.22 (App. 3D, Fig. 7). Dissolution of K-feldspar, which was cemented by Fe-calcite, followed by precipitation of Mn-calcite within secondary porosity. Chlorite and muscovite between Fe-calcite and K-feldspar.

minerals include Fe and Mn-calcite, ankerite, pyrite, chlorite, and TiO_2 minerals. Calcite is the major cement in this sample, occurring as Mn-calcite and Fe-calcite. Relics of detrital spessartine garnet are found cemented by Mn-calcite. This area of calcite is enriched in manganese because of the breakdown of spessartine giving extra ions of manganese to be incorporated into the formation of Mn-calcite. Pyrite (Fig. 4.10D) forms along intergranular boundaries of detrital grains of quartz, K-feldspar, and albite, forming often a small concretion. The pyrite contains dissolution voids. A lithic clast (Fig. 4.10E), composed mainly of quartz and muscovite, has been partially plastically deformed between grains of quartz and K-feldspar. Partially dissolved detrital K-feldspar (Fig. 4.10F) is bordered by Fe-calcite. Chloritized muscovite may be detrital, or the chloritization may be the result of diagenesis. Chlorite and minor muscovite (forming pseudomatrix) formed along the boundary between K-feldspar and Fe-calcite. Mn-calcite fills secondary porosity created by K-feldspar dissolution. This suggests that Fe-calcite formed cement in primary porosity before, or near the initiation, of K-feldspar dissolution. Once dissolution had progressed far enough, Mn-calcite was then precipitating, filling secondary porosity. Therefore, it seems Mn-calcite postdates Fe-calcite, with K-feldspar dissolution occurring between the two events. Minor amounts of ankerite are present, filling dissolution voids in calcite.

Summary: Detrital minerals present are K-feldspar, muscovite, albite, quartz, garnet-spessartine, zircon and lithic clasts. Diagenetic minerals are calcite (Fe and Mn rich), ankerite, pyrite, chlorite and TiO_2 minerals. Important textures are dissolution of detrital grains, and plastic deformation of lithic clasts and plastic minerals (e.g. muscovite) creating this pseudomatrix. The paragenetic sequence is pyrite precipitation,

Fe-calcite precipitation, feldspar dissolution, Mn-calcite precipitation, ankerite precipitation, and TiO_2 mineral precipitation. The formation of chlorite within the paragenetic sequence is uncertain.

4.1.3 Coated Grains and Phosphorites

4.1.3.1 Background

Coated grains and phosphorites have both been identified within the Scotian Basin. Coated grains of Upper Jurassic – Lower Cretaceous age were studied by Okwese et al. (2012). Lower Cretaceous phosphorites of the Orpheus Graben were studied by Pe-Piper and Weir-Murphy (2008). These two studies serve as a comparison in this study of the coated grains and phosphorites found within studied samples. These grains were found in 5 analyzed sites within the wells Mohican I-100 and Wyandot E-53. No coated grains or phosphorites were recognized in the studied samples of Mic Mac H-86.

Coated grains from the wells Thebaud C-74 and Peskowesk A-99 (Okwese et al., 2012) were analyzed and four varieties of coated grains types were noted. Type A coated grains are Fe-rich, and usually composed of siderite or glauconite ± chlorite ± francolite. Intergranular cements can be Fe-calcite, calcite, siderite, minor pyrite, and chlorite. Type B coated grains are composed of Fe-calcite and chlorite in alternating layers. Type C coated grains a mainly composed of calcite, Fe-calcite, and pyrite. Clay minerals, likely detrital, may be present within the center of the type C coated grain. Type D coated grains have an outermost layer of Mg-calcite, with ankerite, Fe-calcite, pyrite, and clay minerals within the interior.

Phosphorites from the Orpheus Graben in the Scotian Basin were studied (Pe-Piper and Weir-Murphy, 2008). These are carbonate-fluorapatite rocks that contain at least 15 wt% P_2O_5. They are present in the Scotian Basin as intraformational clasts, intraformational nodules, in coated grains, and as skeletal fragments. Content of fluorine is generally >3 wt% in phosphorites.

4.1.3.2 Description of Studied Samples

Mohican I-100

Sample 3694.38 site 4: This sample has an analyzed site that contains a columnar fragment (Fig. 4.11A) that is composed mainly of fluorapatite and pyrite. Based on chemical analysis and habit of this fragment, this is likely a bone fragment. This grain is classified as a phosphorite because it is likely a bone fragment and it is composed mostly of fluorapatite with pyrite.

Sample 3696.69 site 4: This sample has an analyzed site that contains a columnar fragment (Fig. 4.11B). However, this fragment is composed of apatite, anhydrite and halite. The sample is also likely to be a bone fragment. The presence of anhydrite suggests that this fragment contained pores (more evidence of being a bone) which incorporated anhydrite during diagenesis. The grain is classified as a phosphorite because it is likely a bone fragment.

Sample 3697.36B site 7: This sample contains an ovoid grain (Fig. 4.11C) composed of fluorapatite, apatite, pyrite and marcasite (distinguished from pyrite in

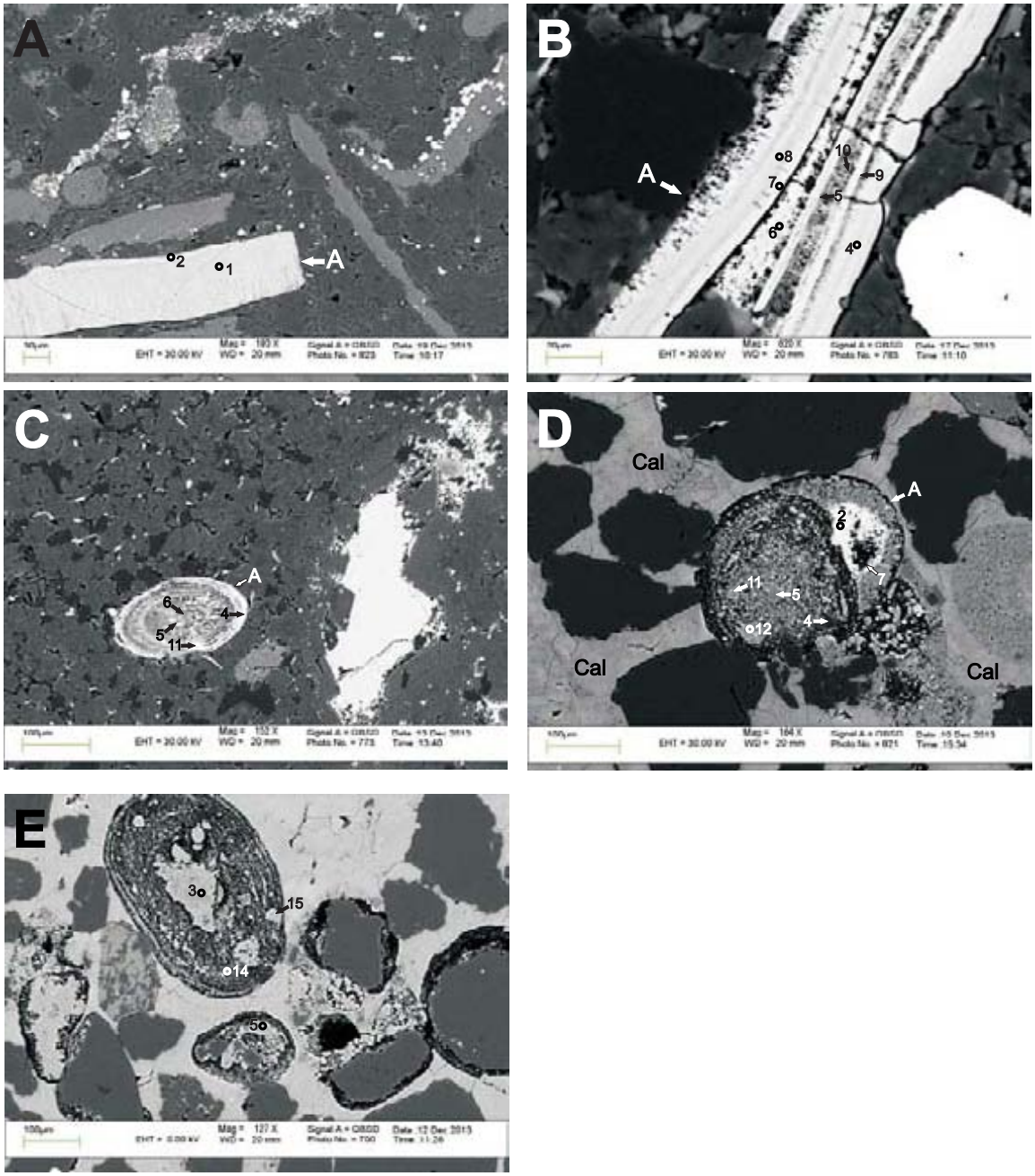

Figure 4.11: Representative backscattered electron images of coated grains and phosphorites from Mohican I-100 and Wyandot E-53 wells. **A:** I-100: 3694.38 (App. 2C, Fig. 4). Phosphorite (position A) (likely a bone fragment) composed of fluorapatite and pyrite. **B:** I-100: 3696.69 (App. 2D, Fig. 4). Phosphorite (position A)(likely a bone fragment) composed of apatite, anhydrite and halite (spots 4-10). Anhydrite formed in pore spaces during diagenesis. **C:** I-100: 3697.36B (App. 2E, Fig. 7). Coated grain (position A) composed of fluorapatite & pyrite (spots 4 & 6), marcasite and apatite (spot 5), and fluorapatite, chlorite and illite (spot 11). **D:** E-53: 2873.10 (App. 3A, Fig. 2). Phosphorite (position A) composed of fluorapatite (spot 2), calcite (spots 5, 11 & 12), quartz (spot 4) and apatite and chlorite (spot 7) surrounded by calcite cement. **E:** E-53: 2873.10 (App. 3A, Fig. 6). Coated grains, mostly calcite (spots 3, 5), Fe-calcite (spot 15) and mixture of chlorite, illite and calcite (spot 14).

chemical analysis by the presence of CuO and As_2O_3). This is considered a coated grain because it has clear concentric layers. However, this coated grain does not fit into any of the types as proposed by Okwese et al. (2012), due to the presence of apatite and fluorapatite.

Wyandot E-53

Sample 2873.10 site 2: This sample contains a round coated grain (Fig. 4.11D) composed mainly of fluorapatite and calcite. Concentric layers can be seen around the edge of the grain. This grain has been cemented by calcite. The presence of fluorapatite and calcite in this grain suggests that this may be a phosphorite.

Sample 2873.10 site 6: This sample contains several coated grains (Fig. 4.11E), mostly calcite rich, including Fe-calcite, and minor amount of ankerite. These grains are cemented by calcite. These grains are considered as coated grains, of type D, because of the presence of calcite and ankerite.

4.1.4 Barite

Barite may be either diagenetic or from drilling mud. Determination as to the classification of each barite analysis was based on several factors, as proposed by Pe-Piper et al. 2014. These factors are crystal outlines, mode of occurrence, and texture relationship between barite and other grains, including both framework grains and diagenetic minerals. Barite found within open pore space is considered to be from

drilling mud. Barite is considered diagenetic if it forms straight crystal outlines, such as when it is replacing another mineral.

4.2 X-Ray Diffraction

X-ray diffraction (XRD) is often used to study clay minerals which can be difficult to distinguish petrographically given that the majority of clay minerals are less than 2 microns (Moore & Reynolds, 1997). The d-spacing, given in ångströms (Å), is the distance between crystal atomic planes. For most samples of this study (Table 4.2 for XRD data), clay minerals identified from diffractograms are similar to those found elsewhere in the Scotian Basin and are most clearly distinguished in the <2 micron oriented mounts, because grains will orient their 00*l* planes parallel to the slide, and therefore only 00*l* reflections appear in the data. For example, illite peaks that are commonly found are those of 001, 002, and 003 reflections, corresponding to 10.1Å, 5Å and 3.33Å, respectively. However, the 3.33Å (003) peak for illite is often overlapped with the principal quartz peak. The principal minerals are identified using criteria summarized by Aneja (2012) and White (2014).

Well	Depth (m)	Observations
Mic Mac H-86 *No kaolinite in BSE	4717.78	- small 001 illite peak at 10Å, increases intensity and shows a second peak (mixed layer of illite chlorite?) during run 2, intensity increases slightly with heat - small 002 illite peak at 5Å, increases intensity during run 2, increases intensity slightly when heat is added - small chlorite and/or kaolinite, peak at 7.1Å, increases very slightly in run 2, heat and glycolation have no real effect . However, no peak at 3.57Å and thus this peak must be chlorite - 4.7Å chlorite peak, showing off the side of the 002 illite peak in run 2, slightly increase in intensity with heat - 3.52Å chlorite peak

Mic Mac H-86 **No kaolinite in BSE*	4719.78	- small 001 illite peak at 10Å, increases in intensity during run 2 with presence of a second 11Å peak of a mixed layer, intensity increases slightly with heat – illite chlorite mixed layer? - 7.1Å peak – kaolinite and/or chlorite – appearing with oriented samples, small and doesn't increase much with temperature, but no kaolinite peak at 3.57Å – thus all must be chlorite - 5Å 002 illite peak, intensity increase with oriented sample, still present in heated sample - small 4.7Å chlorite, or mixed layer, peak, does not increase in intensity over samples
Mohican I-100 **No kaolinite in BSE*	3692.42	- 001 illite at 10Å, intensity increases with oriented mount - very small chlorite peak at 7Å, intensity increases with oriented mount - chlorite peak at 4.7Å, no change between runs - 5Å 002 illite peak appears in the oriented run - no glycolation or heat treatment on this sample - 14Å peak of chlorite in the oriented mount - small peak at 11Å and 7.8Å in oriented mount – likely mixed layer of illite-chlorite - peak around 3.5Å suggests only chlorite is present, with no kaolinite present
Mohican I-100	3696.55 shale	- 001 10Å illite peak shows in methanol mount, increases intensity in oriented run #2; secondary peak at 11Å may represent a mixed layer with chlorite - illite - 7Å chlorite peak - 5Å illite peak and 4.7Å chlorite peak shows more overlap during run 2 - 3.52Å chlorite peak, shows second peak in run 1, which disappears for run 2 - no glycolation or heat treatment on this sample - no evidence for kaolinite in 3.52Å. No evidence for calcite or dolomite, although 3.1Å peak might be a carbonate
Mohican I-100	3697.95	- small 001 illite peak at 10Å in run 1, intensity increases in oriented mount (2) and it shows a second peak on it at about 11Å, possibly showing a mixed layer with chlorite, intensity increases slightly during heat treatment - small chlorite peak at 14Å appears during oriented mount and remains for heat treatment - 002 illite peak at 5Å, increases with oriented mount, no change between different heat stages - 7Å chlorite peak increases with intensity with each run, and with added heat - peak at ~3.85Å in methanol mount that mostly disappears in oriented mount and heat treatments - peak at 3.54Å of chlorite in the oriented mount, intensity increasing with temperature
Wyandot E-53	2876.35	- rutile peak at 2.28Å - 3.52Å – probably chlorite (not so much anatase to be detected by XRD) - no 001 illite peak with methanol mount, but small peak appears during oriented run 2 at 10Å - chlorite 7Å barely present in methanol mount, small peak appears in oriented run. This may be either chlorite and/or kaolinite - possible illite peak with quartz peak at 3.35Å and 10Å not visible with oriented mount - no glycolation or heat treatment on this sample

Wyandot E-53 **kaolinite in BSE*	2876.81	- no illite peaks - Trace peak at 7Å,may be chlorite or kaolinite, no change with run #2 - no glycolation or heat treatment on this sample - virtually no clay minerals in this samples
Wyandot E-53	2877.03	- very small 001 illite peak at 10Å, becomes much more intense with oriented mount and shows a second peak at 10.9Å showing a possible mixed layer, illite peak becomes more intense with heat, but the second peak almost collapsed at 300 degrees - Peak at 7.1Å increases intensity with oriented mount, still present with heat – after heating to 300°C; although not certain could be chlorite + kaolinite mixture - 3.58Å kaolinite, or chlorite, peak with oriented mount, slight intensity increase with heat, no collapse at 300°C - small peak at 3.51Å – possible anatase, no change with heat - 5Å peak 002 illite barely present in methanol mount, increases intensity in oriented mount, collapses slightly between 150-300 degrees - no visible 003 illite peak present

Table 4.2: Data for X-Ray diffraction samples.

4.2.1 Illite

Illite shows clear diffractions at 10.1Å (001) and 5Å (002), but the (003) peak at 3.33Å is overlapped by the principal quartz peak. The 003 illite and quartz peaks do not separate so it is difficult to determine if a 003 illite peak is really present. The intensity of illite, when present, generally increases from random methanol mount, to <2 micron oriented and heat treatment. Many samples show a second peak during the <2 micron mount which represents a chlorite-illite mixed layer. Sample 2876.81 (Fig. 4.17) from Wyandot E-53 shows no illite peak in either random methanol mount or in <2 micron oriented mount. This is consistent with data collected from the scanning electron microscope that shows no analyses of illite present. All other samples have an illite peak either appearing in the random mount or not until the oriented <2 micron mount as in Wyandot E-53 2876.35 (Fig. 4.17).

4.2.2 Chlorite

Chlorite produces diffractions at 14Å (001), 7Å (002), 4.7Å (003) and 3.54Å (004). The chlorite 002 peak and the kaolinite 001 peak overlap, and the chlorite 004 peak and the kaolinite 002 peak overlap. In samples 4717.78 (Fig. 4.12) and 4719.78 (Fig. 4.13) of Mic Mac H-86, and in 3692.42 (Fig. 4.16) and 3697.95 (Fig. 4.14) of Mohican I-100, there is a 7.1Å peak and this is determined to be chlorite because scanning electron microscope and backscattered electron images, of this study, show there being no kaolinite present in this sample depth. Sample 2876.81 (Fig. 4.17) from Wyandot E-53 shows a trace peak at 7Å that may be a mixture of chlorite and kaolinite. Backscattered images of this sample show both chlorite and kaolinite present, but at limited amounts. Sample 2877.03 (Fig. 4.15) has an overlap of kaolinite 002 and chlorite 004, as best seen in the bulk run (Fig. 4.18), which was run from 2 to 40 degrees 2θ (scattering angle) at half the normal clay run scan speed in order to better separate the overlapping peaks.

4.2.3 Kaolinite

Kaolinite produces diffractions at 7.1Å (001) and 3.57Å (002). These are often found overlapping with chlorite (002) and (004) respectively. Kaolinite is present in Wyandot E-53 2876.81 (Fig. 4.17) in XRD and in SEM analyses and BSE. Kaolinite may be present in Wyandot E-53 2876.35 (Fig. 4.17) and 2877.03 (Fig. 4.15), overlapping with chlorite. However, it is not likely present in either Mic Mac H-86 (Figs. 4.12 & 4.13) samples or Mohican I-200 3692.42 (Fig. 4.16) as SEM analyses and BSE do not show this mineral present.

4.2.4 Mixed Layer Clays

Mixed layer clays appear to be mostly illite-chlorite (I-C) layers. These appear in many samples that contain illite. When samples are run as <2 micron oriented slides then mixed layer clays appear with illite 001 that shows a second peak representing a chlorite mixed layer, as can be seen in Fig. 4.15 of Mohican I-100 3697.95. The mixed layers are not likely to be smectite-illite layers because there is no smectite peak present at 14-16Å.

4.2.5 Quartz

Quartz is present in all samples (Figs. 4.12-4.18), showing peaks at 4.26Å and 3.35Å. The peak at 3.35Å also overlaps with the 003 illite peak which prevents definite determination of illite 003.

4.2.6 Zincite

Zincite peaks are present at 2.48Å, 2.6Å and 2.8Å because a zinc oxide standard was added to the <2 micron samples before centrifuging. Zincite and quartz peaks were added to XRD diffractograms to align the diffractograms, and are present in diffractograms showing <2 micron oriented mounts.

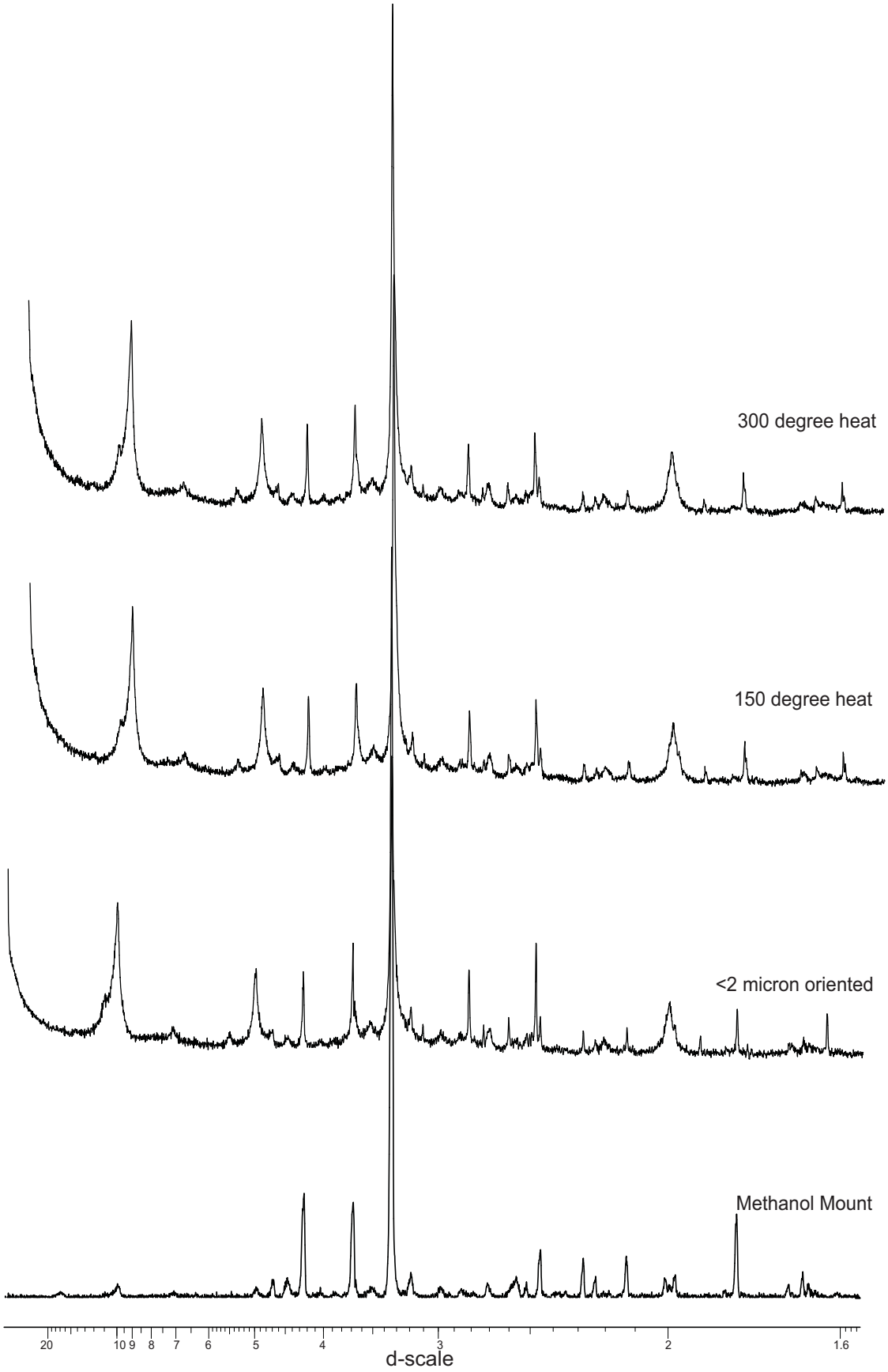

Fig. 4.12: X-Ray Diffractograms for Mic Mac H-86 well at 4717.78m

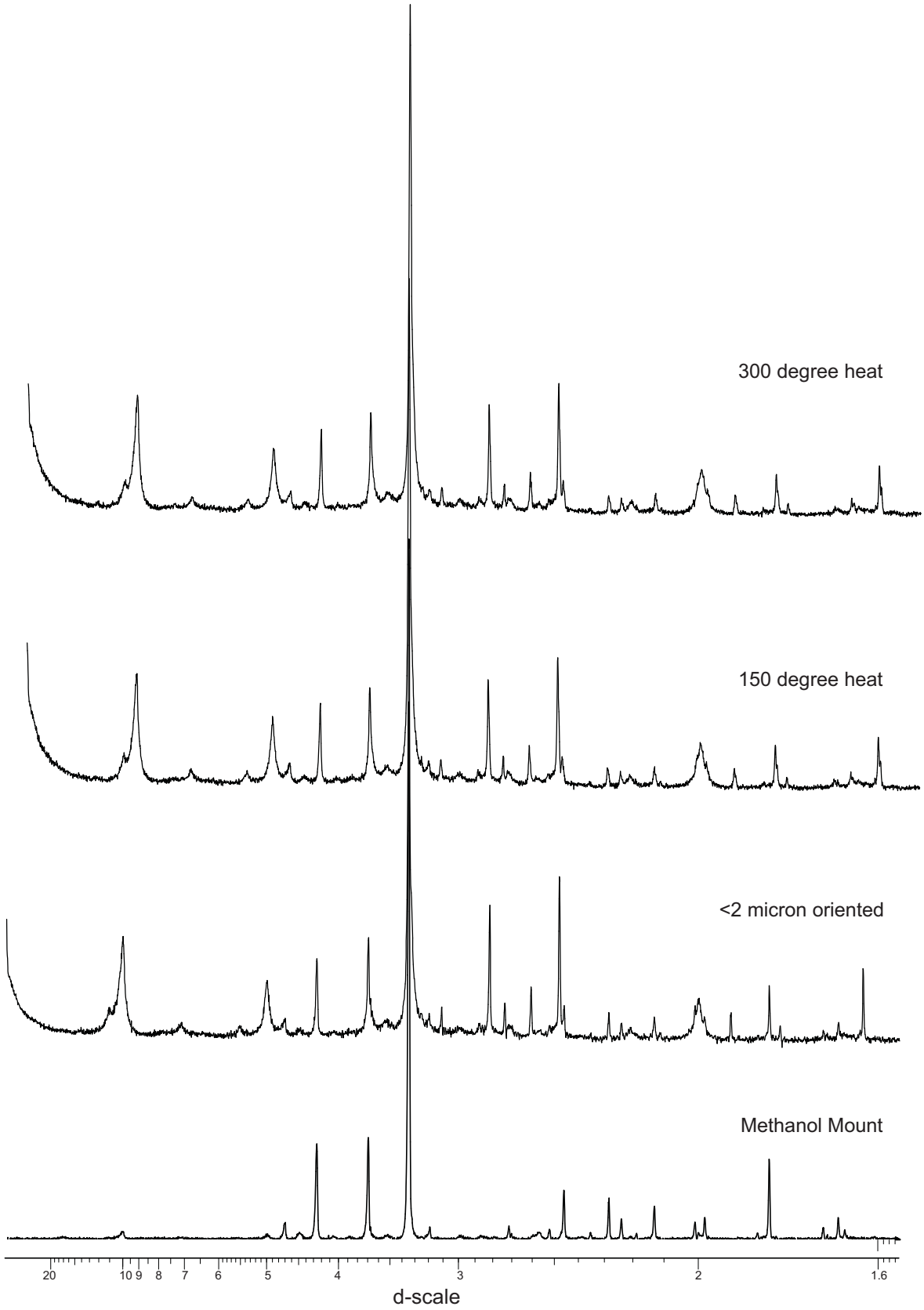

Fig. 4.13: X-Ray Diffractograms for Mic Mac H-86 well at 4719.78m

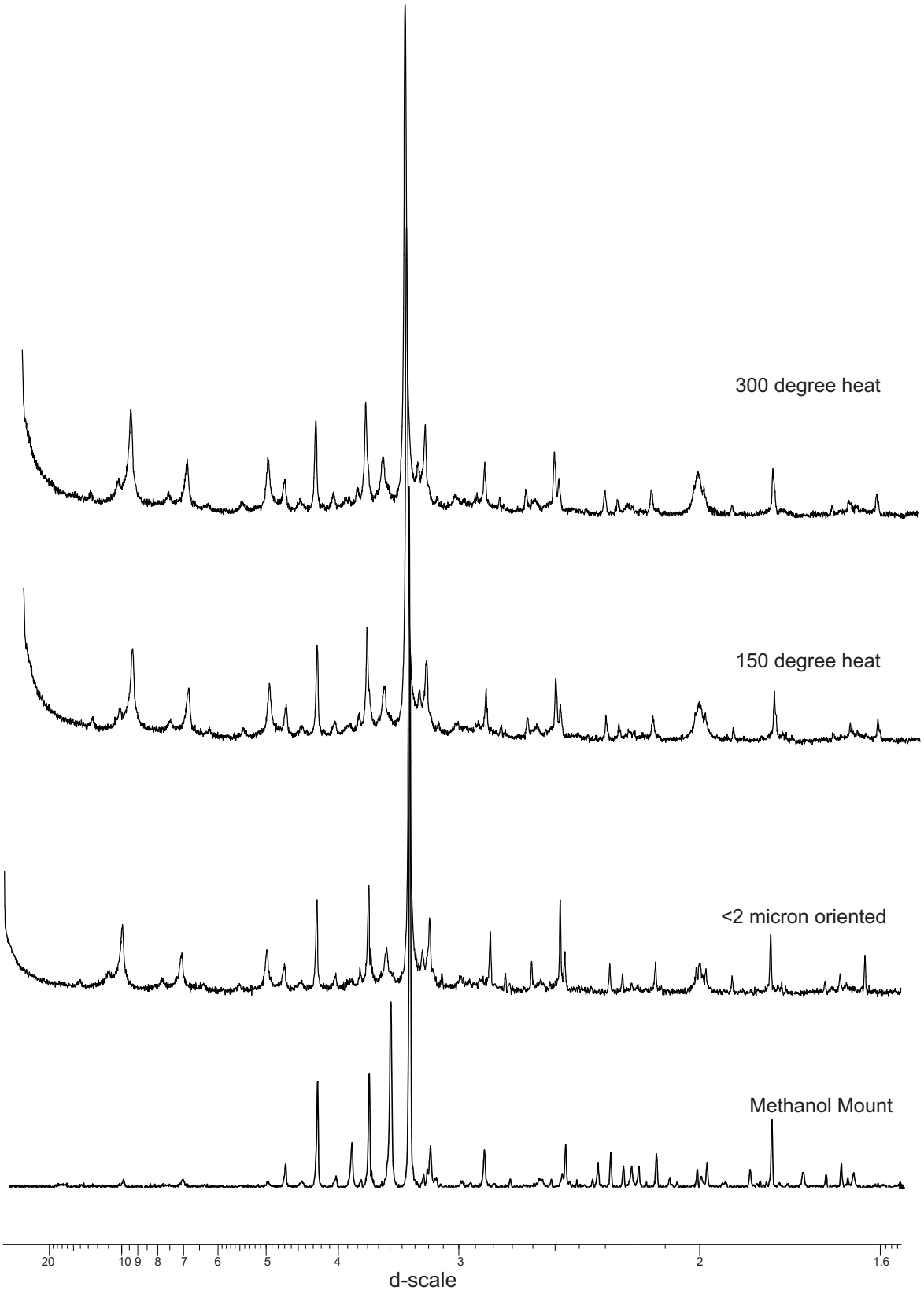

Fig. 4.14: X-Ray Diffractograms for Mohican I-100 at 3697.95m

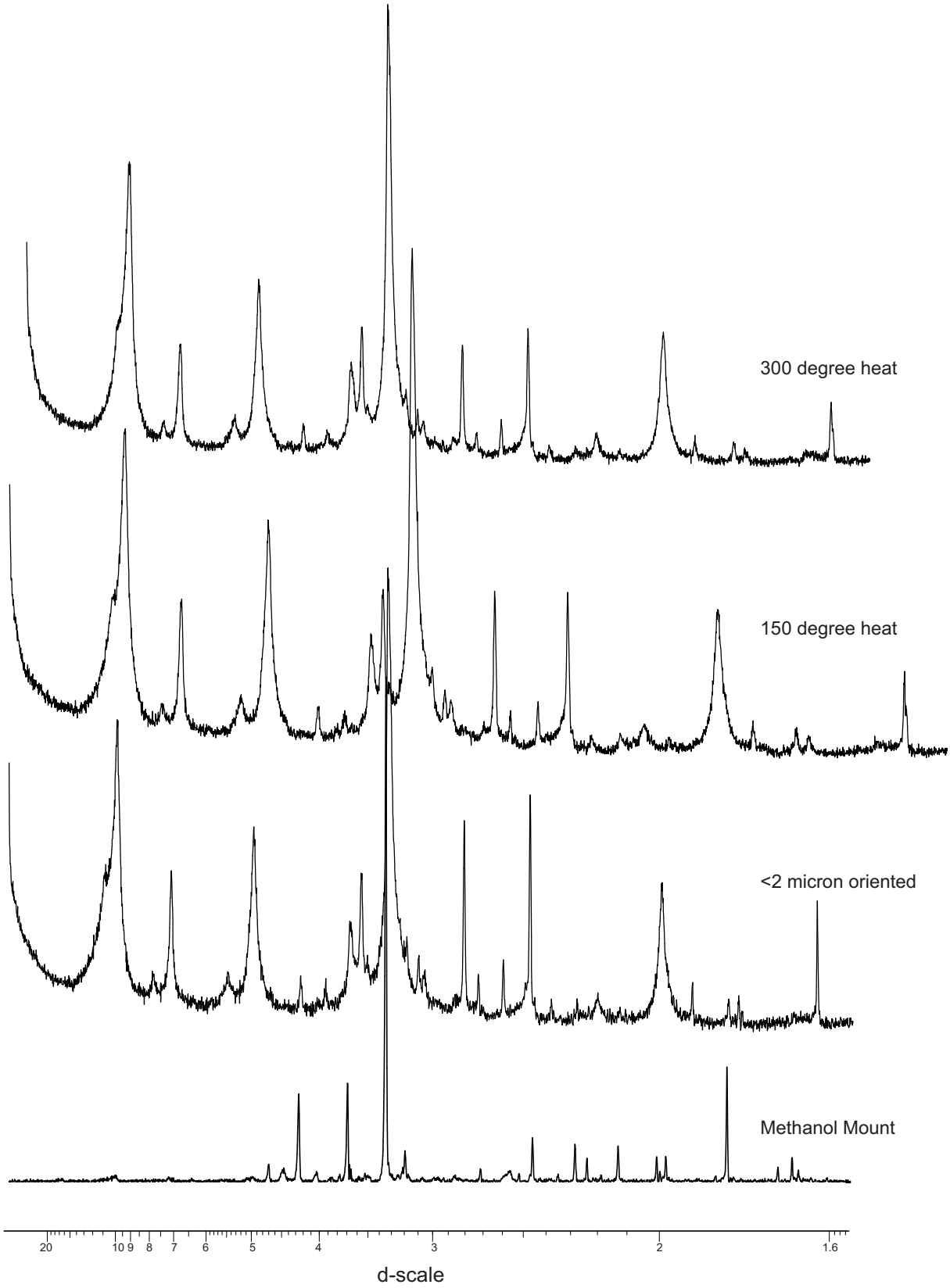

Fig. 4.15: X-Ray Diffractograms for Wyandot E-53 at 2877.03m

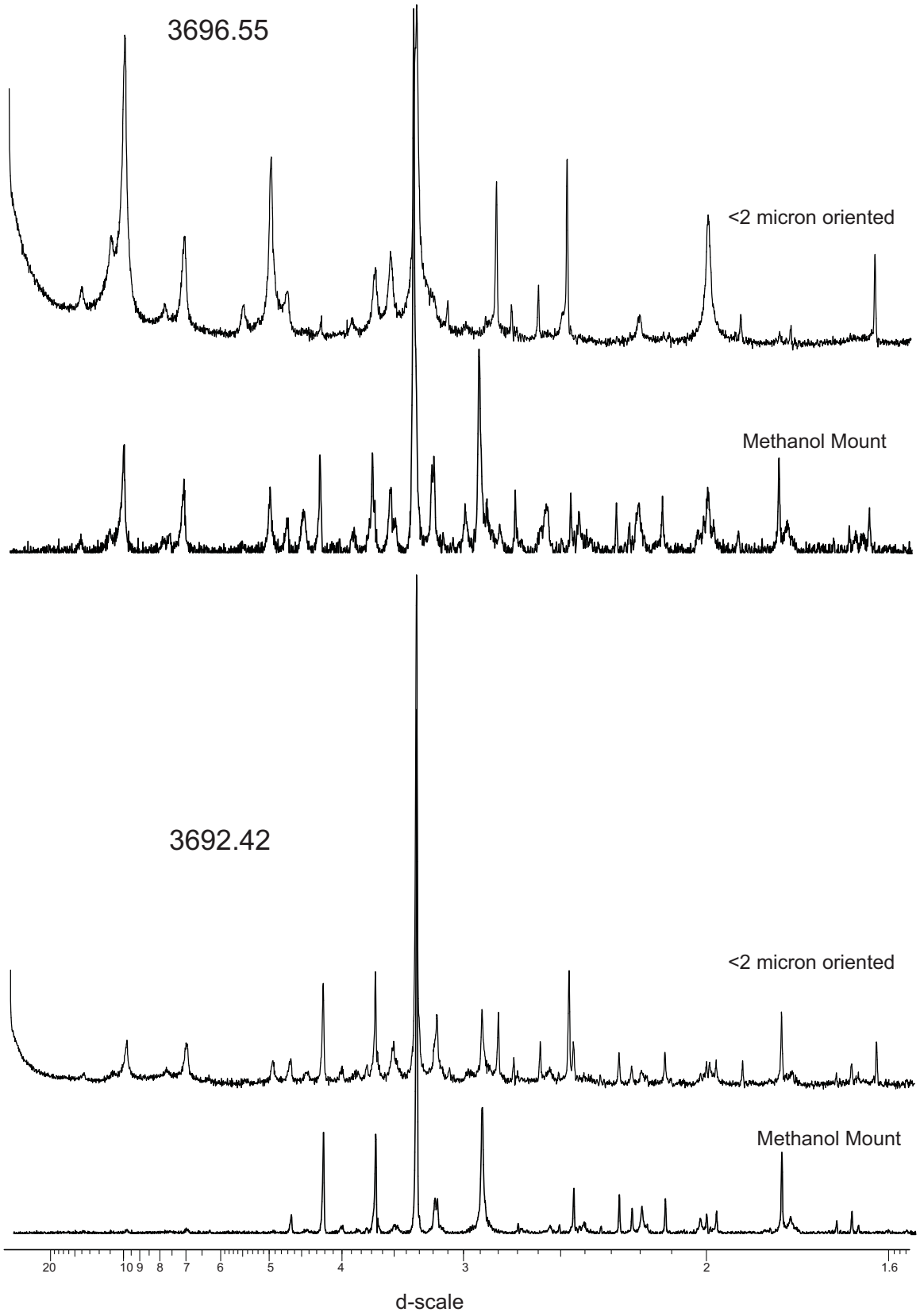

Fig. 4.16: X-Ray Diffractograms for Mohican I-100 at 3692.42m and 3696.55m.

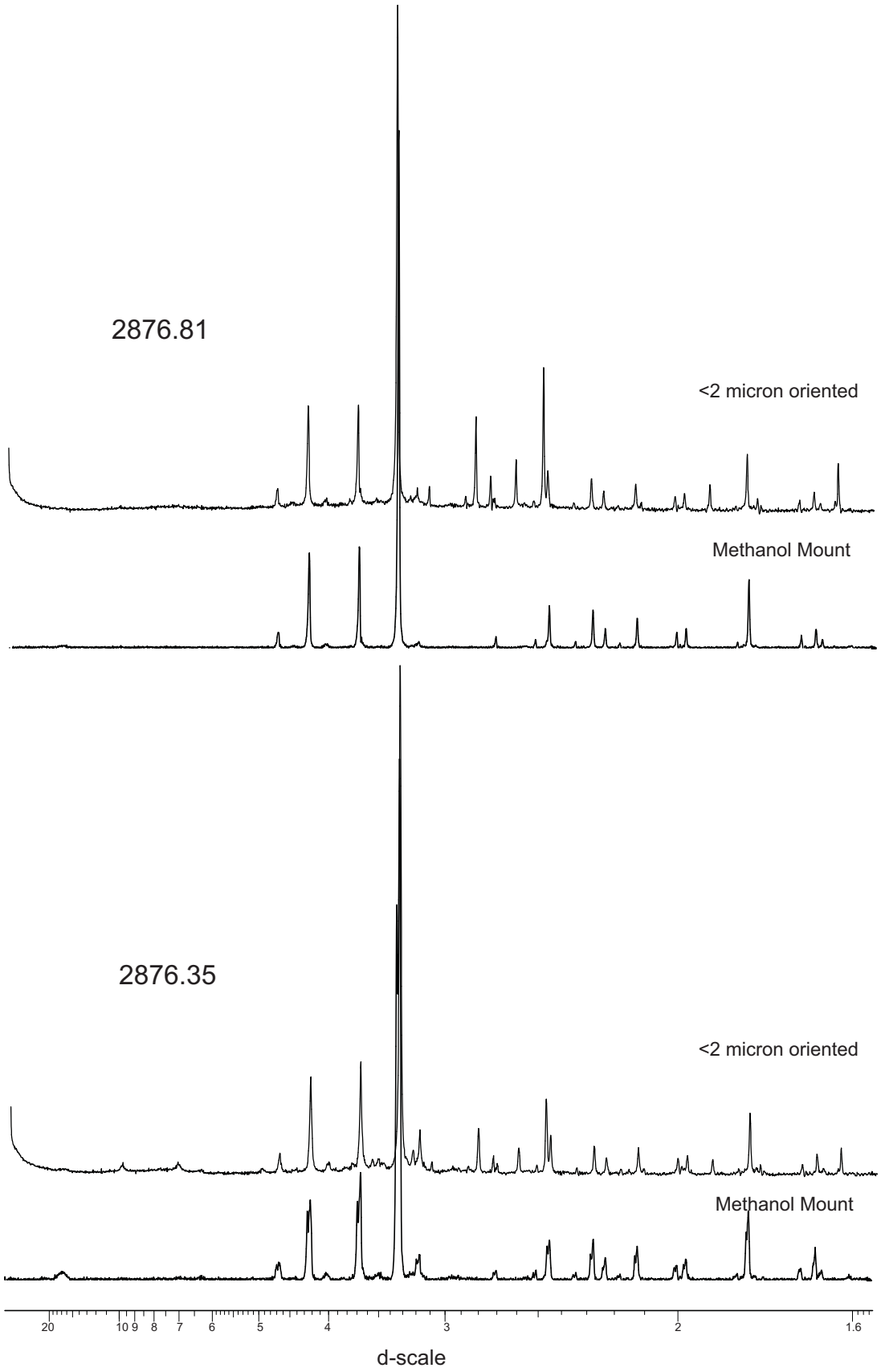

Fig. 4.17: X-Ray Diffractograms for Wyandot E-53 at 2876.35m and 2876.81m.

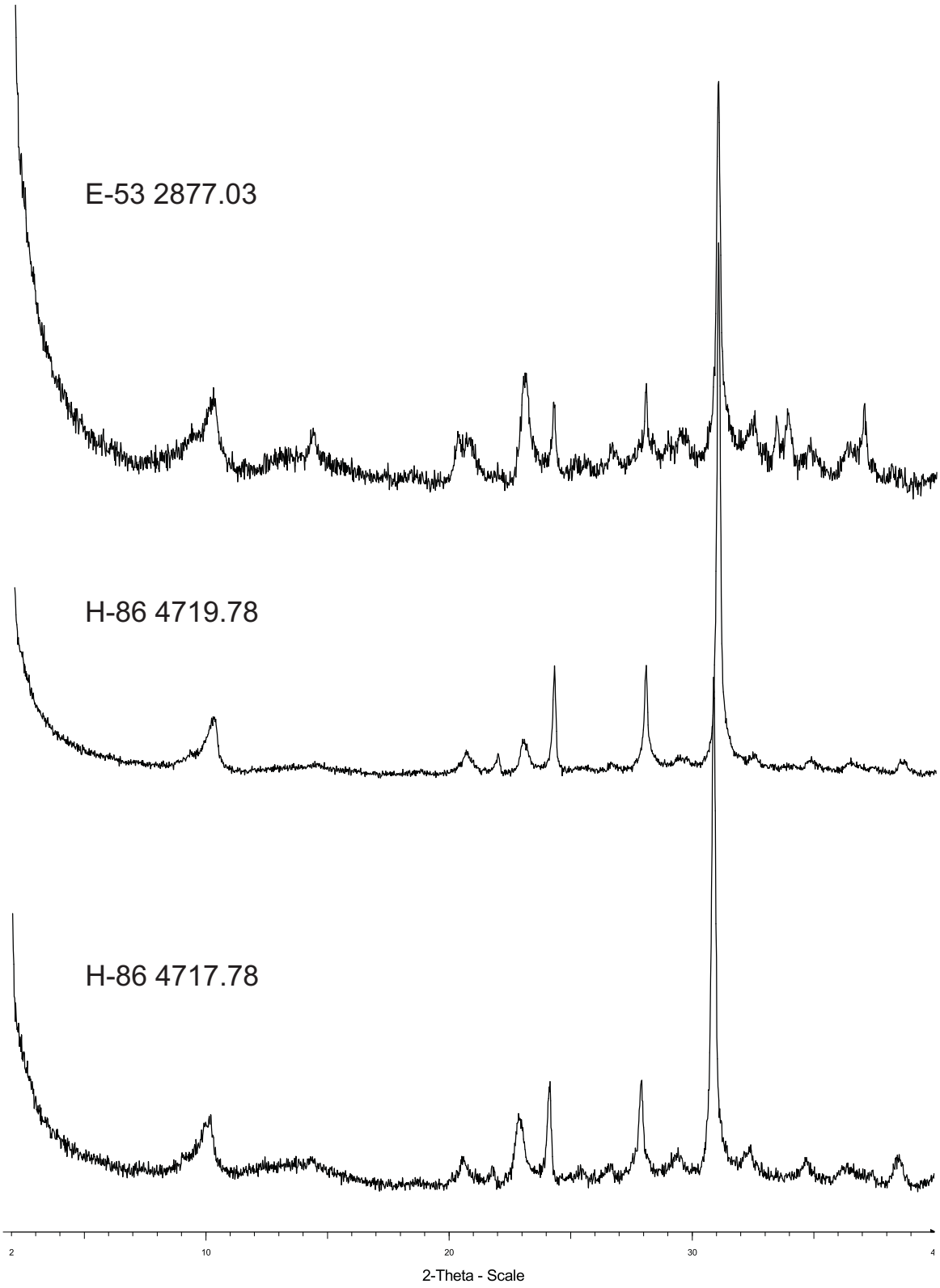

Fig. 4.18: X-Ray Diffractograms for bulk runs

Chapter 5: Discussion

5.1 Coated Grains

5.1.1 Origin

Coated grains are formed in a variety of environments (Okwese et al., 2012). Type A coated grains are found in retrogradational units. Fe-chlorite and siderite are present, and pyrite is absent, which indicates type A grains precipitated during diagenesis in the ferrugineous zone where high iron concentration and low concentration of organic matter inhibits sulphate reduction. Type B coated grains are found reworked in river-mouth sediments. Type B coated grains are intermediate in composition between type A and type C. It is suggested that they may originally be type A grains, and the original carbonate was replaced by Fe-calcite. Type C coated grains were found in retrogradational units, and sometimes reworked into delta top turbidites. It is suggested that Fe-calcite precipitated in the sulphidic or methanic zone during final burial because small crystals of pyrite and Fe-calcite are present in the outer rim. Type D coated grains were found only in oolitic limestones. The outer rim of Mg-calcite is similar to those of limestones ooids which formed during seafloor precipitation. Inner zones of the coated grain are similar to those of type C coated grains, and are not present normally in ooids. These inner zones were reworked and then transported into an ooid-forming zone where the outer coating of Mg-calcite formed. Ankerite present in type D is commonly a late diagenetic mineral and its origin in coated grains is uncertain, however it is thought that it may be early diagenetic in this case because of the lack of mesodiagenetic ankerite in the host rock.

Phosphorites (Pe-Piper & Weir-Murphy, 2008) are commonly found in shelf-edge environments that contain high organic activity resulting from upwelling. They form from inorganic precipitation from pore water, replacement of carbonates, and by bacterial precipitation. Concentric layers of grains are sometimes asymmetric suggesting they developed in very shallow burial along with periodic reworking on the seafloor where they were eroded. Phosphate precipitation occurs in the suboxic zone. During seafloor diagenesis, dissolved phosphorous is released into the seawater and impeded by sorption to iron oxides and hydroxides. Trapping of phosphorous in early diagenesis is therefore favoured by high iron content in sediments. High iron contents may be contributed, in part, to alteration of ilmenite which releases active Fe into water.

5.1.2 Studied Samples

The coated grains of the studied samples have been compared to the Upper Jurassic-Lower Cretaceous grains studied by Okwese et al. (2012). Two coated grains were analyzed, one from Mohican I-100 (sample 3697.36B, site 7) and one from Wyandot E-53 (sample 2873.10, site 2). The data shows that neither of these grains fits perfectly into the classification scheme as proposed for the Upper Jurassic-Lower Cretaceous grains. The Mohican I-100 sample, although it does contain pyrite (and marcasite), as do type C and D grains, it also contains apatite and fluorapatite, which is not present within any type classification. The Wyandot E-53 sample contains grains that are enriched in Fe-calcite, with only a minor amount of Mg-calcite. Whereas the Upper Jurassic-Lower Cretaceous type D samples are opposite, with a Mg-calcite rim, and minor Fe-calcite in the nucleus. It is possible that magnesium is preferentially taken up

in diagenetic chlorite and its precursors compared with conditions in the Orpheus Graben. The Orpheus Graben contains chlorite that is low in MgO but calcite that is high in MgO, whereas in studied samples, the chlorite is high in MgO and calcite is low in MgO.

Three samples of containing phosphorites appear to be fairly similar to those from the Orpheus Graben (Pe-Piper & Weir-Murphy, 2008). Two of the samples are bone fragments and are from Mohican I-100 (3694.38 site 4, and 3696.69 site 4). The first sample (3694.38) contains pyrite and fluorapatite, suggesting that the pyrite was precipitated within the porous structure of bone during seafloor diagenesis. Pyrite is also present throughout this sample, often times along intergranular boundaries. The second sample (3696.69) contains apatite, anhydrite, and halite. Anhydrite was incorporated into porosity during diagenesis. And the presence of both anhydrite and halite suggest that at this depth seafloor diagenesis occurred in a sabkha environment. Halite presence suggests sea environment, and anhydrite shows that occasional seawater was brought in, then as it evaporated gypsum formed within bone porosity, and eventually the gypsum converted to anhydrite upon loss of water during burial. The third phosphorite is from Wyandot E-53 (2873.10 site 2) and contains calcite and fluorapatite, appearing in concentric layers as a coated grain, classified as a phosphorite based on abundance of fluorapatite.

5.2 Chemical Mineralogy

The chemical mineralogy of the studied samples can be used to analyze the diagenetic processes that are occurring in the Middle Jurassic sandstones of the Mohican Formation. The chemical composition is also useful in determining the provenance of

these rocks. In analyzing samples for diagenesis and provenance, the data from both polished thin sections and powdered samples were used. Thin sections were studied with the petrographic microscope, scanning electron microscope, and electron microprobe. Powdered samples were studied using X-Ray diffraction, for purposes of distinguishing between mineral grains that were too small to determine with confidence using thin sections. These results were used to determine the overall diagenesis and diagenetic paragenesis within each well, and the provenance of the Mohican Formation sandstones.

5.2.1 Diagenesis

The diagenesis of the Middle Jurassic sandstone of the Mohican Formation may be important in understanding the diagenetic processes that might take place in Meguma-derived sandstones in the undrilled deep water Shelburne sub-basin. The study of the diagenesis of the Mohican Formation sedimentary rocks help us to get information on how compaction proceeds before complete lithification. In two of the three wells studied, Mic Mac and Wyandot, we see texturally immature sandstones with very good development of a pseudomatrix that is responsible for most lithification and loss of porosity. This pseudomatrix is created by the plastic deformation of plastic minerals (muscovite, biotite, and chlorite), plastic clasts (mica-rich shales/slates), and mica-rich matrix (Figs. 4.5C, 4.6A & B, 4.10E). Such minerals and clasts are very common in these two wells.

5.2.1.1. Muscovite

Muscovite is a detrital mineral; it does not form diagenetically in the Mohican Formation as it did not reach high enough temperatures for this process. However, muscovite is subjected to processes that do occur during compaction and diagenesis, such as plastic deformation, transformation to hydromuscovite, expansion of its cleavage planes and precipitation of diagenetic minerals (e.g. kaolinite &/or illite) along these planes. When muscovite is plotted based on Al and K (in atomic formula units, a.f.u., using Si = 8)(Fig. 5.1) some analyses plot within the metasedimentary and igneous fields (Reynolds et al., 2010)(Fig. 5.2), and some analyses plot outside of both of these two fields. Muscovite plotting outside the proposed fields are mostly showing <5.0 Al (a.f.u.). Back-scattered image analysis shows that some of these muscovite are those that have been diagenetically altered, or weathered, to form hydromuscovite. These muscovites occur as fine grains, usually within matrix or as relics in secondary porosity. Other grains of muscovite show expansion and fanning of cleavage planes followed by precipitation of kaolinite along the cleavage planes (App. 3C, Fig. 5 & App. 4C, Fig. 6). On the contrary, muscovite grains that plot within the metasedimentary and igneous fields are mostly well formed muscovite laths suggesting detrital origin. The muscovite analyses, along with muscovite analyses from the Meguma Terrane, were also plotted separately in the following diagrams: FeO^t/MgO vs. SiO_2 (Figs. 5.3 & 5.4), K_2O vs. SiO_2 (Figs. 5.5 & 5.6), Al_2O_3 vs. SiO_2 (Figs. 5.7 & 5.8), Na_2O vs. SiO_2 (Figs. 5.9 & 5.10), TiO_2 vs. SiO_2 (Figs. 5.11 & 5.12), and Cl vs. SiO_2 (Fig. 5.13). On each diagram a line was drawn at 50wt% SiO_2 to distinguish detrital from diagenetic muscovite as those containing lower amounts

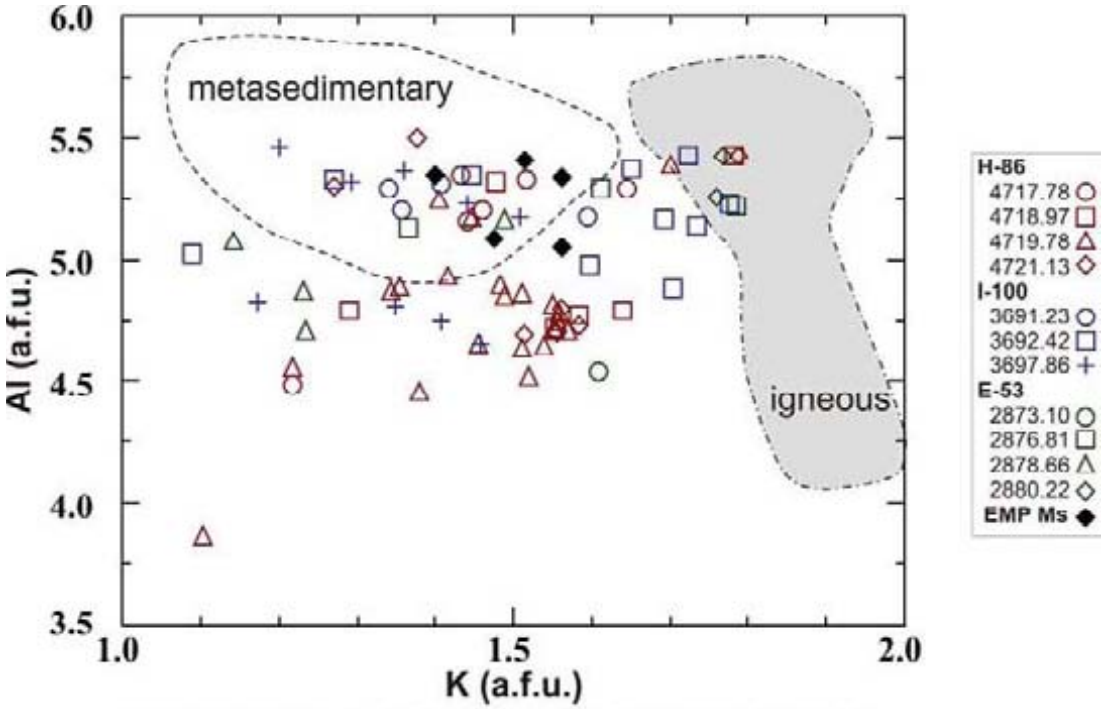

Figure 5.1: Al vs K (a.f.u.) of muscovites from studied wells. The igneous and metasedimentary fields are as specified in Fig. 5.2, and using criteria from studied wells. For more details see Reynolds et al. (2010).

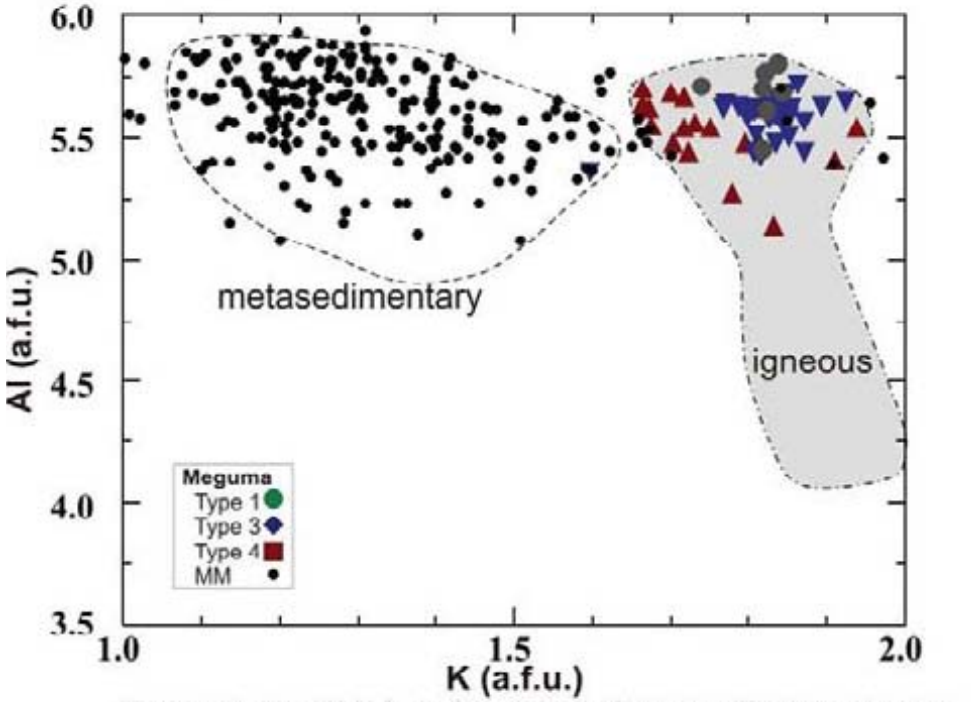

Figure 5.2: Al vs K (a.f.u.) of muscovite of Meguma Terrane, with types as specified in Fig. 5.4. The igneous and metasedimentary fields are based on these sets of analyses, and using criteria for quality of analyses the same as in the studied wells. For more details see Reynolds et al. (2010).

of Al (a.f.u.) were found to have SiO_2 concentrations of >50wt%. On the FeO^t/MgO vs. SiO_2 diagram (Fig. 5.3), diagenetically-altered muscovite all showed low FeO^t/MgO ratios, with none greater than ~2.5, whereas detrital muscovite had a wider range of ratios. The majority of these diagenetically-altered grains are from Mic Mac H-86 well (all samples), but also with a few grains from Mohican I-100 (3697.86) and Wyandot E-53 (2878.66 & 2873.10). In comparison, almost all the grains from Meguma Terrane (Fig 5.4) plot in the detrital field. On the K_2O vs. SiO_2 diagram (Fig. 5.5), the K_2Owt% for diagenetically-altered muscovite was similar that of detrital muscovite, however not reaching as high concentrations as seen in the studied wells and in Meguma Terrane wells (Fig. 5.6). As seen previously, the majority of the diagenetically-altered grains come from Mic Mac H-86 well (all samples), with a few grains from Mohican I-100 (3697.86 & 3692.42) and Wyandot E-53 (2878.66 & 2873.10). On the Al_2O_3 vs. SiO_2 diagram (Fig. 5.7), most of the diagenetically-altered muscovite showed a lower concentration of Al_2O_3 than did most detrital muscovite both from studied wells and Meguma Terrane (Fig. 5.8). Those samples showing diagenetic alteration are the same as those from the K_2O vs. SiO_2 plot. On the Na_2O vs. SiO_2 plot (Fig. 5.9), the concentrations of Na_2O were similar between diagenetically-altered and detrital muscovite from both studied wells and Meguma Terrane (Fig. 5.10). Those samples showing diagenetic-alteration are the same as stated in previous plots. On the TiO_2 vs. SiO_2 plot (Fig. 5.11), the concentrations of TiO_2 of diagenetically-altered muscovite were similar to the detrital muscovite from studied wells and from Meguma Terrane (Fig. 5.12). Although, most diagenetically-altered muscovite had 0wt% of TiO_2 and there were more detrital grains showing TiO_2 concentration. Of the grains that have been both diagenetically-altered and show some

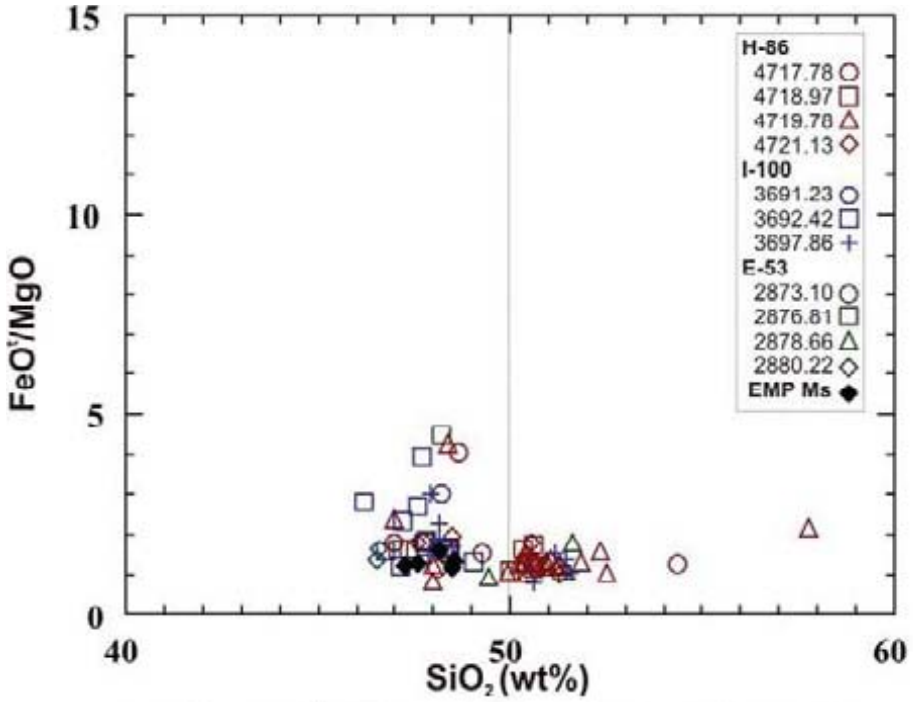

Figure 5.3: FeO'/MgO vs SiO_2 of muscovite from studied wells.

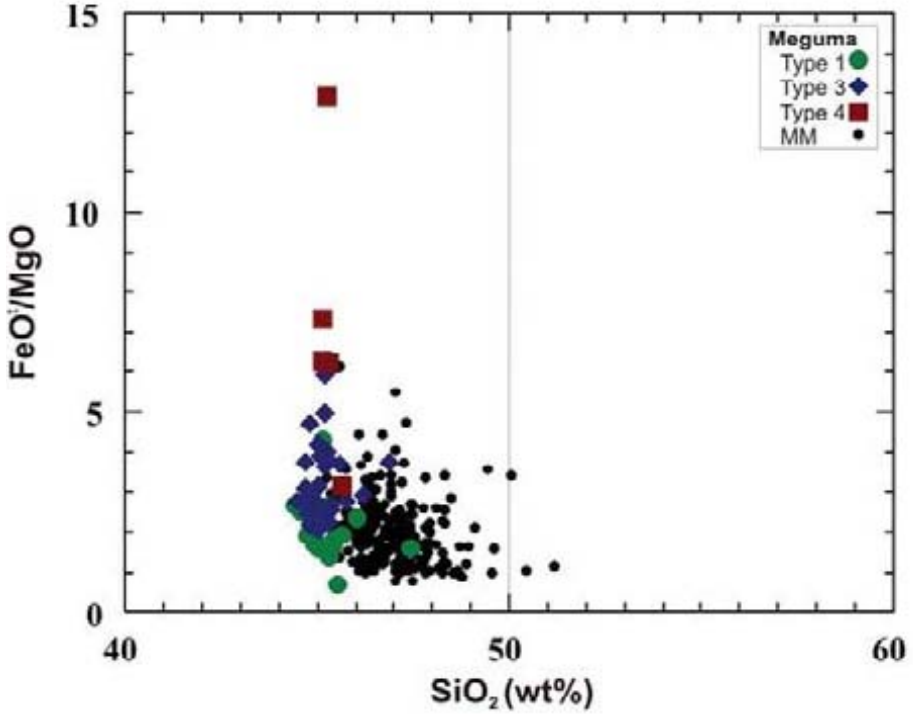

Figure 5.4: FeO'/MgO vs SiO_2 of muscovite from Meguma Terrane, specifically type 1=South Mountain Batholith, 2=East Kemptville leucogranite (not present in this data), type 3=eastern Meguma primary plutons, 4=eastern Meguma secondary plutons, and MM=Meguma metasediments, from Reynolds et al. (2010).

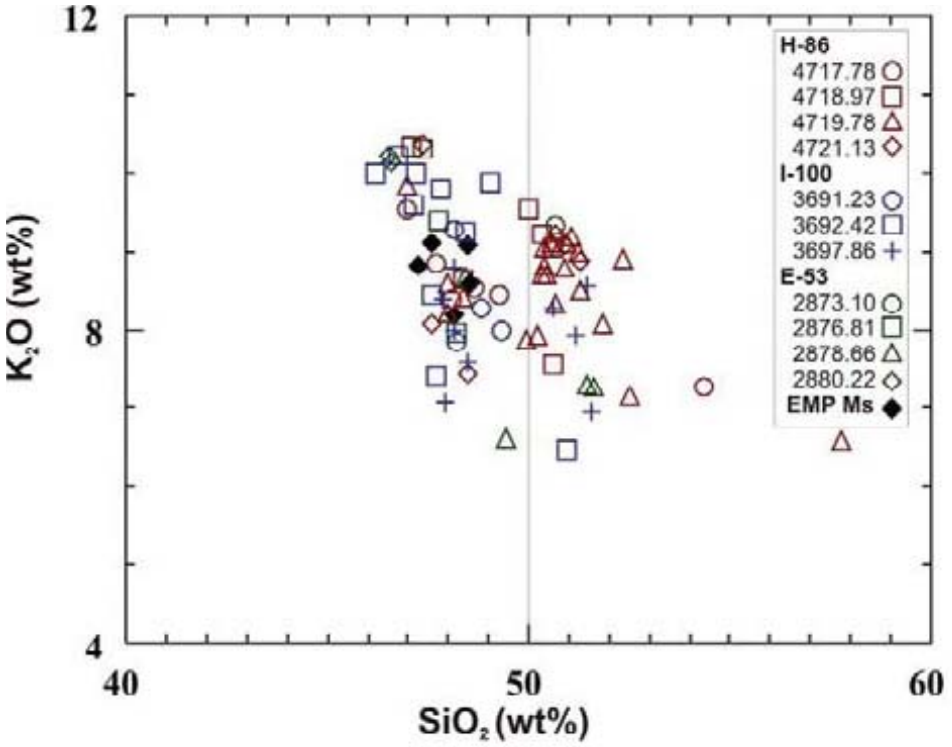

Figure 5.5: K_2O vs SiO_2 of muscovite from studied wells.

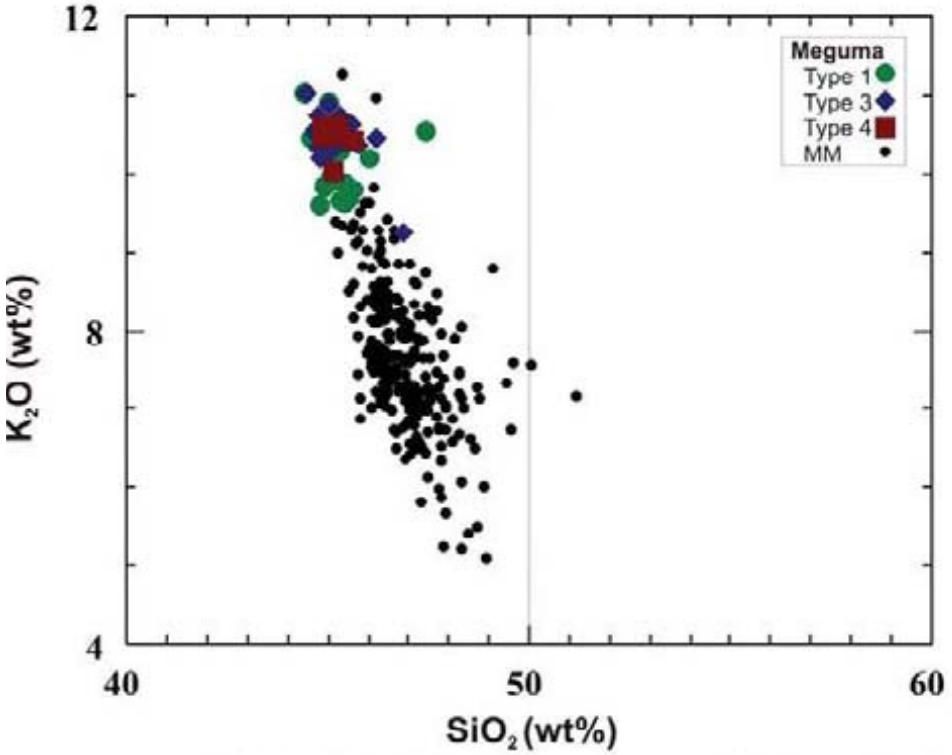

Figure 5.6: K_2O vs SiO_2 of muscovite from Meguma Terrane, with types as specified in Fig. 5.4.

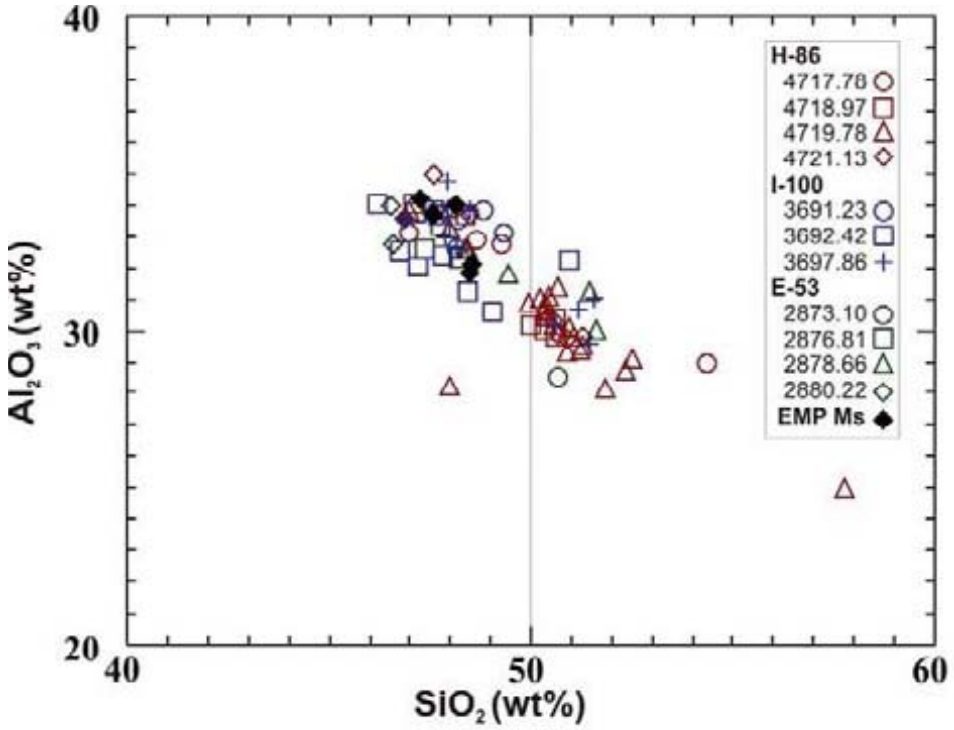

Figure 5.7: Al_2O_3 vs SiO_2 of muscovite from studied wells

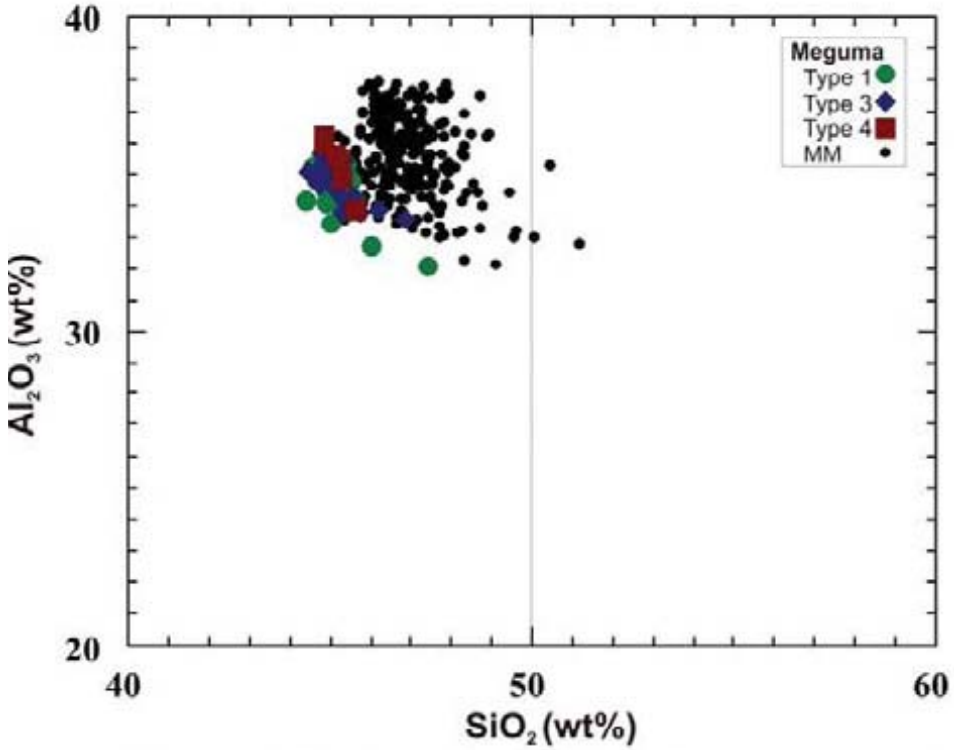

Figure 5.8: Al_2O_3 vs SiO_2 of muscovite from Meguma Terrane, with types as specified in Fig. 5.4.

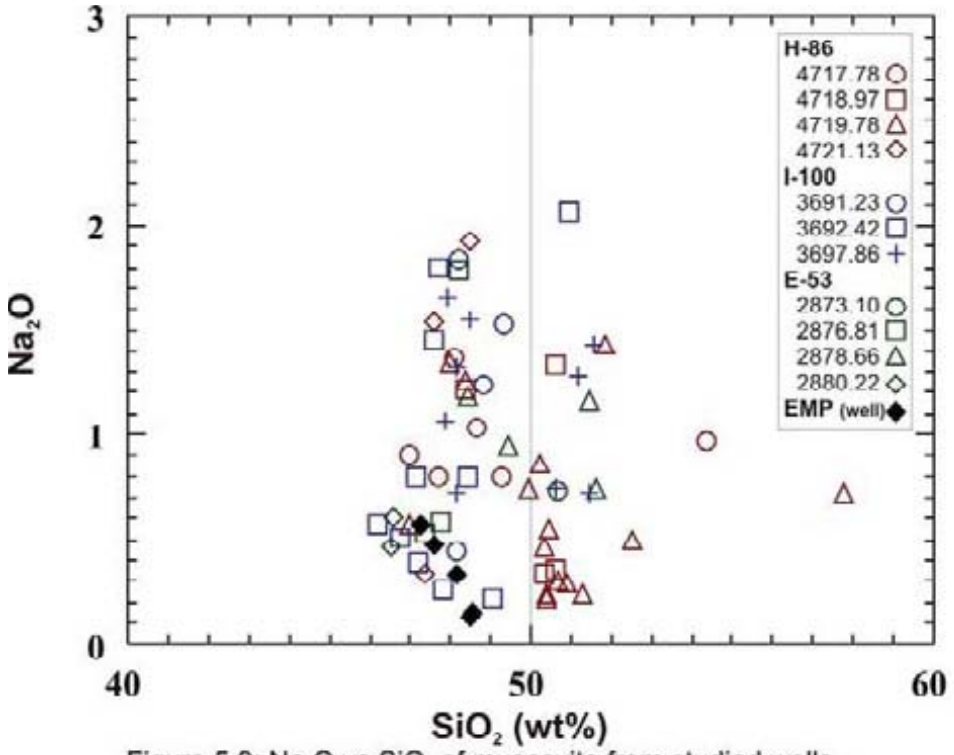

Figure 5.9: Na_2O vs SiO_2 of muscovite from studied wells.

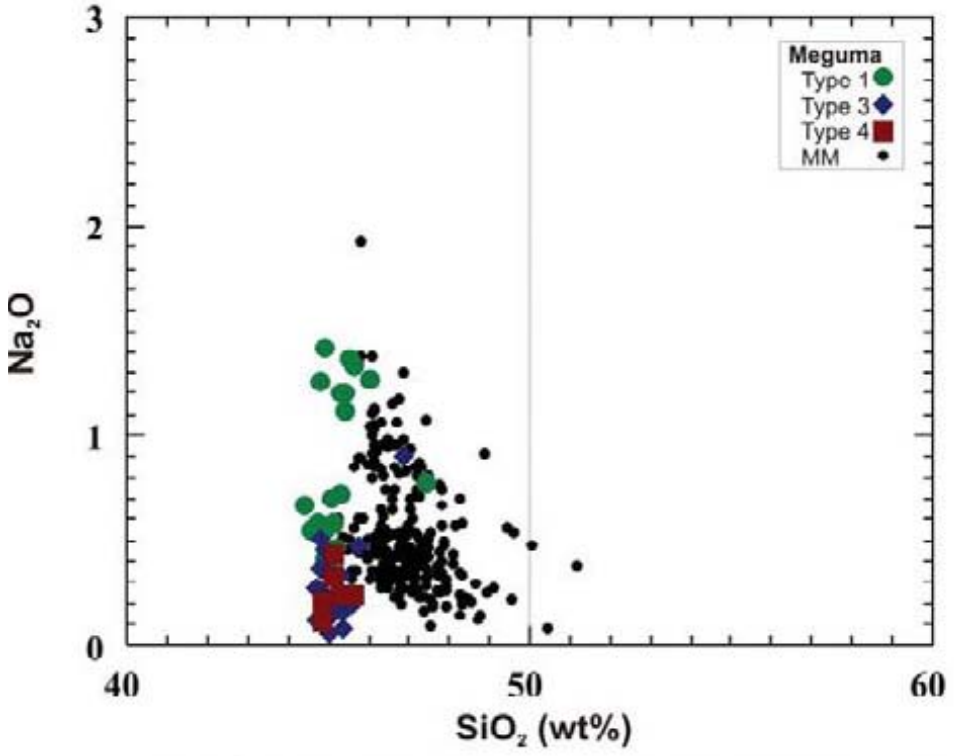

Figure 5.10: Na_2O vs SiO_2 of muscovite from Meguma Terrane, with types as specified in Fig. 5.4.

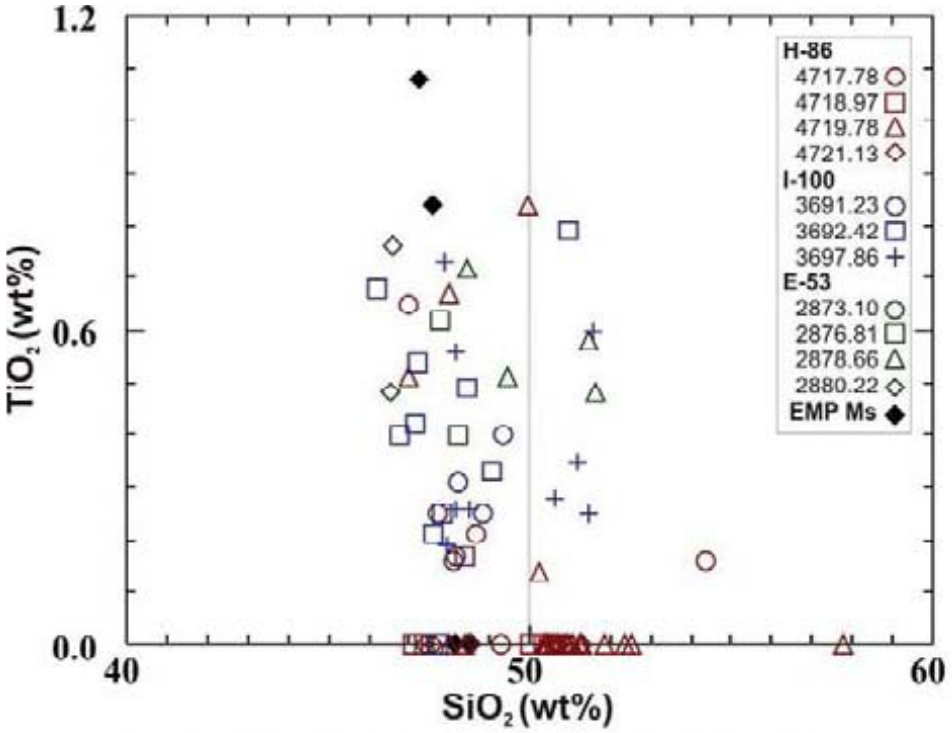

Figure 5.11: TiO_2 vs SiO_2 of muscovite from studied wells

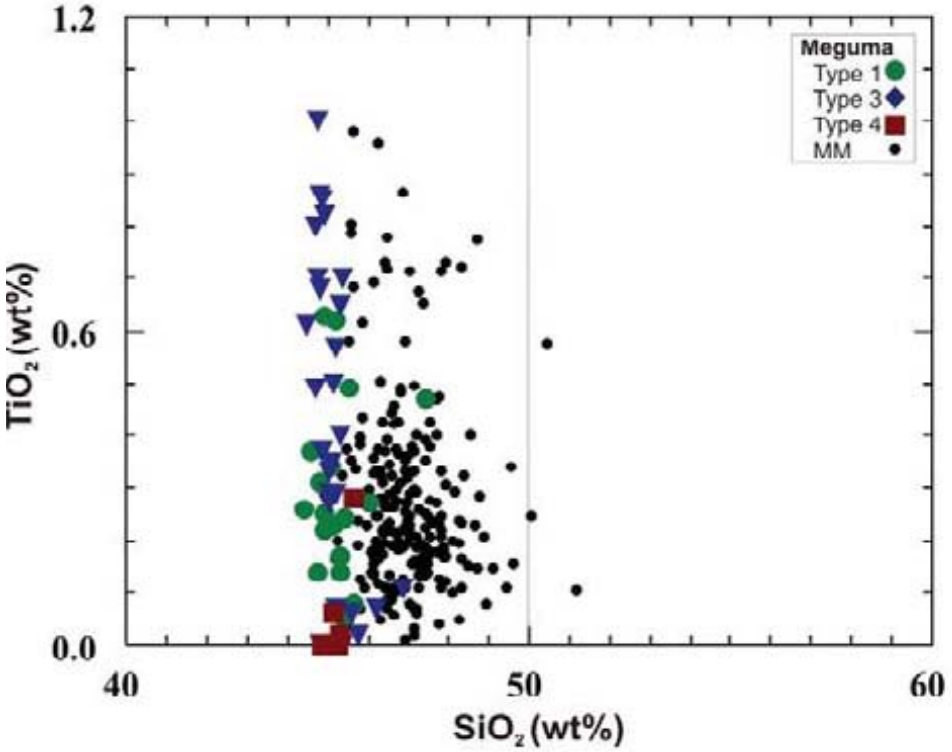

Figure 5.12: TiO_2 vs SiO_2 of muscovite from Meguma Terrane, with types as specified in Fig. 5.4.

presence of TiO_2, they are located mostly in Mohican I-100 well (3692.42 & 3697.86), with a couple grains of Mic Mac H-86 (4717.78 & 4719.78) and Wyandot E-53 (2878.66). On the Cl vs. SiO_2 plot (Fig. 5.13), the concentrations of Cl were similar for both diagenetically-altered and detrital muscovite, however only 12 grains showed analyzed chlorine in their grains, and of these 8 of them are considered diagenetically-altered. These are from Mic Mac H-86 (4718.97 & 4719.78) and Wyandot E-53 (2878.66).

Summary: Muscovites in the studied wells were determined to be both detrital and diagenetic. Diagenetic muscovite includes those that have been compacted and plastically deformed, those that have been altered or weathered to hydromuscovite, those that have expansion along their cleavage planes with precipitation of illite or kaolinite within these planes. Chemically, diagenetic muscovite can be distinguished from detrital muscovite mainly on the basis of Al (a.f.u.), Al_2O_3(wt%), and SiO_2(wt%), but also FeO^t/MgO ratio. In diagenetic muscovite, Al (a.f.u) and Al_2O_3(wt%) are both lower as compared to detrital muscovite from studied wells as well as those of Meguma Terrane muscovite. Muscovite that contained SiO_2(wt%) greater than 50 is considered to be diagenetically altered muscovite. It is beyond this 50wt% SiO_2 line that differences can be seen regarding other oxides. The FeO^t/MgO ratios are all small for diagenetic muscovite, as compared to detrital muscovite which range from smaller to larger ratios

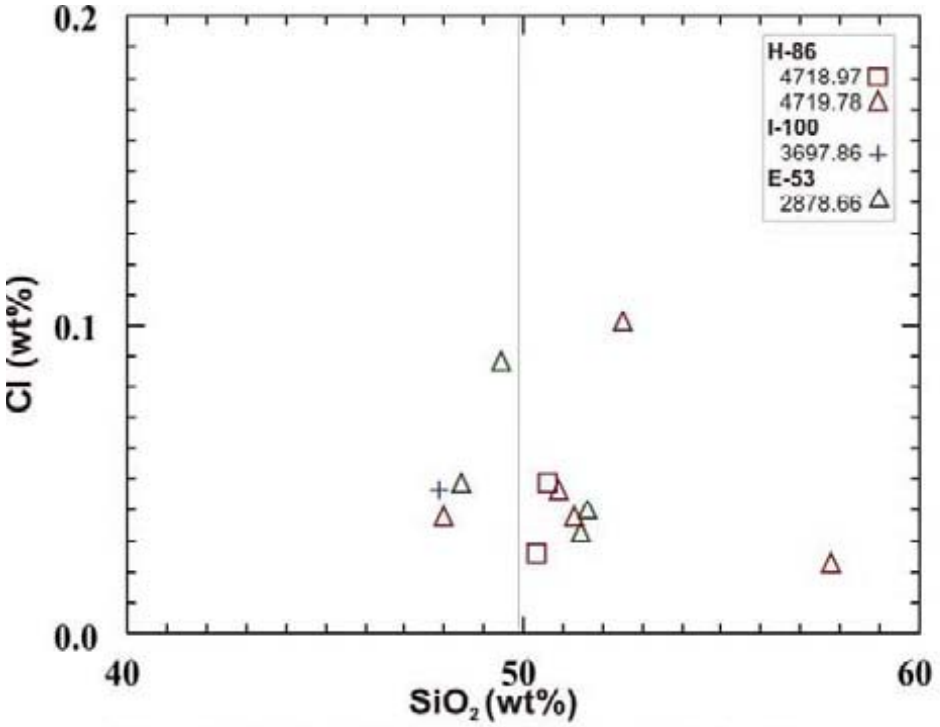

Figure 5.13: Cl vs SiO_2 of muscovite from studied wells.

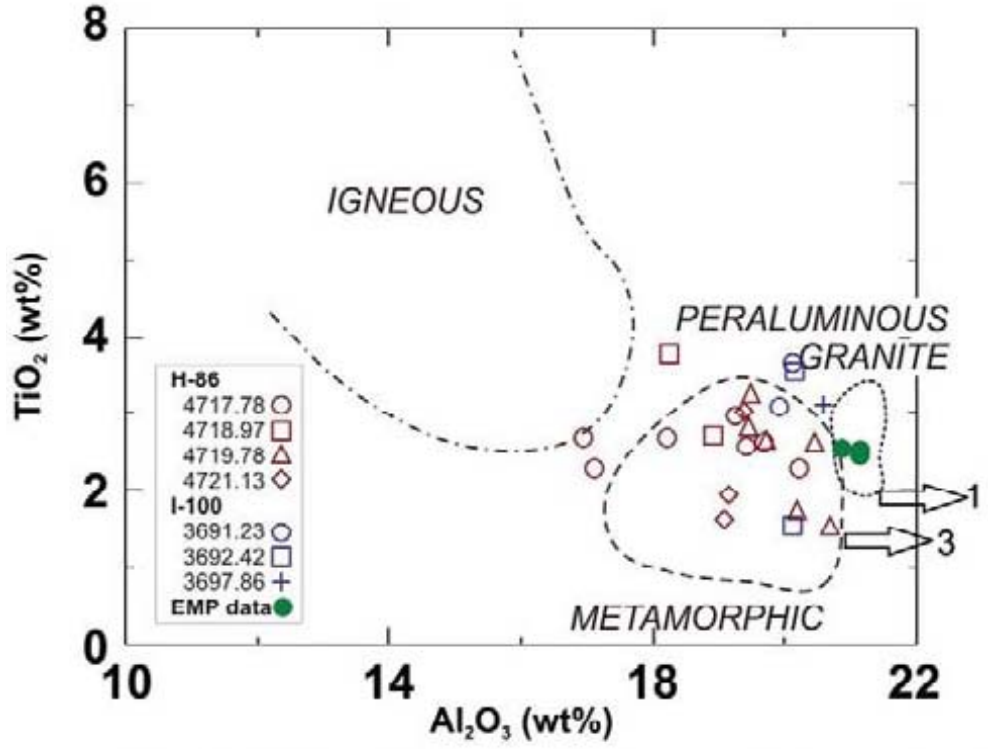

Figure 5.14: TiO_2 vs SiO_2 discrimination diagram of biotite from studied wells, Igneous, metamorphic and peraluminous granite fields from Pe-Piper et al. (2009).

5.2.1.2 Illite

Illite can be both diagenetic and detrital, however in the studied samples most appear to be diagenetic. Illite, found commonly in shales and often in sandstones, is considered to be a mixture of detrital mica grains which often alter during diagenesis, and diagenetic illite which precipitate from the reaction of pore fluid with framework grains (e.g. often within areas of secondary porosity, Pevear, 1999). Illite and muscovite can be chemically and petrographically similar to each other and differentiating between them must take into account the crystal structure and therefore XRD is necessary to determine, with certainty, whether one, or both, are present. Chemically, assumptions can be made regarding illite classification, based on oxide concentrations, and textures visible in BSE. In general, the concentration of SiO_2 of illite is higher than that of muscovite and the concentration of Al_2O_3 and K_2O are lower than that of muscovite. Based on XRD analysis (see Chapter 6) it is determined that illite is present in some of the studied samples, often as a mixed layer with chlorite.

5.2.1.3 Biotite

Biotite is a detrital mineral. However, during diagenesis it undergoes some diagenetic alteration. Within the studied wells, this alteration includes plastic deformation, chloritization, and iron oxide precipitation along its cleavage. In places, biotite has undergone plastic deformation during burial and it is thus squeezed and deformed around more resistant framework grains (App. 1C, Fig. 2, analysis 11), resulting in a pseudomatrix. Biotite grains with iron oxide precipitation along cleavage planes have also often been plastically deformed (App. 1B, Fig. 4). Some grains of

biotite are chloritized, however, much of this chloritization likely occurred at the source as Meguma Terrane slates that also contain biotite that has already been chloritized (App. 5A, Fig. 4). Therefore, it is possible that many of the chloritized biotite grains are from Meguma Terrane, and were already chloritized before burial, and upon burial were then plastically deformed. Biotite was plotted in a TiO_2 vs. SiO_2 discrimination diagram (Fig. 5.14), that shows the detrital nature of the grains as mostly metamorphic with some from peraluminous granite. Some biotite grains also plot outside these fields. Such grains, compared with those that plot within the fields, look more altered and partially plastically deformed in BSE images (App. 1C, Fig. 3). These observations suggest that such grains have been affected by both plastic deformation and iron oxide precipitation along their cleavage planes during burial and subsequent diagenesis.

Summary: Biotite in the studied wells is detrital, however some grains have also been affected by diagenesis. Burial and diagenetic alteration of biotite include plastic deformation of grains, and iron oxide precipitation along cleavage planes of detrital grains, some of which are also plastically deformed.

5.2.1.4 Chlorite

Chlorite appears in these wells as both detrital and diagenetic. It is necessary to chemically distinguish between both detrital and diagenetic chlorite and this was done with a series of diagrams. Data from studied wells was compiled using only good chlorite analyses (those not containing more than 1wt% of CaO, TiO_2, K_2O and Na_2O). First, FeO_t and MgO of chlorite analyses from studied wells were compared with Meguma Group metasediment chlorite analyses (personal communication from Dr. Chris

White). Chlorite data for studied wells was then plotted in a FeO^t/MgO vs. MgO diagram (Fig. 5.15) along with the chlorite data set from the Meguma Group metasediments. This diagram shows that there is a slight reduction in MgO for the studied sample chlorite chemical analyses compared to those of Meguma metasediments. Studied samples were then classified, using BSE image analysis, by their appearance as either crystals (those appearing detrital in origin) or pseudomorphs (those appearing diagenetic in origin), and by their SiO_2 content (<27wt%, 27-30wt%, and >30wt%). By doing this, and plotting them in a FeO^t/MgO vs. MgO diagram (Fig. 5.16), it shows that the pseudomorphs are generally higher in MgO than are the crystals, which are higher in FeO. As well, the pseudomorphs that have higher MgO concentrations than any crystals are also those with SiO_2 content of >30wt%. These two diagrams (Figs. 5.15 & 5.16) suggest that the diagenetic chlorite of the Jurassic sandstones, may have had a MgO rich precursor, likely the Meguma Terrane metasediments, which have slightly higher concentrations of MgO than do the diagenetic chlorite of studied wells.

Next, the chlorite analyses of the studied samples and Meguma Group metasediments were compared with respect to SiO_2 concentrations, along with FeO^t and MgO. First, chlorite data were plotted on a FeO^t vs. SiO_2 diagram (Fig. 5.17) which shows that studied chlorite are higher in SiO_2 (~ >30wt%) and lower in FeO^t than are Meguma chlorite. Next, chlorite was plotted on a MgO vs. SiO_2 diagram (Fig. 5.18), which shows that the chlorite from the studied samples is higher in SiO_2 (~ >30wt%) than Meguma chlorite, and has approximately the same range of MgO concentrations. Next, data was plotted on two diagrams as FeO^t/MgO vs. SiO_2. The first diagram (Fig. 5.19)

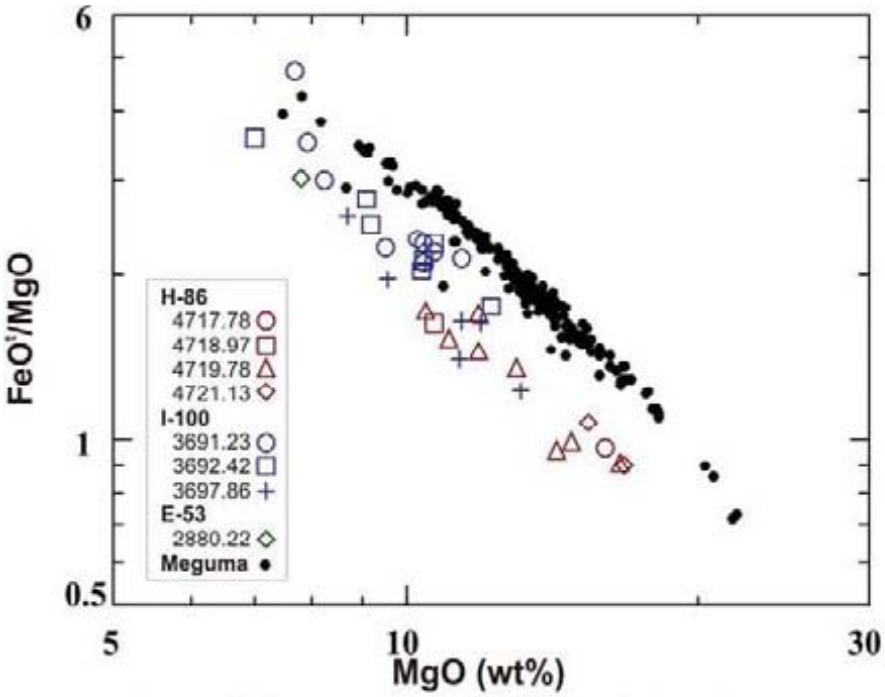

Figure 5.15: Composition of FeO^t/MgO vs MgO variation in chlorite between studied wells and Meguma Group metasediments (personal communication from Dr. Chris White).

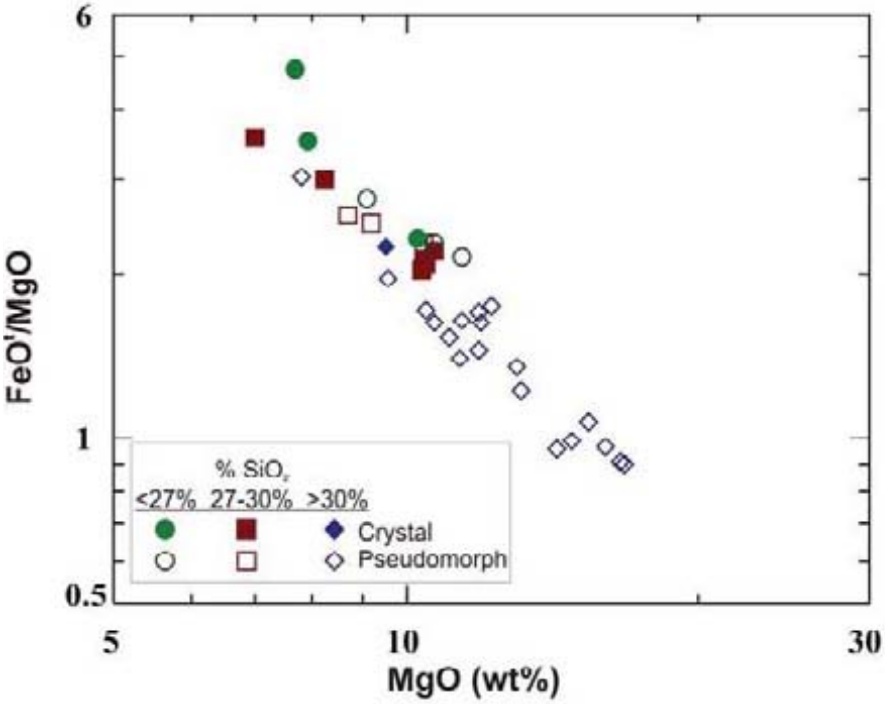

Figure 5.16: FeO^t/MgO vs MgO of chlorite showing relationship of crystals (those that appear to be detrital) and pseudomorphs (those that appear to be of diagenetic origin). SiO_2 content for different types of chlorite grains is also shown.

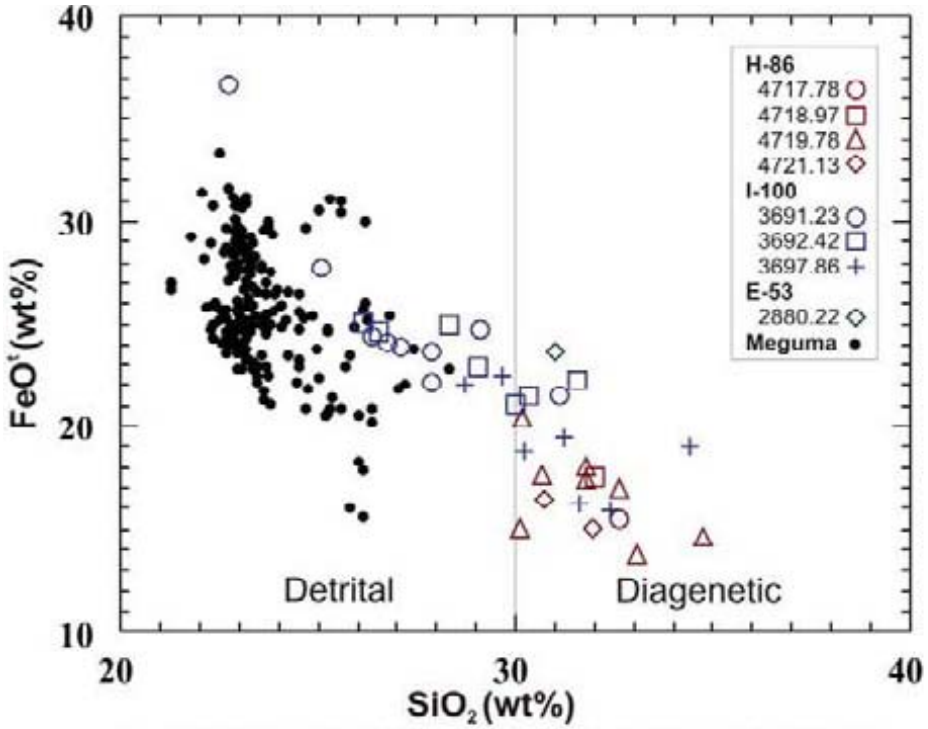

Figure 5.17: FeO^t vs SiO_2 of chlorite, comparing results from the studied wells and from Meguma Group metasediments (personal communication from Dr. Chris White).

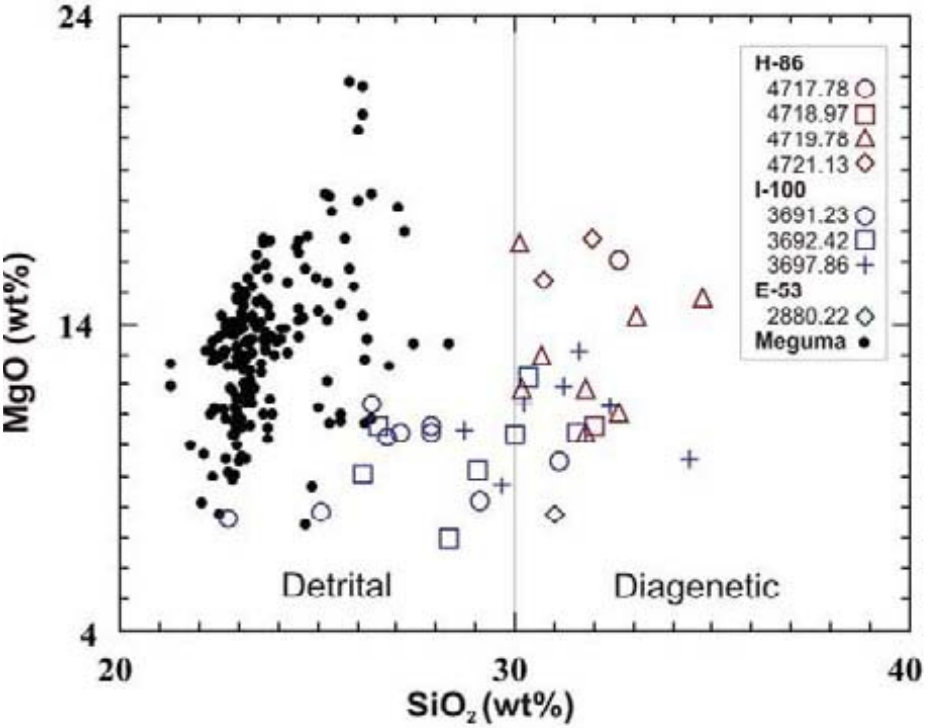

Figure 5.18: MgO vs SiO_2 of chlorite, comparing results from the studied wells and from Meguma Group metasediments (personal communication from Dr. Chris White).

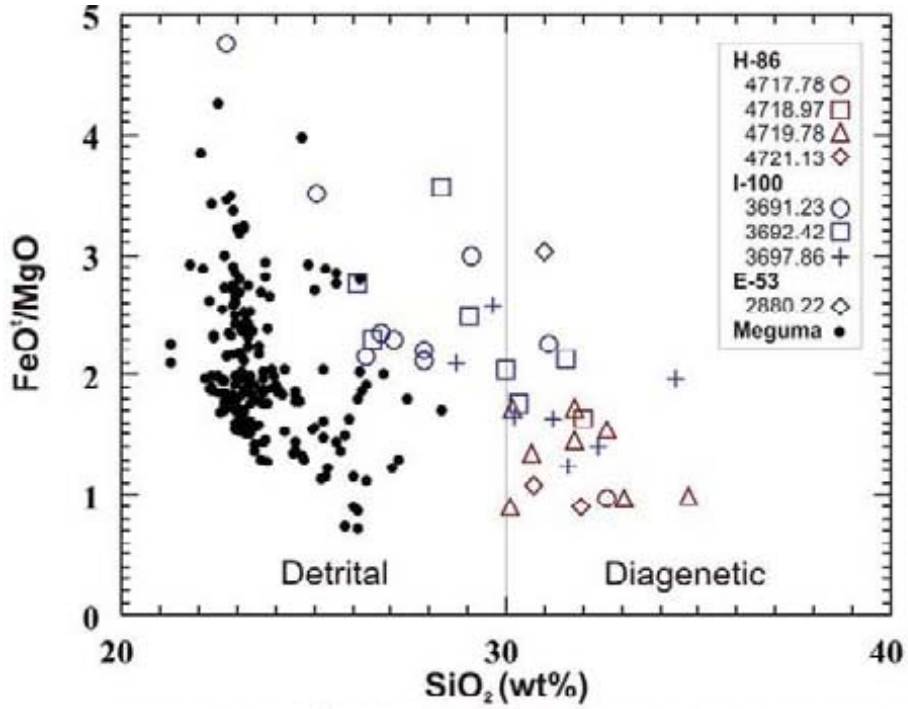

Figure 5.19: FeO'/MgO vs SiO_2 of chlorite, comparing results from the studied wells and from Meguma Group metasediments (personal communication from Dr. Chris White).

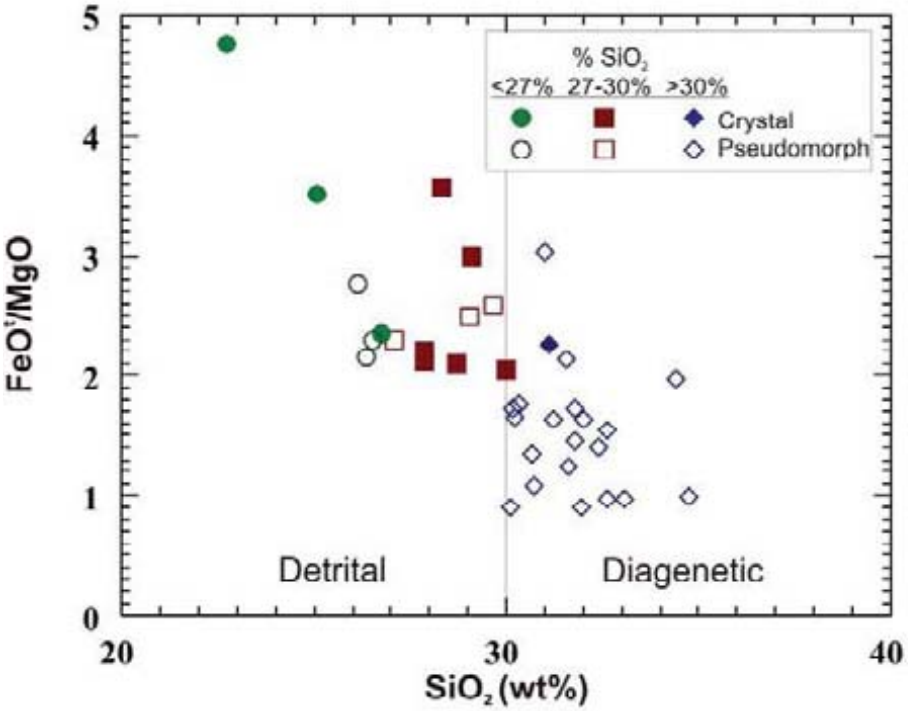

Figure 5.20: FeO'/MgO vs SiO_2 of chlorite showing relationship of crystals (those that appear to be detrital) and pseudomorphs (those that appear to be of diagenetic origin). SiO_2 content for different types of chlorite grains is also shown.

plots the studied samples by well, along with Meguma Group metasediments. This diagram shows that above 30wt% SiO_2 there is a lower ratio of FeO_t/MgO (therefore higher MgO concentration) than below 30wt% SiO_2 (where there is a higher FeO^t concentration. Then plotting the same data from studied wells, except using the SiO_2 content and crystals versus pseudomorphs (Fig. 5.20), it shows that chlorite plotting above 30wt% SiO_2 are mostly pseudomorphs, and contain lower FeO^t/MgO concentration. Most of the crystals plot below 30wt% SiO_2 and have a higher ratio and have higher FeO^t concentration compared to MgO. These diagrams (Figs. 5.17-5.20) show that Meguma chlorite, through diagenesis, increases in SiO_2 and retains high MgO. The best discrimination for detrital versus diagenetic chlorite, in these wells, seems to be SiO_2 concentration. These diagenetic chlorites are higher in MgO compared with diagenetic chlorites from other studied parts of the Scotian Basin, because the parent mineral (i.e., Meguma chlorites) is Mg-rich.

Discrimination diagrams of FeO^t/MgO vs. SiO_2/Al_2O_3 (Figs. 5.21-5.24) were plotted with fields for diagenetic, metamorphic (detrital), and igneous (detrital) types of chlorite. These fields were determined by Pe-Piper and Weir-Murphy (2008) which used data from chlorites from Cretaceous rocks from the Orpheus Graben (Weir-Murphy, 2004). The chlorite from Weir-Murphy (2004) were plotted (Fig. 5.21) using the same standards for contaminants as the studied sample. These chlorite samples show that diagenetic chlorites from Orpheus Graben have higher FeO^t than MgO concentrations. This same plot was used to plot the data of Gould (2007) which studied chlorite rims from the Venture field of the Scotian Basin. The chlorite data of Gould (2007) is diagenetic and is classified in more detail into chlorite rims, expanded mica, pore filling,

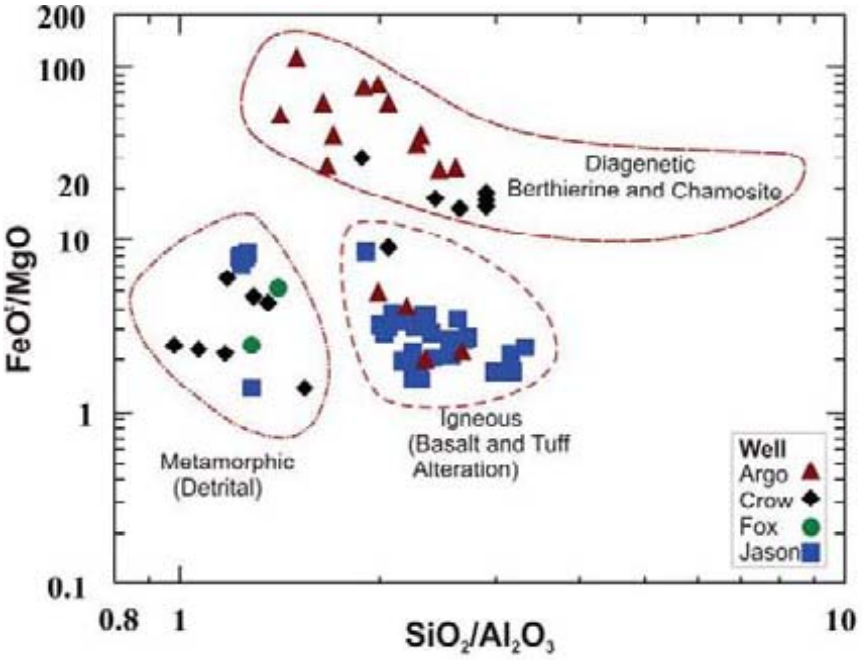

Figure 5.21: FeO^t/MgO vs SiO_2/Al_2O_3 discrimination diagram of chlorite. The discrimination fields (Pe-Piper et al., 2011) for chlorite were drawn using the chlorite analyses for the Cretaceous rocks from Orpheus Graben (Weir-Murphy, 2004).

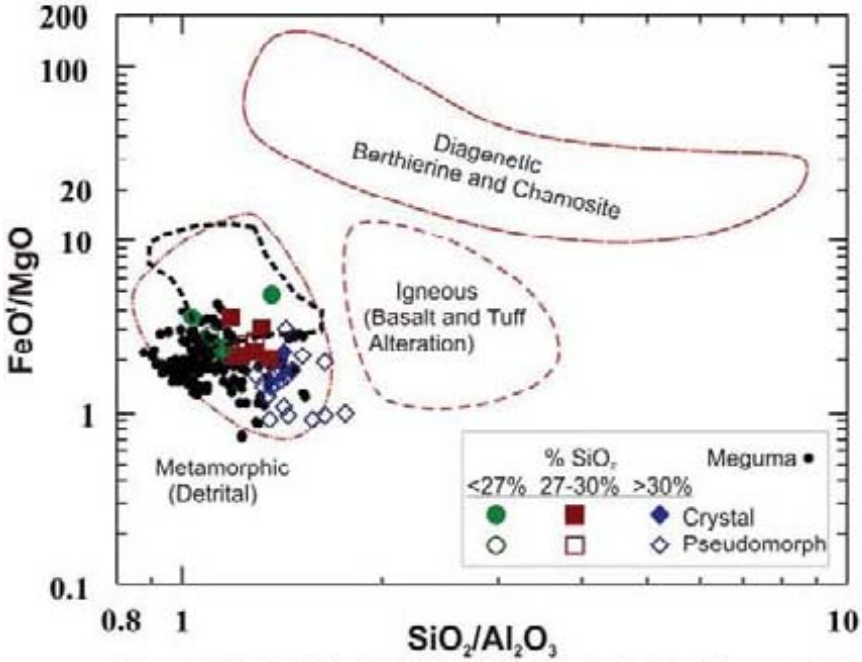

Figure 5.22: FeO^t/MgO vs SiO_2/Al_2O_3 discrimination diagram of chlorite from studied samples, showing relationship of crystals (those that appear to be detrital) and pseudomorphs (those that appear to be of diagenetic origin). SiO_2 content for different types of chlorite grains is also shown. Also shown are chlorite analyses from Meguma Group metasediments (personal communication from Dr. Chris White). The discrimination fields are the same as in Fig. 5.21 & 5.23, with added field around main diagenetic chlorite of Gould, 2007 from the Venture field.

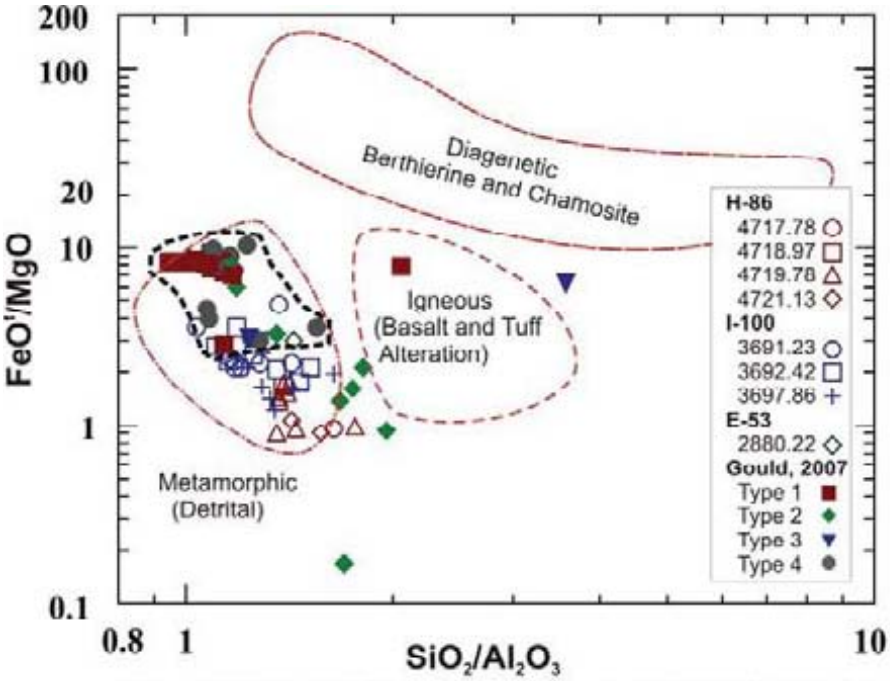

Figure 5.23: FeO'/MgO vs SiO_2/Al_2O_3 discrimination diagram of chlorite, for the studied wells. For comparison the analyses of Gould (2007): type 1=chlorite rims, 2=expanded mica, 3=pore filling, 4=grain replacement, are also shown. The discrimination fields are the same as in Fig. 5.21, with added field around main diagenetic field of Gould, 2007.

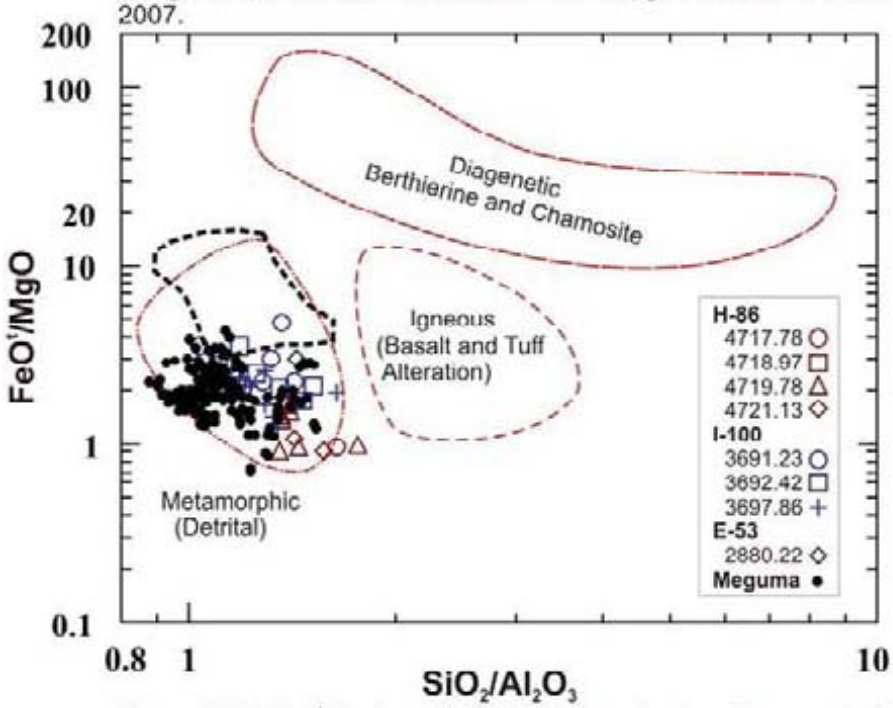

Figure 5.24: FeO'/MgO vs SiO_2/Al_2O_3 discrimination diagram of chlorite with chlorite analyses from the Meguma Group metasediments (personal communication from Dr. Chris White). The discrimination fields are the same as in Fig. 5.21.

and grain replacement. All these chlorite analyses plot in the field for detrital metamorphic chlorites (Fig. 5.23) of Pe-Piper and Weir-Murphy (2008). This suggests that for the purposes of Gould (2007) these fields do not apply probably because of a variation in diagenetic conditions and variation in precursor minerals. Therefore, using Gould (2007) data, a new field has been drawn around the main cluster of diagenetic chlorite from the Sable Basin (Fig. 5.23). By plotting the chlorites of the studied samples, using the crystals vs. pseudomorphs (Fig. 5.22) it shows that the crystals of chlorite, those that are likely detrital, plot in the centre of the metamorphic field, with only a few samples plotting in the diagenetic field of Gould (2007). The diagenetic chlorites, as pseudomorphs, for the studied samples, plot to the lower portion of the detrital metamorphic field, and slightly outside of it. This suggests that the conditions of diagenesis, and the precursor, for the studied samples is different from that of Gould (2007), in addition to being different from Weir-Murphy (2004). Finally, the studied wells are plotted (Fig. 5.24), along with Meguma Group metasediments. Meguma metasediments fall within the lower left of the detrital metamorphic field, and the chlorites of the studied samples (both detrital and diagenetic) plot to the right, with some overlap with Meguma metasediments. Overall, these discrimination diagrams suggest that the diagenesis of Jurassic chlorites is chemically different than that of the Lower Cretaceous. The Jurassic chlorites of studied samples have higher SiO_2, higher MgO, and lower FeO^t. The chlorites of the Lower Cretaceous have lower SiO_2, lower MgO, and high FeO^t.

Chlorite and biotite were plotted together on an Al_2O_3 vs. SiO_2 plot (Fig. 5.25), which does not distinguish the various sample wells and depths. Chlorite shows a

negative trend, where SiO_2 content increases as Al_2O_3 content decreases. Biotite shows a positive trend, with (slightly) increasing SiO_2 with greater increases in Al_2O_3. There is a mixing line (ml) present which contains a higher amount of Al_2O_3 than the rest of the chlorites, and intermediate to high SiO_2 concentrations, this is where there may be alteration occurring such as chloritization of biotite such a process may produce chlorites of mixed layers with other minerals, such as illite, so that they retain higher SiO_2 concentrations.

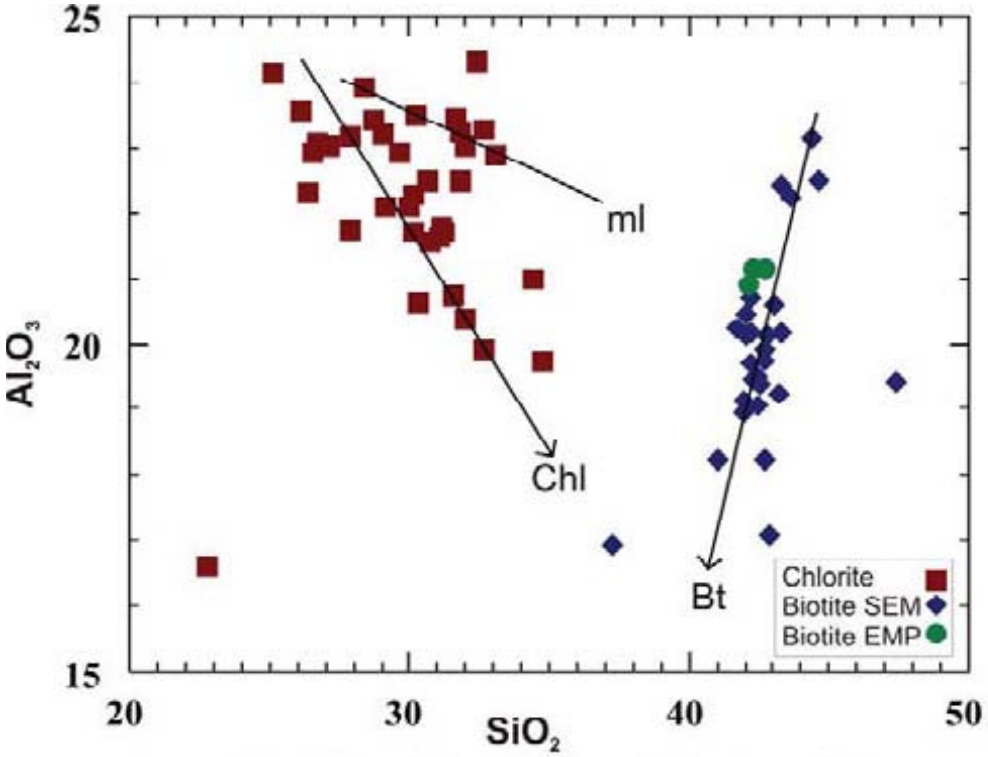

Figure 5.25: Al_2O_3 vs SiO_2 comparison of chlorite and biotite (including electron microprobe data) from studied wells. Chl = chlorite, Bt = biotite, ml = mixing line between chlorite and biotite.

Nomenclature of chlorite was expressed based on the system of Hey (1954), which plots $Fe^t/(Fe^t + Mg)$ vs. Si. These were plotted and compared with those of Meguma Terrane (Fig. 5.26) and those of the Lower Mississauga Formation (Fig. 5.27) (Gould, 2007). Chlorites of the Meguma Terrane, which are detrital, mostly fall within

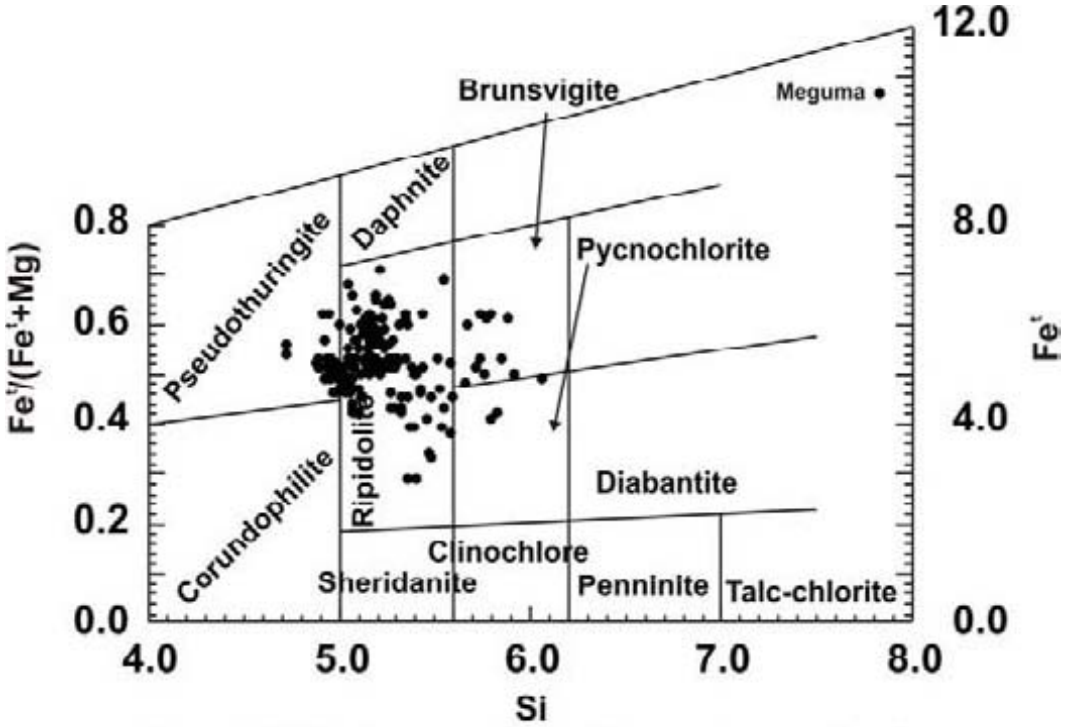

Figure 5.26: Chlorite nomenclature of Meguma Group metasediments (personal communication from Dr. Chris White) as comparison to chlorites in the studied wells (Fig. 5.22), based on system of Hey (1954).

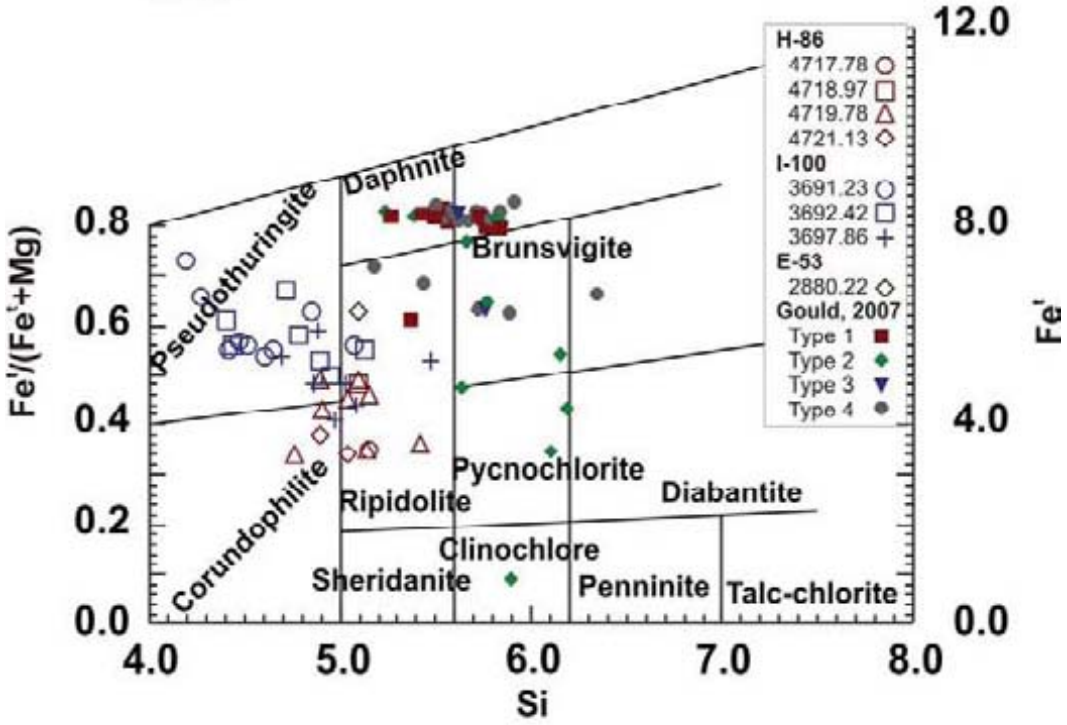

Figure 5.27: Chlorite nomenclature based on system of Hey (1954), with comparison to Gould (2007),with Type 1=chlorite rims, 2=expanded mica, 3=pore filling, and 4=grain replacement.

the ripidolite field. Chlorites of studied wells plot partly in the ripidolite field (largely Mic Mac H-86) and within pseudothuringite (almost exclusively Mohican I-100). Those diagenetic chlorites from Gould (2007), plot mostly outside the ripidolite field, mostly as daphnite. These data suggest that chlorite with Si between 5.0-5.5, are detrital and the others are diagenetic.

Summary: Chlorite is both of detrital and diagenetic origin within the studied wells. The studied diagenetic chlorites contain high MgO and SiO_2(>30wt%), and low FeO^t. The diagenetic chlorites in this study contrast with those of the Cretaceous rocks in the Orpheus Graben in which diagenetic chlorite was found to have low MgO and high FeO^t whereas studied samples has high MgO and low FeO^t. This suggests that the diagenesis of chlorite is variable throughout the Scotian Basin, and the Middle Jurassic sandstones are different from those of the Lower Cretaceous sandstones. In many samples that contain illite, there are often illite-chlorite mixed layers, which became apparent during XRD with a <2 micron oriented run.

5.2.1.5 Carbonate Minerals

Carbonate minerals are present only as diagenetic minerals, mostly as cement, but also found in coated grains or phosphorites. They are present only in studied samples of Mohican I-100 and Wyandot E-53. These were plotted in two ternary diagrams, as a $FeCO_3$-$CaCO_3$-$MgCO_3$ plot (Fig. 5.28), and as a $MnCO_3$-$CaCO_3$-$MgCO_3$ plot (Fig. 5.29). Carbonate minerals present in the studied samples are calcite, Fe-calcite, Mn-calcite, Mg-calcite, dolomite, Fe-dolomite, and ankerite. As Fig. 5.28 shows, most carbonates plot either at the $CaCO_3$ apex, as calcite, or midway between $CaCO_3$ and $MgCO_3$, as dolomite

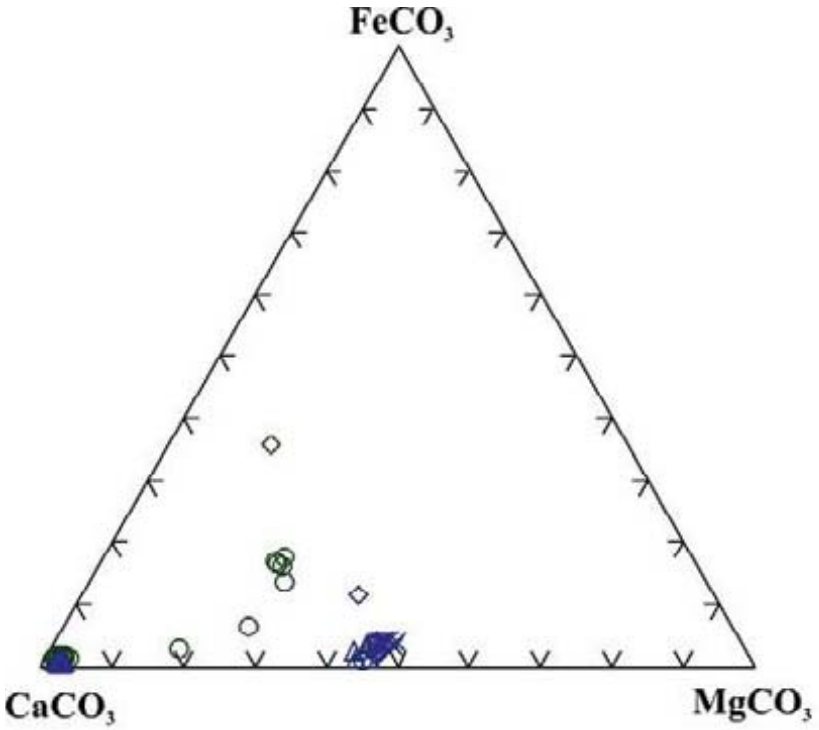

Figure 5.28: $FeCO_3$ - $CaCO_3$ - $MgCO_3$ ternary showing carbonate cements from studied wells.

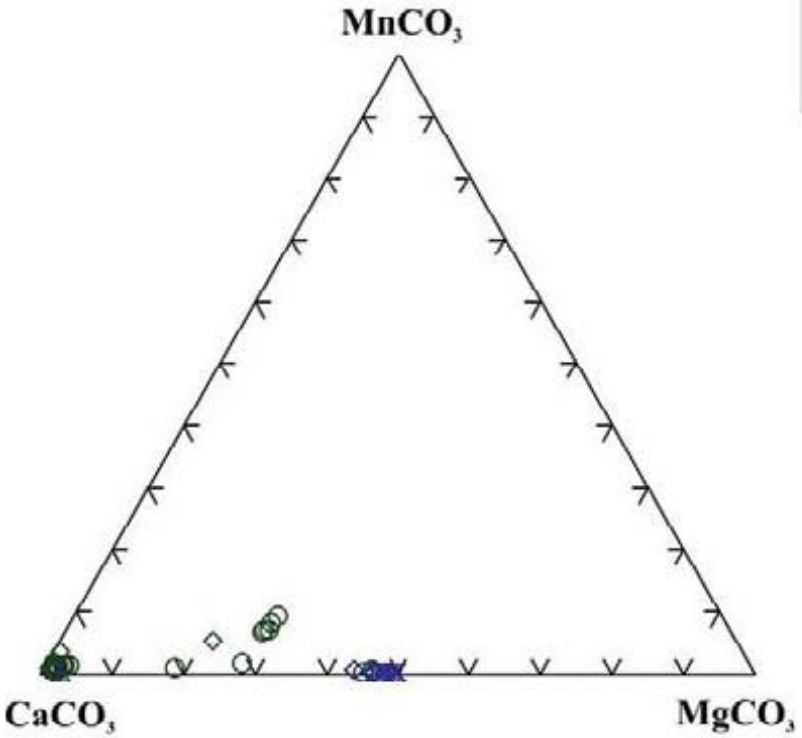

Figure 5.29: $MnCO_3$ - $CaCO_3$ - $MgCO_3$ ternary showing carbonate cements from studied wells.

(almost exclusively in Mohican I-100). A few analyses show concentrations of >5% $FeCO_3$ and these are ankerite, iron-rich dolomite and iron-rich calcite. In Fig. 5.29, most carbonates again plot at the $CaCO_3$ apex, or midway between $CaCO_3$ and $MgCO_3$ (almost exclusively in Mohican I-100). However, there are a few analyses that are minimally concentrated in $MnCO_3$ (only present in samples from Wyandot E-53), appearing as Mn-rich calcite.

5.2.1.5a Dolomite

Dolomite is present mostly in Mohican I-100, but also within one sample of Wyandot E-53. Within Mohican, dolomite is normally present in two stages. Early dolomite precipitated during seafloor diagenesis, in places replacing aragonitic mud (Fig. 4.7D), or forming zones of dolomitization around calcite nodules (Fig. 4.7E). Later diagenetic dolomite occurred by forming dolomite overgrowths on early diagenetic dolomite crystals (Fig. 4.8D).

5.2.1.5b Calcite

Calcite is present only in Mohican I-100 and Wyandot E-53 wells. It is present as calcite, Fe-calcite, Mn-calcite and Mg-calcite. In Wyandot E-53 sample 2880.22 (App. 3D, Fig. 3, analysis 2), Mn-calcite is present and it surrounds and cements two crystals of spessartine garnet which have partially dissolved or broken down. This dissolution created an abundance of manganese to be available which became incorporated into calcite as it was precipitating, causing it to be Mn-rich. In Mohican I-100, calcite is seen to be partly replaced by later anhydrite, and dolomite in places (Fig. 4.7D).

5.2.1.5c Ankerite

Ankerite was found in only three samples. In Mohican I-100 3696.69 it is found rimming early diagenetic dolomite crystals (Fig. 4.7D, position B). In Wyandot E-53 2873.10, ankerite commonly precipitates within secondary porosity from dissolution of both K-feldspar (Fig. 4.9C) and bioclasts (Fig. 4.9A & B).

5.2.1.6 Pyrite

Pyrite is a diagenetic mineral, found in the studied samples as both early and later diagenetic mineral. It is found in several samples, often occurring as framboidal pyrite forming in intergranular boundaries, especially between diagenetic dolomite grains. Later diagenetic pyrite crystallized within dissolution voids.

5.2.1.7 Anhydrite

Anhydrite, found only in Mohican I-100, and forms in multiple stages during diagenesis. Very early anhydrite forms during seafloor diagenesis as concretions, such as seen in sample 3697.36B (App. 2E, Fig. 2). Late anhydrite forms during the later stages of diagenesis and it replaces the earlier formed calcite, possibly from having been remobilized in veins. This mineral is key in determining that the paleoenvironment, in this part of the Mohican Formation and in this well, was that of a sabkha, or salt flat (see section 5.2.2).

5.2.1.8 Kaolinite

Kaolinite was found, for certain, in only two samples from Wyandot E-53 (2876.81, and 2878.66). In sample 2876.81, kaolinite was found both with BSE and SEM, as well as XRD. Sample 2878.66 did not have an XRD sample, however SEM and BSE show that kaolinite is present filling in secondary porosity, as well as precipitating within expanding cleavage planes of muscovite (Fig. 4.10A & B). Kaolinite overlaps with chlorite in a diffractogram, therefore it may be present in XRD samples 2876.35 and 2877.03 from Wyandot, however petrographic analysis was not conducted at these depths to have a definite identification of minerals. Based on XRD, within Mic Mac H-86 and Mohican I-100 wells it appears that kaolinite it not likely present, even though it may be overlapped with chlorite, however, kaolinite was not found in any of the studied samples, from either well, based on SEM analyses.

5.2.1.9 TiO_2 Minerals

TiO_2 minerals such as rutile, anatase and brookite, together with the mineral pseudorutile, mostly form during transport and diagenesis from the alteration of ilmenite as it loses Fe, as seen in Lower Cretaceous sandstones onshore (Pe-Piper et al. 2005). The free iron is then made available to form other diagenetic minerals, such as magnetite, hematite, pyrite, and chlorite. Ilmenite alteration occurs in warm, humid conditions, and it may happen during fluvial transport and pedogenesis (Temple, 1966). The presence of rutile, or other TiO_2 minerals, in most cases in the studied samples, is considered of diagenetic origin because of their mode of occurrence (filling secondary porosity or replacing earlier cements).

5.2.1.10 Late Magnetite

Late diagenetic magnetite is present in Mic Mac 4718.97 (Fig. 4.5F), where it cuts fractures. The precipitation of magnetite is considered to be favoured by bacteria. The late appearance of the magnetite in this study may coincide with the hydrocarbon movement in this area and may suggest the favourable influence of CO_2 on diagenetic crystallization (Kostka & Nealson, 1995). To form diagenetic magnetite requires presence of both bacteria and hydrocarbons. The presence of CO_2 helps in the activity of bacteria to aid magnetite precipitation.

5.2.1.11 Fe-oxyhydroxides

Fe-oxyhydroxides are present as magnetite, hematite and goethite, although limonite may also be present. However many analyses appear to be mixed and their exact nature was undeterminable, and thus they were classified as "iron oxides". These minerals occur only in Mic Mac H-86 well. Fe-oxyhydroxides had to be analyzed on the electron microprobe for more accurate chemical analyses of "iron oxides" in order to distinguish between the different minerals. Other than a few grains of diagenetic magnetite, most of the analyses were contained within lithic clasts. These clasts look like pieces of detrital Meguma clasts, and therefore originally they probably contained pyrrhotite or pyrite, and probably converted to Fe-oxyhydroxides during transport and diagenesis. Pyrrhotite was found to be the most abundant sulphide in the Halifax Formation slates (Haysom, 1994), commonly texturally found as elongated masses, parallel to cleavage. Pyrite is also found in the slates, and forms as either a direct replacement of pyrrhotite (Haysom, 1994), or as independent subhedral to anhedral

grains. Pyrite, which has replaced pyrrhotite, has two distinct habits: either as colloform or as birds-eye-structure, and often forms pyrite stringers which branch off along cleavage planes (Haysom, 1994). Fe-oxyhydroxides that form from oxidation of pyrrhotite, mainly include goethite and ferrihydrite (Belzile et al. 2004). Oxidation of pyrrhotite is favoured by humid conditions, and with increasing temperature (Belzile et al. 2004), both conditions that were present during the Middle Jurassic in the study area. Therefore, it is likely that the lithic clasts within the Mic Mac H-86 well, which contain Fe-oxyhydroxides, are probably from the Meguma Supergroup, and likely converted to Fe-oxyhydroxides during transport and diagenesis.

Summary: Diagenetic minerals in the studied samples are hydromuscovite, illite, kaolinite, chlorite, carbonates, anhydrite, pyrite, and "iron oxides". Minerals such as the carbonates and pyrite form only during diagenesis. XRD data show that most studied samples closely resemble the Scotian Basin clay assemblages in shales and muddy bioturbated sandstones (Aneja, 2012). This suggests that the clay minerals of this study have gone through normal burial diagenetic processes.

5.2.2 Paragenetic Sequences

The overall paragenetic sequence for each well (Figs. 5.30-5.32) was determined using textural criteria between different minerals in contact. Textures include: (i) replacement of one mineral by another, such that the mineral being replaced is older, (ii) engulfment of one mineral by another, such that the mineral being engulfed is older, (iii) presence of one mineral impedes growth of another, such that the impeding mineral is

younger, and (iv) dissolution of framework grains and secondary porosity in cements (Karim et al., 2008).

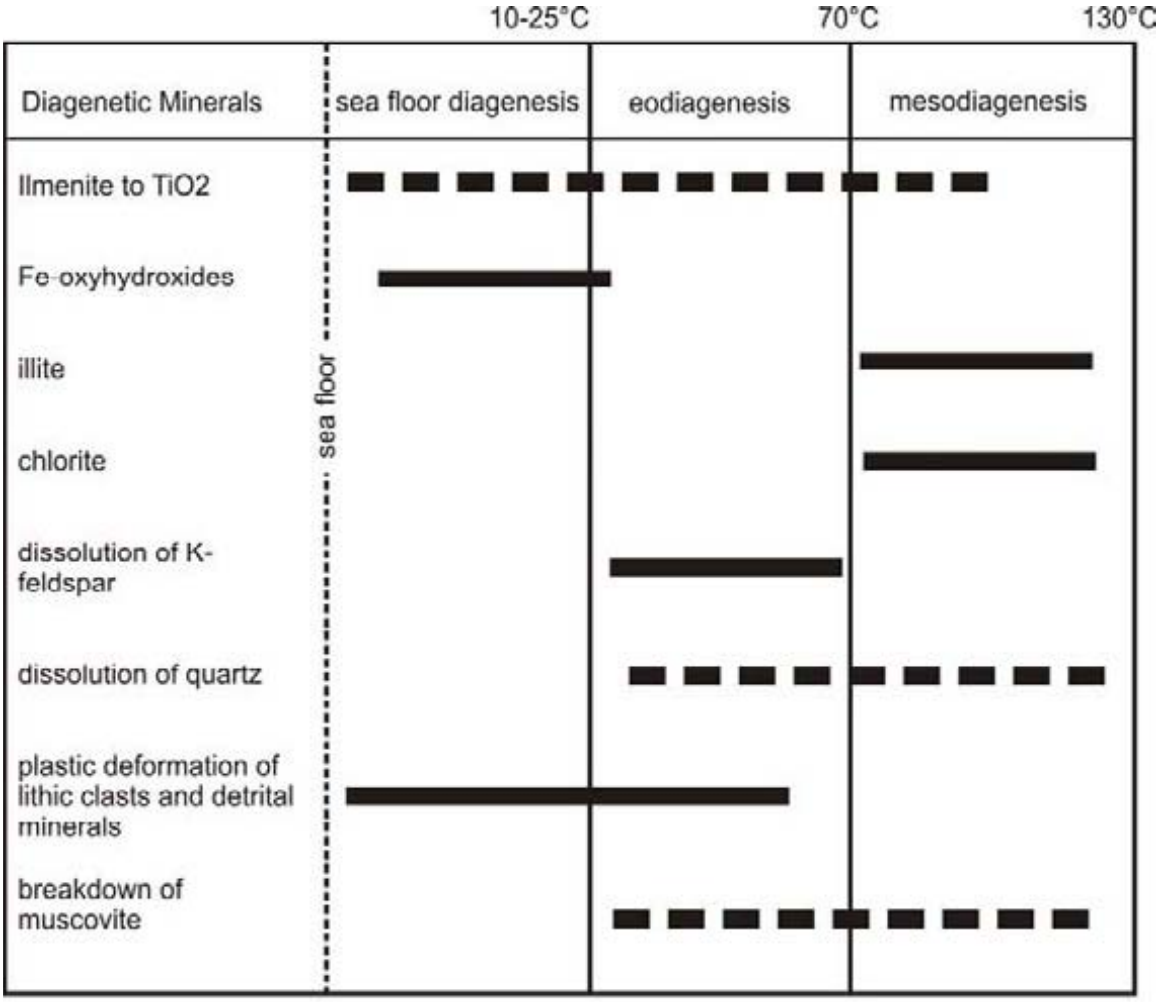

Fig. 5.30: Paragenetic sequence determined from textural relationships from samples from Mic Mac H-86 well. The boundary between eodiagenesis and mesodiagenesis was determined by Morad et al. (2000) and El Ghali et al. (2006).

The Middle Jurassic sandstones in the Mic Mac and Wyandot wells are mostly subarkose in contrast to the Upper Jurassic-Lower Cretaceous wells where quartz arenites predominate. Mic Mac and Wyandot also have a high proportion of Meguma-derived phyllosilicate minerals and pelitic lithic clasts. Due to these lithological differences mechanical compaction predominates in Mic Mac and Wyandot wells, and early cementation is dominant in the Upper Jurassic-Lower Cretaceous sandstones. Wyandot

also had a depositional environment that was predominately marine, and Mic Mac had a depositional environment that was coastal to marine.

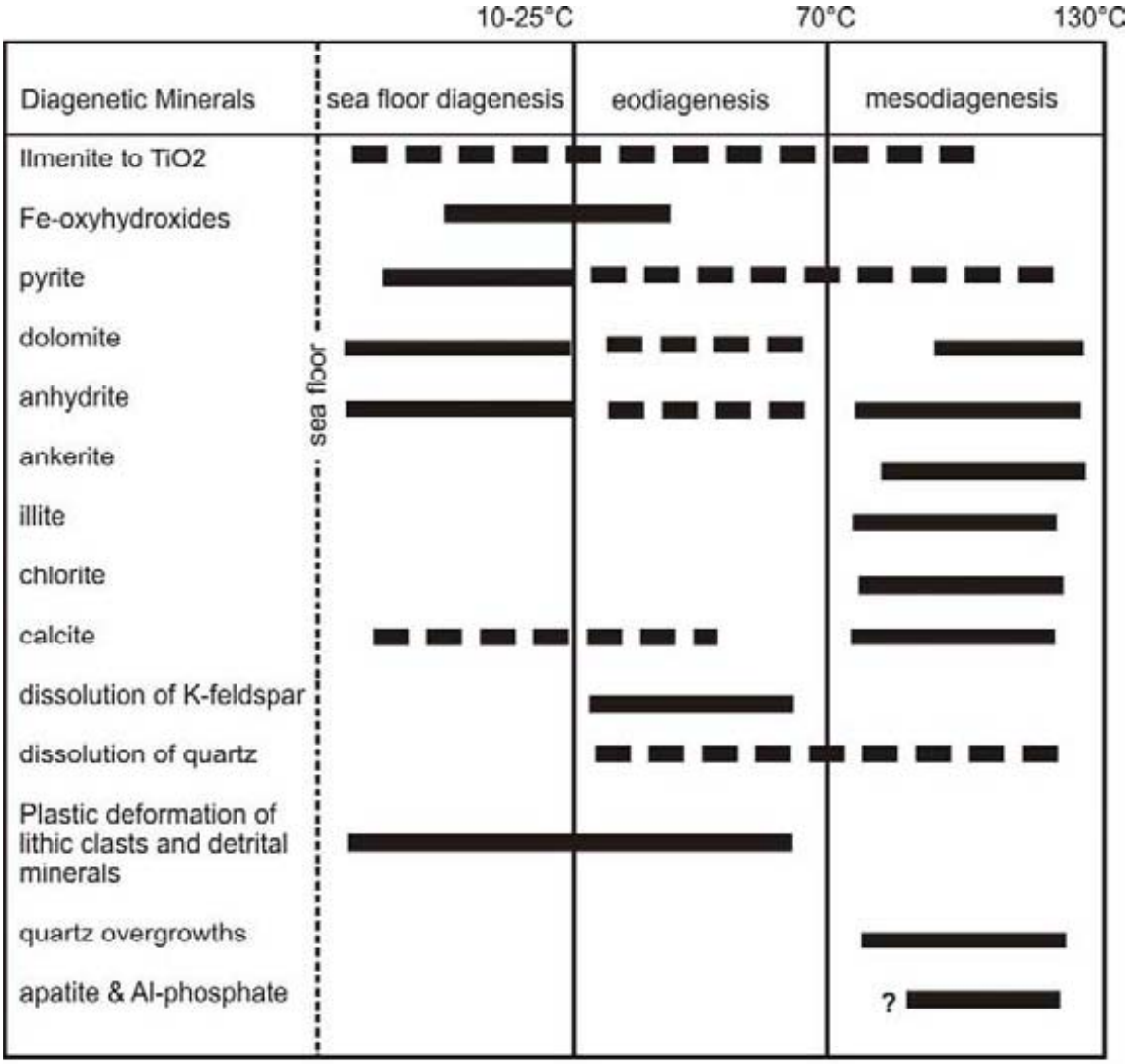

Fig. 5.31: Paragenetic sequence determined from textural relationships from samples from Mohican I-100 well. The boundary between eodiagenesis and mesodiagenesis was determined by Morad et al. (2000) and El Ghali et al. (2006).

Early diagenesis in the Mohican Formation, in the Mohican I-100 well, is consistent with a sabkha environment. This environment forms on a supratidal flat on which occasional storms bring seawater containing carbonate muds. When the seawater

evaporates, gypsum crystals precipitate at the top of the water table. During burial at the

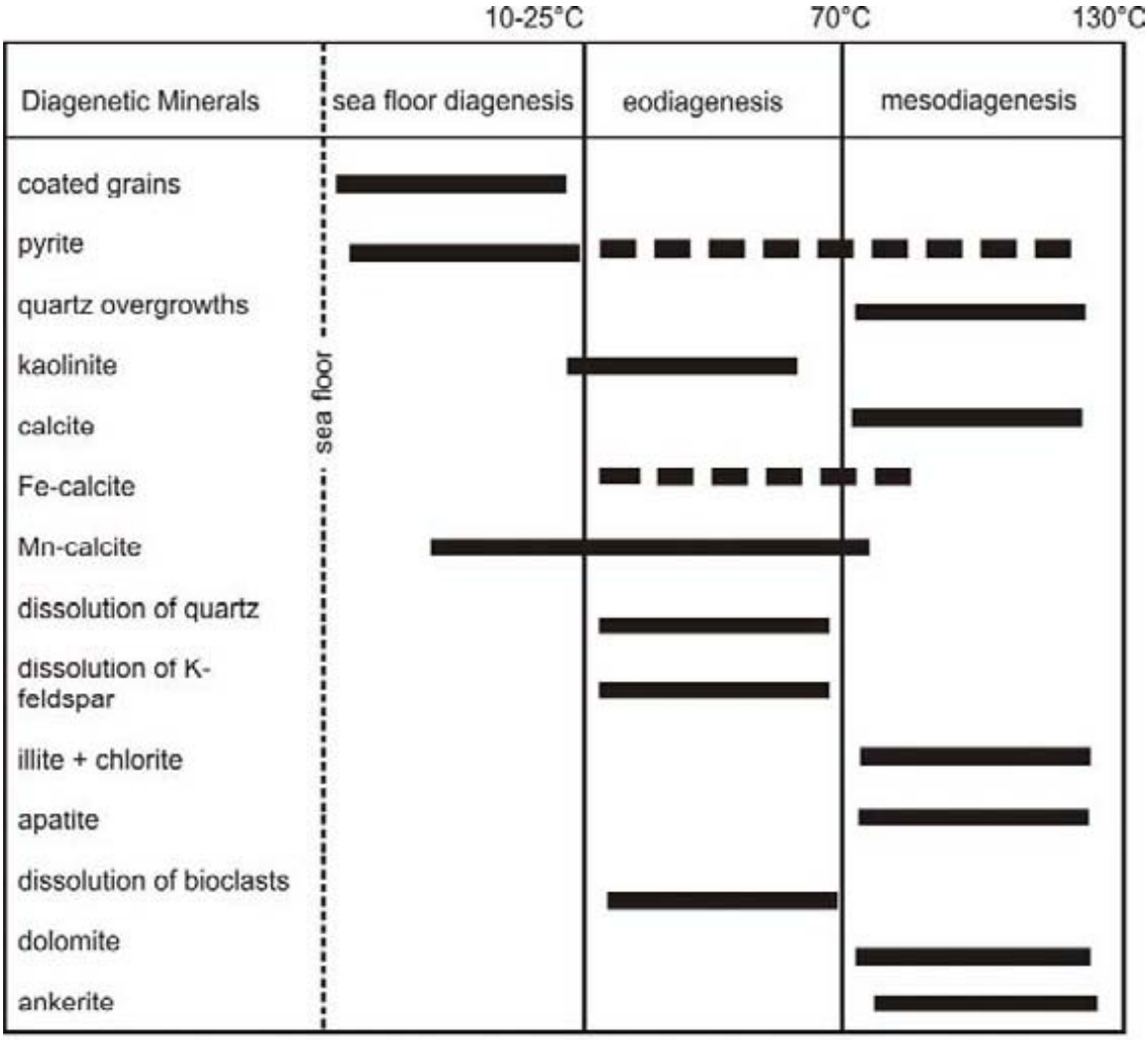

Fig. 5.32: Paragenetic sequence determined from textural relationships from samples from Wyandot E-53 well. The boundary between eodiagenesis and mesodiagenesis was determined by Morad et al. (2000) and El Ghali et al. (2006).

seafloor diagenesis stage, gypsum then converts to anhydrite, as seen in Mohican I-100, as both nodules and cement that predate significant compaction. Thus anhydrite is common in such environments. Anhydrite is a mobile mineral, and can be seen in more than one generation in sedimentary sequences. Also occurring during seafloor diagenesis in Mohican I-100 is the formation of calcite nodules, early dolomite, and early pyrite which can precipitate within ~8 cm depth.

Overall, the paragenetic sequence appears, in general, similar to that of the Lower Cretaceous sandstones (Karim et al., 2008). However, there is an absence of siderite and chlorite rims in the studied samples suggesting a lack of these minerals during the Middle Jurassic in this part of the Scotian Basin, as compared with Lower Cretaceous sandstones in the basin in which siderite and chlorite rims are fairly abundant. The main difference between diagenesis between these two time periods is in the chemical makeup of minerals, such as in the previously discussed high MgO concentration in chlorite of the studied samples compared to Cretaceous rocks which have high FeO^t.

5.2.3 Provenance

Provenance studies the rock sources from which framework grains have originated. There are many methods available to study provenance. Petrography can be used to compare textural relationships of detrital grains to potential source rocks, as well as to study lithic clasts which provide a rock fragment directly from the source. Dating methods are useful in some cases, and minerals used in dating for provenance are usually zircon, monazite, muscovite and K-feldspar. Field work, when possible, can locate the source of paleocurrents to determine their flow direction and therefore where they transported detrital grains and clasts. Hot and cold cathodoluminescence can distinguish between the origin of grains of the same type, commonly done with quartz. Modal composition of detrital grains and lithic clasts can determine the paleotectonic setting (as described in section 4.1.1.2 on paleotectonic classification). Specialized minerals, such as garnet, tourmaline and ilmenite, can also be studied to see where common textural and chemical relationships occur between those that have been transported and those in their

original source rock. In this study, petrography (lithic clasts), modal composition, and studying garnet and ilmenite, were used to determine the provenance of the studied samples.

5.2.3.1 Garnet

Garnet was found only in Wyandot E-53 well at 2880.22 m, and were plotted on an almandine-grossular-spessartine plane (Fig. 5.33). Pyrope is <10% so this end member was not plotted. Both garnet grains were classified as Type 5 garnets which are spessartine with prominent almandine substitution. As seen in the BSE image (App. 3D, Fig. 3, analysis 1), garnet has been partly dissolved, and this likely accounts for the surrounding calcite cement being Mn-rich (App. 3D, Fig. 3, analysis 2). Garnet was found to be abundant in places in Meguma Group Mn-rich metasedimentary rocks (Li et al., 2012).

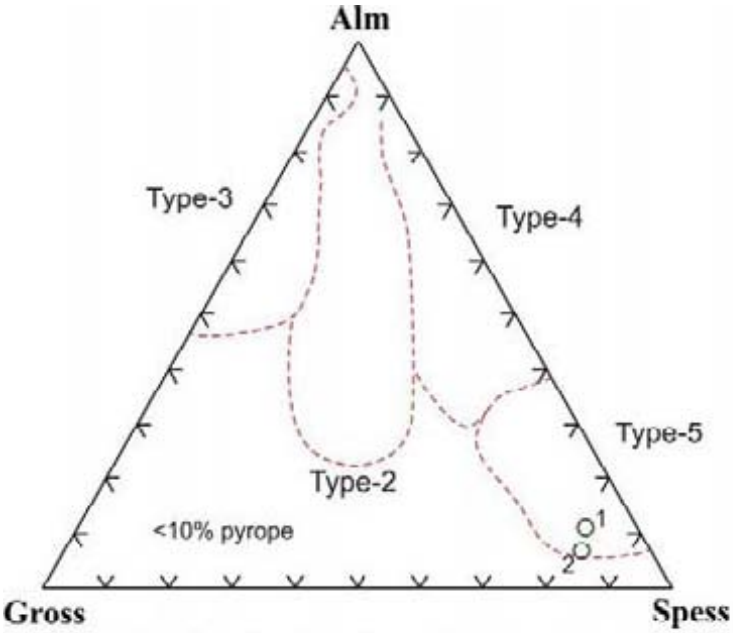

Figure 5.33: Classification of garnet as Type 5 (spessartine with prominent almandine substitutions) from Wyandot E-53 well at 2880.22m depth projected onto an Almandine-Grossular-Spessartine Plane (pyrope <10% so this end member was not used).. End members for the analyzed garnet grains are: Alm (10.946), Gross (7.986), Spess (79.351) and Py (1.716) for sample 1, and Alm (6.536), Gross (10.663), Spess (79.797) and Py (3.004) for sample 2. Type fields from Pe-Piper et al. (2009).

5.2.3.2 Ilmenite

Ilmenite grains found in the Middle Jurassic sandstones in the Mohican Formation are likely originating from the Meguma Terrane. This is likely because those ilmenite in the Mohican Formation are similar in texture and inclusions as those of the Chaswood Formation (Pe-Piper et al., 2005). Ilmenite is most abundant in Mohican I-100 well. Detrital ilmenite grains, that have undergone alteration, often contain inclusions of quartz (App. 2B, Fig. 4, analyses 3 & 4), muscovite (App. 2B, Fig. 4, analysis 2), and tourmaline, and these grains are generally inherited from a peraluminous granitic or metamorphic (pelitic) protolith (Pe-Piper et al. 2005). During diagenesis, ilmenite often alters and forms TiO_2 minerals as a byproduct (see section 5.2.1.9 on TiO_2 minerals).

5.2.3.3 Modal Composition

As previously discussed in section 4.1.1.2, modal composition can determine probable paleotectonic setting, by using the QFL and QmFLt diagrams of Dickinson et al. (1983). Studied samples from Mic Mac H-86 plot as quartzose recycled orogen. The samples from Mohican I-100 are split between recycled orogen and continental block. The samples from Wyandot E-53 are divided between continental block and recycled orogen.

5.2.3.4 Lithic Clasts

Lithic clasts are important in both provenance and diagenesis. For studying provenance the mineralogy and texture is important, for diagenesis their alteration upon burial is important (as shown in section 4.1: Petrography where lithic clasts were often

found partially plastically deformed). Two samples from Meguma supergroup metasediments were studied petrographically (App. 5A) to determine main minerals and textures present in each. One sample was of a slate (sample 8) and the other was a meta-sandstone (sample 10). The meta-sandstone (App. 5A, Figs. 1-4), was found to contain fine grained intergranular muscovite (App. 5A, Fig. 1), opaque minerals forming along cleavage planes of muscovite (App. 5A, Fig. 2 & 3), and chloritized biotite (App. 5A, Fig. 4). The slate (App. 5A, Figs. 5 & 6), was found to contain chlorite and quartz grains (App. 5A, Fig. 3), with fine grained intergranular muscovite, as well as an opaque mineral forming along cleavage planes of chlorite (App. 5A, Fig. 6).

In looking at the studied wells, the Mic Mac H-86 samples have chloritized biotite (App. 4A, Fig. 7 & 8), similar to the Meguma supergroup meta-sandstone. Clasts of Mic Mac H-86 contain muscovite as well as abundant opaque minerals, identified to be various iron oxides or Fe-oxyhydroxides, which are also present in cleavage planes of muscovite and chlorite grains of both Meguma supergroup samples. Large perthite grains (App. 1D, Fig. 3), in Mic Mac H-86, also suggest clasts from granitoid rocks. Lithic clasts were most abundant in Mohican I-100 (App. 4B & 5B) appear abundant in a combination of quartz, chlorite and biotite. The variety of clasts found in this well include: quartzite (App. 4B, Fig. 1), greenschist (App. 5B, Fig. 2 & 5), and rhyolite (App. 5B, Fig. 4). Clasts of Wyandot E-53 (App. 4C), are mostly quartzite (App. 4C, Fig. 4 & 5), with some quartz and muscovite slates (App. 4C, Fig. 10). There are also various types of bioclasts present in Wyandot E-53.

Overall, the clasts correspond to source rock type consistent with the Meguma supergroup, and show both some slate and some meta-sandstones. The clasts in the

studied wells vary between more rounded, and minimally deformed clasts, which generally are those that are quartzite (App. 4B, Fig. 1), and those that have been more partially plastically deformed, which tended to be those richer in muscovite and chlorite (App. 4A, Figs. 6, 9 & 11).

5.3 Lithofacies

The lithofacies scheme proposed by Gould et al. (2010), for the Early Cretaceous Missisauga and Logan Canyon Formations, was used in determining the classification of the Middle Jurassic sandstones of the Mohican Formation in Gould et al. (2011). This classification scheme was useful in classifying both Mic Mac H-86 and Wyandot E-53 wells. However, in the Mohican Formation of the Mohican I-100 well, the lithofacies scheme does not fit. They were originally described by Gould et al. (2011) as four depositional environments: transgression, tidal, coastal, and shelf. However, through further core logging and petrographic analysis in this study, it seems that the entire section of the core is actually from a tidal flat environment. This is suggested as the environment because of the presence of anhydrite, coal, and phytodetritus. Anhydrite forms in a sabkha environment, where there is a periodic influx of seawater. Coal is present in this well, however it is not found in a shelf environment because it requires vegetation to be present. Therefore, the pieces of phytodetritus and coal present in this core mean that the depositional environment was not shelf, and was most likely tidal flats situated close to river input.

5.4 Porosity and Permeability

Porosity and permeability data was obtained from the Canada-Nova Scotia Offshore Petroleum Board. Data was only available for Mic Mac H-86 and Wyandot E-53 wells. In Mic Mac H-86 (Table 5.1), porosity is low in most samples, and the main diagenetic minerals found in all are illite and chlorite.

Sample Depth (m)	Measured Interval (m)	Porosity (%)	Permeability – Kmax (md)	Lithofacies	Lithology	Diagenetic Minerals Present
4717.78	4717.75-4717.84	0.2	25.7	2b	Sandy mudstone	illite, chlorite, iron oxides, TiO_2 minerals
4718.97	4718.97-4719.25	4.1	4.17	9s/9g	Fine grain sandstone	illite, chlorite, iron oxides
4719.78	4718.64-4720.1	1.1	0.45	9s/9g	Sandstone	illite, chlorite, iron oxides, TiO_2 minerals
4721.13	4720.98-4721.14	5.7	39.8	9s/9g	Fine grained sandy mudstone	illite and chlorite

Table 5.1: Porosity and permeability data for studied samples of Mic Mac H-86 well

Lower permeability of samples 4718.97 and 4719.78 may be attributed to the abundance of partially plastically deformed lithic clasts and detrital grains which create a plug before framework grains, preventing the movement of hydrocarbons. Sample 4717.78 has chlorite and illite often along grain boundaries and filling dissolution voids. Voids, in this sample, are more abundant within the matrix than they are within framework grains.

In Wyandot E-53 (Table 5.2) porosity is also low in the samples, with only one sample being considerably higher than the rest (2876.81 m). This sample also contains the highest permeability, with a Kmax of 91.3 md. This sample does not contain illite (based on SEM and BSE images as well as XRD). Although this sample has kaolinite, it is in minimal amounts, and is found filling dissolution voids. Abundant porosity is

visible in BSE images, mostly within the matrix, but some also in partly dissolved clasts. This is also the only sample in which coal was observed.

Sample Depth (m)	Measured Interval (m)	Porosity (%)	Permeability – Kmax (md)	Lithofacies	Lithology	Diagenetic Minerals Present
2873.10	2872.98-2873.20	4.5	0.535	9s	Carbonate	calcite, ankerite, dolomite, pyrite, illite, quartz overgrowths, coated grains
2876.81	2876.67-2877.01	19	91.3	4x	Coarse grain sandstone	kaolinite, TiO_2 minerals, coal, apatite
2878.66	2878.47-2878.81	9.9	30.1	4x	Coarse grain sandstone	kaolinite, illite, TiO_2 minerals, pyrite
2880.22	2879.75-2880.36	3.9	3.42	9g	carbonate	calcite, ankerite, chlorite, pyrite, TiO_2 minerals

Table 5.2: Porosity and permeability data for studied samples of Wyandot E-53 well

Sample 2878.66 of Wyandot E-53 has higher porosity, mostly from highly dissolved framework grains, some of which have chlorite and kaolinite filling void spaces. Sample 2880.22 has carbonate cement in places, reducing permeability. In some places, dissolution of framework grains is nearly complete. There is also plastically deformed lithic clasts present, which also contribute to reduced permeability, as they are squeezed between framework grains.

Overall, permeability is lower in samples that contain carbonate cement throughout, even when porosity is higher. Permeability is higher in samples that have high dissolution of framework grains, abundant voids within the matrix, and are lacking illite (either absent, or in minimal amounts found). Mic Mac H-86 shows that a higher value of porosity does not always coincide with higher permeability, possibly an effect of

pseudomatrix. As it is normally expected, samples in Wyandot E-53 with higher porosity tend to also have higher permeability values.

Porosity and permeability also varies between different lithofacies. In Mac Mac H-86 well, sample 4717.78 has a 2b facies designation as a mudstone, and it has a very low porosity (0.2%). The other three samples have a 9s/9g designation, varying from fine to coarse sandstone, and the porosity is higher in these samples. In Wyandot E-53, samples 2873.10 and 2880.22 are both lithofacies 9 and have a lower porosity and permeability. Samples 2876.81 and 2878.66 are both lithofacies 4x, which is medium to coarse sandstone and can include coal, and these two samples have a higher porosity and permeability. This shows that lithofacies, can indicate the general porosity and permeability present. Therefore, it may be a good indicator of reservoir potential by suggesting which types of lithofacies that hydrocarbons would more easily be transported through and situated in.

Chapter 6: Conclusion

The purpose of this study was to study the diagenesis and provenance of the Middle Jurassic sandstones, found in the Mohican Formation of the Scotian Basin, and to compare these to the younger, more well-known Cretaceous sandstones to give insight into the reservoir potential of the Mohican Formation.

1) Provenance data showed that detrital minerals in the studied samples come from the Meguma Supergroup and Meguma Terrane, in general. Spessartine garnet comes from Mn-rich metasedimentary rocks of the Meguma Supergroup, either as a first or second cycle detritus. Ilmenite also seems to originate from the Meguma Terrane (granites and meta-sediments), then alters during diagenesis, as similarly occurred during the development of the Cretaceous Chaswood Formation sands onshore. Lithic clasts are similar in mineralogical composition and texture with the slates and meta-sandstones of the Meguma Supergroup. Fe-oxyhydroxides occur in lithic clasts and probably derive from alteration during transport and diagenesis from pyrrhotite or pyrite, thus suggesting an origin from the Halifax Group slates.

2) Diagenetic paragenesis in the Middle Jurassic is generally similar to the Lower Cretaceous sandstones. However, there is an absence of siderite and chlorite rims in the studied samples compared with the Lower Cretaceous (and chemical differences in specific minerals).

3) Chlorite diagenesis is variable throughout the Scotian Basin, with Middle Jurassic diagenetic chlorite being chemically different than Lower Cretaceous diagenetic chlorite. This is also evident in the studied coated grains and phosphorites.

4) The depositional environment of the entire Middle Jurassic Mohican Formation in the Mohican I-100 well was determined to be from a tidal flat environment, and formed in a sabkha environment.

5) The type of lithofacies appears to correlate with relative porosity and permeability in the studied wells, suggesting that lithofacies can be a predictor of reservoir quality.

6) There is secondary porosity present in the studied samples, some of which, however, has been partially filled with late diagenetic minerals, suggesting that mineral dissolution may not always contribute to a good reservoir quality.

REFERENCES

Anjea, N., 2013. Clay mineral analysis of shales from the Mesozoic strata, Scotian Basin. Technical Report, Department of Geology, Saint Mary's University, p.1-21.

Belzile, N., Chen, Y.W., Cai, M.F., and Li, Y. 2004. A review of pyrrhotite oxidation. Journal of Geochemical Exploration, **84:** 65-76.

CNOSPB, 2000. Technical summaries of Scotian Shelf significant and commercial discoveries, November 2000 edition, 275p.

Dickinson, W.R., Beard, L.S., Brakenridge, G.R., Erjavec, J.L., Ferguson, R.C., Inman, K.F., Knepp, R.A., Lindberg, F.A., and Ryberg, P.T., 1983. Provenance of North American Phanerozoic sandstones in relation to tectonic setting. Geological Society of America Bulletin, **94:** 222-235.

El-Ghali, M.A.K., Morad, S., Al-Aasm, I., Ramseyer, K. and Mansurberg, H., 2006. Distribution of diagenetic alterations in glaciogenic sandstones within a depositional facies and sequence stratigraphic framework: evidence from the Upper Ordovician of the Murzuq Basin, SW Libya. Sedimentary Geology, **190**: 299-327.

Encana, 2014. http://www.encana.com.

Folk, R.L., 1968. Petrology of sedimentary rocks. Austin, University of Texas publication, 170p.

Gould, K.M., 2007. Chlorite diagenesis in reservoir sandstones of the Lower Missisauga formation, offshore Nova Scotia. Masters thesis, Saint Mary's University, Halifax, N.S., Canada.

Gould, K.M., Karim, A., Piper, D.J.W, and Pe-Piper, G. 2010. A standard lithofacies scheme for the Mississauga and Logan Canyon formations of the Scotian Basin and its application to long sections of conventional cores. Geological Survey of Canada, open file 6745.

Gould, K.M., Karim, A., Piper, D.J.W., and Pe-Piper, G. 2011. Lithofacies and diagenesis of selected conventional core from Jurassic and Early Cretaceous terrigenous clastic rocks, Scotian Basin. Geological Survey of Canada, open file 6945.

GSC Atlantic, 2014. NRCAN Basin Database. http://basin.gdr.nrcan.gc.ca/wells

Haysom, S.J., 1994. The opaque mineralogy, petrology, and geochemistry of the Meguma Group metasediments, Rawdon area, Nova Scotia. Honours thesis, Saint Mary's University, Halifax, N.S., Canada.

Hey, M.H., 1954. A new review of the chlorites. The Mineralogical Magazine, **224:** 277-292.

Karim, A., Pe-Piper, G., and Piper, D.J.W. 2008. Distribution of diagenetic minerals in Lower Cretaceous sandstones and their relationship to stratigraphy and lithofacies: Glenelg, Thebaud and Chebucto fields, offshore Scotian basin. Geological Survey of Canada, open file 5880.

Karim, A., Pe-Piper, G., and Piper, D.J.W. 2010. Controls on diagenesis of Lower Cretaceous reservoir sandstones in the western Sable Subbasin, offshore Nova Scotia. Sedimentary Geology, **224(1):** 65-83.

Kostka, J.E. and Nealson, K.H., 1995. Dissolution and reduction of magnetite by bacteria. Environmental Science and Technology, **29(10):** 2535-2540.

Li, G., Pe-Piper, G., and Piper, DJW. 2012. The provenance of Middle Jurassic sandstones in the Scotian Basin: petrographic evidence of passive margin tectonics. Canadian Journal of Earth Sciences, **49:** 1463-1477.

Moore, D.M., and Reynolds, R.C. Jr., 1997. X-ray diffraction and the identification of clay minerals, 2nd ed. 378p.

Morad, S., Ketzer, J.M., and De Ros, L.F. 2000. Spatial and temporal distribution of diagenetic alterations in siliciclastic rocks: implications for mass transfer in sedimentary basins. Sedimentology, **47(1):** 95-120.

Okwese, A.C., Pe-Piper, G., and Piper, D.J.W. 2012. Controls on regional variability in marine pore-water diagenesis below the seafloor in Upper Jurassic-Lower Cretaceous prodeltaic sandstone and shales, Scotian Basin, Eastern Canada. Marine and Petroleum Geology, **29:** 175-191.

Pe-Piper, G., and Weir-Murphy, S., 2008. Early diagenesis of inner-shelf phosphorite and iron-silicate minerals, Lower Cretaceous of the Orpheus graben, southeastern Canada: implications for the origin of chlorite rims. American Association of Petroleum Geologists Bulletin, **92(9):** 1153-1168.

Pe-Piper, G., Tsikouras, B., Piper, D.J.W., and Triantaphyllidis, S. 2009. Chemical fingerprinting of detrital minerals in the Upper Jurassic-Lower Cretaceous sandstones, Scotian Basin. Geological Survey of Canadam open file 6288.

Pe-Piper, G., Karim, A., and Piper, D.J.W. 2011. Authigenesis of titania minerals and the mobility of Ti: new evidence from pro-deltaic sandstones, Cretaceous Scotian Basin, Canada. Journal of Sedimentary Research, **81:** 762-773.

Pe-Piper, G., Piper, D.J.W., and Dolansky, L. 2005. Alteration of ilmenite in the Cretaceous sandstones of Nova Scotia, southeastern Canada. Clay and Clay Minerals, **53(5)**: 490-510.

Pe-Piper, G., Piper, D.J.W., Zhang, Y., and Chavez, I. 2014. Diagenetic barite and sphalerite in Middle Mesozoic sandstones, Scotian Basin, as tracers for basin hydrology. American Association of Petroleum Geologists *IN REVIEW*

Pevear, D.R., 1999. Illite and hydrocarbon exploration. Proceedings of the National Academy of Sciences of the United States of America, **96:**

Reynolds, P.H., Pe-Piper, G., and Piper, D.J.W., 2010. Sediment sources and dispersion as revealed by single-grain $^{40}Ar/^{39}Ar$ ages of detrital muscovite from Carboniferous and Cretaceous rocks in mainland Nova Scotia. Canadian Journal of Earth Sciences, **47**: 957-970.

Shell Canada Limited. 1971a. Well History Report – Mic Mac H-86.

Shell Canada Limited. 1971b. Well History Report – Wyandot E-53.

Shell Canada Limited. 1972. Well History Report – Mohican I-100.

Temple, A.K., 1966. Alteration of ilmenite. Economic Geology, **61:** 695-714.

Wade, J.A., and MacLean, B.C., 1990. Aspects of the geology of the Scotian Basin from recent seismic and well data, in M.J. Keen and G.L. Williams, eds., Geology of the continental margin of eastern Canada: Geological Survey of Canada, Geology of Canada, **2:** 190-238.

Weir-Murphy, S.L., 2004. The Cretaceous rocks of the Orpheus graben, offshore Nova Scotia. Masters thesis, Saint Mary's University, Halifax, Nova Scotia, Canada.

Weston, J.F., MacRae, R.A., Ascoli, P., Cooper, M.K.E., Fensom, R.A., Shaw, D., and Williams, G.L., 2012. A revised biostratigraphic and well-log sequence-stratigraphic framework for the Scotian Margin, offshore eastern Canada. Canadian Journal of Earth Sciences, **49:** 1417-1462.

White, D.C., 2014. Variation in style of overpressure in Scotian Shelf wells, Scotian Basin. Honours thesis. Saint Mary's University, Halifax, Nova Scotia, Canada.

Appendix 1A: Scanning Electron Microscope Backscattered Electron Images for Mic Mac H-86 well with EDS Mineral Analyses Sample 4717.78

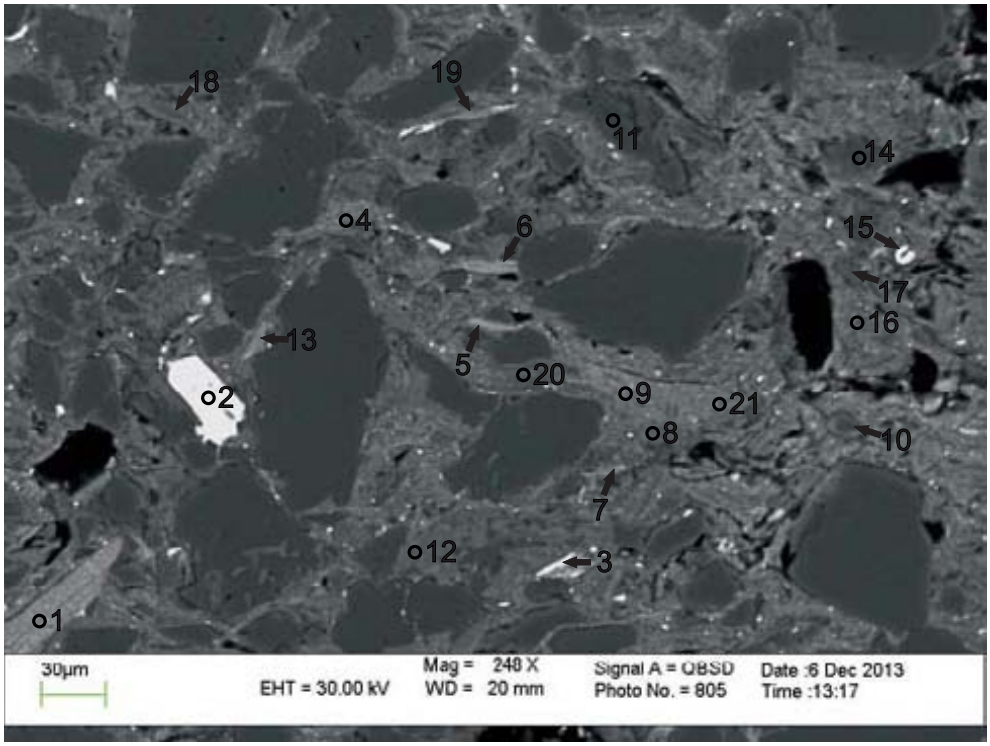

1: Biotite
2: Ilmenite
3: Chlorite + Muscovite
4-7: Illite
8: Muscovite
9: Illite
10: Quartz
11: Quartz
12: Illite
13: Illite
14: Albite
15: Iron oxide + Illite
16: Illite
17: Quartz
18: Muscovite
19: Biotite
20: Muscovite + Chlorite
21: Illite

Figure 1: Mic Mac H-86: 4717.78 site 1. Detrital grains, mostly quartz and albite, surrounded by a matrix of partially plastically deformed muscovite, chlorite and illite.

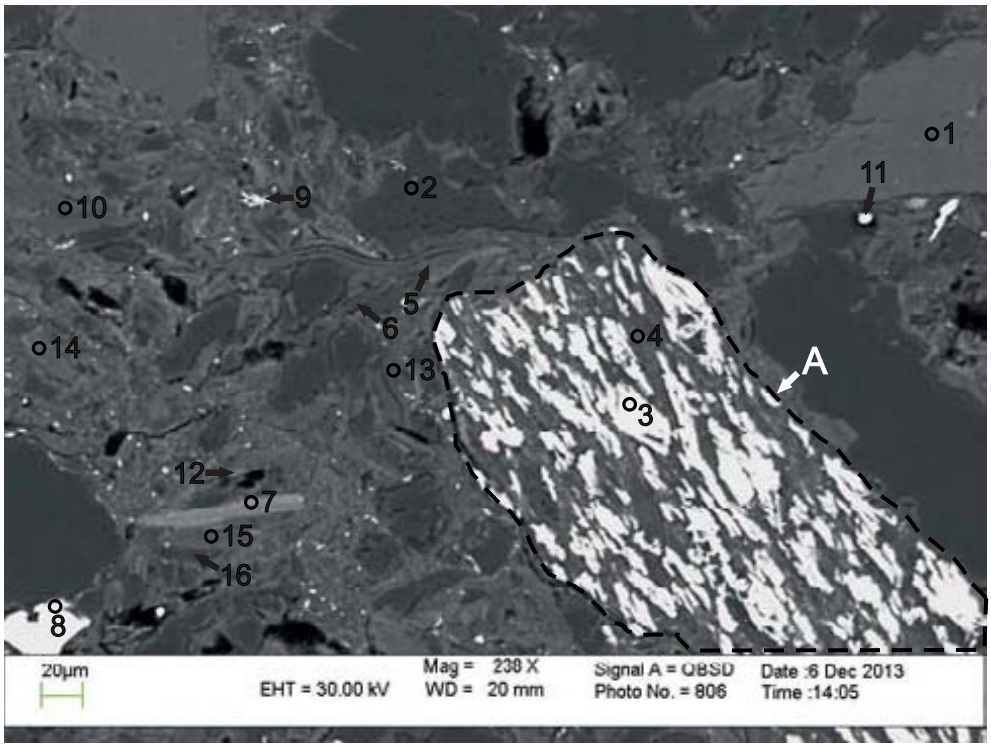

1: K-feldspar
2: Albite
3: Hematite
4: Muscovite + Hematite
5: Muscovite
6: Quartz
7: Biotite
8: Iron oxide + other
9: Altered Ilmenite + K-feldspar
10: Muscovite + Chlorite
11: Barite (drilling mud) + Muscovite
12: Illite
13: Muscovite
14: Illite
15: Chlorite + other
16: Quartz

Figure 2: Mic Mac H-86: 4717.78 site 2. Lithic clast (position A, and see App. 4A, Fig. 1) composed of hematite and muscovite (see Fig. 7 and Table 2A for electron microprobe analyses of this clast)

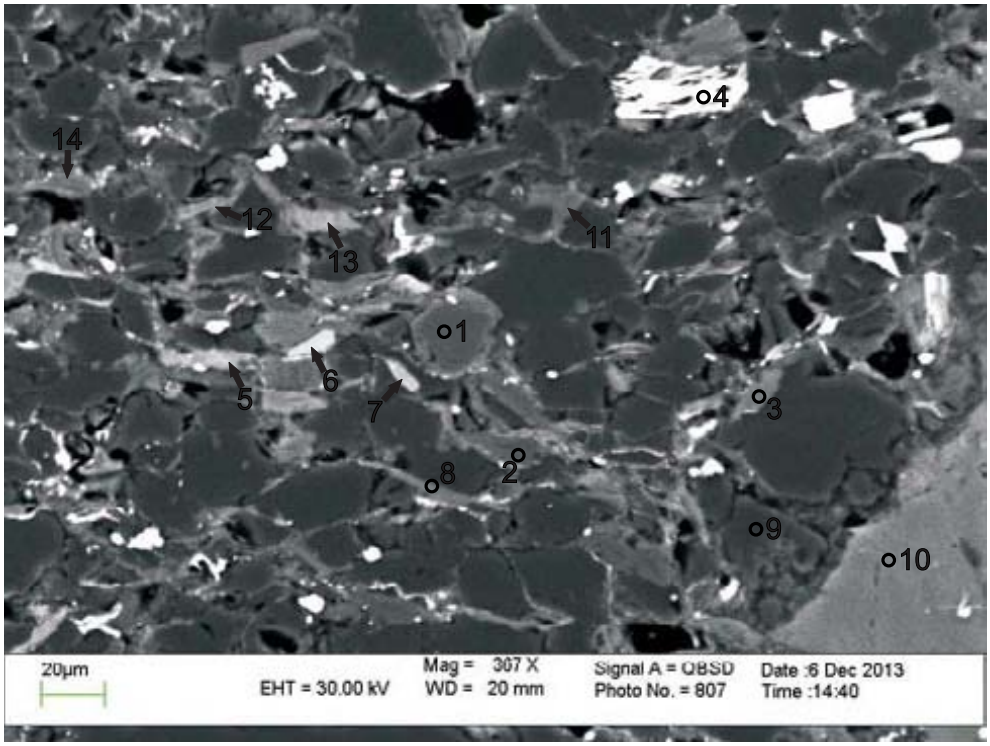

1: Mix
2: Muscovite
3: Muscovite + Chlorite
4: Altered Ilmenite + Muscovite
5: Chlorite
6: Illite
7: Illite
8: Muscovite
9: Quartz
10: K-feldspar
11: Muscovite + Chlorite
12: Muscovite
13: Chlorite + other
14: Muscovite + Quartz

Figure 3: Mic Mac H-86: 4717.78 site 3. Detrital grains of quartz and K-feldspar enclosed by a matrix of partially plastically deformed chlorite, muscovite and illite.

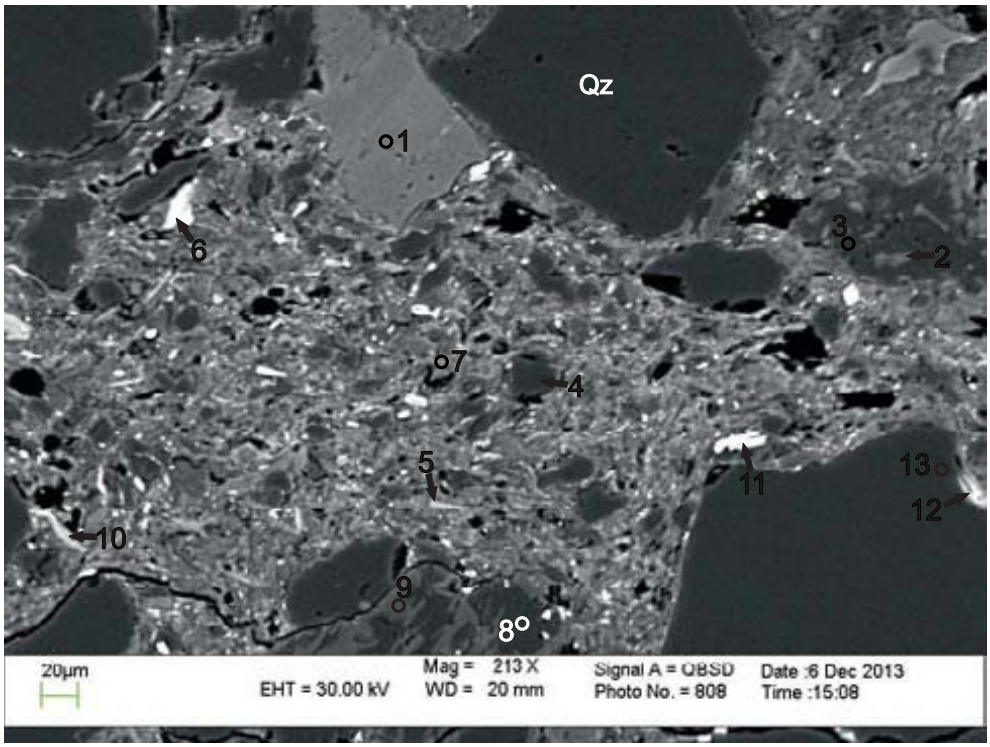

1: K-feldspar
2: Muscovite
3: Albite
4: Quartz
5: Illite
6: Apatite
7: Muscovite + Chlorite
8: Quartz
9: Muscovite
10: Illite
11: Altered Ilmenite + Muscovite
12: Biotite + Chlorite
13: Quartz

Figure 4: Mic Mac H-86: 4717.78 site 4. Muscovite, chlorite and illite rich muddy matrix. Some framework minerals, such as K-feldspar (analysis 1) and quartz contain dissolution voids.

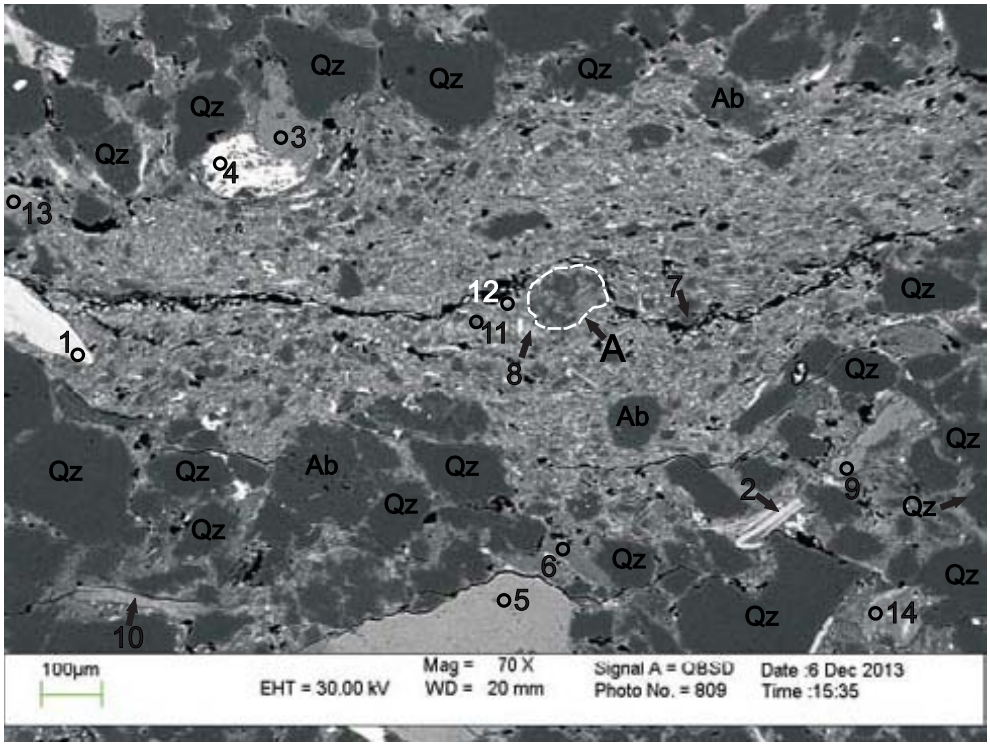

1: Biotite
2: Biotite
3: K-feldspar
4: Iron oxide + Muscovite
5: K-feldspar
6: Muscovite
7: Quartz
8: Illite
9: K-feldspar
10: Chlorite + Muscovite
11: Muscovite + Chlorite
12: Illite
13: Chlorite
14: Muscovite + Chlorite

Figure 5: Mic Mac H-86: 4717.78 site 5. Quartz and muscovite-rich lithic clast (position A) within muddy matrix (see App. 4A, Fig 2)(see Fig. 8 and Table 2A for electron microprobe analyses of this site).

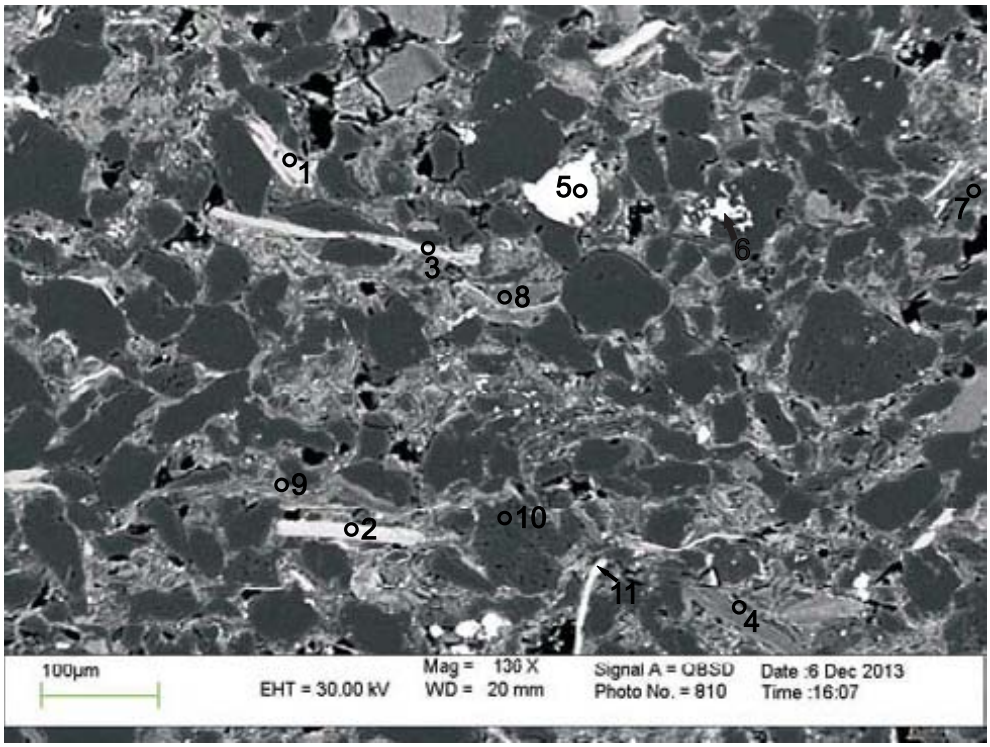

1: Biotite
2: Biotite
3: Biotite
4: Muscovite
5: Iron oxide
6: Rutile
7: Muscovite
8: Muscovite + Chlorite
9: Muscovite + Chlorite
10: Albite
11: Biotite

Figure 6: Mic Mac H-86: 4717.78 site 6. Dissolution voids in detrital albite (analysis 10). Biotite (analyses 1 and 3) within intergranular boundary between framework grains.

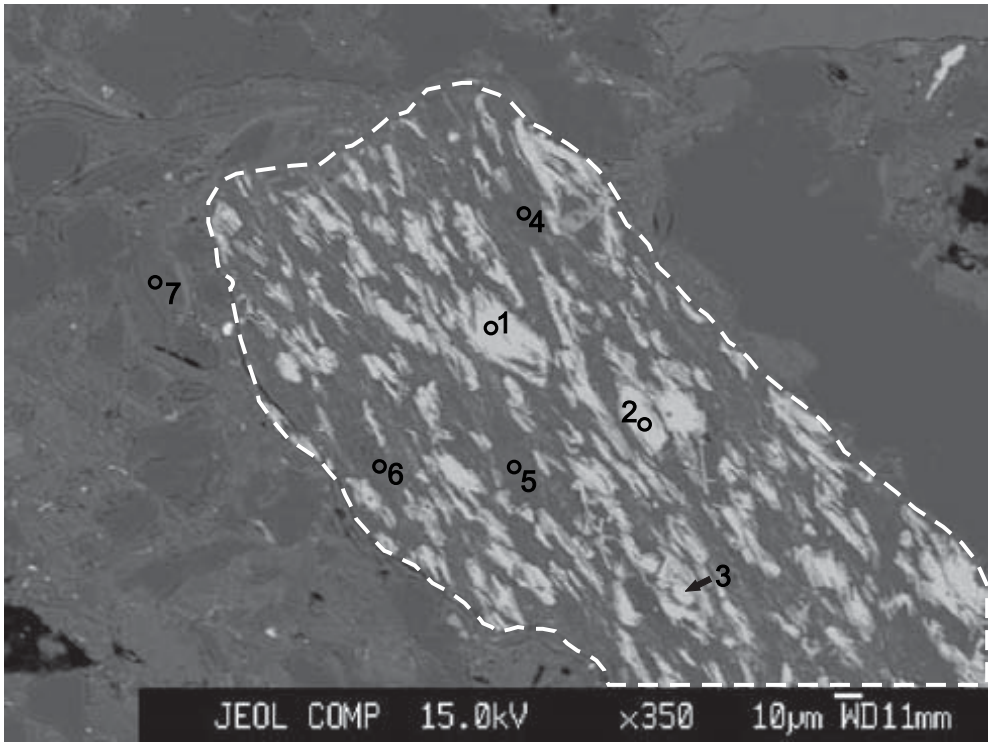

1: Hematite + other
2: Hematite + other
3: Iron oxide + other
4: Muscovite + Chlorite
5: Muscovite
6: Muscovite + Chlorite
7: Muscovite

Figure 7: Electron microprobe analysis for Mic Mac H-86 4717.78 site 7 (from Fig. 2). Lithic clast made up of mainly muscovite and hematite.

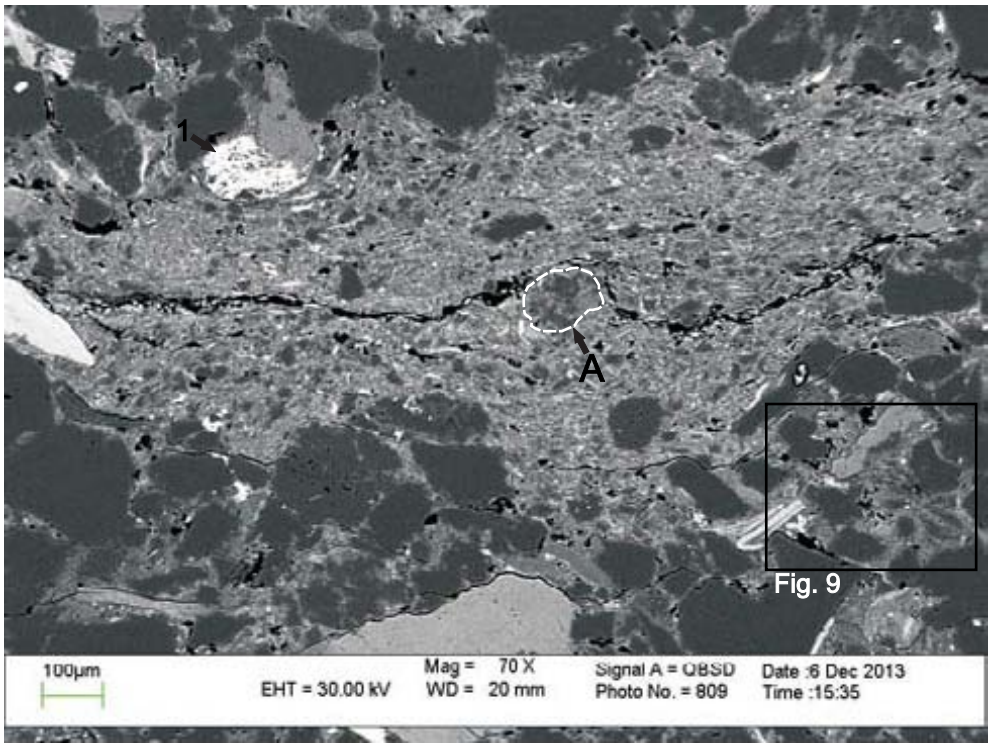

1: Muscovite + Iron oxide

Figure 8: Electron microprobe analysis for Mic Mac H-86 4717.78 site 8 (from Fig. 5). Quartz and muscovite-rich lithic clast (position A, and see App. 4A, Fig. 2)(See Fig. 9 and Table 2A for electron microprobe analyses of matrix).

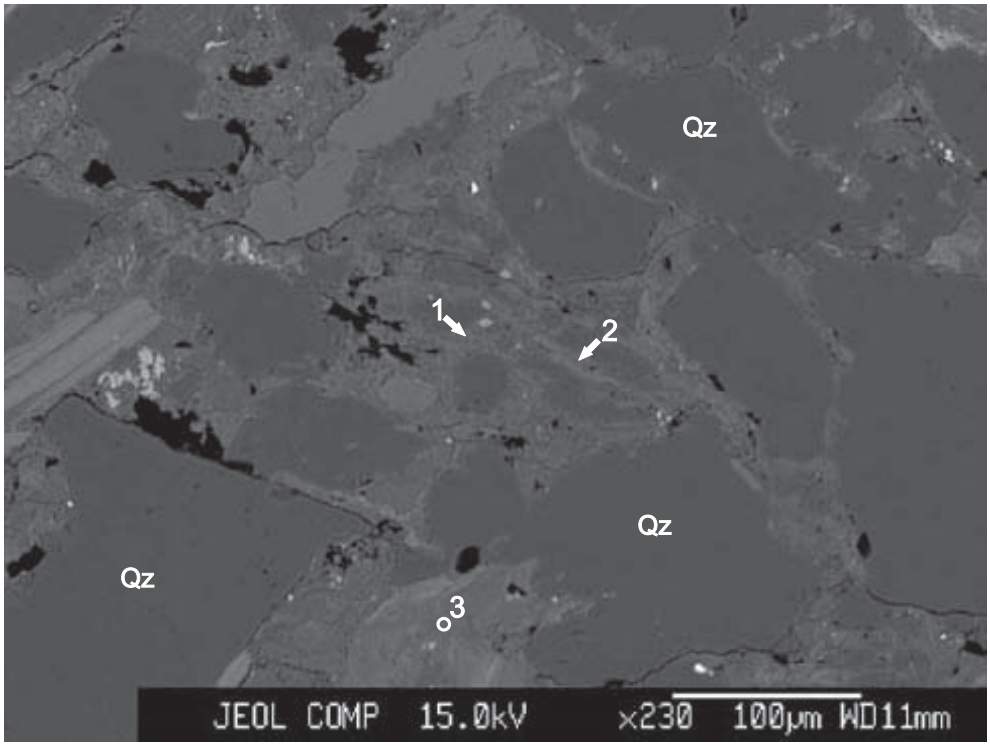

1: Muscovite + Chlorite
2: Muscovite
3: Muscovite + Chlorite

Figure 9: Electron microprobe analysis for Mic Mac H-86 4717.78 site 9 (from Fig. 8). Muscovite and chlorite fibers partially plastically deformed enclosing detrital grains, which are mostly quartz.

Table 1A: Scanning electron microscope chemical analyses of minerals from representative sites for Mic Mac H-86 well at 4717.78m depth

Sample	Site	Position	Mineral	SiO_2	TiO_2	Al_2O_3	FeO	MnO	MgO	CaO	Na_2O	K_2O	P_2O_5	SO_3	F	Cl	SrO	BaO	Total	Actual Total
H-86-4717.78	1	1	Biotite	42.91	2.27	17.10	17.14	0.25	12.20			7.94				0.18			100.00	101.50
H-86-4717.78	1	2	Ilmenite	1.80	60.58	1.06	35.97	0.37								0.22			100.00	93.67
H-86-4717.78	1	3	Chlorite + Muscovite	36.47	1.12	19.05	31.16	0.40	7.49		0.38	3.93							100.00	104.79
H-86-4717.78	1	4	Illite	45.32	0.74	24.03	10.42		1.75		0.50	7.25							90.00	100.49
H-86-4717.78	1	5	Illite	42.20	1.49	18.71	13.54		6.44		0.32	7.21				0.11			90.00	112.37
H-86-4717.78	1	6	Illite	42.08	1.65	16.80	14.52	0.21	6.53		0.31	7.93							90.00	107.20
H-86-4717.78	1	7	Illite	45.63	1.04	19.06	11.96	0.13	5.19		0.38	6.53				0.12			90.00	108.84
H-86-4717.78	1	8	Muscovite	48.58		29.00	3.84		1.68			9.90							93.00	110.81
H-86-4717.78	1	9	Illite	43.45	0.97	23.65	12.08	0.20	2.06		0.40	7.20							90.00	102.36
H-86-4717.78	1	10	Quartz	90.92	0.18	3.61	3.28		0.28			1.71							100.00	126.71
H-86-4717.78	1	11	Quartz	99.99															100.00	120.20
H-86-4717.78	1	12	Illite	48.25	0.29	23.78	6.58	0.14	4.26			6.72							90.00	101.67
H-86-4717.78	1	13	Illite	38.57	1.76	20.36	13.75	0.13	8.60		0.35	6.38				0.11			90.00	106.11
H-86-4717.78	1	14	Albite	67.56		19.88	0.44			0.11	11.18	0.83							100.00	120.96
H-86-4717.78	1	15	Iron oxide + Illite	19.70	17.80	8.96	48.23	0.25	2.80	0.21		2.05							100.00	107.95
H-86-4717.78	1	16	Illite	46.90	0.34	23.69	9.42		2.34		0.31	6.82				0.18			90.00	114.51
H-86-4717.78	1	17	Quartz	88.54	0.30	5.71	2.66		0.55			2.23							100.00	123.37
H-86-4717.78	1	18	Muscovite	47.69	0.25	33.67	1.13		0.63		0.80	8.84							93.00	112.41
H-86-4717.78	1	19	Biotite	44.65	1.08	22.49	16.69	0.21	8.11		0.40	6.38							100.00	102.45
H-86-4717.78	1	20	Muscovite + Chlorite	48.75	1.07	33.37	4.63		2.84		0.51	8.83							100.00	110.78
H-86-4717.78	1	21	Illite	45.34	0.45	24.15	9.77		2.21		0.38	7.57				0.14			90.00	103.31
H-86-4717.78	2	1	K-feldspar	65.93		18.08					0.58	15.41							100.00	120.02
H-86-4717.78	2	2	Albite	67.77		19.59	0.13			0.85	11.65								100.00	119.19
H-86-4717.78	2	3	Hematite + other	4.34	0.87	2.44	90.53	1.28				0.54							100.00	86.47
H-86-4717.78	2	4	Muscovite + Hematite	48.17	0.70	32.33	8.99	0.14	1.08		0.78	7.78							100.00	117.48
H-86-4717.78	2	5	Muscovite	46.56	0.44	32.38	2.63		1.19		0.54	9.27							93.00	110.80
H-86-4717.78	2	6	Quartz	94.15		3.16	1.09		0.70			0.90							100.00	117.52
H-86-4717.78	2	7	Biotite	41.74	2.27	20.24	17.37	0.21	10.23		0.31	7.49				0.16			100.00	102.68
H-86-4717.78	2	8	Iron oxide + other	3.98	5.24	1.78	88.75	0.25											100.00	84.76
H-86-4717.78	2	9	Altered Ilmenite + Muscovite	36.39	38.12	11.94	9.13		0.61			3.82							100.00	97.18
H-86-4717.78	2	10	Muscovite + Chlorite	54.27	0.23	30.52	3.19		1.69			10.11							100.00	106.47
H-86-4717.78	2	11	Barite (drilling mud) + Muscovite	26.40		8.82	0.90		0.80		0.47	1.65		22.37			0.97	37.62	100.00	116.55
H-86-4717.78	2	12	Illite	37.94	0.18	23.91	13.10		11.57			3.32							90.00	104.61
H-86-4717.78	2	13	Muscovite	49.26		32.75	1.05		0.70		0.80	8.44							93.00	109.12
H-86-4717.78	2	14	Illite	41.53	0.18	25.03	9.71	0.16	8.37			5.02							90.00	100.23
H-86-4717.78	2	15	Chlorite + other	40.79	0.25	24.90	16.02	0.41	16.12		0.28	1.10				0.13			100.00	93.00
H-86-4717.78	2	16	Quartz	90.68		4.61	2.30		1.09			1.30							100.00	115.85
H-86-4717.78	3	1	Mix	45.54	0.25	37.94	9.30		5.14		1.83								100.00	100.86
H-86-4717.78	3	2	Muscovite	48.64	0.21	32.91	1.33		0.33		1.03	8.53							93.00	112.45
H-86-4717.78	3	3	Muscovite + Chlorite	53.03	0.40	30.16	4.31		1.39		0.39	10.31							100.00	112.49
H-86-4717.78	3	4	Altered Ilmenite + Muscovite	39.49	0.85	13.72	41.60	0.67			0.63	3.02							100.00	113.13
H-86-4717.78	3	5	Chlorite	32.53		20.96	19.24	0.37	10.41	0.14		1.33							85.00	100.25

Table 1A: Scanning electron microscope chemical analyses of minerals from representative sites for Mic Mac H-86 well at 4717.78m depth

Sample	Site	Position	Mineral	SiO_2	TiO_2	Al_2O_3	FeO	MnO	MgO	CaO	Na_2O	K_2O	P_2O_5	SO_3	F	Cl	SrO	BaO	Total	Actual Total
H-86-4717.78	3	6	Illite	40.90	2.06	18.96	12.93	0.15	6.62		0.40	7.97							90.00	106.04
H-86-4717.78	3	7	Illite	44.42		17.48	16.29	0.24	10.59			0.97							90.00	110.59
H-86-4717.78	3	8	Muscovite	53.00	0.62	26.37	2.59		1.19		0.30	8.92							93.00	115.38
H-86-4717.78	3	9	Quartz	99.09		0.51	0.15					0.23							100.00	122.10
H-86-4717.78	3	10	K-feldspar	66.08		17.97					0.75	15.19							100.00	119.37
H-86-4717.78	3	11	Muscovite + Chlorite	55.81	0.30	29.42	3.42		1.56		0.26	9.23							100.00	113.17
H-86-4717.78	3	12	Muscovite	52.06	0.23	25.74	4.20		1.59		0.32	8.84							93.00	112.44
H-86-4717.78	3	13	Chlorite + other	43.23		22.60	19.75		13.00			1.42							100.00	100.50
H-86-4717.78	3	14	Muscovite + Quartz	54.72	0.22	31.67	2.68		1.46		0.38	8.87							100.00	114.35
H-86-4717.78	4	1	K-feldspar	66.12		18.08					0.67	15.12							100.00	116.12
H-86-4717.78	4	2	Muscovite	52.74		26.75	2.21		1.62		1.52	8.17							93.00	116.61
H-86-4717.78	4	3	Albite	68.18		19.35	0.17			0.27	11.76	0.28							100.00	123.01
H-86-4717.78	4	4	Quartz	99.77			0.23												100.00	120.00
H-86-4717.78	4	5	Illite	41.90	0.77	21.97	11.21	0.14	6.37		0.50	7.04				0.13			90.00	107.49
H-86-4717.78	4	6	Apatite	0.75		0.68	0.24			47.63		0.23	43.56		6.93				100.00	116.34
H-86-4717.78	4	7	Muscovite + Chlorite	52.07	0.38	31.44	4.99		2.44		0.40	8.25							100.00	114.95
H-86-4717.78	4	8	Quartz	99.47		0.40						0.12							100.00	118.72
H-86-4717.78	4	9	Muscovite	48.08	0.16	33.94	0.56		0.49		1.37	8.39							93.00	109.25
H-86-4717.78	4	10	Illite	41.86	1.51	21.89	9.46		6.42		0.28	8.58							90.00	99.20
H-86-4717.78	4	11	Altered Ilmenite + Muscovite	17.54	67.44	10.96	1.35				0.78	1.95							100.00	114.05
H-86-4717.78	4	12	Biotite + Chlorite	36.52	1.12	19.78	26.45	0.36	12.39			3.40							100.00	103.46
H-86-4717.78	4	13	Quartz	99.99															100.00	122.88
H-86-4717.78	5	1	Biotite	42.68	2.67	18.22	17.42	0.25	9.70			9.06							100.00	96.17
H-86-4717.78	5	2	Biotite	42.23	2.62	19.69	14.81	0.30	12.17		0.31	7.87							100.00	117.04
H-86-4717.78	5	3	K-feldspar	65.35		18.76	0.35				0.38	15.15							100.00	114.66
H-86-4717.78	5	4	Iron oxide + Muscovite	20.94	1.43	11.98	61.76	0.87		0.34	1.75	0.92							100.00	101.91
H-86-4717.78	5	5	K-feldspar	65.18		18.22					0.77	14.65						1.18	100.00	119.84
H-86-4717.78	5	6	Muscovite	46.96	0.65	33.15	1.17		0.66		0.90	9.52							93.00	114.50
H-86-4717.78	5	7	Quartz	99.86			0.13												100.00	128.61
H-86-4717.78	5	8	Illite	49.35	0.60	21.41	7.03		5.04		0.29	6.27							90.00	121.09
H-86-4717.78	5	9	K-feldspar	65.99		17.89	0.12				0.50	15.50							100.00	126.82
H-86-4717.78	5	10	Chlorite + Muscovite	40.69	0.20	22.13	16.58	0.25	18.29			1.88							100.00	96.03
H-86-4717.78	5	11	Muscovite + Chlorite	54.59	0.25	29.02	3.32		3.03		0.31	9.47							100.00	108.62
H-86-4717.78	5	12	Illite	49.84	0.30	24.08	6.44		2.04		0.27	7.01							90.00	107.64
H-86-4717.78	5	13	Chlorite	32.64		19.93	15.50	0.31	16.04			0.59							85.00	88.90
H-86-4717.78	5	14	Muscovite + Chlorite	46.27	0.42	29.67	11.64		3.68		0.35	7.99							100.00	122.72
H-86-4717.78	6	1	Biotite	44.39	1.87	23.13	13.19	0.19	7.96			9.27							100.00	103.14
H-86-4717.78	6	2	Biotite	43.23	2.95	19.24	14.63	0.22	10.51		0.32	8.89							100.00	107.15
H-86-4717.78	6	3	Biotite	47.40	2.55	19.41	14.76	0.23	7.96			7.67							100.00	110.23
H-86-4717.78	6	4	Muscovite	47.25	0.65	32.22	2.10		0.73		1.09	8.94							93.00	110.06
H-86-4717.78	6	5	Iron oxide	2.08	2.04	0.96	94.05	0.88											100.00	90.77
H-86-4717.78	6	6	Rutile	1.84	94.25	0.93	3.00												100.00	108.46

Table 1A: Scanning electron microscope chemical analyses of minerals from representative sites for Mic Mac H-86 well at 4717.78m depth

Sample	Site	Position	Mineral	SiO_2	TiO_2	Al_2O_3	FeO	MnO	MgO	CaO	Na_2O	K_2O	P_2O_5	SO_3	F	Cl	SrO	BaO	Total	Actual Total
H-86-4717.78	6	7	Muscovite	54.37	0.16	28.96	0.72		0.59		0.97	7.26							93.00	120.31
H-86-4717.78	6	8	Muscovite + Chlorite	50.51	0.50	34.22	3.45		1.38		0.53	9.43							100.00	114.98
H-86-4717.78	6	9	Muscovite + Chlorite	52.56	0.32	29.38	5.20		2.19		0.39	9.96							100.00	111.51
H-86-4717.78	6	10	Albite	68.60		19.03	0.14			0.25	11.85	0.13							100.00	122.28
H-86-4717.78	6	11	Biotite	37.26	2.67	16.95	27.72	0.54	7.40		0.50	6.96							100.00	113.50

Table 2A: Electron microprobe chemical analyses of iron oxides and micas from representative sites for Mic Mac H-86 well at 4717.78m depth

Sample	Figure	Position	Mineral	No.	SiO_2	TiO_2	Al_2O_3	FeO	MnO	MgO	CaO	Na_2O	K_2O	Cr_2O_3	V_2O_3	Total
4717.78	7	1	Hematite + other	13	1.67	0.57	0.72	83.85	1.04	0.07	0.16	-	-	0.01	0.14	88.23
4717.78	7	2	Hematite + other	14	1.47	0.72	0.72	83.81	1.34	0.08	0.17	-	-	0.01	0.15	88.47
4717.78	7	3	Iron oxide + other	15	8.14	0.53	5.44	74.31	1.18	0.25	0.16	-	-	0.03	0.08	90.11
4717.78	7	4	Muscovite + Chlorite	19	48.04	0.66	31.02	5.95	0.08	1.10	0.10	0.54	8.22	0.00	-	95.71
4717.78	7	5	Muscovite	20	46.34	0.25	33.87	2.15	0.01	0.96	0.00	0.86	8.73	0.00	-	93.18
4717.78	7	6	Muscovite + Chlorite	21	44.04	0.20	31.49	7.46	0.10	0.86	0.09	0.57	8.28	0.00	-	93.09
4717.78	7	7	Muscovite	22	48.13	0.00	33.94	1.44	0.00	0.92	0.02	0.33	8.20	0.00	-	92.99
4717.78	8	1	Muscovite + Iron oxide	16	48.43	0.89	11.72	35.53	0.52	0.58	0.12	-	-	0.01	0.05	97.84
4717.78	9	1	Muscovite + Chlorite	23	47.57	0.13	27.55	7.92	0.07	2.42	0.25	0.26	7.83	0.00	-	94.01
4717.78	9	2	Muscovite	24	46.56	0.34	32.13	2.55	0.01	1.28	0.05	0.40	9.73	0.00	-	93.04
4717.78	9	3	Muscovite + Chlorite	25	45.34	3.47	25.91	6.59	0.10	1.87	0.20	0.28	7.81	0.00	-	91.56

* In this and all subsequent similar Tables, Fe-oxides minerals and micas were analyzed using different standards so if silicate minerals were analyzed together with Fe-oxide minerals do not include Na_2O and K_2O determinations.

Appendix 1B: Scanning Electron Microscope Backscattered Electron Images for Mic Mac H-86 well with EDS Mineral Analyses Sample 4718.97

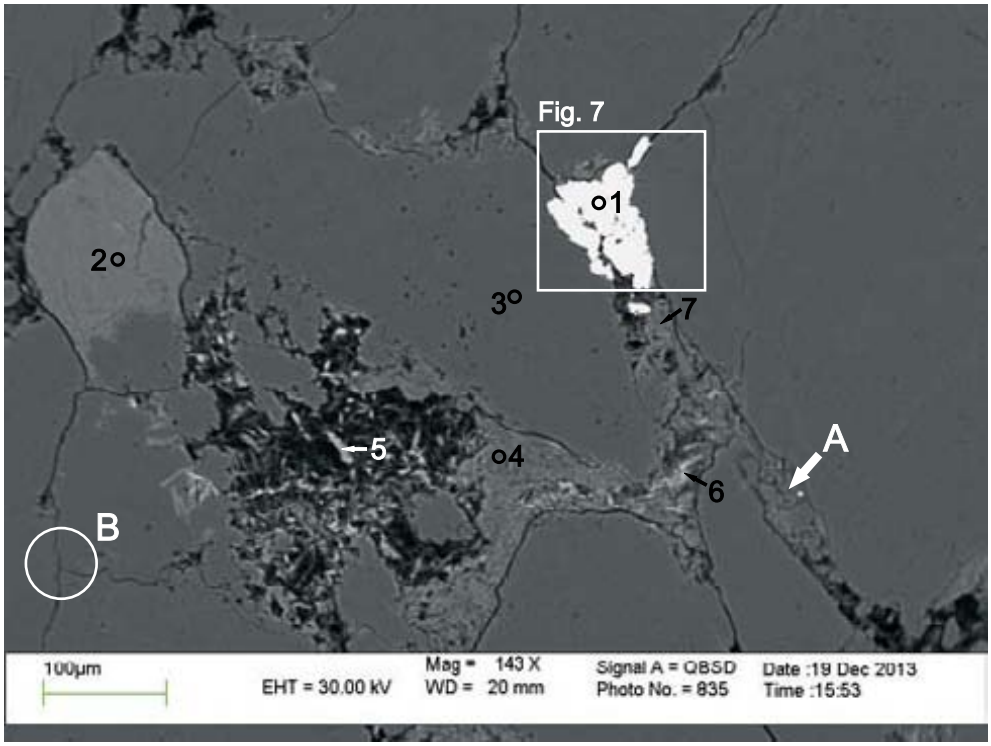

1: Hematite + other
2: Muscovite
3: Quartz
4: Muscovite
5: Muscovite + Chlorite
6: Chlorite
7: Muscovite

Figure 1: Mic Mac H-86: 4718.97 site 1. Compacted sandstone with pseudomatrix (position A, and see App. 4A, Fig. 4). Several areas of dissolution create secondary porosity where mica (analysis 5) might have precipitated. The precursor of some of this porosity may be detrital muscovite (analysis 4). Apparent triple point in quartz overgrowths (position B, see App. 4A, Fig. 3) occured during diagenesis. Diagenetic hematite (analysis 1) fills fractures (see Fig. 7 and Table 2B for electron microprobe analyses).

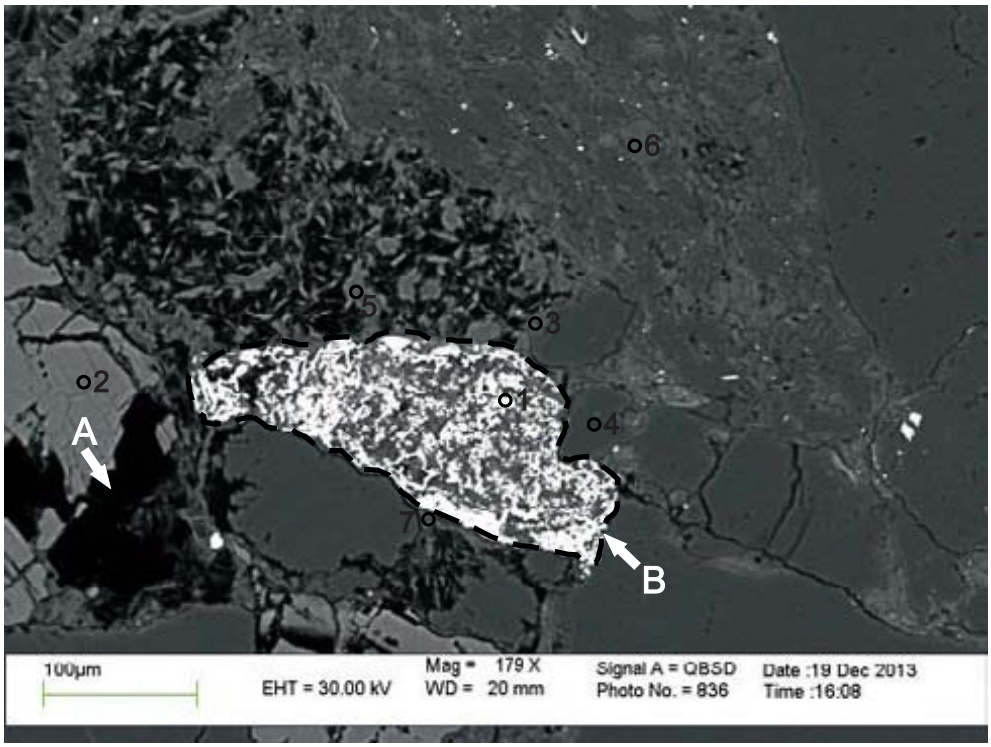

1: Iron oxide + other
2: K-feldspar
3: Muscovite
4: Quartz
5-7: Muscovite

Figure 2: Mic Mac H-86: 4718.97 site 2. Secondary porosity within K-feldspar (position A, and see App. 4A, Fig. 5). Some porosity is partly filled in or lined with muscovite (analysis 5). Lithic clast (position B) that has partially plastically deformed around framework grains, is composed of an iron oxide (see Fig. 8 and Table 2B for microprobe analyses).

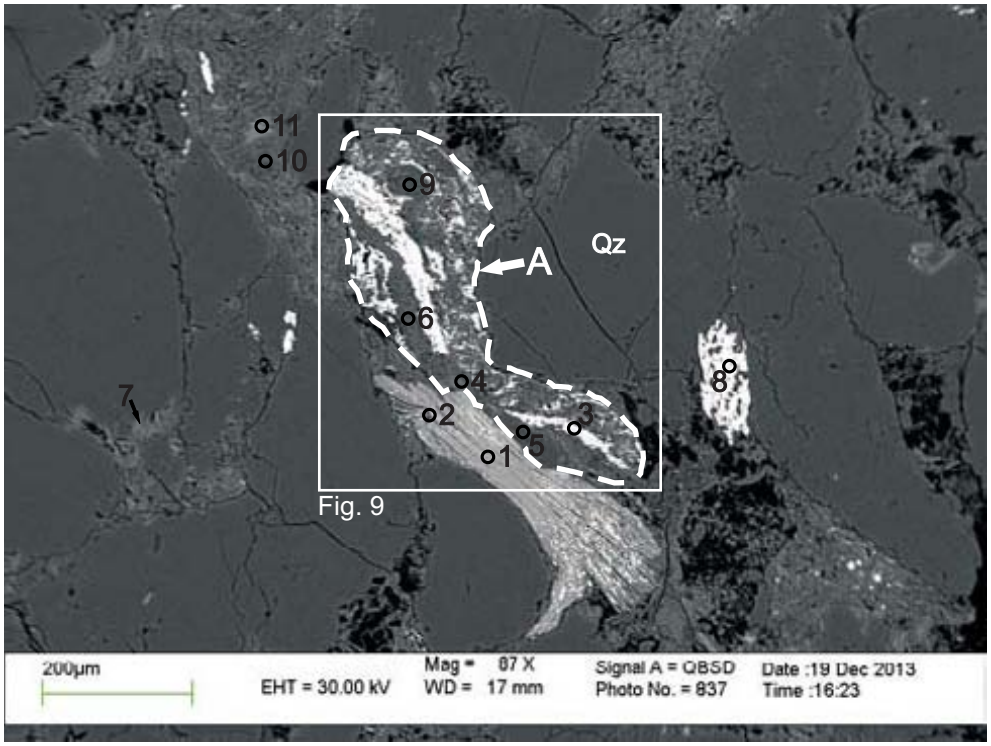

1: Biotite
2: Biotite + other
3: Iron oxide + other
4: Muscovite
5: Quartz
6: Muscovite + Chlorite
7: Muscovite + Chlorite
8: Altered Ilmenite
9: Quartz
10: Illite
11: Chlorite

Figure 3: Mic Mac H-86: 4718.97 site 3. Plastically deformed clast (position A, and see App. 4A, Fig. 6) that has plastically deformed around quartz grains, and contains an iron oxide (see Fig. 9 and Table 2B for electron microprobe analyses).

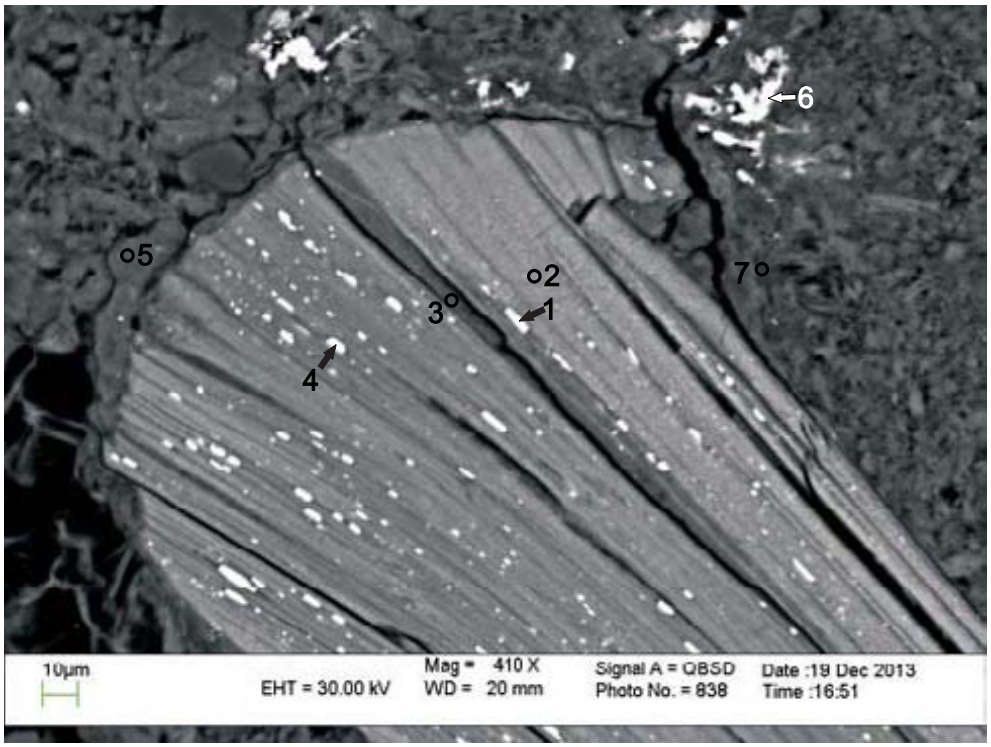

1: Biotite + Iron oxide
2: Biotite
3: Illite + Chlorite
4: Biotite + Iron oxide
5: K-feldspar
6: Altered Ilmenite
7: Illite

Figure 4: Mic Mac H-86: 4718.97 site 4. Plastically deformed (see App. 4A, Fig. 7) detrital biotite with iron oxide exsolution along cleavage planes (see App 4A, Fig.8 and see Fig. 10 and Table 2B for electron microprobe analyses).

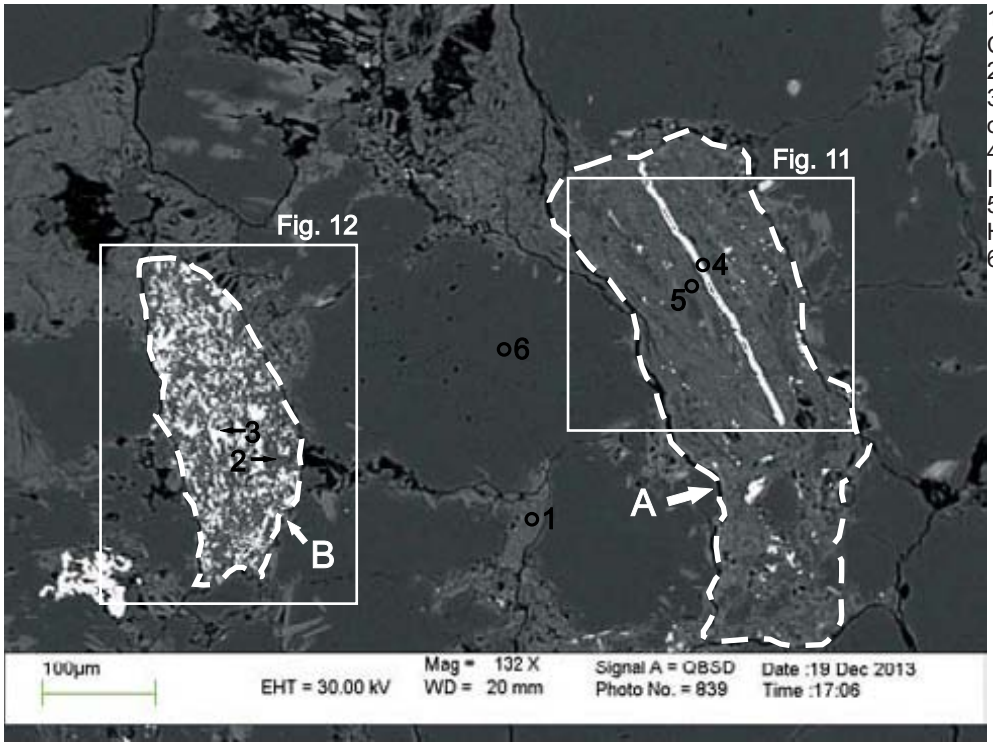

1: Muscovite + Chlorite
2: K-feldspar
3: Iron oxide + other
4: Muscovite + Iron oxide
5: Illite or Hydromuscovite
6: Quartz

Figure 5: Mic Mac H-86: 4718.97m site 5. Plastically deformed lithic clast (position A, and see App. 4A, Fig. 9) composed of illite/hydromuscovite (analysis 5) and fracture filled iron oxide (analysis 4). Lithic clast (position B) composed of K-feldspar, muscovite, illite, and iron oxide. (See Figs. 11 and 12, and Table 2B for electron microprobe analyses of lithic clasts at positions A and B).

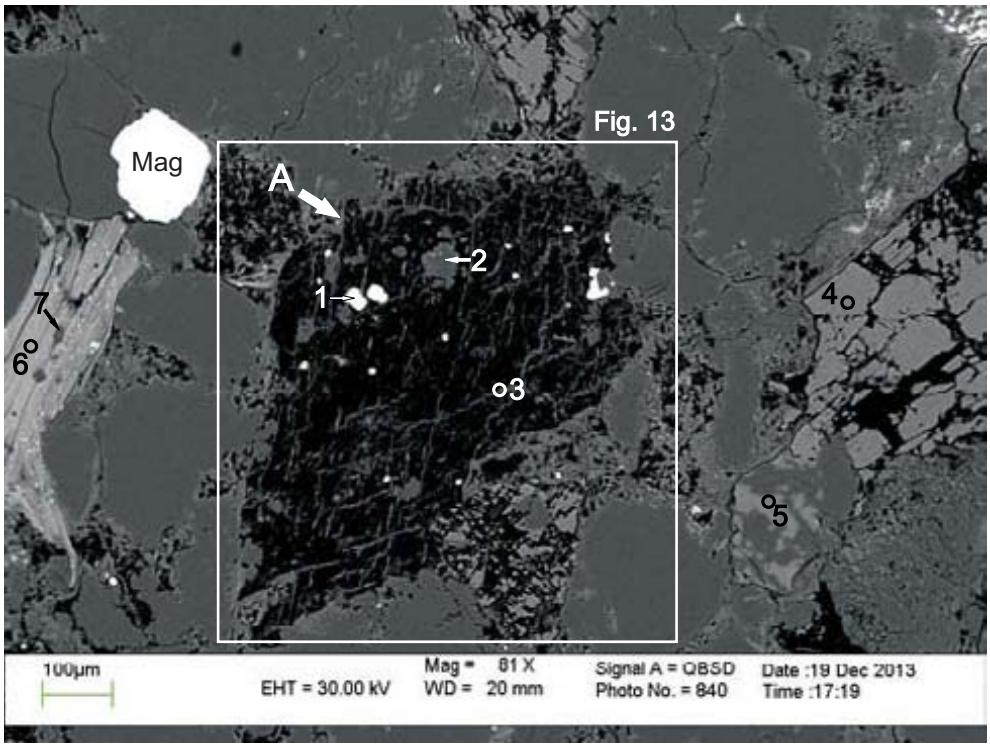

1: Barite (drilling mud)
2: Quartz
3: Muscovite
4: K-feldspar
5: K-feldspar
6: Biotite
7: Quartz

Figure 6: Mic Mac H-86: 4718.97 site 6. Highly dissolved mineral crystal (position A), with fine grain mineral precipitaion along its cleavage planes (see Fig. 13 and Table 2B for electron microprobe analyses). Biotite (analysis 6) is plastically deformed within intergranular boundaries of framework grains. K-feldspar has been partly dissolved (analysis 4). Magnetite (Mag) analysis determined using electron microprobe (see Table 2B).

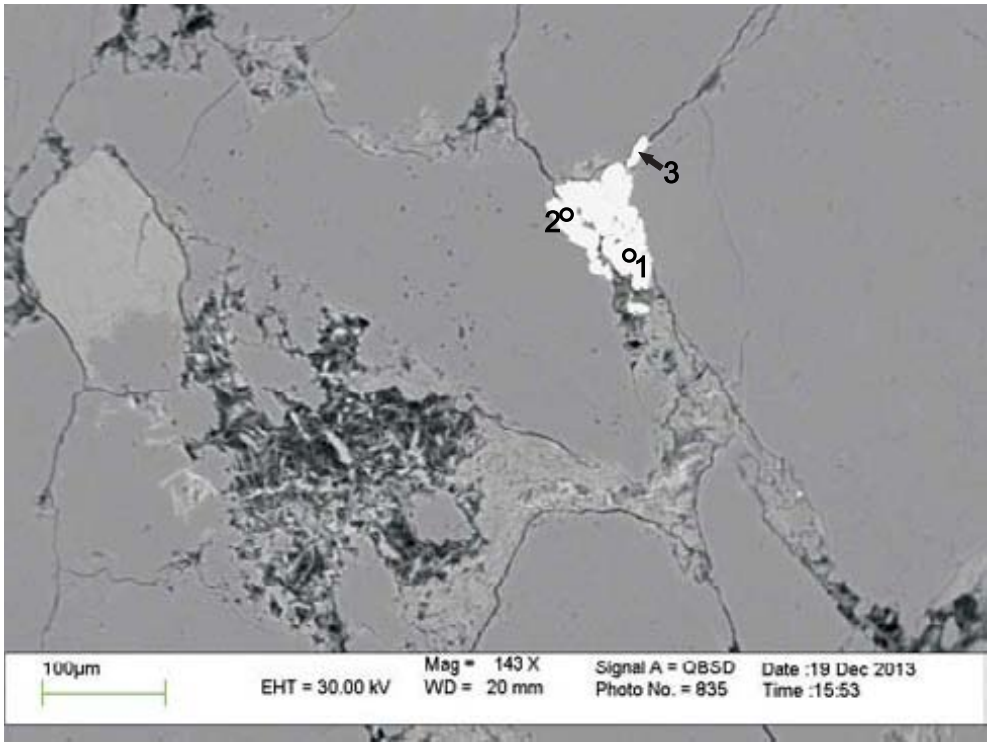

1: Hematite
2: Hematite + other
3: Hematite + other

Figure 7: Electron microprobe analysis for Mic Mac H-86 4718.97 site 7 (from Fig. 1). Diagenetic hematite and goethite form in intergranular boundaries.

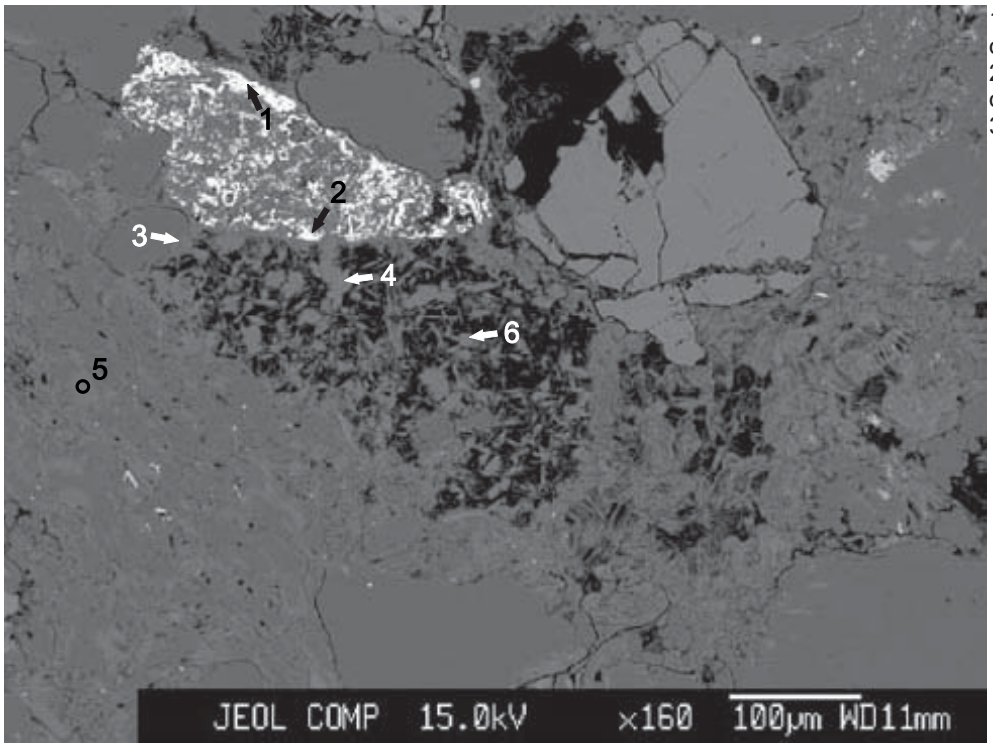

1: Iron oxide + other
2: Iron oxide + other
3-6: Mix - voids

Figure 8: Electron microprobe analyses for Mic Mac H-86 4718.97 site 8 (from Fig. 2). Low data totals (see Table 2B) for muscovite (as determined on scanning electron microscope, see Fig. 2 and Table 1B) because area has many dissolution voids.

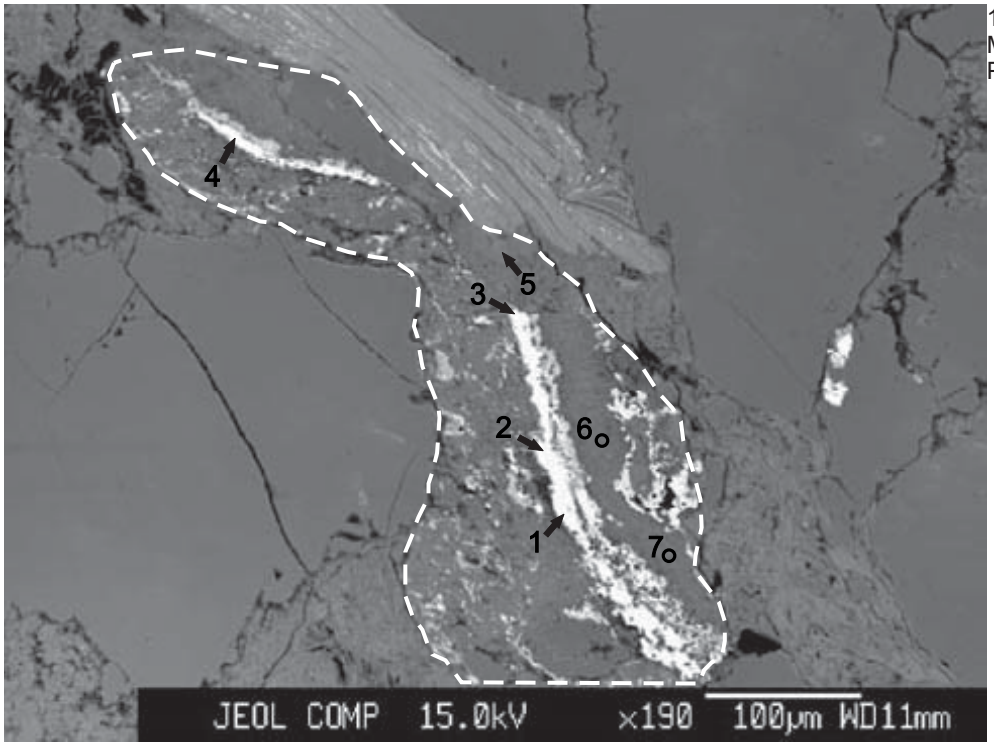

1-7:
Microcrystalline
Patches

Figure 9: Electron microprobe analyses for Mic Mac H-86 4718.97 site 9 (from Fig. 3). Lithic clasts containing microcrystalline grains of muscovite, quartz, and chlorite (from scanning electron microscope, Fig. 3 and Table 1B).

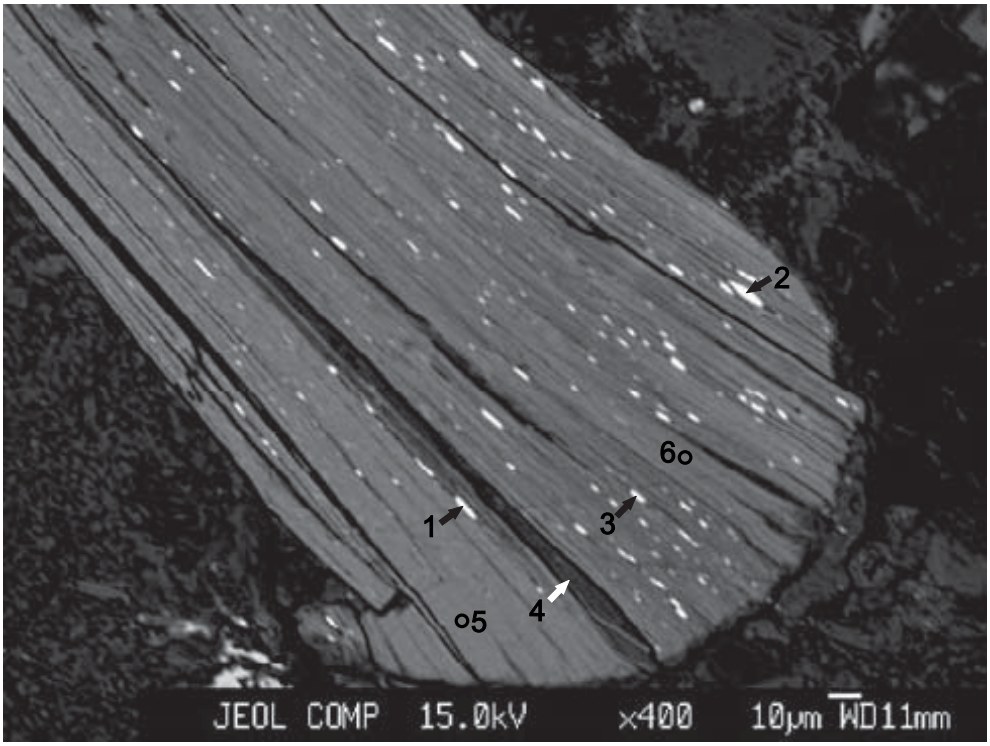

1-3: Iron oxide
+ other
4-6: Biotite

Figure 10: Electron microprobe image for Mic Mac H-86 4718.97 site 10 (from Fig. 4). Iron oxides forming in spaces along cleavage planes of detrital biotite.

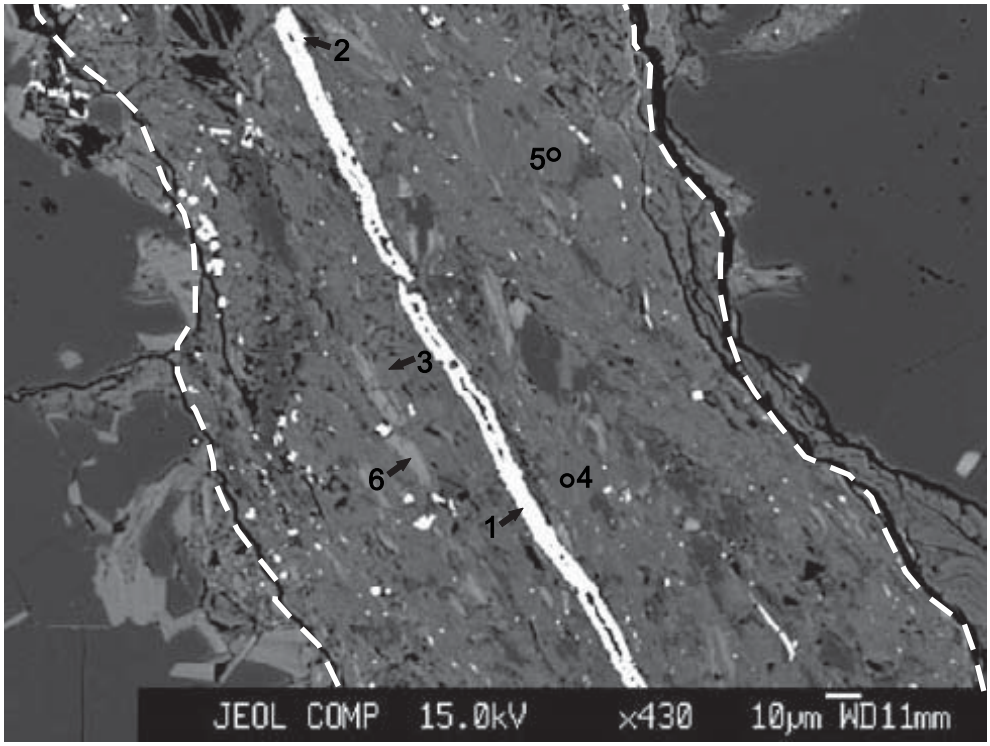

1: Iron oxide + other
2: Iron oxide + other
3-6: Illite or Hydromuscovite

Figure 11: Electron microprobe analyses for Mic Mac H-86 4718.97 site 11 (from Fig. 5). Lithic clast made up mostly of muscovite (see Fig. 5 and Table 1B), illite, hydromuscovite, and an iron oxide (see Table 2B for electron microprobe analyses).

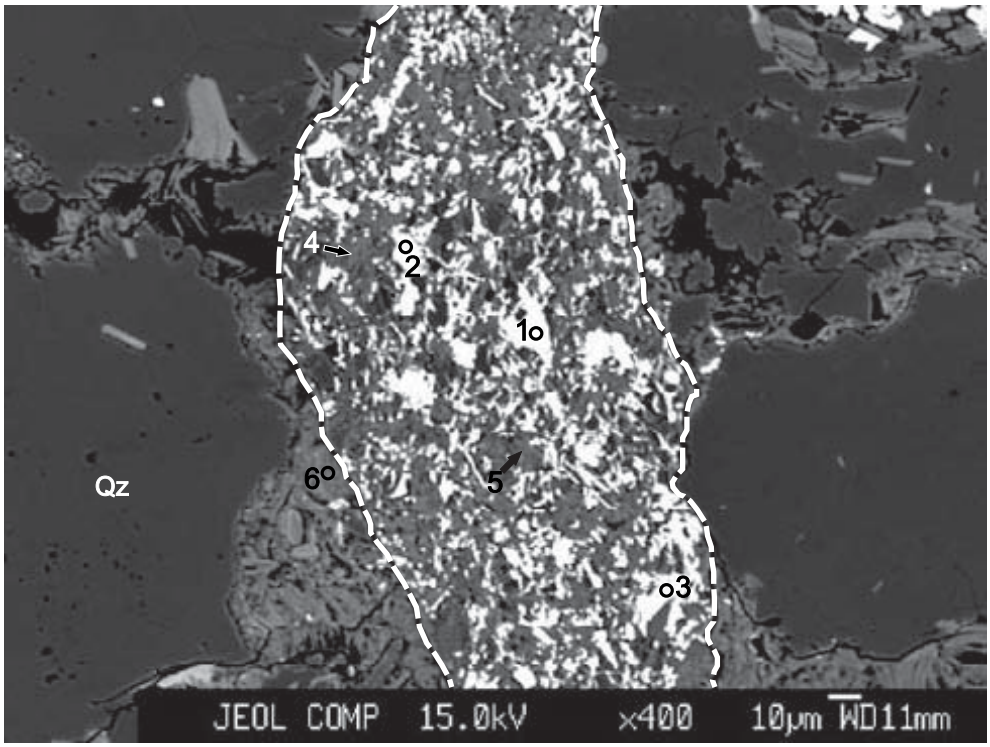

1-3: Iron oxide + other
4: K-feldspar
5: Illite
6: Muscovite or Hydromuscovite

Figure 12: Electron microprobe image for Mic Mac H-86 4718.97 site 12 (from Fig. 5). Lithic clast made up of K-feldspar, illite, and an iron oxide. Muscovite and hydromuscovite (analysis 6) found within intergranular boundary between clast and quartz grain.

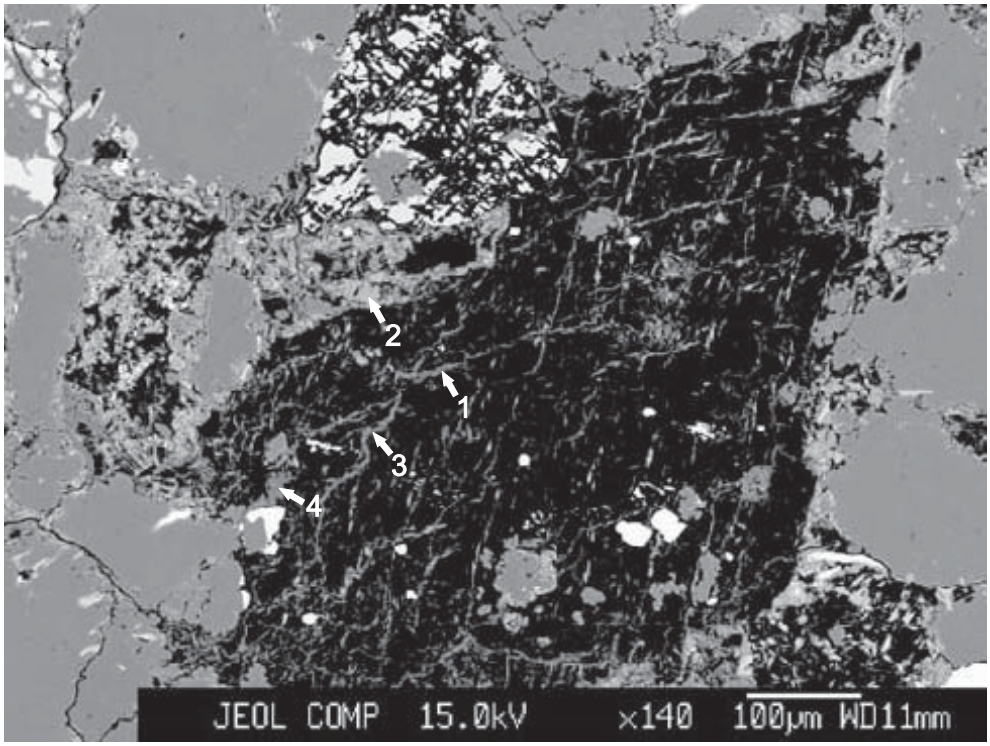

1: Void
2: Muscovite + Chlorite
3: Muscovite + Chlorite
4: Muscovite + Void

Figure 13: Electron microprobe analyses for Mic Mac H-86 4718.97 site 13 (from Fig. 6). Fine grained muscovite and chlorite forming along cleavage planes of dissolved mineral.

Table 1B: Scanning electron microscope chemical analyses of minerals from representative sites for Mic Mac H-86 well at 4718.97m depth

Sample	Site	Position	Mineral	SiO_2	TiO_2	Al_2O_3	FeO	MnO	MgO	CaO	Na_2O	K_2O	SO_3	Cl	SrO	BaO	Total	Actual Total
H-86-4718.97	1	1	Hematite + other	2.48	0.45	1.78	95.28										100.00	84.36
H-86-4718.97	1	2	Muscovite	47.11		34.06	0.92		0.57			10.33					93.00	94.73
H-86-4718.97	1	3	Quartz	99.99													100.00	108.86
H-86-4718.97	1	4	Muscovite	50.63		29.79	1.58		1.38		0.36	9.05		0.21			93.00	94.51
H-86-4718.97	1	5	Muscovite + Chlorite	51.32	0.18	29.17	8.83		1.77		0.36	8.14		0.22			100.00	89.32
H-86-4718.97	1	6	Chlorite	31.09		22.47	17.89	0.22	11.57	0.26		1.19		0.30			85.00	85.78
H-86-4718.97	1	7	Muscovite	50.33		30.03	1.84		1.13		0.33	9.21		0.11			93.00	95.71
H-86-4718.97	2	1	Iron oxide + other	8.77	1.70	4.35	82.66	0.58				1.95					100.00	71.91
H-86-4718.97	2	2	K-feldspar	65.82		17.99					0.77	15.41					100.00	96.61
H-86-4718.97	2	3	Muscovite	50.59		30.40	1.96		1.15		1.33	7.55					93.00	97.44
H-86-4718.97	2	4	Quartz	99.79			0.19										100.00	105.74
H-86-4718.97	2	5	Muscovite	50.00		30.17	1.71		1.57			9.53					93.00	91.88
H-86-4718.97	2	6	Muscovite	48.39	0.17	33.72	0.55		0.33		1.22	8.65					93.00	97.93
H-86-4718.97	2	7	Muscovite	50.07		29.17	2.85		1.39			9.26		0.27			93.00	85.55
H-86-4718.97	3	1	Biotite	41.03	3.75	18.23	17.47	0.28	9.53		0.27	9.25		0.18			100.00	170.49
H-86-4718.97	3	2	Biotite + other	48.07	0.98	26.87	12.00	0.14	3.05			8.60		0.28			100.00	174.53
H-86-4718.97	3	3	Iron oxide + other	5.18	1.42	2.21	89.32	1.86									100.00	145.84
H-86-4718.97	3	4	Muscovite	50.73	0.14	28.63	2.24		1.71			9.43		0.12			93.00	172.24
H-86-4718.97	3	5	Quartz	99.79			0.19										100.00	191.38
H-86-4718.97	3	6	Muscovite + Chlorite	55.70		28.85	3.63		2.22			9.15		0.42			100.00	171.72
H-86-4718.97	3	7	Muscovite + Chlorite	51.04	0.33	29.99	4.76		1.82		0.34	11.72					100.00	162.15
H-86-4718.97	3	8	Altered Ilmenite	5.09	73.78	1.00	19.35	0.36		0.27				0.16			100.00	170.05
H-86-4718.97	3	9	Quartz	99.84			0.17										100.00	192.99
H-86-4718.97	3	10	Illite	52.87		24.59	4.21	0.13	1.58		1.22	5.40					90.00	183.61
H-86-4718.97	3	11	Chlorite	31.99		23.04	17.52	0.65	10.68		0.27	0.86					85.00	157.74
H-86-4718.97	4	1	Biotite + Iron oxide	23.02	2.44	11.43	53.40	0.44	4.23			5.06					100.00	84.38
H-86-4718.97	4	2	Biotite	41.93	2.70	18.93	17.74	0.21	9.65			8.56		0.27			100.00	93.58
H-86-4718.97	4	3	Illite + Chlorite	52.90	0.43	28.80	5.24		2.79			9.62		0.21			100.00	88.13
H-86-4718.97	4	4	Biotite + Iron oxide	22.83	1.63	12.91	54.38		4.46			3.81					100.00	97.85
H-86-4718.97	4	5	K-feldspar	66.91		20.63	3.72		1.36			7.25		0.15			100.00	99.06
H-86-4718.97	4	6	Altered Ilmenite	7.92	84.22	4.33	1.60					1.77		0.17			100.00	88.46
H-86-4718.97	4	7	Illite	42.93	0.20	26.27	6.79	0.23	7.57			5.62		0.42			90.00	81.23
H-86-4718.97	5	1	Muscovite + Chlorite	52.86	0.18	28.76	6.78		2.29			8.99		0.15			100.00	94.85
H-86-4718.97	5	2	K-feldspar	65.69	0.27	22.88	3.41		0.91		0.78	6.05					100.00	96.44
H-86-4718.97	5	3	Iron oxide + other	4.88	0.75	2.06	90.90	1.42									100.00	74.6
H-86-4718.97	5	4	Muscovite + Iron oxide	57.27	0.53	13.26	20.53	0.30	0.76			7.36					100.00	72.78

Table 1B: Scanning electron microscope chemical analyses of minerals from representative sites for Mic Mac H-86 well at 4718.97m depth

Sample	Site	Position	Mineral	SiO_2	TiO_2	Al_2O_3	FeO	MnO	MgO	CaO	Na_2O	K_2O	SO_3	Cl	SrO	BaO	Total	Actual Total
H-86-4718.97	5	5	Illite/Hydromuscovite	45.50	2.59	30.69	7.85		7.76		0.43	5.17					100.00	100.63
H-86-4718.97	5	6	Quartz	99.99													100.00	106.6
H-86-4718.97	6	1	Barite (drilling mud)										38.78		1.75	59.48	100.00	98.45
H-86-4718.97	6	2	Quartz	89.89		7.44	0.57					2.10					100.00	107.05
H-86-4718.97	6	3	Muscovite	50.77		28.38	1.88		1.50	1.49		8.51		0.48			93.00	83.22
H-86-4718.97	6	4	K-feldspar	65.87		17.88					0.59	15.67					100.00	114.44
H-86-4718.97	6	5	K-feldspar	65.65		17.95					1.04	14.72				0.64	100.00	112.35
H-86-4718.97	6	6	Biotite	43.32	1.33	22.41	16.17		8.77			7.99					100.00	85.96
H-86-4718.97	6	7	Quartz	94.72		2.66	0.94			0.35	0.97	0.36					100.00	93.61

Table 2B: Electron microprobe chemical analyses of iron oxides and micas from representative sites for Mic Mac H-86 well at 4718.97m depth

Sample	Figure	Position	Mineral	No.	SiO_2	TiO_2	Al_2O_3	FeO	MnO	MgO	CaO	Na_2O	K_2O	Cr_2O_3	V_2O_3	Total
4718.97	6	Mag	Magnetite	38	0.02	0.01	0.01	90.24	0.00	0.00	0.02	-	-	0.02	0.09	90.42
4718.97	7	1	Hematite	17	0.23	0.07	0.10	88.85	0.02	0.00	0.02	-	-	0.02	0.15	89.46
4718.97	7	2	Hematite + other	18	0.35	3.41	0.16	86.16	0.19	0.00	0.02	-	-	0.03	0.05	90.37
4718.97	7	3	Hematite + other	19	4.74	0.00	0.25	84.72	0.02	0.00	0.11	-	-	0.05	0.11	90.00
4718.97	8	1	Iron oxide + other	20	10.24	1.32	7.39	67.18	1.11	0.11	0.11	-	-	0.00	0.03	87.49
4718.97	8	2	Iron oxide + other	21	2.00	1.62	1.03	81.70	1.19	0.05	0.08	-	-	0.01	0.02	87.69
4718.97	8	3	Mix - voids	26	23.30	0.00	13.92	1.06	0.00	0.79	0.37	0.10	4.80	0.00	-	44.33
4718.97	8	4	Mix - voids	27	25.05	0.00	14.65	1.16	0.00	0.84	0.41	0.11	5.01	0.00	-	47.22
4718.97	8	5	Mix - voids	28	25.62	0.00	14.91	1.18	0.00	0.83	0.41	0.10	5.14	0.00	-	48.19
4718.97	8	6	Mix - voids	29	26.66	0.00	15.39	1.20	0.00	0.89	0.35	0.12	5.34	0.00	-	49.95
4718.97	9	1	Microcrystalline patches	22	26.45	0.06	17.17	3.46	0.05	1.27	0.24	-	-	0.02	0.01	48.72
4718.97	9	2	Microcrystalline patches	23	24.11	0.18	20.71	8.96	0.03	1.48	0.32	-	-	0.00	0.02	55.80
4718.97	9	3	Microcrystalline patches	24	26.12	0.32	16.12	17.89	0.11	2.63	0.16	-	-	0.00	0.01	63.36
4718.97	9	4	Microcrystalline patches	25	31.29	0.07	18.63	3.21	0.02	1.30	0.16	-	-	0.01	0.04	54.73
4718.97	9	5	Microcrystalline patches	30	37.03	0.00	24.60	0.76	0.00	1.01	0.15	0.79	5.38	0.00	-	69.72
4718.97	9	6	Microcrystalline patches	31	36.51	0.00	25.64	0.77	0.00	0.92	0.16	0.65	4.67	0.00	-	69.32
4718.97	9	7	Microcrystalline patches	32	37.07	0.00	26.03	0.71	0.00	0.87	0.14	0.56	4.21	0.00	-	69.60
4718.97	10	1	Iron oxide + other	26	13.88	2.21	6.55	54.42	0.12	3.82	0.08	-	-	0.01	0.05	81.16
4718.97	10	2	Iron oxide + other	27	5.56	1.33	2.85	75.70	0.06	1.57	0.04	-	-	0.02	0.01	87.13
4718.97	10	3	Iron oxide + other	28	19.71	1.66	8.73	45.72	0.12	3.69	0.05	-	-	0.03	0.00	79.69
4718.97	10	4	Biotite	33	38.70	2.34	19.18	14.58	0.24	8.13	0.13	0.18	8.43	0.00	-	91.91
4718.97	10	5	Biotite	34	38.99	2.34	19.49	14.51	0.27	8.19	0.10	0.17	8.14	0.02	-	92.22
4718.97	10	6	Biotite	35	39.29	2.27	19.43	14.51	0.24	8.19	0.10	0.15	7.79	0.02	-	91.99
4718.97	11	1	Iron oxide + other	29	24.32	0.64	15.10	33.71	0.28	1.53	0.16	-	-	0.00	0.06	75.79
4718.97	11	2	Iron oxide + other	30	4.47	1.22	2.95	64.30	0.86	0.27	0.13	-	-	0.00	0.06	74.26
4718.97	11	3	Illite/Hydromuscovite	42	53.06	0.41	26.53	3.06	0.00	2.41	0.08	0.57	6.27	0.00	-	92.40
4718.97	11	4	Illite/Hydromuscovite	43	49.13	0.26	26.17	3.27	0.02	2.43	0.09	0.53	5.98	0.00	-	87.88
4718.97	11	5	Illite/Hydromuscovite	44	51.52	0.72	26.99	3.27	0.01	2.58	0.12	0.37	5.66	0.00	-	91.24
4718.97	11	6	Illite/Hydromuscovite	45	49.78	0.62	28.40	3.24	0.02	2.59	0.09	0.35	5.27	0.00	-	90.35
4718.97	12	1	Iron oxide + other	31	1.77	0.93	1.12	77.49	1.02	0.02	0.14	-	-	0.01	0.07	82.57
4718.97	12	2	Iron oxide + other	32	10.44	0.73	4.23	62.86	0.65	0.10	0.10	-	-	0.02	0.05	79.19
4718.97	12	3	Iron oxide + other	33	12.01	1.30	8.77	67.45	0.24	0.91	0.15	-	-	0.02	0.04	90.87
4718.97	12	4	K-feldspar	46	65.65	2.56	17.52	2.44	0.00	0.96	0.09	0.50	4.66	0.00	-	94.37
4718.97	12	5	Illite	47	54.89	0.20	19.80	9.57	0.00	0.81	0.11	0.44	5.28	0.00	-	91.11
4718.97	12	6	Muscovite/Hydromuscovite	48	48.34	0.01	29.05	2.33	0.00	1.67	0.07	0.17	8.90	0.00	-	90.55
4718.97	13	1	Void	49	11.04	0.00	7.20	0.42	0.00	0.22	0.44	0.01	2.58	0.00	-	21.91
4718.97	13	2	Muscovite + Chlorite	50	46.54	0.00	28.28	3.96	0.03	1.80	0.63	0.22	8.23	0.00	-	89.69

Table 2B: Electron microprobe chemical analyses of iron oxides and micas from representative sites for Mic Mac H-86 well at 4718.97m depth

4718.97	13	3	Muscovite + Chlorite	51	47.90	0.03	28.76	4.06	0.03	1.83	0.68	0.23	8.47	0.00	-	91.99
4718.97	13	4	Muscovite + Void	52	26.41	0.00	17.23	0.92	0.00	0.70	0.46	0.06	5.09	0.00	-	50.85

Appendix 1C: Scanning Electron Microscope Backscattered Electron Images for Mic Mac H-86 well with EDS Mineral Analyses Sample 4719.78

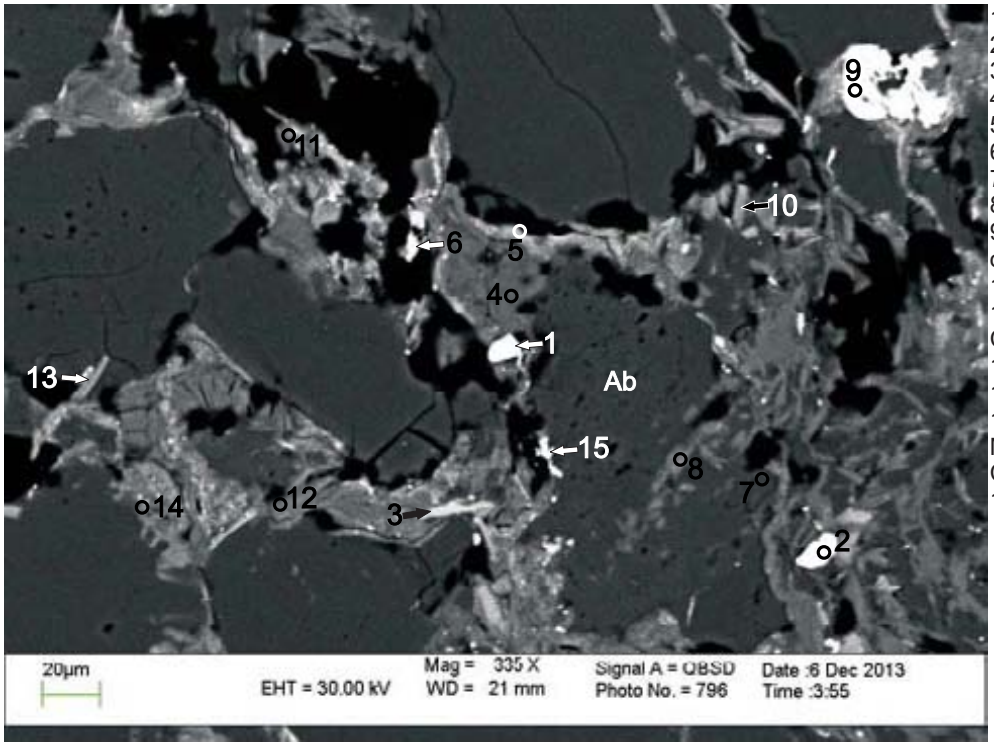

1: Zircon
2: Zircon
3: Illite
4: Muscovite
5: Illite
6: Illite
7: Albite
8: Muscovite
9: Iron oxide + other
10: Muscovite
11: Muscovite + Chlorite
12: Muscovite
13: Quartz
14: Quartz + Muscovite + Chlorite
15: Mix

Figure 1: Mic Mac H-86: 4719.78 site 1. Muscovite (analysis 4) seems to be converted into illite (analysis 5) within secondary porosity. Dissolution voids in detrital albite (analysis 7) are partly filled by muscovite (analysis 8).

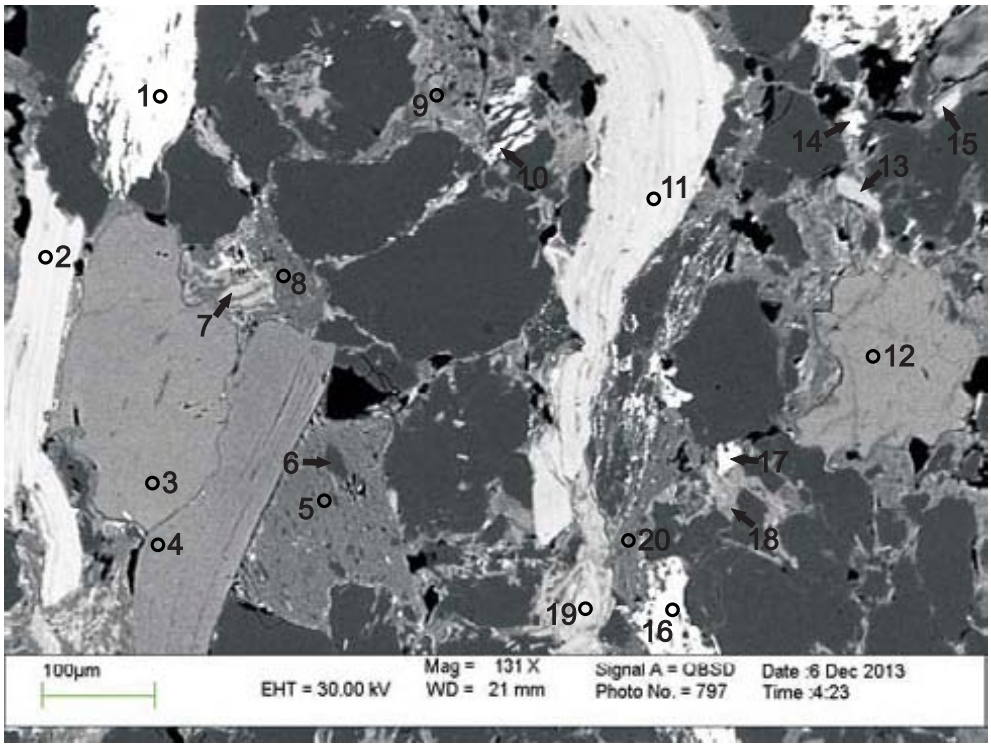

1: Iron oxide + other
2: Biotite
3: K-feldspar
4: Muscovite
5: Muscovite
6: Quartz
7: Chlorite
8: Muscovite
9: K-feldspar
10: Altered Ilmenite + other
11: Biotite
12: K-feldspar
13: Chlorite
14: Chlorite
15: Chlorite
16: Iron oxide
17: Rutile
18: Chlorite
19: Chlorite
20: Muscovite

Figure 2: Mic Mac H-86: 4719.78 site 2. Detrital muscovite (analysis 4) fills intergranular boundary between K-feldspar (analysis 3) and quartz and muscovite-rich clast (analyses 5 & 6, and see App. 4A, Fig. 10). Plastically deformed biotite (analysis 11) has become partially chloritzed at its tail (analysis 19).

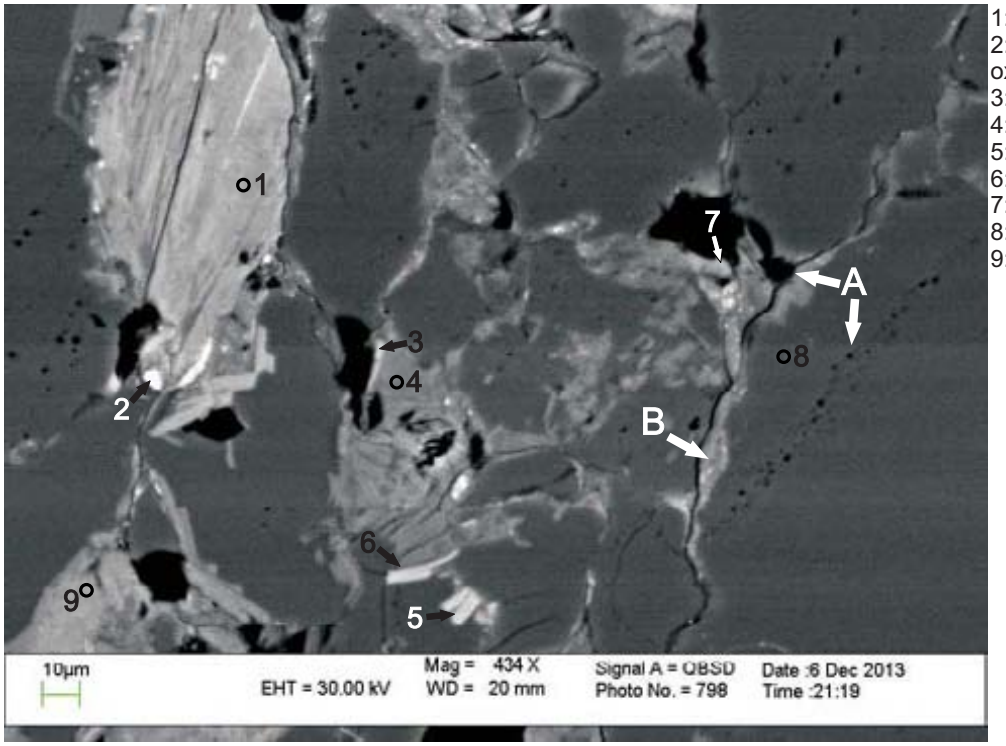

1: Chlorite
2: Chlorite + Iron oxide
3: Illite
4: Muscovite
5: Illite
6: Illite
7: Muscovite
8: Quartz
9: Illite

Figure 3: Mic Mac H-86: 4719.78 site 3. Quartz overgrowths (position A) separated from the detrital quartz by a dissolution zone. Mica seems to fill secondary porosity (position B) and composed the intergranular space.

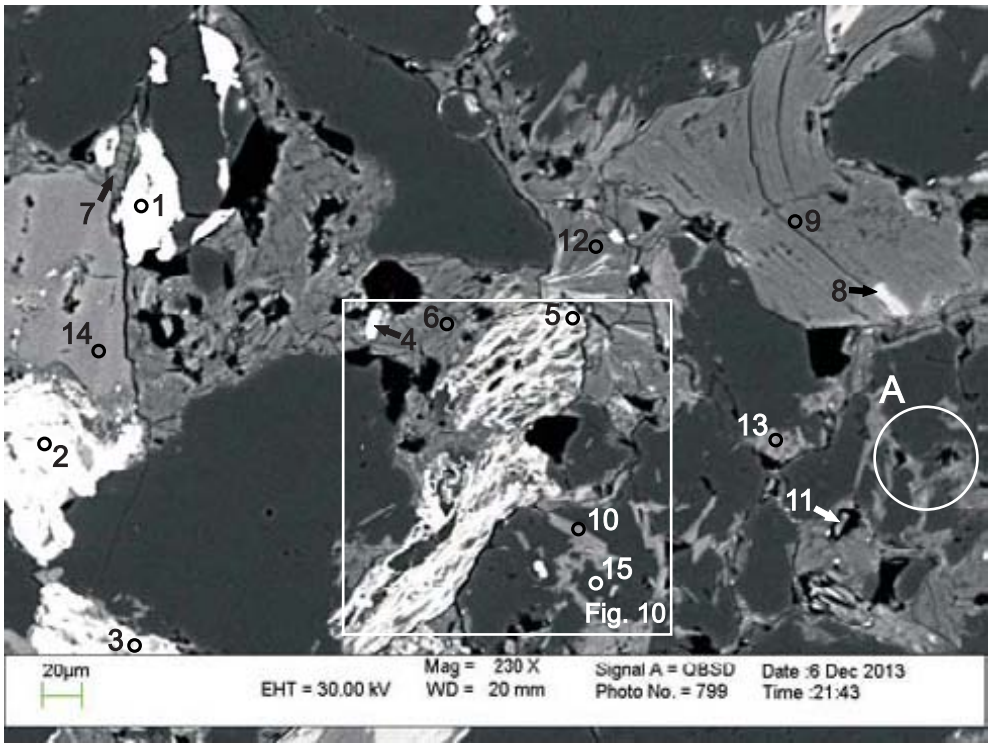

1: Hematite + other
2: Iron oxide + Muscovite
3: Iron oxide + Muscovite
4: Zircon
5: Chlorite + Muscovite + Iron oxide
6: Muscovite
7: Muscovite
8: Chlorite + other
9: Muscovite
10: Muscovite + Chlorite
11: Quartz
12: Muscovite
13: Illite
14: K-feldspar
15: Quartz

Figure 4: Mic Mac H-86: 4719.78 site 4. Mica seems to fill secondary porosity (position A). Detrital muscovite (analysis 9) showing slight plastic deformation. (See Figs. 9 and 10 and Table 2C for electron microprobe data of this site).

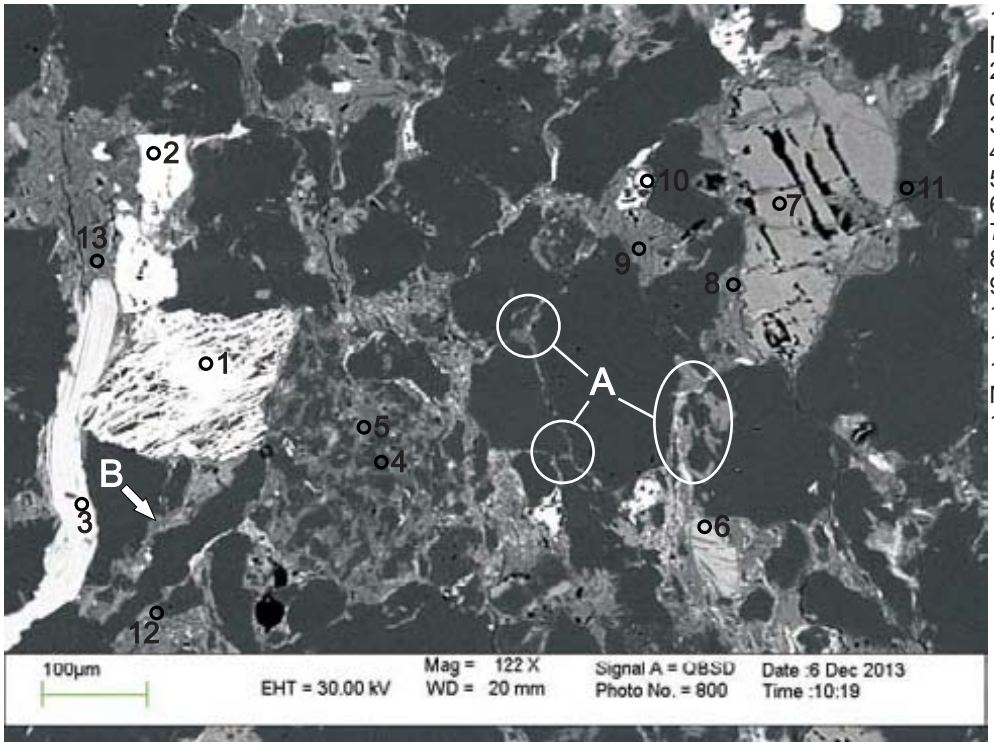

1: Hematite + Muscovite
2: Hematite + other
3: Biotite
4: Quartz
5: Muscovite
6: Chlorite
7: K-feldspar
8: Muscovite
9: Muscovite
10: TiO_2 + Quartz
11: Quartz
12: Quartz + Muscovite
13: Muscovite

Figure 5: Mic Mac H-86: 4719.78 site 5. Detrital biotite (analysis 3) is plastically deformed filling intergranular boundary between framework grains. Mica seems to fill secondary porosity (positions A and B). (See Fig. 11 and Table 2C for electron microprobe analyses of this site).

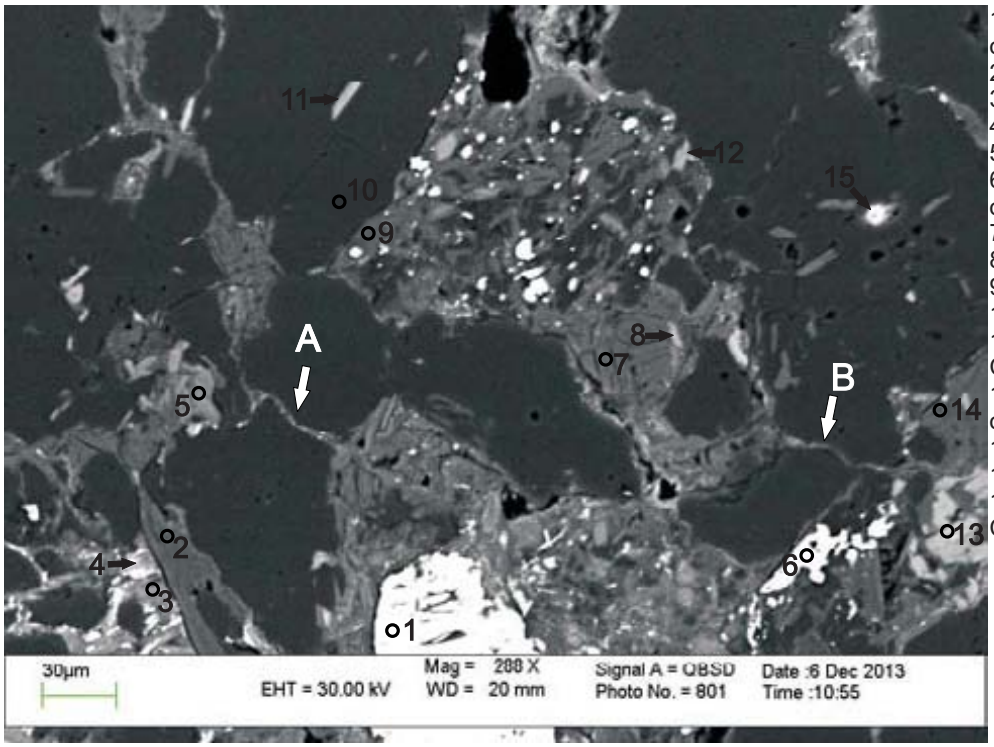

1: Iron oxide + other
2: Muscovite
3: Chlorite
4: Chlorite
5: Chlorite
6: Iron oxide + other
7: Muscovite
8: Altered Biotite
9: Muscovite
10: Quartz
11: Quartz + Chlorite
12: Chlorite + other
13: Chlorite
14: Muscovite
15: Quartz + Chlorite

Figure 6: Mic Mac H-86: 4719.78 site 6. Mica seems to fill secondary porosity , including fractures, contributing at the same time to the pseudomatrix (positions A and B). (See Fig. 13 and Table 2C for electron microprobe analyses of this site).

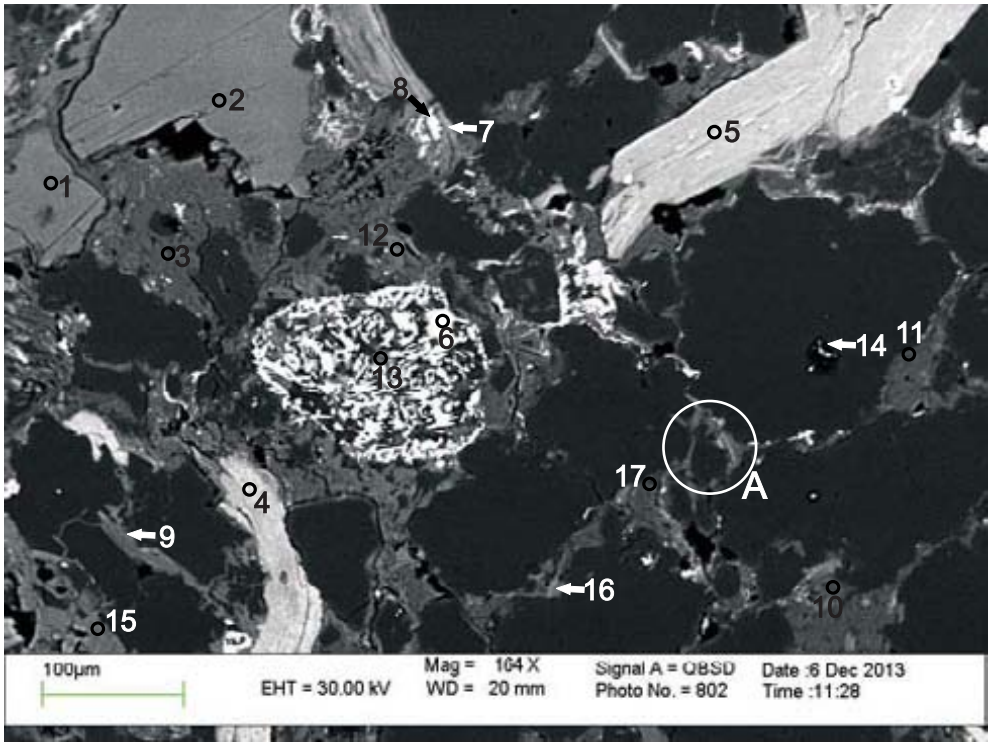

1: K-feldspar
2: K-feldspar
3: Muscovite
4: Biotite
5: Biotite
6: Rutile
7: Altered Biotite
8: Rutile + other
9: Muscovite
10: Muscovite
11: Muscovite
12: Muscovite + Chlorite
13: Chlorite + other
14: Quartz
15: Illite + Chlorite
16: Chlorite + other
17: Muscovite

Figure 7: Mic Mac H-86: 4719.78 site 7. Quartz and muscovite fill secondary porosity, including intergranular boundaries (position A, and see Fig. 15 and Table 2C for electron microprobe analyses).

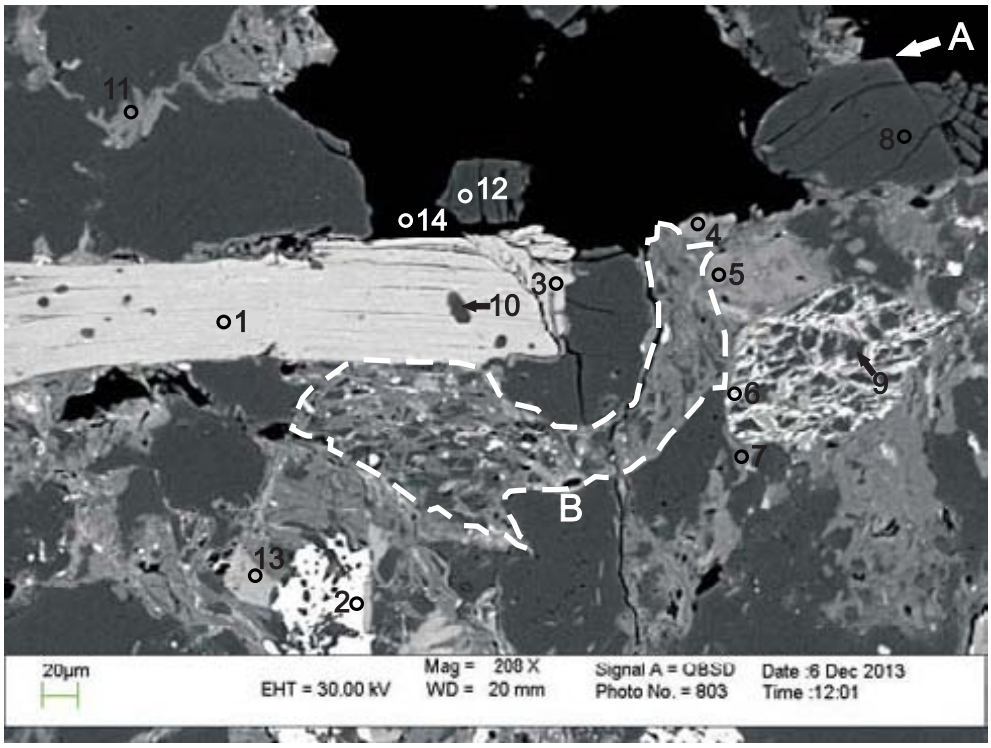

1: Biotite
2: Rutile
3: Biotite
4: K-feldspar
5: K-feldspar
6: Muscovite
7: Muscovite
8: Quartz
9: Quartz
10: Quartz + Biotite
11: Quartz
12: Quartz
13: Chlorite
14: Porosity

Figure 8: Mic Mac H-86: 4719.78 site 8. Quartz overgrowth (position A) faces secondary porosity. Plastically deformed muscovite-rich lithic clast (position B, and see App. 4A, Fig. 11) bends around framework grain.

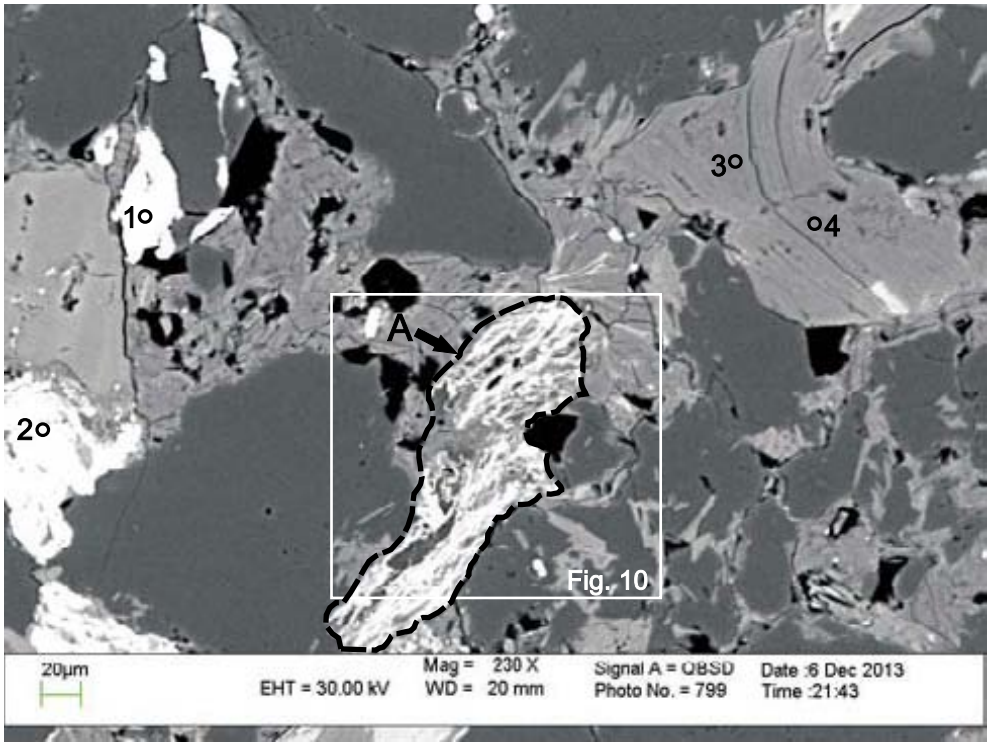

1: Hematite + other
2: Iron oxide + other
3: Muscovite
4: Muscovite

Figure 9: Electron microprobe analyses for Mic Mac H-86 4719.78 site 9 (from Fig. 4). Muscovite (analyses 3 and 4) and lithic clast (position A, and see Fig. 10, and Table 2C) showing slight plastic deformation.

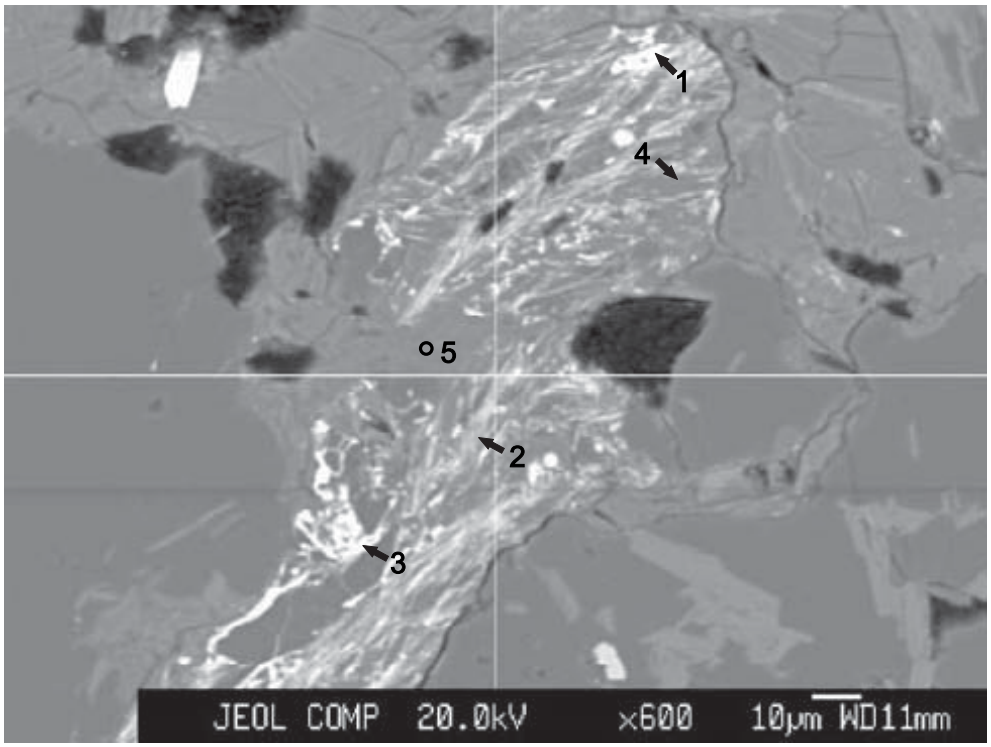

1: Iron oxide + other
2: Mix
3: Iron oxide + other
4: Chlorite + Muscovite
5: Chlorite + Muscovite

Figure 10: Electron microprobe analyses for Mic Mac H-86 4719.78 site 10 (from Fig. 4). This is a clast made up of iron oxide, muscovite and chlorite, and shows slight plastic deformation.

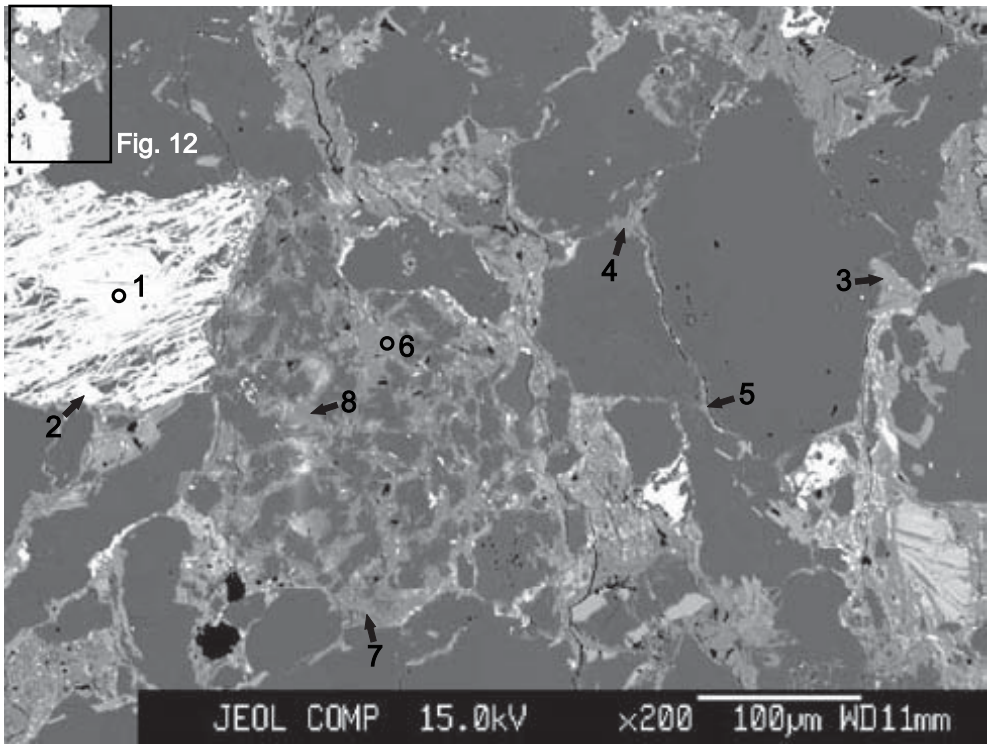

1: Hematite + other
2: Hematite + other
3: Quartz
4-6: Muscovite
7: Muscovite + Chlorite
8: Muscovite

Figure 11: Electron microprobe analyses for Mic Mac H-86 4719.78 site 11 (from Fig. 5). Intergranular boundaries are composed mainly of muscovite and chlorite (analysis 4-8). (See Fig. 12 and Table 2C for electron microprobe analyses of iron oxides).

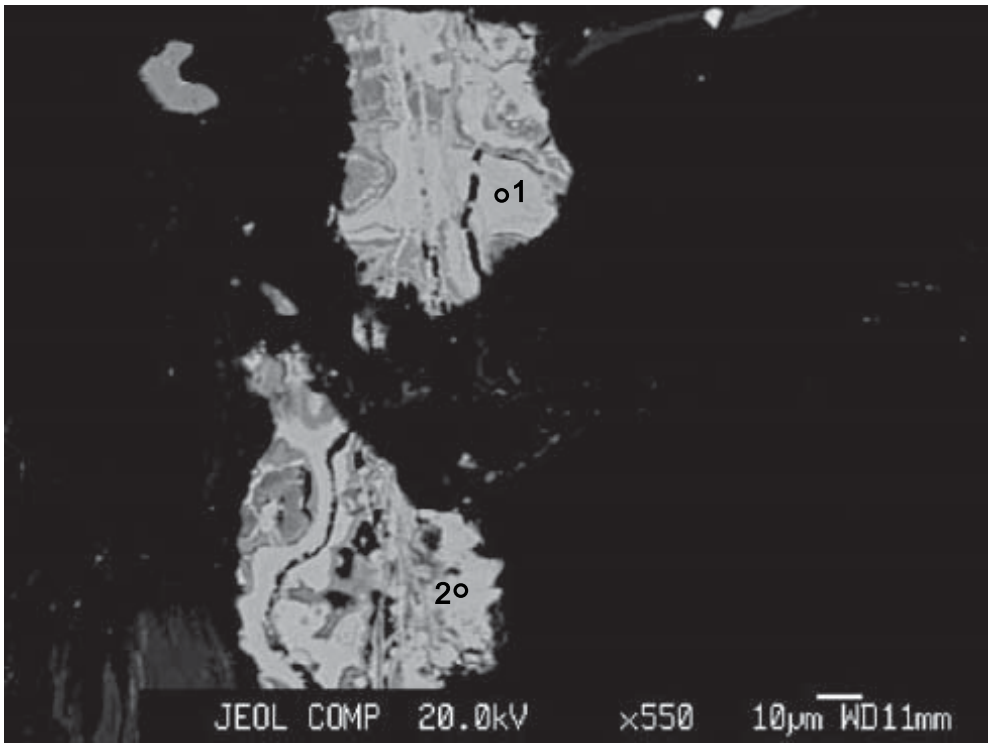

1: Hematite + other
2: Hematite + other

Figure 12: Electron microprobe analyses for Mic Mac H-86 4719.78 site 12 (from Fig. 11). Iron oxide, likely hematite.

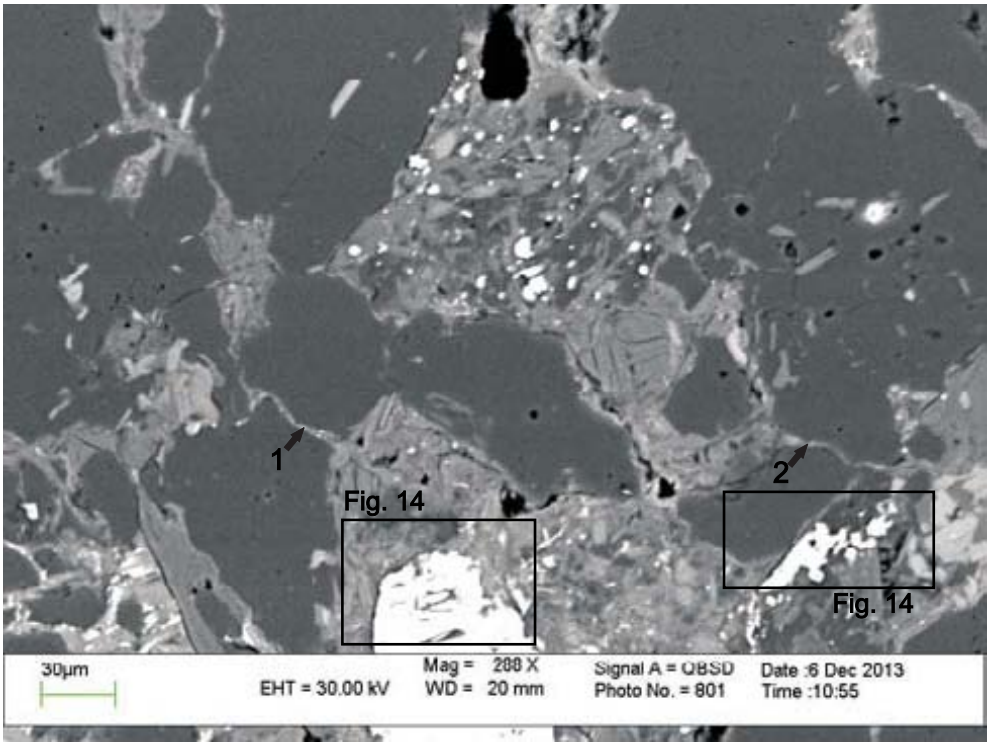

1: Quartz + Mica
2: Quartz + Mica

Figure 13: Electron microprobe analyses for Mic Mac H-86 4719.78 site 13 (from Fig. 6). Intergranular boundaries are likely composed of micas (such as muscovite, illite, and chlorite), however due to small intergranular space the analysis shows the beam was position mostly over the detrital quartza grains.

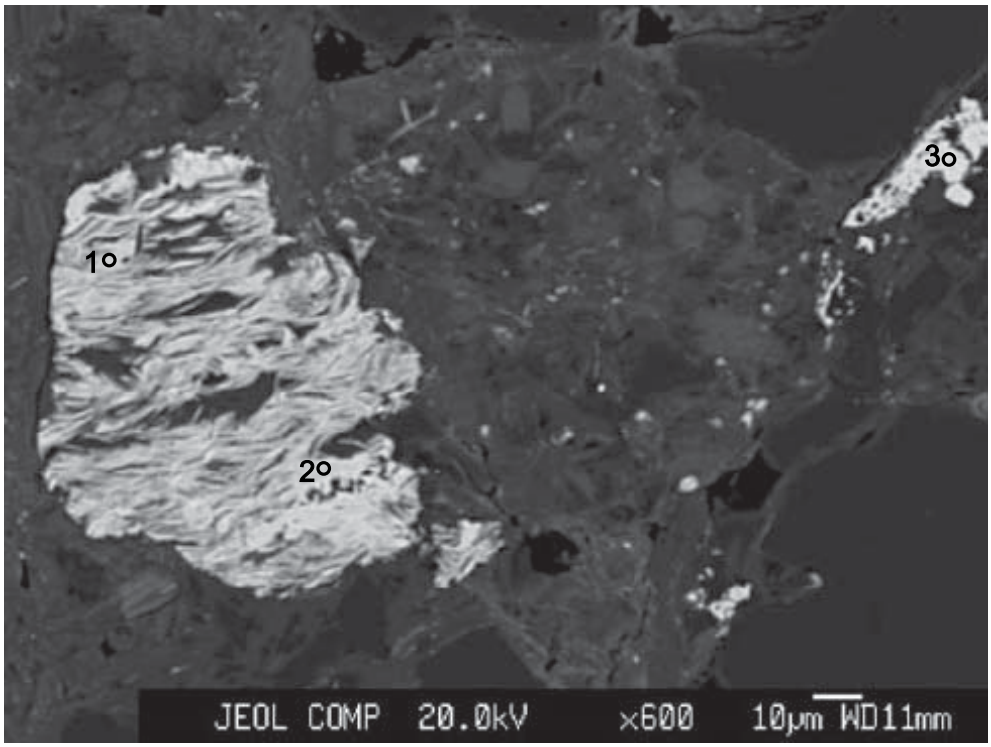

1: Hematite + other
2: Goethite + other
3: Iron oxide + other

Figure 14: Electron microprobe analyses for Mic Mac H-86 4719.78 site 14 (from Fig. 13). Clast compoaed of hematite, geothite, and silicate minerals (analysis 1 and 2).

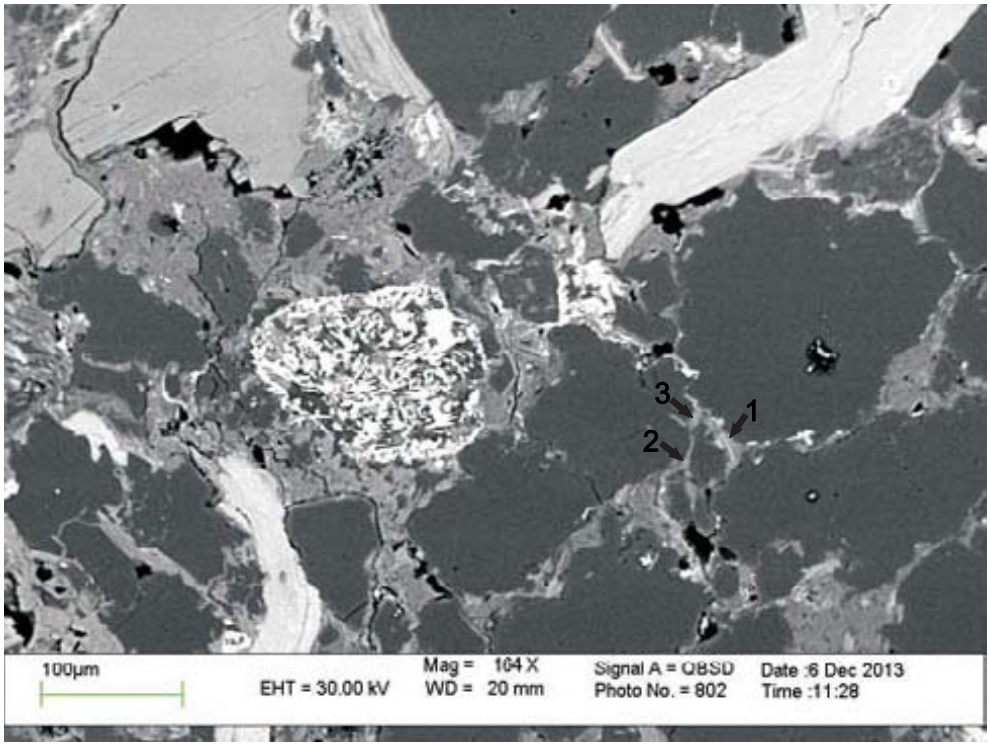

1-3: Quartz + Mica (Muscovite)

Figure 15: Electron microprobe analyses for Mic Mac H-86 4719.78 site 15 (from Fig. 7). Mica (likely muscovite) fills intergranular boundaries between detrital quartz grains.

Table 1C: Scanning electron microscope chemical analyses of minerals from representative sites for Mic Mac H-86 well at 4719.78m depth

Sample	Site	Position	Mineral	SiO_2	TiO_2	Al_2O_3	FeO	MnO	MgO	CaO	Na_2O	K_2O	P_2O_5	SO_3	F	Cl	Y_2O_3	ZrO_2	BaO	HfO_2	Total	Actual Total
H-86-4719.78	1	1	Zircon	33.29		6.46	4.36		0.46	0.43		1.54				0.22	2.03	49.01		2.19	100.00	84.5
H-86-4719.78	1	2	Zircon	35.98		0.91	0.36			0.36							1.35	60.07		0.97	100.00	97.25
H-86-4719.78	1	3	Illite	46.04	1.55	20.36	10.09		5.53			6.45									90.00	84.63
H-86-4719.78	1	4	Muscovite	50.68		31.39	1.26		1.03		0.30	8.33									93.00	81.18
H-86-4719.78	1	5	Illite	50.92	0.27	24.18	5.59		2.11			6.32				0.59					90.00	56.15
H-86-4719.78	1	6	Illite	42.20	1.71	19.73	11.57	0.12	7.92			6.52				0.23					90.00	78.91
H-86-4719.78	1	7	Albite	68.03		19.22					12.17	0.43				0.14					100.00	79.68
H-86-4719.78	1	8	Muscovite	51.87		28.19	1.96		1.48		1.43	8.06									93.00	84.74
H-86-4719.78	1	9	Iron oxide + other	22.95	0.93	15.08	56.06	0.98	0.56			2.82	0.62								100.00	76.1
H-86-4719.78	1	10	Muscovite	49.24	0.28	30.44	2.62		1.08		0.66	8.70									93.00	85.43
H-86-4719.78	1	11	Muscovite + Chlorite	54.23		30.35	4.52		2.01			8.41				0.50					100.00	64.13
H-86-4719.78	1	12	Muscovite	52.50		29.10	1.66		1.64		0.50	7.17				0.45					93.00	51.50
H-86-4719.78	1	13	Quartz	94.89		1.64	2.97					0.48									100.00	88.12
H-86-4719.78	1	14	Quartz + Muscovite + Chlorite	70.27		18.27	3.86		1.56			5.70				0.31					100.00	91.16
H-86-4719.78	1	15	Mix	38.38	30.03	20.46	4.23		1.97		1.24	3.38				0.28					100.00	83.16
H-86-4719.78	2	1	Iron oxide + other	19.32	1.37	15.46	59.99	0.39		0.22	1.19	2.08									100.00	80.56
H-86-4719.78	2	2	Biotite	42.31	2.82	19.46	15.01	0.25	10.96		0.35	8.85									100.00	82.69
H-86-4719.78	2	3	K-feldspar	66.17		18.25					0.98	14.60									100.00	91.43
H-86-4719.78	2	4	Muscovite	46.37	0.98	32.07	2.34		0.73		0.50	10.03									93.00	84.05
H-86-4719.78	2	5	Muscovite	50.42		31.12	1.13		1.10		0.55	8.70									93.00	86.54
H-86-4719.78	2	6	Quartz	99.99																	100.00	93.65
H-86-4719.78	2	7	Chlorite	32.62		23.26	17.03	0.29	11.09			0.71									85.00	75.14
H-86-4719.78	2	8	Muscovite	50.23	0.14	31.05	1.53		1.25		0.86	7.94									93.00	88.41
H-86-4719.78	2	9	K-feldspar	62.27		22.54	1.61		0.50		0.32	12.58				0.18					100.00	81.48
H-86-4719.78	2	10	Altered Ilmenite + other	9.24	77.58	3.95	7.42	0.18	0.55	0.25		0.66				0.15					100.00	80.91
H-86-4719.78	2	11	Biotite	42.06	2.62	20.46	16.62	0.22	11.19			6.70				0.15					100.00	85.15
H-86-4719.78	2	12	K-feldspar	66.27		18.06					1.02	14.65									100.00	100.79
H-86-4719.78	2	13	Chlorite	37.32	1.21	17.80	11.21	0.16	11.36			5.96									85.00	90.31
H-86-4719.78	2	14	Chlorite	32.40	0.82	18.20	28.47	0.41	0.88		0.36	3.49									85.00	97.97
H-86-4719.78	2	15	Chlorite	37.22	1.43	17.82	13.78	0.14	8.50			5.96				0.14					85.00	90.89
H-86-4719.78	2	16	Iron oxide	4.32		2.38	90.99	0.88		0.29		0.33		0.57		0.24					100.00	67.02
H-86-4719.78	2	17	Rutile	2.72	96.38		0.90														100.00	82.27
H-86-4719.78	2	18	Chlorite	30.13	0.21	22.28	15.05	0.19	16.60	0.29		0.26									85.00	82.84
H-86-4719.78	2	19	Chlorite	30.17		21.72	20.42	0.31	11.91			0.49									85.00	79.78
H-86-4719.78	2	20	Muscovite	49.96	0.84	30.93	1.37		1.31		0.74	7.88									93.00	88.31
H-86-4719.78	3	1	Chlorite	31.78		23.24	17.40	0.38	11.91			0.28									85.00	73.68
H-86-4719.78	3	2	Chlorite + Iron oxide	35.90	1.20	16.02	41.69	0.54	1.59			2.79				0.26					100.00	91.02
H-86-4719.78	3	3	Illite	42.51		25.14	8.68	0.13	7.62		0.35	5.43				0.16					90.00	104.72
H-86-4719.78	3	4	Muscovite	50.97		30.10	1.59		1.24			9.10									93.00	105.3
H-86-4719.78	3	5	Illite	37.45		21.32	18.63	0.24	9.32			2.86				0.17					90.00	105.88
H-86-4719.78	3	6	Illite	43.86		22.52	12.41	0.14	7.24			3.70				0.14					90.00	119.22
H-86-4719.78	3	7	Muscovite	50.87		29.30	1.95		1.60		0.29	8.80				0.20					93.00	125.55
H-86-4719.78	3	8	Quartz	99.99																	100.00	143.84
H-86-4719.78	3	9	Illite	37.64		21.29	14.80	0.15	15.28			0.85									90.00	112.86
H-86-4719.78	4	1	Hematite + other	3.32	0.68	1.17	94.00	0.84													100.00	116.55

Table 1C: Scanning electron microscope chemical analyses of minerals from representative sites for Mic Mac H-86 well at 4719.78m depth

Sample	Site	Position	Mineral	SiO_2	TiO_2	Al_2O_3	FeO	MnO	MgO	CaO	Na_2O	K_2O	P_2O_5	SO_3	F	Cl	Y_2O_3	ZrO_2	BaO	HfO_2	Total	Actual Total
H-86-4719.78	4	2	Iron oxide + Muscovite	10.55	2.27	6.61	77.16	1.83		0.32		1.23									100.00	124.29
H-86-4719.78	4	3	Iron oxide + Muscovite	18.97	1.90	10.58	63.42	1.19	0.88			2.84				0.2					100.00	130.71
H-86-4719.78	4	4	Zircon	32.86		2.83	0.98			0.25		0.84						61.23		1	100.00	179.21
H-86-4719.78	4	5	Chlorite + Muscovite + Iron oxide	37.37	1.07	22.01	32.68	0.23	0.73		1.00	4.91									100.00	156.96
H-86-4719.78	4	6	Muscovite	50.31		30.70	1.59		1.24		0.46	8.71									93.00	165.66
H-86-4719.78	4	7	Muscovite	50.23		29.96	2.77		1.19			8.70				0.14					93.00	168.03
H-86-4719.78	4	8	Chlorite + other	42.36	3.22	20.10	15.68	0.22	8.97		0.34	9.13									100.00	171.67
H-86-4719.78	4	9	Muscovite	46.96	0.51	33.80	0.91		0.38		0.57	9.86									93.00	173.71
H-86-4719.78	4	10	Muscovite + Chlorite	54.46	0.30	28.48	4.32		1.99		0.24	10.19									100.00	173.97
H-86-4719.78	4	11	Quartz	93.95		3.80	0.59		0.35	0.11		1.13				0.07					100.00	295.16
H-86-4719.78	4	12	Muscovite	50.57		30.21	1.83		1.28			9.10									93.00	173.29
H-86-4719.78	4	13	Illite	42.24	0.14	25.17	9.87	0.17	7.24			5.15									90.00	174.5
H-86-4719.78	4	14	K-feldspar	66.02		18.03	0.12				0.63	15.20									100.00	178.39
H-86-4719.78	4	15	Quartz	99.90			0.09														100.00	191.66
H-86-4719.78	5	1	Hematite + Muscovite	23.15	1.23	15.85	54.65	0.41	0.80		0.49	3.43									100.00	156.66
H-86-4719.78	5	2	Hematite + other	1.97	2.10	1.45	93.49	0.75								0.21					100.00	118.12
H-86-4719.78	5	3	Biotite	42.44	3.24	19.50	15.14	0.27	10.38			9.00									100.00	161.86
H-86-4719.78	5	4	Quartz	95.39		3.38	0.23					1.01									100.00	183
H-86-4719.78	5	5	Muscovite	55.20	1.19	26.67	2.13		1.73		0.47	5.59									93.00	171.04
H-86-4719.78	5	6	Chlorite	30.66		22.50	17.60	0.82	13.00			0.43									85.00	158.69
H-86-4719.78	5	7	K-feldspar	66.17		18.08					0.70	15.03									100.00	189.41
H-86-4719.78	5	8	Muscovite	57.77		25.05	1.88		0.88		0.72	6.58				0.10					93.00	172.69
H-86-4719.78	5	9	Muscovite	50.40		30.50	1.58		1.24		0.24	9.06									93.00	169.05
H-86-4719.78	5	10	TiO2 + Quartz	19.38	80.18		0.44														100.00	138.89
H-86-4719.78	5	11	Quartz	99.99																	100.00	177.75
H-86-4719.78	5	12	Quartz + Muscovite	60.56		26.47	3.52		1.63			7.65				0.16					100.00	139.3
H-86-4719.78	5	13	Muscovite	51.27		29.54	1.82		1.45		0.24	8.50				0.17					93.00	140.9
H-86-4719.78	6	1	Iron oxide + other	10.35	1.52	7.20	78.31	0.84			0.59	1.19									100.00	108.52
H-86-4719.78	6	2	Muscovite	47.97	0.67	33.28	0.70		0.84		1.34	8.21									93.00	131.72
H-86-4719.78	6	3	Chlorite	34.75	0.15	19.74	14.67	0.13	14.82			0.74									85.00	116.78
H-86-4719.78	6	4	Chlorite	28.86	0.34	17.35	23.52	0.21	13.70			1.02									85.00	123.09
H-86-4719.78	6	5	Chlorite	33.06		22.90	13.75	0.18	14.29			0.81									85.00	117.15
H-86-4719.78	6	6	Iron oxide + other	4.32	1.95	1.63	91.24	0.85													100.00	105.36
H-86-4719.78	6	7	Muscovite	51.05		29.83	1.70		1.25			9.18									93.00	132.27
H-86-4719.78	6	8	Altered Biotite	42.66		28.32	14.61	1.01	10.33			3.06									100.00	127.16
H-86-4719.78	6	9	Muscovite	48.39		32.65	1.84		0.43		1.26	8.42									93.00	129.85
H-86-4719.78	6	10	Quartz	99.99																	100.00	140.61
H-86-4719.78	6	11	Quartz + Chlorite	56.07		16.51	13.91	0.58	12.75			0.20									100.00	138.01
H-86-4719.78	6	12	Chlorite + other	43.75	0.87	24.81	14.82	0.67	12.92			2.18									100.00	126.05
H-86-4719.78	6	13	Chlorite	31.78		22.50	18.13	0.97	10.49	0.24		0.92									85.00	118.7
H-86-4719.78	6	14	Muscovite	50.40		30.80	1.66		1.10		0.22	8.83									93.00	133.19
H-86-4719.78	6	15	Quartz + Chlorite	50.66	0.27	10.64	28.06	0.23	1.01		0.44	2.78			5.60	0.32					100.00	134.1
H-86-4719.78	7	1	K-feldspar	65.84		18.05					0.71	14.84							0.55		100.00	131.7
H-86-4719.78	7	2	K-feldspar	65.74		18.33					0.77	14.41							0.75		100.00	136.33
H-86-4719.78	7	3	Muscovite	47.99		28.23	1.96		1.54			8.60			4.52	0.16					93.00	128.62

Table 1C: Scanning electron microscope chemical analyses of minerals from representative sites for Mic Mac H-86 well at 4719.78m depth

Sample	Site	Position	Mineral	SiO_2	TiO_2	Al_2O_3	FeO	MnO	MgO	CaO	Na_2O	K_2O	P_2O_5	SO_3	F	Cl	Y_2O_3	ZrO_2	BaO	HfO_2	Total	Actual Total
H-86-4719.78	7	4	Biotite	43.28	1.73	20.18	17.68	0.25	9.30			7.56									100.00	121.67
H-86-4719.78	7	5	Biotite	42.74	2.65	19.73	15.22	0.27	10.63		0.36	8.40									100.00	127.54
H-86-4719.78	7	6	Rutile	0.83	98.27		0.90														100.00	118.71
H-86-4719.78	7	7	Altered Biotite	44.47	0.20	22.11	17.12	0.31	14.11			1.67									100.00	119.87
H-86-4719.78	7	8	Rutile + other	5.03	86.92	3.74	2.12		1.92			0.28									100.00	116.47
H-86-4719.78	7	9	Muscovite	51.64	0.31	27.30	2.85		1.52		0.72	8.69									93.00	128.88
H-86-4719.78	7	10	Muscovite	49.48		28.73	2.43		1.92			8.53			1.82	0.10					93.00	135.6
H-86-4719.78	7	11	Muscovite	52.36		28.72	1.84		1.17			8.91									93.00	131.63
H-86-4719.78	7	12	Muscovite + Chlorite	52.82	0.25	30.04	4.32		1.79		0.30	10.48									100.00	124.68
H-86-4719.78	7	13	Chlorite + other	44.79	3.99	24.22	12.84		11.86			2.29									100.00	116.2
H-86-4719.78	7	14	Quartz	96.86		0.57	0.15				1.40	0.35				0.65					100.00	121.52
H-86-4719.78	7	15	Illite + Chlorite	53.86	0.20	28.15	4.86		2.60			10.32									100.00	125
H-86-4719.78	7	16	Chlorite + other	50.59		22.56	11.14	0.17	12.57			2.95									100.00	120.51
H-86-4719.78	7	17	Muscovite	51.22		29.43	1.82		1.53			8.99									93.00	126.49
H-86-4719.78	8	1	Biotite	42.21	1.53	20.71	18.02	0.15	9.24			7.94				0.20					100.00	120.55
H-86-4719.78	8	2	Rutile	0.96	98.23	0.53	0.28														100.00	116.79
H-86-4719.78	8	3	Biotite	43.62	1.52	22.24	15.57	0.15	8.66		0.38	7.87									100.00	125.27
H-86-4719.78	8	4	K-feldspar	65.63		18.54					1.05	13.84							0.94		100.00	128.16
H-86-4719.78	8	5	K-feldspar	65.48		18.50	0.17				0.89	14.08							0.89		100.00	138.36
H-86-4719.78	8	6	Muscovite	40.20	0.49	27.30	16.59	0.18	1.17		0.94	6.10									93.00	128.85
H-86-4719.78	8	7	Muscovite	52.60		27.01	2.80		1.96		0.21	8.42									93.00	129.84
H-86-4719.78	8	8	Quartz	99.99																	100.00	142.75
H-86-4719.78	8	9	Quartz	96.86		1.93	0.68					0.52									100.00	140.5
H-86-4719.78	8	10	Quartz + Biotite	87.79	0.42	3.78	4.59		1.23			2.18									100.00	141.88
H-86-4719.78	8	11	Quartz	91.22		5.37	0.89					2.51									100.00	131.2
H-86-4719.78	8	12	Quartz	99.99																	100.00	136.22
H-86-4719.78	8	13	Chlorite	34.02	0.20	21.99	15.68	0.88	11.11			1.12									85.00	111.61
H-86-4719.78	8	14	Porosity													100					100.00	1.16

Table 2C: Electron microprobe chemical analyses of iron oxides and micas from representative sites for Mic Mac H-86 well at 4719.78m depth

Sample	Figure	Position	Mineral	No.	SiO_2	TiO_2	Al_2O_3	FeO	MnO	MgO	CaO	Na_2O	K_2O	Cr_2O_3	V_2O_3	Total
4719.78	9	1	Hematite + other	39	0.82	1.54	0.28	85.23	0.34	0.04	0.06	-	-	0.01	0.07	88.39
4719.78	9	2	Iron oxide + other	40	1.82	1.95	0.89	79.35	2.35	0.09	0.22	-	-	0.03	0.03	86.72
4719.78	9	3	Muscovite	79	45.44	0.45	35.10	1.05	0.02	0.58	0.04	0.45	9.89	0.00	-	93.01
4719.78	9	4	Muscovite	80	46.08	0.50	35.54	1.05	0.01	0.60	0.04	0.33	9.37	0.03	-	93.53
4719.78	10	1	Iron oxide + other	41	4.36	1.63	2.34	80.90	0.16	0.14	0.06	-	-	0.02	0.04	89.64
4719.78	10	2	Mix	42	33.48	1.32	20.62	32.37	0.17	0.78	0.17	-	-	0.02	0.05	88.97
4719.78	10	3	Iron oxide + other	43	20.62	1.42	2.26	67.07	0.71	0.12	0.19	-	-	0.02	0.03	92.43
4719.78	10	4	Chlorite + Muscovite	81	34.65	0.80	26.28	25.24	0.19	0.55	0.14	0.71	6.54	0.08	-	95.18
4719.78	10	5	Chlorite + Muscovite	82	35.96	0.82	27.22	23.68	0.15	0.54	0.19	0.71	6.75	0.08	-	96.10
4719.78	11	1	Hematite + other	46	2.07	0.64	1.19	83.56	0.69	0.06	0.14	-	-	0.02	0.11	88.48
4719.78	11	2	Hematite + other	47	2.03	0.41	0.83	83.41	0.61	0.07	0.16	-	-	0.01	0.08	87.60
4719.78	11	3	Quartz	68	94.09	0.00	0.00	0.00	0.00	0.00	0.00	0.00	0.02	0.00	-	94.11
4719.78	11	4	Muscovite	69	46.46	0.01	31.26	2.30	0.01	1.38	0.13	0.13	9.27	0.00	-	90.95
4719.78	11	5	Muscovite	70	46.59	0.01	30.03	2.53	0.01	1.84	0.14	0.13	8.90	0.00	-	90.17
4719.78	11	6	Muscovite	71	48.07	0.14	34.01	1.12	0.01	0.90	0.04	0.49	9.18	0.00	-	93.95
4719.78	11	7	Muscovite + Chlorite	72	55.78	0.05	24.88	3.37	0.03	1.49	0.16	0.15	7.71	0.00	-	93.61
4719.78	11	8	Muscovite	73	48.38	0.19	35.00	1.09	0.02	0.92	0.04	0.58	9.04	0.01	-	95.25
4719.78	12	1	Hematite + other	44	2.23	1.04	1.24	82.18	1.03	0.02	0.17	-	-	0.02	0.07	88.00
4719.78	12	2	Hematite + other	45	1.17	0.93	1.11	83.21	0.66	0.01	0.16	-	-	0.00	0.05	87.30
4719.78	13	1	Quartz	74	94.51	0.00	1.60	0.57	0.02	0.10	0.01	0.02	0.57	0.00	-	97.39
4719.78	13	2	Quartz	75	94.07	0.00	1.61	0.31	0.02	0.14	0.00	0.03	0.46	0.00	-	96.65
4719.78	14	1	Hematite + other	48	2.70	0.36	1.84	81.01	0.70	0.09	0.15	-	-	0.04	0.06	86.94
4719.78	14	2	Goethite + other	49	1.67	0.18	1.76	80.14	0.45	0.15	0.19	-	-	0.02	0.07	84.62
4719.78	14	3	Iron oxide + other	50	10.85	1.24	0.55	79.68	0.80	0.01	0.08	-	-	0.02	0.07	93.29
4719.78	15	1	Quartz + Mica (muscovite)	76	87.34	0.00	6.82	1.59	0.00	0.46	0.06	0.07	1.95	0.00	-	98.30
4719.78	15	2	Quartz + Mica (muscovite)	77	86.26	0.00	6.80	1.54	0.02	0.47	0.06	0.07	1.88	0.00	-	97.10
4719.78	15	3	Quartz + Mica (muscovite)	78	86.70	0.00	6.69	1.55	0.01	0.47	0.06	0.09	1.73	0.00	-	97.31

Appendix 1D: Scanning Electron Microscope Backscattered Electron Images for Mic Mac H-86 well with EDS Mineral Analyses Sample 4721.13

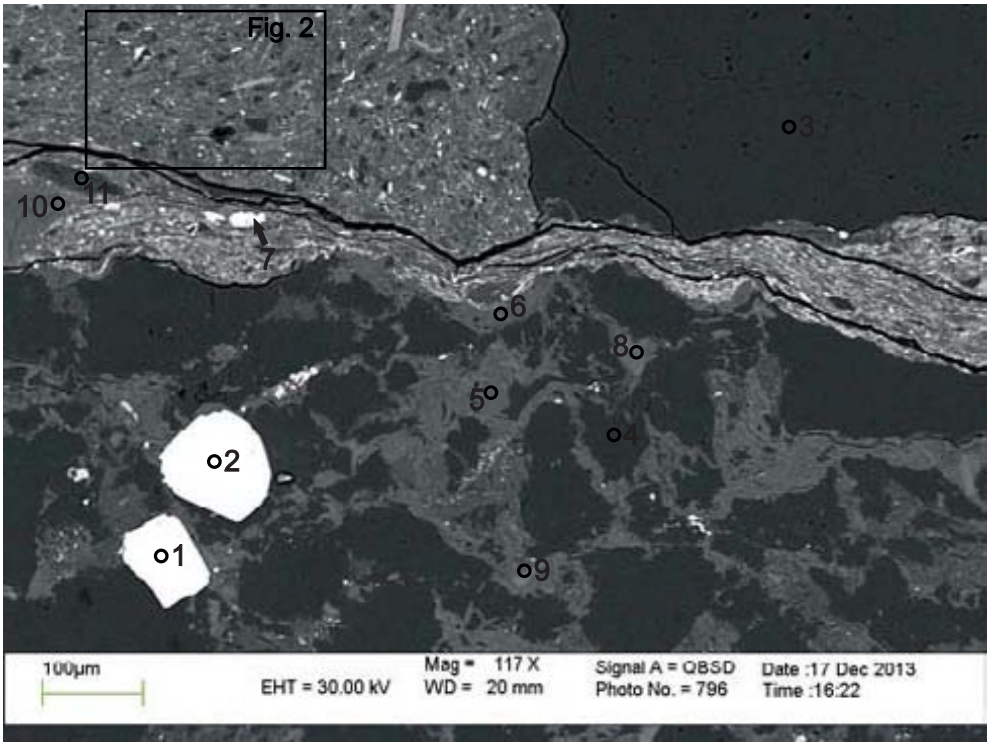

Figure 1: Mic Mac H-86: 4721.13 site 1. Contact between a probable extrabasinal rounded lithic clast and a mudstone host (see Fig. 2 and Table 1D for host analyses, and see Fig. 6 and Table 2D for electron microprobe analyses).

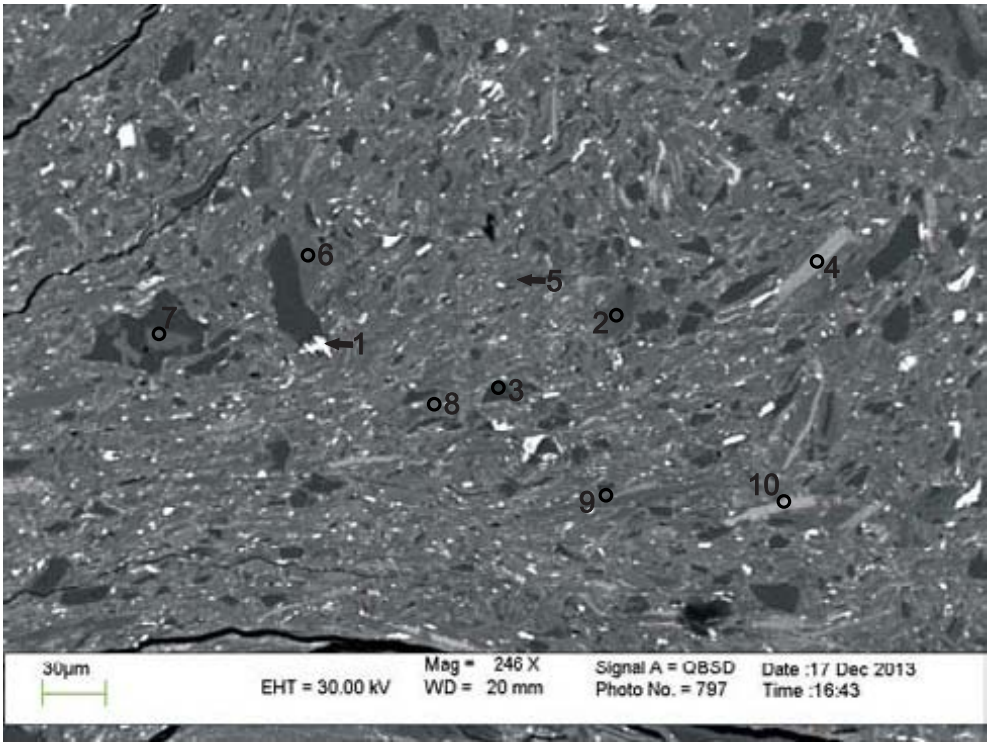

Figure 2: Mic Mac H-86: 4721.13 site 2. Mudstone host made up primarily of fine grained quartz, muscovite, biotite and chlorite.

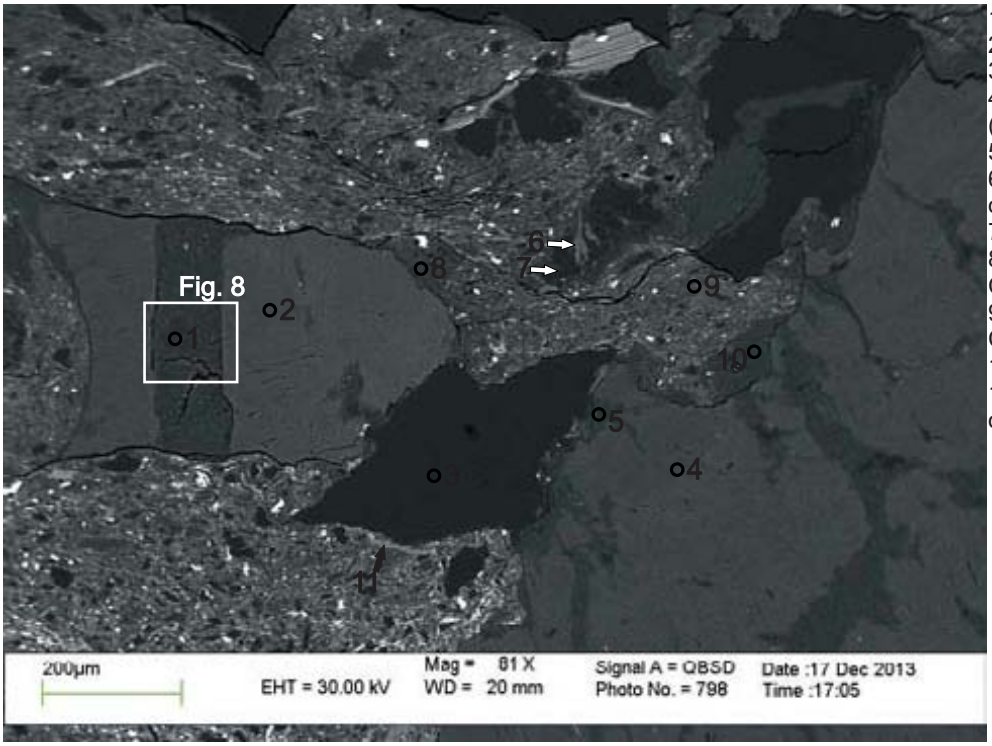

1: Muscovite
2: K-feldspar
3: Quartz
4: K-feldspar (Microcline)
5: Muscovite
6: Chlorite + other
7: Quartz
8: Muscovite + Chlorite
9: Muscovite + Chlorite
10: Muscovite
11: Muscovite + other

Figure 3: Mic Mac H-86: 4721.13 site 3. Mudstone host with large detrital K-feldspar (analysis 2) and microcline grains (analyses 4, and see App. 4A, Fig. 12) with exsolution of perthite. Muscovite (analysis 1) fills in fracture within detrital K-feldspar (see Fig. 7, and Table 2D for electron microprobe analyses)

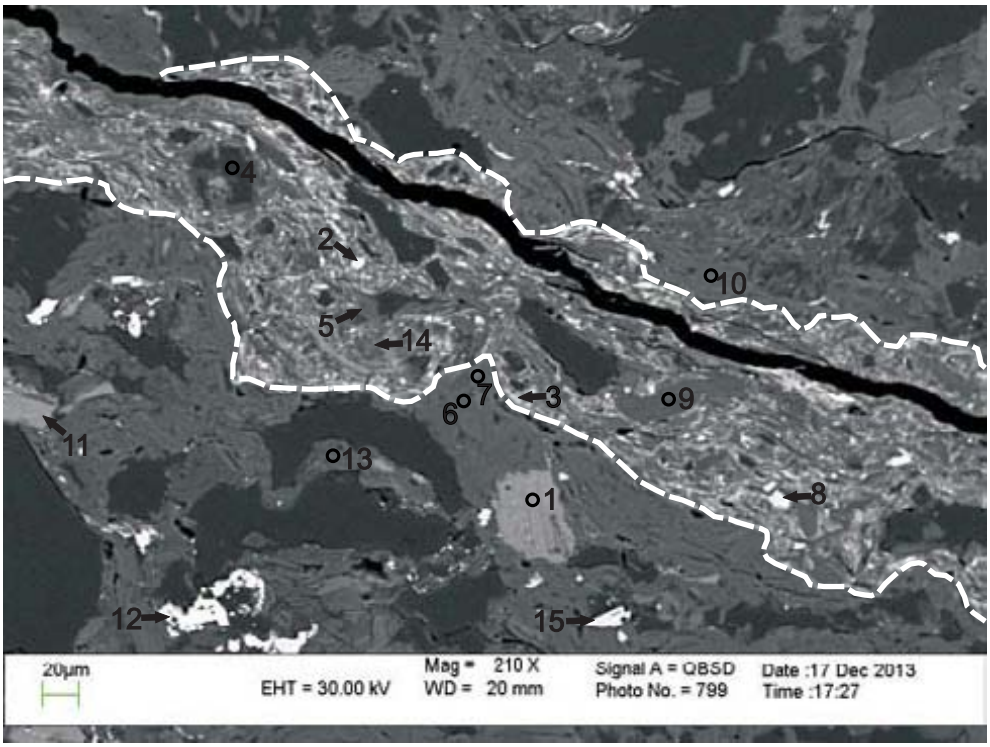

1: Biotite
2: Altered Ilmenite + other
3: Chlorite + Muscovite
4: Albite
5-7: Muscovite + Chlorite
8: Iron oxide + other
9: Muscovite
10: Muscovite + Chlorite
11: Biotite
12: Altered Ilmenite
13: Muscovite
14: Muscovite
15: Quartz + TiO_2

Figure 4: Mic Mac H-86: 4721.13 site 4. Two lithic clasts with a thin band of mudstone host between them.

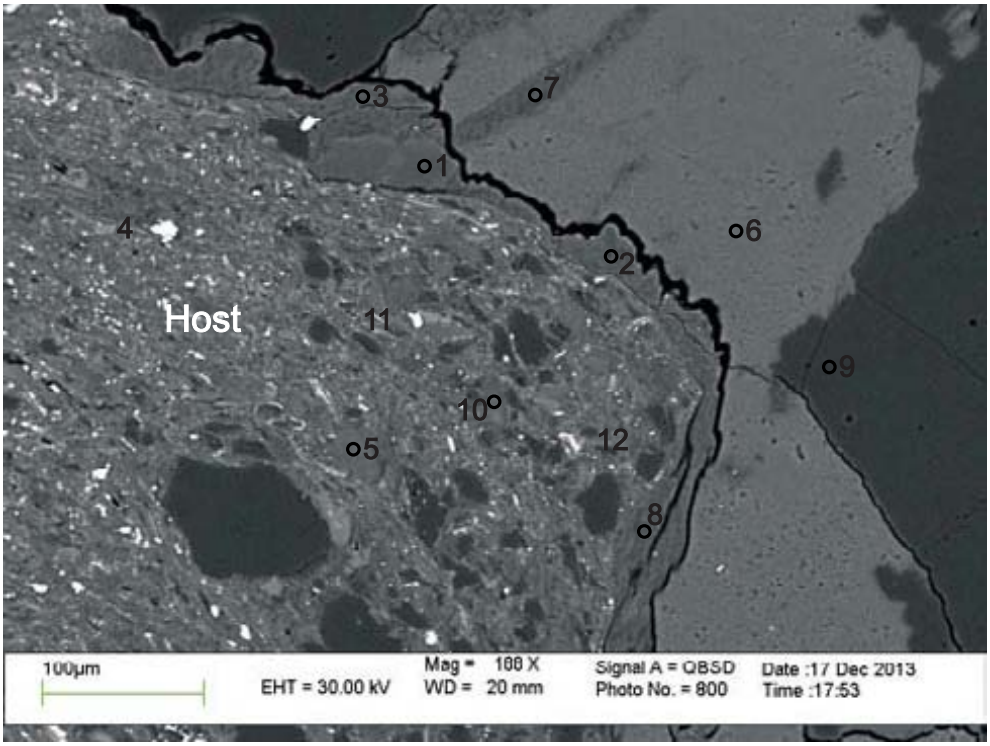

1: Muscovite
2: Muscovite
3: Muscovite
4: Iron oxide + other
5: Muscovite + Chlorite
6: K-feldspar
7: Muscovite (Sericite)
8: Muscovite
9: Quartz
10: Muscovite + Chlorite
11: TiO_2 + other
12: Chlorite + Muscovite

Figure 5: Mic Mac H-86: 4721.13 site 5. Contact between the lithic clast and the host rock.

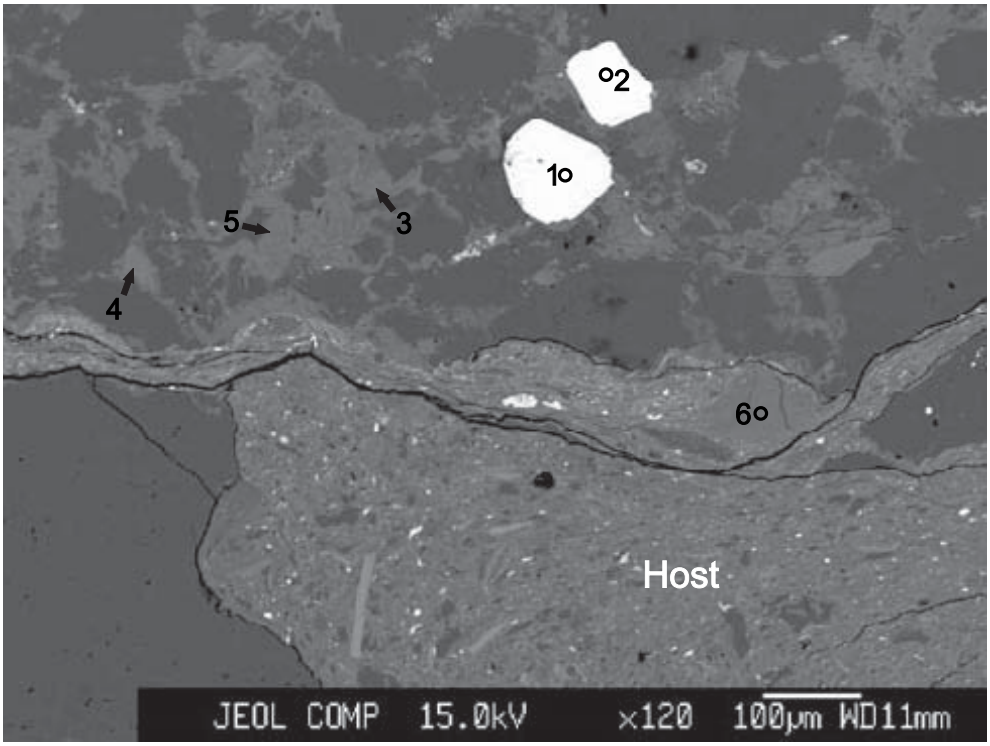

1: Magnetite
2: Magnetite
3-6: Muscovite + Chlorite

Figure 6: Electron microprobe analyses for Mic Mac H-86 4721.13 site 6 (from Fig. 1). Lithic clast composed of quartz (see Fig. 1, and Table 1D), muscovite, chlorite, and magnetite. Clast is in contact with a muddy host.

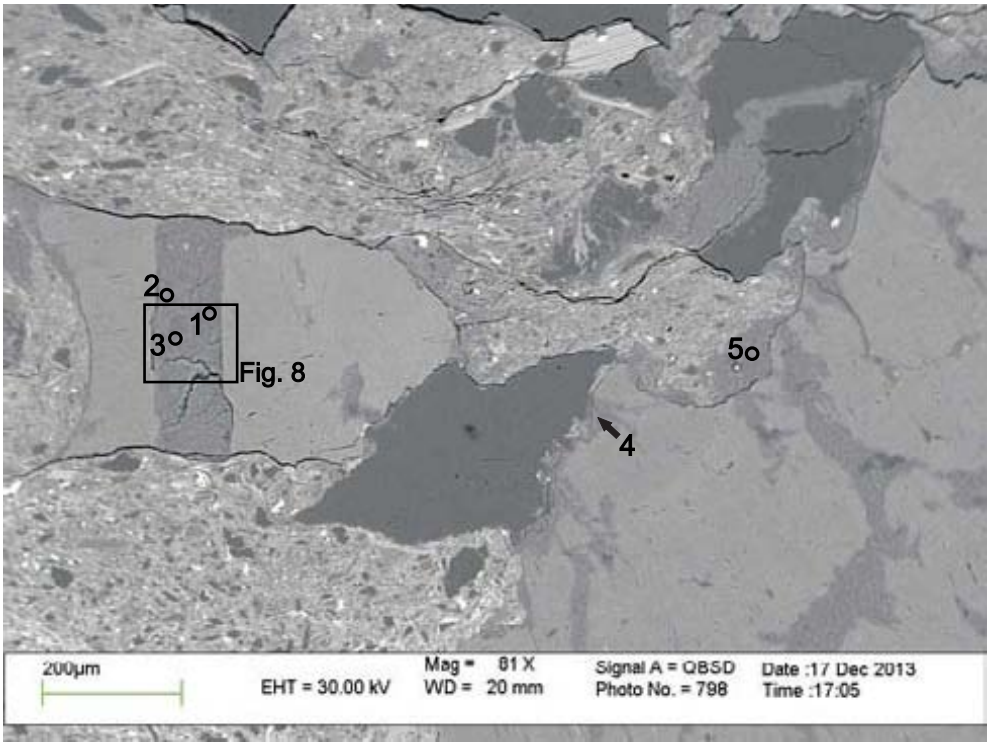

1-3: Muscovite + Chlorite
4-5: Muscovite

Figure 7: Electron microprobe analyses for Mic Mac H-86 4721.13 site 7 (from Fig. 3). Fine grained muscovite and chlorite fills in fracture within a detrital K-feldspar grain (see Fig. 8 for zoomed in image).

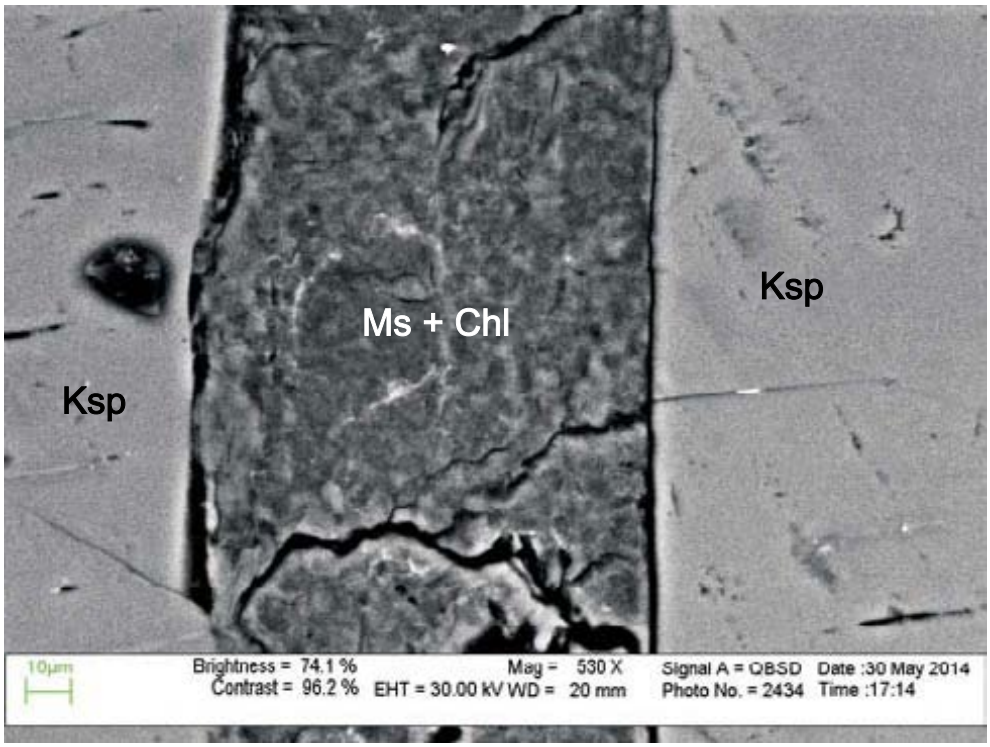

Figure 8: Mic Mac H-86: 4721.13 site 6. Fine grained muscovite and chlorite fills in a fracture in detrital K-feldspar grain.

Table 1D: Scanning electron microscope chemical analyses for representative sites for Mic Mac H-86 well at 4721.13m depth

Sample	Site	Position	Mineral	SiO_2	TiO_2	Al_2O_3	FeO	MnO	MgO	Na_2O	K_2O	Cl	BaO	Total	Actual Total
H-86-4721.13	1	1	Magnetite	0.75			99.24							100.00	78.37
H-86-4721.13	1	2	Magnetite	0.90			99.10							100.00	79.87
H-86-4721.13	1	3	Quartz	99.99										100.00	126.58
H-86-4721.13	1	4	Quartz	99.99										100.00	124.03
H-86-4721.13	1	5	Muscovite + Chlorite	51.30		30.25	7.69	0.14	2.84		7.79			100.00	108.01
H-86-4721.13	1	6	Muscovite + Chlorite	52.45	0.32	30.50	4.18		1.81		10.77			100.00	111.81
H-86-4721.13	1	7	Muscovite + Iron Oxide	19.87	1.58	15.95	58.75		0.51	0.54	2.77			100.00	99.14
H-86-4721.13	1	8	Chlorite	31.95		20.37	15.10	0.43	16.79		0.37			85.00	102.38
H-86-4721.13	1	9	Chlorite	30.73		21.56	16.49	0.29	15.38		0.56			85.00	103.93
H-86-4721.13	1	10	Muscovite + Chlorite	52.28	0.53	28.25	8.01		2.65		8.12	0.13		100.00	104.72
H-86-4721.13	1	11	Muscovite	48.48		33.70	0.96		0.49	1.92	7.45			93.00	102.36
H-86-4721.13	2	1	Quartz + TiO2	20.02	75.85	2.21	1.26				0.51	0.14		100.00	106.00
H-86-4721.13	2	2	Muscovite	47.57		34.95	0.56		0.31	1.54	8.07			93.00	114.17
H-86-4721.13	2	3	Quartz	98.81		0.60	0.42				0.17			100.00	114.54
H-86-4721.13	2	4	Biotite	42.57	3.02	19.39	15.17	0.21	11.28		8.25	0.13		100.00	108.22
H-86-4721.13	2	5	Muscovite + Chlorite	53.39	0.25	29.46	5.61		2.14	0.28	8.85			100.00	109.09
H-86-4721.13	2	6	Muscovite + Chlorite	52.99	0.25	31.16	3.69		1.74	0.35	9.83			100.00	106.61
H-86-4721.13	2	7	Muscovite + Chlorite	57.05		25.91	3.94		2.64	0.31	10.17			100.00	107.71
H-86-4721.13	2	8	Muscovite + Chlorite	52.41	0.52	29.46	6.86		1.81	0.35	8.60			100.00	109.46
H-86-4721.13	2	9	Muscovite + Chlorite	55.85	0.30	30.14	3.37		1.36	0.40	8.56			100.00	111.78
H-86-4721.13	2	10	Chlorite + other	43.77	2.14	20.50	16.29	0.26	9.02		8.03			100.00	109.59
H-86-4721.13	3	1	Muscovite	52.32		27.85	2.58		2.02	0.35	7.76	0.13		93.00	98.70
H-86-4721.13	3	2	K-feldspar	65.82		18.35				1.39	13.82		0.60	100.00	111.64
H-86-4721.13	3	3	Quartz	99.99										100.00	116.20
H-86-4721.13	3	4	K-feldspar (Microcline)	66.49		17.97				0.57	14.97			100.00	120.58
H-86-4721.13	3	5	Muscovite	50.37		29.49	2.02		1.36		9.78			93.00	108.93
H-86-4721.13	3	6	Chlorite + other	40.17		26.57	18.65	0.30	12.19		2.11			100.00	100.85
H-86-4721.13	3	7	Quartz	98.40		0.91	0.27				0.41			100.00	121.16
H-86-4721.13	3	8	Muscovite + Chlorite	53.27		30.88	4.71		1.44	0.31	9.27	0.12		100.00	105.74
H-86-4721.13	3	9	Muscovite + Chlorite	50.87	0.67	28.38	8.79		2.27	0.30	8.71			100.00	111.11
H-86-4721.13	3	10	Muscovite	50.91		29.75	1.80		1.45		9.08			93.00	121.03
H-86-4721.13	3	11	Muscovite + other	44.07	2.00	21.65	16.62	0.15	7.06		8.46			100.00	104.21

Table 1D: Scanning electron microscope chemical analyses for representative sites for Mic Mac H-86 well at 4721.13m depth

Sample	Site	Position	Mineral	SiO_2	TiO_2	Al_2O_3	FeO	MnO	MgO	Na_2O	K_2O	Cl	BaO	Total	Actual Total
H-86-4721.13	4	1	Biotite	41.97	1.93	19.14	17.56	0.17	11.04		8.05	0.14		100.00	104.35
H-86-4721.13	4	2	Altered Ilmenite + other	15.96	45.80	10.54	23.94	0.26	1.14		2.35			100.00	96.77
H-86-4721.13	4	3	Chlorite + Muscovite	39.53	1.80	22.69	24.70	0.19	3.70	0.49	6.88			100.00	107.22
H-86-4721.13	4	4	Albite	68.01		19.22	0.24			12.13	0.40			100.00	117.30
H-86-4721.13	4	5	Muscovite + Chlorite	59.68	0.25	26.21	3.67		2.09		8.12			100.00	108.00
H-86-4721.13	4	6	Muscovite + Chlorite	52.13	0.32	31.40	3.40		1.69	0.55	10.52			100.00	109.15
H-86-4721.13	4	7	Muscovite + Chlorite	47.98	0.25	29.63	7.47		6.65	0.28	7.72			100.00	107.83
H-86-4721.13	4	8	Iron oxide + other	24.04	1.67	16.33	53.22	0.50	0.65	0.65	2.94			100.00	108.30
H-86-4721.13	4	9	Muscovite	48.01	0.47	30.64	2.39		1.17	0.69	9.63			93.00	111.95
H-86-4721.13	4	10	Muscovite + Chlorite	52.17	0.27	30.14	4.73		1.79		10.90			100.00	110.46
H-86-4721.13	4	11	Biotite	42.48	1.62	19.07	17.50		11.24		7.94	0.14		100.00	98.66
H-86-4721.13	4	12	Altered Ilmenite	5.11	41.78	2.51	49.79	0.30			0.52			100.00	89.30
H-86-4721.13	4	13	Muscovite	47.87	0.28	29.65	4.05		2.04		9.10			93.00	105.05
H-86-4721.13	4	14	Muscovite	46.54	0.67	27.28	7.98		2.06	0.36	8.13			93.00	107.02
H-86-4721.13	4	15	Quartz + TiO2	8.39	83.97		7.29				0.17	0.17		100.00	104.07
H-86-4721.13	5	1	Muscovite	47.35		34.08	0.88			0.33	10.36			93.00	109.80
H-86-4721.13	5	2	Muscovite	50.57		30.31	1.93		1.08		9.10			93.00	108.60
H-86-4721.13	5	3	Muscovite	50.69		29.91	1.79		1.36		9.23			93.00	107.61
H-86-4721.13	5	4	Iron oxide + other	12.43	1.53	8.31	74.29	1.15		0.66	1.61			100.00	85.02
H-86-4721.13	5	5	Muscovite + Chlorite	52.82	0.18	31.27	3.37		1.87	0.66	9.84			100.00	106.77
H-86-4721.13	5	6	K-feldspar	66.55		17.91				0.32	15.21			100.00	122.80
H-86-4721.13	5	7	Muscovite (Sericite)	51.29		29.79	1.52		1.54		8.87			93.00	114.37
H-86-4721.13	5	8	Muscovite	50.55		30.14	2.12		1.08		9.13			93.00	108.79
H-86-4721.13	5	9	Quartz	99.99										100.00	125.78
H-86-4721.13	5	10	Muscovite + Chlorite	52.95		30.50	4.19		1.94		10.44			100.00	110.06
H-86-4721.13	5	11	TiO2 + other	6.59	83.79	4.46	2.89		1.63		0.66			100.00	98.60
H-86-4721.13	5	12	Chlorite + Muscovite	43.32	0.65	25.94	21.06	0.28	1.59	0.80	6.35			100.00	105.58

Table 2D: Electron microprobe chemical analyses of iron oxides and micas from representative sites for Mic Mac H-86 well at 4721.13m depth

Sample	Figure	Position	Mineral	No.	SiO_2	TiO_2	Al_2O_3	FeO	MnO	MgO	CaO	Na_2O	K_2O	Cr_2O_3	V_2O_3	Total
4721.13	6	1	Magnetite	51	0.34	0.01	0.05	90.09	0.06	0.00	0.02	-	-	0.01	0.07	90.64
4721.13	6	2	Magnetite	52	0.11	0.04	0.06	90.43	0.00	0.02	0.00	-	-	0.00	0.05	90.72
4721.13	6	3	Muscovite + Chlorite	53	40.60	0.22	27.06	8.58	0.06	1.79	0.11	0.22	8.76	0.01	-	87.41
4721.13	6	4	Muscovite + Chlorite	54	42.24	0.25	27.58	9.02	0.06	1.84	0.10	0.14	6.83	0.02	-	88.07
4721.13	6	5	Muscovite + Chlorite	55	42.52	0.29	27.95	9.22	0.06	1.83	0.08	0.12	5.74	0.00	-	87.80
4721.13	6	6	Muscovite + Chlorite	56	43.37	0.28	28.40	9.27	0.06	1.84	0.09	0.12	4.85	0.01	-	88.28
4721.13	7	1	Muscovite + Chlorite	57	49.94	0.03	29.89	4.53	0.05	2.09	0.53	0.31	8.41	0.00	-	95.77
4721.13	7	2	Muscovite + Chlorite	58	50.64	0.03	29.88	4.52	0.05	2.11	0.47	0.29	8.22	0.00	-	96.20
4721.13	7	3	Muscovite + Chlorite	59	51.03	0.03	30.03	4.55	0.05	2.08	0.48	0.28	8.05	0.00	-	96.59
4721.13	7	4	Muscovite	60	47.90	0.00	31.41	1.76	0.02	1.57	0.12	0.12	8.96	0.00	-	91.86
4721.13	7	5	Muscovite	61	48.80	0.00	32.28	1.98	0.02	1.49	0.13	0.16	8.64	0.00	-	93.49

Appendix 2A: Scanning Electron Microscope Backscattered Electron Images for Mohican I-100 well with EDS Mineral Analyses Sample 3691.23A

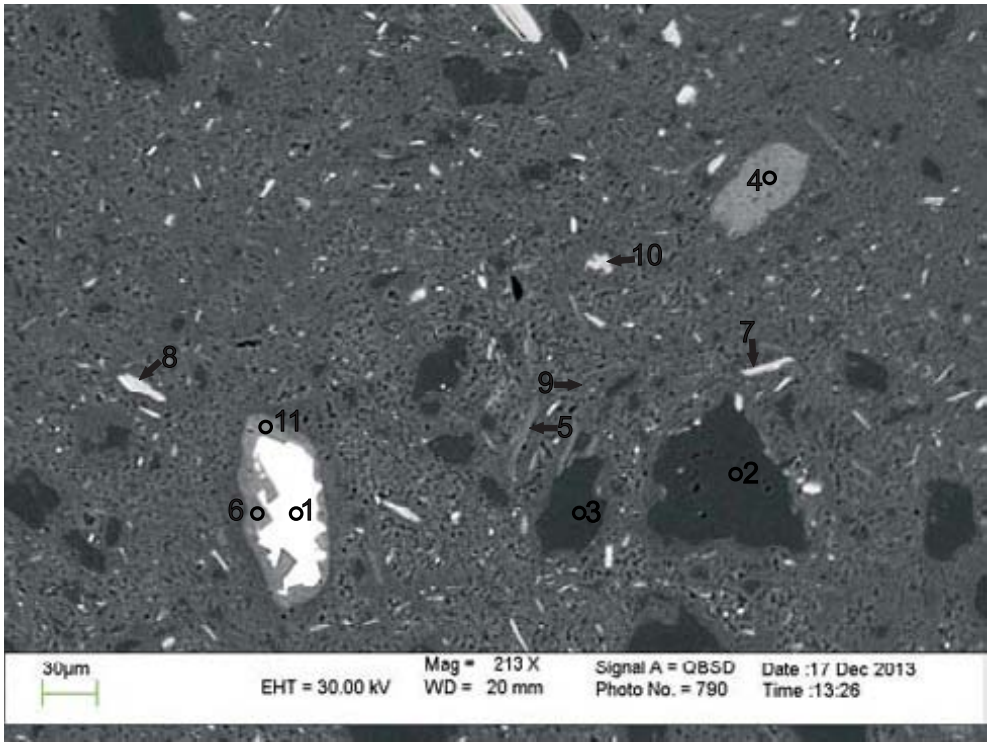

1: Barite + Dolomite
2: Quartz + other
3: Dolomite + Illite
4: Dolomite + Illite + other
5: Quartz
6: Barite + Dolomite
7: Quartz + Dolomite
8: Dolomite + Illite
9: Dolomite + Illite + other
10: Dolomite + Muscovite
11: Barite

Figure 1: Mohican I-100: 3691.23A site 1. Fine grained carbonate pocket, mainly of dolomite. This pocket is situated within a larger muddy host.

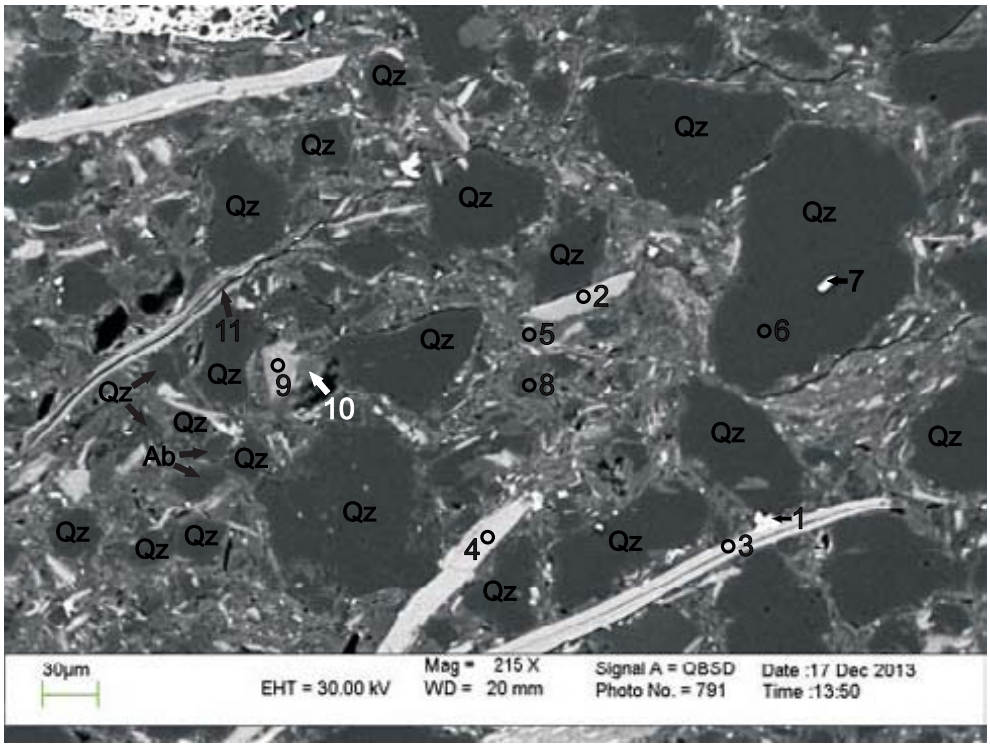

1: Ilmenite + Quartz
2: Chlorite
3: Biotite
4: Chlorite
5: Muscovite + Chlorite
6: Quartz
7: Ilmenite + Quartz
8: Albite
9: Chlorite + Illite
10: Muscovite + Chlorite
11: Muscovite + Chlorite

Figure 2: Mohican I-100: 3691.23A site 2. Framework grains of mostly quartz with minor amounts of albite situated within a muddy host composed mainly of muscovite and chlorite.

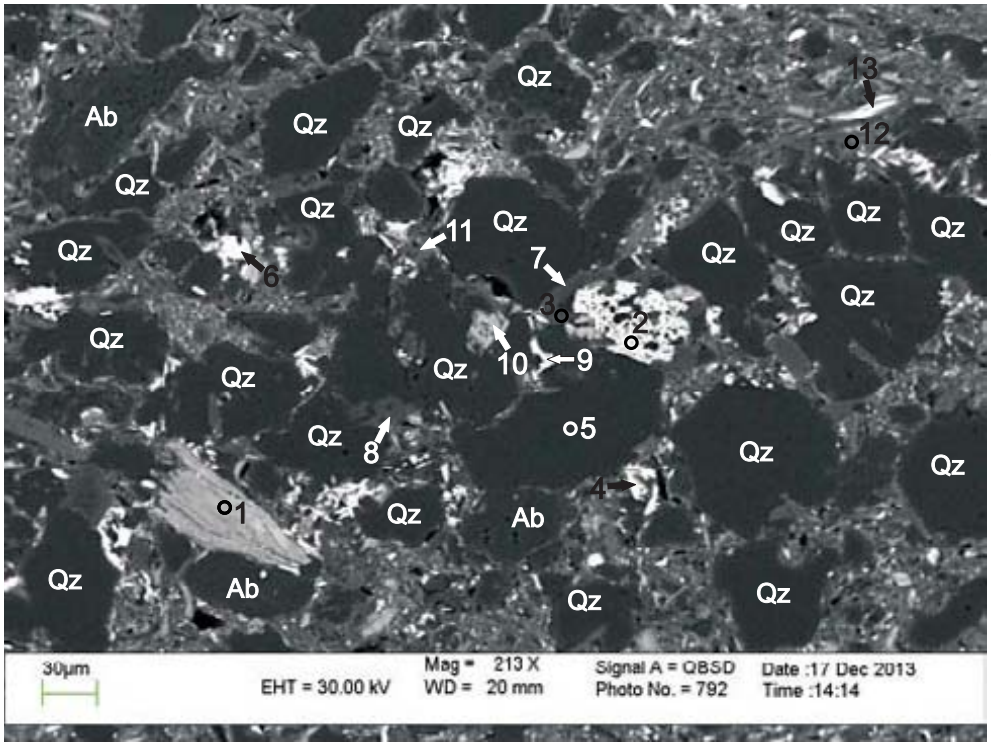

1: Chlorite
2: Altered Ilmenite + Muscovite
3: Muscovite
4: Chlorite + Muscovite
5: Quartz
6: Altered Ilmenite + Quartz
7: Muscovite
8: Muscovite
9: Quartz + Iron oxide + other
10: Chlorite
11: Muscovite + Chlorite
12: K-feldspar
13: Chlorite

Figure 3: Mohican I-100: 3691.23A site 3. Framework grains, mostly quartz hosted in a muddy matrix. Other detrital grains include chlorite (analysis 1) and ilmenite which has been altered and contains inclusions of muscovite (analysis 2).

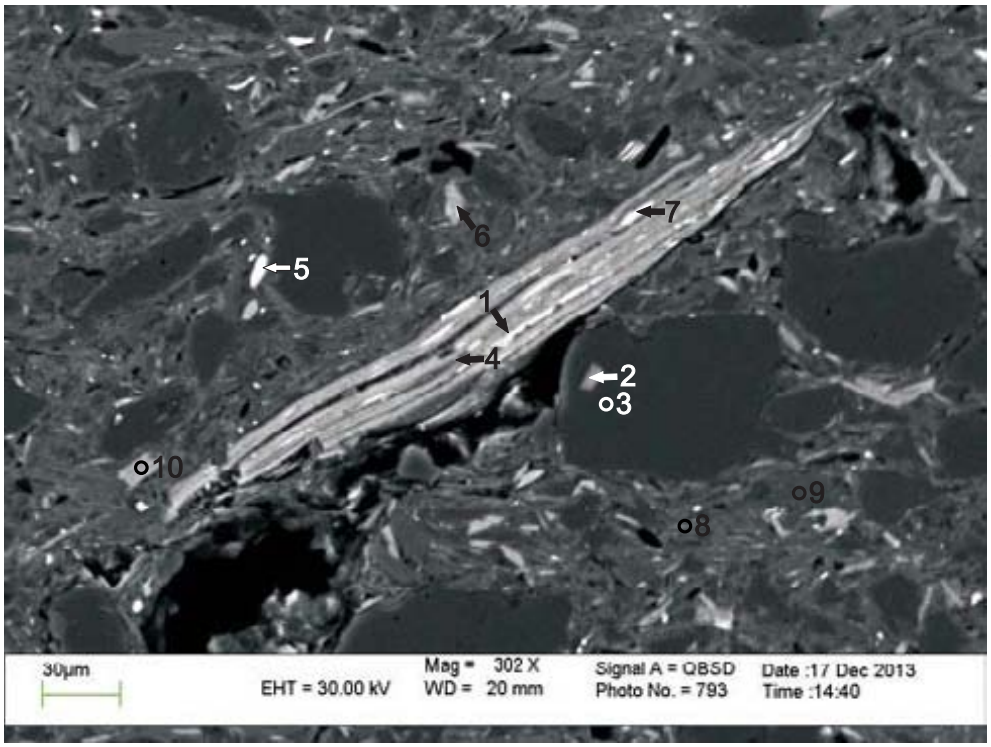

1: Chlorite + Muscovite
2: Chlorite + Quartz
3: Quartz
4: Illite
5: Chlorite + Muscovite
6: Chlorite + Muscovite
7: Chlorite + Muscovite
8: Muscovite + Chlorite
9: Muscovite
10: Chlorite

Figure 4: Mohican I-100: 3691.23A site 4. Detrital muscovite grain, that has been chloritized, sits within a muddy matrix composed of much finer grains of muscovite and chlorite.

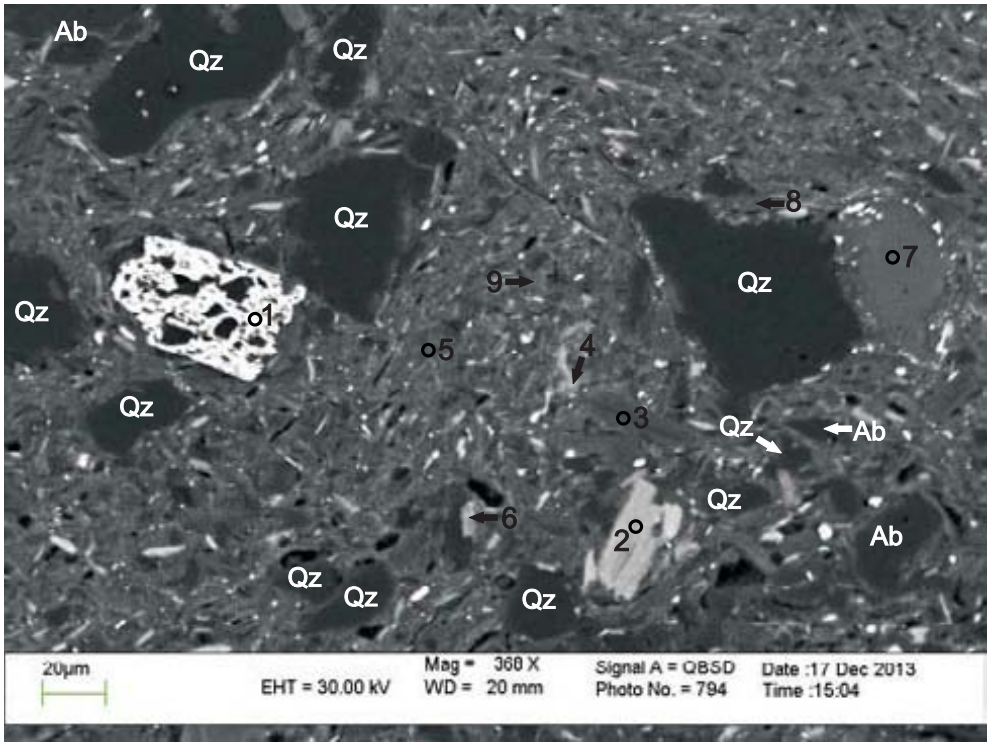

1: Altered Ilmenite + Muscovite
2: Chlorite
3: Muscovite
4: Illite + Chlorite
5: Muscovite + Chlorite
6: Illite + Chlorite
7: K-feldspar
8: Muscovite + Chlorite
9: Muscovite + Chlorite

Figure 5: Mohican I-100: 3691.23A site 5. Matrix-supported grains of altered ilmenite (analysis 1) with inclusions of muscovite situated among quartz and K-feldspar in a matrix of muscovite and chlorite.

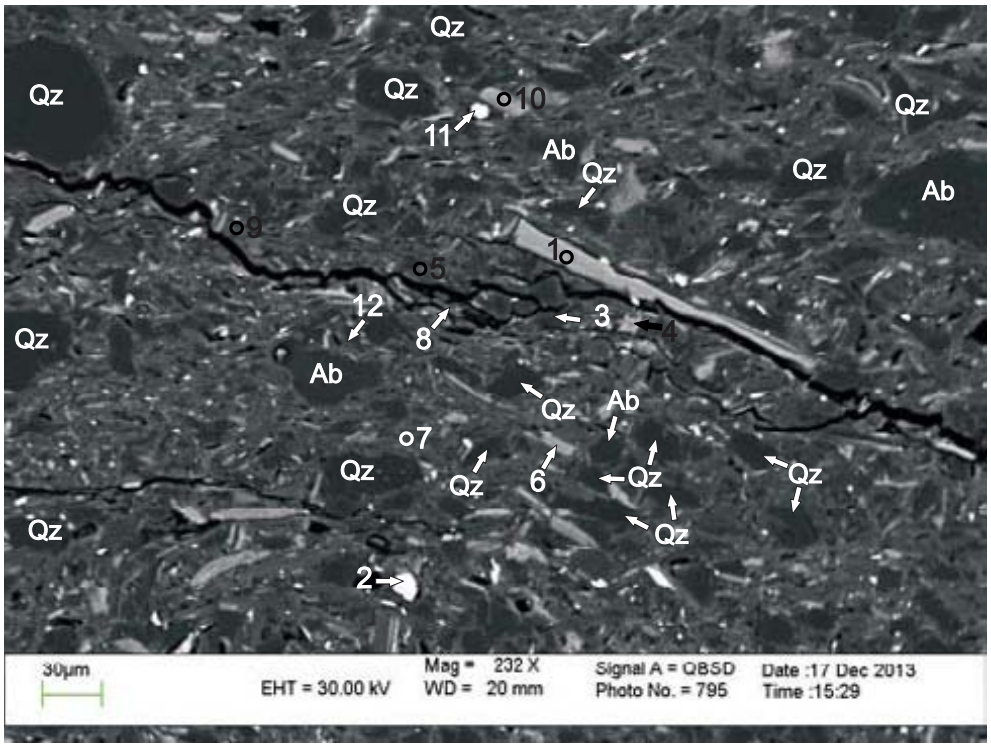

1: Biotite
2: Iron oxide + Muscovite + Chlorite
3: Quartz
4: Anhydrite + Muscovite
5: Muscovite + Chlorite
6: Chlorite
7: Muscovite + Chlorite
8: Muscovite
9: Muscovite
10: Chlorite
11: Iron oxide + Muscovite
12: Muscovite + Chlorite

Figure 6: Mohican I-100: 3691.23A site 6. Smaller grains of detrital minerals of quartz, biotite and albite, siting within a muddy matrix of muscovite and chlorite. Iron oxides present (analyses 2 and 11) are likely diagenetic as they are not hosted within a clast, and they appear to have formed in void space.

Table 1A: Scanning electron microscope chemical analyses of minerals from representative sites for Mohican I-100 well at 3691.23Am depth

Sample	Site	Position	Mineral	SiO_2	TiO_2	Al_2O_3	FeO	MnO	MgO	CaO	Na_2O	K_2O	P_2O_5	SO_3	Cl	V_2O_5	SrO	BaO	Total	Actual Total
I-100-3691.23A	1	1	Barite + Dolomite				0.68		3.02	2.88				43.25			8.53	41.66	100.00	97.00
I-100-3691.23A	1	2	Quartz + other	97.38		0.51	0.22		0.60	1.15		0.16							100.00	107.25
I-100-3691.23A	1	3	Dolomite + Illite	23.45		11.30	6.07		21.03	35.46		2.70							100.00	69.61
I-100-3691.23A	1	4	Dolomite + Illite + other	40.28		6.16	3.23		16.93	32.04		1.37							100.00	81.00
I-100-3691.23A	1	5	Quartz	99.99															100.00	115.30
I-100-3691.23A	1	6	Barite + Dolomite				2.56		2.82	9.98				35.31			9.50	39.84	100.00	98.85
I-100-3691.23A	1	7	Quartz + Dolomite	85.40		1.51	1.53		2.32	8.55		0.70							100.00	102.91
I-100-3691.23A	1	8	Dolomite + Illite	16.54	1.95	8.67	6.00		22.73	42.21		1.90							100.00	63.58
I-100-3691.23A	1	9	Dolomite + Illite + other	15.40	20.42	7.88	3.45		20.69	30.42		1.75							100.00	76.19
I-100-3691.23A	1	10	Dolomite + Muscovite	34.83		12.04	3.52		13.68	28.98	5.45	1.51							100.00	82.99
I-100-3691.23A	1	11	Barite			0.47				0.38				40.95			11.05	47.17	100.00	103.34
I-100-3691.23A	2	1	Ilmenite + Quartz	8.58	56.10	1.30	31.35	2.23				0.41							100.00	95.62
I-100-3691.23A	2	2	Chlorite	31.11		21.76	21.51		9.55		0.30	0.77							85.00	96.84
I-100-3691.23A	2	3	Biotite	42.70	3.07	19.92	17.83	0.22	7.38			8.72			0.15				100.00	106.90
I-100-3691.23A	2	4	Chlorite	25.08		24.14	27.72	0.16	7.90										85.00	93.63
I-100-3691.23A	2	5	Muscovite + Chlorite	51.17	0.25	33.96	3.43		1.38	0.45	1.42	7.95							100.00	104.35
I-100-3691.23A	2	6	Quartz	99.99															100.00	118.30
I-100-3691.23A	2	7	Ilmenite + Quartz	31.08	42.29		24.16	2.45											100.00	118.14
I-100-3691.23A	2	8	Albite	63.94		21.90	1.94		0.55	0.46	9.38	1.83							100.00	113.88
I-100-3691.23A	2	9	Chlorite + Illite	35.45		23.54	18.42		11.82	3.75		2.37	4.63						100.00	91.68
I-100-3691.23A	2	10	Muscovite + Chlorite	51.51	0.45	33.71	3.19		1.14		0.50	9.49							100.00	106.49
I-100-3691.23A	2	11	Muscovite + Chlorite	49.65	1.18	26.13	9.57	0.15	5.12		0.51	7.67							100.00	100.78
I-100-3691.23A	3	1	Chlorite	29.13		22.10	24.71		8.26			0.78							85.00	92.15
I-100-3691.23A	3	2	Altered Ilmenite + Muscovite	7.74	78.98	3.89	7.22		1.54			0.63							100.00	91.81
I-100-3691.23A	3	3	Muscovite	48.22	0.31	33.56	0.91		0.30		1.84	7.85							93.00	105.65
I-100-3691.23A	3	4	Chlorite + Muscovite	31.70	1.22	21.88	39.06				0.59	5.53							100.00	98.19
I-100-3691.23A	3	5	Quartz	99.99															100.00	115.99
I-100-3691.23A	3	6	Altered Ilmenite + Quartz	4.96	93.33	0.62	0.86					0.24							100.00	98.20
I-100-3691.23A	3	7	Muscovite	49.34	0.40	33.13	0.63				1.53	7.98							93.00	105.38
I-100-3691.23A	3	8	Muscovite	48.83	0.25	33.80	0.64				1.24	8.26							93.00	105.08
I-100-3691.23A	3	9	Quartz + Iron oxide + other	23.79	3.00	6.42	62.54		1.39		1.89	0.67				0.29			100.00	98.51
I-100-3691.23A	3	10	Chlorite	27.09		23.02	23.90	0.23	10.43			0.34							85.00	98.37
I-100-3691.23A	3	11	Muscovite + Chlorite	50.85	0.55	33.88	3.07		1.38		0.55	9.73							100.00	103.83
I-100-3691.23A	3	12	K-feldspar	63.32	0.28	19.56	2.51		0.58		1.01	12.73							100.00	111.33
I-100-3691.23A	3	13	Chlorite	22.73	0.44	16.61	36.61		7.68			0.94							85.00	104.70
I-100-3691.23A	4	1	Chlorite + Muscovite	32.34	3.44	15.00	35.34		7.06			6.62			0.2				100.00	96.32
I-100-3691.23A	4	2	Chlorite + Quartz	55.02		15.82	17.77	0.37	11.03										100.00	111.07
I-100-3691.23A	4	3	Quartz	99.86			0.14												100.00	118.17
I-100-3691.23A	4	4	Illite	44.13	2.20	18.79	11.50		6.00		0.42	6.98							90.00	100.48
I-100-3691.23A	4	5	Chlorite + Muscovite	26.03	1.50	16.42	51.09		1.21			3.75							100.00	104.20

Table 1A: Scanning electron microscope chemical analyses of minerals from representative sites for Mohican I-100 well at 3691.23Am depth

Sample	Site	Position	Mineral	SiO_2	TiO_2	Al_2O_3	FeO	MnO	MgO	CaO	Na_2O	K_2O	P_2O_5	SO_3	Cl	V_2O_5	SrO	BaO	Total	Actual Total
I-100-3691.23A	4	6	Chlorite + Muscovite	34.91		26.38	27.12		10.43			1.17							100.00	94.52
I-100-3691.23A	4	7	Chlorite + Muscovite	35.47	2.69	16.93	30.67		8.39			5.85							100.00	118.76
I-100-3691.23A	4	8	Muscovite + Chlorite	52.37	0.37	27.73	8.19		3.88		0.62	6.83							100.00	102.82
I-100-3691.23A	4	9	Muscovite	48.62	1.10	33.39	0.53				1.57	7.79							93.00	105.41
I-100-3691.23A	4	10	Chlorite	26.35		22.31	24.46	0.23	11.40			0.26							85.00	93.36
I-100-3691.23A	5	1	Altered Ilmenite + Muscovite	11.34	73.09	5.61	7.77		1.54			0.63							100.00	90.84
I-100-3691.23A	5	2	Chlorite	26.73		23.06	24.13	0.26	10.30			0.51							85.00	95.75
I-100-3691.23A	5	3	Muscovite	48.18	0.17	32.63	1.42		0.88		0.44	9.27							93.00	106.35
I-100-3691.23A	5	4	Illite + Chlorite	43.64	0.43	25.72	16.33		8.85		0.32	4.71							100.00	102.12
I-100-3691.23A	5	5	Muscovite + Chlorite	53.76	0.32	29.80	5.52		1.81		1.07	7.75							100.00	103.61
I-100-3691.23A	5	6	Illite + Chlorite	43.15		24.07	22.35		9.09	0.27		1.08							100.00	98.63
I-100-3691.23A	5	7	K-feldspar	65.69		17.91	0.15				0.55	15.68							100.00	113.17
I-100-3691.23A	5	8	Muscovite + Chlorite	53.37	0.23	31.01	4.44		1.51		1.07	8.36							100.00	106.94
I-100-3691.23A	5	9	Muscovite + Chlorite	51.94	0.33	31.91	5.20		1.48		1.12	8.01							100.00	109.01
I-100-3691.23A	6	1	Biotite	42.08	3.64	20.12	16.29	0.28	7.88			9.55			0.14				100.00	103.65
I-100-3691.23A	6	2	Iron oxide + Muscovite + Chlorite	16.32	2.32	8.07	67.69		3.86	0.63		1.07							100.00	87.59
I-100-3691.23A	6	3	Quartz	93.87	0.20	3.95	0.76					1.22							100.00	116.07
I-100-3691.23A	6	4	Anhydrite + Muscovite	12.81		3.85	0.51			29.83	1.21	0.55		51.21					100.00	112.24
I-100-3691.23A	6	5	Muscovite + Chlorite	53.99	0.35	29.63	4.86		1.81	0.88	1.05	7.41							100.00	107.61
I-100-3691.23A	6	6	Chlorite	27.87	0.15	23.18	22.14	0.26	10.45			0.95							85.00	97.19
I-100-3691.23A	6	7	Muscovite + Chlorite	51.62	0.32	33.27	3.80		0.99		1.19	8.82							100.00	107.47
I-100-3691.23A	6	8	Muscovite	48.18	0.26	32.38	2.01		0.84		0.80	8.49							93.00	103.45
I-100-3691.23A	6	9	Muscovite	51.61	0.31	24.74	5.94		2.11	0.47	0.76	7.01							93.00	102.45
I-100-3691.23A	6	10	Chlorite	27.87		21.74	23.66	0.37	10.70			0.64							85.00	96.59
I-100-3691.23A	6	11	Iron oxide + Muscovite	8.60	2.45	5.61	80.62		1.18	0.66		0.88							100.00	90.74
I-100-3691.23A	6	12	Muscovite + Chlorite	61.67	0.58	21.94	6.63		2.44		0.59	6.17							100.00	103.57

Appendix 2B: Scanning Electron Microscope Backscattered Electron Images for Mohican I-100 well with EDS Mineral Analyses Sample 3692.42

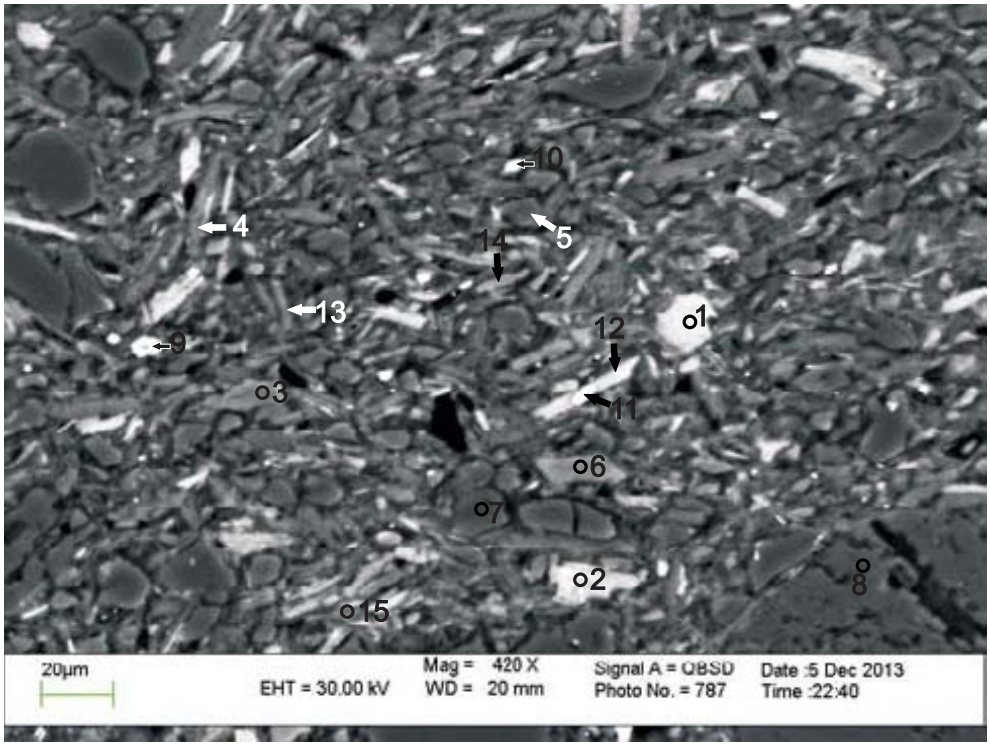

1: Chlorite
2: Chlorite
3: Muscovite
4: Muscovite
5: Quartz
6: Muscovite
7: Albite
8: Albite
9-11: TiO_2 + Muscovite
12: Muscovite + Chlorite
13: Muscovite
14: Illite + Quartz
15: Illite

Figure 1: Mohican I-100: 3692.42 site 1. Dissolution of albite (analysis 8) surrounded by muddy matrix composed of muscovite, illite, and chlorite.

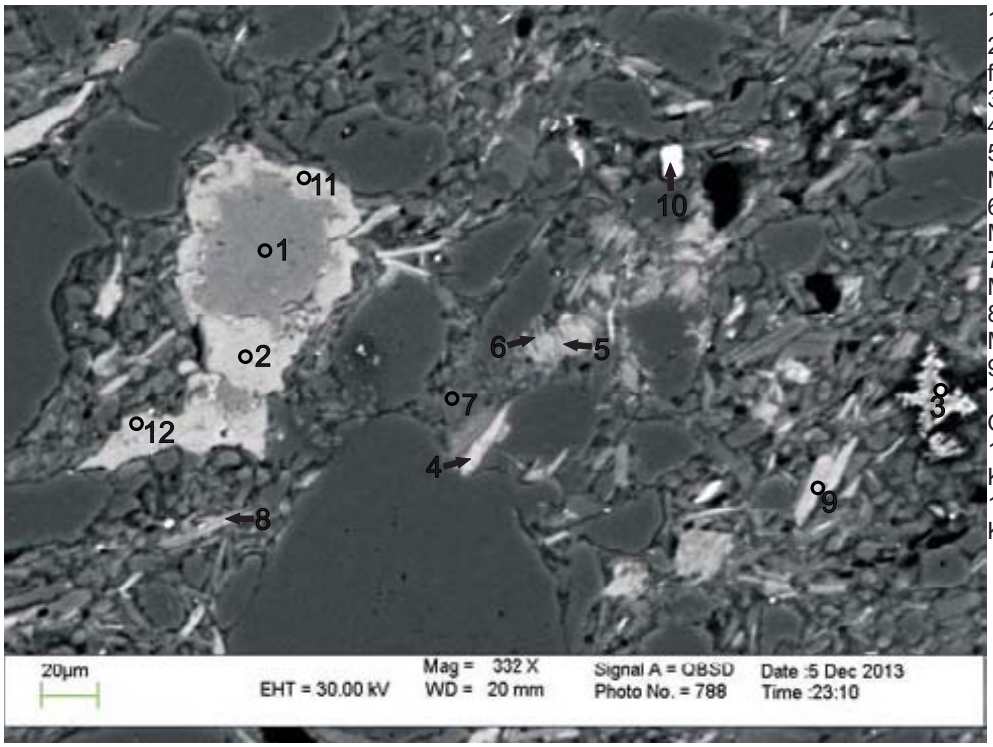

1: K-feldspar
2: Anhydrite + K-feldspar
3: Halite + other
4: Chlorite
5: Chlorite + Muscovite
6: Chlorite + Muscovite
7: K-feldspar + Muscovite
8: Chlorite + Muscovite
9: Chlorite
10: TiO_2 + Quartz
11: Anhydrite + K-feldspar
12: Anhydrite + K-feldspar

Figure 2: Mohican I-100: 3692.42 site 2. Replacement of K-feldspar (analysis 1) by anhydrite (analyses 2 and 11).

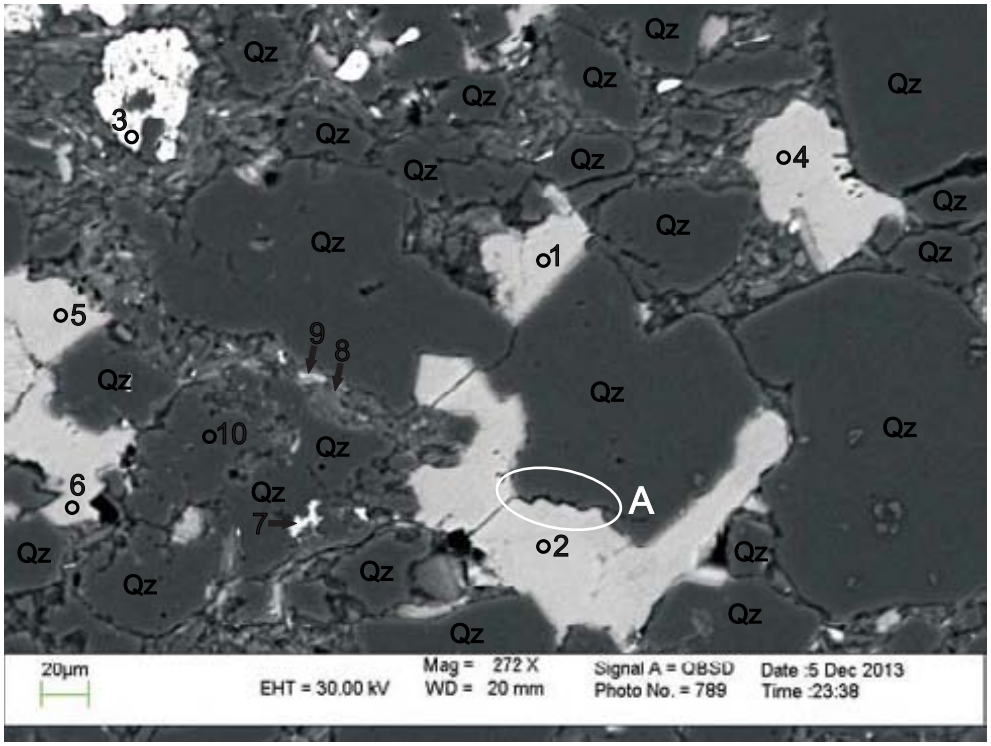

1: Anhydrite
2: Anhydrite
3: Altered Ilmenite + Quartz
4: Anhydrite
5: Anhydrite
6: Anhydrite
7: Altered Ilmenite + Muscovite
8: Muscovite
9: Chlorite + TiO_2
10: Quartz

Figure 3: Mohican I-100: 3692.42 site 3. Quartz dissolution (position A) against anhydrite cement.

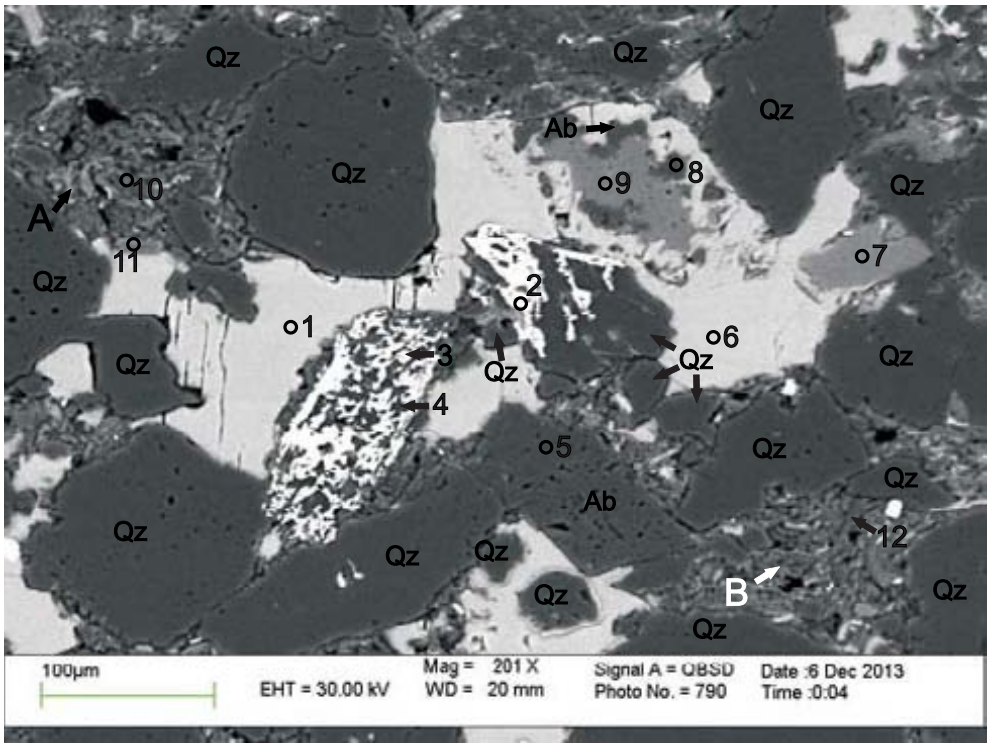

1: Anhydrite
2: Altered Ilmenite + Muscovite
3: Altered Ilmenite + Quartz
4: Quartz + Altered Ilmenite
5: Albite
6: Anhydrite
7: K-feldspar
8: Albite
9: K-feldspar
10: Mix
11: Muscovite
12: Quartz + Muscovite

Figure 4: Mohican I-100: 3692.42 site 4. Framework grains, mainly quartz with minor albite, supported by a muddy matrix (positions A and B) and cemented by anhydrite (analyses 1 and 6). This site is the transition between the matrix-supported area (as seen in Fig. 1) and the area cemented by anhydrite (as seen in Figs. 5-7).

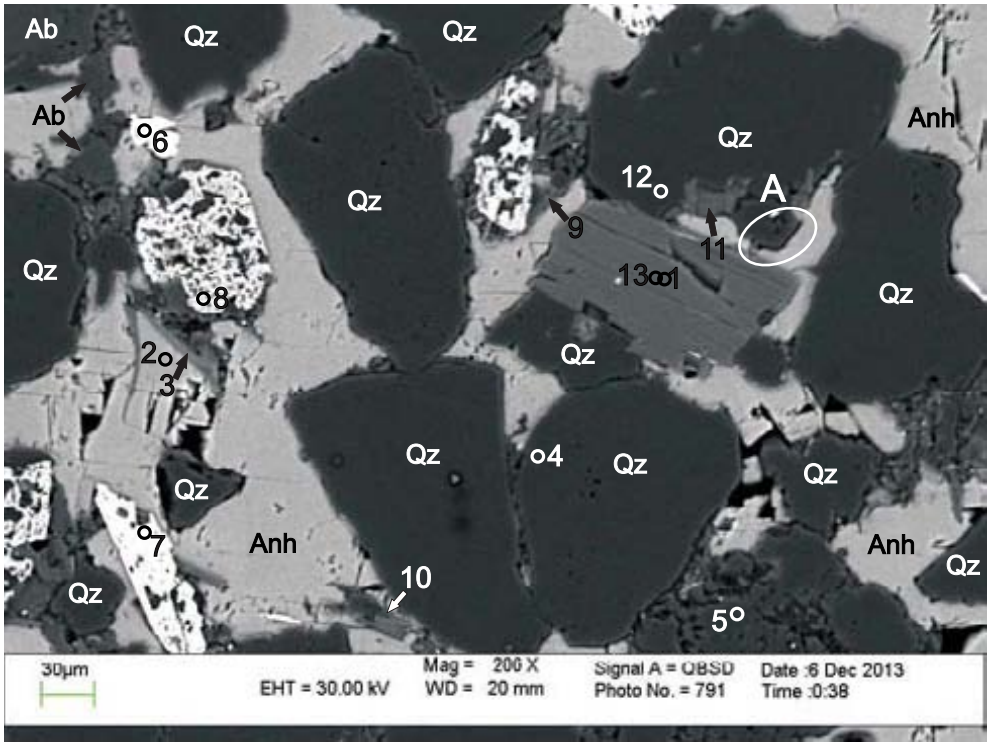

1: Muscovite
2: Anhydrite
3: Muscovite + Anhydrite
4: Quartz
5: Quartz
6: Al-phosphate
7: Altered Ilmenite + other
8: Altered Ilmenite + other
9-11: Muscovite + Chlorite
10: Muscovite + Chlorite
12: Quartz
13: Muscovite

Figure 5: Mohican I-100: 3692.42 site 5. Quartz overgrowths (position A) forming during diagenesis. Framework grains cemented by diageneitc anhydrite. Abundant altered ilmenite grains within this site is characteristic of the sample as a whole.

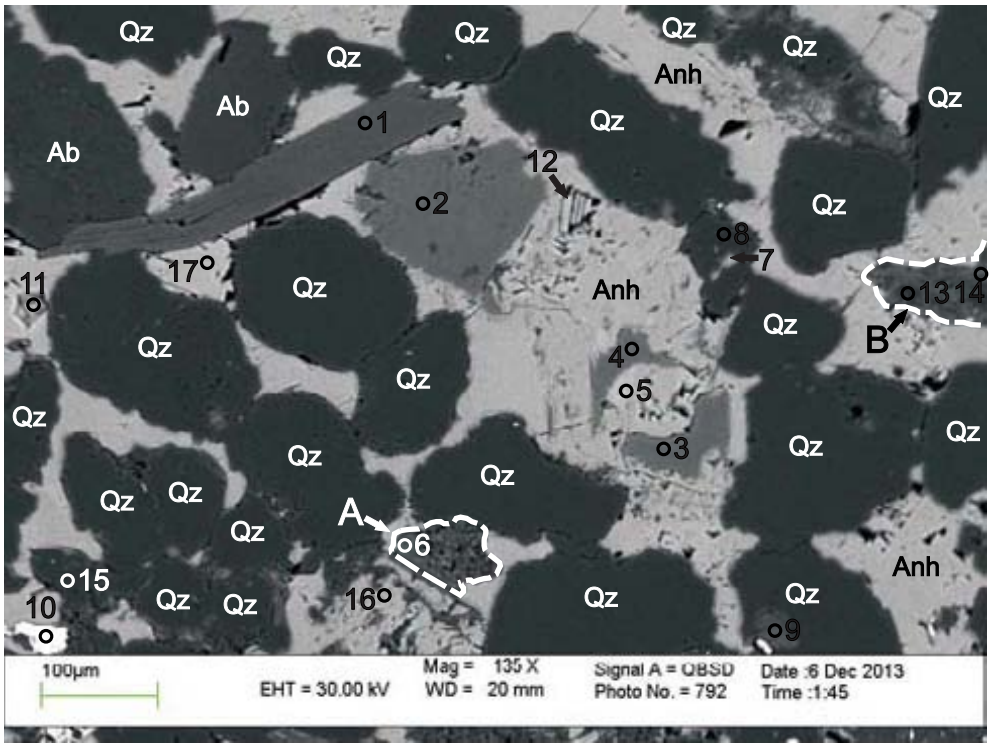

1: Muscovite
2-4: K-feldspar
5: Anhydrite
6: Muscovite
7: Chlorite
8: Quartz
9: Muscovite
10: Altered Ilmenite + Anhydrite
11: Anhydrite
12: Anhydrite
13: Quartz
14: Muscovite
15: Quartz
16: Anhydrite +Muscovite
17: Anhydrite

Figure 6: Mohican I-100: 3692.42 site 6. Replacement of K-feldspar (analyses 3 and 4) by anhydrite cement (analysis 5). Lithic clasts (positions A and B) are composed of muscovite along with chlorite and quartz.

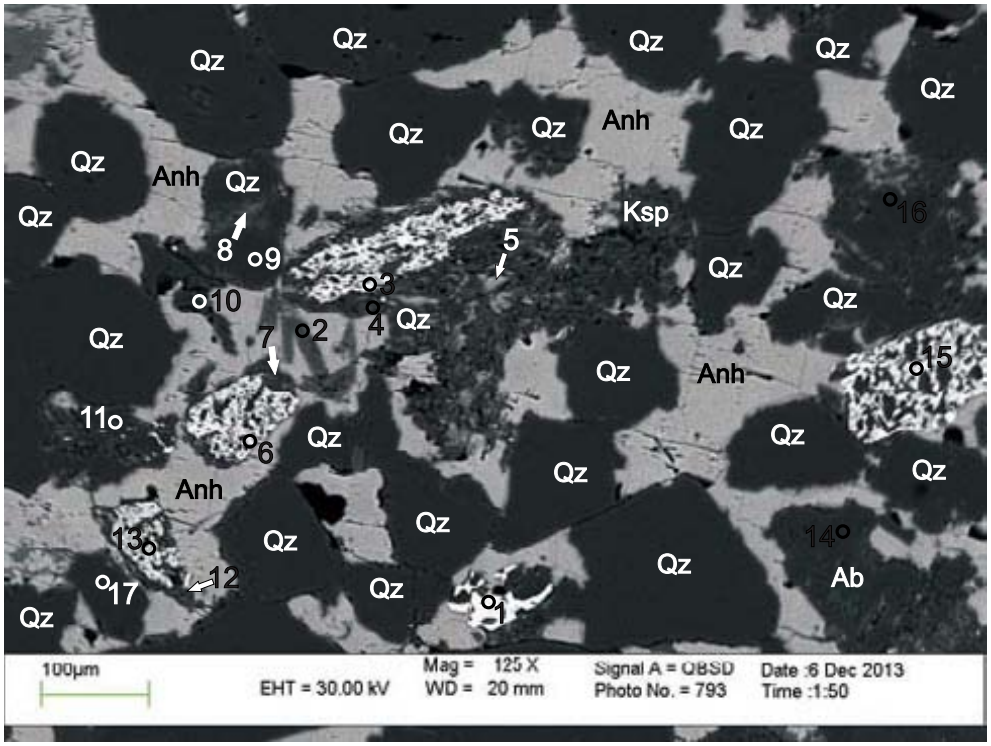

1: Rutile
2: Muscovite
3: Altered Ilmenite
4: Muscovite
5: Chlorite
6: Altered Ilmenite
7: Muscovite
8: Illite
9: Quartz
10: Quartz
11: Quartz + other
12: Muscovite + Chlorite
13: Altered Ilmenite
14: Albite
15: Altered Ilmenite
16: Quartz
17: Quartz

Figure 7: Mohican I-100: 3692.42 site 7. Quartz (analysis 16) and albite (analysis 14) with dissolution voids that have been partly filled by anhydrite.

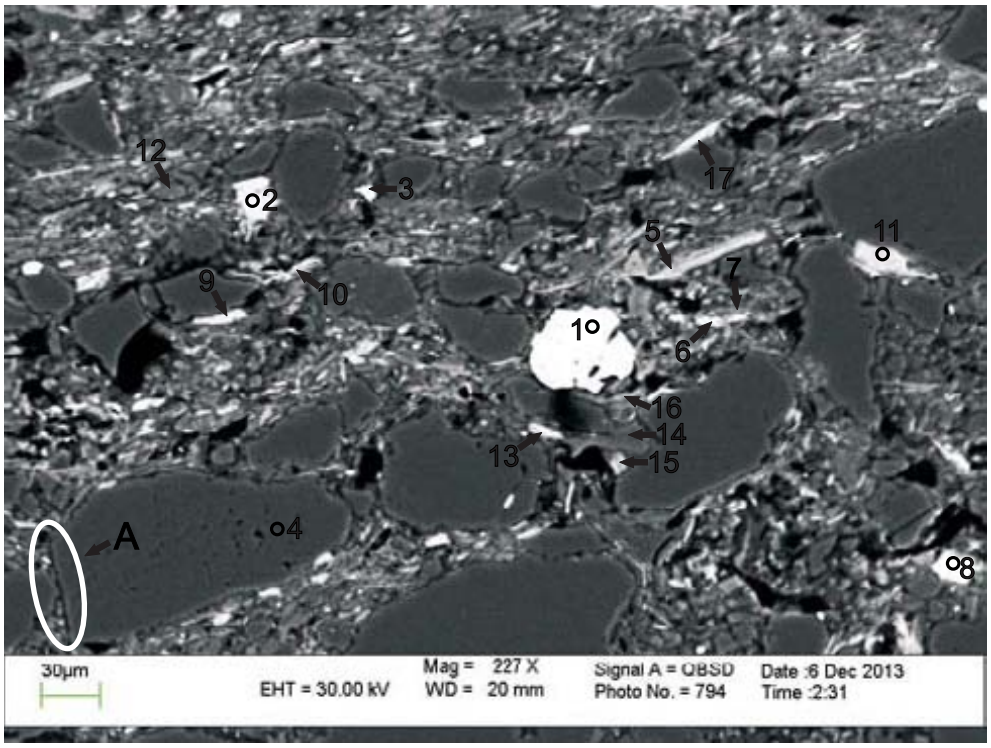

1: Altered Ilmenite
2: Anhydrite
3: Illite + TiO_2
4: Quartz
5: Chlorite
6: Chlorite
7: Muscovite
8: Fluorapatite
9: Chlorite
10: Muscovite + Chlorite
11: Chlorite
12: Muscovite
13: Chlorite
14: Albite
15: Chlorite + Muscovite
16: Muscovite
17: Chlorite + Muscovite

Figure 8: Mohican I-100: 3692.42 site 8. Matrix supported lamination. Quartz (analysis 4) has some dissolution voids as well as overgrowths along a line of dissolution (position A).

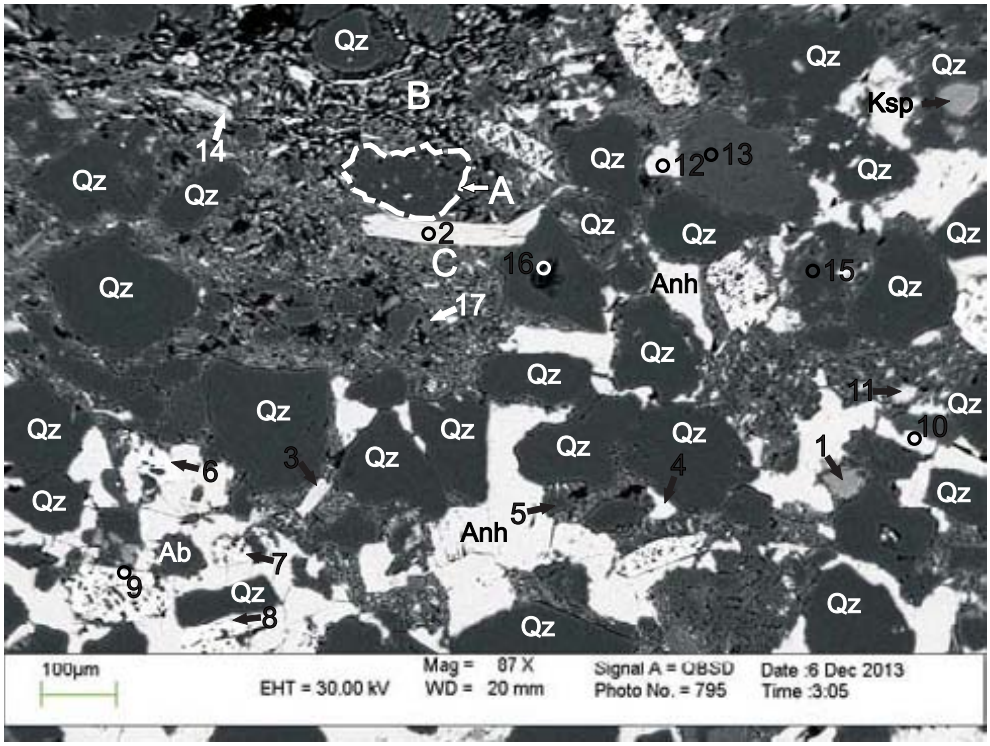

1: K-feldspar
2: Biotite
3: Biotite
4: Anhydrite
5: Quartz
6: Altered Ilmenite
7: Rutile
8: Altered Ilmenite
9: Altered Ilmenite
10: Anhydrite
11: Chlorite
12: Anhydrite
13: Albite
14: Chlorite + Muscovite
15: Quartz
16: Quartz
17: Muscovite

Figure 9: Mohican I-100: 3692.42 site 9. Quartzite clast (position A, and see App. 4B, Fig. 1) enclosed by a muddy matrix (position B). Matrix is becoming more compacted (position C) with lower porosity, perhaps due to compression by growing anhydrite nodules. This compacted matrix serves as a transition zone between all matrix and all cement.

Table 1B: Scanning electron microscope chemical analyses of minerals from representative sites for Mohican I-100 well at 3692.42m depth

Sample	Site	Position	Mineral	SiO_2	TiO_2	Al_2O_3	FeO	MnO	MgO	CaO	Na_2O	K_2O	P_2O_5	SO_3	F	Cl	Cr_2O_3	SrO	BaO	La_2O_3	Ce_2O_3	Nd_2O_3	WO_3	Total	Actual Total
I-100 3692.42	1	1	Chlorite	26.13		23.56	25.08	0.65	9.10			0.47												85.00	104.93
I-100 3692.42	1	2	Chlorite	27.42	1.59	22.21	23.73	0.22	9.46			0.36												85.00	102.63
I-100 3692.42	1	3	Muscovite	47.19	0.54	32.07	1.96		0.85		0.39	9.99												93.00	115.48
I-100 3692.42	1	4	Muscovite	49.84	0.21	30.60	2.74		1.59		1.04	6.97												93.00	121.06
I-100 3692.42	1	5	Quartz	96.73		2.00	0.42		0.25			0.59												100.00	127.79
I-100 3692.42	1	6	Muscovite	48.60	0.49	29.69	2.71		1.19		0.78	9.53												93.00	117.81
I-100 3692.42	1	7	Albite	68.73		18.88				0.28	11.96	0.14												100.00	126.91
I-100 3692.42	1	8	Albite	65.16		21.24	0.22			0.98	10.66	1.75												100.00	128.90
I-100 3692.42	1	9	TiO2 + Muscovite	12.81	75.00	6.22	2.21		1.39	0.38	0.74	1.06				0.18								100.00	96.45
I-100 3692.42	1	10	TiO2 + Muscovite	40.07	38.67	13.25	1.58		0.70	0.28	1.52	2.77			1.18									100.00	124.49
I-100 3692.42	1	11	TiO2 + Muscovite	21.48	35.16	12.75	24.15	0.19	3.08			3.19												100.00	102.87
I-100 3692.42	1	12	Muscovite + Chlorite	45.50	1.10	23.49	15.81		6.73		0.35	7.03												100.00	115.17
I-100 3692.42	1	13	Muscovite	50.37	0.25	30.52	2.17		0.96		1.40	7.33												93.00	119.40
I-100 3692.42	1	14	Illite + Quartz	73.87	0.27	16.12	3.76		1.54		0.46	3.99												100.00	131.17
I-100 3692.42	1	15	Illite	45.32	0.18	22.08	12.00		6.73		0.27	3.44												90.00	111.63
I-100 3692.42	2	1	K-feldspar	65.84		17.91					0.54	15.06							0.65					100.00	121.22
I-100 3692.42	2	2	Anhydrite + K-feldspar	3.29		1.00				35.85		0.81		59.06										100.00	121.02
I-100 3692.42	2	3	Halite + other	15.59	0.25	5.59	1.34				37.13	11.61		0.40		28.10								100.00	129.65
I-100 3692.42	2	4	Chlorite	28.33		23.94	24.96	0.15	6.99			0.61												85.00	106.21
I-100 3692.42	2	5	Chlorite + Muscovite	39.06		27.23	23.40	0.15	7.89		0.43	1.83												100.00	103.50
I-100 3692.42	2	6	Chlorite + Muscovite	42.72		27.72	19.61		6.37		0.53	3.06												100.00	102.39
I-100 3692.42	2	7	K-feldspar + Muscovite	60.37	0.18	29.33	1.72		0.56		0.97	6.88												100.00	112.91
I-100 3692.42	2	8	Chlorite + Muscovite	43.70	0.18	25.38	17.62	0.28	8.59	0.80		2.85	0.60											100.00	108.17
I-100 3692.42	2	9	Chlorite	29.99	0.28	22.08	21.12	0.22	10.37			0.94												85.00	102.01
I-100 3692.42	2	10	TiO2 + Quartz	8.71	87.76	2.49	0.45					0.60												100.00	105.82
I-100 3692.42	2	11	Anhydrite + K-feldspar	2.80		1.00				36.58		0.51		59.11										100.00	118.60
I-100 3692.42	2	12	Anhydrite + K-feldspar	5.37		1.81	0.30			34.73		1.16		56.66										100.00	115.59
I-100 3692.42	3	1	Anhydrite							37.74				61.83				0.45						100.00	121.58
I-100 3692.42	3	2	Anhydrite							37.54				61.63				0.85						100.00	121.54
I-100 3692.42	3	3	Altered Ilmenite + Quartz	2.33	89.87	0.64	6.97					0.19												100.00	97.59
I-100 3692.42	3	4	Anhydrite	0.36		0.25				37.93				61.48										100.00	122.28
I-100 3692.42	3	5	Anhydrite				0.14			37.72				61.58				0.54						100.00	118.24
I-100 3692.42	3	6	Anhydrite	0.90		0.28				37.02		0.19		61.03				0.58						100.00	116.91
I-100 3692.42	3	7	Altered Ilmenite + Muscovite	25.58	62.32	7.94	1.99		0.68			1.48												100.00	114.62
I-100 3692.42	3	8	Muscovite	47.83	0.25	32.42	1.57		0.86		0.26	9.80												93.00	112.64
I-100 3692.42	3	9	Chlorite + TiO2	43.45	2.89	25.85	17.42		7.43			2.96												100.00	123.78
I-100 3692.42	3	10	Quartz	99.88			0.13																	100.00	146.54
I-100 3692.42	4	1	Anhydrite							38.23				61.78										100.00	137.83
I-100 3692.42	4	2	Altered Ilmenite + Muscovite	7.29	61.15	4.80	23.22	0.96	2.14			0.45												100.00	114.03
I-100 3692.42	4	3	Altered Ilmenite + Quartz	15.47	83.74	0.30	0.18			0.18		0.12												100.00	133.35
I-100 3692.42	4	4	Quartz + Altered Ilmenite	86.77	12.83	0.40																		100.00	142.71
I-100 3692.42	4	5	Albite	68.88		19.03	0.14				11.76	0.20												100.00	150.80
I-100 3692.42	4	6	Anhydrite							38.27				61.73										100.00	147.55
I-100 3692.42	4	7	K-feldspar	65.72		17.95					0.51	15.27							0.55					100.00	153.80
I-100 3692.42	4	8	Albite	68.13		18.67	0.37			0.53	11.68	0.14		0.47										100.00	155.65
I-100 3692.42	4	9	K-feldspar	66.36		17.82					1.09	14.72												100.00	150.91
I-100 3692.42	4	10	Mix	63.66	0.30	27.30	1.08		0.45		1.47	5.76												100.00	153.30
I-100 3692.42	4	11	Muscovite	46.77	1.10	32.48	1.53		0.84		0.55	9.37		0.37										93.00	135.93
I-100 3692.42	4	12	Quartz + Muscovite	94.77		3.48	0.44		0.27			1.06												100.00	157.67
I-100 3692.42	5	1	Muscovite	46.19	0.31	32.38	2.88		0.54		0.59	10.09												93.00	132.05
I-100 3692.42	5	2	Anhydrite							37.72				61.73				0.56						100.00	130.38
I-100 3692.42	5	3	Muscovite + Anhydite	40.05		25.74	5.20		3.90	5.21	0.35	7.77		11.81										100.00	127.18

Table 1B: Scanning electron microscope chemical analyses of minerals from representative sites for Mohican I-100 well at 3692.42m depth

Sample	Site	Position	Mineral	SiO_2	TiO_2	Al_2O_3	FeO	MnO	MgO	CaO	Na_2O	K_2O	P_2O_5	SO_3	F	Cl	Cr_2O_3	SrO	BaO	La_2O_3	Ce_2O_3	Nd_2O_3	WO_3	Total	Actual Total
I-100 3692.42	5	4	Quartz	99.99																				100.00	135.50
I-100 3692.42	5	5	Quartz	99.99																				100.00	134.36
I-100 3692.42	5	6	Al-phosphate			34.99	0.99			1.46			37.14	0.95	-0.44	0.22		3.76		4.96	11.58	4.40		100.00	102.81
I-100 3692.42	5	7	Altered Ilmenite + other	3.79	64.79	1.11	26.55	3.29		0.48														100.00	97.11
I-100 3692.42	5	8	Altered Ilmenite + other	14.65	70.28	6.14	5.30		3.20	0.20		0.23												100.00	106.67
I-100 3692.42	5	9	Muscovite + Chlorite	47.45	0.27	31.05	11.22	0.18	3.15	0.95	1.43	3.93		0.37										100.00	118.07
I-100 3692.42	5	10	Muscovite + Chlorite	53.22	0.30	30.18	3.20		1.79	0.46	0.30	9.77		0.77										100.00	118.04
I-100 3692.42	5	11	Muscovite + Chlorite	52.52	0.50	32.52	2.03		1.51		0.35	10.56												100.00	120.91
I-100 3692.42	5	12	Quartz	99.99																				100.00	131.35
I-100 3692.42	5	13	Muscovite	46.16	0.31	32.51	2.87		0.47		0.57	10.12												93.00	120.00
I-100 3692.42	6	1	Muscovite	46.75	0.40	32.58	1.53		0.99		0.51	10.23												93.00	142.28
I-100 3692.42	6	2	K-feldspar	66.19		17.82					0.50	15.48												100.00	151.27
I-100 3692.42	6	3	K-feldspar	66.32		17.84					0.71	15.13												100.00	155.03
I-100 3692.42	6	4	K-feldspar	65.97		17.86					0.73	15.07							0.37					100.00	152.33
I-100 3692.42	6	5	Anhydrite							37.23				61.55				1.22						100.00	141.10
I-100 3692.42	6	6	Muscovite	50.73		29.28	2.38		1.38		0.33	8.57							0.35					93.00	135.45
I-100 3692.42	6	7	Chlorite	31.57		20.72	22.29		10.43															85.00	129.42
I-100 3692.42	6	8	Quartz	99.99																				100.00	153.42
I-100 3692.42	6	9	Muscovite	47.13	0.42	33.74	0.73		0.60		0.80	9.59												93.00	141.51
I-100 3692.42	6	10	Altered Ilmenite + Anhydrite	0.62	66.72		30.01	1.07		1.08				0.50										100.00	100.84
I-100 3692.42	6	11	Anhydrite							37.86				62.15										100.00	120.07
I-100 3692.42	6	12	Anhydrite							38.00				62.00										100.00	126.10
I-100 3692.42	6	13	Quartz	99.32		0.49						0.19												100.00	133.91
I-100 3692.42	6	14	Muscovite	49.02	0.33	30.58	1.68		1.29		0.22	9.87												93.00	125.44
I-100 3692.42	6	15	Quartz	99.99																				100.00	118.23
I-100 3692.42	6	16	Anhydrite + Muscovite	2.57		1.11	0.36			36.62		0.48		58.86										100.00	117.13
I-100 3692.42	6	17	Anhydrite							37.67				61.68				0.65						100.00	116.34
I-100 3692.42	7	1	Rutile	0.66	98.42	0.45	0.26			0.21														100.00	106.83
I-100 3692.42	7	2	Muscovite	46.19	0.68	34.04	0.93		0.33		0.57	9.98		0.30										93.00	109.57
I-100 3692.42	7	3	Altered Ilmenite	13.20	76.16	6.10	2.75		0.85		0.36	0.57												100.00	112.18
I-100 3692.42	7	4	Muscovite	50.26	0.31	31.65	2.05		0.40		2.22	6.12												93.00	103.35
I-100 3692.42	7	5	Chlorite	29.05		23.21	22.90	0.14	9.21			0.49												85.00	102.69
I-100 3692.42	7	6	Altered Ilmenite	17.07	74.41	2.23	4.30		0.65	0.69				0.65										100.00	104.44
I-100 3692.42	7	7	Muscovite	50.93	0.79	32.26	0.50				2.06	6.47												93.00	111.19
I-100 3692.42	7	8	Illite	50.70	0.42	24.18	3.65		1.79			9.26												90.00	111.15
I-100 3692.42	7	9	Quartz	99.99																				100.00	118.98
I-100 3692.42	7	10	Quartz	97.38		1.34	0.41			0.24		0.63												100.00	117.05
I-100 3692.42	7	11	Quartz + other	90.66	1.15	5.27	0.75					2.17												100.00	118.27
I-100 3692.42	7	12	Muscovite + Chlorite	69.22	1.50	19.12	1.27		0.68		0.74	4.66			2.80									100.00	115.96
I-100 3692.42	7	13	Altered Ilmenite	14.12	75.65	6.90	0.77		0.53	0.39		1.46				0.20								100.00	97.51
I-100 3692.42	7	14	Albite	76.07		15.06				0.17	8.71													100.00	124.87
I-100 3692.42	7	15	Altered Ilmenite	15.83	76.25	4.59	1.02					0.75			1.55									100.00	124.38
I-100 3692.42	7	16	Quartz	98.94		0.42	0.64																	100.00	130.67
I-100 3692.42	7	17	Quartz	99.99																				100.00	115.32
I-100 3692.42	8	1	Altered Ilmenite	0.71	70.49	0.53	27.61	0.67																100.00	93.65
I-100 3692.42	8	2	Anhydrite	0.66			0.14			37.65		0.18		61.35										100.00	110.52
I-100 3692.42	8	3	Illite + TiO2	20.94	60.77	11.47	1.98		0.73			4.12												100.00	97.75
I-100 3692.42	8	4	Quartz	99.99																				100.00	115.26
I-100 3692.42	8	5	Chlorite	33.92		23.63	17.06		8.89			1.50												85.00	99.01
I-100 3692.42	8	6	Chlorite	30.49	0.21	23.72	19.58	0.22	9.38			1.42												85.00	103.20
I-100 3692.42	8	7	Muscovite	43.99	0.34	32.35	5.93		1.66		1.22	6.31			1.1997									93.00	113.49
I-100 3692.42	8	8	Fluorapatite	0.39		0.34				46.75			44.73		7.90								-0.09	100.00	128.28

Table 1B: Scanning electron microscope chemical analyses of minerals from representative sites for Mohican I-100 well at 3692.42m depth

Sample	Site	Position	Mineral	SiO_2	TiO_2	Al_2O_3	FeO	MnO	MgO	CaO	Na_2O	K_2O	P_2O_5	SO_3	F	Cl	Cr_2O_3	SrO	BaO	La_2O_3	Ce_2O_3	Nd_2O_3	WO_3	Total	Actual Total
I-100 3692.42	8	9	Chlorite	28.80	0.17	22.87	21.73	0.19	10.22			1.04												85.00	94.18
I-100 3692.42	8	10	Muscovite + Chlorite	57.89	0.32	26.55	4.13		2.26		2.04	5.37			1.46									100.00	117.83
I-100 3692.42	8	11	Chlorite	30.33		20.62	21.54		12.23			0.28												85.00	101.40
I-100 3692.42	8	12	Muscovite	47.61	0.21	33.80	1.08		0.40		1.45	8.44												93.00	103.85
I-100 3692.42	8	13	Chlorite	33.95	0.21	22.60	17.49	0.14	9.33			1.28												85.00	103.95
I-100 3692.42	8	14	Albite	65.03		21.67				2.99	10.21	0.10												100.00	119.62
I-100 3692.42	8	15	Chlorite + Muscovite	40.45	0.17	26.36	18.09		12.47	0.50		1.39	0.57											100.00	108.69
I-100 3692.42	8	16	Muscovite	48.41	0.49	31.25	1.74		1.06		0.80	9.26												93.00	108.14
I-100 3692.42	8	17	Chlorite + Muscovite	39.68	0.83	25.79	21.16	0.70	9.07			2.61					0.15							100.00	105.63
I-100 3692.42	9	1	K-feldspar	66.14		17.99					0.57	15.29												100.00	125.24
I-100 3692.42	9	2	Biotite	42.25	3.52	20.16	15.18	0.26	8.87			9.74												100.00	106.26
I-100 3692.42	9	3	Biotite	42.78	1.53	20.14	18.80		9.53			7.22												100.00	97.27
I-100 3692.42	9	4	Anhydrite							38.14				61.88										100.00	119.22
I-100 3692.42	9	5	Quartz	99.13	0.18	0.34	0.18					0.16												100.00	120.79
I-100 3692.42	9	6	Altered Ilmenite	0.83	67.92	0.74	28.79	0.67		0.50				0.52										100.00	86.90
I-100 3692.42	9	7	Rutile	1.45	97.08	0.70	0.17			0.59														100.00	96.93
I-100 3692.42	9	8	Altered Ilmenite	1.24	62.15	0.53	34.26	1.59		0.22														100.00	86.80
I-100 3692.42	9	9	Altered Ilmenite	11.36	74.18	6.41	4.68		2.57	0.21		0.59												100.00	94.87
I-100 3692.42	9	10	Anhydrite							38.04				61.95										100.00	126.73
I-100 3692.42	9	11	Chlorite	26.51		22.92	24.63	0.22	10.70															85.00	105.56
I-100 3692.42	9	12	Anhydrite							38.20				61.80										100.00	117.45
I-100 3692.42	9	13	Albite	65.48		21.31				2.67	10.31	0.22												100.00	122.29
I-100 3692.42	9	14	Chlorite + Muscovite	40.32		26.08	21.48		9.73			2.40												100.00	86.62
I-100 3692.42	9	15	Quartz	99.99																				100.00	127.69
I-100 3692.42	9	16	Quartz	99.99																				100.00	133.46
I-100 3692.42	9	17	Muscovite	47.73		33.72	1.85		0.47		1.80	7.41												93.00	115.40

Appendix 2C: Scanning Electron Microscope Backscattered Electron Images for Mohican I-100 well with EDS Mineral Analyses Sample 3694.38

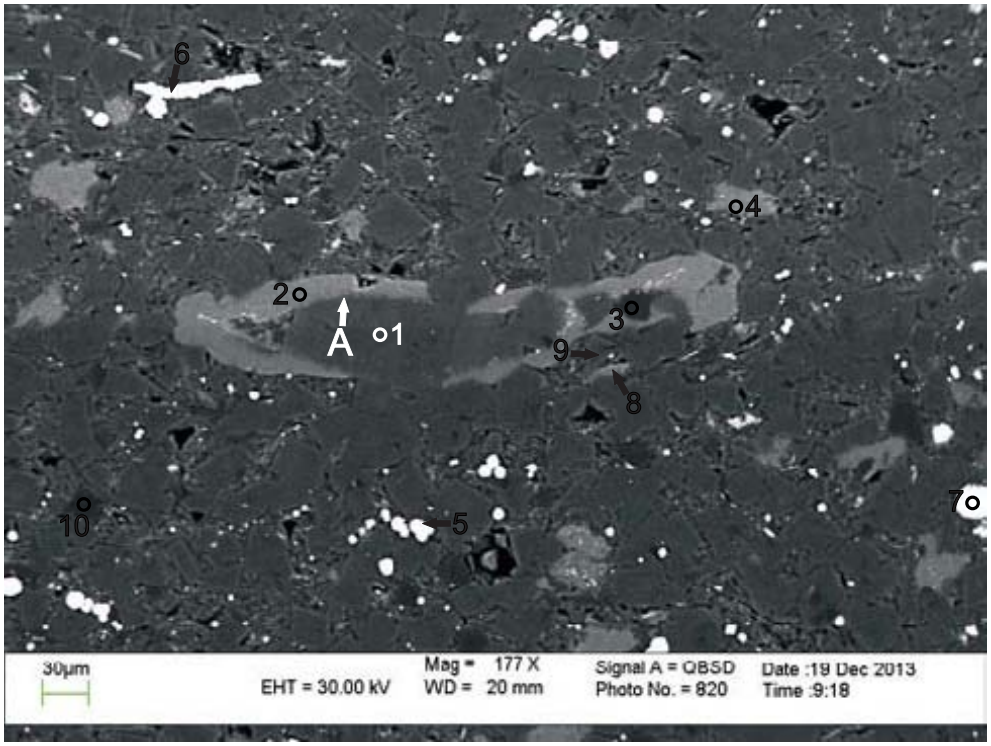

1: Dolomite
2: Calcite
3: Quartz
4: Calcite
5-7: Pyrite
8: Calcite
9: Dolomite
10: Quartz

Figure 1: Mohican I-100: 3694.38 site 1. Abundant dolomite formed in two stages, during early and late diagenesis. Calcite probably formed in between events, or syn-late diagenesis because calcite prevents overgrowths of late diagenetic dolomite from forming where calcite and dolomite are in contact (position A). .

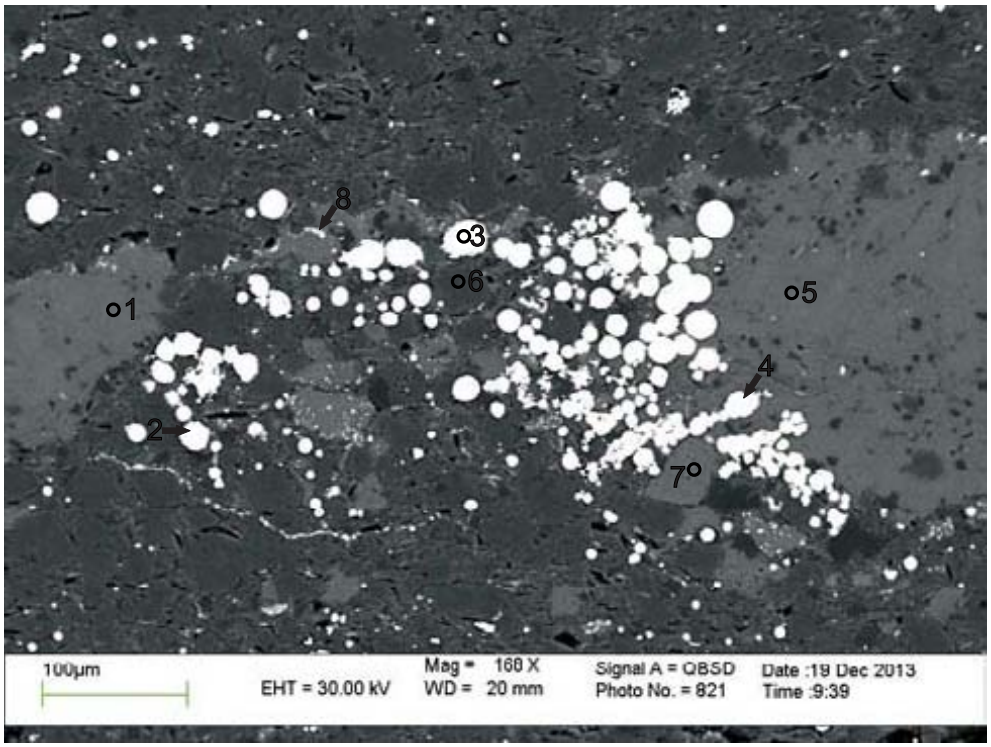

1: Calcite
2-4: Pyrite
5: Calcite
6: Dolomite + other
7: Calcite
8: Pyrite + Calcite + Chlorite

Figure 2: Mohican I-100: 3694.38 site 2. Diagenetic framboidal pyrite (analysis 3) formed in intergranular spaces.

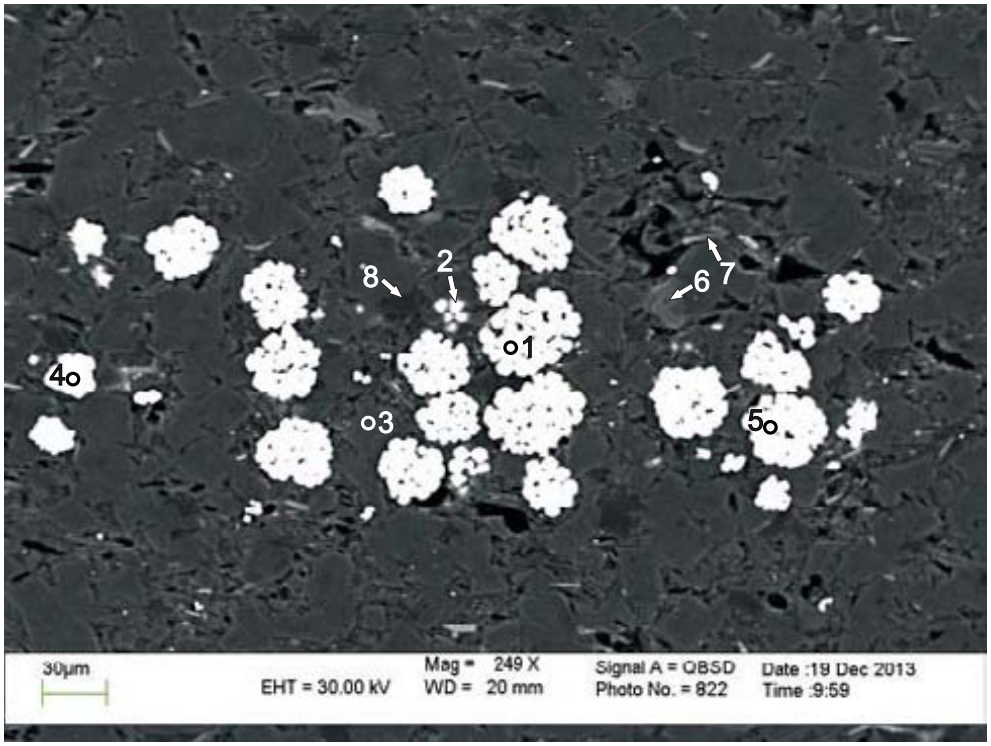

1: Pyrite
2: Pyrite + Chlorite
3: Dolomite
4: Pyrite
5: Pyrite
6: Mix
7: Chlorite + Dolomite
8: Quartz

Figure 3: Mohican I-100: 3694.38 site 3. Framboidal pyrite (analyses 1, 4 and 5) formed in intergranular spaces between early diagenetic dolomite. Chlorite grains found rimming some dolomite grains (analysis 7).

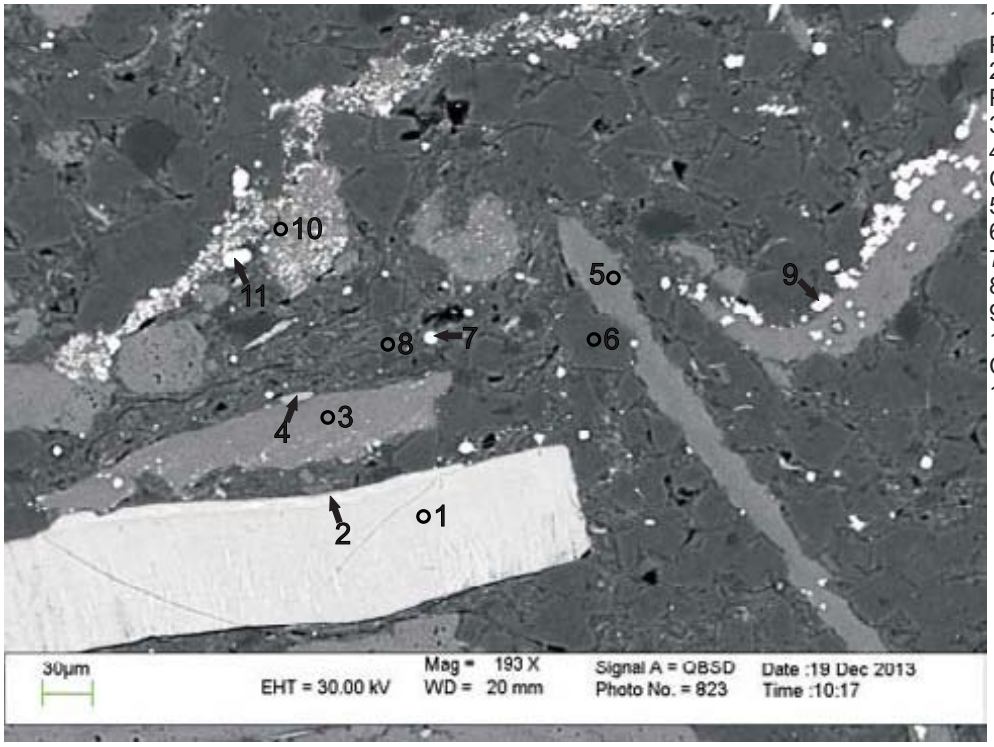

1: Fluorapatite + Pyrite
2: Fluorapatite + Pyrite
3: Calcite
4: Chlorite + Calcite
5: Calcite
6: Dolomite
7: Pyrite + other
8: Illite
9: Pyrite
10: Chlorite + Calcite
11: Pyrite

Figure 4: Mohican I-100: 3694.38 site 4. This site contains phosphorite (probably a piece of bone) (analyses 1 and 2) with pyrite forming within fractures or pores. Location of pyrite within calcite and along boundaries between calcite and dolomite suggests that early diagenetic pyrite formed after the first stage of dolomite in open pore spaces and then calcite (analyses 3 and 10) precipitated filling in the remainder of pore space, enclosing pyrite.

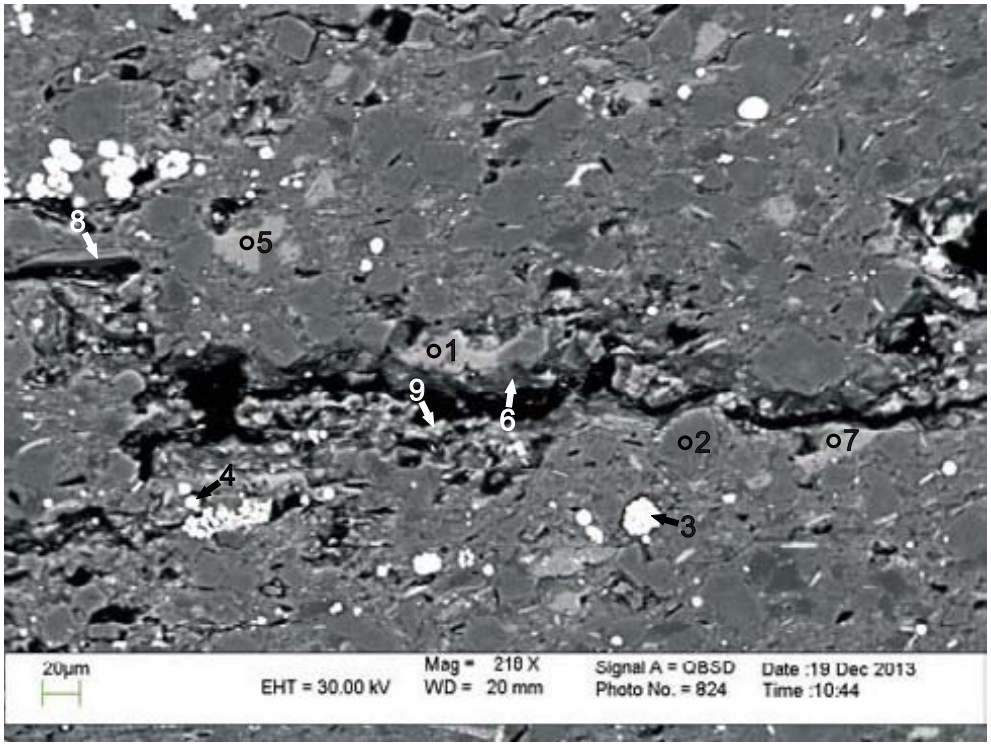

1: Calcite + Chlorite
2: Dolomite + Muscovite
3: Pyrite
4: Pyrite + other
5: Calcite
6: Muscovite + Calcite
7: Calcite + Muscovite
8: Muscovite
9: Dolomite + Muscovite

Figure 5: Mohican I-100: 3694.38 site 5. Calcite and muscovite are present along fracture within dolomite. Calcite did not completely fill the fracture.

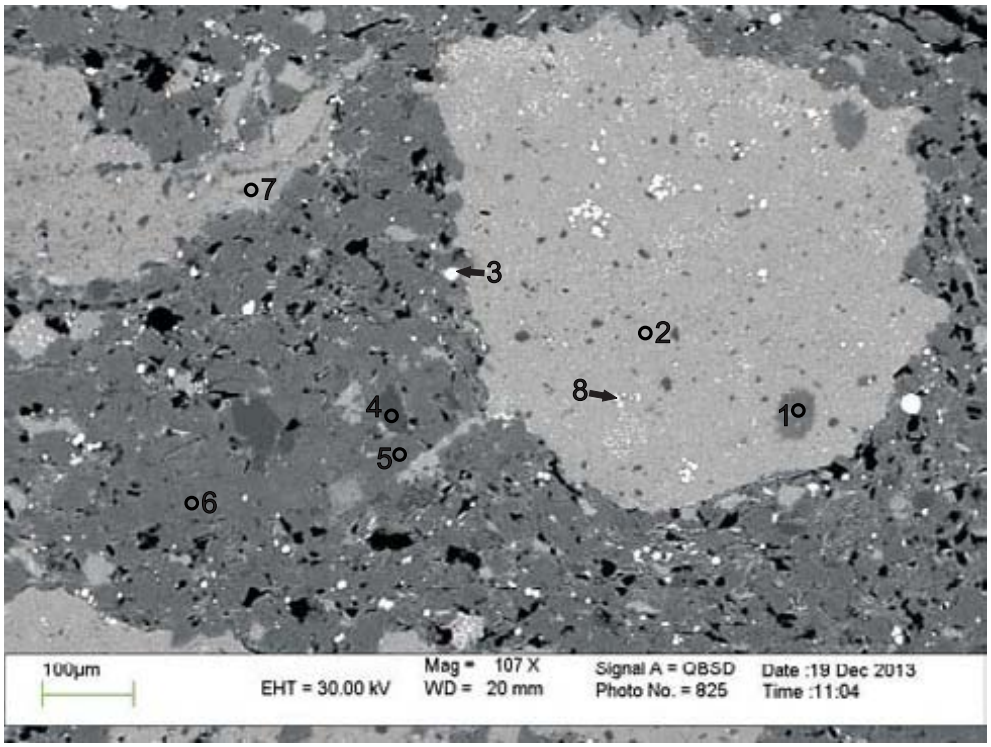

1: Dolomite
2: Calcite + Chlorite
3: Pyrite
4: Quartz
5: Dolomite
6: Dolomite + Muscovite
7: Calcite + Chlorite + Muscovite
8: Pyrite + Calcite + Chlorite

Figure 6: Mohican I-100: 3694.38 site 6. Calcite nodule (analysis 2) containing diagenetic pyrite (analysis 8), and grains of dolomite (analysis 1) which were enclosed in calcite during calcite precipitation.

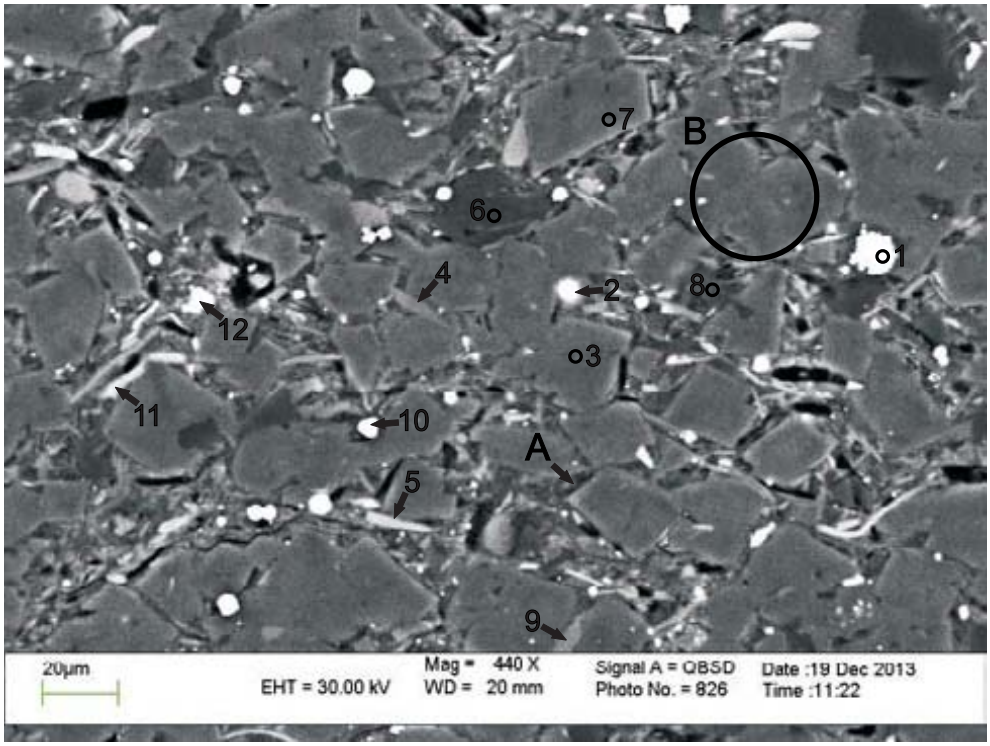

1: Pyrite + other
2: Pyrite + other
3: Dolomite
4: Muscovite
5: Chlorite + Illite
6: Albite
7: Dolomite
8: Quartz
9: Muscovite + Dolomite
10: Pyrite + other
11: Chlorite + Illite
12: Pyrite + other

Figure 7: Mohican I-100: 3694.38 site 7. Early diagenetic dolomite crystals with late diagenetic overgrowths (position A). Overgrowths occur where dolomite was exposed to porosity or matrix, and not when it is in contact with each other (position B).

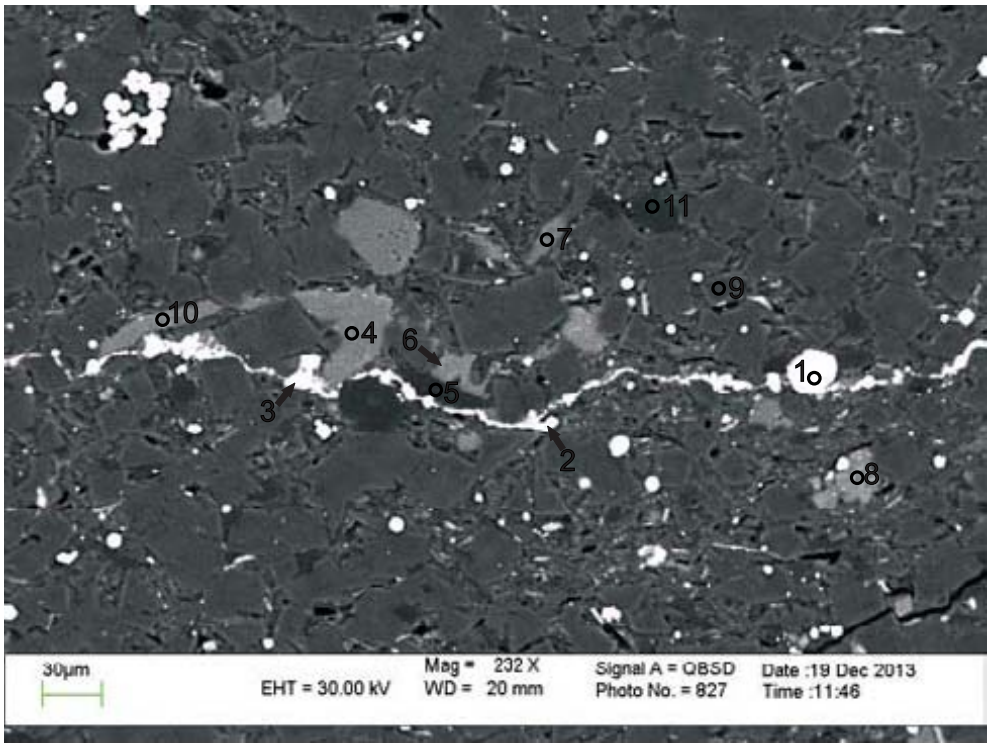

1: Pyrite
2: Pyrite + other
3: Pyrite + other
4: Calcite
5: Quartz
6: Calcite + other
7: Calcite + Muscovite
8: Fe-Calcite
9: Dolomite
10: Calcite
11: Albite

Figure 8: Mohican I-100: 3694.38 site 8. Diagenetic pyrite forms along a previous fracture or dissolution zone.

Table 1C: Scanning electron microscope chemical analyses of minerals from representative sites for Mohican I-100 well at 3694.38m depth

Sample	Site	Position	Mineral	SiO_2	TiO_2	Al_2O_3	FeO	MnO	MgO	CaO	Na_2O	K_2O	P_2O_5	SO_3	F	Cl	NiO	CuO	Total	Actual Total
I-100-3694.38	1	1	Dolomite				2.00		18.68	31.32									52.00	50.55
I-100-3694.38	1	2	Calcite						1.06	54.94									56.00	47.34
I-100-3694.38	1	3	Quartz	99.73						0.27									100.00	108.53
I-100-3694.38	1	4	Calcite				0.32		0.85	53.36		0.07		1.38					56.00	50.18
I-100-3694.38	1	5	Pyrite	0.17			26.64			0.38				72.81					100.00	189.09
I-100-3694.38	1	6	Pyrite	1.28		0.87	27.23			0.36		0.14		70.12					100.00	169.26
I-100-3694.38	1	7	Pyrite	0.75		0.34	27.45		0.22	0.32				70.92					100.00	187.85
I-100-3694.38	1	8	Calcite	1.14		0.74	0.40		1.43	52.07		0.22							56.00	49.33
I-100-3694.38	1	9	Dolomite	0.56			2.68		18.27	30.40		0.10							52.00	50.14
I-100-3694.38	1	10	Quartz	99.28			0.12			0.60									100.00	98.77
I-100-3694.38	2	1	Calcite	0.76		0.34	0.60	0.168	1.04	53.10									56.00	44.65
I-100-3694.38	2	2	Pyrite				26.90			0.21				72.89					100.00	175.38
I-100-3694.38	2	3	Pyrite	0.19			26.89			0.20				72.74					100.00	182.08
I-100-3694.38	2	4	Pyrite	0.13			26.72			0.28				72.86					100.00	188.91
I-100-3694.38	2	5	Calcite	0.78		0.48	0.56		1.20	52.98									56.00	48.13
I-100-3694.38	2	6	Dolomite + other	5.03		2.70	4.49		31.89	54.47		0.61		0.82					100.00	51.84
I-100-3694.38	2	7	Calcite				0.38		0.83	54.40				0.38					56.00	48.07
I-100-3694.38	2	8	Pyrite + Calcite + Chlorite	4.62		3.70	13.15		1.24	41.79	0.47	0.52		34.51					100.00	82.98
I-100-3694.38	3	1	Pyrite				27.34							72.66					100.00	185.58
I-100-3694.38	3	2	Pyrite + Chlorite	2.61		1.98	25.76		0.61	0.32		0.23		68.49					100.00	183.57
I-100-3694.38	3	3	Dolomite	1.57		0.98	1.63		17.53	29.71		0.22		0.36					52.00	49.54
I-100-3694.38	3	4	Pyrite	0.15			27.21	0.13		0.18				72.32					100.00	177.42
I-100-3694.38	3	5	Pyrite				27.07	0.28						72.64					100.00	187.58
I-100-3694.38	3	6	Mix	30.98		9.09	9.06	0.53	11.57	32.97	0.50	5.32							100.00	70.68
I-100-3694.38	3	7	Chlorite + Dolomite	31.77		23.49	15.37	0.39	19.82	8.27		0.90							100.00	86.82
I-100-3694.38	3	8	Quartz	96.26		1.32	0.54		0.32	0.88		0.67							100.00	102.71
I-100-3694.38	4	1	Fluorapatite + Pyrite				0.24			45.70	1.62		38.82	4.17	9.26	0.21			100.00	98.90
I-100-3694.38	4	2	Fluorapatite + Pyrite			0.25	1.96		0.32	43.00	1.54	0.13	36.55	7.77	8.29	0.24			100.00	102.48
I-100-3694.38	4	3	Calcite				0.36		1.13	53.54				0.98					56.00	46.81
I-100-3694.38	4	4	Chlorite + Calcite	32.71		25.62	24.15	0.59	13.08	3.47		0.37							100.00	84.27
I-100-3694.38	4	5	Calcite				0.20		1.01	53.89		0.09		0.81					56.00	48.44
I-100-3694.38	4	6	Dolomite	1.20			1.21		17.57	31.67				0.35					52.00	50.25
I-100-3694.38	4	7	Pyrite + other	1.56		1.13	26.33	0.10		0.27		0.18		70.42					100.00	179.03
I-100-3694.38	4	8	Illite	44.72	0.54	23.78	7.34		4.30	3.83	0.69	4.82							90.00	91.85
I-100-3694.38	4	9	Pyrite	0.17			25.87	0.18		1.92				71.62			0.11	0.14	100.00	178.93
I-100-3694.38	4	10	Chlorite + Calcite	2.33		1.25	2.88		1.72	85.37		0.35		6.09					100.00	51.46
I-100-3694.38	4	11	Pyrite	0.28			26.59			0.42				72.71					100.00	178.53
I-100-3694.38	5	1	Calcite + Chlorite	1.45		0.87	0.51		2.22	93.82	0.75	0.39							100.00	47.46
I-100-3694.38	5	2	Dolomite + Muscovite	8.32		5.12	3.89		29.65	51.17		1.13		0.72					100.00	55.10

Table 1C: Scanning electron microscope chemical analyses of minerals from representative sites for Mohican I-100 well at 3694.38m depth

Sample	Site	Position	Mineral	SiO_2	TiO_2	Al_2O_3	FeO	MnO	MgO	CaO	Na_2O	K_2O	P_2O_5	SO_3	F	Cl	NiO	CuO	Total	Actual Total
I-100-3694.38	5	3	Pyrite	0.51		0.28	26.81			0.27				72.14					100.00	184.93
I-100-3694.38	5	4	Pyrite + other	3.81		2.23	24.08	0.17	0.60	1.23		0.49		67.40					100.00	170.68
I-100-3694.38	5	5	Calcite				0.52		1.15	53.92				0.40					56.00	45.81
I-100-3694.38	5	6	Muscovite + Calcite	43.34	0.47	19.90	3.96		2.42	22.00	0.71	6.38		0.82					100.00	52.92
I-100-3694.38	5	7	Calcite + Muscovite	3.51		2.91	0.46		1.79	89.86		0.45		1.02					100.00	51.67
I-100-3694.38	5	8	Muscovite	47.64	0.35	31.14	2.50		1.06	0.71	1.16	8.42							93.00	92.54
I-100-3694.38	5	9	Dolomite + Muscovite	6.93		3.99	3.54		32.45	51.41		0.63		1.07					100.00	55.23
I-100-3694.38	6	1	Dolomite				1.78		17.93	32.29									52.00	52.01
I-100-3694.38	6	2	Calcite + Chlorite	2.33		1.23	1.20		2.19	90.46		0.30		2.27					100.00	51.01
I-100-3694.38	6	3	Pyrite				26.91	0.15		0.21				72.71					100.00	183.81
I-100-3694.38	6	4	Quartz	99.99															100.00	103.99
I-100-3694.38	6	5	Dolomite				0.99		18.38	32.23				0.39					52.00	49.02
I-100-3694.38	6	6	Dolomite + Muscovite	7.34		4.99	2.95		30.36	53.39		0.99							100.00	51.58
I-100-3694.38	6	7	Calcite + Chlorite + Muscovite	12.92		7.39	1.29		1.94	74.23		1.57		0.67					100.00	52.53
I-100-3694.38	6	8	Pyrite + Calcite + Chlorite	10.23		5.23	13.61	0.19	1.51	30.81		0.87		37.56					100.00	79.06
I-100-3694.38	7	1	Pyrite + other	1.63		0.77	24.49	0.25	0.33	2.53		0.28		69.57				0.15	100.00	161.64
I-100-3694.38	7	2	Pyrite + other	1.82		1.27	22.38	0.54	10.15	6.88		0.29		56.66					100.00	152.45
I-100-3694.38	7	3	Dolomite	0.50		0.40	1.09		18.78	30.76				0.45					52.00	50.08
I-100-3694.38	7	4	Muscovite	46.10	0.31	30.49	2.22		2.16	2.85	1.49	7.37							93.00	95.39
I-100-3694.38	7	5	Chlorite + Illite	41.46		20.56	17.51	0.28	15.27	3.29		1.61							100.00	87.11
I-100-3694.38	7	6	Albite	67.98		19.22	0.15			0.35	11.93	0.36							100.00	105.61
I-100-3694.38	7	7	Dolomite	1.11		0.47	1.06		18.19	30.73		0.12		0.32					52.00	50.64
I-100-3694.38	7	8	Quartz	95.37		2.49	0.49		0.35	0.56		0.75							100.00	103.39
I-100-3694.38	7	9	Muscovite + Dolomite	48.90	0.40	29.21	3.40		3.35	4.39	0.43	9.89							100.00	93.88
I-100-3694.38	7	10	Pyrite + other	3.17	0.25	2.27	23.36		2.02	3.97		0.43		64.52					100.00	154.97
I-100-3694.38	7	11	Chlorite + Illite	34.57		24.04	15.31	0.28	13.35	11.33		1.12							100.00	87.19
I-100-3694.38	7	12	Pyrite + other	8.36		5.61	23.47	0.19	0.95	0.41	0.35	0.82		59.85					100.00	184.33
I-100-3694.38	8	1	Pyrite				27.30			0.11				72.59					100.00	191.83
I-100-3694.38	8	2	Pyrite + other	7.38		3.51	22.49	0.31	0.40	0.39		0.65		64.85					100.00	184.69
I-100-3694.38	8	3	Pyrite + other	2.10		1.25	25.43	0.22	0.81	4.53		0.24		65.42					100.00	156.67
I-100-3694.38	8	4	Calcite				0.20		1.24	54.47		0.09							56.00	46.49
I-100-3694.38	8	5	Quartz	98.92			0.26			0.29				0.55					100.00	101.90
I-100-3694.38	8	6	Calcite + other	4.88		2.36	1.18		2.37	88.05		0.55		0.60					100.00	49.57
I-100-3694.38	8	7	Calcite + Muscovite	18.89		8.43	2.96		2.32	63.08		3.63		0.70					100.00	54.08
I-100-3694.38	8	8	Fe-Calcite				1.56		0.94	50.18				3.32					56.00	51.97
I-100-3694.38	8	9	Dolomite	1.22		0.70	1.10		17.96	30.42		0.12		0.47					52.00	51.21
I-100-3694.38	8	10	Calcite	0.57		0.44	0.42		1.01	52.74		0.13		0.70					56.00	47.96
I-100-3694.38	8	11	Albite	68.99		18.42	0.17			0.60	11.70	0.12							100.00	109.00

Appendix 2D: Scanning Electron Microscope Backscattered Electron Images for Mohican I-100 well with EDS Mineral Analyses Sample 3696.69

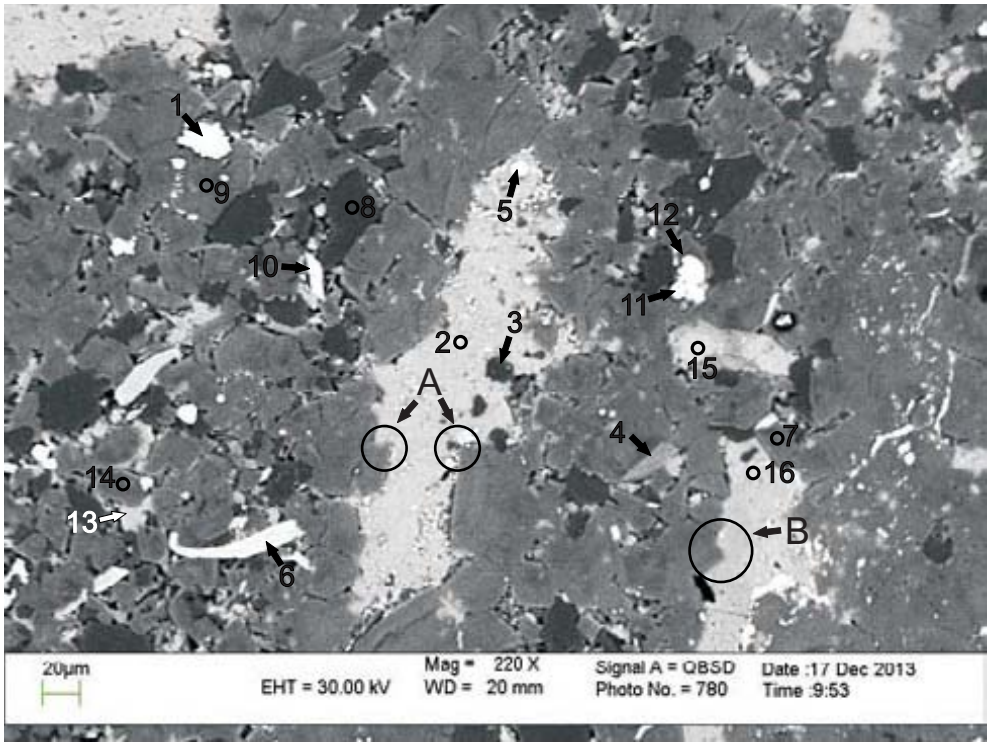

1: Pyrite + Chlorite + Calcite
2: Calcite
3: Calcite + Quartz + Chlorite
4: Dolomite + Chlorite + Muscovite
5: Pyrite + Calcite + other
6: Dolomite + Chlorite
7: Fe-Dolomite + Muscovite
8-9: Quartz + Dolomite
10: Dolomite + Chlorite
11: Dolomite + Chlorite + Pyrite 12: Pyrite + Dolomite + K-feldspar
13: Fe-Dolomite + K-feldspar
14: Calcite + Dolomite + K-feldspar
15: Fe-Dolomite + K-feldspar
16: Calcite

Figure 1: Mohican I-100: 3696.69 site 1. Dolomite cross cutting into calcite (positions A and B).

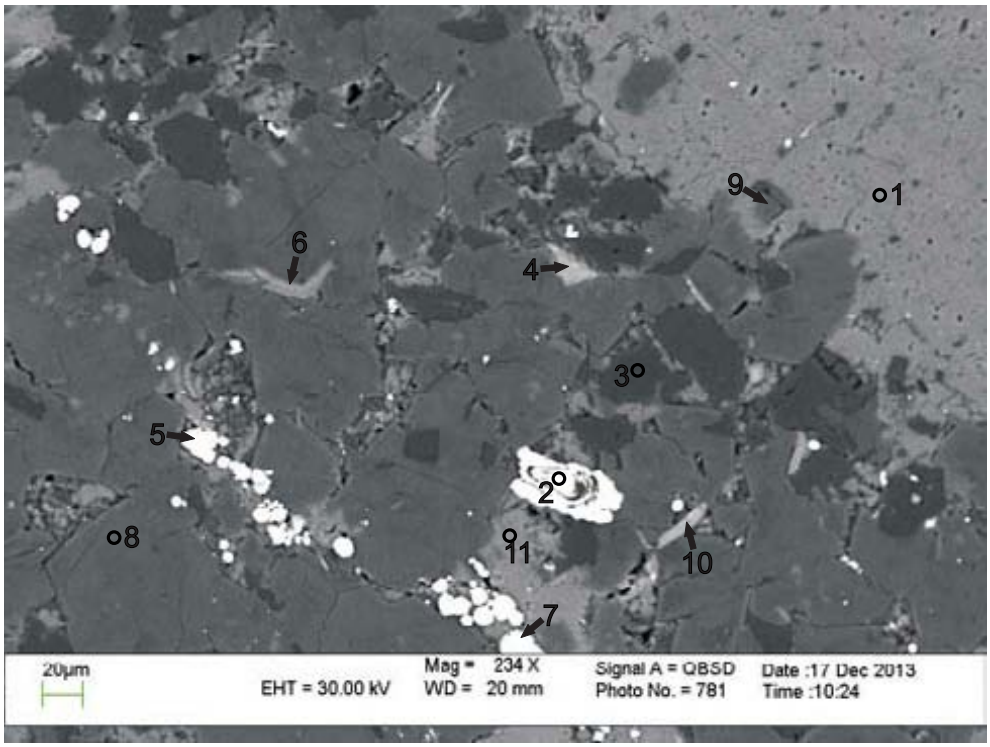

1: Calcite
2: Zircon
3: Quartz
4: Chlorite + Calcite
5: Pyrite
6: Chlorite + Dolomite
7: Pyrite
8: Dolomite
9: Dolomite + Chlorite
10: Chlorite
11: Calcite

Figure 2: Mohican I-100: 3696.69 site 2. Calcite nodule (analysis 1) formed after early dolomite, engulfing some dolomite grains (analysis 9). Diagenetic pyrite (analysis 5) formed along a linear zone of dissolution.

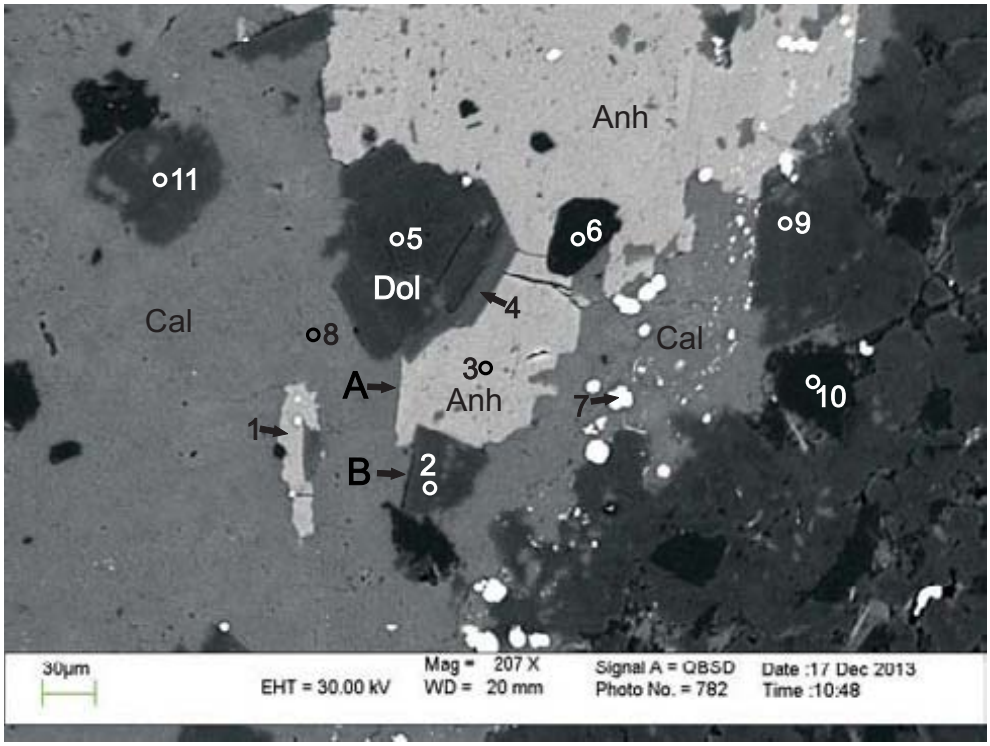

1: Anhydrite
2: Dolomite
3: Anhydrite
4: Ankerite
5: Dolomite
6: Quartz
7: Pyrite
8: Calcite
9: Dolomite
10: Quartz
11: Dolomite

Figure 3: Mohican I-100: 3696.69 site 3. Calcite is replaced by anhydrite (position A); dolomite replaces aragonitic lime mud and bioclasts. There was probably two phases of dolomite separated by the formation of sparry calcite (see App. 4B, Fig. 2). Dolomite overgrowths are later than calcite evidenced by straight grain boundary (position B).

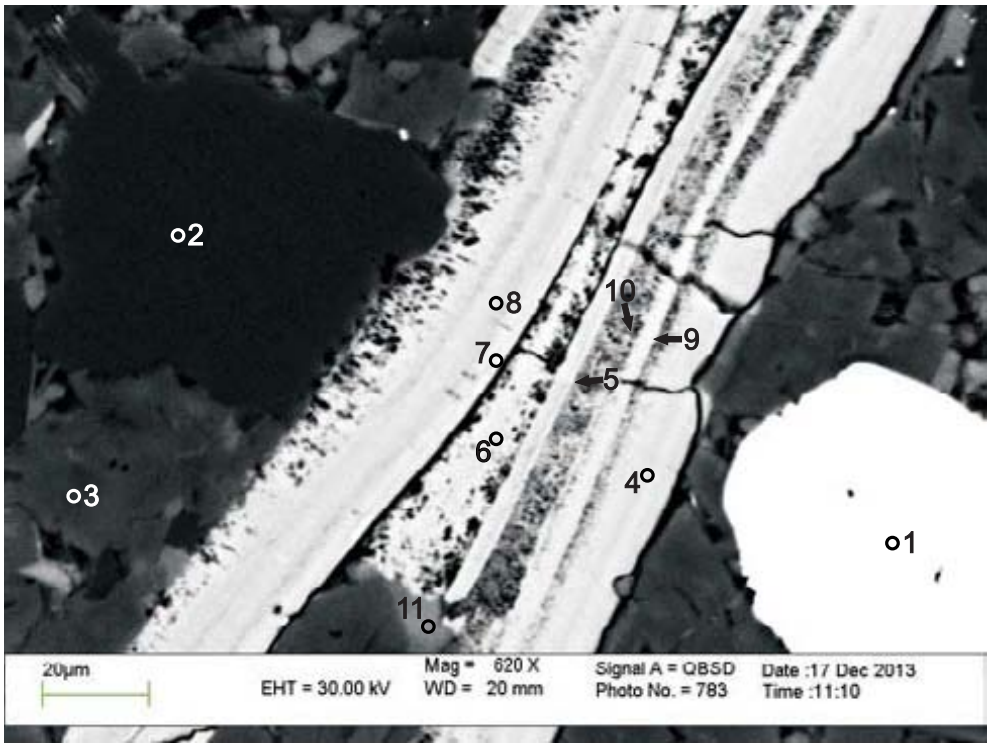

1: Pyrite
2: Quartz
3: Dolomite + Chlorite
4-10: Apatite + Anhydrite + Halite
11: Calcite + Chlorite

Figure 4: Mohican I-100: 3696.69 site 4. Phosphorite, likely a bone fragment, composed of apatite, anhydrite and halite (see App. 4B, Fig. 3 and 4). Anhydrite likely formed in pore spaces of the bone during diagenesis.

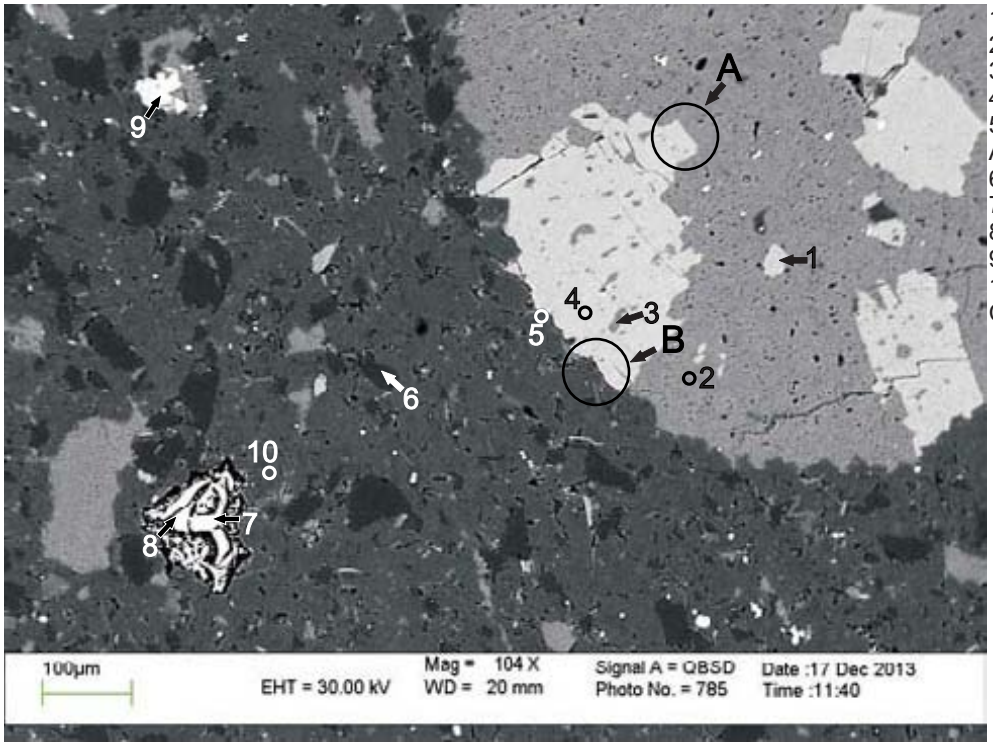

1: Anhydrite
2: Calcite
3: Anhydrite
4: Anhydrite
5: Dolomite + Anhydrite + other
6: Quartz
7: Pyrite
8: Pyrite
9: Pyrite + other
10: Dolomite + Chlorite

Figure 5: Mohican I-100: 3696.69 site 5. Late mobility of anhydrite: precipitating in voids in calcite (analysis 1). Anhydrite, which converted during diagenesis from gypsum, forms from calcite (position A). Zone of dolomitization of calcite (position B), (See App. 4B, Fig. 5).

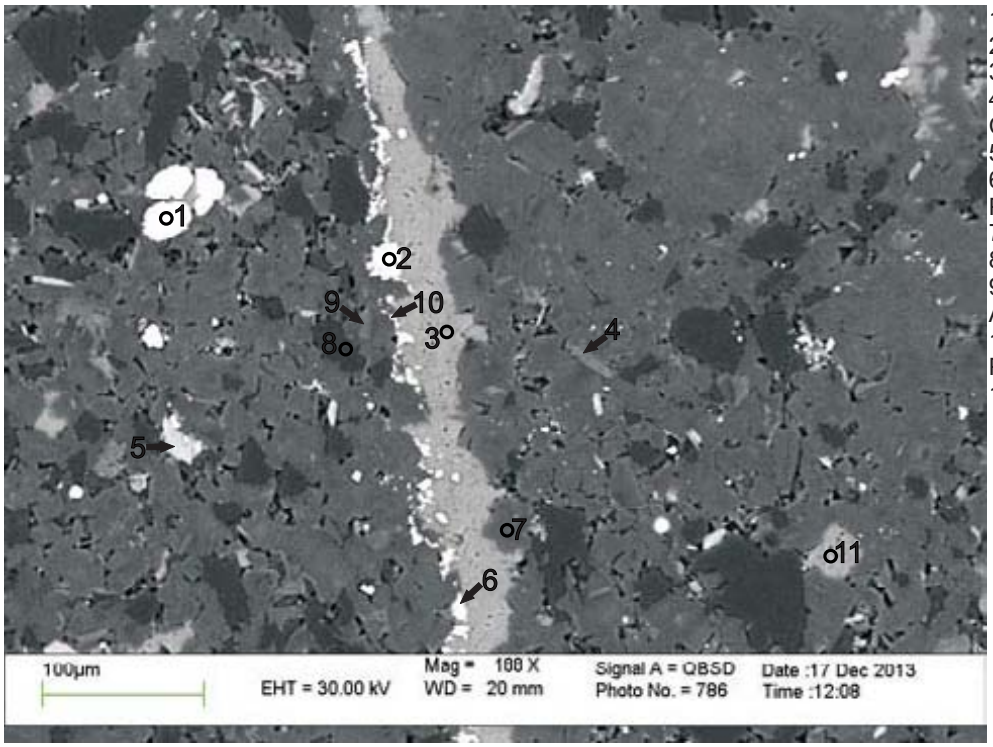

1: Pyrite
2: Pyrite
3: Calcite
4: Dolomite + Chlorite
5: Chlorite + other
6: Anhydrite + Pyrite
7: Dolomite
8: Quartz
9: Dolomite + Ankerite
10: Dolomite + Pyrite
11: Calcite

Figure 6: Mohican I-100: 3696.69 site 6. Vein of calcite (analysis 3) and pyrite (analysis 2) formed in a linear zone of porosity caused by fracturing and dissolution.

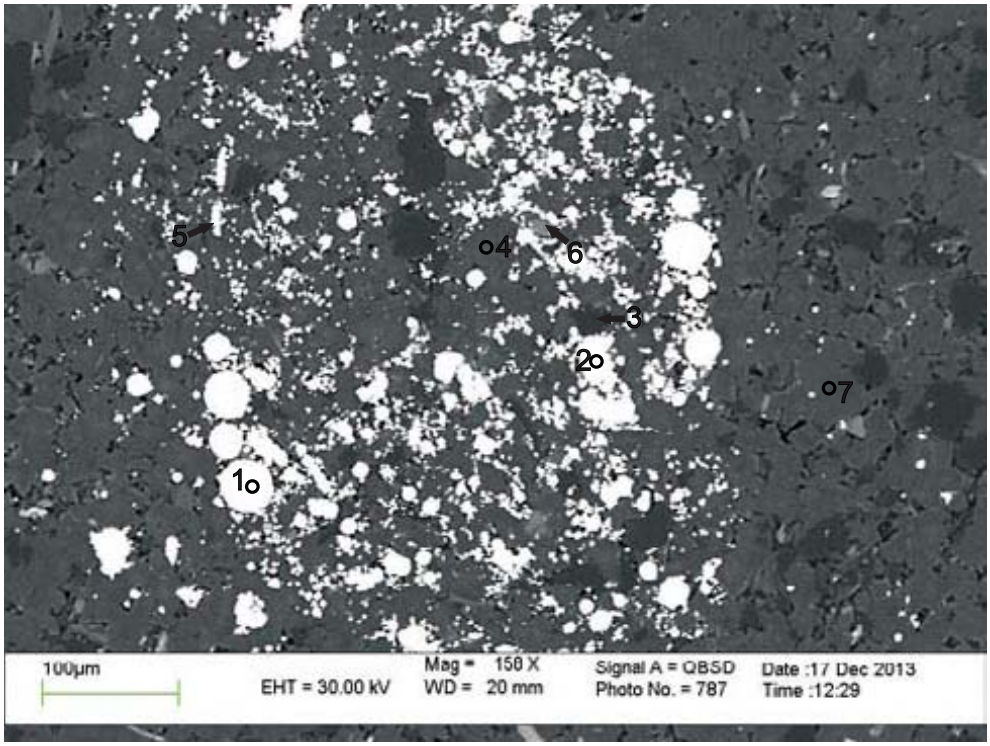

1: Pyrite
2: Pyrite
3: Quartz
4: Dolomite + Pyrite
5: Dolomite + Pyrite
6: Anhydrite + Chlorite
7: Dolomite

Figure 7: Mohican I-100: 3696.69 site 7. Subspherical area of diagenetic pyrite forms in intergranular spaces between early diagenetic dolomite.

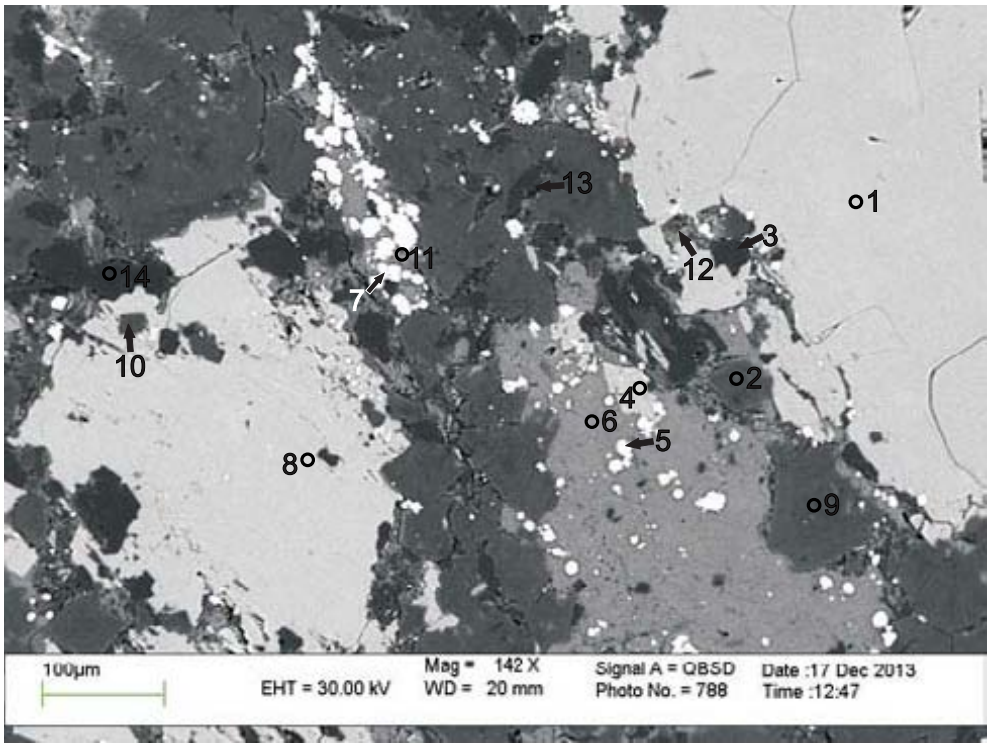

1: Anhydrite
2: Dolomite
3: Quartz
4: Anhydrite
5: Pyrite + Calcite
6: Calcite
7: Pyrite + Calcite
8: Anhydrite
9: Dolomite + Chlorite
10: Dolomite + other
11: Calcite + Chlorite + Pyrite
12: Calcite + Chlorite
13: Quartz
14: Quartz

Figure 8: Mohican I-100: 3696.69 site 8. Pyrite (analysis 5) replaced or displaced earlier calcite cement (analysis 6) formed in intergranular boundaries between early diagenetic dolomite. Anhydrite has partly replaced the calcite cement (analysis 4). Larger anhydrite nodules (analyses 1 and 8) were likely converted from gypsum during diagenesis.

Table 1D: Scanning electron microscope chemical analyses of minerals from representative sites for Mohican I-100 well at 3696.69m depth

Sample	Site	Position	Mineral	SiO_2	TiO_2	Al_2O_3	FeO	MnO	MgO	CaO	Na_2O	K_2O	P_2O_5	SO_3	Cl	As_2O_3	ZrO_2	HfO_2	Total	Actual Total
I-100-3696.69	1	1	Pyrite + Chlorite + Calcite	2.05		1.32	23.17		2.59	3.64		0.24		67.00					100.00	165.88
I-100-3696.69	1	2	Calcite				0.20		1.10	54.72									56.00	46.09
I-100-3696.69	1	3	Calcite + Quartz + Chlorite	74.08		1.28	0.36			23.35		0.36		0.55					100.00	91.09
I-100-3696.69	1	4	Dolomite + Chlorite + Muscovite	8.56		8.22	3.13		33.74	45.10		1.28							100.00	57.45
I-100-3696.69	1	5	Pyrite + Calcite + other	4.30		2.57	16.93		2.54	26.85		0.60		46.20					100.00	108.59
I-100-3696.69	1	6	Dolomite + Chlorite	12.24		10.81	10.78	0.28	27.58	38.04		0.26							100.00	62.21
I-100-3696.69	1	7	Fe-Dolomite + Muscovite	17.26		12.30	10.82		25.12	33.59		0.92							100.00	66.81
I-100-3696.69	1	8	Quartz + Dolomite	88.80		0.98	0.82		3.58	5.55		0.26							100.00	103.55
I-100-3696.69	1	9	Quartz + Dolomite	41.03			1.79		23.18	34.00									100.00	64.84
I-100-3696.69	1	10	Dolomite + Chlorite	1.69		1.04	3.24		36.61	57.19		0.23							100.00	52.16
I-100-3696.69	1	11	Dolomite + Chlorite + Pyrite	3.06		1.83	3.60		34.08	56.40		0.39		0.65					100.00	55.00
I-100-3696.69	1	12	Pyrite + Dolomite + K-feldspar	11.85		6.03	15.58		13.45	19.81		1.42		31.89					100.00	98.71
I-100-3696.69	1	13	Fe-Dolomite + K-feldspar	19.38		4.02	5.26	0.34	28.85	41.37	0.77								100.00	59.02
I-100-3696.69	1	14	Calcite + Dolomite + K-feldspar	8.39		2.80	1.81		6.25	80.19		0.57							100.00	48.21
I-100-3696.69	1	15	Fe-Dolomite + K-feldspar	26.03		7.26	3.78	0.28	10.16	46.76		5.70							100.00	71.46
I-100-3696.69	1	16	Calcite				0.27		0.92	54.38				0.45					56.00	50.10
I-100-3696.69	2	1	Calcite				0.21		1.03	54.76									56.00	50.41
I-100-3696.69	2	2	Zircon	37.54		0.32	0.81			0.53							59.85	0.94	100.00	109.05
I-100-3696.69	2	3	Quartz	99.77						0.22									100.00	113.60
I-100-3696.69	2	4	Chlorite + Calcite	29.37		26.51	22.82	0.30	13.36	6.39		0.17		1.05					100.00	91.65
I-100-3696.69	2	5	Pyrite				26.31			0.36				73.34					100.00	190.98
I-100-3696.69	2	6	Chlorite + Dolomite	32.90	1.33	18.84	14.10	0.21	17.38	12.19		3.05							100.00	84.26
I-100-3696.69	2	7	Pyrite	0.21			26.42			0.59				72.76					100.00	193.56
I-100-3696.69	2	8	Dolomite				1.83		19.66	30.51									52.00	50.08
I-100-3696.69	2	9	Dolomite + Chlorite	2.48		2.42	4.95	0.28	32.78	56.85		0.22							100.00	55.14
I-100-3696.69	2	10	Chlorite	31.51		21.43	19.52	0.23	11.16	1.04		0.12							85.00	101.02
I-100-3696.69	2	11	Calcite				0.40		0.87	54.73									56.00	48.68
I-100-3696.69	3	1	Anhydrite			0.32				37.67				62.00					100.00	100.61
I-100-3696.69	3	2	Dolomite				2.66	0.14	18.83	30.37									52.00	50.83
I-100-3696.69	3	3	Anhydrite							37.62				62.38					100.00	103.84
I-100-3696.69	3	4	Ankerite				8.72	0.45	16.79	30.04									56.00	53.77
I-100-3696.69	3	5	Dolomite				1.74		19.57	30.69									52.00	51.73
I-100-3696.69	3	6	Quartz	99.99															100.00	112.39
I-100-3696.69	3	7	Pyrite				26.12			0.78				73.11					100.00	199.21
I-100-3696.69	3	8	Calcite				0.32		0.76	50.27				4.66					56.00	51.60
I-100-3696.69	3	9	Dolomite				2.96	0.15	18.93	29.96									52.00	53.38
I-100-3696.69	3	10	Quartz	99.86						0.14									100.00	114.70
I-100-3696.69	3	11	Dolomite	0.68			2.71		18.61	30.00									52.00	51.02
I-100-3696.69	4	1	Pyrite	0.15			26.57							73.29					100.00	199.66
I-100-3696.69	4	2	Quartz	99.99															100.00	112.14
I-100-3696.69	4	3	Dolomite + Chlorite	6.74		3.40	3.31		35.57	49.39		1.58							100.00	54.59
I-100-3696.69	4	4	Apatite + Anhydrite + Halite						0.38	50.67	1.60		43.01	4.07	0.27				100.00	95.51

Table 1D: Scanning electron microscope chemical analyses of minerals from representative sites for Mohican I-100 well at 3696.69m depth

Sample	Site	Position	Mineral	SiO_2	TiO_2	Al_2O_3	FeO	MnO	MgO	CaO	Na_2O	K_2O	P_2O_5	SO_3	Cl	As_2O_3	ZrO_2	HfO_2	Total	Actual Total
I-100-3696.69	4	5	Apatite + Anhydrite + Halite	0.51		0.26				49.98	1.91		42.19	4.79	0.35				100.00	87.22
I-100-3696.69	4	6	Apatite + Anhydrite + Halite							50.87	1.52		43.51	3.75	0.34				100.00	91.88
I-100-3696.69	4	7	Apatite + Anhydrite + Halite						0.40	49.73	1.81		43.08	4.64	0.35				100.00	91.96
I-100-3696.69	4	8	Apatite + Anhydrite + Halite						0.45	49.10	2.18		42.21	5.59	0.48				100.00	95.58
I-100-3696.69	4	9	Apatite + Anhydrite + Halite							50.93	1.36		43.51	3.85	0.35				100.00	87.97
I-100-3696.69	4	10	Apatite + Anhydrite + Halite							50.43	1.58		43.63	4.00	0.36				100.00	87.82
I-100-3696.69	4	11	Calcite + Chlorite	2.76		1.63	1.29	0.36	1.59	90.23		0.48	1.65						100.00	51.51
I-100-3696.69	5	1	Anhydrite							37.86				62.13					100.00	101.67
I-100-3696.69	5	2	Calcite						1.24	54.76									56.00	47.19
I-100-3696.69	5	3	Anhydrite						1.01	73.28				25.72					100.00	61.92
I-100-3696.69	5	4	Anhydrite							37.72				62.28					100.00	96.90
I-100-3696.69	5	5	Dolomite + Anhydrite + other	3.27			4.19		35.58	55.06				1.90					100.00	50.85
I-100-3696.69	5	6	Quartz	99.84						0.15									100.00	101.03
I-100-3696.69	5	7	Pyrite				26.39							73.61					100.00	170.66
I-100-3696.69	5	8	Pyrite				26.53			0.22		0.13		72.79		0.32			100.00	143.34
I-100-3696.69	5	9	Pyrite + other	0.56		0.34	23.18			9.53			2.11	64.30					100.00	135.46
I-100-3696.69	5	10	Dolomite + Chlorite	7.19		5.80	3.45		31.99	50.87		0.70							100.00	50.84
I-100-3696.69	6	1	Pyrite	0.15			26.45			0.22				73.19					100.00	196.09
I-100-3696.69	6	2	Pyrite	0.11			26.01			0.50				73.39					100.00	196.48
I-100-3696.69	6	3	Calcite				0.23		0.82	54.95									56.00	49.34
I-100-3696.69	6	4	Dolomite + Chlorite	3.74		3.80	1.72		34.62	54.93		0.47		0.72					100.00	55.97
I-100-3696.69	6	5	Chlorite + other	28.04		23.64	18.78	0.19	14.26	11.57		0.31		3.20					100.00	83.51
I-100-3696.69	6	6	Anhydrite + Pyrite	0.68		0.57	14.24		2.30	47.49				34.71					100.00	80.00
I-100-3696.69	6	7	Dolomite				1.49		19.86	30.66									52.00	52.31
I-100-3696.69	6	8	Quartz	96.03		1.55	0.39		0.50	1.06		0.45							100.00	112.41
I-100-3696.69	6	9	Dolomite + Ankerite				10.10	0.59	35.60	53.70									100.00	52.39
I-100-3696.69	6	10	Dolomite + Pyrite	0.71		0.62	5.47		31.47	50.68				11.06					100.00	60.22
I-100-3696.69	6	11	Calcite				0.21		1.02	54.78									56.00	51.11
I-100-3696.69	7	1	Pyrite				26.23							73.76					100.00	197.00
I-100-3696.69	7	2	Pyrite	0.17			26.55			0.13				73.14					100.00	200.01
I-100-3696.69	7	3	Quartz	99.11			0.32			0.57									100.00	115.22
I-100-3696.69	7	4	Dolomite + Pyrite	0.90			5.25		35.02	57.82				1.02					100.00	54.02
I-100-3696.69	7	5	Dolomite + Pyrite	2.40		0.93	17.95		13.86	20.50		0.51		43.87					100.00	81.73
I-100-3696.69	7	6	Anhydrite + Chlorite	14.20	0.62	4.08	7.02		1.08	54.44		0.64		17.90					100.00	71.79
I-100-3696.69	7	7	Dolomite				1.20		19.84	30.96									52.00	54.62
I-100-3696.69	8	1	Anhydrite							37.74				62.28					100.00	111.20
I-100-3696.69	8	2	Dolomite				2.33		19.23	30.44									52.00	54.68
I-100-3696.69	8	3	Quartz	99.99															100.00	115.58
I-100-3696.69	8	4	Anhydrite							37.64				62.35					100.00	106.88
I-100-3696.69	8	5	Pyrite + Calcite				26.09			5.40				68.52					100.00	172.35
I-100-3696.69	8	6	Calcite				0.33		1.10	54.57									56.00	50.15
I-100-3696.69	8	7	Pyrite + Calcite				25.12			1.72				73.16					100.00	194.33

Table 1D: Scanning electron microscope chemical analyses of minerals from representative sites for Mohican I-100 well at 3696.69m depth

Sample	Site	Position	Mineral	SiO_2	TiO_2	Al_2O_3	FeO	MnO	MgO	CaO	Na_2O	K_2O	P_2O_5	SO_3	Cl	As_2O_3	ZrO_2	HfO_2	Total	Actual Total
I-100-3696.69	8	8	Anhydrite	0.77						37.16				62.08					100.00	103.11
I-100-3696.69	8	9	Dolomite + Chlorite	1.18		0.81	2.96		36.21	58.84									100.00	55.46
I-100-3696.69	8	10	Dolomite + Anhydrite	0.92			1.99		37.96	57.82				1.32					100.00	50.14
I-100-3696.69	8	11	Calcite + Chlorite + Pyrite	5.22		3.50	2.60		1.29	79.77		0.55		6.84	0.22				100.00	57.51
I-100-3696.69	8	12	Calcite + Chlorite	18.44		10.28	1.63		3.86	62.94		1.94		0.92					100.00	64.34
I-100-3696.69	8	13	Quartz	96.37		1.68	0.23		0.56	0.81		0.35							100.00	106.32
I-100-3696.69	8	14	Quartz	99.99															100.00	108.44

Appendix 2E: Scanning Electron Microscope Backscattered Electron Images for Mohican I-100 well with EDS Mineral Analyses Sample 3697.36

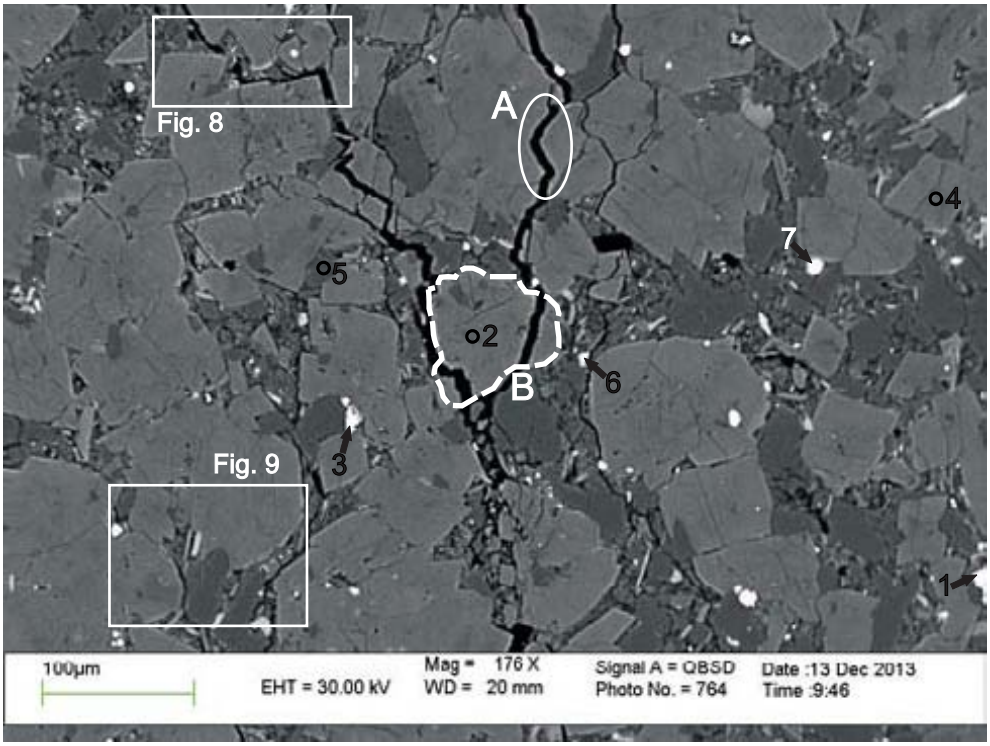

1: Pyrite
2: Dolomite + Chlorite
3: Quartz
4: Dolomite + Chlorite
5: Dolomite + Muscovite
6: K-feldspar + Fe-Dolomite
7: Quartz + other

Figure 1: Mohican I-100: 3697.36B site 1. Fracturing of early diagenetic dolomite grains (position A and B) and subsequent later diagenetic dolomite precipitation along dolomite grains exposed to porosity (position A). (See Figs. 8 and 9 for analyes of intergranular space).

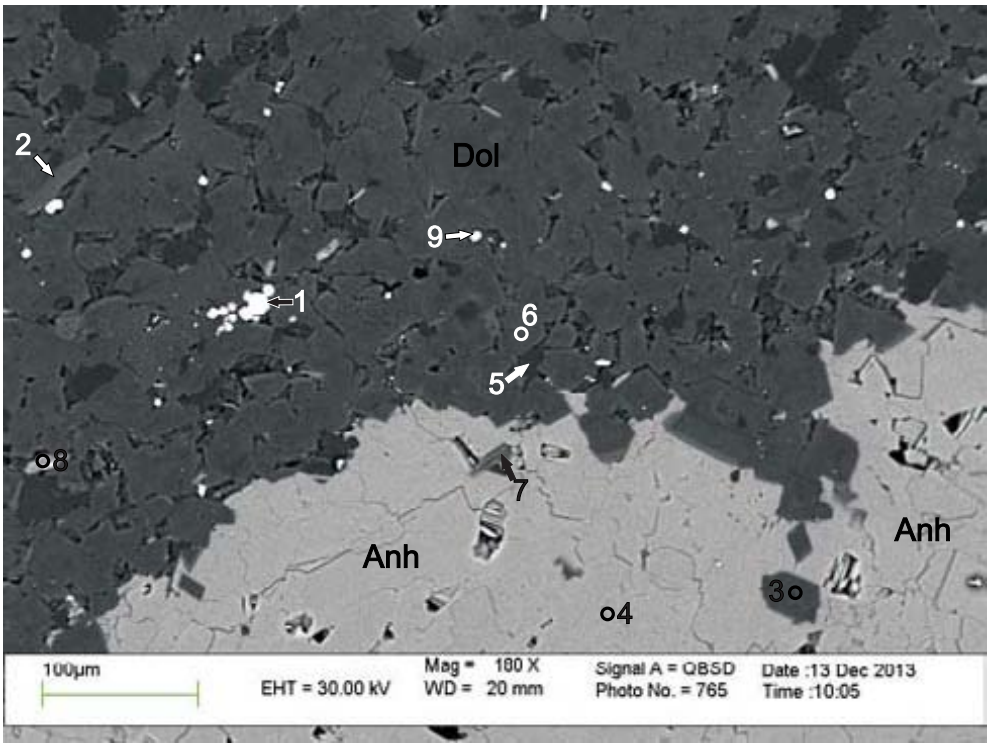

1: Pyrite
2: Muscovite + other
3: Dolomite + other
4: Anhydrite
5: Albite + Calcite
6: Dolomite + other
7: Anhydrite + other
8: Illite + other
9: Dolomite

Figure 2: Mohican I-100: 3697.36B site 2. Zone of dolomitization of anhydrite nodule (see App. 4B, Fig 6.).

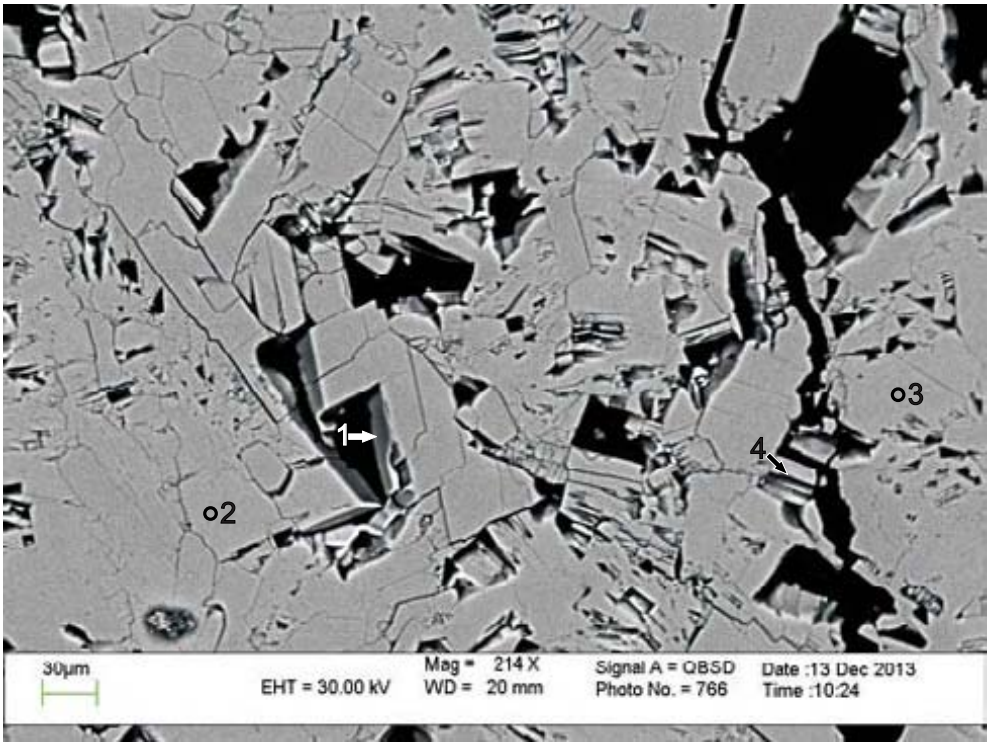

1-4: Anhydrite

Figure 3: Mohican I-100: 3697.36B site 3. Anhydrite nodule. Grains appear in a mostly lath or columnar habit (see App. 4B, Fig. 6).

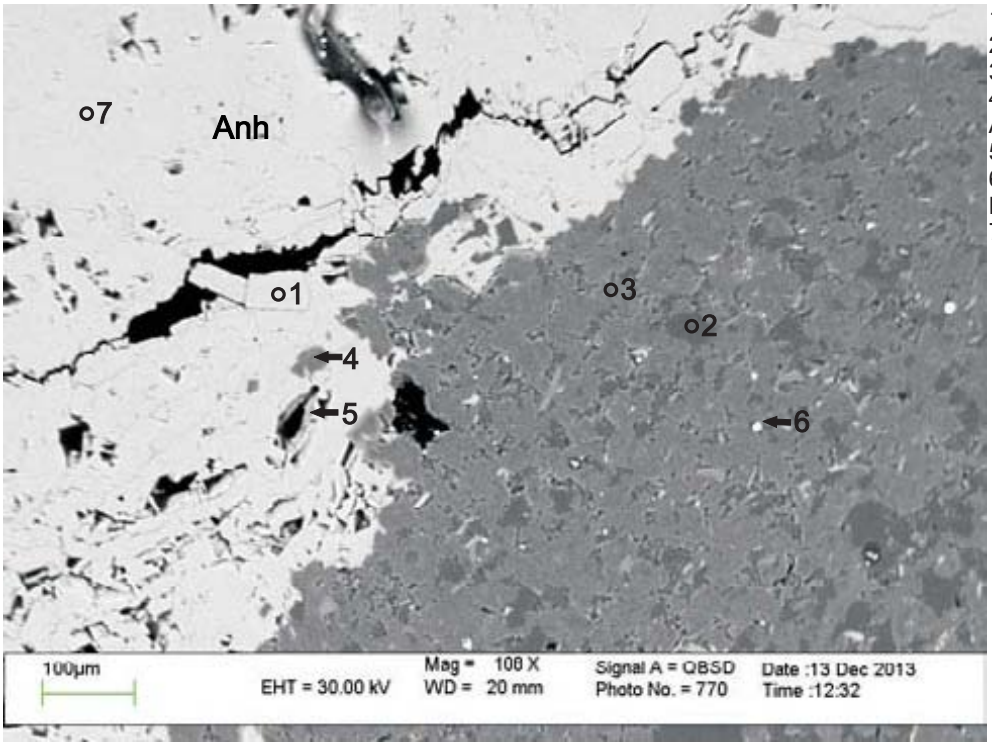

1: Anhydrite
2: Quartz
3: Quartz
4: Anhydrite + Ankerite
5: Anhydrite
6: Dolomite + Pyrite
7: Anhydrite

Figure 4: Mohican I-100: 3697.36B site 4. Zone of dolomitization of anhydrite nodule. Anhydrite nodule likely formed from dehydration of gypsum upon burial and was dolomitized.

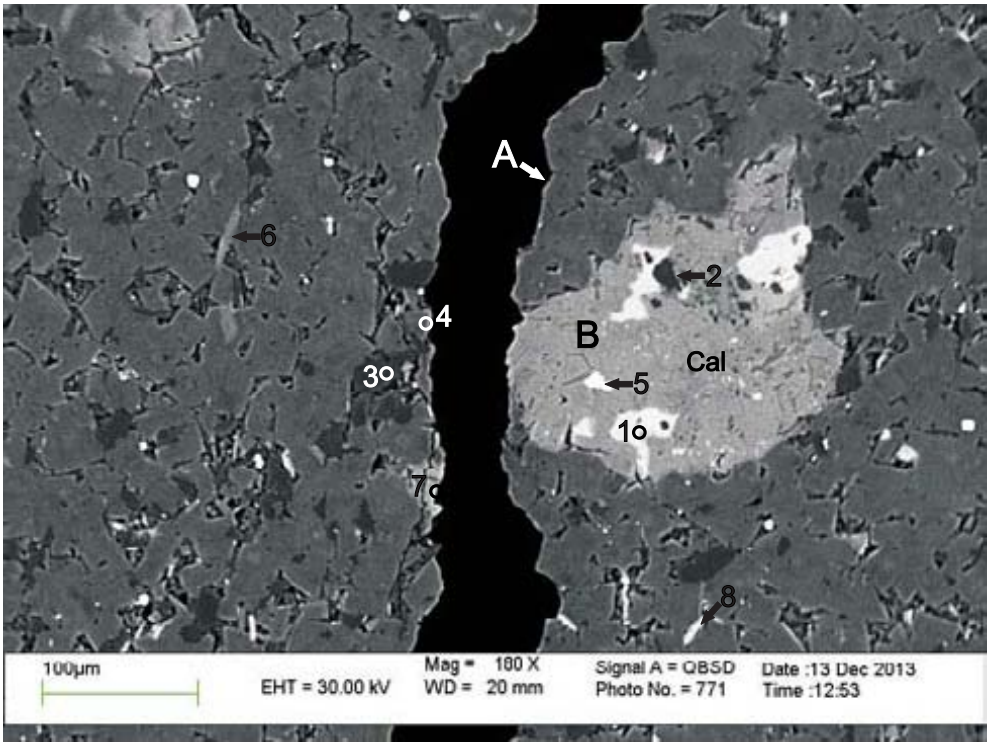

1: Anhydrite
2: Albite + Calcite
3: Quartz
4: Dolomite
5: Barite + Dolomite
6: Muscovite
7: Dolomite + other
8: Quartz + Muscovite + Chlorite

Figure 5: Mohican I-100: 3697.36B site 5. Fracture occured prior to later diagenetic dolomite overgrowths as can be seen by the presence of overgrowths (position A) bordering the fracture. Small calcite nodule (position B) has been partly replaced by anhydrite.

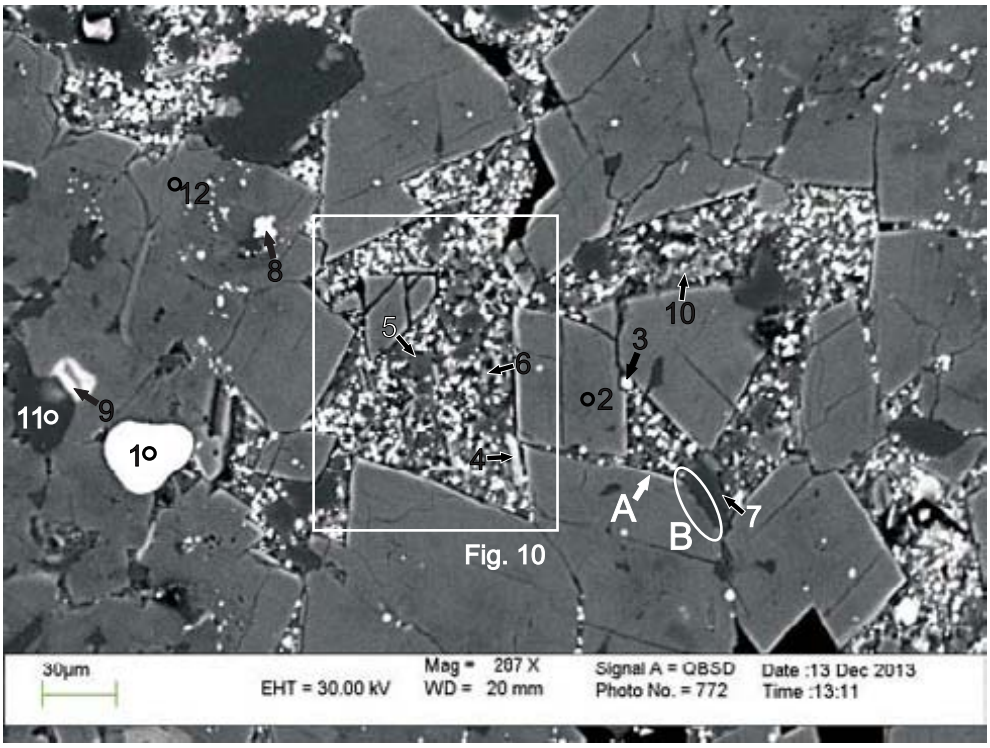

1: Pyrite
2: Dolomite
3: Dolomite + Illite
4: Dolomite + Illite
5: Muscovite + other
6: Pyrite + Illite
7: Quartz + other
8: Dolomite + Pyrite
9: Fe-Dolomite
10: Illite + Pyrite + Dolomite
11: Quartz
12: Dolomite

Figure 6: Mohican I-100: 3697.36B site 6. Overgrowths on dolomite seen where dolomite was exposed to porosity in the past (position A) and it is not seen when dolomite is in contact with framework grains, such as quartz (position B). See Fig. 10 for mineral details in microporosity.

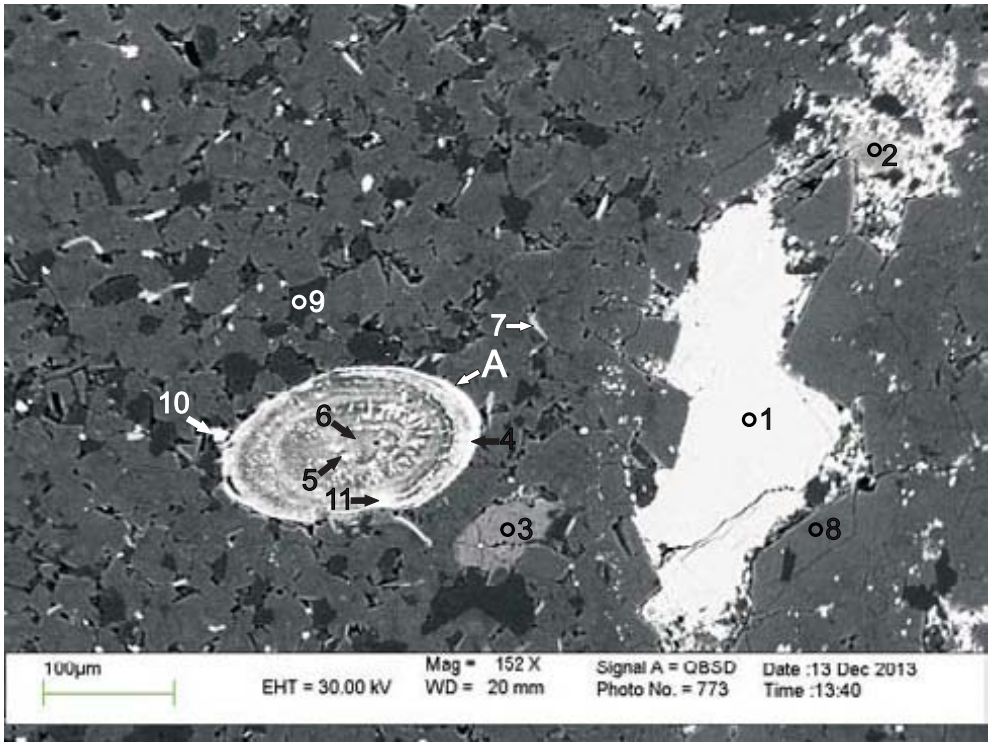

1: Anhydrite
2: Dolomite + Pyrite + Muscovite
3: K-feldspar
4: Fluorapatite + Pyrite
5: Marcasite + Apatite
6: Fluorapatite + Pyrite
7: Muscovite + Chlorite + Calcite
8: Dolomite
9: Quartz
10: Muscovite + Pyrite + Calcite
11: Fluorapatite + Chlorite + Illite

Figure 7: Mohican I-100: 3697.36B site 7. Coated grain or phosphorite (position A), consisting of pyrite, marcasite, fluorapatite, and chlorite.

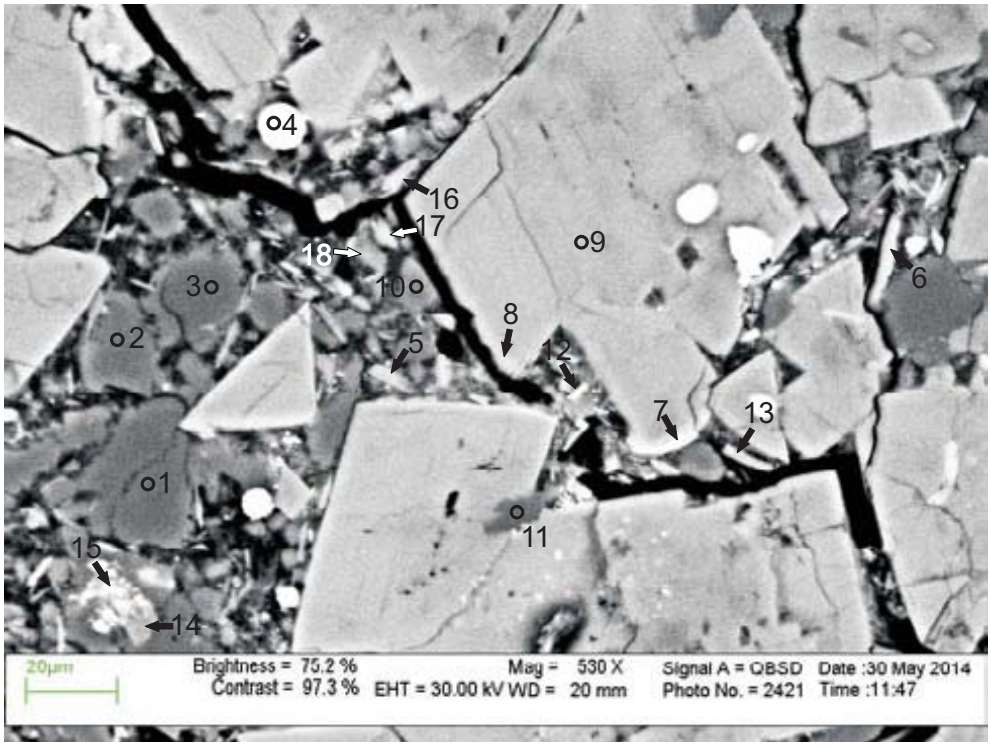

1: Quartz
2: Albite
3: Quartz + Muscovite
4: Fe-Dolomite
5: Quartz + Muscovite
6: Fe-Dolomite + Muscovite
7: Fe-Dolomite + Muscovite
8: Muscovite + Dolomite
9: Fe-Dolomite
10: Muscovite + Dolomite
11: Fe-Dolomite
12: Fe-Dolomite + Quartz
13: Fe-Dolomite + Muscovite
14: Quartz + Muscovite
15: Muscovite + Pyrite

Figure 8: Mohican I-100: 3697.36B site 8 (from Fig. 1). Fine grained matrix in intergranular boundary between dolomite. Matrix is composed of muscovite, K-feldspar, and dolomite.

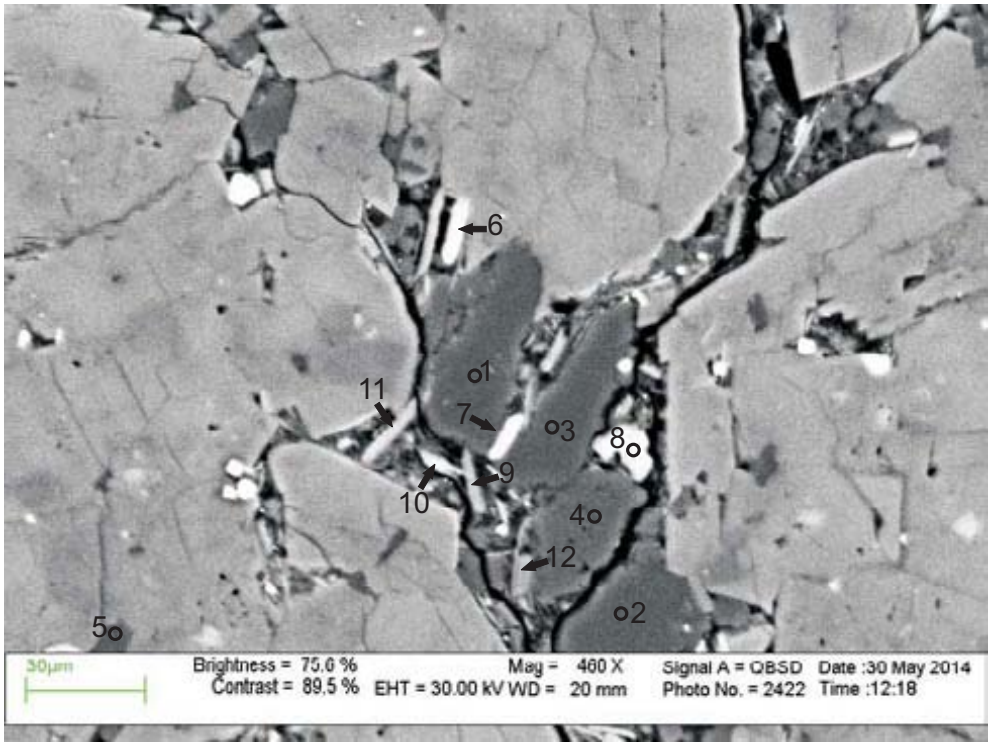

1-3: Quartz
4: Albite
5: Fe-Dolomite + Quartz
6: Muscovite + Chlorite
7: Quartz
8: Quartz + Muscovite + Pyrite
9: Muscovite + Fe-Dolomite
10: Muscovite
11: Fe-Dolomite
12: Quartz + Muscovite

Figure 9: Mohican I-100: 3697.36B site 9 (from Fig. 1). Grains of sparry dolomite appear to have displaced original detrital quartz, feldspar, and chloritized muscovite, into linear patches.

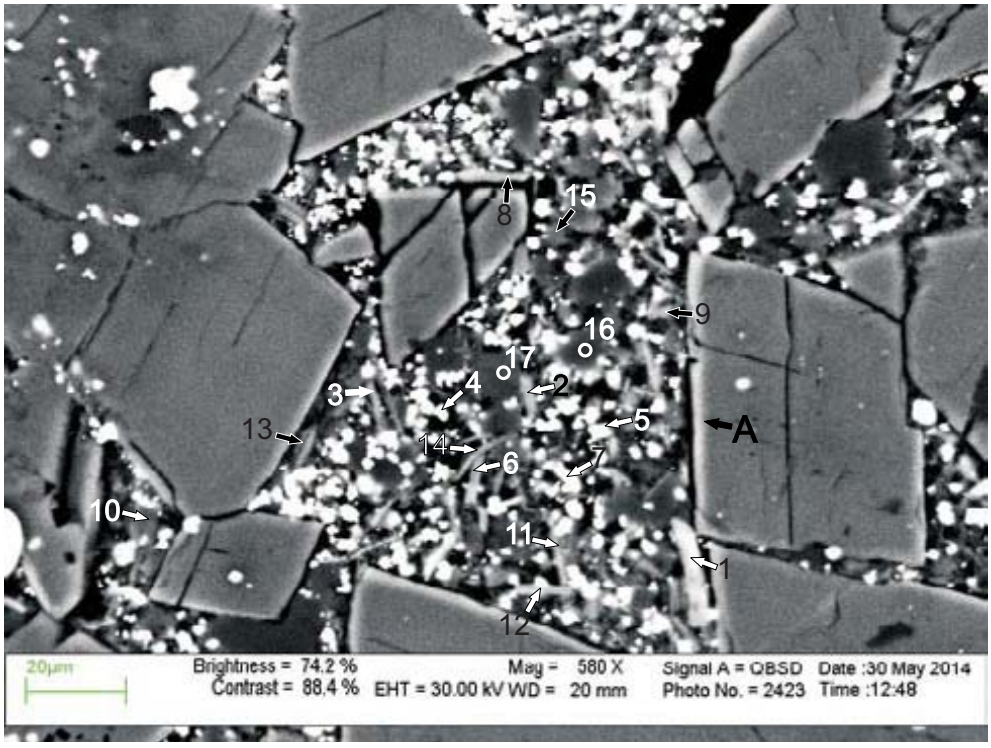

1: Fe-Dolomite + Pyrite + Illite
2: Fe-Dolomite + Pyrite + Illite
3: Muscovite + Pyrite
4: Pyrite + Dolomite + Muscovite
5-8: Pyrite + Dolomite + Illite
9: Fe-Dolomite + Pyrite + Muscovite
10: Dolomite + Pyrite + Muscovite
11: Pyrite + Dolomite + Muscovite
12: Pyrite + Dolomite + Muscovite
13-15: Quartz + Pyrite + Muscovite

Figure 10: Mohican I-100 3697.36B site 10 (from Fig. 6). Microporosity composed of diagenetic pyrite, dolomite, muscovite and illite. Late diagenetic overgrowths on early diagenetic dolomite is most visible here (position A).

Table 1E: Scanning electron microscope chemical analyses of minerals from representative sites for Mohican I-100 well at 3697.36Bm depth

Sample	Site	Position	Mineral	SiO_2	TiO_2	Al_2O_3	FeO	MnO	MgO	CaO	Na_2O	K_2O	P_2O_5	SO_3	F	Cl	CuO	As_2O_3	SrO	BaO	Total	Actual Total
I-100-3697.36B	1	1	Pyrite				25.97							74.04							100.00	228.08
I-100-3697.36B	1	2	Dolomite + Chlorite	1.60		1.13	4.99	0.28	39.17	52.82											100.00	57.54
I-100-3697.36B	1	3	Quartz	99.99																	100.00	120.31
I-100-3697.36B	1	4	Dolomite + Chlorite	1.03			4.35		38.55	56.08											100.00	59.60
I-100-3697.36B	1	5	Dolomite + Muscovite	4.73		1.74	4.71	0.35	35.07	53.18		0.24									100.00	58.58
I-100-3697.36B	1	6	Muscovite + Fe-Dolomite	65.44	0.33	22.77	2.32		2.69	0.35	0.89	5.00				0.22					100.00	112.58
I-100-3697.36B	1	7	Quartz + other	84.22		9.58	0.81		0.58		0.59	1.98		1.30					0.59	0.35	100.00	125.76
I-100-3697.36B	2	1	Pyrite				26.64			0.24				73.11							100.00	220.45
I-100-3697.36B	2	2	Muscovite + other	37.39	0.30	27.34	4.09		6.48	17.81	1.05	5.54									100.00	98.61
I-100-3697.36B	2	3	Dolomite + other	4.02		2.12	3.58		33.64	55.18		0.64		0.82							100.00	61.13
I-100-3697.36B	2	4	Anhydrite							37.54				62.45							100.00	116.50
I-100-3697.36B	2	5	Albite + Calcite	61.18		17.12	1.47		1.53	6.49	12.21										100.00	121.99
I-100-3697.36B	2	6	Dolomite + other	1.69		0.79	2.98	0.28	36.05	53.34		0.18			4.68						100.00	61.35
I-100-3697.36B	2	7	Anhydrite + other	66.42			2.65	0.15	2.59	17.38				10.79							100.00	108.47
I-100-3697.36B	2	8	Illite + other	47.92		21.35	4.19		6.10	13.42	4.64	2.38									100.00	96.54
I-100-3697.36B	2	9	Dolomite				2.43	0.16	20.44	28.97											52.00	56.86
I-100-3697.36B	3	1	Anhydrite							36.13				63.88							100.00	126.48
I-100-3697.36B	3	2	Anhydrite							37.22				62.78							100.00	111.38
I-100-3697.36B	3	3	Anhydrite							37.36				62.65							100.00	118.35
I-100-3697.36B	3	4	Anhydrite	0.90					0.48	36.09	0.53			62.00							100.00	118.50
I-100-3697.36B	4	1	Anhydrite							37.40				62.60							100.00	103.30
I-100-3697.36B	4	2	Quartz	99.49			0.12			0.38											100.00	121.42
I-100-3697.36B	4	3	Quartz	86.81		0.43	0.73		2.82	9.04		0.17									100.00	106.35
I-100-3697.36B	4	4	Anhydrite + Ankerite				2.92	0.21	4.21	41.25				51.44							100.00	84.43
I-100-3697.36B	4	5	Anhydrite							36.91				63.10							100.00	110.43
I-100-3697.36B	4	6	Dolomite + Pyrite	2.99		1.77	2.02		17.47	27.03		0.36		0.36							52.00	62.12
I-100-3697.36B	4	7	Anhydrite							37.32				62.68							100.00	100.56
I-100-3697.36B	5	1	Anhydrite	0.73						37.34				61.95							100.00	116.69
I-100-3697.36B	5	2	Albite + Calcite	64.18		17.95	0.42		0.55	2.91	12.17	0.12		1.70							100.00	131.71
I-100-3697.36B	5	3	Quartz	99.41		0.43				0.15											100.00	123.13
I-100-3697.36B	5	4	Dolomite	1.92		1.14	1.36	0.13	19.15	28.13		0.17									52.00	58.52
I-100-3697.36B	5	5	Barite + Dolomite				1.94		3.93	6.44				37.08					4.15	46.47	100.00	102.44
I-100-3697.36B	5	6	Muscovite	41.98	0.23	26.25	3.01		5.89	8.12	0.66	6.85									93.00	104.48
I-100-3697.36B	5	7	Dolomite + other	3.87		1.49	16.42	0.93	25.35	50.82		1.11									100.00	36.12
I-100-3697.36B	5	8	Quartz + Muscovite + Chlorite	70.79	0.58	11.60	8.10		3.73	1.82	0.78	2.58									100.00	110.29
I-100-3697.36B	6	1	Pyrite				26.10			0.15				73.74							100.00	215.29
I-100-3697.36B	6	2	Dolomite				2.94	0.22	19.31	29.53											52.00	59.30
I-100-3697.36B	6	3	Dolomite + Illite	13.97		9.39	11.77	0.36	21.19	33.22		1.08		8.84		0.17					100.00	76.82
I-100-3697.36B	6	4	Dolomite + Illite	3.66		3.10	12.41	0.70	29.68	49.22		0.31		0.92							100.00	63.23
I-100-3697.36B	6	5	Muscovite + other	53.16	0.25	29.16	3.04		1.08	0.57	2.01	7.18		3.55							100.00	124.02
I-100-3697.36B	6	6	Pyrite + Illite	38.70		11.13	12.14		1.39	0.76	0.31	2.59		32.96							100.00	164.33
I-100-3697.36B	6	7	Quartz + other	89.03		5.44	1.16		0.85	0.35	0.34	1.24		1.60							100.00	131.70
I-100-3697.36B	6	8	Dolomite + Pyrite	2.27		1.00	7.80	0.37	31.92	46.64		0.18		9.79							100.00	61.44
I-100-3697.36B	6	9	Fe-Dolomite				5.83	0.36	39.03	54.78											100.00	55.50
I-100-3697.36B	6	10	Illite + Pyrite + Dolomite	38.70		18.86	6.64	0.17	6.70	15.91	4.72	2.61		5.69							100.00	108.91
I-100-3697.36B	6	11	Quartz	97.87			0.26		0.60	1.26											100.00	120.46

Table 1E: Scanning electron microscope chemical analyses of minerals from representative sites for Mohican I-100 well at 3697.36Bm depth

Sample	Site	Position	Mineral	SiO_2	TiO_2	Al_2O_3	FeO	MnO	MgO	CaO	Na_2O	K_2O	P_2O_5	SO_3	F	Cl	CuO	As_2O_3	SrO	BaO	Total	Actual Total
I-100-3697.36B	6	12	Dolomite				3.04	0.19	19.46	28.96				0.35							52.00	57.45
I-100-3697.36B	7	1	Anhydrite							37.25				62.40					0.35		100.00	119.81
I-100-3697.36B	7	2	Dolomite + Pyrite + Muscovite	8.19		5.44	11.39	0.57	17.76	45.32	1.35	0.52		9.46							100.00	73.17
I-100-3697.36B	7	3	K-feldspar	66.98		18.10					0.27	14.65									100.00	125.50
I-100-3697.36B	7	4	Fluorapatite + Pyrite				0.28			42.98	1.94		41.64	3.52	9.38	0.27					100.00	122.34
I-100-3697.36B	7	5	Marcastie + Apatite				22.98			8.88	0.54		8.11	58.68		0.25	0.15	0.42			100.00	167.16
I-100-3697.36B	7	6	Fluorapatite + Pyrite				1.85			40.65	1.70		38.20	7.84	9.41	0.37					100.00	95.67
I-100-3697.36B	7	7	Muscovite + Chlorite + Calcite	34.53		25.40	15.75		14.23	8.77	0.39	0.94									100.00	100.71
I-100-3697.36B	7	8	Dolomite				3.32	0.18	19.69	28.80											52.00	60.33
I-100-3697.36B	7	9	Quartz	99.88						0.13											100.00	122.88
I-100-3697.36B	7	10	Muscovite + Pyrite + Calcite	26.33		16.78	13.41	0.18	5.24	6.90	0.50	3.07		27.39		0.23					100.00	87.98
I-100-3697.36B	7	11	Fluorapatite + Chlorite + Illite	2.97		2.48	2.02		0.35	33.59	1.52	0.77	34.67	3.60	17.74	0.28					100.00	128.55
I-100-3697.36B	8	1	Quartz	99.99																	99.99	2.70
I-100-3697.36B	8	2	Albite	63.85		21.37	0.53		0.65	0.59	9.71	1.88			1.42						100.00	111.68
I-100-3697.36B	8	3	Quartz + Muscovite	86.38	0.23	8.86	0.73		1.16		0.36	2.26									99.98	105.54
I-100-3697.36B	8	4	Fe-Dolomite	0.42			2.93	0.20	19.31	29.14											52.00	50.32
I-100-3697.36B	8	5	Quartz + Muscovite	73.57	0.22	16.74	1.49		1.34	0.91	0.32	4.72		0.47		0.21					99.99	98.74
I-100-3697.36B	8	6	Fe-Dolomite + Muscovite	21.84	0.62	4.84	5.53	0.40	26.23	39.19		1.32									99.97	60.41
I-100-3697.36B	8	7	Fe-Dolomite + Muscovite	24.73		12.98	5.89	0.22	21.95	29.61		2.94		1.70							100.02	66.82
I-100-3697.36B	8	8	Muscovite + Dolomite	56.18	0.28	31.03	1.63		1.84	0.90	0.88	7.08				0.21					100.03	91.20
I-100-3697.36B	8	9	Fe-Dolomite				2.87	0.17	19.13	29.84											52.00	47.98
I-100-3697.36B	8	10	Muscovite + Dolomite	57.05	0.35	27.66	3.45		3.81	0.42	0.63	6.37				0.26					100.00	90.47
I-100-3697.36B	8	11	Fe-Dolomite				2.80	0.16	19.13	29.91											52.00	47.66
I-100-3697.36B	8	12	Fe-Dolomite + Quartz	1.45			6.11	0.39	35.45	56.60											100.00	48.04
I-100-3697.36B	8	13	Fe-Dolomite + Muscovite	5.75		3.63	10.99	0.62	30.23	48.29		0.51									100.00	50.88
I-100-3697.36B	8	14	Quartz + Muscovite	77.82	1.53	11.72	0.75		1.38		0.36	2.75			3.68						100.00	103.22
I-100-3697.36B	8	15	Muscovite + Pyrite	55.70	0.27	25.26	2.17		3.20		0.73	6.59		0.52	5.30	0.23					100.00	94.72
I-100-3697.36B	8	16	Fe-Dolomite + Muscovite	19.85		16.14	4.88	0.31	18.31	38.74		1.76									100.00	60.28
I-100-3697.36B	8	17	Muscovite + Fe-Dolomite	55.96	1.00	22.77	3.50		4.74	5.32	0.40	5.71		0.42		0.19					100.00	77.25
I-100-3697.36B	8	18	Muscovite + Fe-Dolomite	46.27	0.83	19.59	3.51		8.62	13.66		6.28				1.24					100.00	26.85
I-100-3697.36B	9	1	Quartz	99.99																	100.00	116.74
I-100-3697.36B	9	2	Quartz	99.99																	100.00	121.53
I-100-3697.36B	9	3	Quartz	99.99																	100.00	113.14
I-100-3697.36B	9	4	Albite	68.48		19.01				0.20	12.34										100.00	112.04
I-100-3697.36B	9	5	Fe-Dolomite + Quartz	2.10			3.06		37.13	57.56		0.17									100.00	50.23
I-100-3697.36B	9	6	Muscovite + Chlorite	61.07	1.87	23.30	3.47		2.39	0.70	0.70	6.18				0.31					100.00	90.53
I-100-3697.36B	9	7	Quartz	99.99																	100.00	107.84
I-100-3697.36B	9	8	Quartz + Muscovite + Pyrite	90.62		5.65	0.87		0.66			1.65		0.42		0.12					100.00	103.23
I-100-3697.36B	9	9	Muscovite + Fe-Dolomite	65.22		17.35	6.42		6.33	1.74	0.36	2.43				0.15					100.00	97.23
I-100-3697.36B	9	10	Muscovite	51.88	0.60	28.10	2.12		1.97		0.89	7.29				0.13					93.00	94.94
I-100-3697.36B	9	11	Fe-Dolomite				2.77	0.15	19.54	29.54											52.00	49.29
I-100-3697.36B	9	12	Quartz + Muscovite	92.46		4.89	0.55		0.58			1.51									100.00	101.62
I-100-3697.36B	10	1	Fe-Dolomite + Pyrite + Illite	22.87		14.02	17.60	0.48	8.32	14.65		2.71		19.15		0.22					100.00	80.72
I-100-3697.36B	10	2	Fe-Dolomite + Pyrite + Illite	40.54		18.46	7.90		2.92	5.37	0.63	4.48		16.16	3.36	0.20					100.00	104.19
I-100-3697.36B	10	3	Muscovite + Pyrite	55.60		21.88	4.93		1.38	0.57	1.00	5.36		9.09		0.18					100.00	102.22
I-100-3697.36B	10	4	Pyrite + Dolomite + Muscovite	52.15		26.13	5.07		1.82	0.95	1.94	6.13	0.66	4.84		0.26					100.00	96.31

Table 1E: Scanning electron microscope chemical analyses of minerals from representative sites for Mohican I-100 well at 3697.36Bm depth

Sample	Site	Position	Mineral	SiO_2	TiO_2	Al_2O_3	FeO	MnO	MgO	CaO	Na_2O	K_2O	P_2O_5	SO_3	F	Cl	CuO	As_2O_3	SrO	BaO	Total	Actual Total
I-100-3697.36B	10	5	Pyrite + Dolomite + Illite	47.23	0.30	22.79	6.29		2.79	1.36	0.57	5.94		7.29	5.30	0.14					100.00	105.56
I-100-3697.36B	10	6	Pyrite + Dolomite + Illite	89.85	0.30	4.65	1.31		0.56	0.21		1.16		1.97							100.00	105.52
I-100-3697.36B	10	7	Pyrite + Dolomite + Illite	23.21	0.13	14.10	15.40		1.66	0.81	0.44	3.06		41.00		0.18					100.00	147.36
I-100-3697.36B	10	8	Pyrite + Dolomite + Illite	51.32	0.32	21.54	7.40		2.50	1.08	2.75	4.70	0.71	7.47		0.24					100.00	103.90
I-100-3697.36B	10	9	Fe-Dolomite + Pyrite + Muscovite	11.04		7.20	12.27	0.67	24.01	41.56		1.01		2.22							100.00	63.94
I-100-3697.36B	10	10	Dolomite + Pyrite + Muscovite	25.41		12.72	10.48		16.43	24.91		2.43		7.42		0.21					100.00	76.05
I-100-3697.36B	10	11	Pyrite + Dolomite + Muscovite	36.20	0.27	18.99	8.05		2.34	3.75	0.78	4.93		18.28	6.22	0.20					100.00	110.40
I-100-3697.36B	10	12	Pyrite + Dolomite + Muscovite	19.49		12.75	16.29		1.28	2.14	0.61	2.79		44.65							100.00	144.10
I-100-3697.36B	10	13	Quartz + Pyrite + Muscovite	72.09		7.95	5.85		0.95	0.55	0.40	1.99		9.99		0.21					100.00	109.33
I-100-3697.36B	10	14	Quartz + Pyrite + Muscovite	75.36	0.72	13.83	2.21		1.16	0.66	0.31	3.29	0.44	2.00							100.00	109.59
I-100-3697.36B	10	15	Quartz + Pyrite + Muscovite	78.98	0.23	8.30	3.91		1.03	0.29		2.71		4.52							100.00	107.93
I-100-3697.36B	10	16	Pyrite + Muscovite	55.45	0.42	19.37	6.90		2.45	0.70	0.39	5.61		6.74	1.81	0.15					100.00	101.86
I-100-3697.36B	10	17	Muscovite + Pyrite	48.58	0.73	22.66	7.86		3.37	0.69	1.07	5.24		7.02	2.63	0.19					100.00	96.92

Appendix 2F: Scanning Electron Microscope Backscattered Electron Images for Mohican I-100 well with EDS Mineral Analyses Sample 3697.86

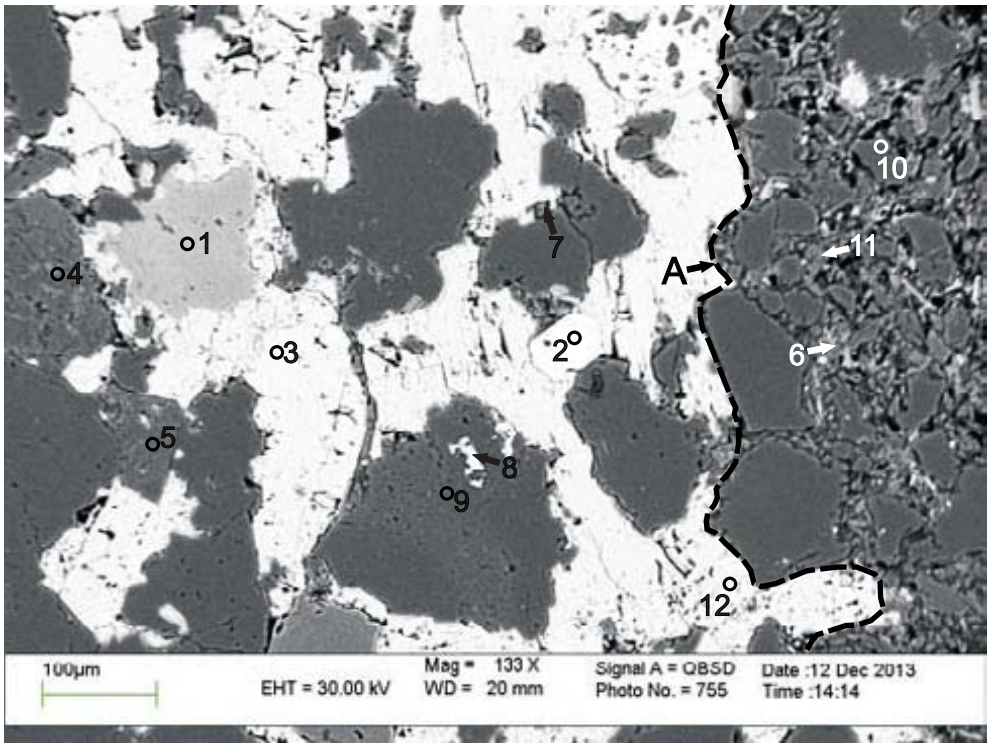

1: K-feldspar
2: Zircon
3: Anhydrite
4: Albite w/Perthite
5: Albite
6: Chlorite + Muscovite
7: Anhydrite
8: Quartz + TiO_2
9: Albite
10-12: Anhydrite + Muscovite

Figure 1: Mohican I-100: 3697.86 site 1. Contact (position A) between a matrix supported zone, rich in muscovite and chlorite (analysis 6) and a zone cemented by anhydrite (analyses 3 and 12).

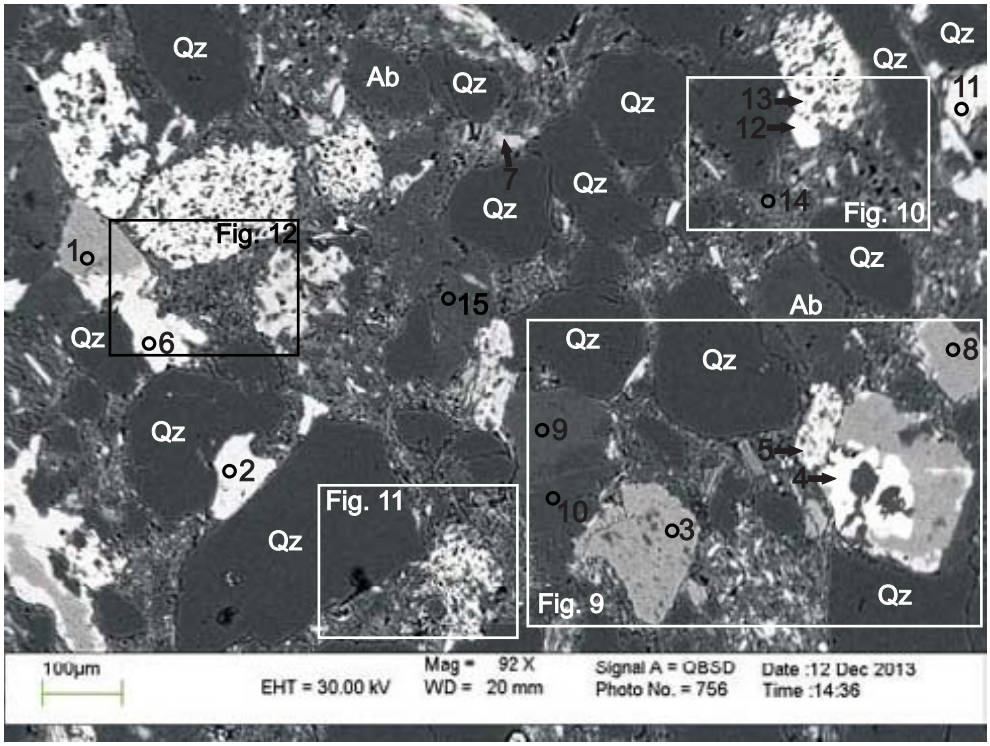

1: K-feldspar
2: Anhydrite
3: K-feldspar
4: Chalcopyrite
5: Altered Ilmenite + other
6: Anhydrite
7: Chlorite
8: K-feldspar
9: Albite
10: Albite
11: Anhydrite
12: Altered Ilmenite + other
13: Altered Ilmenite + other
14: K-feldspar
15: Albite

Figure 2: Mohican I-100: 3697.86 site 2. For mineralogical detals of fine grained areas in this site see Figs. 9, 10, 11 and 12.

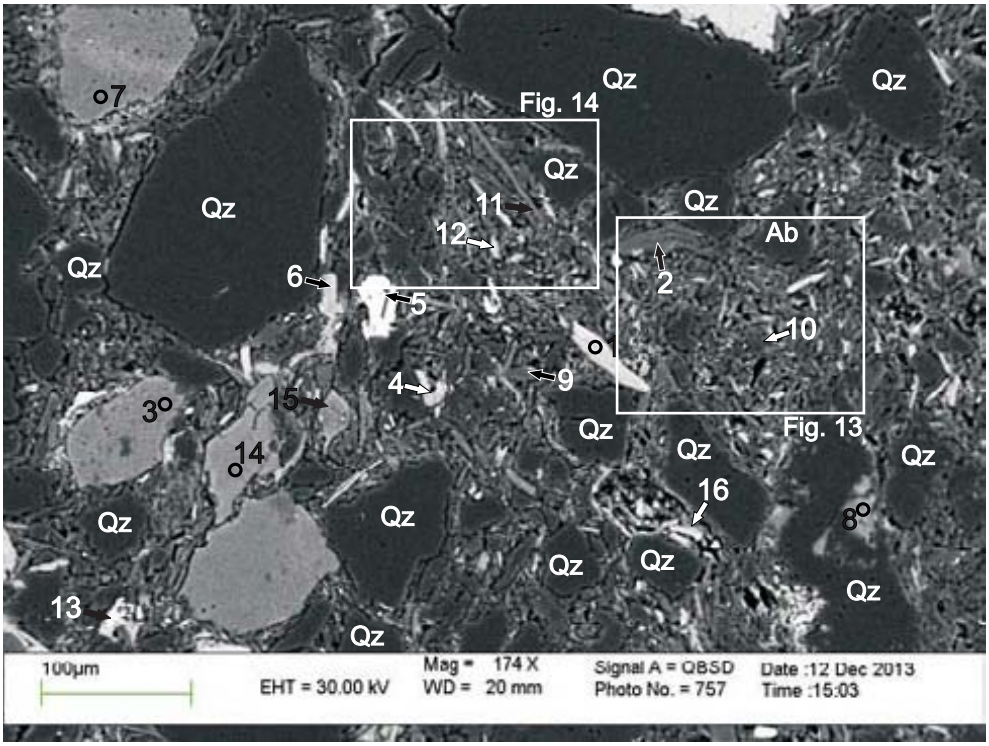

1: Chlorite
2: Muscovite
3: K-feldspar
4: Chlorite
5: Monazite + Chlorite
6: Chlorite
7: K-feldspar
8: K-feldspar
9: Muscovite
10: Albite
11: Muscovite
12: Chlorite + Muscovite
13: Altered Ilmenite + Muscovite
14: K-feldspar
15: K-feldspar
16: Chlorite

Figure 3: Mohican I-100: 3697.86 site 3. For mineralogical details of the matrix in this site see Figs. 13 and 14.

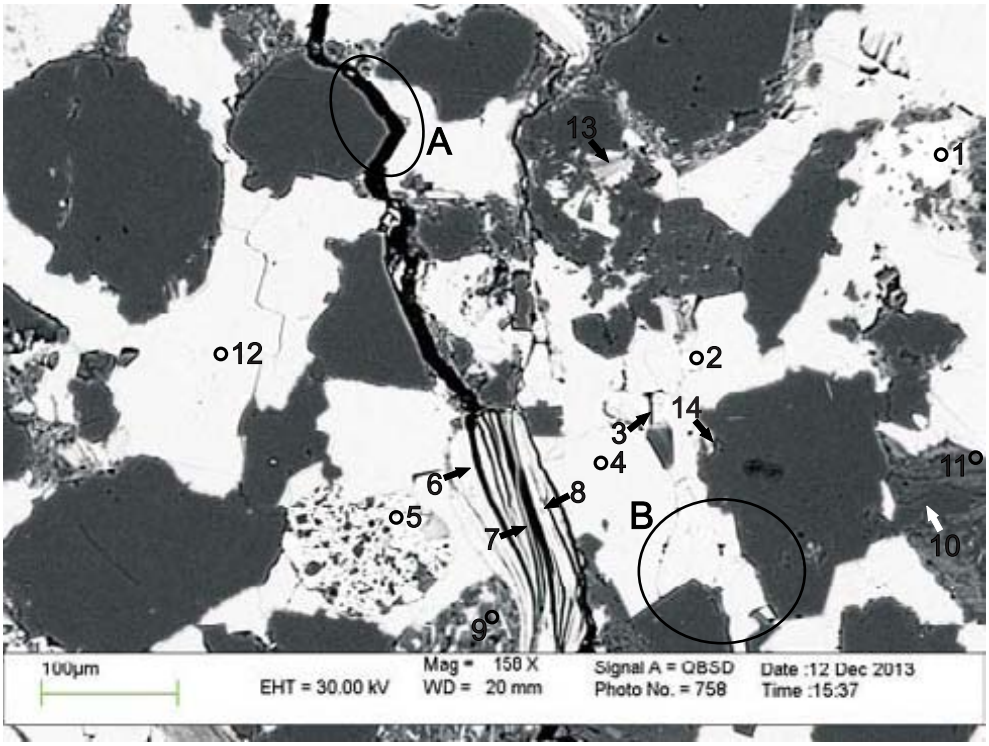

1: Altered Ilmenite
2: Anhydrite + TiO_2
3: Anhydrite
4: Anhydrite
5: Altered Ilmenite
6: Chlorite
7: Muscovite
8: Chlorite after Muscovite
9: Muscovite
10: Quartz
11: Chlorite + Anhydrite + Muscovite
12: Anhydrite
13: Chlorite + Muscovite
14: Quartz

Figure 4: Mohican I-100: 3697.86 site 4. Quartz overgrowths (positions A and B), along a thin linear dissolution zone, suggesting that dissolution occured after cementation by anhydrite and then the quartz overgrowths formed.

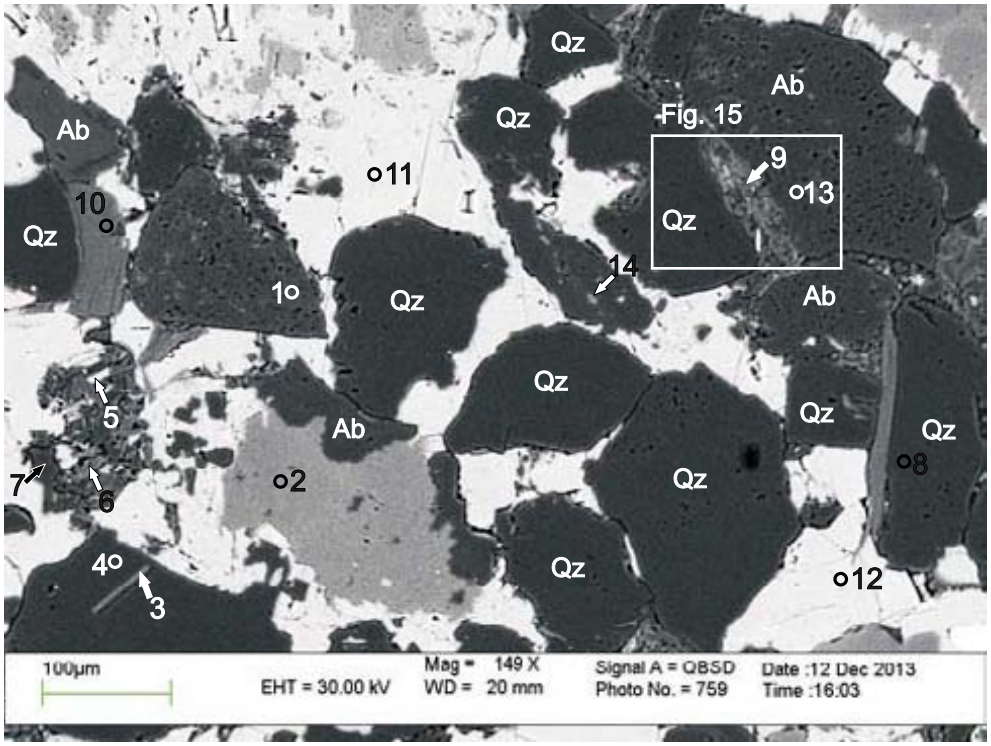

1: Albite
2: K-feldspar
3: Muscovite + Quartz
4: Quartz
5: Quartz
6: Muscovite
7: Quartz
8: Quartz
9: Muscovite
10: Muscovite
11: Anhydrite
12: Anhydrite
13: Albite + K-feldspar
14: Albite

Figure 5: Mohican I-100: 3697.86 site 5. Albite contains dissolution voids. Lithic clast forms pseudomatrix between detrital quartz and albite (see Fig. 15).

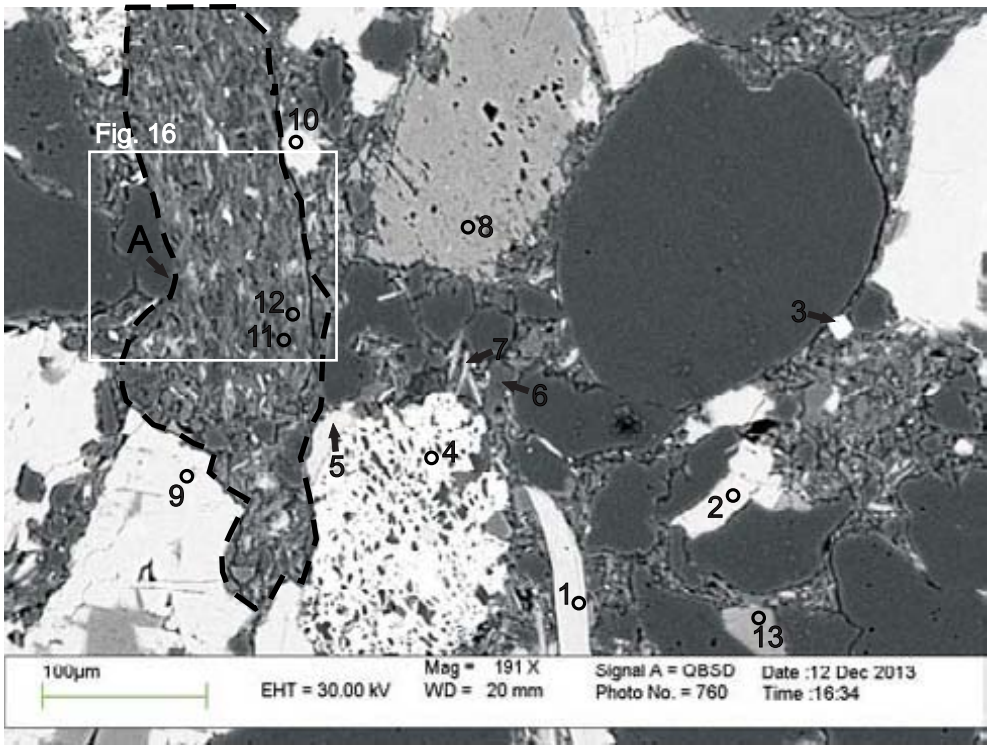

1: Biotite
2: Anhydrite
3: Quartz + other
4: Quartz + TiO_2
5: Anhydrite
6: Muscovite
7: Quartz
8: K-feldspar
9: Anhydrite
10: Anhydrite + Chlorite
11:TiO_2 + Muscovite
12: Muscovite
13: K-feldspar + Chlorite

Figure 6: Mohican I-100: 3697.86 site 6. Lithic clast (position A) composed of quartz, muscovite and chlorite (see Fig. 16 and App. 4B, Fig. 7).

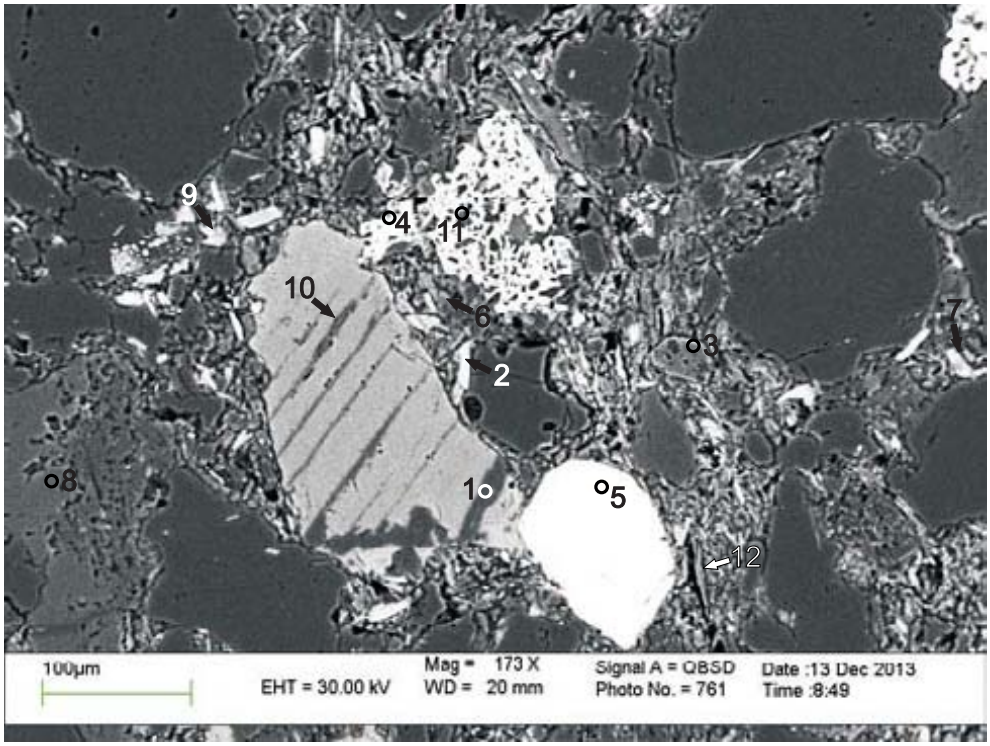

1: Albite
2: Chlorite
3: Chlorite + Muscovite
4: Altered Ilmenite
5: Fluorapatite
6: Chlorite + other
7: Muscovite
8: Albite
9: Illite
10: K-feldspar w/Perthite
11: Altered Ilmenite + Quartz
12: Illite

Figure 7: Mohican I-100: 3697.86 site 7. Detrital minerals of perthitic K-feldspar (analysis 10), fluorapatite (analysis 5) and ilmenite (analysis 11).

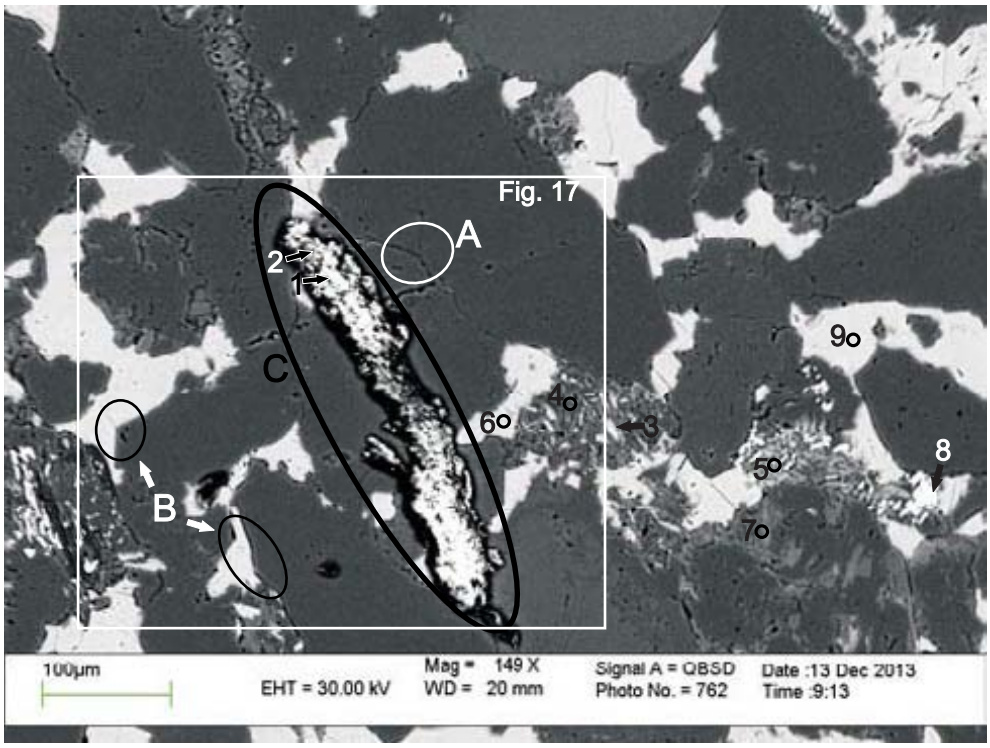

1-2: SEM charging - unreliable data
3: Chlorite + Illite
4: Illite + other
5: Illite
6: Anhydrite
7: Muscovite
8: Altered Ilmenite + Quartz
9: Anhydrite

Figure 8: Mohican I-100: 3697.86 site 8. Apparent triple point (position A) and quartz overgrowths (position B). SEM charging occured (analyses 1 and 2, and position C) producing poor results in this area, see Fig. 17 for cleaner image and for mineralogical details in this site.

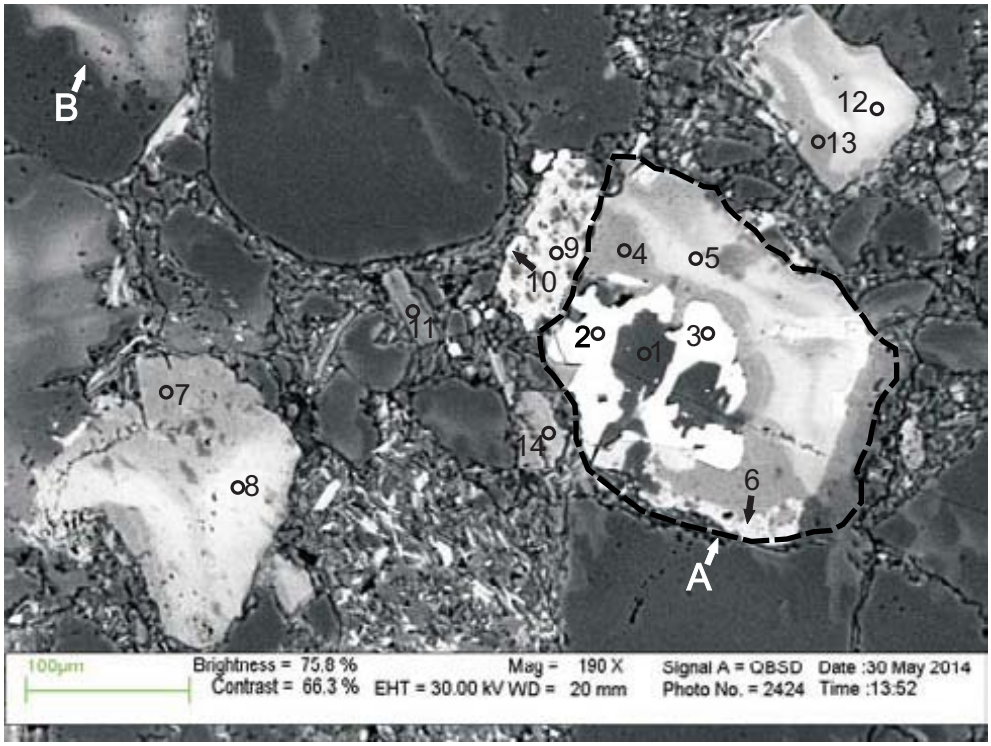

1: Albite
2: Chalcopyrite
3: Chalcopyrite + Albite
4: Chalcopyrite + K-feldspar
5: K-feldspar
6: Quartz
7: Fe-Dolomite + Muscovite
8: K-feldspar
9: Altered Ilmenite + Albite
10: Quartz + other
11: K-feldspar + other
12: K-feldspar
13: Quartz + K-feldspar + other
14: K-feldspar

Figure 9: Mohican I-100 3697.86 site 9 (from Fig. 2). Lithic clast (position A) made up of K-feldspar, albite, and chalcopyrite. Discolouration of mineral (position B) is not due to chemical variation but is from SEM charging.

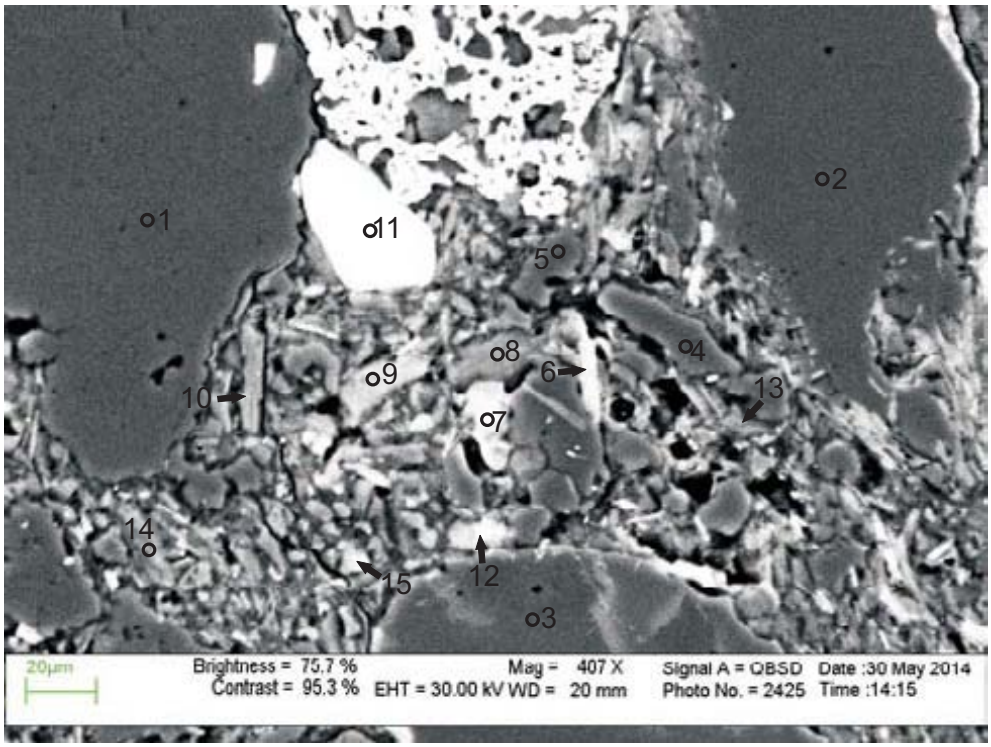

1-3: Quartz
4: Quartz + other
5: Quartz
6: Quartz + other
7-10: Muscovite + Chlorite
11: Ilmenite + Muscovite
12: Quartz + Muscovite
13: Muscovite + Chlorite
14: Albite
15: K-feldspar

Figure 10: Mohican I-100 3697.86 site 10 (from Fig. 2). Matrix composed mostly of muscovite and chlorite.

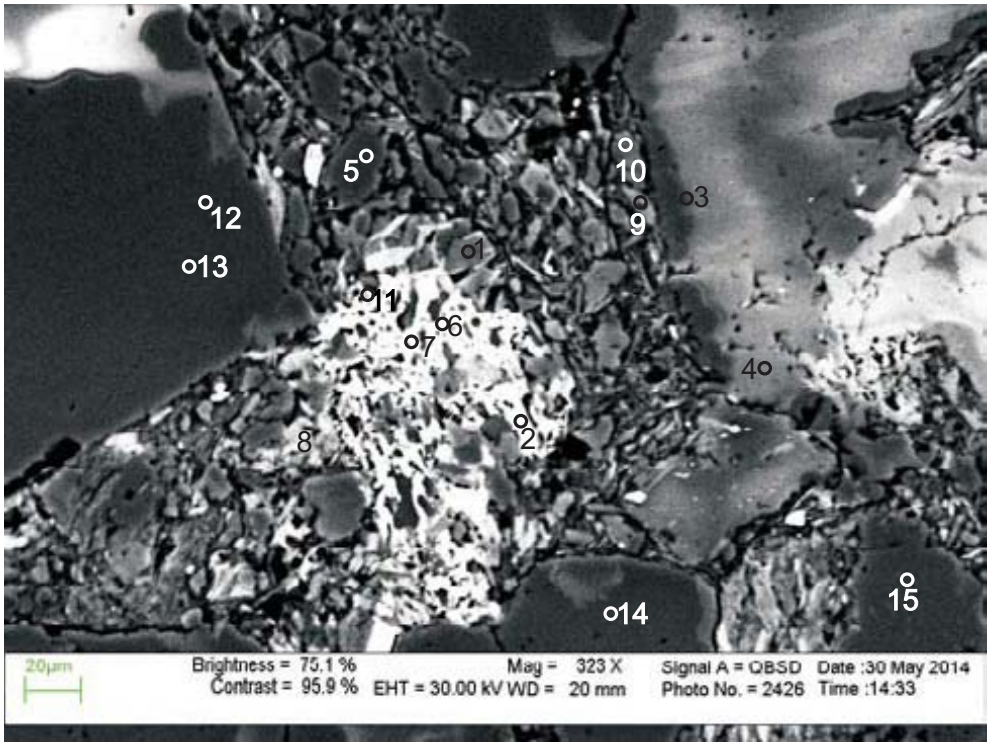

1: Muscovite
2: Muscovite + Altered Ilmenite
3: Albite
4: Albite
5: Quartz + Muscovite + Chlorite
6: Altered Ilmenite + Muscovite
7: Quartz + Altered Ilmenite + other
8: Muscovite + Quartz
9: Muscovite
10: Quartz + Muscovite
11: TiO_2 + Chlorite
12-15: Quartz

Figure 11: Mohican I-100 3697.86 site 11 (from Fig. 2). Altered ilmenite with muscovite inclusions (analysis 2). Discolouration of some grains is not caused by chemical variation (analyses 3 and 4, and see Table 1F) but is from charging on SEM lilkely due to uneven carbon coating.

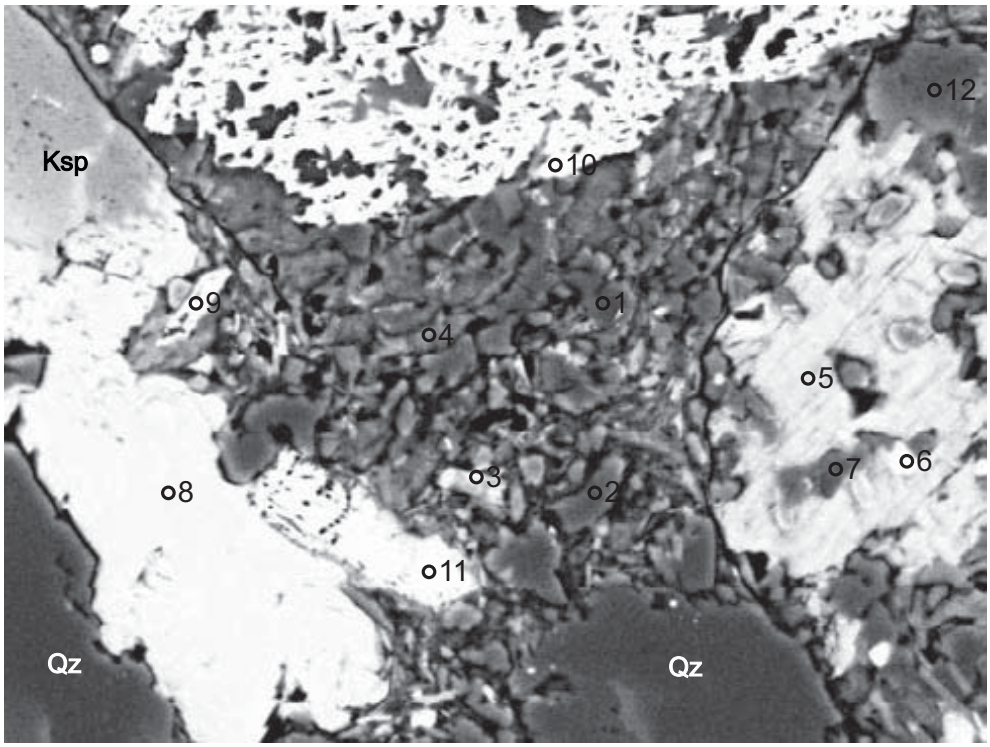

1: Muscovite + Chlorite
2: Quartz + Muscovite
3: Muscovite + Chlorite
4: Quartz + Muscovite
5: Albite + Chlorite
6: Chlorite + TiO_2
7: Muscovite + Chlorite
8: Anhydrite + Quartz
9: Muscovite + Anhydrite
10: Quartz + Muscovite
11: Anhydrite + Pyrite + Muscovite
12: Muscovite + Chlorite

Figure 12: Mohican I-100 3697.86 side 12 (from Fig. 2). Fine grained matrix composed of muscovite, chlorite, and fragments of detrital quartz (analysis 4), adjacent to anhydrite (analysis 8) that cements K-feldspar and quartz.

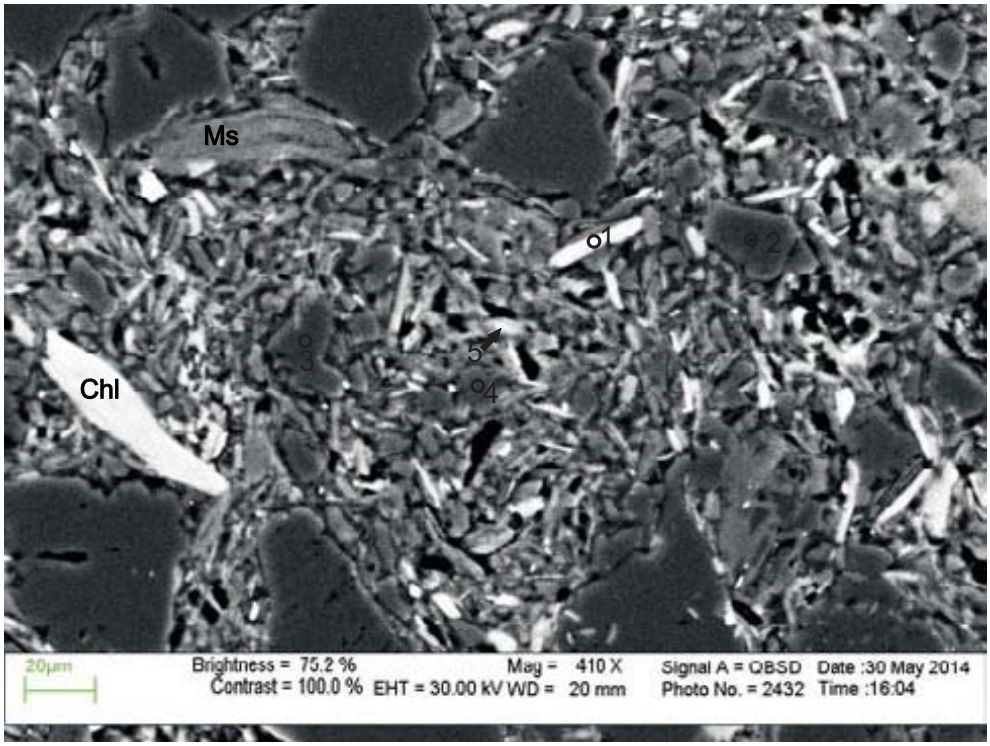

1: Muscovite + Chlorite
2: Quartz
3: Quartz
4: Albite
5: Muscovite + Chlorite

Figure 13: Mohican I-100 3697.86 site 13 (from Fig. 3). Chlorite and muscovite is present as both matrix (analysis 5), and as larger framework grains.

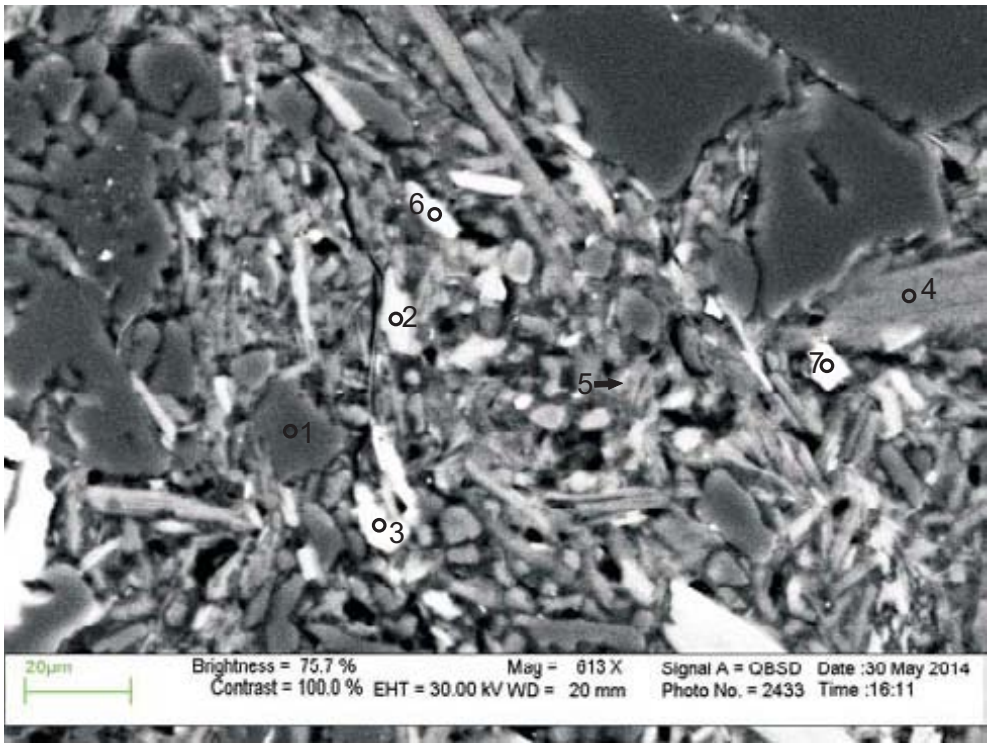

1: Albite
2: Muscovite + Chlorite
3: Muscovite + TiO_2
4: Muscovite
5: Muscovite + other
6: Muscovite + Chlorite
7: Muscovite + other

Figure 14: Mohican I-100 3697.86 site 14 (from Fig. 3). Fine grained matrix composed mostly of muscovite and chlorite.

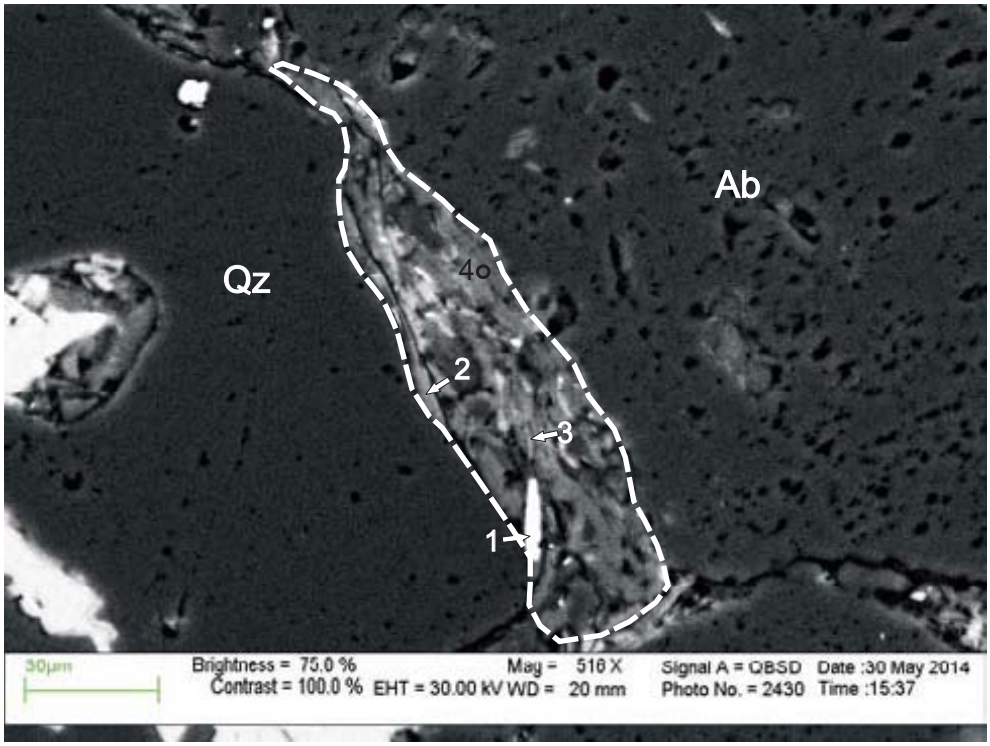

1: Muscovite + TiO_2
2: Muscovite
3: Muscovite + Chlorite
4: Muscovite + other

Figure 15: Mohican I-100 3697.86 site 15 (from Fig. 5). Muscovite and chlorite rich lithic clast forms pseudomatrix between detrital grains of quartz and albite (see App. 4B, Fig. 8).

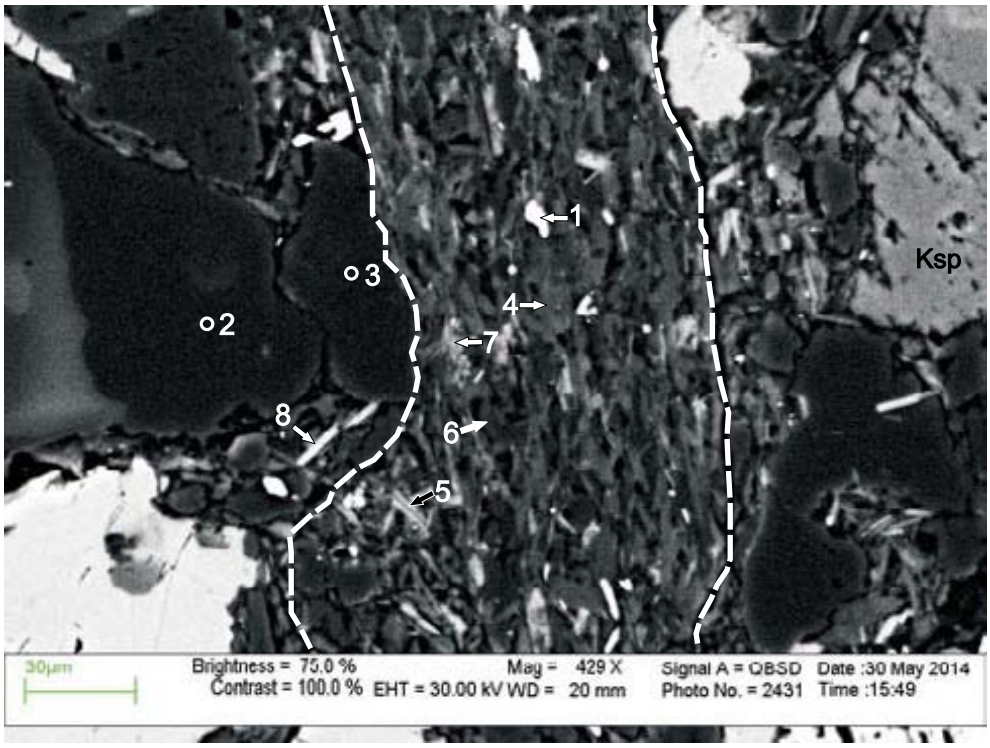

1: Muscovite + TiO_2
2: Quartz
3: Quartz
4: Muscovite + TiO_2
5: Muscovite + Chlorite
6-8: Quartz + Muscovite

Figure 16: Mohican I-100 3697.86 site 16 (from Fig. 6). Lithic clast made up of K-feldspar, quartz, muscovite and TiO_2. Orientation of the grains in the clast show that this is likely a slate, probably from the Meguma Group.

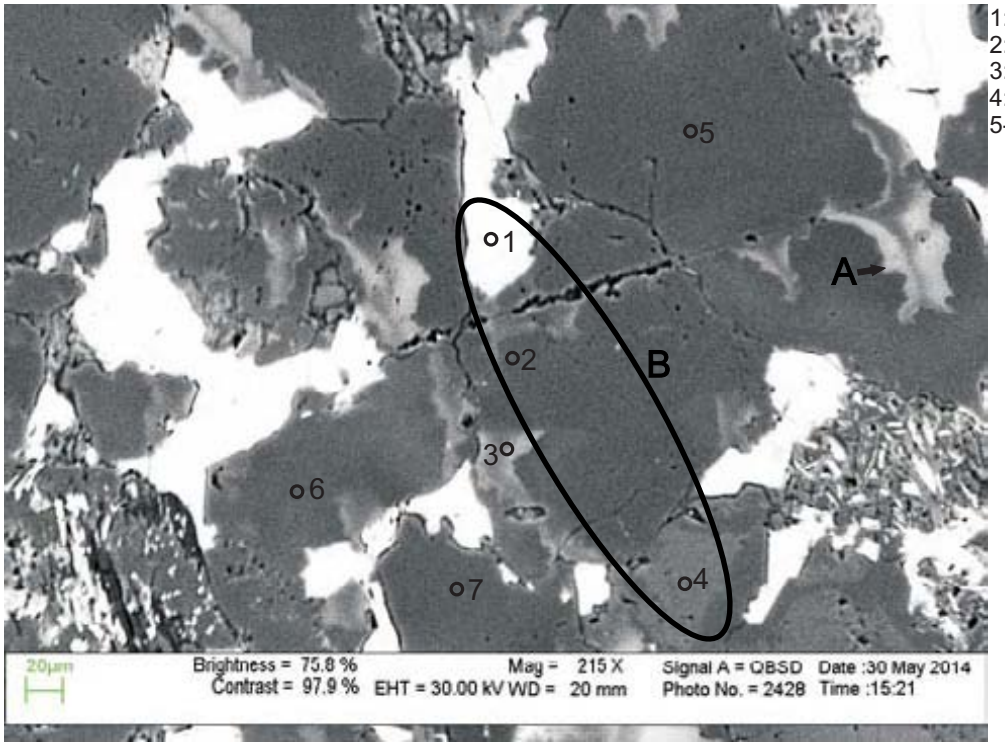

1: Anhydrite
2: Quartz
3: Quartz
4: Albite
5-7: Quartz

Figure 17: Mohican I-100 3697.86 site 17 (from Fig, 8). Variation in colour between analyses 2 and 3 and position A are from SEM charging and not due to variations in mineral composition. Area containing anhydrite (analysis 1), quartz (analysis 2) and albite (analysis 4) all within position B, is the same area seen in Fig. 8 position C.

Table 1F: Scanning electron microscope chemical analyses of minerals from representative sites for Mohican I-100 well at 3697.86m depth

Sample	Site	Position	Mineral	SiO_2	TiO_2	Al_2O_3	FeO	MnO	MgO	CaO	Na_2O	K_2O	P_2O_5	SO_3	F	Cl	CuO	SrO	ZrO_2	BaO	La_2O_3	Ce_2O_3	Nd_2O_3	HfO_2	Total	Actual Total
I-100-3697.86	1	1	K-feldspar	65.84		18.20					0.66	14.76								0.55					100.00	116.75
I-100-3697.86	1	2	Zircon	31.68															67.30					1.03	100.00	128.04
I-100-3697.86	1	3	Anhydrite							37.72				61.70				0.57							100.00	114.31
I-100-3697.86	1	4	Albite w/Perthite	59.83		25.96	0.28			0.42	8.66	4.85													100.00	121.03
I-100-3697.86	1	5	Albite	66.10		21.09	0.32			0.92	10.60	0.98													100.00	118.00
I-100-3697.86	1	6	Chlorite + Muscovite	69.78	0.30	17.95	5.63		2.32		1.21	2.79													100.00	121.44
I-100-3697.86	1	7	Anhydrite	0.79						37.32				61.90											100.00	115.14
I-100-3697.86	1	8	Quartz + TiO2	80.20	19.58		0.19																		100.00	123.72
I-100-3697.86	1	9	Albite	68.22		19.24				0.35	12.19														100.00	125.30
I-100-3697.86	1	10	Anhydrite + Muscovite	55.45		6.20	0.72		0.41	9.79	1.82	1.19		23.52											100.00	131.05
I-100-3697.86	1	11	Anhydrite + Muscovite	52.84	0.98	5.80	0.71		0.46	10.89	1.46	1.17		25.69											100.00	129.94
I-100-3697.86	1	12	Anhydrite + Muscovite	52.90	0.97	5.71	0.66		0.35	10.89	1.66	1.18		25.69											100.00	129.75
I-100-3697.86	2	1	K-feldspar	66.61		18.27	0.21				0.46	14.45													100.00	109.74
I-100-3697.86	2	2	Anhydrite							37.15				62.18				0.69							100.00	105.98
I-100-3697.86	2	3	K-feldspar	66.46		18.46					0.59	14.49													100.00	124.93
I-100-3697.86	2	4	Chalcopyrite	0.19			21.02							56.96			21.84								100.00	188.20
I-100-3697.86	2	5	Altered Ilmenite + other	24.58	65.57	2.40	6.47			0.45		0.24				0.30									100.00	89.12
I-100-3697.86	2	6	Anhydrite							36.90				62.53				0.57							100.00	102.55
I-100-3697.86	2	7	Chlorite	31.62		23.47	16.22		13.13		0.37	0.20													85.00	100.26
I-100-3697.86	2	8	K-feldspar	66.74		18.39					1.08	13.80													100.00	132.46
I-100-3697.86	2	9	Albite	65.42		21.09				2.01	10.96	0.51													100.00	128.16
I-100-3697.86	2	10	Albite	68.58		18.71					12.71														100.00	129.72
I-100-3697.86	2	11	Anhydrite			0.32				36.97				62.15				0.58							100.00	119.47
I-100-3697.86	2	12	Altered Ilmenite + other	4.64	83.10	2.15	7.87		1.36	0.64						0.23									100.00	80.52
I-100-3697.86	2	13	Altered Ilmenite + other	18.61	74.63	4.18	1.08		0.46			1.06													100.00	99.33
I-100-3697.86	2	14	K-feldspar	61.22	0.43	26.51	2.19		2.14		0.80	6.59				0.15									100.00	118.84
I-100-3697.86	2	15	Albite	66.87		19.84	0.17			0.53	12.08	0.49													100.00	126.74
I-100-3697.86	3	1	Chlorite	28.70		23.42	22.00		10.50			0.38													85.00	105.25
I-100-3697.86	3	2	Muscovite	48.13	0.56	32.72	1.39		0.74		0.72	8.78													93.00	117.72
I-100-3697.86	3	3	K-feldspar	66.55		18.06					0.46	14.94													100.00	120.36
I-100-3697.86	3	4	Chlorite	32.40		24.32	15.96	0.15	11.33			0.84													85.00	112.34
I-100-3697.86	3	5	Monazite + Chlorite	18.10	2.10	11.64	13.23		5.55			0.70	17.76								5.63	17.18	8.12		100.00	82.03
I-100-3697.86	3	6	Chlorite	34.42		21.00	19.00	0.16	9.60			0.84													85.00	105.23
I-100-3697.86	3	7	K-feldspar	66.53		18.23					1.23	14.01													100.00	120.22
I-100-3697.86	3	8	K-feldspar	65.74		18.39					1.04	13.82								1.02					100.00	129.29
I-100-3697.86	3	9	Muscovite	48.18	0.26	34.02	0.86		0.38		1.32	7.98													93.00	120.28
I-100-3697.86	3	10	Albite	69.69		18.52	0.27				11.14	0.39													100.00	131.32
I-100-3697.86	3	11	Muscovite	51.47	0.25	29.61	1.38		1.03		0.72	8.55													93.00	109.44
I-100-3697.86	3	12	Chlorite + Muscovite	40.20	0.18	27.42	18.96		10.91			2.34													100.00	104.71
I-100-3697.86	3	13	Altered Ilmenite + Muscovite	19.77	63.55	12.21	0.98		0.41			3.08													100.00	104.34
I-100-3697.86	3	14	K-feldspar	66.17		18.37					0.81	14.21								0.46					100.00	122.03
I-100-3697.86	3	15	K-feldspar	66.04		18.31	0.62				0.31	14.70													100.00	123.73
I-100-3697.86	3	16	Chlorite	31.24		21.70	19.43	0.22	11.93			0.48													85.00	106.94
I-100-3697.86	4	1	Altered Ilmenite	3.49	81.65	2.25	11.58			0.57		0.45													100.00	96.90
I-100-3697.86	4	2	Anhydrite + TiO2	0.81	39.20	0.43	8.92	0.36		20.32				29.99											100.00	105.32
I-100-3697.86	4	3	Anhydrite							37.44				62.55											100.00	117.95
I-100-3697.86	4	4	Anhydrite							37.25				62.75											100.00	118.30
I-100-3697.86	4	5	Altered Ilmenite	25.01	66.21	4.63	1.98		1.16	0.24		0.78													100.00	99.51
I-100-3697.86	4	6	Chlorite	29.64		22.93	22.43	0.26	8.71	0.19		0.64				0.20									85.00	72.45
I-100-3697.86	4	7	Muscovite	47.87	0.73	33.01	1.04		0.71		1.07	8.39				0.20									93.00	78.68
I-100-3697.86	4	8	Chlorite after Muscovite	39.98		27.32	18.56	0.25	11.94	0.28	0.36	1.31													100.00	107.20
I-100-3697.86	4	9	Muscovite	46.61	0.16	33.53	3.08		1.36		1.59	6.67													93.00	111.92
I-100-3697.86	4	10	Quartz	99.99																					100.00	132.74

Table 1F: Scanning electron microscope chemical analyses of minerals from representative sites for Mohican I-100 well at 3697.86m depth

Sample	Site	Position	Mineral	SiO_2	TiO_2	Al_2O_3	FeO	MnO	MgO	CaO	Na_2O	K_2O	P_2O_5	SO_3	F	Cl	CuO	SrO	ZrO_2	BaO	La_2O_3	Ce_2O_3	Nd_2O_3	HfO_2	Total	Actual Total
I-100-3697.86	4	11	Chlorite + Anhydrite + Muscovite	37.82		28.34	11.42		5.60	3.89	0.70	3.55		8.66											100.00	122.73
I-100-3697.86	4	12	Anhydrite							37.34				62.65											100.00	112.10
I-100-3697.86	4	13	Chlorite + Muscovite	46.53		32.44	9.80		5.02		3.03	3.19													100.00	115.93
I-100-3697.86	4	14	Quartz	99.99																					100.00	132.03
I-100-3697.86	5	1	Albite	65.27		21.67				1.80	10.69	0.57													100.00	128.77
I-100-3697.86	5	2	K-feldspar	66.61		18.46					0.57	14.37													100.00	123.45
I-100-3697.86	5	3	Muscovite + Quartz	63.32	0.60	23.58	2.83		1.51		0.51	7.67													100.00	113.84
I-100-3697.86	5	4	Quartz	99.99																					100.00	121.40
I-100-3697.86	5	5	Quartz	92.05		4.91	1.30		0.65		0.27	0.84													100.00	112.07
I-100-3697.86	5	6	Muscovite	47.94	0.19	34.79	1.00		0.33		1.66	7.07													93.00	117.79
I-100-3697.86	5	7	Quartz	99.99																					100.00	119.32
I-100-3697.86	5	8	Quartz	99.39		0.60																			100.00	126.42
I-100-3697.86	5	9	Muscovite	48.66	2.34	29.17	3.51		2.46		2.05	4.82													93.00	124.00
I-100-3697.86	5	10	Muscovite	50.61	0.28	30.15	1.30		1.65		0.74	8.26													93.00	111.93
I-100-3697.86	5	11	Anhydrite							37.26				62.75											100.00	112.55
I-100-3697.86	5	12	Anhydrite							37.12				62.88											100.00	120.87
I-100-3697.86	5	13	Albite + K-feldspar	57.16		30.06	0.23				5.51	7.02													100.00	130.91
I-100-3697.86	5	14	Albite	68.45		18.91					12.63														100.00	135.96
I-100-3697.86	6	1	Biotite	43.08	3.09	20.61	13.97	0.19	10.05			9.01													100.00	117.17
I-100-3697.86	6	2	Anhydrite	0.34						37.09				62.55											100.00	120.06
I-100-3697.86	6	3	Quartz + other	77.80	0.32	10.90	1.33		1.34	1.90		3.52	2.91												100.00	131.91
I-100-3697.86	6	4	Quartz + TiO2	77.31	22.70																				100.00	111.91
I-100-3697.86	6	5	Anhydrite							37.36				62.65											100.00	112.64
I-100-3697.86	6	6	Muscovite	48.46	0.26	33.86	0.80		0.47		1.55	7.60													93.00	123.53
I-100-3697.86	6	7	Quartz	97.27		1.93	0.18		0.25			0.37													100.00	129.44
I-100-3697.86	6	8	K-feldspar	66.87		18.23					0.36	14.51													100.00	126.60
I-100-3697.86	6	9	Anhydrite	0.68		0.32				36.85		0.10		62.05											100.00	113.96
I-100-3697.86	6	10	Anhydrite + Chlorite	7.77		7.01	2.96		3.02	27.59		0.39		51.24											100.00	125.05
I-100-3697.86	6	11	TiO2 + Muscovite	71.19	2.34	19.25	1.08		0.53		0.85	4.75													100.00	120.64
I-100-3697.86	6	12	Muscovite	51.76	0.20	28.19	4.04		2.10		1.22	5.49													93.00	114.79
I-100-3697.86	6	13	K-feldspar + Chlorite	63.96	0.27	23.35	2.55		1.87	0.55	0.74	6.73													100.00	116.28
I-100-3697.86	7	1	Albite	67.60		18.97					11.74	1.69													100.00	129.56
I-100-3697.86	7	2	Chlorite	30.23		23.49	18.87	0.26	11.40			0.73													85.00	101.57
I-100-3697.86	7	3	Chlorite + Muscovite	56.05	1.72	24.51	4.00		3.43	1.16	0.62	7.23	0.87			0.42									100.00	96.89
I-100-3697.86	7	4	Altered Ilmenite	62.12	14.80	13.53	2.07		1.66	2.46		3.22				0.13									100.00	110.87
I-100-3697.86	7	5	Fluorapatite							46.52			46.15		7.33										100.00	119.71
I-100-3697.86	7	6	Chlorite + other	71.81	0.58	17.44	2.62		2.29		0.36	4.67				0.20									100.00	121.21
I-100-3697.86	7	7	Muscovite	52.96		27.91	2.66		1.93	0.33	3.55	3.54				0.12									93.00	120.07
I-100-3697.86	7	8	Albite	65.40		20.44	0.19			0.74	10.29	2.93													100.00	131.95
I-100-3697.86	7	9	Illite	52.06	0.63	22.62	6.47		3.24		0.50	4.47													90.00	112.29
I-100-3697.86	7	10	K-feldspar w/Perthite	67.13		19.03					2.26	10.95	0.62												100.00	119.61
I-100-3697.86	7	11	Altered Ilmenite + Quartz	75.41	22.80	0.93	0.58					0.28													100.00	121.32
I-100-3697.86	7	12	Illite	47.90	0.27	23.44	7.59		3.86	0.22	4.01	2.72													90.00	114.56
I-100-3697.86	8	1	SEM charging - unreliable data	11.12		5.46	0.28		1.74	80.17				1.22											100.00	48.23
I-100-3697.86	8	2	SEM charging - unreliable data	12.79		8.62			1.79	56.05				20.75											100.00	65.35
I-100-3697.86	8	3	Chlorite + Illite	43.02	0.57	31.10	15.26		4.73		1.36	3.99													100.00	101.21
I-100-3697.86	8	4	Illite + other	64.48	0.23	26.64	1.26		0.71	0.62	1.85	4.23													100.00	124.75
I-100-3697.86	8	5	Illite	40.68	0.72	24.57	7.79		9.45	1.22		4.00		1.58											90.00	115.69
I-100-3697.86	8	6	Anhydrite							37.40				62.60											100.00	110.25
I-100-3697.86	8	7	Muscovite	51.57	0.60	31.05	0.72		0.71		1.43	6.95													93.00	127.01
I-100-3697.86	8	8	Altered Ilmenite + Quartz Inclusions	8.83	87.17	1.76	0.71		0.68	0.57		0.29													100.00	101.32
I-100-3697.86	8	9	Anhydrite							37.26				62.75											100.00	114.95
I-100-3697.86	9	1	Albite	68.58		18.82	0.19				12.40														100.00	105.50

Table 1F: Scanning electron microscope chemical analyses of minerals from representative sites for Mohican I-100 well at 3697.86m depth

Sample	Site	Position	Mineral	SiO_2	TiO_2	Al_2O_3	FeO	MnO	MgO	CaO	Na_2O	K_2O	P_2O_5	SO_3	F	Cl	CuO	SrO	ZrO_2	BaO	La_2O_3	Ce_2O_3	Nd_2O_3	HfO_2	Total	Actual Total
I-100-3697.86	9	2	Chalcopyrite	0.28			21.69							55.58			22.44								100.00	151.68
I-100-3697.86	9	3	Chalcopyrite + Albite	37.69		12.00	10.77			0.21	10.34			20.75			8.25								100.00	150.06
I-100-3697.86	9	4	Chalcopyrite + K-feldspar	20.71	0.22	7.60	23.80			0.27		2.73		31.01			13.67								100.00	133.99
I-100-3697.86	9	5	K-feldspar	65.89		18.31	0.14				1.86	13.82													100.00	101.23
I-100-3697.86	9	6	Quartz	99.99																					100.00	101.74
I-100-3697.86	9	7	Ferroan Dolomite + Muscovite	26.14		11.81	8.48	0.52	17.29	31.76		4.01													100.00	60.48
I-100-3697.86	9	8	K-feldspar	66.14		18.29					1.27	14.29													100.00	90.03
I-100-3697.86	9	9	Altered Ilmenite + Albite	37.46	48.69	6.67	4.28			0.50	1.83	0.29				0.26									100.00	68.52
I-100-3697.86	9	10	Quartz + other	95.04	1.10	2.14	0.64		0.25			0.82													100.00	97.54
I-100-3697.86	9	11	K-feldspar + other	67.90	0.17	21.13	2.84		2.09		0.47	5.41													100.00	95.02
I-100-3697.86	9	12	K-feldspar	67.09		18.40					1.29	13.21													100.00	99.44
I-100-3697.86	9	13	Quartz + K-feldspar + other	94.15		3.46	0.62		0.51	0.34		0.93													100.00	95.93
I-100-3697.86	9	14	K-feldspar	67.23		17.95						14.82													100.00	97.72
I-100-3697.86	10	1	Quartz	99.99																					100.00	100.14
I-100-3697.86	10	2	Quartz	99.99																					100.00	105.72
I-100-3697.86	10	3	Quartz	99.99																					100.00	106.57
I-100-3697.86	10	4	Quartz + other	94.79	0.17	2.57	1.07		0.53			0.89													100.00	97.49
I-100-3697.86	10	5	Quartz	99.99																					100.00	95.86
I-100-3697.86	10	6	Quartz + other	98.32		1.27	0.27					0.13													100.00	92.72
I-100-3697.86	10	7	Muscovite + Chlorite	52.03	0.25	20.69	16.47	0.57	5.52		0.98	3.49													100.00	62.26
I-100-3697.86	10	8	Muscovite + Chlorite	41.95	0.20	30.27	12.72	0.57	9.27		0.63	4.38													100.00	85.76
I-100-3697.86	10	9	Muscovite + Chlorite	64.71	0.43	19.69	4.21		5.79		0.40	4.76													100.00	94.13
I-100-3697.86	10	10	Muscovite + Chlorite	54.16	0.20	31.14	3.73		2.16		0.82	7.78													100.00	81.25
I-100-3697.86	10	11	Ilmenite + Muscovite	31.68	31.76	24.79	4.13		1.23	0.59	1.16	4.52				0.15									100.00	74.18
I-100-3697.86	10	12	Quartz + Muscovite	91.15	1.07	4.91	0.75		0.41			1.70													100.00	96.84
I-100-3697.86	10	13	Muscovite + Chlorite	56.13	0.30	28.74	2.87		2.24		0.78	7.19			1.58	0.14									100.00	91.98
I-100-3697.86	10	14	Albite	68.13		19.07	0.12				12.34	0.33													100.00	99.01
I-100-3697.86	10	15	K-feldspar	63.92	0.20	20.41	1.16		1.26		0.57	11.03			1.47										100.00	92.72
I-100-3697.86	11	1	Muscovite	46.59	1.16	33.53	2.31		0.49		1.87	7.05													93.00	86.14
I-100-3697.86	11	2	Muscovite + Altered Ilmenite	47.94	8.71	33.14	1.51		0.33		2.14	6.24													100.00	94.00
I-100-3697.86	11	3	Albite	67.62		19.90	0.22			0.32	11.43	0.51													100.00	106.67
I-100-3697.86	11	4	Albite	66.27		19.82	0.81		0.30	0.28	11.10	1.42													100.00	99.13
I-100-3697.86	11	5	Quartz + Muscovite + Chlorite	80.48	0.18	9.24	3.78		3.22		0.36	2.76													100.00	80.53
I-100-3697.86	11	6	Ilmenite + Muscovite	28.43	48.82	15.95	2.41		1.28		0.50	2.64													100.00	79.10
I-100-3697.86	11	7	Quartz + Ilmenite + other	50.16	34.18	5.57	7.05		2.55	0.27						0.22									100.00	79.94
I-100-3697.86	11	8	Muscovite + Quartz	70.57		20.96	1.17		1.48		2.02	3.81													100.00	79.76
I-100-3697.86	11	9	Muscovite	48.69	0.58	25.05	2.52		2.46	3.11	0.91	6.18	3.35			0.15									93.00	87.89
I-100-3697.86	11	10	Quartz + Muscovite	92.78		4.97	0.42		0.28			1.55													100.00	96.62
I-100-3697.86	11	11	TiO2 + Chlorite	28.69	50.88	11.36	4.79		2.52		0.44	1.19				0.16									100.00	75.75
I-100-3697.86	11	12	Quartz	99.99																					100.00	93.31
I-100-3697.86	11	13	Quartz	99.99																					100.00	93.08
I-100-3697.86	11	14	Quartz	99.99																					100.00	98.70
I-100-3697.86	11	15	Quartz	99.99																					100.00	98.34
I-100-3697.86	12	1	Muscovite + Chlorite	68.30	0.30	16.33	8.08		4.58		0.50	1.90													100.00	93.10
I-100-3697.86	12	2	Quartz + Muscovite	94.15		3.65	0.58		0.40			1.24													100.00	94.30
I-100-3697.86	12	3	Muscovite + Chlorite	66.64	0.40	21.71	3.04		2.82		0.35	5.05													100.00	84.47
I-100-3697.86	12	4	Quartz + Muscovite	93.14		4.61	0.31		0.48		0.31	1.17													100.00	90.48
I-100-3697.86	12	5	Albite + Chlorite	56.84	0.97	20.61	7.05	0.13	2.44	0.20	10.33	1.43													100.00	101.86
I-100-3697.86	12	6	Chlorite + TiO2	40.77	1.70	24.83	19.64	0.35	10.79			1.92													100.00	78.37
I-100-3697.86	12	7	Muscovite + Chlorite	44.15	1.33	24.30	17.88	0.31	9.65			2.37													100.00	83.50
I-100-3697.86	12	8	Anhydrite + Quartz	1.16						36.45				61.60				0.79							100.00	88.47
I-100-3697.86	12	9	Muscovite + Anhydrite	50.01	0.45	29.70	1.76		1.49	2.46		9.12		4.97											100.00	88.76
I-100-3697.86	12	10	Quartz + Muscovite	85.85	0.20	9.24	0.69		0.41		0.44	2.10			1.04										100.00	96.31

Table 1F: Scanning electron microscope chemical analyses of minerals from representative sites for Mohican I-100 well at 3697.86m depth

Sample	Site	Position	Mineral	SiO_2	TiO_2	Al_2O_3	FeO	MnO	MgO	CaO	Na_2O	K_2O	P_2O_5	SO_3	F	Cl	CuO	SrO	ZrO_2	BaO	La_2O_3	Ce_2O_3	Nd_2O_3	HfO_2	Total	Actual Total
I-100-3697.86	12	11	Anhydrite + Pyrite + Muscovite	45.01	0.28	21.31	3.91		2.87	5.88	0.93	5.34		14.48											100.00	91.72
I-100-3697.86	12	12	Muscovite + Chlorite	46.27	1.03	28.72	12.11	0.18	7.13		0.58	3.99													100.00	90.60
I-100-3697.86	13	1	Muscovite + Chlorite	48.97	0.63	21.37	18.45	0.22	8.92			1.42													100.00	85.31
I-100-3697.86	13	2	Quartz	99.99																					100.00	105.48
I-100-3697.86	13	3	Quartz	99.99																					100.00	96.01
I-100-3697.86	13	4	Albite	65.61		20.37	1.03				11.14	1.85													100.00	100.05
I-100-3697.86	13	5	Muscovite + Chlorite	60.15	0.40	24.53	3.94		2.57		0.84	5.90			1.66										100.00	92.51
I-100-3697.86	14	1	Albite	68.84		18.84	0.14				12.17														100.00	97.56
I-100-3697.86	14	2	Muscovite + Chlorite	41.82	0.32	27.34	17.71		10.26	0.20		2.32													100.00	83.53
I-100-3697.86	14	3	Muscovite + TiO2	51.06	34.13	8.45	2.96		2.37			1.05													100.00	90.64
I-100-3697.86	14	4	Muscovite	50.02	0.53	29.91	2.66		1.40		0.62	7.87													93.00	85.02
I-100-3697.86	14	5	Muscovite + other	63.36	0.53	23.83	3.87		2.30		0.70	5.40													100.00	92.79
I-100-3697.86	14	6	Muscovite + Chlorite	52.45	0.47	28.66	6.09		4.00		0.38	6.37			1.58										100.00	88.32
I-100-3697.86	14	7	Muscovite + other	66.36	0.78	22.58	2.29		1.56		0.53	5.90													100.00	84.98
I-100-3697.86	15	1	Muscovite + TiO2	62.85	16.73	12.60	3.10		1.44		0.77	2.52													100.00	74.42
I-100-3697.86	15	2	Muscovite	51.17	0.35	30.66	0.96		0.63		1.28	7.94													93.00	82.93
I-100-3697.86	15	3	Muscovite + Chlorite	48.02		28.63	11.71		7.23		0.96	3.44													100.00	86.71
I-100-3697.86	15	4	Muscovite + other	53.54	0.22	34.94	0.71				3.36	7.24													100.00	90.23
I-100-3697.86	16	1	Muscovite + TiO2	65.25	7.66	17.97	2.89		0.80		0.80	4.64													100.00	81.83
I-100-3697.86	16	2	Quartz	99.99																					100.00	106.53
I-100-3697.86	16	3	Quartz	99.99																					100.00	103.41
I-100-3697.86	16	4	Muscovite + TiO2	47.66	18.15	26.26	0.89		0.73		1.69	4.61													100.00	98.18
I-100-3697.86	16	5	Muscovite + Chlorite	52.97	0.38	28.14	7.10		4.03		0.75	6.47				0.16									100.00	80.21
I-100-3697.86	16	6	Quartz + Muscovite	83.64	1.12	11.36	0.36				0.40	3.10													100.00	98.66
I-100-3697.86	16	7	Quartz + Muscovite	71.64		21.31	0.84		0.45		1.09	4.66													100.00	101.40
I-100-3697.86	16	8	Quartz + Muscovite	84.99		9.26	0.95		0.58		2.80	1.41													100.00	91.44
I-100-3697.86	17	1	Anhydrite							37.82				62.18											100.00	91.11
I-100-3697.86	17	2	Quartz	99.99																					100.00	100.48
I-100-3697.86	17	3	Quartz	99.99																					100.00	107.73
I-100-3697.86	17	4	Albite	65.31		21.58				2.50	10.31	0.29													100.00	101.17
I-100-3697.86	17	5	Quartz	99.99																					100.00	103.41
I-100-3697.86	17	6	Quartz	99.99																					100.00	112.18
I-100-3697.86	17	7	Quartz	99.99																					100.00	108.76

Appendix 3A: Scanning Electron Microscope Backscattered Electron Images for Wyandot E-53 well with EDS Mineral Analyses Sample 2873.10

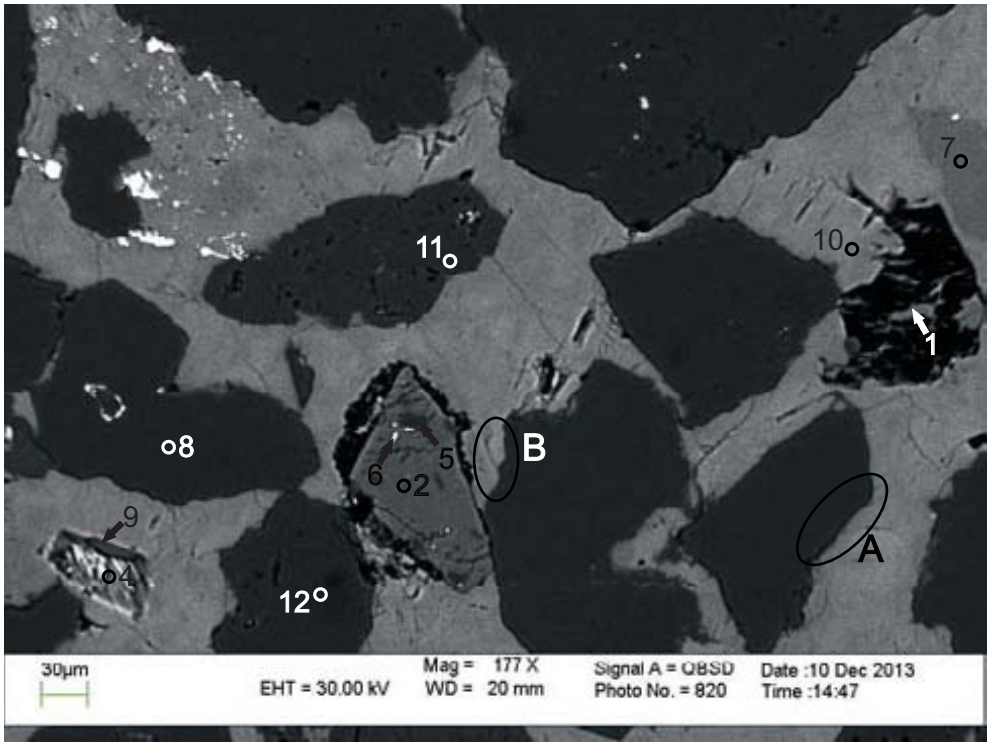

1: K-feldspar
2: K-feldspar
3: Calcite + Pyrite
4: Fe-Calcite
5: Albite
6: K-feldspar + Pyrite
7: Calcite
8: Quartz
9: Fe-Calcite
10: Fe-Calcite
11: Albite
12: Quartz

Figure 1: Wyandot E-53: 2873.10 site 1. Quartz overgrowths (positions A and B) separated from calcite cement by thin dissolution zone.

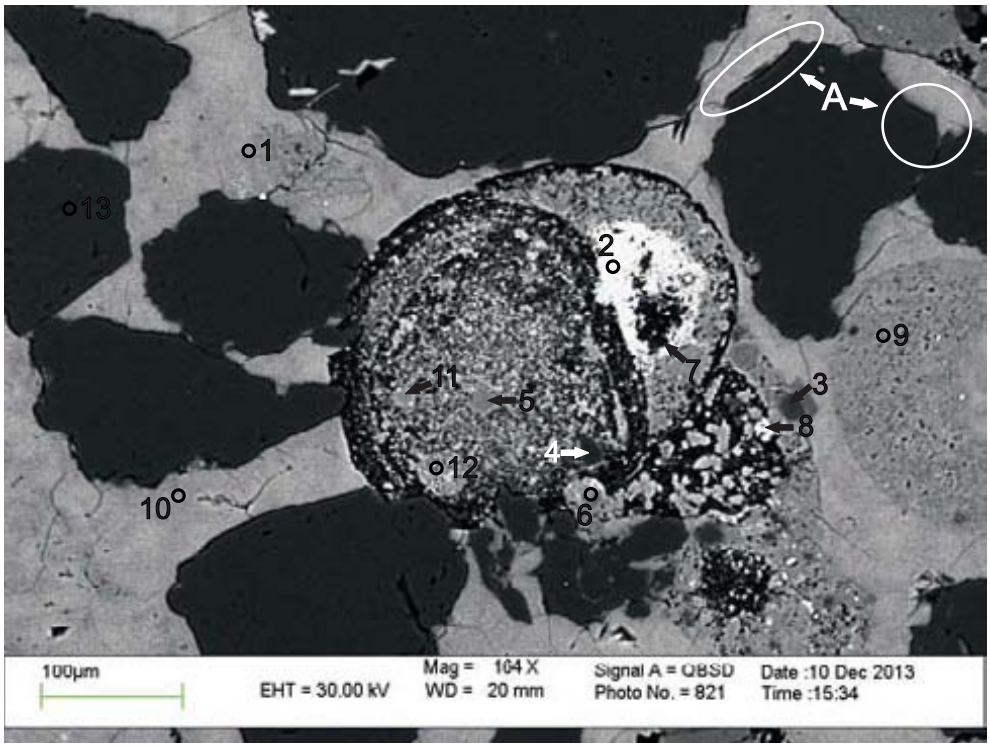

1: Fe-Calcite
2: Fluorapatite
3: Dolomite
4: Quartz
5: Calcite
6: Calcite
7: Apatite + Chlorite
8: TiO_2 + other
9: Fe-Calcite
10: Fe-Calcite
11: Calcite
12: Calcite + other
13: Albite

Figure 2: Wyandot E-53: 2873.10 site 2. Coated grain, composed of fluorapatite and calcite, and detrital quartz grains in mostly calcite cement, along with presence of quartz overgrowths (position A).

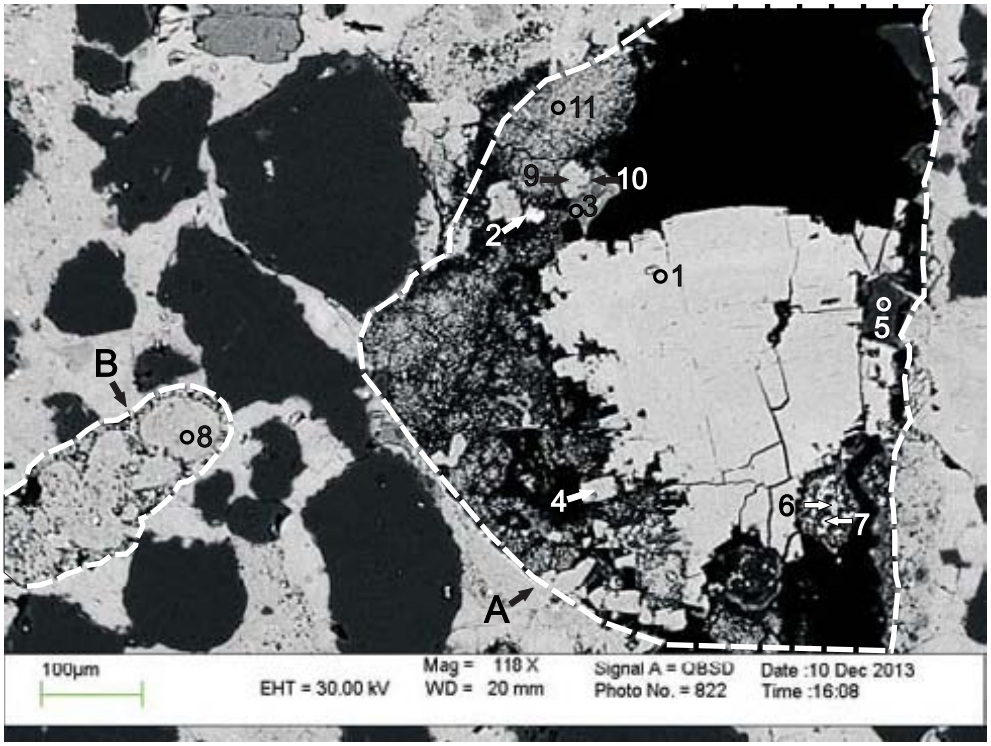

1: Ankerite
2: TiO_2 + Calcite
3: Fluorapatite
4: Ankerite
5: Quartz
6: Fe-Calcite
7: Fluorapatite
8: Calcite
9: Calcite
10: Calcite + other
11: Calcite

Figure 3: Wyandot E-53: 2873.10 site 3. Bioclast (position A), with sparry calcite in places, underwent dissolution and then was partly replaced by ankerite (analysis 1). Partial dissolution of bioclast (position B) composed of calcite (analysis 8).

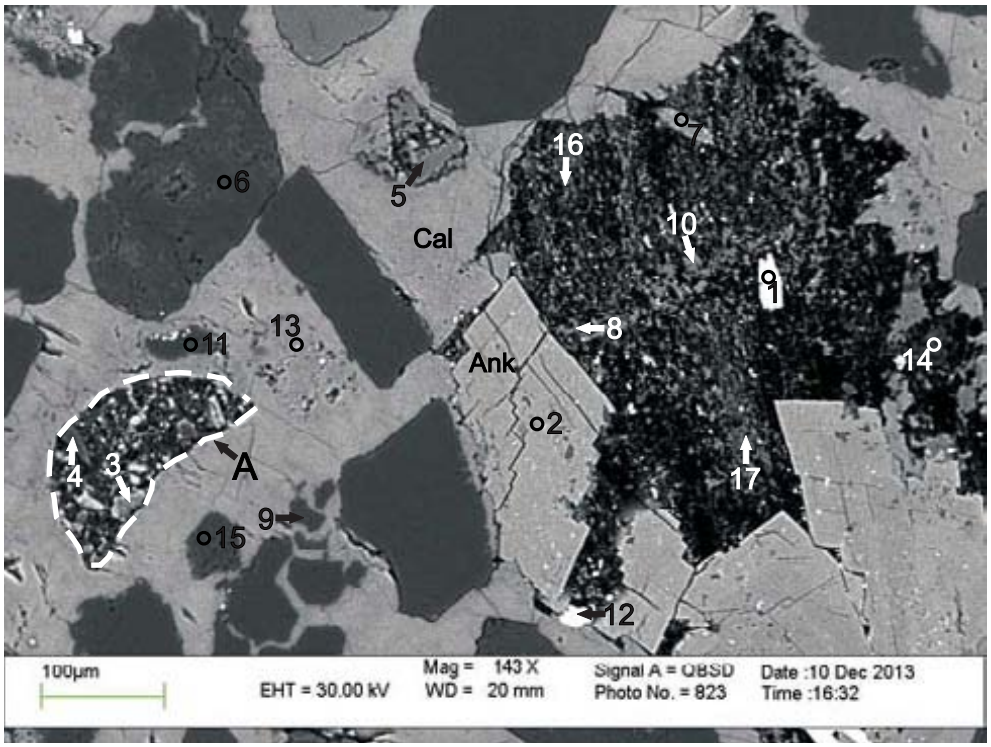

1: Barite
2: Ankerite
3: Calcite + Dolomite
4: Quartz
5: K-feldspar
6: Quartz
7: Fe-Calcite + K-feldspar
8: K-feldspar
9: Quartz
10: K-feldspar
11: Quartz
12: Barite + Feldspar
13: Fe-Calcite
14: Illite
15: Quartz + Albite
16: K-feldspar
17: K-feldspar

Figure 4: Wyandot E-53: 2873.10 site 4. Dissolution of K-feldspar (analyses 8,10, 16 and 17) with dissolution void partly replaced by ankerite (analysis 2). Dissolution of bioclast (position A), with replacement by calcite and dolomite (analysis 3) and quartz fragment (analysis 4).

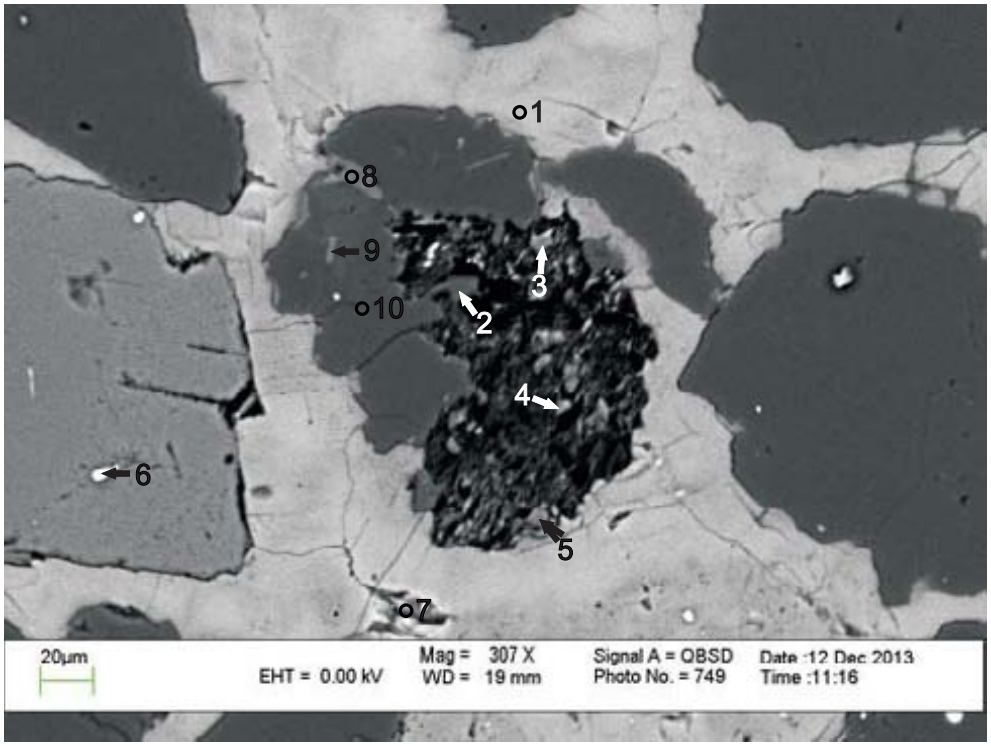

1: Calcite
2: Quartz + other
3: Muscovite + Chlorite
4: Illite
5: Muscovite + Chlorite
6: K-feldspar + Pyrite
7: Fe-Calcite
8: Muscovite
9: K-feldspar
10: Quartz

Figure 5: Wyandot E-53: 2873.10 site 5. Porosity filled in with kaolinite (analyses 3 and 5), illite (analysis 4), muscovite and chlorite (analysis 3).

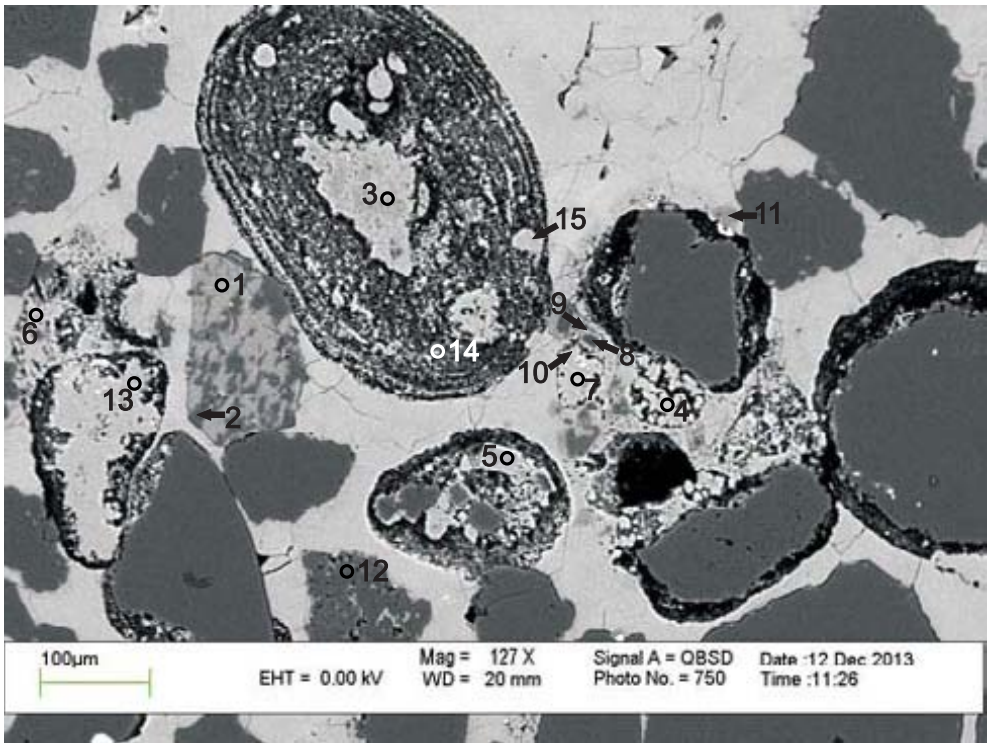

1: K-feldspar
2: Albite
3: Calcite
4: Fe-Calcite
5: Calcite
6: Fe-Calcite
7: Fe-Calcite
8: Dolomite
9: Ankerite
10: Fe-Calcite
11: Mg-Calcite
12: Quartz
13: Fe-Calcite
14: Chlorite + Calcite + Illite
15: Fe-Calcite

Figure 6: Wyandot E-53: 2873.10 site 6. Coated grains composed of mostly of calcite (analyses 3, 5 and 13). Albitization of K-feldspar (analyses 1 and 2).

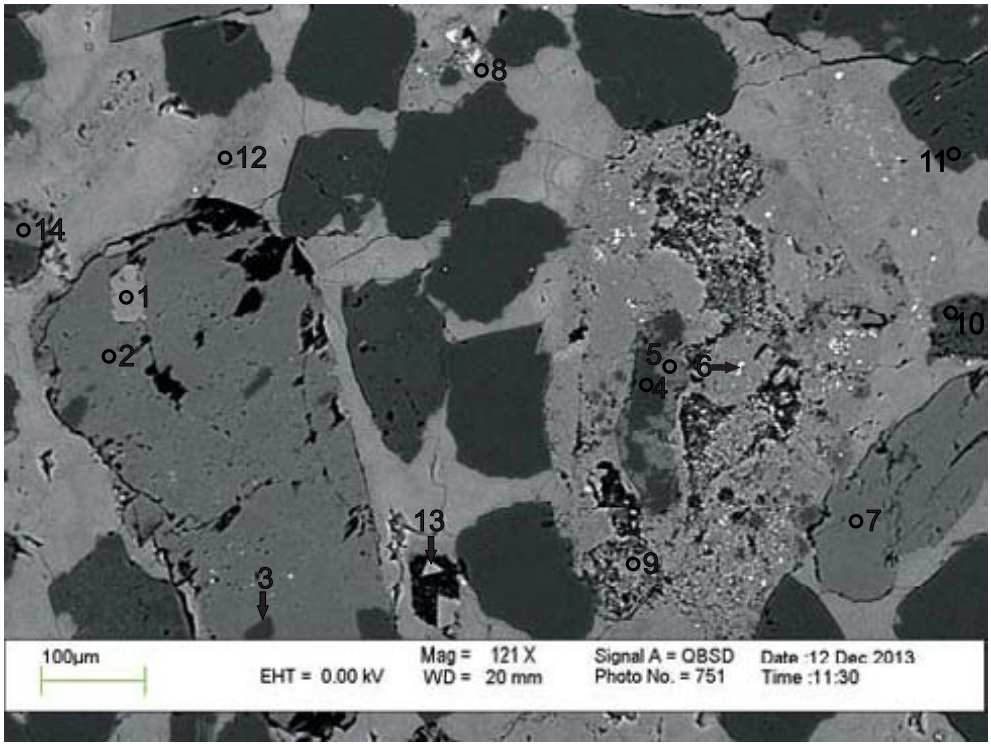

1: Chlorite + Calcite + K-feldspar
2: K-feldspar
3: Albite
4: Quartz
5: Muscovite + Chlorite
6: Pyrite + Calcite
7: K-feldspar
8: Fe-Calcite
9: Fe-Calcite
10: Quartz
11: Albite
12: Mg-Calcite
13: Ankerite
14: K-feldspar

Figure 7: Wyandot E-53: 2873.10 site 7. Partial dissolution of K-feldspar (analyses 2 and 7), with porosity partially infilled with calcite and chlorite.

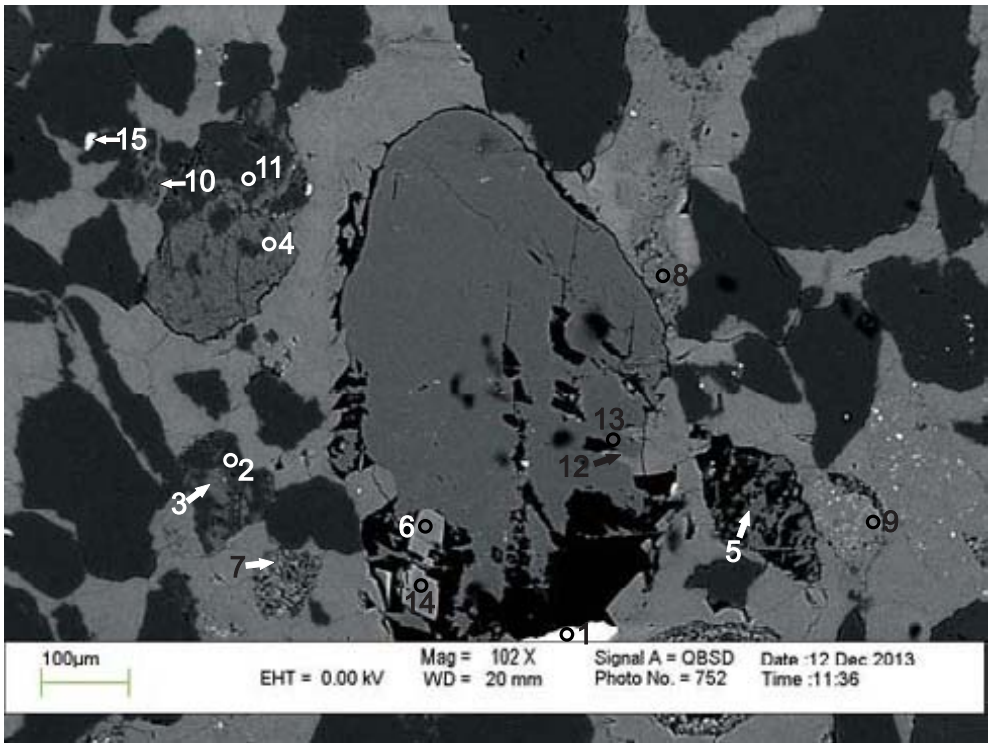

1: Barite (drilling mud)
2: Quartz
3: K-feldspar
4: K-feldspar
5: K-feldspar
6: Ankerite
7: Calcite
8: Fe-Calcite
9: Fe-Calcite
10: Illite
11: Albite
12: Calcite + K-feldspar
13: K-feldspar
14: Ankerite
15: Rutile

Figure 8: Wyandot E-53: 2873.10 site 8. Fe-Calcite (analysis 12) replaces K-feldspar (analysis 13). Barite (analysis 1) is likely from drilling mud as it fills in pore space and does not form straight grain boundaries with other mineral grains (see App. 4C, Fig. 1).

Table 1A: Scanning electron microscope chemical analyses of minerals from representative sites for Wyandot E-53 well at 2873.10m depth

Sample	Site	Position	Mineral	SiO_2	TiO_2	Al_2O_3	FeO	MnO	MgO	CaO	Na_2O	K_2O	P_2O_5	SO_3	F	Cl	SrO	BaO	WO_3	Total	Actual Total
E53-2873.10	1	1	K-feldspar	65.87		17.99					0.57	14.74						0.84		100.00	115.86
E53-2873.10	1	2	K-feldspar	66.53		17.76						15.70								100.00	108.45
E53-2873.10	1	3	Calcite + Pyrite	1.24			14.43	0.66	0.71	47.99				34.96						100.00	84.54
E53-2873.10	1	4	Fe-Calcite				1.03	0.82	0.66	53.49										56.00	43.85
E53-2873.10	1	5	Albite	69.07		18.73				0.17	11.34	0.69								100.00	112.86
E53-2873.10	1	6	K-feldspar + Pyrite	61.31		16.72	1.74				0.28	14.29		5.67						100.00	114.96
E53-2873.10	1	7	Calcite						0.72	54.52				0.76						56.00	54.60
E53-2873.10	1	8	Quartz	99.99																100.00	107.67
E53-2873.10	1	9	Fe-Calcite				1.00	0.90	1.36	52.74										56.00	48.58
E53-2873.10	1	10	Fe-Calcite				1.01	0.86	1.00	48.71					4.41					56.00	56.42
E53-2873.10	1	11	Albite	67.77		19.22	0.13			0.48	12.00	0.40								100.00	110.44
E53-2873.10	1	12	Quartz	99.86			0.14													100.00	114.62
E53-2873.10	2	1	Fe-Calcite				1.13	0.84	1.00	53.03										56.00	49.12
E53-2873.10	2	2	Fluorapatite	1.16		0.93	0.17			45.74	0.63	0.20	39.83	1.17	10.16				0.04	100.00	109.58
E53-2873.10	2	3	Dolomite				0.67	0.17	18.78	31.88				0.50						52.00	53.02
E53-2873.10	2	4	Quartz	99.43						0.56										100.00	110.17
E53-2873.10	2	5	Calcite						1.16	54.13				0.71						56.00	49.85
E53-2873.10	2	6	Calcite				0.56	0.43	0.51	54.49										56.00	50.10
E53-2873.10	2	7	Apatite + Chlorite	17.28		11.36	6.37		3.48	34.60		1.30	24.50	0.80		0.33				100.00	82.35
E53-2873.10	2	8	TiO2 + other	4.86	80.02	3.51	2.79		0.81	7.79		0.20								100.00	91.78
E53-2873.10	2	9	Fe-Calcite	0.57			1.15	0.73	0.50	53.06										56.00	52.57
E53-2873.10	2	10	Fe-Calcite				1.03	0.82	0.99	53.16										56.00	46.60
E53-2873.10	2	11	Calcite				0.83	0.50	0.86	53.82										56.00	48.16
E53-2873.10	2	12	Calcite + other	8.69		4.27	4.01	0.81	1.39	76.24		0.83		3.72						100.00	56.56
E53-2873.10	2	13	Albite	68.41		19.27				0.49	11.82									100.00	104.73
E53-2873.10	3	1	Ankerite				10.93	4.38	9.84	30.85										56.00	54.75
E53-2873.10	3	2	TiO2 + Calcite	6.12	69.81	3.57	2.24		0.80	15.18		0.63	0.96	0.67						100.00	80.54
E53-2873.10	3	3	Fluorapatite				1.08			47.07	0.66		39.66	3.32	7.95	0.26				100.00	75.15
E53-2873.10	3	4	Ankerite				9.18	4.73	9.62	31.43			1.04							56.00	54.01
E53-2873.10	3	5	Quartz	95.88		2.02	0.68		0.36	0.83		0.24								100.00	98.51
E53-2873.10	3	6	Fe-Calcite				1.06	0.81	0.72	50.56			2.50	0.36						56.00	52.43
E53-2873.10	3	7	Fluorapatite				0.66	0.50	0.56	63.33	0.58		26.67	1.10	6.59					100.00	75.42
E53-2873.10	3	8	Calcite	0.92		0.46	0.92	0.94	0.75	51.92		0.10								56.00	46.92
E53-2873.10	3	9	Calcite				0.93	0.77	0.73	51.81					1.76					56.00	49.83
E53-2873.10	3	10	Calcite + other	9.54		0.94	1.87	1.01	0.55	75.36			4.31	1.17	5.03	0.22				100.00	53.71
E53-2873.10	3	11	Calcite				0.95	1.05	0.46	52.98				0.57						56.00	47.25
E53-2873.10	4	1	Barite	1.54		0.47						0.41		38.43			3.09	56.07		100.00	102.01
E53-2873.10	4	2	Ankerite				11.74	4.76	9.49	29.64				0.39						56.00	53.34

Table 1A: Scanning electron microscope chemical analyses of minerals from representative sites for Wyandot E-53 well at 2873.10m depth

Sample	Site	Position	Mineral	SiO_2	TiO_2	Al_2O_3	FeO	MnO	MgO	CaO	Na_2O	K_2O	P_2O_5	SO_3	F	Cl	SrO	BaO	WO_3	Total	Actual Total
E53-2873.10	4	3	Calcite + Dolomite	1.37		0.59	6.69	1.16	21.71	63.31				5.17						100.00	55.69
E53-2873.10	4	4	Quartz	99.77						0.22										100.00	102.28
E53-2873.10	4	5	K-feldspar	66.36		17.99					1.95	13.70								100.00	106.02
E53-2873.10	4	6	Quartz	98.45		1.10	0.19					0.26								100.00	100.87
E53-2873.10	4	7	Fe-Calcite + K-feldspar	5.03		1.87	2.35	2.78	0.83	84.78		1.00		1.40						100.00	54.16
E53-2873.10	4	8	K-feldspar	65.89		17.61	0.69				0.32	14.85		0.62						100.00	96.03
E53-2873.10	4	9	Quartz	98.75						1.26										100.00	101.94
E53-2873.10	4	10	K-feldspar	65.72		17.88	0.46				0.44	15.09		0.40						100.00	101.68
E53-2873.10	4	11	Quartz	96.97		0.93	0.82		0.33	0.80		0.14								100.00	99.45
E53-2873.10	4	12	Barite + Feldspar	19.06		6.42	0.30			0.62	4.15	0.76		26.99			3.87	37.82		100.00	115.81
E53-2873.10	4	13	Fe-Calcite	0.41			2.93	0.64	0.50	48.75				2.77						56.00	50.51
E53-2873.10	4	14	Illite	51.36	0.39	21.94	3.88	0.15	2.84	0.95		5.82			2.50	0.15				90.00	94.05
E53-2873.10	4	15	Quartz + Albite	86.92	0.22	7.37	0.18			0.31	4.89	0.12								100.00	98.61
E53-2873.10	4	16	K-feldspar	62.72		16.08	1.35				0.34	15.91		1.30	2.31					100.00	68.80
E53-2873.10	4	17	K-feldspar	64.90		16.97	0.30					16.32			1.52					100.00	74.19
E53-2873.10	5	1	Calcite				1.06	0.92	1.04	52.98										56.00	52.33
E53-2873.10	5	2	Quartz + other	83.92	0.18	9.60	2.44		1.34	0.38	0.36	1.77								100.00	104.71
E53-2873.10	5	3	Muscovite + Chlorite	47.81	0.38	32.75	7.72		6.72	0.57	2.53	1.49								100.00	97.16
E53-2873.10	5	4	Illite	46.02	0.39	24.70	5.25		4.15	0.62	1.81	5.68		1.13		0.28				90.00	45.49
E53-2873.10	5	5	Muscovite + Chlorite	45.33	1.03	33.50	8.72		6.78	1.54	2.08	0.99								100.00	99.81
E53-2873.10	5	6	K-feldspar + Pyrite	36.49		11.21	9.88					8.61		33.84						100.00	155.00
E53-2873.10	5	7	Fe-Calcite	0.45			1.13	1.04	0.93	52.47										56.00	51.65
E53-2873.10	5	8	Muscovite	50.68		28.52	1.99		1.76		0.73	9.33								93.00	111.21
E53-2873.10	5	9	K-feldspar	66.19	0.27	22.96	1.13		0.96	0.48	2.55	5.47								100.00	122.92
E53-2873.10	5	10	Quartz	98.72		0.72					0.57									100.00	115.54
E53-2873.10	6	1	K-feldspar	67.17		18.12					0.44	14.26								100.00	109.82
E53-2873.10	6	2	Albite	68.39		19.08				0.42	11.63	0.48								100.00	117.12
E53-2873.10	6	3	Calcite				0.71	0.36	2.05	51.69				1.18						56.00	55.07
E53-2873.10	6	4	Fe-Calcite	1.13		0.56	1.58	0.77	0.48	51.38		0.11								56.00	56.79
E53-2873.10	6	5	Calcite						2.86	52.70				0.45						56.00	55.25
E53-2873.10	6	6	Fe-Calcite	0.77		0.43	1.15	0.58	0.64	52.44										56.00	50.98
E53-2873.10	6	7	Fe-Calcite	0.42			1.40			54.18										56.00	55.07
E53-2873.10	6	8	Dolomite	0.58		0.27	2.28	0.49	18.21	29.31				0.87						52.00	61.29
E53-2873.10	6	9	Ankerite	1.04		0.52	8.08	0.80	10.96	33.76				0.84						56.00	59.62
E53-2873.10	6	10	Fe-Calcite	2.76		1.39	6.82	0.22	0.94	34.39		0.31	1.31	7.73		0.13				56.00	73.53
E53-2873.10	6	11	Mg-Calcite				4.52	1.10	10.51	38.10					1.78					56.00	59.08
E53-2873.10	6	12	Quartz	98.96		0.87						0.17								100.00	113.50
E53-2873.10	6	13	Fe-Calcite	0.77		0.37	2.35	0.73	0.66	48.74		0.10		2.30						56.00	54.11

Table 1A: Scanning electron microscope chemical analyses of minerals from representative sites for Wyandot E-53 well at 2873.10m depth

Sample	Site	Position	Mineral	SiO_2	TiO_2	Al_2O_3	FeO	MnO	MgO	CaO	Na_2O	K_2O	P_2O_5	SO_3	F	Cl	SrO	BaO	WO_3	Total	Actual Total
E53-2873.10	6	14	Chlorite + Calcite + Illite	17.41		10.90	11.31	0.96	2.97	53.52		1.14		1.25		0.56				100.00	57.17
E53-2873.10	6	15	Fe-Calcite	0.61			1.02	0.89	0.53	52.94										56.00	55.53
E53-2873.10	7	1	Chlorite + Calcite + K-feldspar	33.37		10.81	9.56	4.18	6.30	30.11		5.69								100.00	80.87
E53-2873.10	7	2	K-feldspar	66.36		17.97					0.44	15.21								100.00	110.51
E53-2873.10	7	3	Albite	68.65		18.99				0.15	12.00	0.20								100.00	114.19
E53-2873.10	7	4	Quartz	99.75						0.25										100.00	123.19
E53-2873.10	7	5	Muscovite + Chlorite	52.58	0.33	29.14	4.95		1.64			11.37								100.00	107.98
E53-2873.10	7	6	Pyrite + Calcite	0.81			24.43	0.37	0.50	24.32				49.57						100.00	121.06
E53-2873.10	7	7	K-feldspar	66.32		18.12					1.17	14.39								100.00	123.82
E53-2873.10	7	8	Fe-Calcite	1.79		0.90	1.40	0.88	2.07	48.85		0.10								56.00	58.47
E53-2873.10	7	9	Fe-Calcite	3.51		1.77	1.44	0.63	0.72	47.63		0.31								56.00	58.72
E53-2873.10	7	10	Quartz	89.16		5.52	2.61		0.88	0.36		1.46								100.00	125.28
E53-2873.10	7	11	Albite	69.29		18.84					11.88									100.00	125.92
E53-2873.10	7	12	Mg-Calcite	0.69		0.31	2.09	0.59	7.35	44.50				0.48						56.00	59.40
E53-2873.10	7	13	Ankerite	0.73		0.40	8.93	5.66	9.97	30.14		0.17								56.00	59.87
E53-2873.10	7	14	K-feldspar	66.32		17.99						15.71								100.00	107.89
E53-2873.10	8	1	Barite (drilling mud)											39.63			4.27	56.12		100.00	109.87
E53-2873.10	8	2	Quartz	97.14		1.13					0.24	1.48								100.00	113.23
E53-2873.10	8	3	K-feldspar	66.27		17.78					0.46	15.10						0.38		100.00	111.45
E53-2873.10	8	4	K-feldspar	66.12		17.72	0.26				0.51	15.39								100.00	112.46
E53-2873.10	8	5	K-feldspar	65.76		18.16					0.31	15.29	0.46							100.00	122.77
E53-2873.10	8	6	Ankerite				11.27	4.30	9.50	30.93										56.00	58.91
E53-2873.10	8	7	Calcite	3.01		1.65	0.88	0.40	0.96			0.24		0.45						56.00	55.92
E53-2873.10	8	8	Fe-Calcite	3.01		1.68	1.58	0.55	0.74	43.49		0.29	3.93	0.74						56.00	64.40
E53-2873.10	8	9	Fe-Calcite	0.36			2.72	0.73	0.99	49.56				1.64						56.00	61.79
E53-2873.10	8	10	Illite	42.80		23.35	2.17	0.23	1.81	10.91		8.74								90.00	88.19
E53-2873.10	8	11	Albite	68.50		19.16	0.22			0.32	11.81									100.00	115.12
E53-2873.10	8	12	Calcite + K-feldspar	5.50		1.66	1.20	1.52	0.46	44.55		1.11								56.00	64.12
E53-2873.10	8	13	K-feldspar	66.51		17.99					1.31	14.20								100.00	121.15
E53-2873.10	8	14	Ankerite				11.47	4.00	9.39	31.15										56.00	58.96
E53-2873.10	8	15	Rutile	2.85	93.41	0.42	2.87			0.46										100.00	94.07

Appendix 3B: Scanning Electron Microscope Backscattered Electron Images for Wyandot E-53 well with EDS Mineral Analyses Sample 2876.81

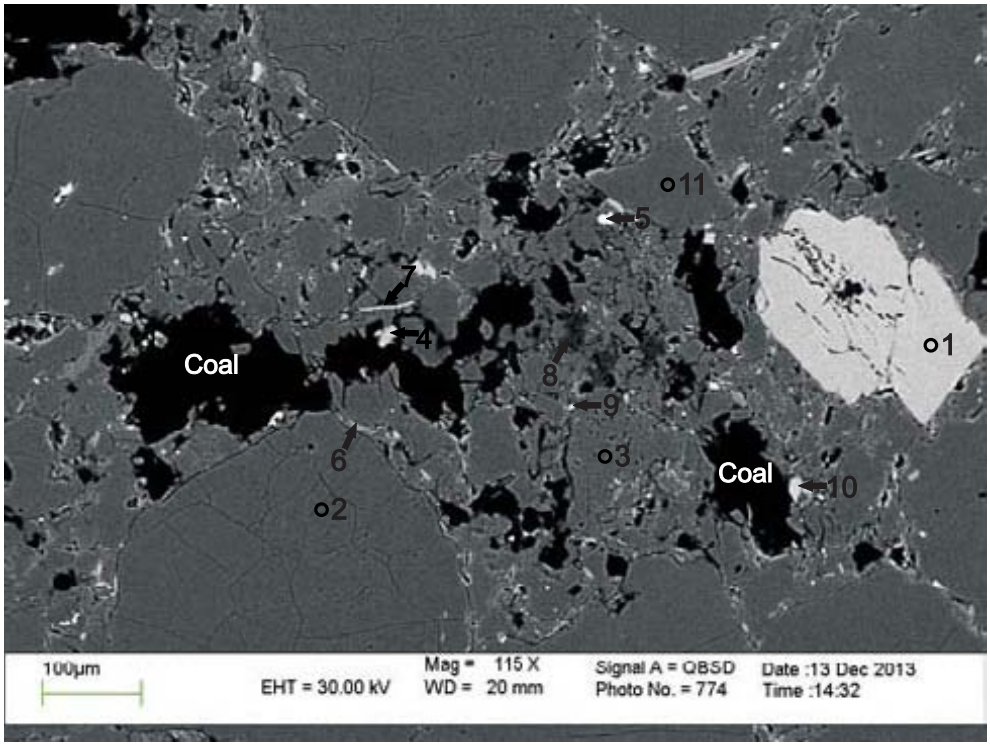

1: K-feldspar
2: Quartz
3: Albite
4: K-feldspar
5: Rutile
6: Muscovite
7: Muscovite
8: Kaolinite
9: Muscovite + TiO_2
10: K-feldspar
11: Quartz

Figure 1: Wyandot E-53: 2876.81 site 1. Quartz grains are highly fractured (analyses 2). Slight dissolution in albite (analysis 3) and K-feldspar (analysis 1). Kaolinite has filled in some pore space (analysis 8). The areas above appearing a black spots are areas where there are coal seams or coal fragments.

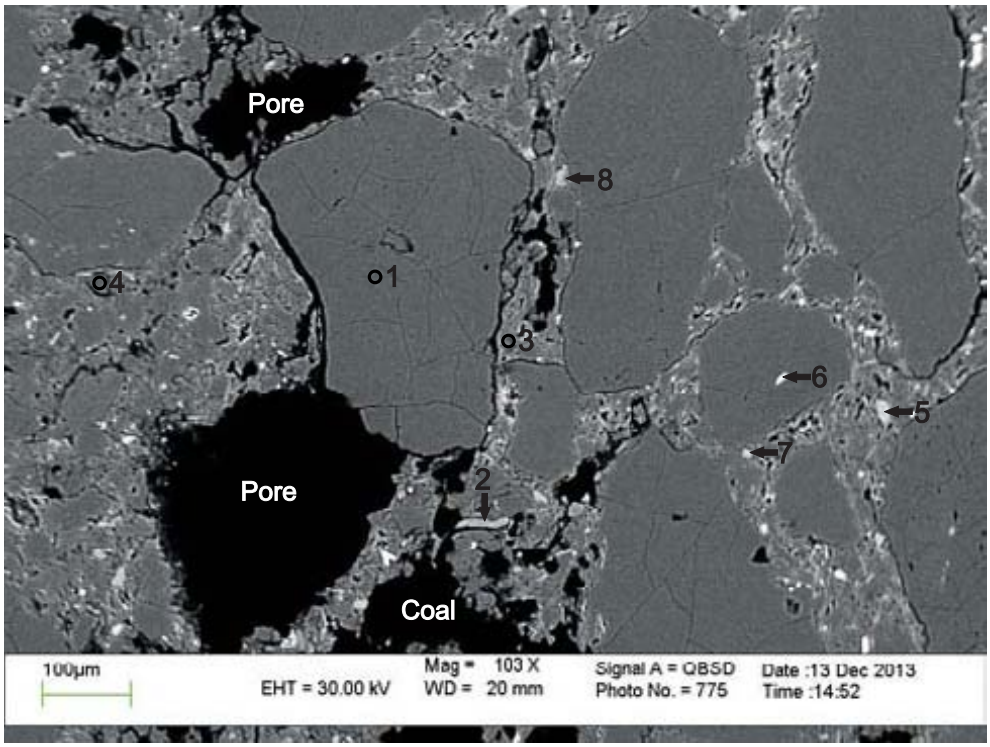

1: Quartz
2: Muscovite
3: Quartz
4: Quartz
5: K-feldspar
6: Quartz + Zircon
7: Muscovite + Chlorite
8: Albite

Figure 2: Wyandot E-53: 2876.81 site 2. This site contains a mixture of porosity and coal, the difference between the two is indistinguishable based on a backscattered image (see App. 4C, Figs. 2 & 3 for microphotos showing difference between porosity and coal in both ppl and xpl).

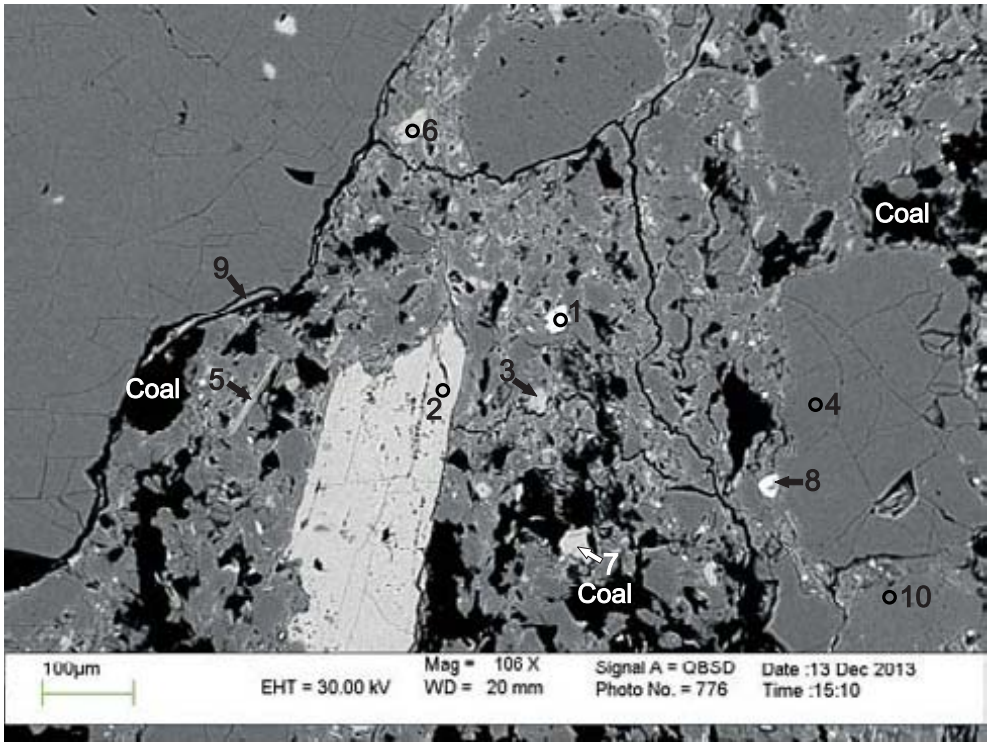

1: Rutile
2: K-feldspar
3: K-feldspar
4: Quartz
5: Muscovite
6: K-feldspar
7: K-feldspar
8: Muscovite + TiO_2
9: Muscovite + Chlorite
10: Albite

Figure 3: Wyandot E-53: 2876.81 site 3. Dissolution within K-feldspar (analysis 3) appears as both voids and along cleavage planes. Coal (black areas) is also present.

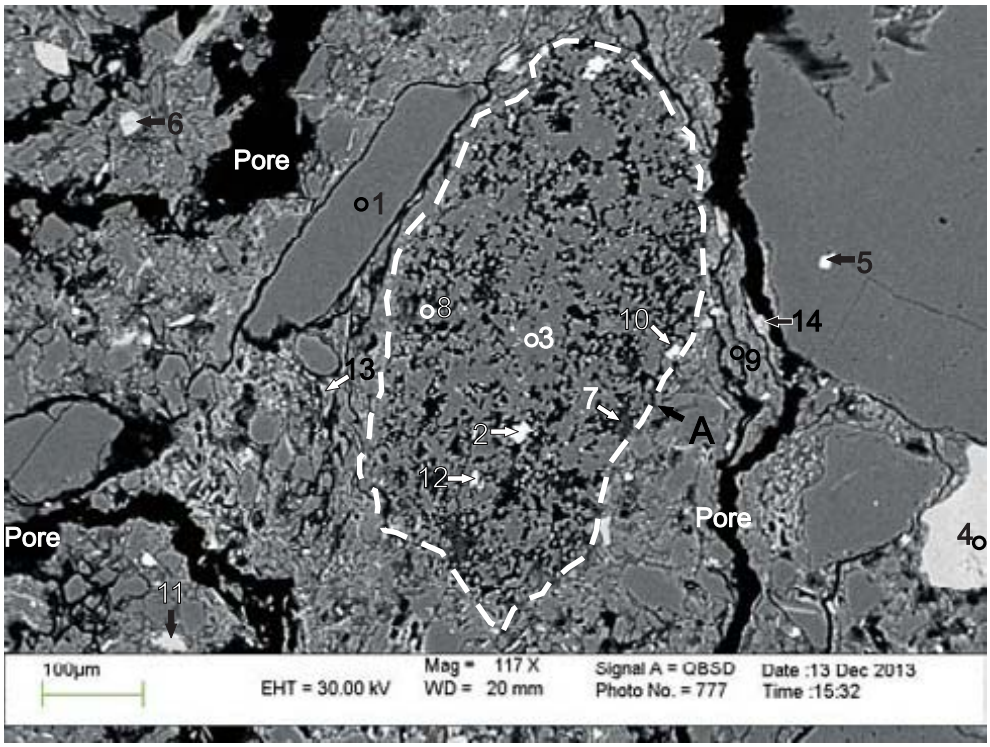

1: Quartz
2: Rutile
3: Quartz
4: K-feldspar
5: Zircon
6: K-feldspar
7: Kaolinite
8: Quartz
9: Feldspar + Quartz
10: Fluorapatite + SiO_2
11: K-feldspar
12: Quartz + TiO_2
13: K-feldspar
14: Quartz + Muscovite

Figure 4: Wyandot E-53: 2876.81 site 4. Dissolution of quartzite clast (position A) with crystallization of diagenetic rutile (analysis 2), apatite (analysis 10, and kaolinite (analysis 7) within voids (see App 4C, Fig. 4). It seems that there are two types of K-feldspar present (analyses 4 and 13). This site is highly porous (black areas) and contains no coal.

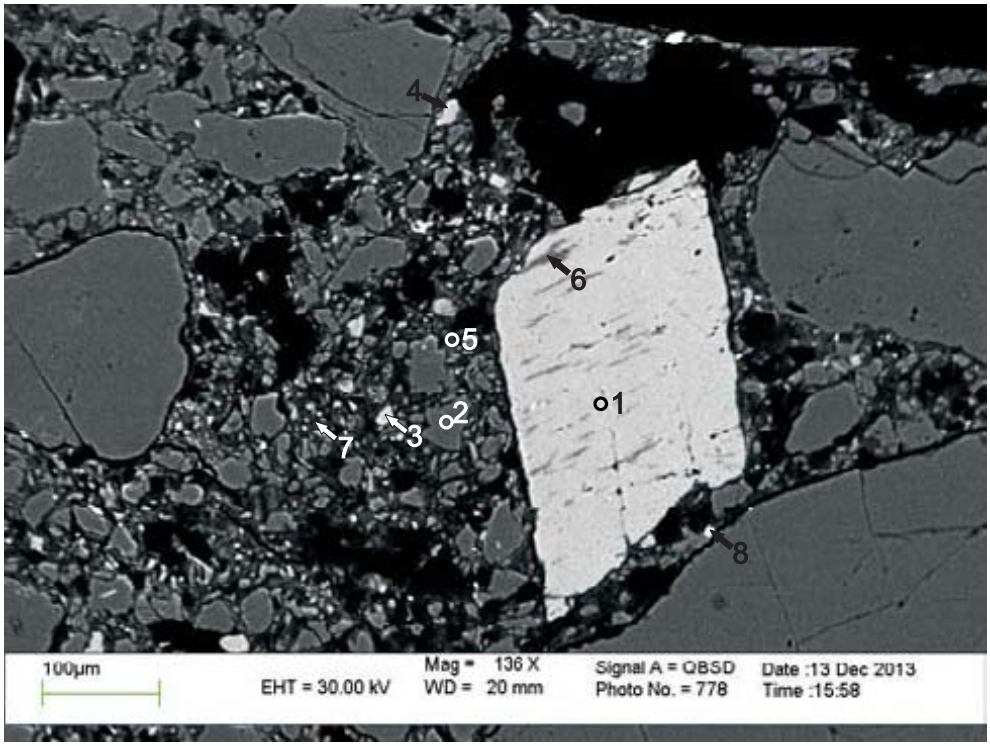

1: K-feldspar
2: Quartz
3: K-feldspar
4: K-feldspar
5: K-feldspar + Kaolinite
6: Albite
7: K-feldspar + other
8: Quartz + TiO_2

Figure 5: Wyandot E-53: 2876.81 site 5. Albitized K-feldspar (analyses 1 and 6) sitting among fragments of dissolved framework grains. This site is highly porous and contains no coal.

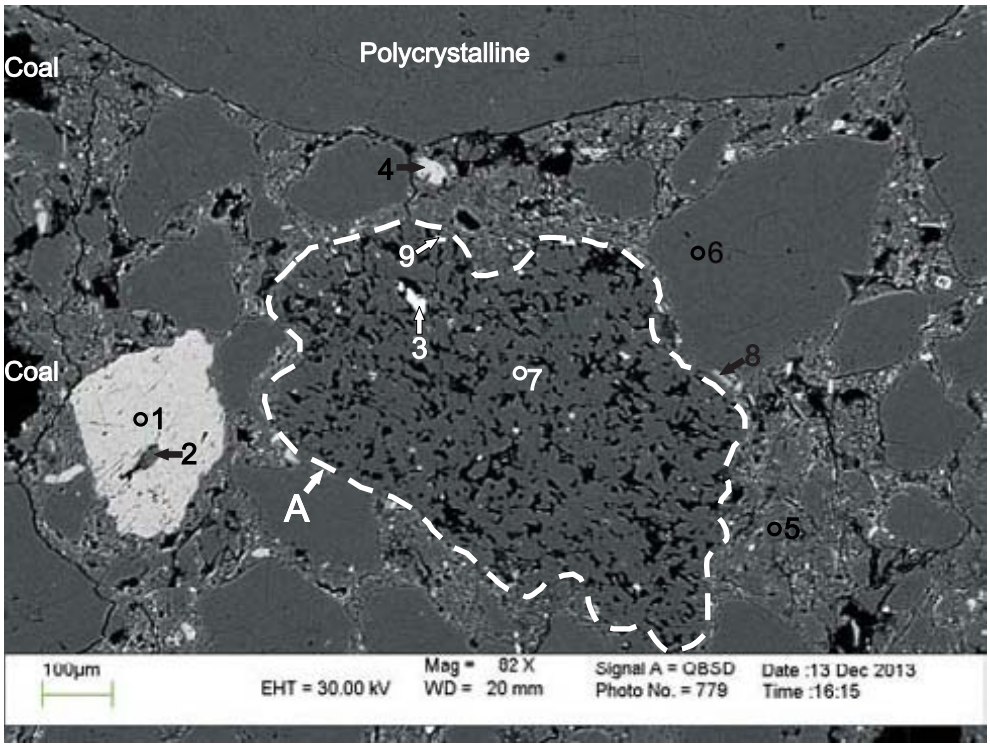

1: K-feldspar
2: Albite
3: Monazite
4: K-feldspar
5: Quartz
6: Quartz
7: Quartz
8: Muscovite
9: Rutile

Figure 6: Wyandot E-53: 2876.81 site 6. Dissolution of quartzite clast (position A, and see App. 4C, Fig. 5). This site contains coal and no porosity except within the lithic clast.

Table 1B: Scanning electron microscope chemical analyses of minerals from representative sites for Wyandot E-53 well at 2876.81m depth

Sample	Site	Position	Mineral	SiO_2	TiO_2	Al_2O_3	FeO	MnO	MgO	CaO	Na_2O	K_2O	P_2O_5	SO_3	F	Cl	Sc_2O_3	Cr_2O_3	Y_2O_3	ZrO_2	BaO	La_2O_3	Ce_2O_3	Nd_2O_3	HfO_2	ThO_2	Total	Actual Total
E-53-2876.81	1	1	K-feldspar	65.69		18.23					1.15	14.90															100.00	130.44
E-53-2876.81	1	2	Quartz	99.99																							100.00	121.44
E-53-2876.81	1	3	Albite	69.03		18.78					12.17																100.00	126.66
E-53-2876.81	1	4	K-feldspar	66.17		18.23					0.81	14.79															100.00	118.69
E-53-2876.81	1	5	Rutile	3.87	92.98	1.91					0.98	0.26															100.00	116.12
E-53-2876.81	1	6	Muscovite	55.47	0.25	25.96	2.30		1.43		0.73	6.86															93.00	109.98
E-53-2876.81	1	7	Muscovite	52.90	0.74	26.59	2.25		1.43		0.55	8.51															93.00	111.66
E-53-2876.81	1	8	Kaolinite	49.29		36.72																					86.00	97.66
E-53-2876.81	1	9	Muscovite & TiO2	37.63	33.26	21.16	1.66		1.48		0.69	3.67		0.45													100.00	121.07
E-53-2876.81	1	10	K-feldspar	65.65		18.06					0.51	15.10									0.65						100.00	128.75
E-53-2876.81	1	11	Quartz	99.99																							100.00	127.52
E-53-2876.81	2	1	Quartz	99.99																							100.00	121.87
E-53-2876.81	2	2	Muscovite	47.35		32.62	1.38		0.84		0.53	10.30															93.00	112.76
E-53-2876.81	2	3	Quartz	96.84		2.34	0.18		0.25			0.40															100.00	117.83
E-53-2876.81	2	4	Quartz	99.99																							100.00	115.09
E-53-2876.81	2	5	K-feldspar	67.13	0.35	18.78	0.73				0.81	12.20															100.00	127.13
E-53-2876.81	2	6	Quartz + Zircon	90.34																9.64							100.00	121.18
E-53-2876.81	2	7	Muscovite + Chlorite	53.35	0.55	29.27	3.91		1.87		0.50	10.55															100.00	118.57
E-53-2876.81	2	8	Albite	64.88	0.77	21.39	0.93		0.46		8.48	3.11															100.00	127.80
E-53-2876.81	3	1	Rutile	0.60	98.57	0.43	0.41																				100.00	112.65
E-53-2876.81	3	2	K-feldspar	65.95		18.31					1.11	14.64															100.00	122.85
E-53-2876.81	3	3	K-feldspar	65.31		18.52					1.12	14.50	0.55														100.00	124.70
E-53-2876.81	3	4	Quartz	99.99																							100.00	134.68
E-53-2876.81	3	5	Muscovite	47.75	0.62	33.35	0.84		0.47		0.58	9.38															93.00	123.91
E-53-2876.81	3	6	K-feldspar	65.89		18.14					0.77	15.19															100.00	121.44
E-53-2876.81	3	7	K-feldspar	65.93		18.03						16.03															100.00	121.80
E-53-2876.81	3	8	Muscovite + TiO2	23.83	55.85	15.55	0.53		0.40		0.42	3.46															100.00	125.00
E-53-2876.81	3	9	Muscovite + Chlorite	60.39	0.45	26.23	2.64		1.96		0.28	7.41		0.52		0.13											100.00	104.92
E-53-2876.81	3	10	Albite	68.92		18.86				0.20	11.92	0.11															100.00	133.48
E-53-2876.81	4	1	Quartz	99.99																							100.00	125.21
E-53-2876.81	4	2	Rutile	1.20	98.80																						100.00	110.10
E-53-2876.81	4	3	Quartz	99.99																							100.00	127.35
E-53-2876.81	4	4	K-feldspar	65.93		18.22					0.54	15.31															100.00	134.17
E-53-2876.81	4	5	Zircon	33.41		1.23	0.26			0.81					2.00		0.61		4.50	56.23					0.96		100.00	125.52
E-53-2876.81	4	6	K-feldspar	65.50		18.35	0.32				0.26	15.56															100.00	110.81
E-53-2876.81	4	7	Kaolinite	50.66		33.51	0.30					0.35			1.01	0.17											86.00	95.48
E-53-2876.81	4	8	Quartz	98.62	0.65	0.74																					100.00	125.27
E-53-2876.81	4	9	Muscovite + Quartz	71.36	0.42	17.78	0.94		0.63	0.24	5.85	2.79															100.00	129.13
E-53-2876.81	4	10	Fluorapatite + SiO2	6.42	0.32		0.14	0.18		44.28			42.05		6.61												100.00	137.65
E-53-2876.81	4	11	K-feldspar	65.54	0.22	18.33					0.57	15.35															100.00	115.35
E-53-2876.81	4	12	Quartz + TiO2	30.40	69.46		0.15																				100.00	112.12
E-53-2876.81	4	13	K-feldspar	67.92	0.25	19.86	1.62		0.86		3.37	6.12															100.00	126.79
E-53-2876.81	4	14	Quartz + Muscovite	61.89	2.09	24.41	2.14		1.49		0.43	7.36				0.19											100.00	104.42
E-53-2876.81	5	1	K-feldspar	65.63		18.16					0.47	15.74															100.00	122.60
E-53-2876.81	5	2	Quartz	99.99																							100.00	123.92
E-53-2876.81	5	3	K-feldspar	66.02		18.76	0.28				0.36	14.59															100.00	119.92
E-53-2876.81	5	4	K-feldspar	66.17		17.91					1.21	14.71															100.00	119.73
E-53-2876.81	5	5	K-feldspar + Kaolinite	62.23	0.67	26.02	2.07		1.82		0.31	6.90															100.00	105.99
E-53-2876.81	5	6	Albite	67.64		18.93				0.31	11.19	1.92															100.00	128.77
E-53-2876.81	5	7	K-feldspar + other	61.59	4.07	21.92	2.79		1.48		0.70	6.97		0.47													100.00	71.10
E-53-2876.81	5	8	Quartz + TiO2	11.85	77.48	5.33	2.20					0.84			1.76	0.16		0.37									100.00	96.82
E-53-2876.81	6	1	K-feldspar	65.25		18.29					0.67	15.21	0.57														100.00	114.56
E-53-2876.81	6	2	Albite	66.21		22.92				0.24	10.17	0.46															100.00	114.65
E-53-2876.81	6	3	Monazite	1.28						1.61			35.65		-0.74							13.16	28.94	9.75		10.37	100.00	114.41
E-53-2876.81	6	4	K-feldspar	65.82		18.22					0.71	15.24															100.00	125.99
E-53-2876.81	6	5	Quartz	99.99																							100.00	138.68

Table 1B: Scanning electron microscope chemical analyses of minerals from representative sites for Wyandot E-53 well at 2876.81m depth

Sample	Site	Position	Mineral	SiO_2	TiO_2	Al_2O_3	FeO	MnO	MgO	CaO	Na_2O	K_2O	P_2O_5	SO_3	F	Cl	Sc_2O_3	Cr_2O_3	Y_2O_3	ZrO_2	BaO	La_2O_3	Ce_2O_3	Nd_2O_3	HfO_2	ThO_2	Total	Actual Total
E-53-2876.81	6	6	Quartz	99.99																							100.00	137.23
E-53-2876.81	6	7	Quartz	99.99																							100.00	132.10
E-53-2876.81	6	8	Muscovite	48.22	0.40	32.30	1.91		0.43		1.78	7.95															93.00	119.66
E-53-2876.81	6	9	Rutile	4.62	95.38																						100.00	116.52

Appendix 3C: Scanning Electron Microscope Backscattered Electron Images for Wyandot E-53 well with EDS Mineral Analyses Sample 2878.66

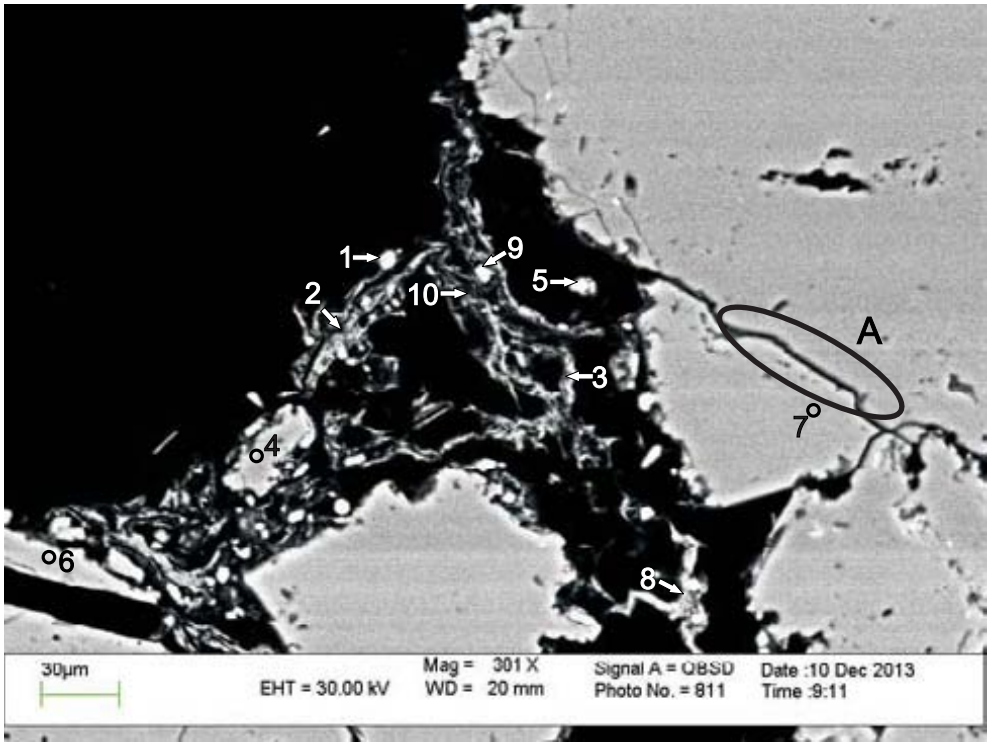

1: K-feldspar + Pyrite
2: Illite
3: Illite
4-7: Quartz
8: Muscovite + Pyrite
9: Muscovite + Pyrite + other
10: Muscovite + Pyrite

Figure 1: Wyandot E-53: 2878.66 site 1. High secondary porosity, with quartz overgrowths (position A) forming in dissolution space between grains.

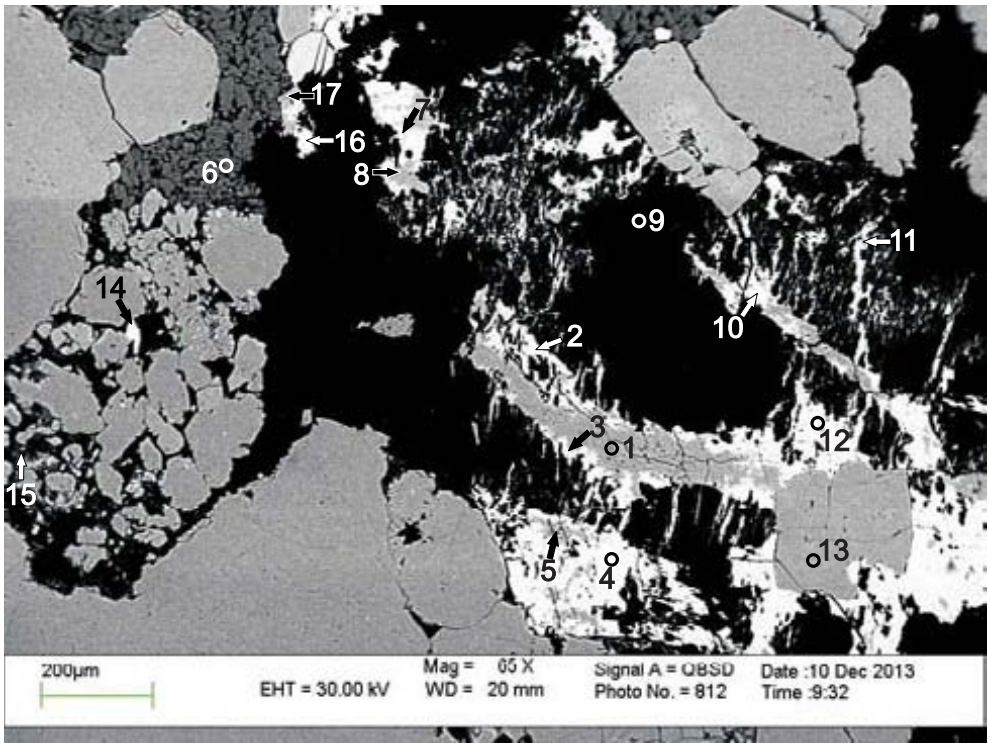

1: Albite
2-4: K-feldspar
5: Albite
6: Kaolinite
7: K-feldspar
8: Albite
9: Porosity
10-12: K-feldspar
13: Albite
14: K-feldspar
15: Quartz + Muscovite + Pyrite
16: K-feldspar
17: Feldspar

Figure 2: Wyandot E-53: 2878.66 site 2. High secondary porosity. Kaolinite (analysis 6) is filling in porosity from dissolution of framework grains, such as K-feldspar (analyses 3 and 16).

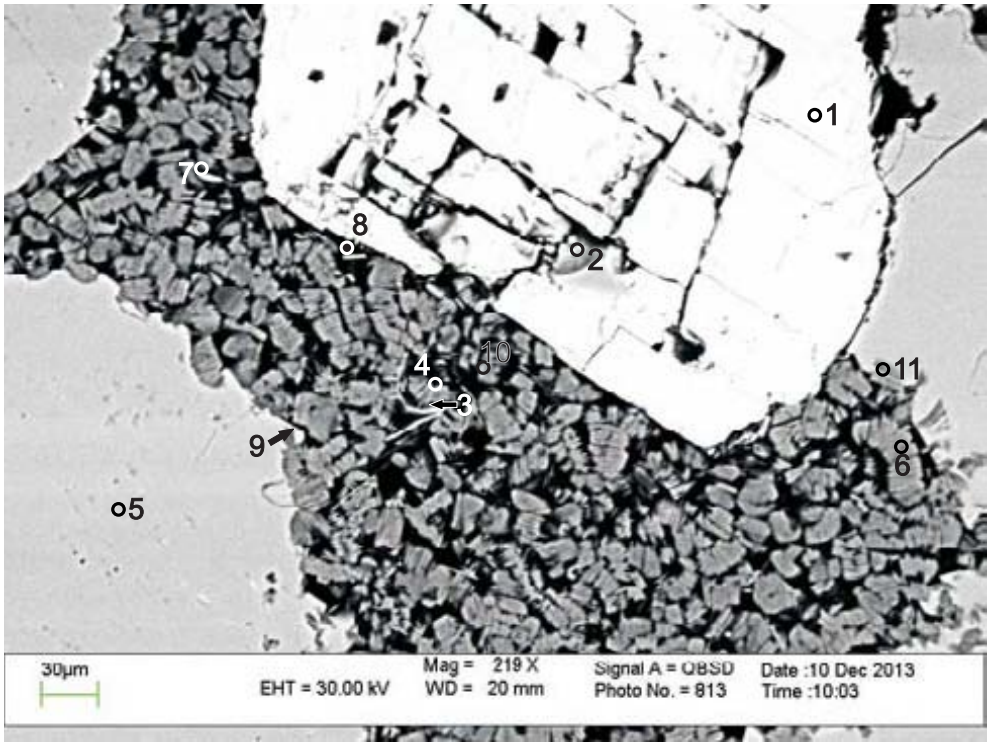

1: K-feldspar
2: Quartz
3: Kaolinite + Muscovite
4: Kaolinite
5: Quartz
6: Kaolinite
7: Quartz
8: Kaolinite
9: Quartz
10: Kaolinite
11: Kaolinite

Figure 3: Wyandot E-53: 2878.66 site 3. Kaolinite precipitated in intergranular space (analyses 3,4,6 and 8). Dissolution of K-feldspar (analysis 1) mostly along cleavage planes.

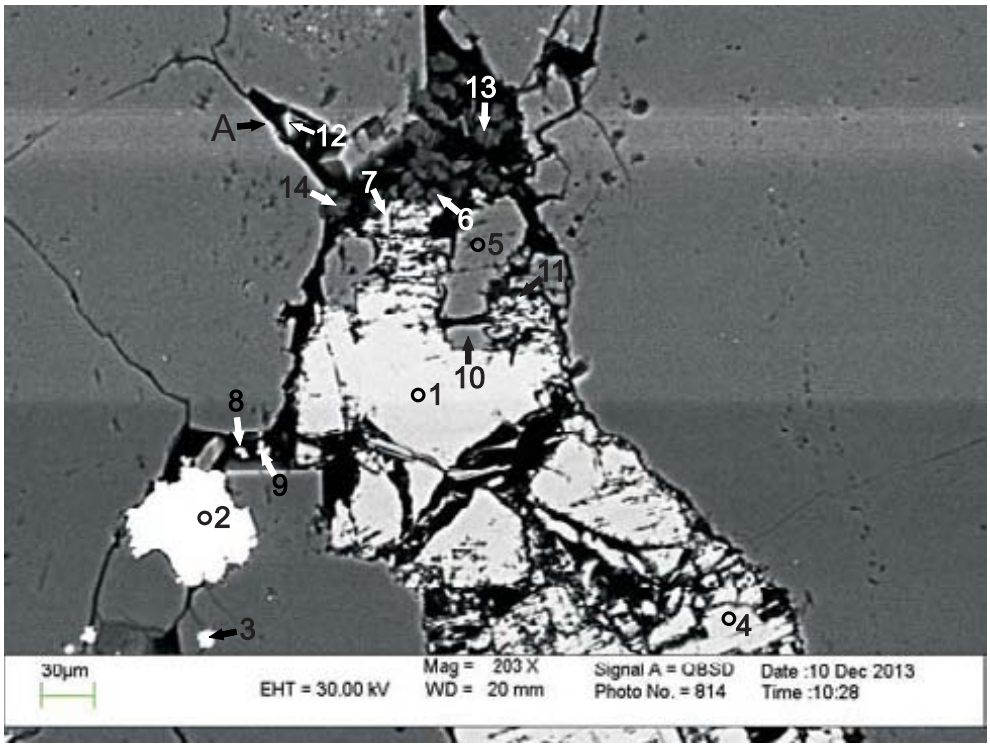

1: K-feldspar
2: Pyrite
3: Pyrite + Quartz
4: K-feldspar
5: Albite
6: Kaolinite
7: K-feldspar
8: Pyrite + other
9: Pyrite + other
10: Albite
11: K-feldspar
12: Quartz
13: Kaolinite
14: Kaolinite

Figure 4: Wyandot E-53: 2878.66 site 4. Dissolution of K-feldspar (analysis 1) and albite (analysis 5) grains leaving secondary porosity where kaolinite precipitated (analysis 13). Diagenetic pyrite forms in intergranular space (analysis 2). Quartz overgrowths formed straight crystal outline adjacent to porosity (position A).

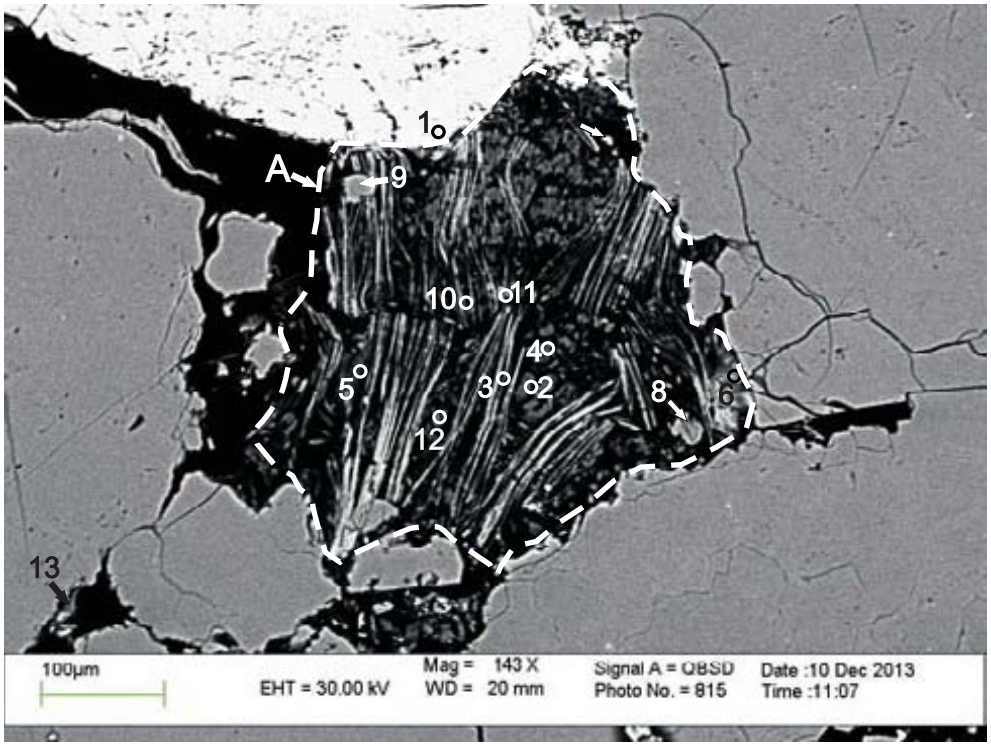

1: K-feldspar
2: Kaolinite
3: Muscovite
4: Kaolinite
5: Muscovite
6: Muscovite
7: Pyrite
8: Quartz
9: Quartz
10: Muscovite + Kaolinite
11: Muscovite
12: Kaolinite
13: K-feldspar + other

Figure 5: Wyandot E-53: 2878.66 site 5. Expansion of the cleavage planes of detrital muscovite and precipitation of kaolinite along these cleavage planes (position A, and see App. 4C, Fig. 6).

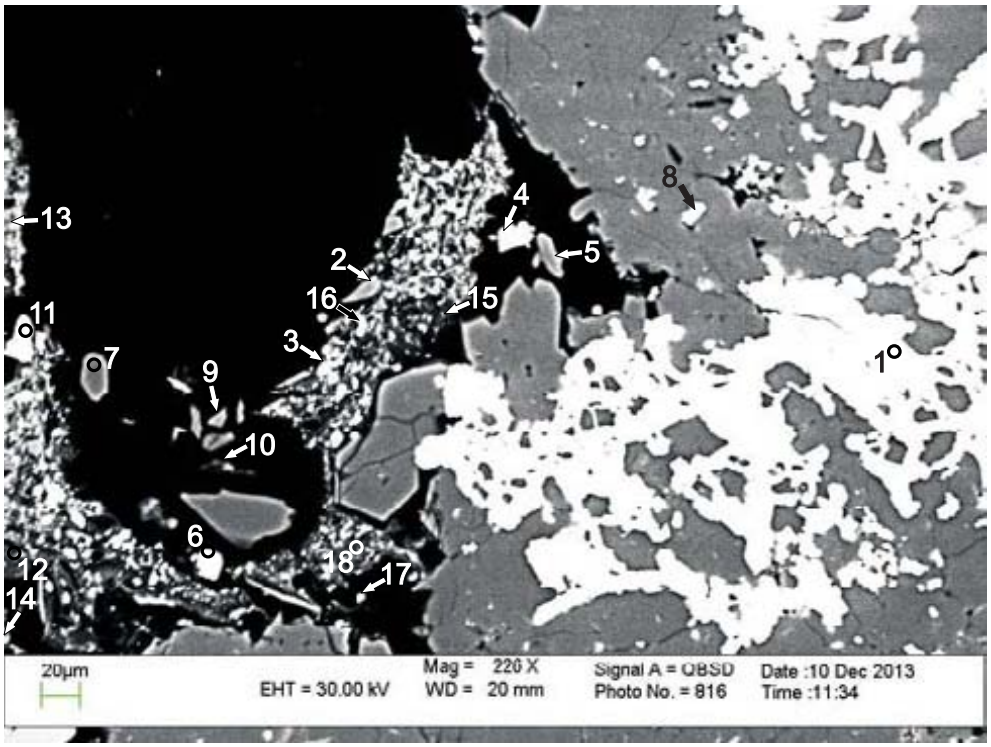

1: Pyrite
2: Quartz
3: Muscovite + Barite (drilling mud) + other
4: Pyrite
5: Quartz
6: Barite (drilling mud)
7: Quartz
8: Pyrite + Quartz
9: Quartz
10: Quartz
11: Barite (drilling mud)
12: Illite
13: Barite (drilling mud) + Illite
14: K-feldspar
15: Muscovite + Barite
16: Muscovite

Figure 6: Wyandot E-53: 2878.66 site 6. Pyrite (analysis 1) formed within secondary porosity in a quartz-rich lithic clast, which also contains minor amounts of albite (see App 4C, Fig. 7). Barite all occurs as drilling mud as it is found in open pore spaces and does not form defined crystal boundaries with other minerals (analyses 3, 5, 11, 13, and 18).

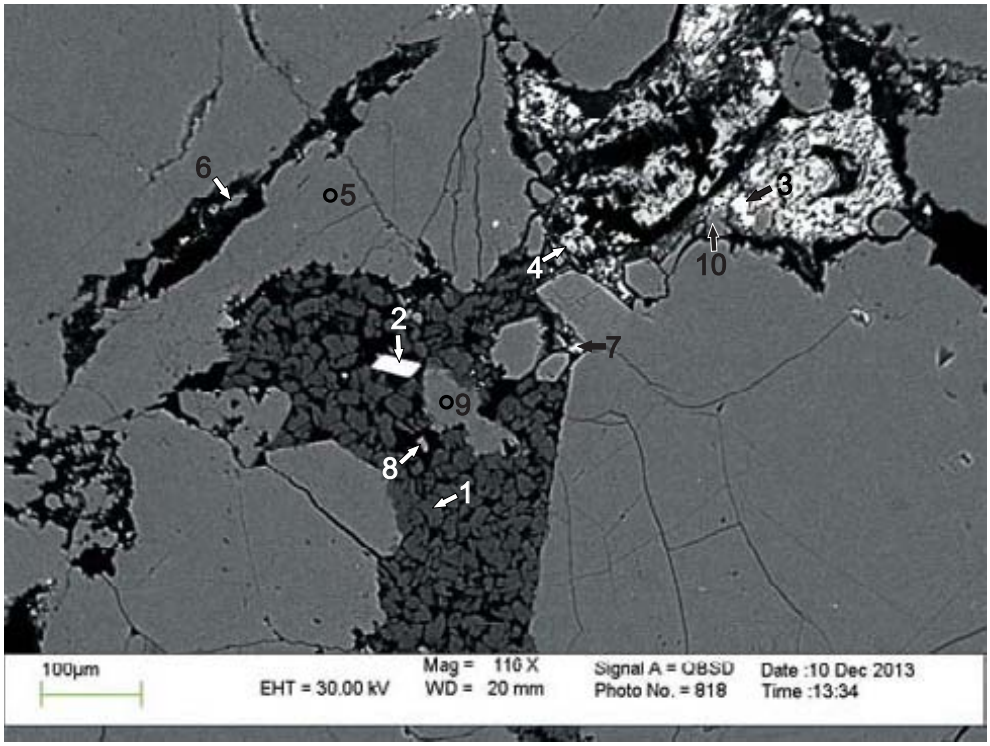

1: Kaolinite
2: Rutile
3: Barite
4: K-feldspar
5: Quartz
6: Quartz
7: Barite (drilling mud) + Kaolinite
8-10: Quartz

Figure 7: Wyandot E-53: 2878.66 site 7. Large pore is filled mostly of kaolinite (analysis 1) and some grains of partially dissolved quartz (analysis 9) and rutile (analysis 2).

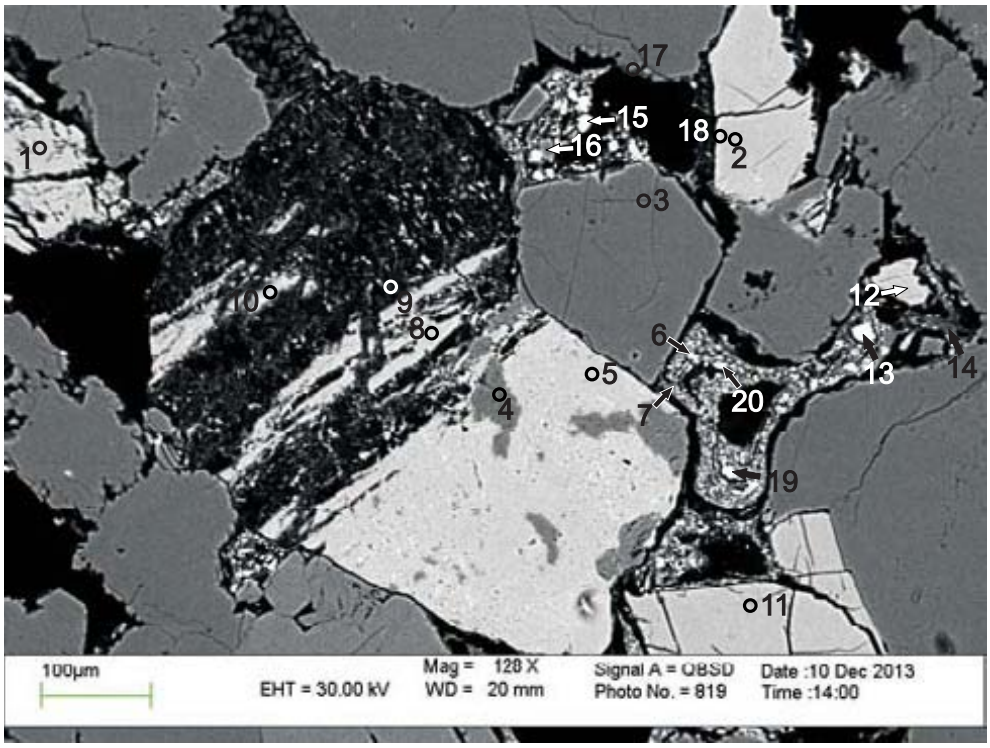

1: K-feldspar
2: K-feldspar
3: Quartz
4: Albite
5: K-feldspar (Albitized)
6: Pyrite + Barite (drilling mud) + K-feldspar
7: Muscovite + Pyrite
8-12: K-feldspar
13: Barite (drilling mud) + Quartz
14-20: Quartz + K-feldspar

Figure 8: Wyandot E-53: 2878.66 site 8. Partial dissolution of albitized K-feldspar grain (analyses 5 and 10).

Table 1C: Scanning electron microscope chemical analyses of minerals from representative sites for Wyandot E-53 well at 2878.66m depth

Sample	Site	Position	Mineral	SiO_2	TiO_2	Al_2O_3	FeO	MnO	MgO	CaO	Na_2O	K_2O	P_2O_5	SO_3	F	Cl	CuO	BaO	Total	Actual Total
E-53-2878.66	1	1	K-feldspar + Pyrite	57.42		21.82	2.57		1.46		3.90	5.00		2.32	4.17	1.33			100.00	39.87
E-53-2878.66	1	2	Illite	47.71		21.17	5.59		1.683		0.765	6.075		6.16		0.85			90.00	75.64
E-53-2878.66	1	3	Illite	46.86	0.29	21.36	6.13		1.683		0.531	6.354		5.44		1.34			90.00	55.84
E-53-2878.66	1	4	Quartz	99.84			0.17												100.00	119.77
E-53-2878.66	1	5	Quartz	97.12		2.04	0.22					0.49				0.12			100.00	118.41
E-53-2878.66	1	6	Quartz	99.99															100.00	118.70
E-53-2878.66	1	7	Quartz	99.99															100.00	125.53
E-53-2878.66	1	8	Muscovite + Pyrite	58.51		20.03	5.93		1.82		0.74	5.78		6.47		0.72			100.00	98.51
E-53-2878.66	1	9	Muscovite + Pyrite + other	74.79		14.11	2.48		1.31		0.35	4.41		1.92		0.62			100.00	95.13
E-53-2878.66	1	10	Muscovite + Pyrite	59.68		22.88	3.89		1.79		0.46	6.73		3.72		0.84			100.00	85.82
E-53-2878.66	2	1	Albite	67.26		19.56	0.45			0.27	11.66	0.52		0.3					100.00	127.14
E-53-2878.66	2	2	K-feldspar	65.63		18.27					1.27	14.29	0.55						100.00	126.94
E-53-2878.66	2	3	K-feldspar	65.20		18.44					0.82	14.78	0.76						100.00	128.93
E-53-2878.66	2	4	K-feldspar	65.87		18.23					1.38	14.15	0.37						100.00	127.35
E-53-2878.66	2	5	Albite	68.63		19.54	0.42			0.25	10.33	0.83							100.00	113.82
E-53-2878.66	2	6	Kaolinite	49.12		36.89													86.00	95.63
E-53-2878.66	2	7	K-feldspar	65.89		18.22					1.6	13.82	0.48						100.00	119.75
E-53-2878.66	2	8	Albite	67.13		18.99	0.50				12.01	0.49	0.39	0.5					100.00	124.24
E-53-2878.66	2	9	Porosity											15.66	63.32	16.66	4.37		100.00	2.05
E-53-2878.66	2	10	K-feldspar	66.04		18.08					0.97	14.91							100.00	134.76
E-53-2878.66	2	11	K-feldspar	65.29		18.42					0.88	14.66	0.76						100.00	138.54
E-53-2878.66	2	12	K-feldspar	66.61		18.25					1.44	13.71							100.00	137.89
E-53-2878.66	2	13	Albite	68.05		19.29				0.56	11.95	0.14							100.00	144.09
E-53-2878.66	2	14	K-feldspar	66.10		18.08					0.77	15.03							100.00	112.66
E-53-2878.66	2	15	Quartz + Muscovite + Pyrite	76.33	0.33	14.30	1.49		1.77		0.42	2.99		1.95		0.4			100.00	82.93
E-53-2878.66	2	16	K-feldspar	66.02		18.33					0.69	14.97							100.00	118.01
E-53-2878.66	2	17	Feldspar	61.03		29.17	0.31				5.84	3.22				0.43			100.00	76.53
E-53-2878.66	3	1	K-feldspar	66.42		18.25					1.12	14.2							100.00	128.55
E-53-2878.66	3	2	Quartz	98.38		0.93						0.67							100.00	145.51
E-53-2878.66	3	3	Kaolinite + Muscovite	52.77		38.41	0.33		0.32		1.32	6.84							100.00	118.07
E-53-2878.66	3	4	Kaolinite	49.01		36.99													86.00	99.23
E-53-2878.66	3	5	Quartz	99.99															100.00	122.11
E-53-2878.66	3	6	Kaolinite	48.93		37.05													86.00	110.65
E-53-2878.66	3	7	Quartz	87.04		12.70	0.14									0.11			100.00	129.20
E-53-2878.66	3	8	Kaolinite	50.96		34.78										0.27			86.00	67.15
E-53-2878.66	3	9	Quartz	90.04		9.96													100.00	105.28
E-53-2878.66	3	10	Kaolinite	50.37		35.62													86.00	102.95
E-53-2878.66	3	11	Kaolinite	59.33		26.67													86.00	117.74
E-53-2878.66	4	1	K-feldspar	66.10		18.25					0.58	15.07							100.00	122.99
E-53-2878.66	4	2	Pyrite	0.24			26.35	0.1			0.53			72.79					100.00	217.63
E-53-2878.66	4	3	Pyrite + Quartz	31.15			18.95					0.11		49.82					100.00	197.90
E-53-2878.66	4	4	K-feldspar	65.82		18.33					0.51	14.95	0.37						100.00	126.36
E-53-2878.66	4	5	Albite	68.30		19.31				0.32	11.9	0.17							100.00	130.82
E-53-2878.66	4	6	Kaolinite	49.77		36.22													86.00	98.92
E-53-2878.66	4	7	K-feldspar	66.40		19.03	0.33				0.75	13.47							100.00	137.92
E-53-2878.66	4	8	Pyrite + other	15.42		1.44	22.10	0.12		0.17	1.17	0.3		58.93		0.34			100.00	171.57
E-53-2878.66	4	9	Pyrite + other	7.94		1.85	22.68	0.1	0.27		0.5	0.29		66.15		0.24			100.00	244.22
E-53-2878.66	4	10	Albite	68.45		19.08				0.28	12.04	0.14							100.00	149.55
E-53-2878.66	4	11	K-feldspar	69.72		20.24	0.30				4.07	5.69							100.00	150.53

Table 1C: Scanning electron microscope chemical analyses of minerals from representative sites for Wyandot E-53 well at 2878.66m depth

Sample	Site	Position	Mineral	SiO_2	TiO_2	Al_2O_3	FeO	MnO	MgO	CaO	Na_2O	K_2O	P_2O_5	SO_3	F	Cl	CuO	BaO	Total	Actual Total
E-53-2878.66	4	12	Quartz	99.99															100.00	152.25
E-53-2878.66	4	13	Kaolinite	49.58		36.43													86.00	118.20
E-53-2878.66	4	14	Kaolinite	49.01		36.99													86.00	115.16
E-53-2878.66	5	1	K-feldspar	65.65		17.88	0.24				0.31	15.31		0.62					100.00	129.86
E-53-2878.66	5	2	Kaolinite	49.27		36.72													86.00	109.45
E-53-2878.66	5	3	Muscovite	48.41	0.72	32.62	0.73		0.4743		1.18	8.67				0.21			93.00	83.46
E-53-2878.66	5	4	Kaolinite	49.34		36.66													86.00	102.63
E-53-2878.66	5	5	Muscovite	49.46	0.51	31.86	0.51		0.5673		0.95	6.61			2.17	0.38			93.00	85.12
E-53-2878.66	5	6	Muscovite	51.43	0.58	31.25	0.60		0.558		1.16	7.29				0.15			93.00	111.76
E-53-2878.66	5	7	Pyrite	4.66		1.91	26.33	0.17		0.35	1.23	0.54		64.5		0.34			100.00	131.35
E-53-2878.66	5	8	Quartz	98.90		1.00						0.10							100.00	140.32
E-53-2878.66	5	9	Quartz	99.99															100.00	134.56
E-53-2878.66	5	10	Muscovite + Kaolinite	55.92	0.27	38.94	0.35				0.62	3.77				0.14			100.00	98.91
E-53-2878.66	5	11	Muscovite	51.61	0.48	30.03	1.71		0.9672		0.74	7.27				0.18			93.00	109.92
E-53-2878.66	5	12	Kaolinite	49.19		35.75	0.31					0.52				0.23			86.00	80.30
E-53-2878.66	5	13	K-feldspar + other	69.01		18.52	2.77		1.72		0.46	4.48		2.57		0.48			100.00	84.77
E-53-2878.66	6	1	Pyrite	0.58		0.32	26.36							72.74					100.00	240.65
E-53-2878.66	6	2	Quartz	93.72		4.01	0.63					0.28		1.00				0.36	100.00	126.07
E-53-2878.66	6	3	Muscovite + Barite (drillng mud) + other	57.27		18.50	2.46		1.34	0.35	0.67	2.65		8.37		0.69		7.72	100.00	91.35
E-53-2878.66	6	4	Pyrite	0.21			26.33							73.44					100.00	249.27
E-53-2878.66	6	5	Quartz	89.31		1.98	4.27					0.71		3.72					100.00	100.61
E-53-2878.66	6	6	Barite (drilling mud)	1.90		0.70								40.2				57.21	100.00	103.24
E-53-2878.66	6	7	Quartz	99.99															100.00	135.37
E-53-2878.66	6	8	Pyrite + Quartz	42.33			13.95							43.72					100.00	213.96
E-53-2878.66	6	9	Quartz	98.38											1.62				100.00	93.61
E-53-2878.66	6	10	Quartz	99.02										0.75		0.22			100.00	80.57
E-53-2878.66	6	11	Barite (drilling mud)											39.63				60.38	100.00	121.43
E-53-2878.66	6	12	Illite	49.89		22.84	3.87		1.503	0.666	0.64	4.00		4.88		0.549		1.17	90.00	90.64
E-53-2878.66	6	13	Barite (drilling mud) + Illite	49.86		17.36	10.01		1.34	0.42	1.97	3.18		12.34		0.53		2.97	100.00	100.52
E-53-2878.66	6	14	K-feldspar	64.95		18.65					1.00	14.48	0.94						100.00	127.65
E-53-2878.66	6	15	Muscovite + Barite	58.40		19.18	3.60		1.82	0.35	0.80	2.96		7.99		0.7		4.19	100.00	122.48
E-53-2878.66	6	16	Muscovite + Barite	59.83		9.54	1.79		0.78	0.28	0.36	0.75		13.01		0.24		13.41	100.00	129.97
E-53-2878.66	6	17	Pyrite + other	20.60		7.26	15.44			0.22		2.11		48.54	3.07	0.88		1.89	100.00	64.27
E-53-2878.66	6	18	Muscovite + Pyrite + Barite (drilling mud)	55.83	0.38	24.85	3.73		1.89		0.62	5.3		4.25		0.60		2.55	100.00	110.23
E-53-2878.66	7	1	Kaolinite	49.06		36.92													86.00	94.31
E-53-2878.66	7	2	Rutile	0.49	97.83	0.49	1.18												100.00	93.94
E-53-2878.66	7	3	Barite	4.28		1.66								33.54				60.53	100.00	96.74
E-53-2878.66	7	4	K-feldspar	66.06		18.37					0.85	14.19	0.55						100.00	118.65
E-53-2878.66	7	5	Quartz	99.99															100.00	112.20
E-53-2878.66	7	6	Quartz	99.49		0.38						0.13							100.00	119.14
E-53-2878.66	7	7	Barite (drilling mud) + Kaolinite	6.10		2.63								36.01				55.27	100.00	109.29
E-53-2878.66	7	8	Quartz	99.99															100.00	108.78
E-53-2878.66	7	9	Quartz	99.99															100.00	120.44
E-53-2878.66	7	10	Quartz	99.43		0.45						0.10							100.00	132.76
E-53-2878.66	8	1	K-feldspar	66.23		18.10					0.75	14.92							100.00	113.73
E-53-2878.66	8	2	K-feldspar	66.19		18.12					0.88	14.83							100.00	123.45
E-53-2878.66	8	3	Quartz	99.99															100.00	121.61
E-53-2878.66	8	4	Albite	68.39		19.22	0.53			0.21	10.96	0.67							100.00	114.67
E-53-2878.66	8	5	K-feldspar (Albitized)	65.91		17.95					0.80	14.97						0.37	100.00	120.72

Table 1C: Scanning electron microscope chemical analyses of minerals from representative sites for Wyandot E-53 well at 2878.66m depth

Sample	Site	Position	Mineral	SiO_2	TiO_2	Al_2O_3	FeO	MnO	MgO	CaO	Na_2O	K_2O	P_2O_5	SO_3	F	Cl	CuO	BaO	Total	Actual Total
E-53-2878.66	8	6	Pyrite + Barite (drilling mud) + K-feldspar	4.02		1.81	25.76				1.44	0.28		61.48				5.23	100.00	167.09
E-53-2878.66	8	7	Muscovite + Pyrite	56.33		21.22	5.60		1.94	0.7	0.51	3.53		4.99		0.39		4.79	100.00	88.53
E-53-2878.66	8	8	K-feldspar	66.72		17.86						15.42							100.00	115.00
E-53-2878.66	8	9	K-feldspar	65.52		16.21						15.19		0.55	2.12	0.42			100.00	58.40
E-53-2878.66	8	10	K-feldspar	66.34		17.99					0.61	15.08							100.00	105.33
E-53-2878.66	8	11	K-feldspar	65.57		18.33					1.59	13.98	0.50						100.00	121.43
E-53-2878.66	8	12	K-feldspar	65.91		18.23					0.74	15.1							100.00	122.23
E-53-2878.66	8	13	Barite (drilling mud) + Quartz	15.83		2.12						0.67		32.21				49.18	100.00	124.08
E-53-2878.66	8	14	Quartz + K-feldspar	81.52		9.49	0.36				1.29	5.84		0.70				0.79	100.00	92.89
E-53-2878.66	8	15	Quartz + K-feldspar	81.44		9.56	0.32				1.29	5.91		0.80				0.67	100.00	93.41
E-53-2878.66	8	16	Quartz + K-feldspar	81.31		9.60	0.35				1.28	6.01		0.72				0.73	100.00	94.03
E-53-2878.66	8	17	Quartz + K-feldspar	81.20		9.56	0.40				1.29	5.89		0.77		0.14		0.74	100.00	93.87
E-53-2878.66	8	18	Quartz + K-feldspar	81.25		9.52	0.41				1.21	5.95		0.75		0.16		0.73	100.00	94.13
E-53-2878.66	8	19	Quartz + K-feldspar	81.18		9.49	0.40				1.39	6.05		0.82				0.68	100.00	93.39
E-53-2878.66	8	20	Quartz + K-feldspar	81.44		9.37	0.37				1.21	6.05		0.85				0.70	100.00	93.29

Appendix 3D: Scanning Electron Microscope Backscattered Electron Images for Wyandot E-53 well with EDS Mineral Analyses Sample 2880.22

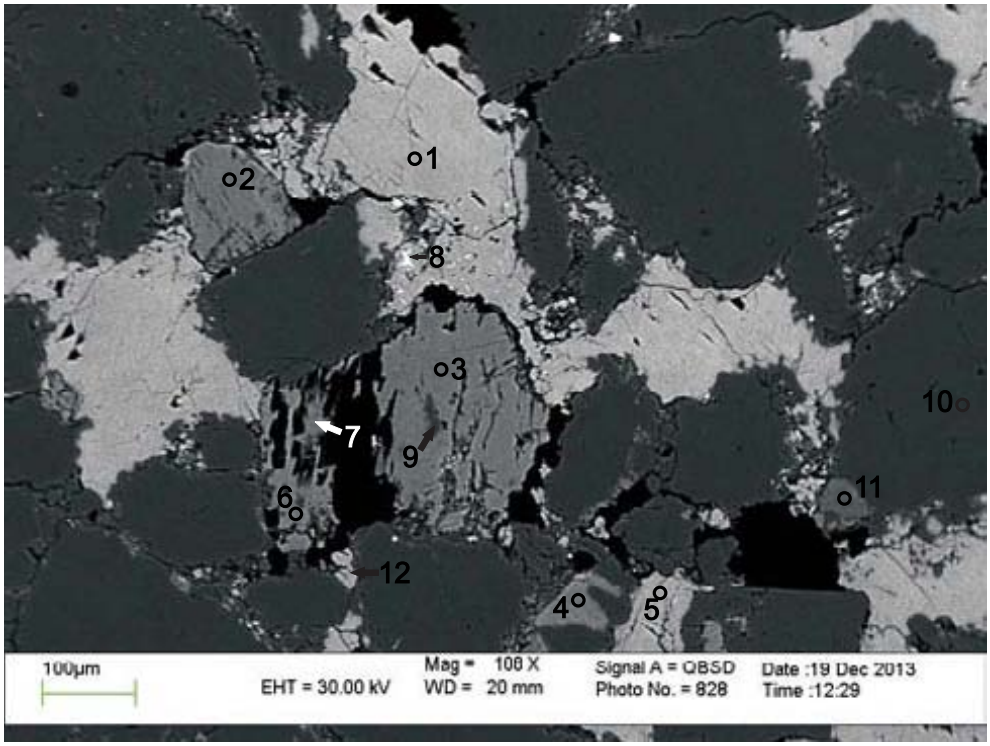

1: Fe-Calcite
2-4: K-feldspar
5: Fe-Calcite
6: K-feldspar
7: K-feldspar
8: Ankerite
9: Albite
10: Quartz
11: Muscovite
12: Mn-Calcite + Quartz

Figure 1: Wyandot E-53: 2880.22 site 1. Dissolution in intergranular space has been replaced by early calcite cement (analysis 5), and followed by dissolution of framework grains, such as K-feldspar (analysis 3).

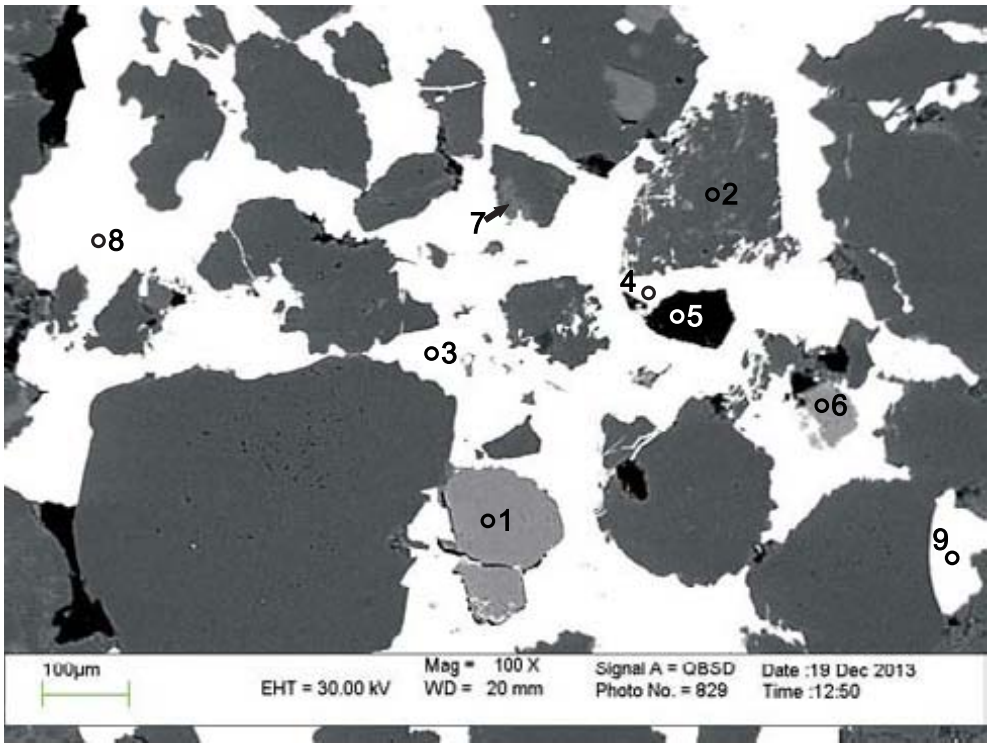

1: K-feldspar
2: Albite
3: Pyrite
4: Rutile
5: Porosity
6: K-feldspar
7: Quartz + Muscovite
8: Pyrite
9: Pyrite

Figure 2: Wyandot E-53: 2880.22 site 2. Diagenetic pyrite has formed a cement around framework grains of quartz, K-feldspar and albite (see App. 4C, Fig. 8).

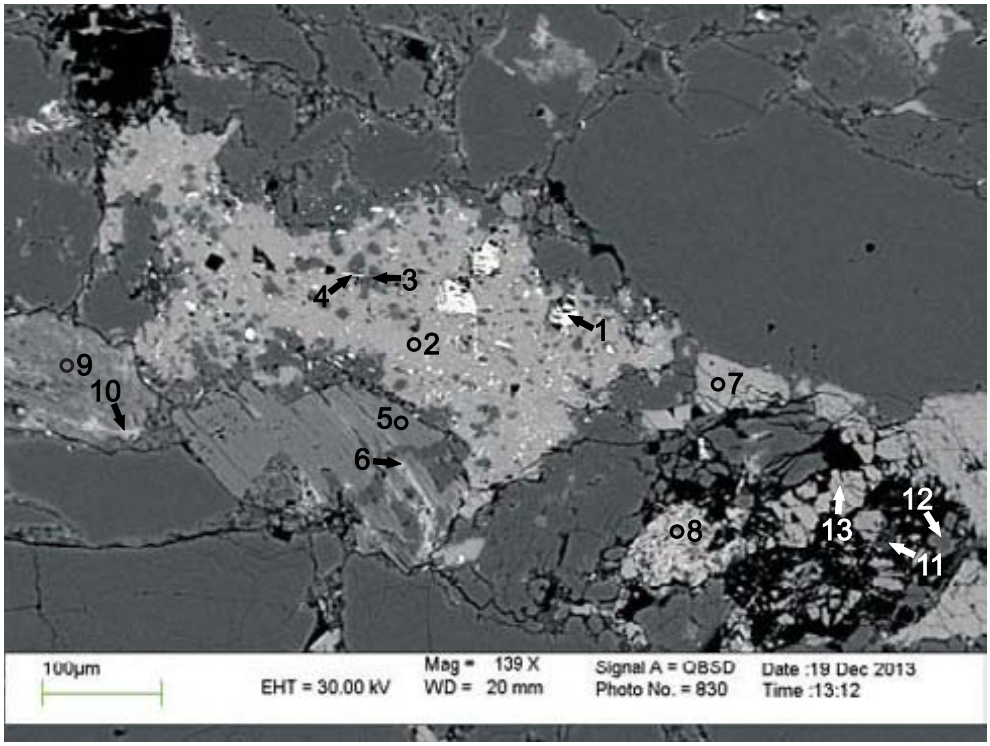

1: Garnet-Spessartine
2: Mn-Calcite
3: Quartz
4: Quartz + TiO_2
5: Muscovite
6: Chlorite
7: Mn-Calcite
8: Chlorite + K-feldspar
9: Muscovite
10: Chlorite + Muscovite
11: Illite
12: Quartz
13: Mn-Calcite

Figure 3: Wyandot E-53: 2880.22 site 3. Relics of detrital Mn-rich garnet (analysis 1, and see App. 4C, Fig. 9) hosted in Mn-rich calcite (analysis 2). Chlorite (analysis 6) forms along cleavage planes of muscovite (analysis 5).

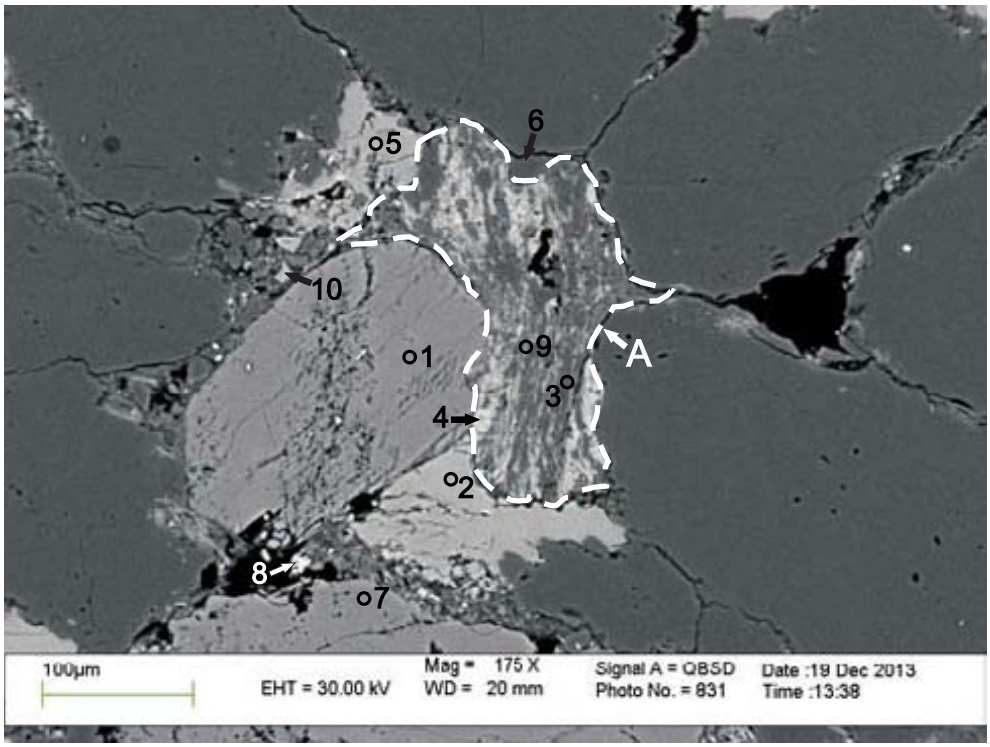

1: K-feldspar
2: Fe-Calcite
3: Quartz
4: Chlorite
5: Fe-Calcite
6: Quartz
7: K-feldspar
8: TiO_2 + Chlorite
9: Muscovite + Illite
10: Calcite

Figure 4: Wyandot E-53: 2880.22 site 4. Plastically deformed lithic clast composed of quartz, muscovite and illite (position A, and see App. 4C, Fig. 10).

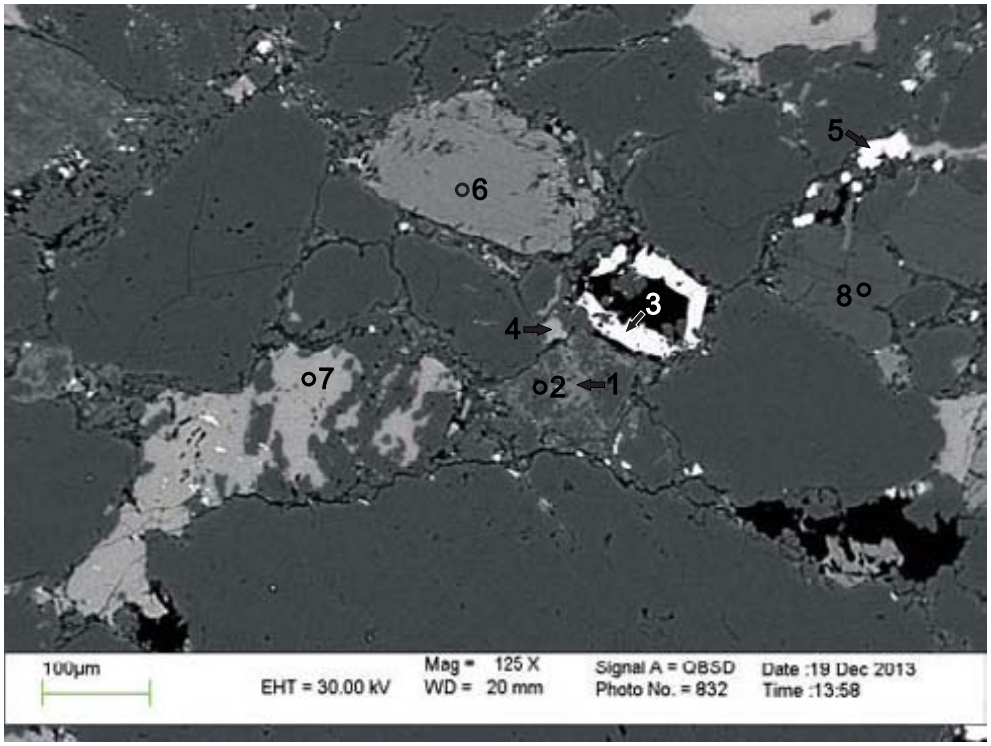

Figure 5: Wyandot E-53: 2880.22 site 5. Fe-calcite forms cement (analysis 7). Fragments of spessartine (Mn-garnet) surround area of porosity (analysis 3).

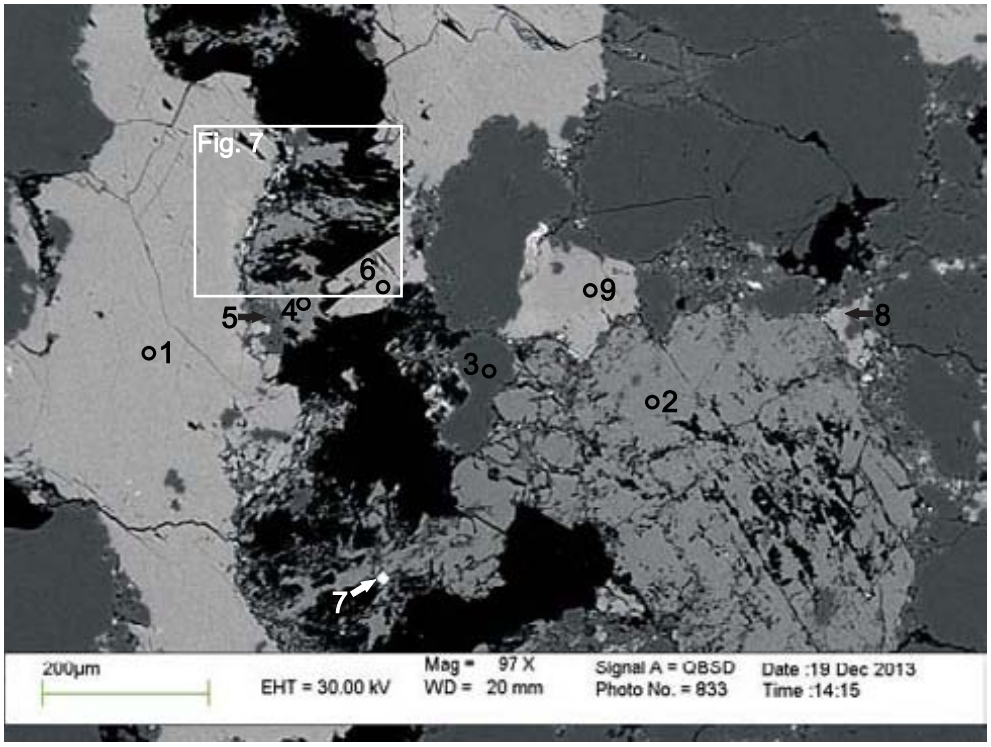

Figure 6: Wyandot E-53: 2880.22 site 6. Dissolution of K-feldspar (analysis 2 and 4) leaves secondary porosity where calcite cement (analyses 1 and 6) precipitated. Fe-calcite (analysis 1) forms cement in intergranular space, and Mn-calcite (analysis 6, and see Fig. 7) forms within space left by K-feldspar dissolution.

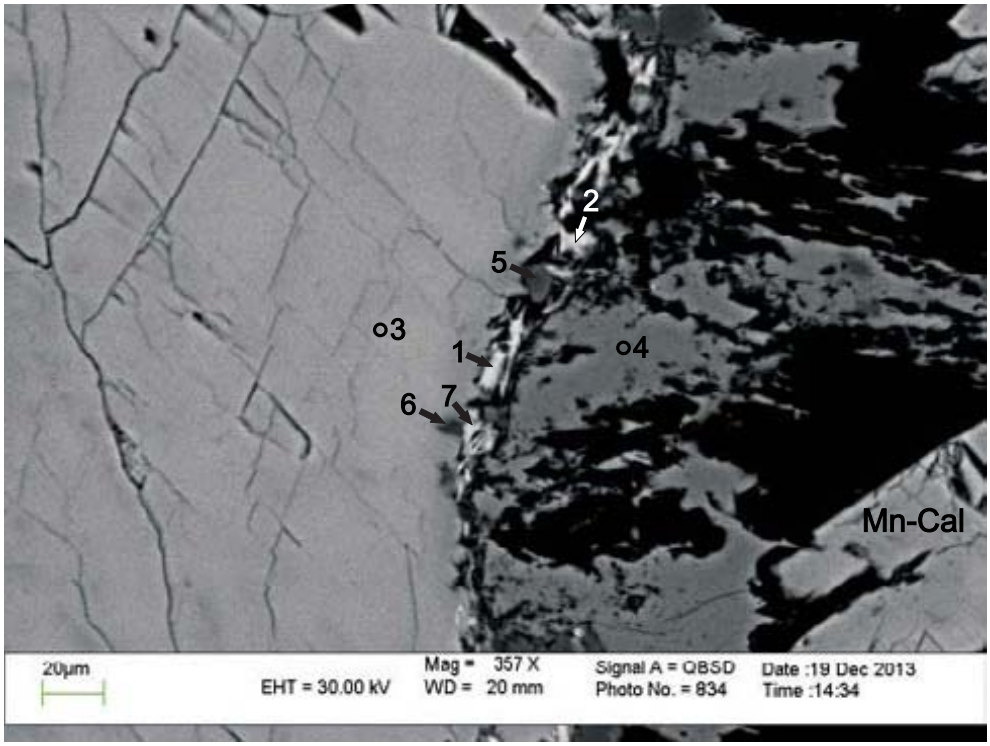

1: Chlorite
2: Chlorite
3: Fe-Calcite
4: K-feldspar
5: Quartz
6: Quartz
7: Chlorite + Muscovite

Figure 7: Wyandot E-53: 2880.22m site 7 (from Fig. 6). Dissolution of K-feldspar (analysis 4), with precipitation of Mn-calcite within porosity. Chlorite, with some muscovite (analysis 7), forms between calcite cement and K-feldspar (analyses 1 and 2).

Table 1D: Scanning electron microscope chemical analyses of minerals from representative sites for Wyandot E-53 well at 2880.22m depth

Sample	Site	Position	Mineral	SiO_2	TiO_2	Al_2O_3	FeO	MnO	MgO	CaO	Na_2O	K_2O	P_2O_5	SO_3	F	Cl	Sc_2O_3	Y_2O_3	ZrO_2	BaO	HfO_2	Total	Actual Total
E-53-2880.22	1	1	Fe-Calcite				1.10	0.60	0.40	53.90												56.00	50.10
E-53-2880.22	1	2	K-feldspar	65.99		18.16					0.81	15.03										100.00	102.50
E-53-2880.22	1	3	K-feldspar	65.91		18.18					1.08	14.44	0.39									100.00	106.75
E-53-2880.22	1	4	K-feldspar	65.99		18.18					0.89	14.50								0.44		100.00	107.63
E-53-2880.22	1	5	Fe-Calcite				1.22	0.96		53.82												56.00	50.15
E-53-2880.22	1	6	K-feldspar	66.23		17.88					0.38	15.51										100.00	100.54
E-53-2880.22	1	7	K-feldspar	65.16		18.44					0.38	15.54	0.48									100.00	101.25
E-53-2880.22	1	8	Ankerite				23.23	2.31	5.30	25.17												56.00	55.96
E-53-2880.22	1	9	Albite	68.56		19.29					11.66	0.49										100.00	105.35
E-53-2880.22	1	10	Quartz	99.99																		100.00	115.17
E-53-2880.22	1	11	Muscovite	46.61	0.76	32.79	1.30		0.80		0.60	10.13										93.00	104.90
E-53-2880.22	1	12	Mn-Calcite + Quartz	7.12		3.16	2.14	1.52	0.73	84.50		0.84										100.00	50.03
E-53-2880.22	2	1	K-feldspar	65.54		18.18					0.96	14.80	0.50									100.00	102.37
E-53-2880.22	2	2	Albite	68.82		19.01	0.13				12.04											100.00	108.78
E-53-2880.22	2	3	Pyrite	0.15			28.02							71.84								100.00	187.53
E-53-2880.22	2	4	Rutile		99.15		0.85															100.00	92.01
E-53-2880.22	2	5	Porosity	17.88			10.64									71.47						100.00	0.93
E-53-2880.22	2	6	K-feldspar	65.76		18.18	0.44				0.82	14.83										100.00	109.47
E-53-2880.22	2	7	Quartz + Muscovite	70.23		19.71	1.75		1.36	0.42	0.31	6.24										100.00	99.38
E-53-2880.22	2	8	Pyrite				27.79							72.22								100.00	176.96
E-53-2880.22	2	9	Pyrite	0.17			27.87							71.97								100.00	207.51
E-53-2880.22	3	1	Garnet-Spessartine	38.46	0.72	20.01	4.32	30.92	0.38	2.46					2.73							100.00	102.90
E-53-2880.22	3	2	Mn-Calcite				0.50	0.97		54.52												56.00	46.59
E-53-2880.22	3	3	Quartz	98.40	0.33		0.19			1.08												100.00	89.38
E-53-2880.22	3	4	Quartz + TiO2	51.81	38.50	0.49	0.41			8.79												100.00	86.56
E-53-2880.22	3	5	Muscovite	46.51	0.48	34.00	0.75		0.56		0.46	10.23										93.00	96.67
E-53-2880.22	3	6	Chlorite	31.84		22.92	21.29		6.94	0.25		1.72										85.00	88.93
E-53-2880.22	3	7	Mn-Calcite				0.70	1.72		53.58												56.00	48.53
E-53-2880.22	3	8	Chlorite + K-feldspar	40.07		25.23	24.93		7.10	0.28	0.50	1.63				0.25						100.00	76.12
E-53-2880.22	3	9	Muscovite	47.05	0.35	32.09	2.29		1.33		0.40	9.49										93.00	92.69
E-53-2880.22	3	10	Chlorite + Muscovite	40.20		27.89	21.27		7.18			3.44										100.00	84.19
E-53-2880.22	3	11	Illite	49.10	0.48	20.88	5.73		2.61	0.56	0.90	5.82			3.59	0.33						90.00	76.78
E-53-2880.22	3	12	Quartz	98.90		0.70						0.40										100.00	112.36
E-53-2880.22	3	13	Mn-Calcite	0.74		0.36	0.97	2.44	0.41	51.08												56.00	49.04
E-53-2880.22	4	1	K-feldspar	65.82		18.33					1.33	14.50										100.00	102.55
E-53-2880.22	4	2	Fe-Calcite				1.01	0.91		54.07												56.00	46.83
E-53-2880.22	4	3	Quartz	95.26	1.05	2.68	0.32					0.67										100.00	104.71
E-53-2880.22	4	4	Chlorite	31.00		22.46	22.95		7.20	0.23		1.16										85.00	85.45
E-53-2880.22	4	5	Fe-Calcite				1.29	0.87	0.37	53.47												56.00	47.37
E-53-2880.22	4	6	Quartz	99.99																		100.00	107.75
E-53-2880.22	4	7	K-feldspar	66.10		18.03					1.25	14.61										100.00	101.74
E-53-2880.22	4	8	TiO2 + Chlorite	8.79	78.33	4.38	6.41		0.96	0.41		0.72										100.00	82.13
E-53-2880.22	4	9	Muscovite + Illite	58.72	1.87	24.92	6.51		1.82		1.08	5.06										100.00	103.69
E-53-2880.22	4	10	Calcite	3.39		1.80	0.63	0.80		48.99		0.38										56.00	51.09
E-53-2880.22	5	1	Muscovite	50.00	0.28	27.26	2.77		2.46			10.23										93.00	98.91

Table 1D: Scanning electron microscope chemical analyses of minerals from representative sites for Wyandot E-53 well at 2880.22m depth

Sample	Site	Position	Mineral	SiO_2	TiO_2	Al_2O_3	FeO	MnO	MgO	CaO	Na_2O	K_2O	P_2O_5	SO_3	F	Cl	Sc_2O_3	Y_2O_3	ZrO_2	BaO	HfO_2	Total	Actual Total
E-53-2880.22	5	2	Quartz	98.51		0.94	0.13					0.42										100.00	105.53
E-53-2880.22	5	3	Garnet-Spessartine	39.21	0.20	20.82	2.56	30.86	0.66	3.26					2.42							100.00	104.38
E-53-2880.22	5	4	Fe-Calcite	0.77			1.18	0.95	0.37	52.74												56.00	48.72
E-53-2880.22	5	5	Rutile	1.65	97.13	0.66	0.35					0.22										100.00	95.06
E-53-2880.22	5	6	K-feldspar	65.63		18.39					0.77	15.21										100.00	101.79
E-53-2880.22	5	7	Fe-Calcite				1.31	0.94	0.43	53.32												56.00	46.06
E-53-2880.22	5	8	Albite	65.89		21.03				2.36	10.61	0.12										100.00	109.81
E-53-2880.22	6	1	Fe-Calcite				1.11	0.89		54.00												56.00	44.54
E-53-2880.22	6	2	K-feldspar	65.63		18.37					0.38	15.63										100.00	107.63
E-53-2880.22	6	3	Quartz	99.99																		100.00	106.64
E-53-2880.22	6	4	K-feldspar	64.88		18.44					0.36	15.45	0.85									100.00	100.76
E-53-2880.22	6	5	Albite	68.07		19.42	0.51			0.15	11.22	0.60										100.00	102.90
E-53-2880.22	6	6	Mn-Calcite	0.42			0.57	2.13		52.88												56.00	47.63
E-53-2880.22	6	7	Zircon	31.15		0.93	0.39			0.57		0.23					0.41	1.22	62.46		2.64	100.00	96.89
E-53-2880.22	6	8	Calcite + Quartz	8.19		2.72	1.84	2.03	0.55	83.81		0.86										100.00	55.51
E-53-2880.22	6	9	Calcite				0.34	0.22		55.45												56.00	49.81
E-53-2880.22	7	1	Chlorite	31.02		21.63	23.63		7.82	0.50		0.39										85.00	83.74
E-53-2880.22	7	2	Chlorite	31.31		21.41	22.36		7.74	0.66		1.39				0.13						85.00	85.56
E-53-2880.22	7	3	Fe-Calcite				1.11	0.83		54.06												56.00	47.00
E-53-2880.22	7	4	K-feldspar	66.29		17.93					0.31	15.48										100.00	104.91
E-53-2880.22	7	5	Quartz	97.65		0.98	0.64		0.23	0.21		0.26										100.00	104.48
E-53-2880.22	7	6	Quartz	93.06		0.89	0.93		0.27	4.69		0.19										100.00	96.90
E-53-2880.22	7	7	Chlorite + Muscovite	53.59		19.24	18.78		6.78	0.80		0.81										100.00	95.28

Appendix 4A: Microphotos of Mineral Grains and Lithic Clasts of Mic Mac H-86 well

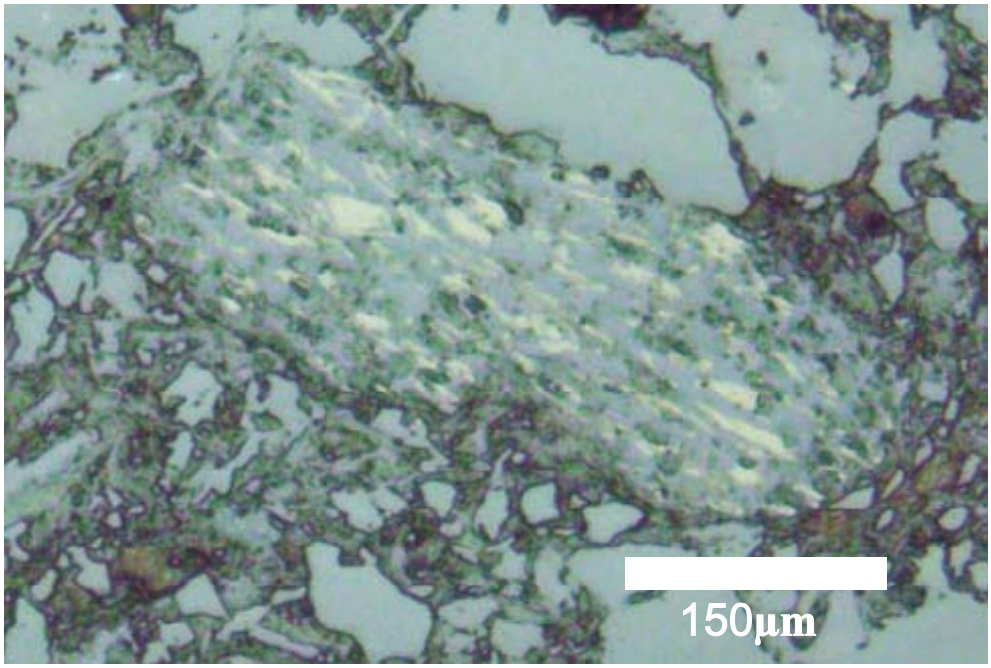

Figure 1: Lithic clast composed of muscovite and goethite/hematite from Mic Mac H-86 4717.78 site 2. 10x magnification, reflected xpl.

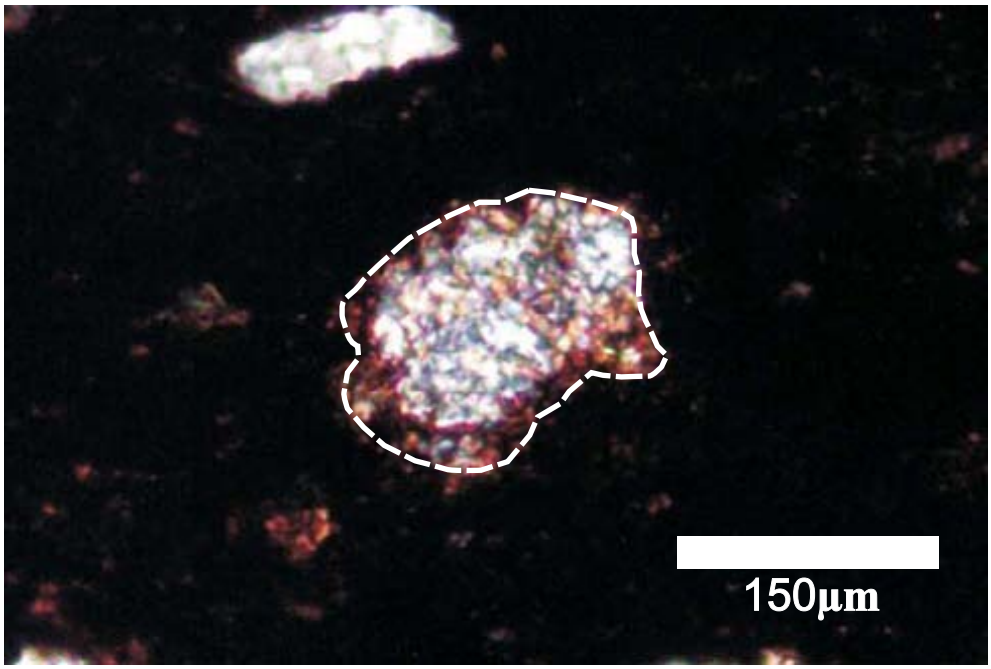

Figure 2: Muscovite and quartz rich litihic clast in muddy matrix from Mic Mac H-86 4717.78 site 5. 10x magnification, xpl.

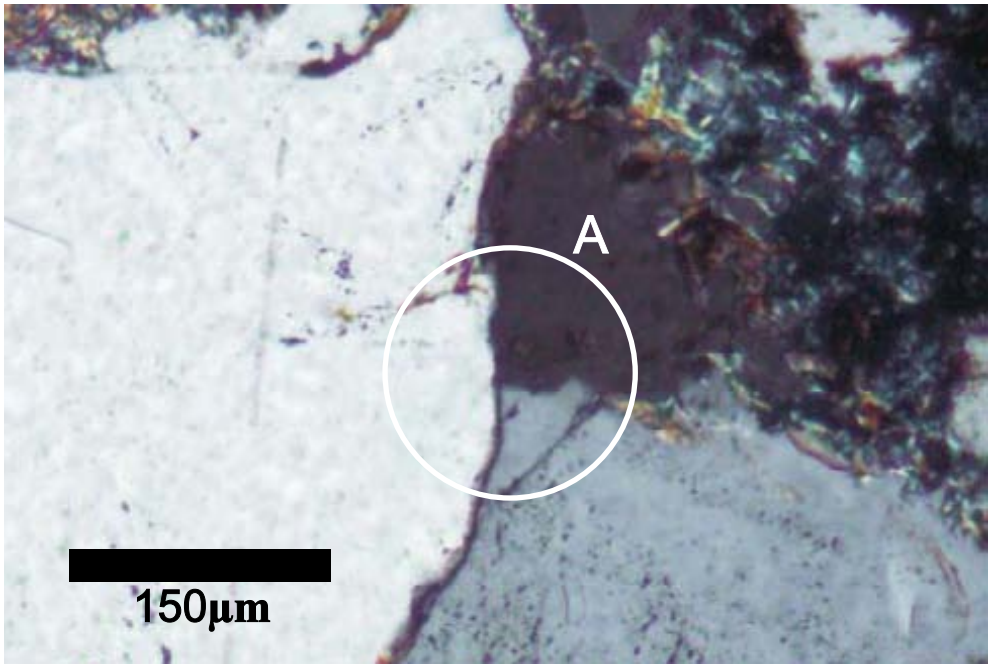

Figure 3: Compacted sandstone from Mic Mac
H-86 4718.97 site 1 with apparent triple point in quartz overgrowths (position A) that occured during diagenesis. 10x magnification, xpl.

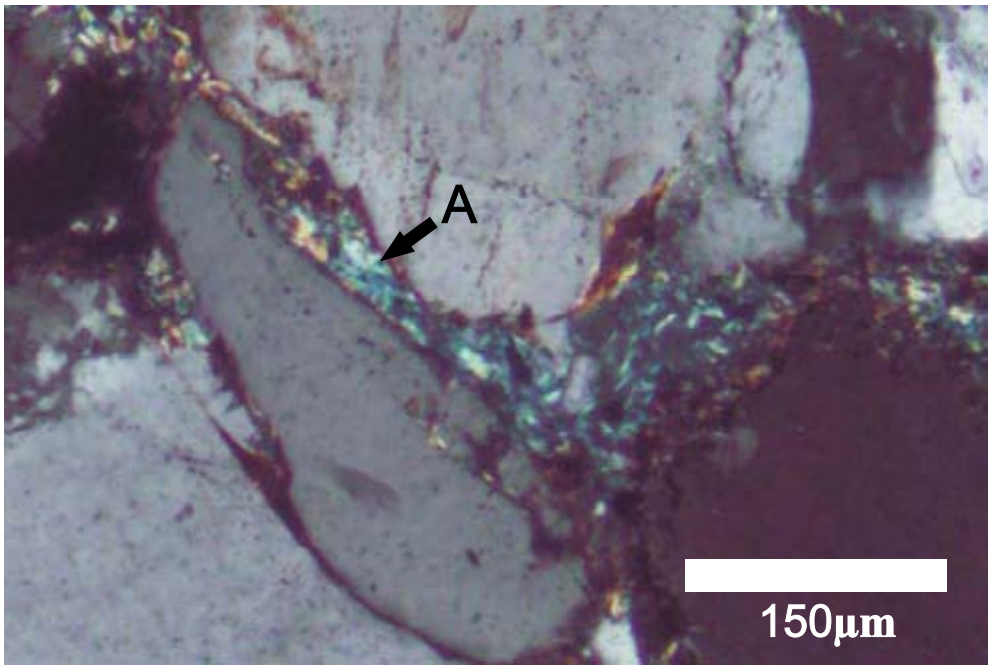

Figure 4: Compacted sandstone from Mic Mac
H-86 4718.97 site 1 with pseudomatrix (position A). 10x magnification, xpl.

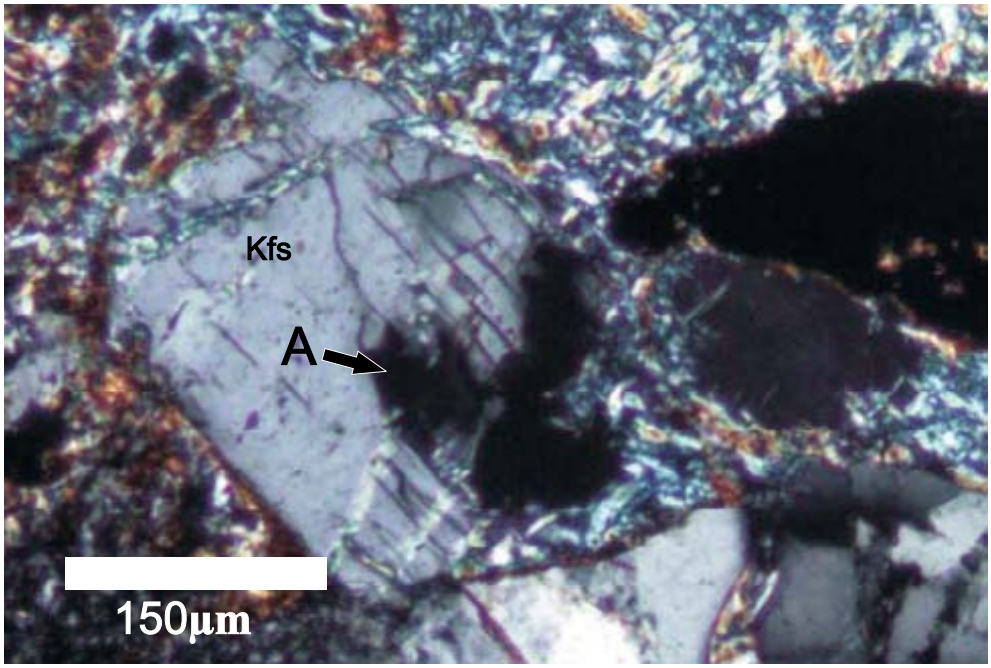

Figure 5: Secondary porosity within K-feldspar from Mic Mac H-86 4718.97 site 2 (position A). 10x magnification, xpl.

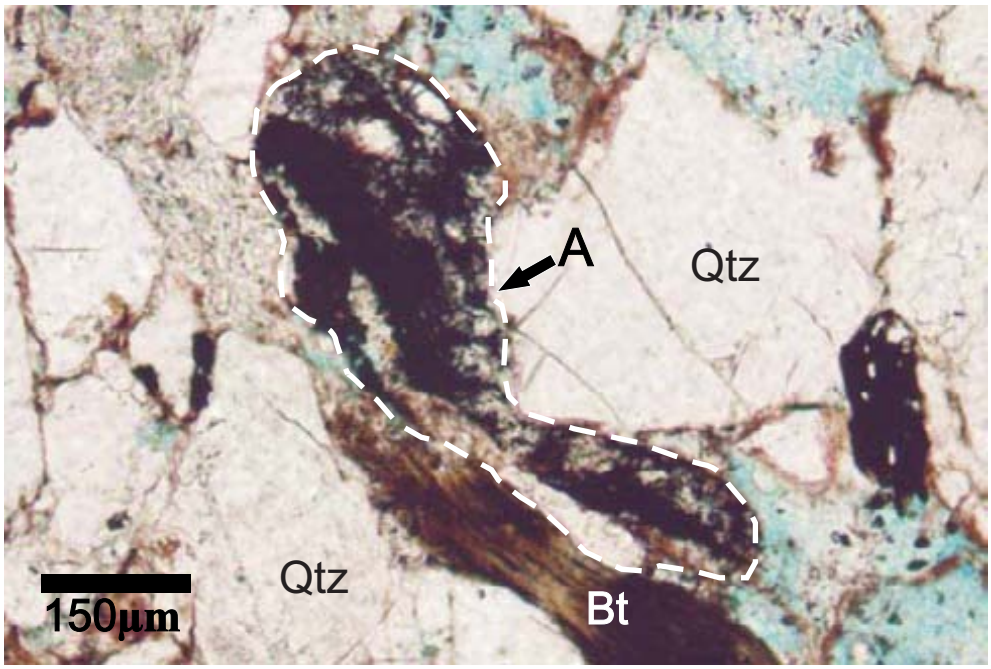

Figure 6: Plastically deformed ithic clast (position A) composed of microcrystalline patches of iron oxides, muscovite and chlorite, from Mic Mac H-86 4718.97 site 3. 10x magnification, ppl.

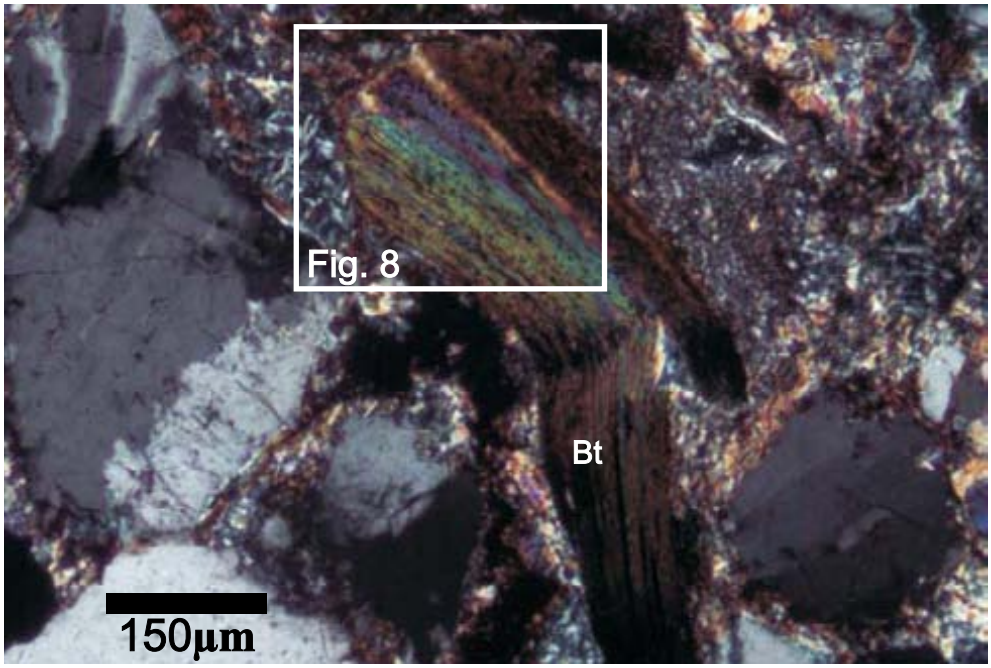

Figure 7: Plastically deformed chloritzed biotite from Mic Mac H-86 4718.97 site 4. 10x magnification, xpl.

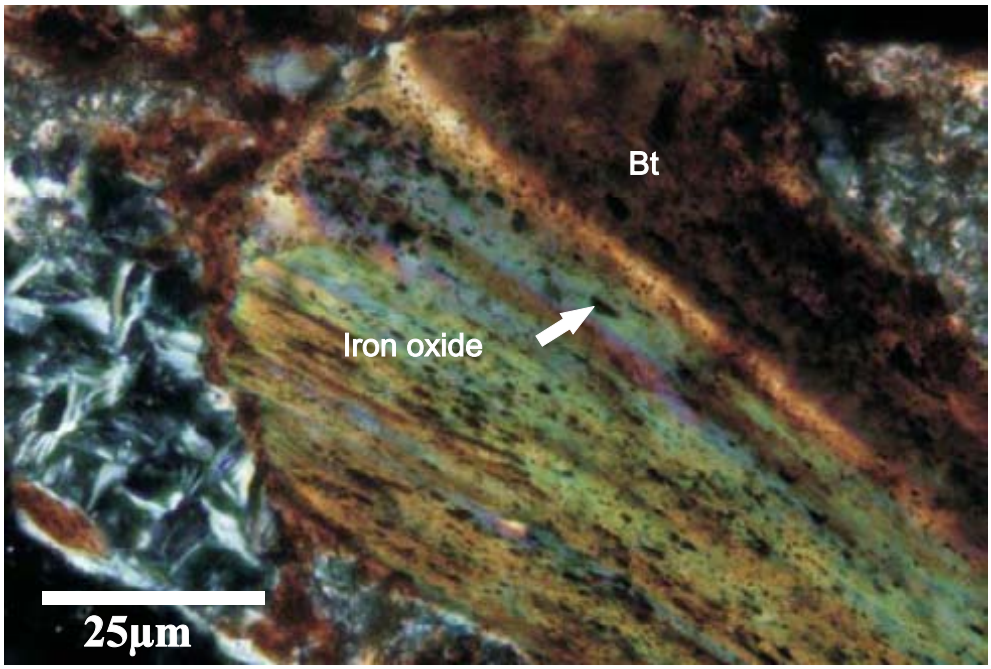

Figure 8: Chloritized biotite with iron oxide inclusions along cleavage planes from Mic Mac H-86 4718.97 site 4. 40x magnification, xpl.

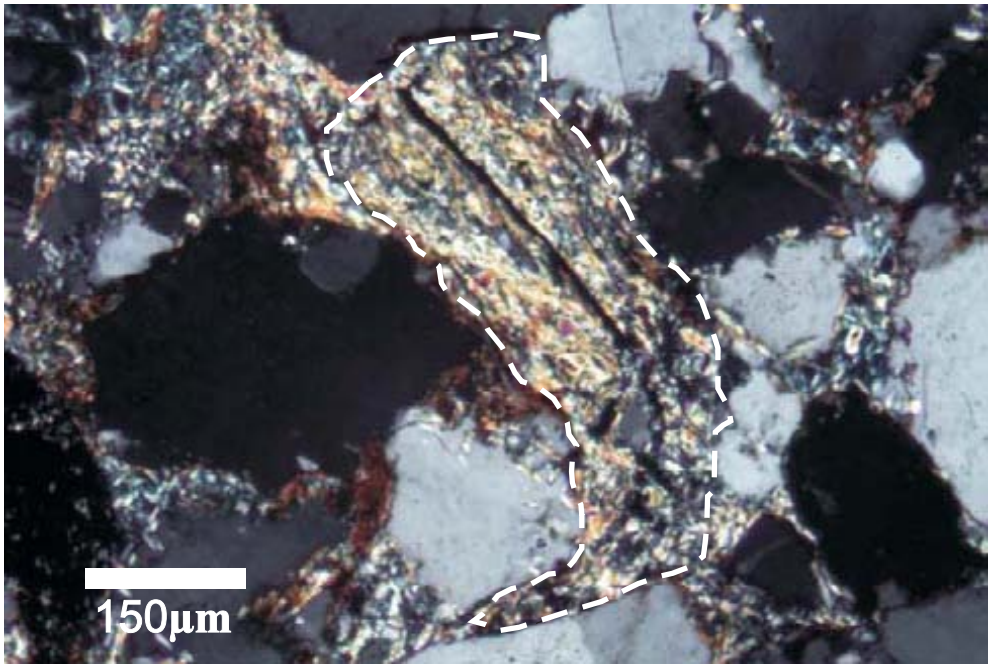

Figure 9: Plastically deformed lithic clast composed of muscovite and chlorite, with iron oxide along a fracture which likely formed from the oxidation of pyrrhotite, from Mic Mac H-86 4718.97 site 5. 10x magnification, xpl.

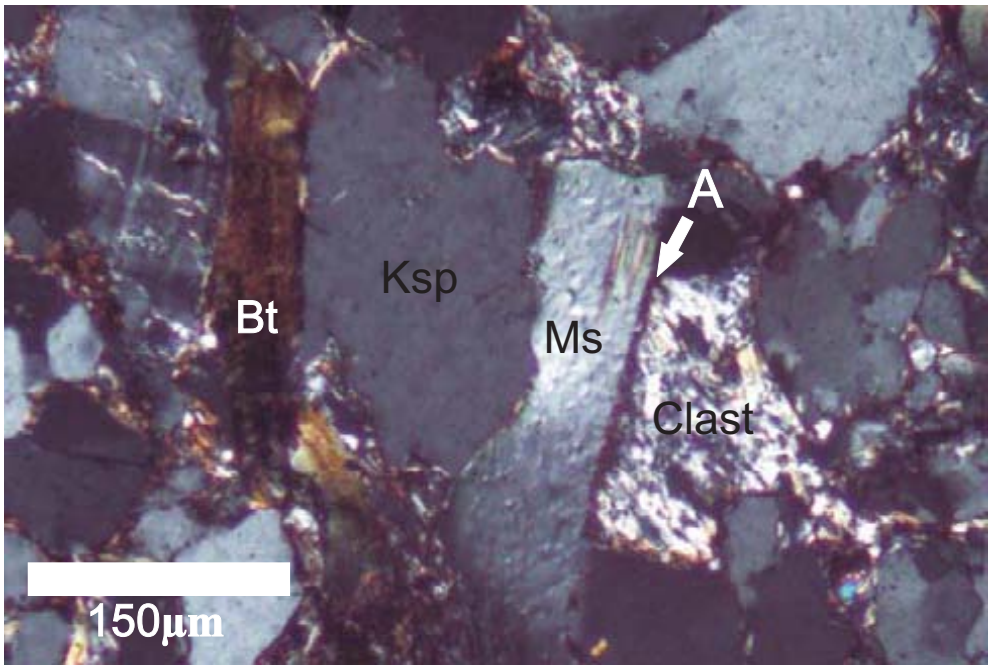

Figure 10: Detrital muscovite in contact with a quartz and muscovite-rich lithic clast (position A) and K-feldspar, from Mic Mac H-86 4719.78 site 2. 10x magnification, xpl.

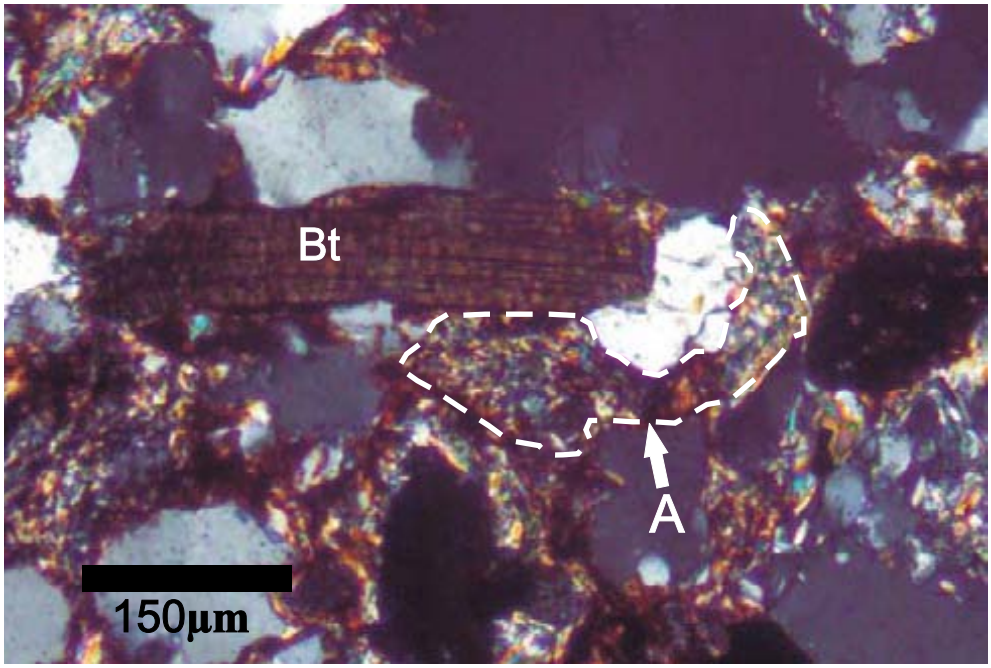

Figure 11: Plastically deformed muscovite-rich lithic clast (position A) from Mic Mac H-86 4719.78 site 8. 10x magnification, xpl.

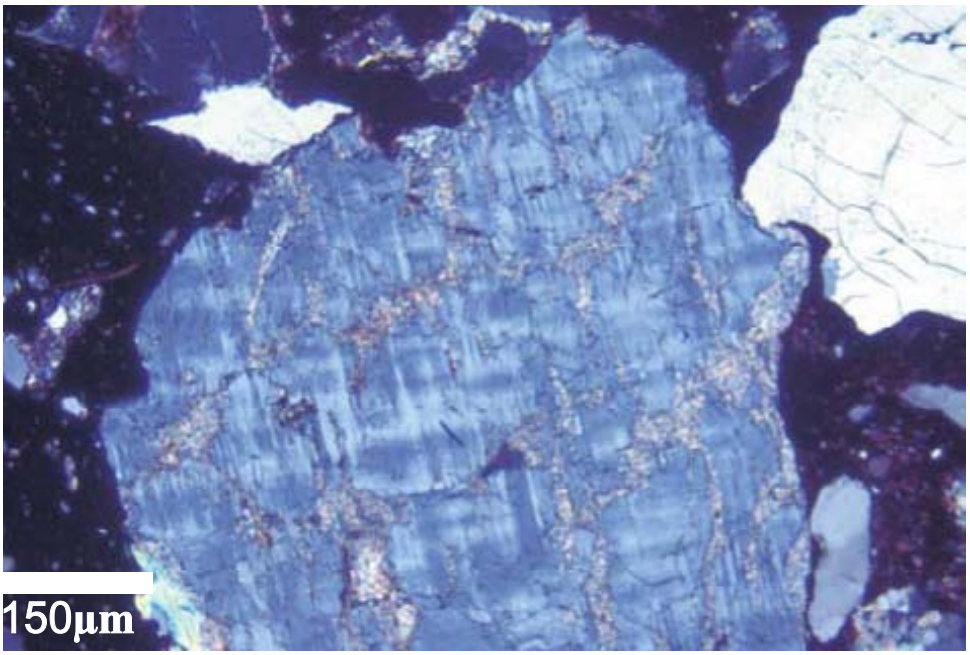

Figure 12: K-feldspar (microcline) with exsolution of perthite, from Mic Mac H-86 4721.13 site 3. 10x magnification, xpl.

Appendix 4B: Microphotos of Mineral Grains and Lithic Clasts of Mohican I-100 well

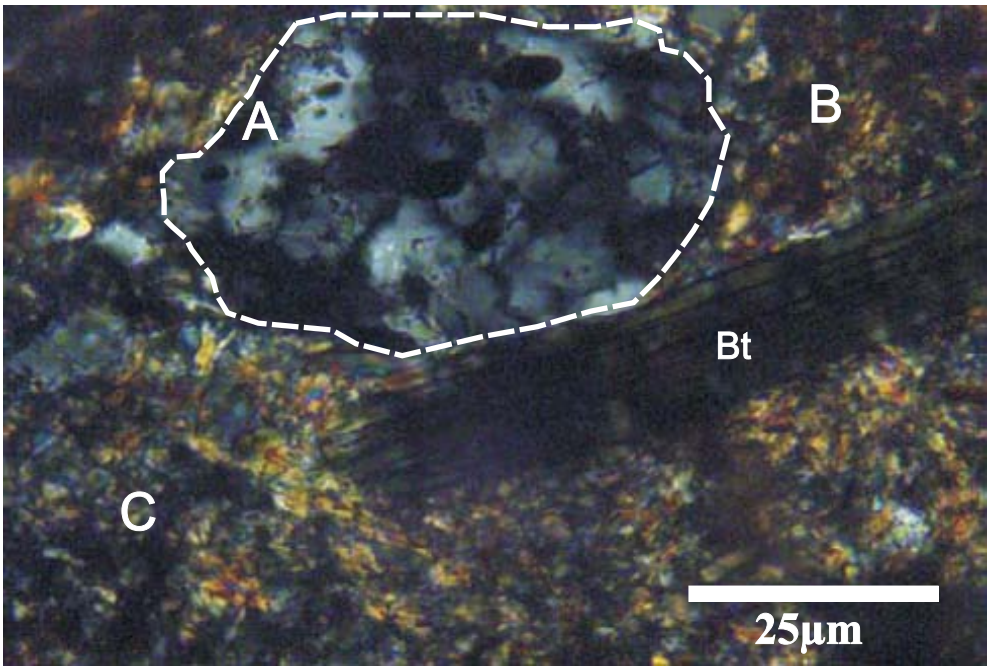

Figure 1: Quartzite lithic clast (position A) and biotite within a muddy muscovite-rich matrix (position B) and more compacted matrix that is at initial stage of cementation (position C), from Mohican I-100 3692.42 site 9. 40x magnification, xpl.

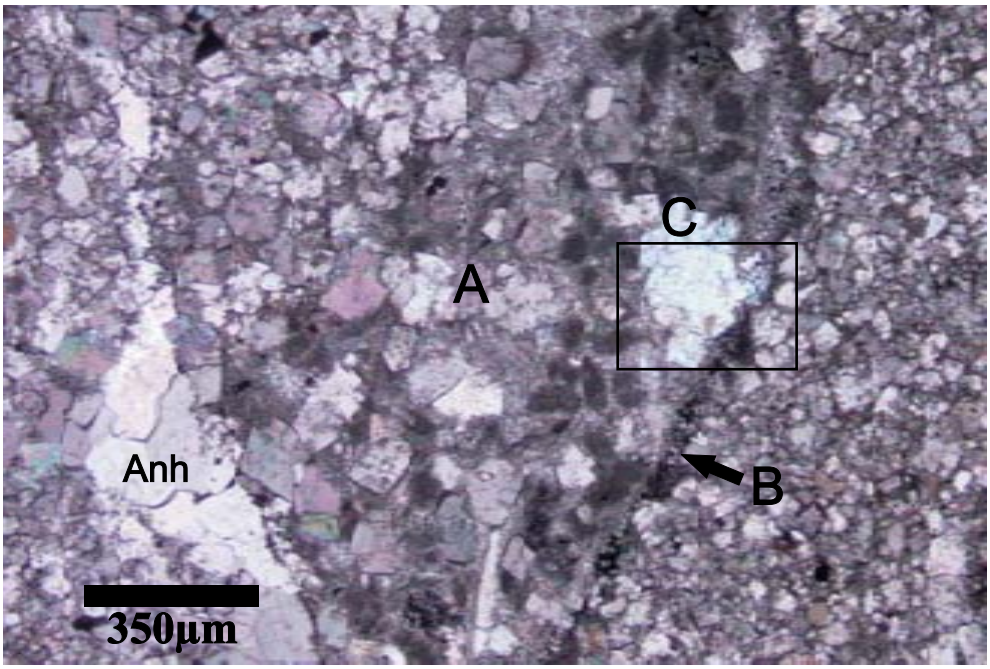

Figure 2: Sparry calcite cement (position A) filling hollow bioclast. Pyrite forms along edge of bioclast (position B). For zoomed in (box C) scanning electron microscope image see App. 2D, Fig. 3. From Mohican I-100 3696.69 site 3. 4x magnification, xpl.

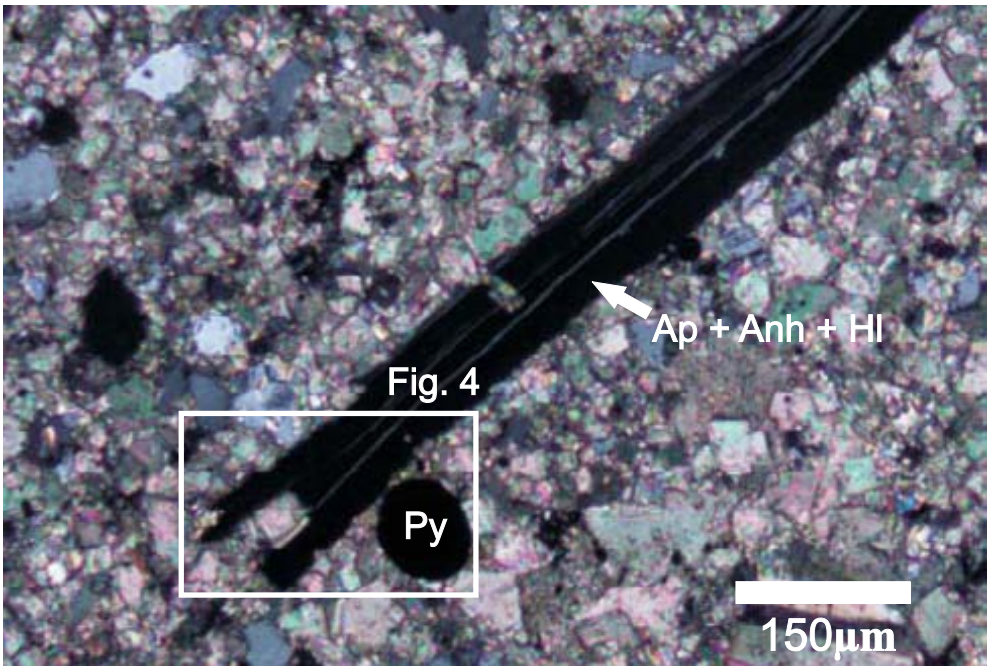

Figure 3: Phosphorite - probably a bone, but possibly some other phosphatic skeletal material, replaced by or host to early diagenetic anhydrite, apatite and halite, from Mohican I-100 3696.69 site 4. 10x magnification, xpl.

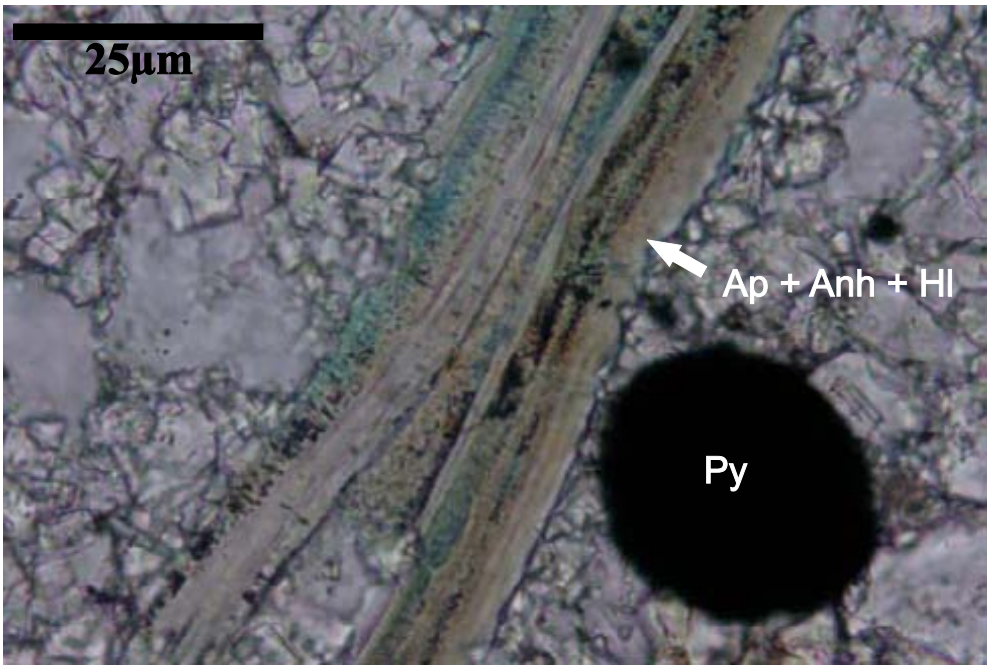

Figure 4: Bone fragment from App. 4A, Fig. 3 showing internal structure, from Mohican I-100 3696.69 site 4. 40x magnification, ppl.

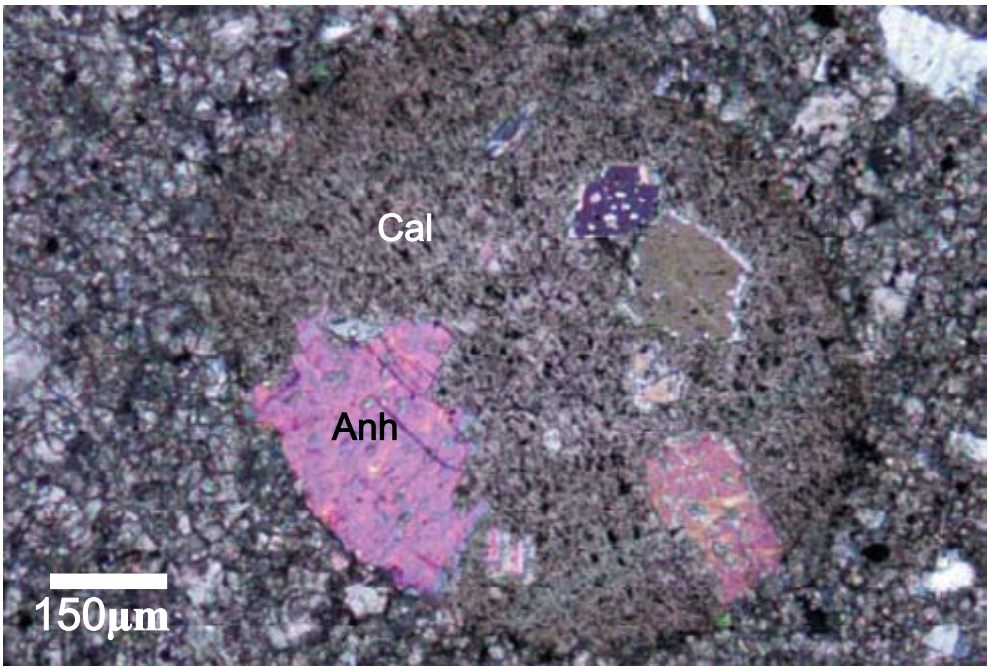

Figure 5: Original calcite bioclast, partly replaced by anhydrite, surrounded by dolomite, presumably replacing original arangonitic lime mud, from Mohican I-100 3696.69 site 5. 10x magnification, xpl.

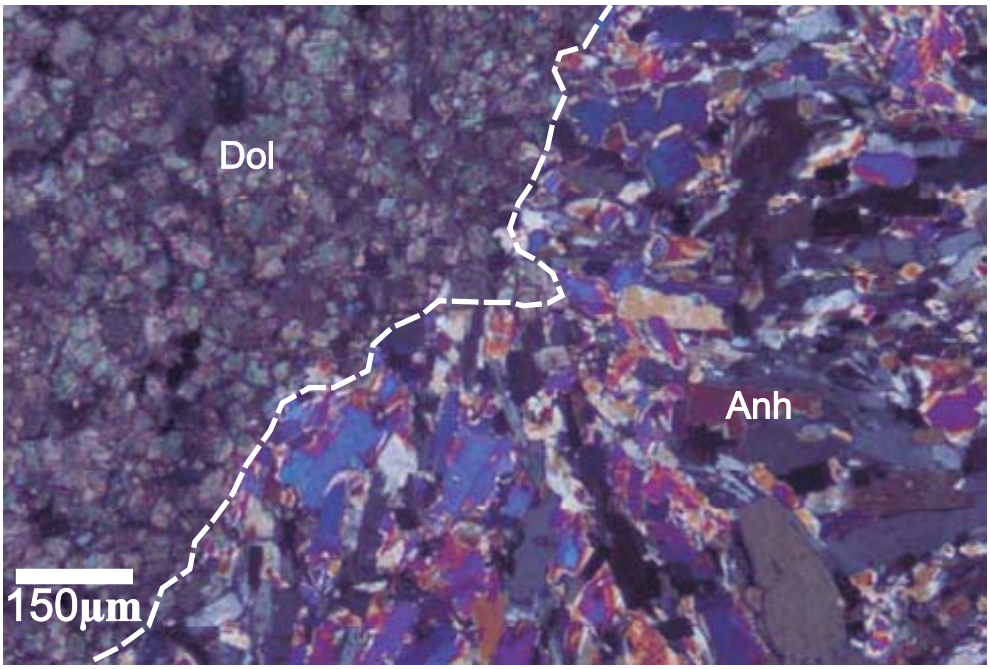

Figure 6: Anhydrite nodule, surrounded by dolomite-rich cement, from Mohican I-100 3697.36B site 2. 10x magnification, xpl.

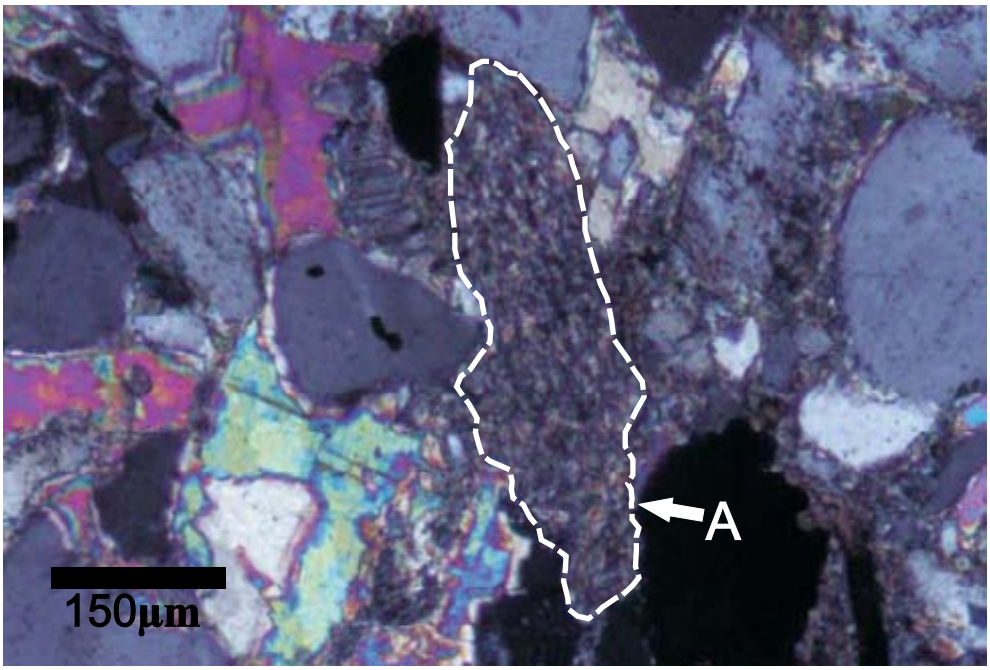

Figure 7: Lithic clast (position A) composed of mostly muscovite and quartz, from Mohican I-100 3697.86 site 6. 10x magnification, xpl.

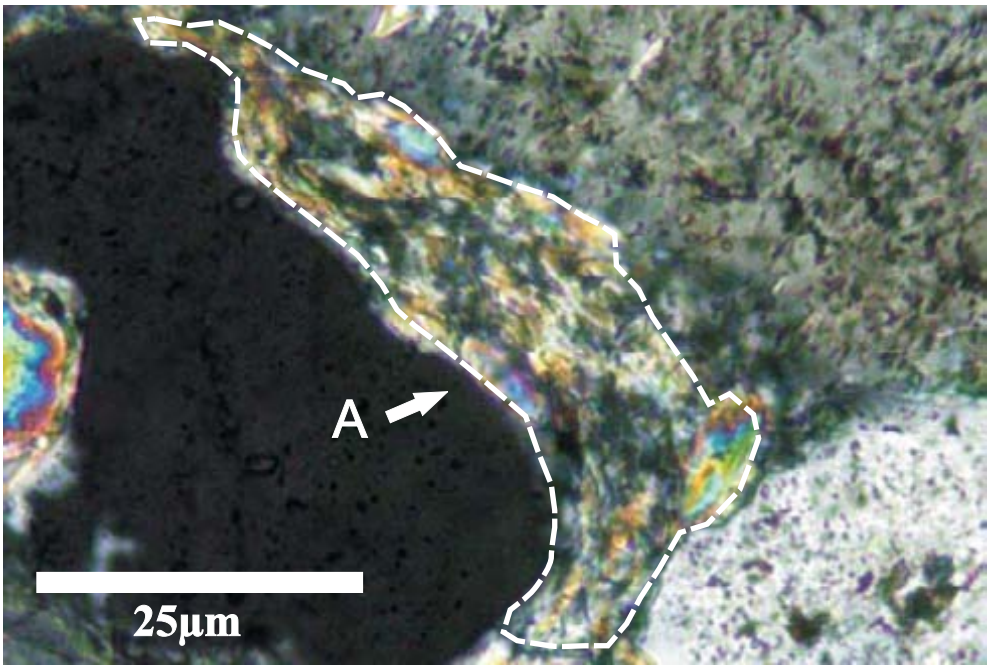

Figure 8: Lithic clast (position A) composed of mostly muscovite and chlorite, forms pseudomatrix, from Mohican I-100 3697.86 site 15. 40x magnification, xpl.

Appendix 4C: Microphotos of Mineral Grains and Lithic Clasts of Wyandot E-53 well

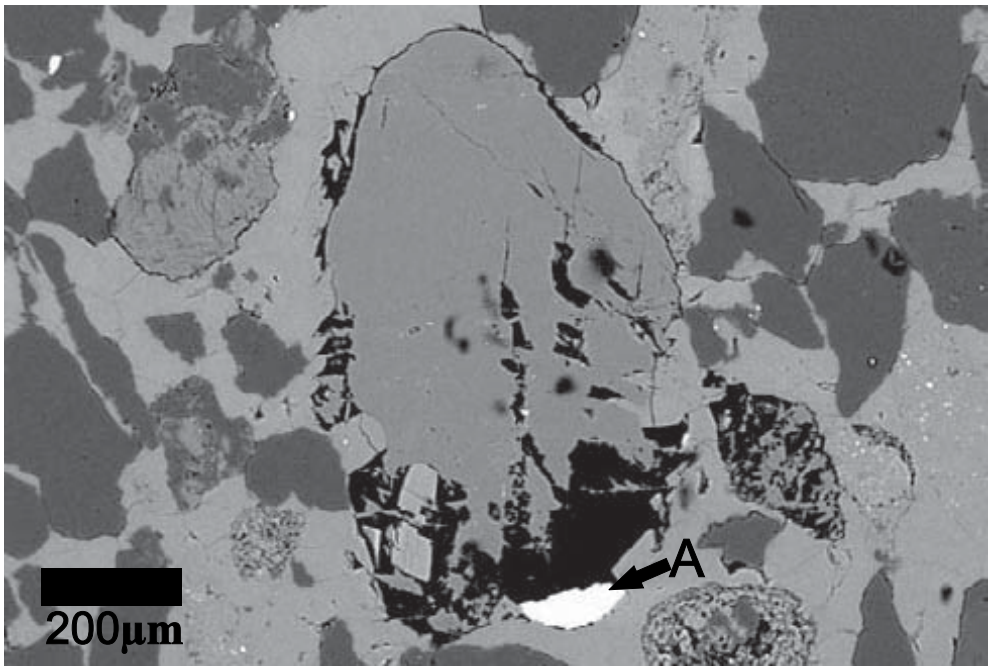

Figure 1: SEM image from Wyandot E-53 2873.10 site 8, showing barite (position A) which appears to be drilling mud because it fills in porosity and does not form straight grain boundaries with other mineral grains.

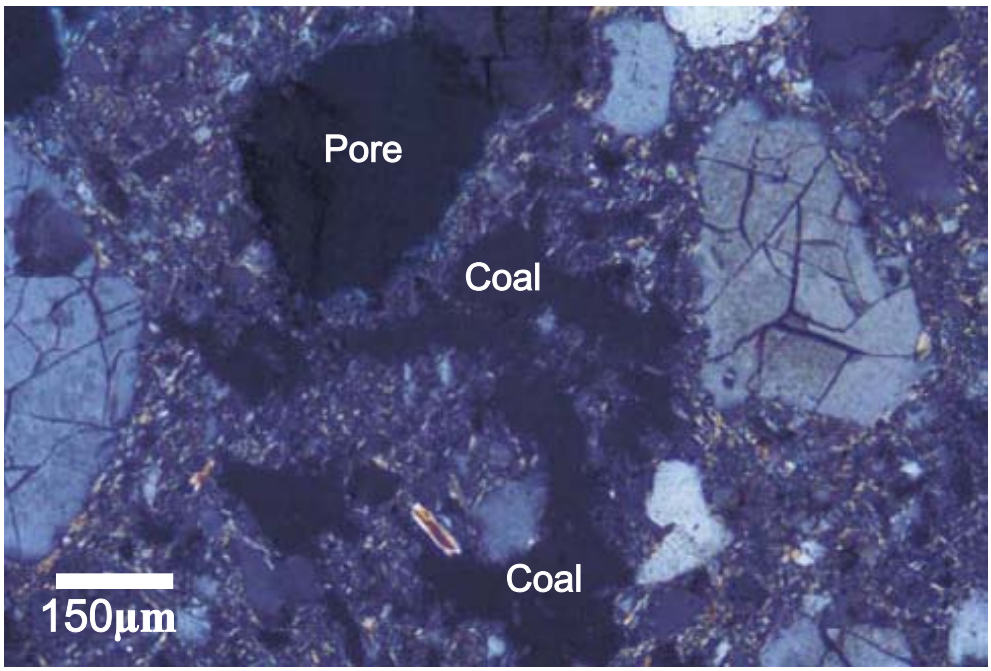

Figure 2: Presence of coal in comparison with porosity (see Fig 3 for image in ppl), from Wyandot E-53 2876.81 site 2. 10x magnification, xpl.

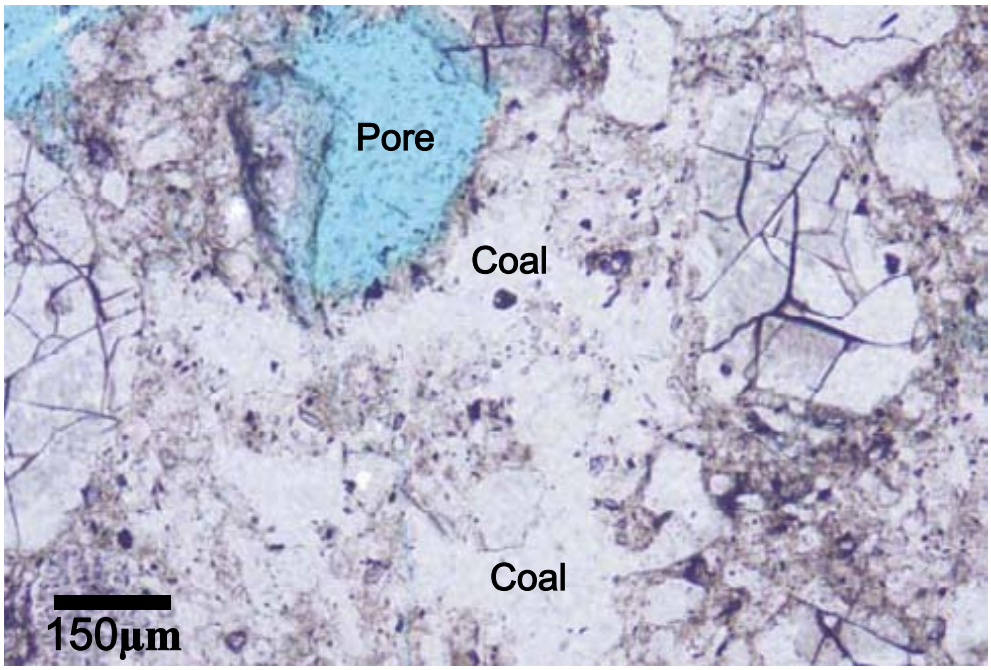

Figure 3 (from Fig. 2): Presence of coal and comparison with porosity. The coal appears as clear masses, while the porosity is seen as clear blue because the samples were impregnanted with blue epoxy to be able to easily see porosity. From Wyandot E-53 2876.81 site 2. 10x magnification, ppl.

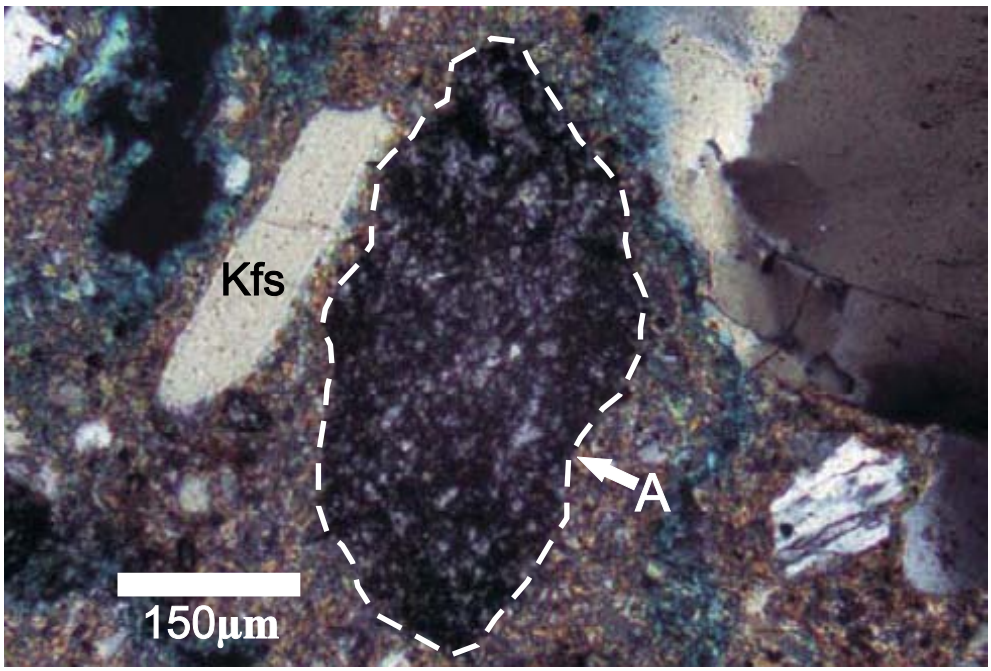

Figure 4: Quartzite-clast (position A), from Wyandot E-53 2876.81 site 4. 10x magnification, xpl.

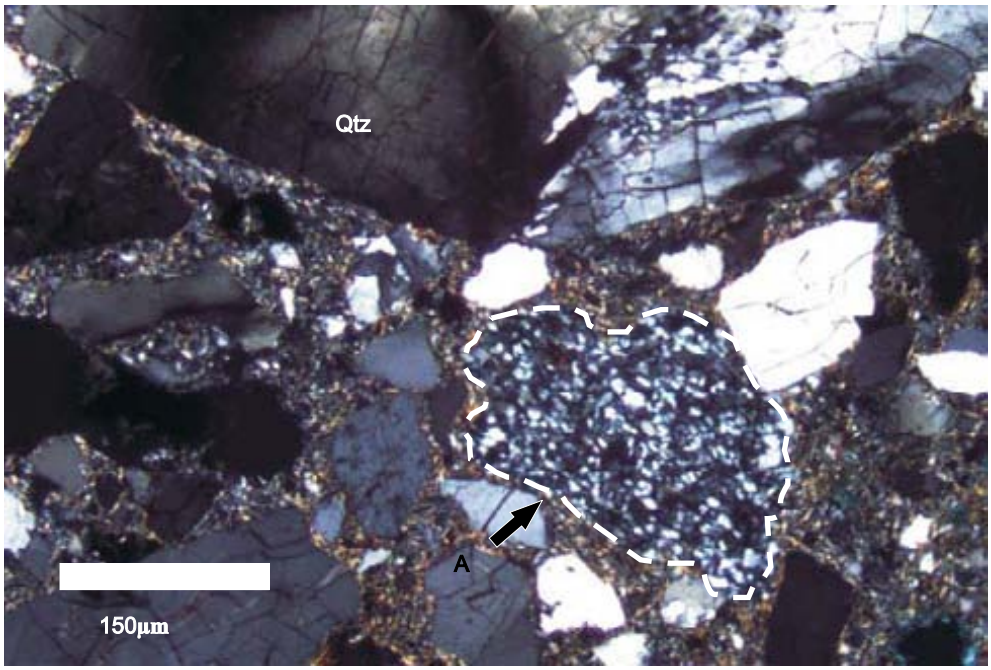

Figure 5: Quartzite-clast (position A) and quartz showing fractures, from Wyandot E-53 2876.81 site 4. 10x magnification, xpl.

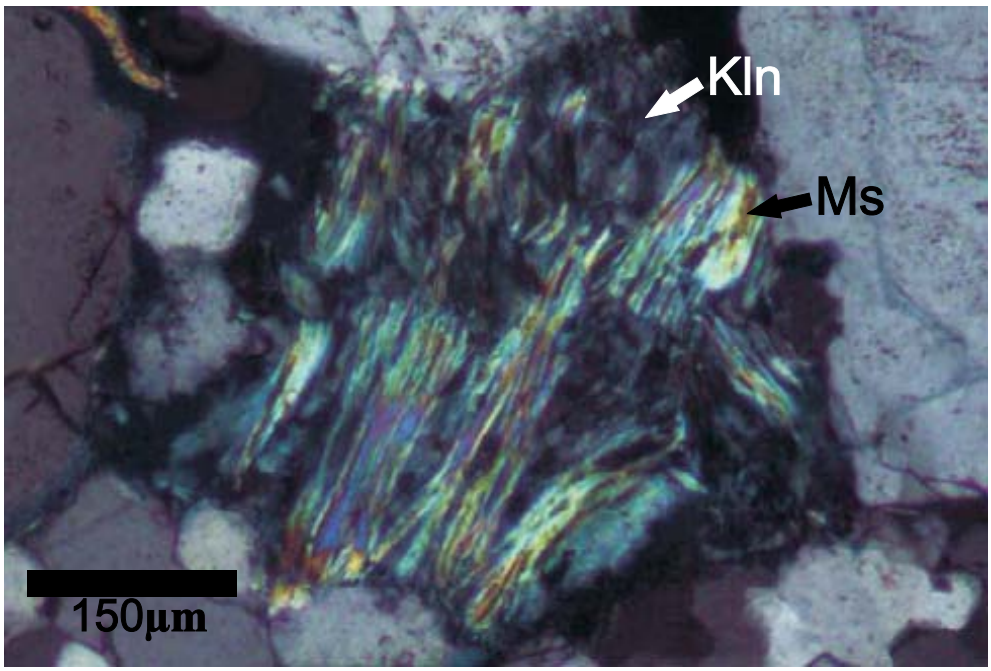

Figure 6: Expansion of the cleavage planes of detrital muscovite and precipitation of kaolinite along these cleavage planes, from Wyandot E-53 2878.66 site 5. 10x magnification, xpl.

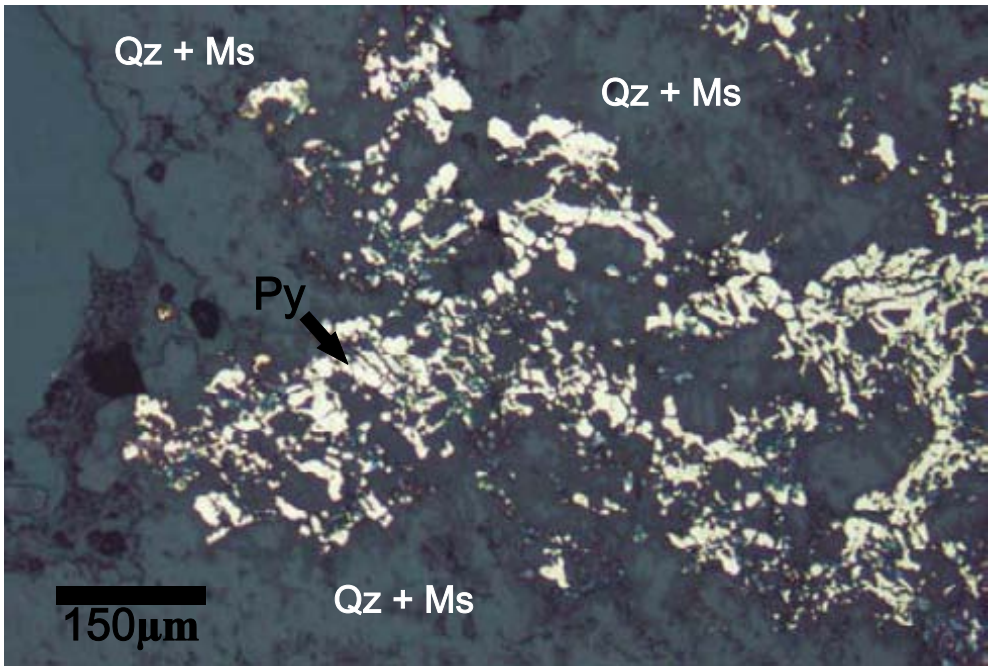

Figure 7: Diagenetic pyrite (py) formed in intergranular space or dissolution within a quartz and muscovite-rich lithic clast, from Wyandot E-53 2878.66 site 6. 10x magnification, reflected ppl.

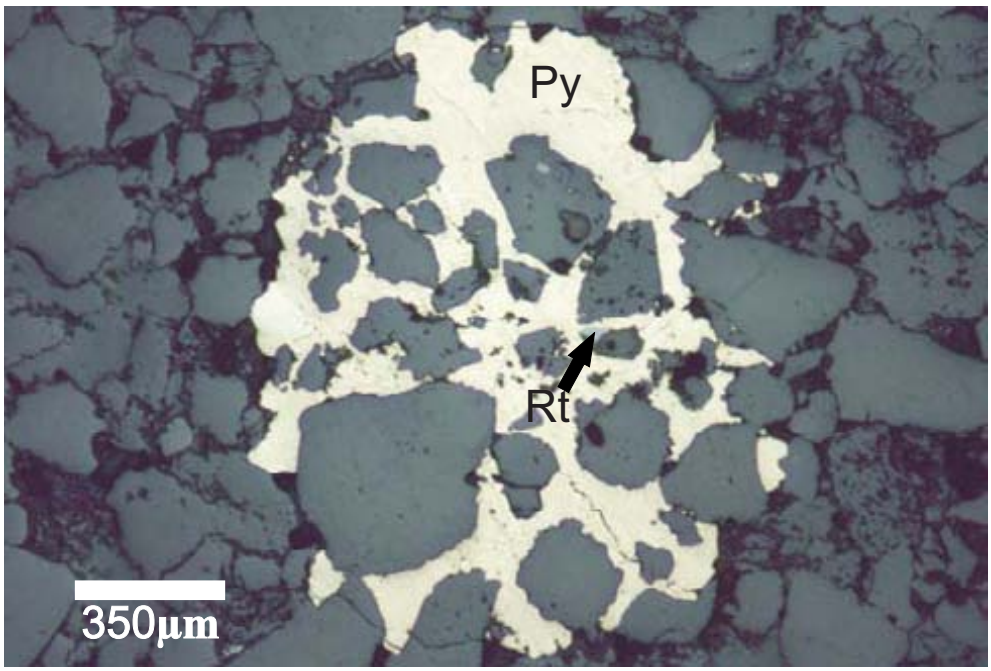

Figure 8: Diagenetic pyrite (Py) within intergranular spaces between framework grains along with rutile (Rt), from Wyandot E-53 2880.22 site 2. 4x magnification, reflected ppl. This may be a very small pyrite concretion.

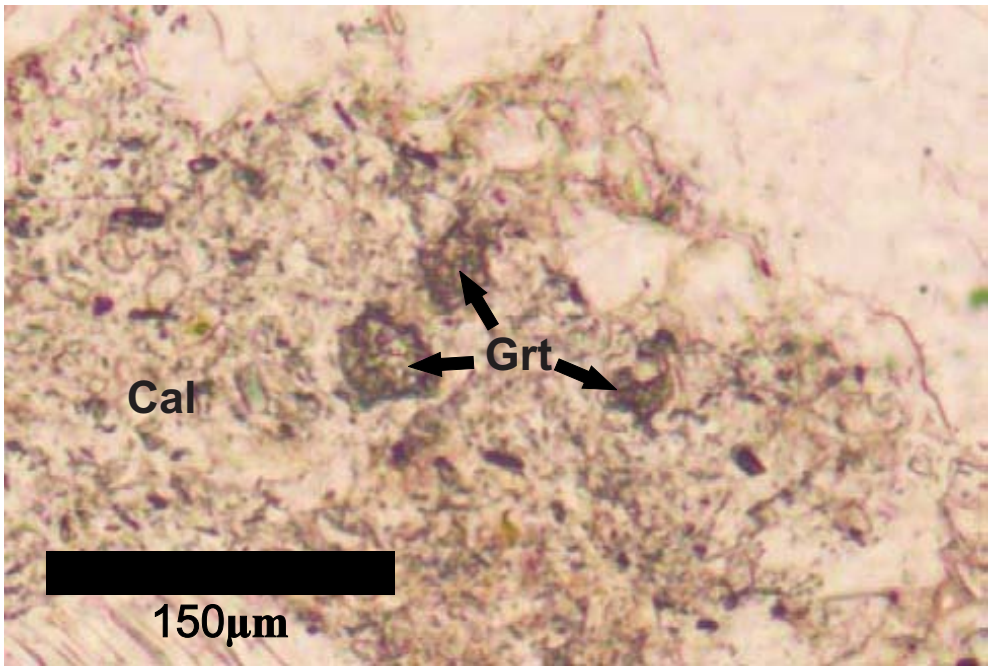

Figure 9: Relics of detrital garnets (Grt) within a calcite (Cal) rich cement, from Wyandot E-53 2880.22 site 3. 10x magnification, ppl.

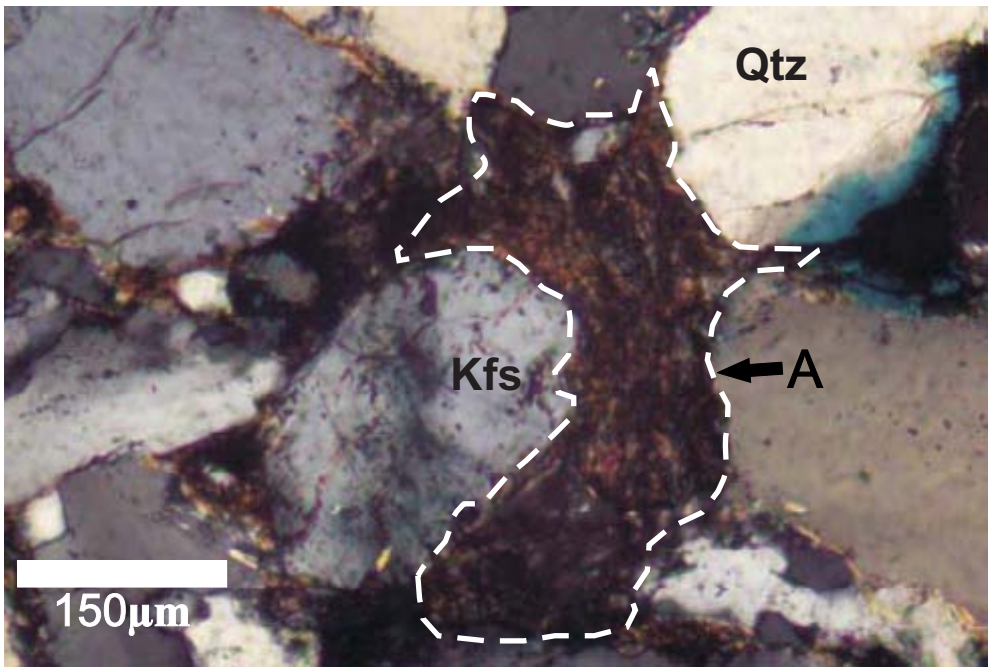

Figure 10: Lithic clast (position A), rich in quartz and muscovite, plastically deformed around detrital K-feldspar grain, from Wyandot E-53 2880.22 site 4. 10x magnification, xpl.

Appendix 5A: Microphotographs of Minerals and Textures of Potential Sources (Meguma Group Slate and Meta-sandstone)

- Sample 8: Slate
- Sample 10: Meta-sandstone

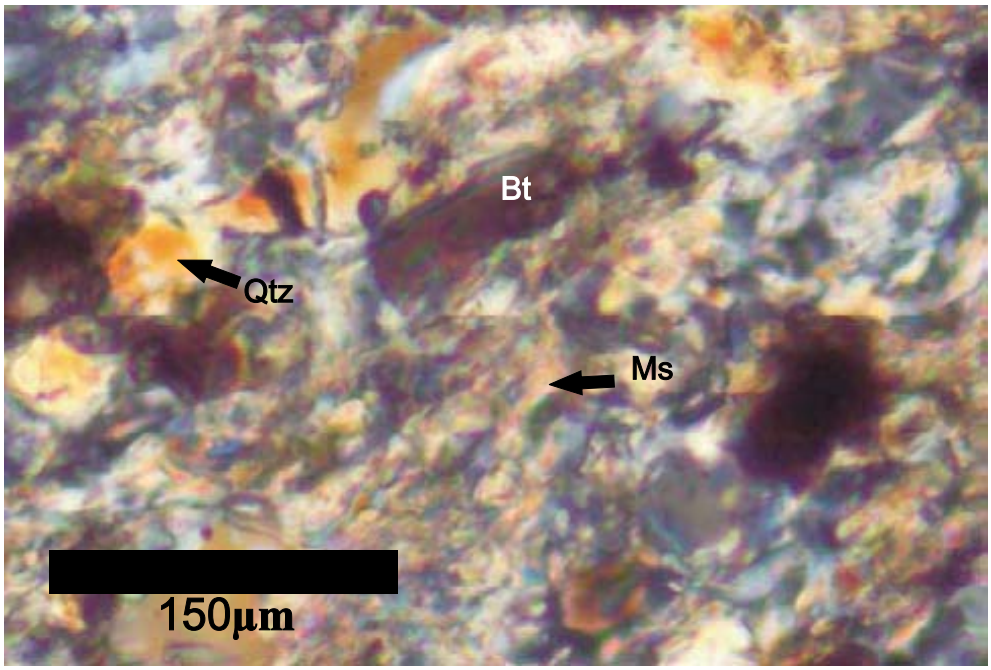

Figure 1: Fine grained intergranular muscovite, from Meguma meta-sandstone (sample 10). 10x magnification, xpl.

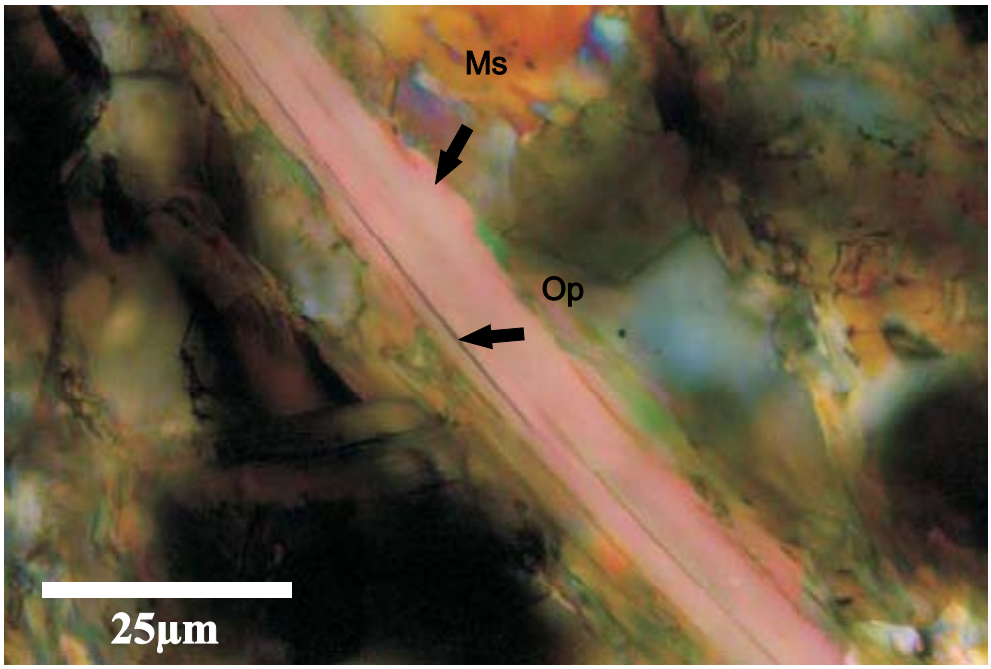

Figure 2: Muscovite grain with opaques (Op) along cleavage planes, from Meguma meta-sandstone (sample 10). 40x magnification, xpl.

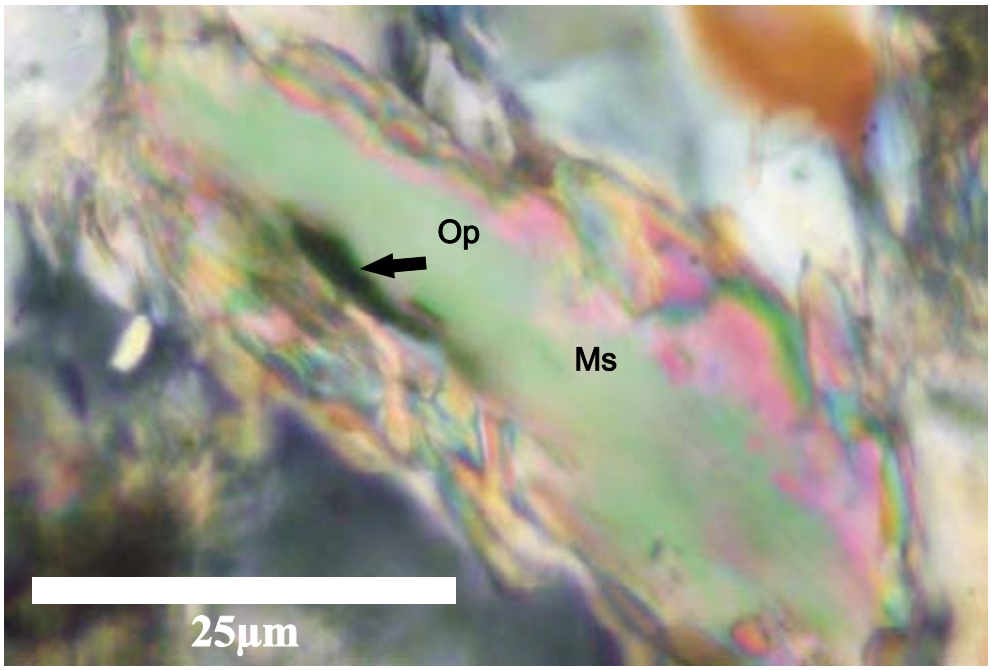

Figure 3: Muscovite grain with opaque inclusion along cleavage plane, from Meguma meta-sandstone (sample 10). 40x magnification, xpl.

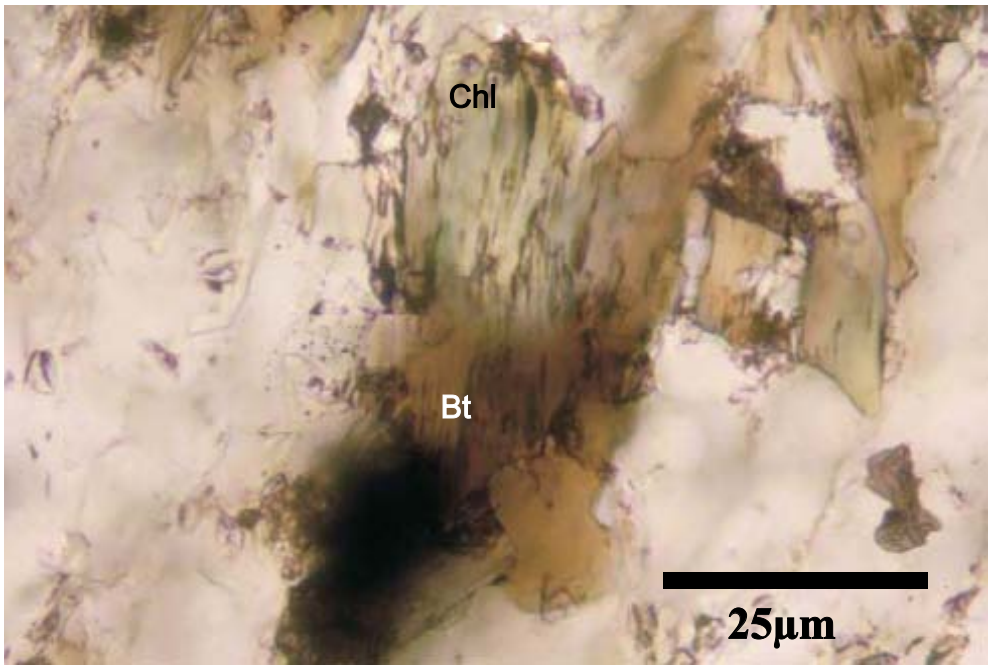

Figure 4: Chloritization of biotite, from Meguma meta-sandstone (sample 10). 40x magnification, ppl.

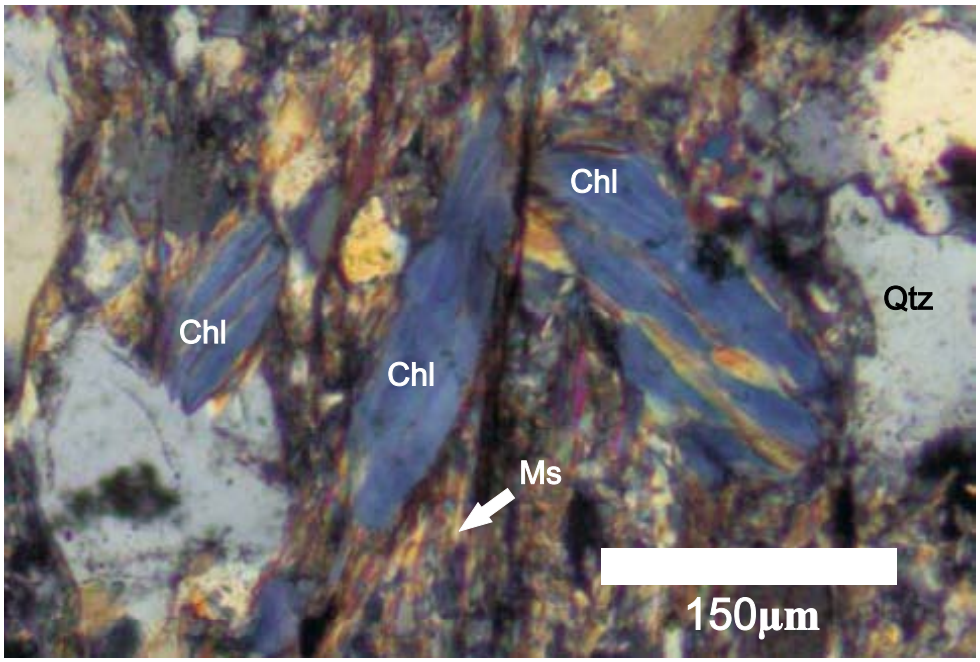

Figure 5: Chlorite and quartz grains with fine grain intergranular muscovite, from Meguma slate (sample 8). 10x magnification, xpl.

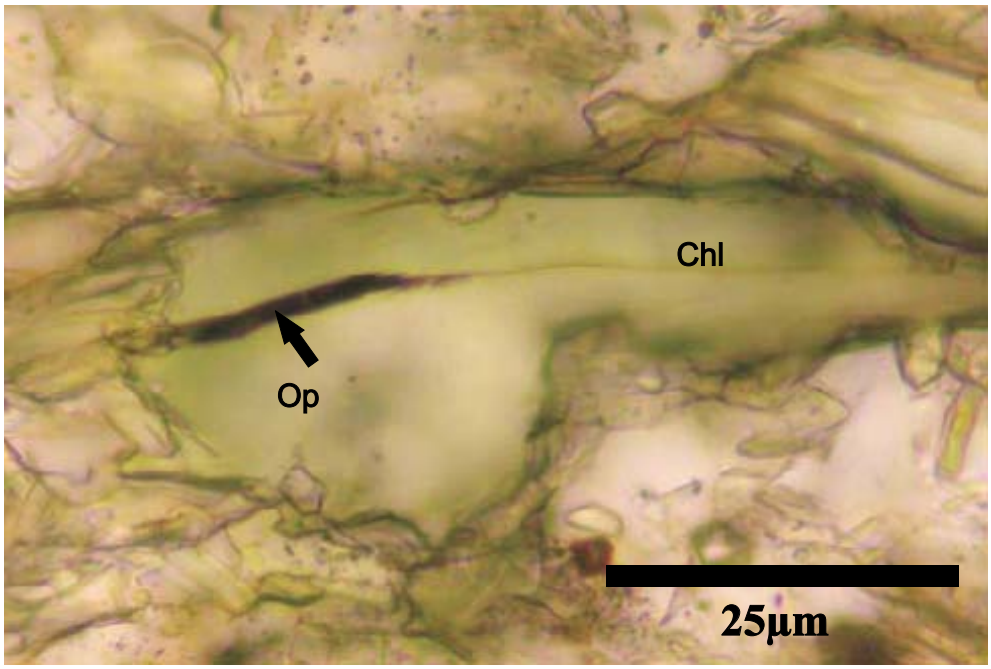

Figure 6: Chlorite grain with an opaque formed along cleavage, from Meguma slate (sample 8). 40x magnification, ppl.

Appendix 5B: Microphotographs of Minerals and Textures of Lithic Clasts from Mohican I-100 Well

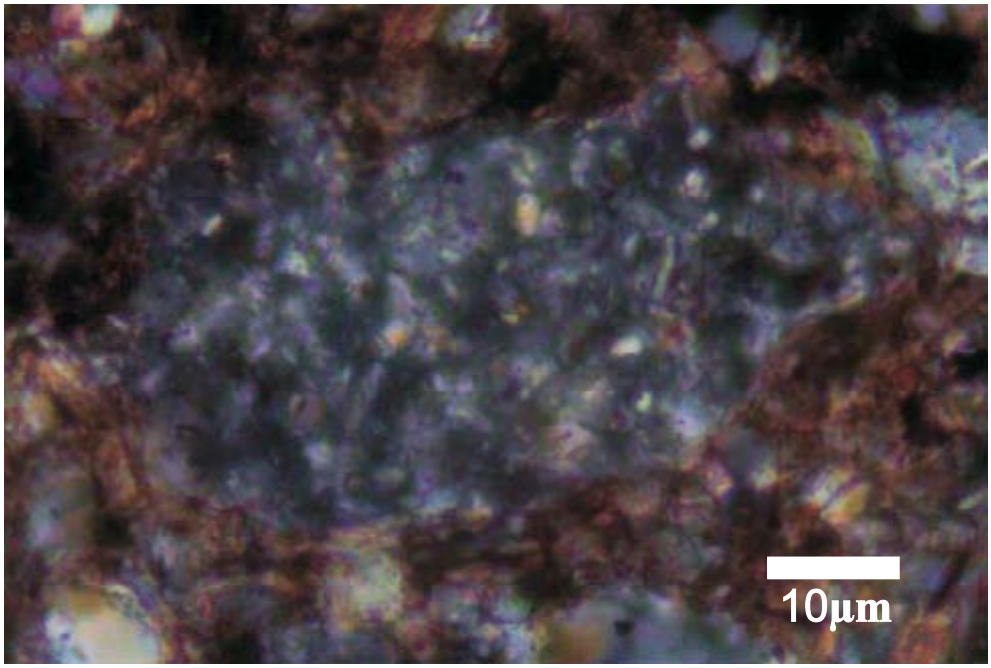

Figure 1: Lithic clast composed of quartz, chlorite and biotite, from Mohican I-100 3691.23A. 40x magnification, xpl.

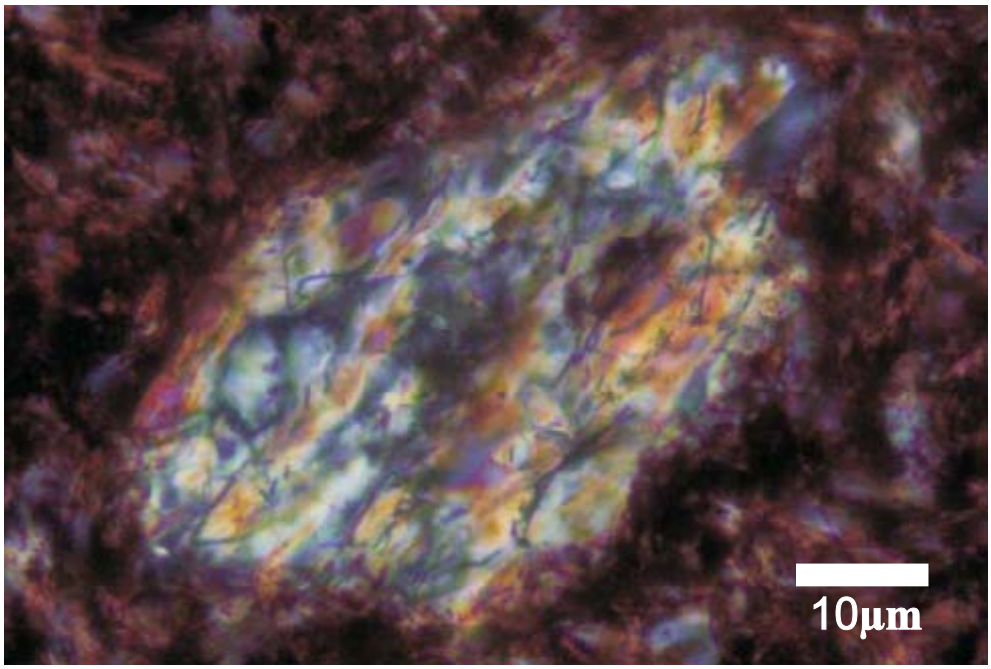

Figure 2: Greenschist lithic clast, composed of quartz with aligned grains of muscovite and chlorite, from Mohican I-100 3691.23A. 40x magnification, xpl.

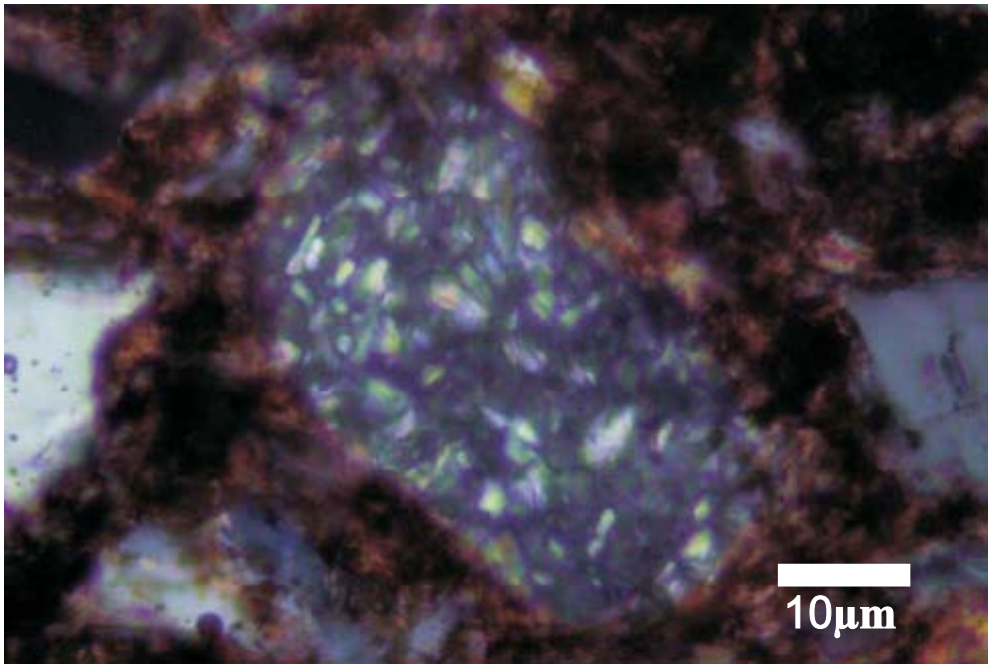

Figure 3: Lithic clast composed of quartz and chlorite, from Mohican I-100 3691.23A. 40x magnification, xpl.

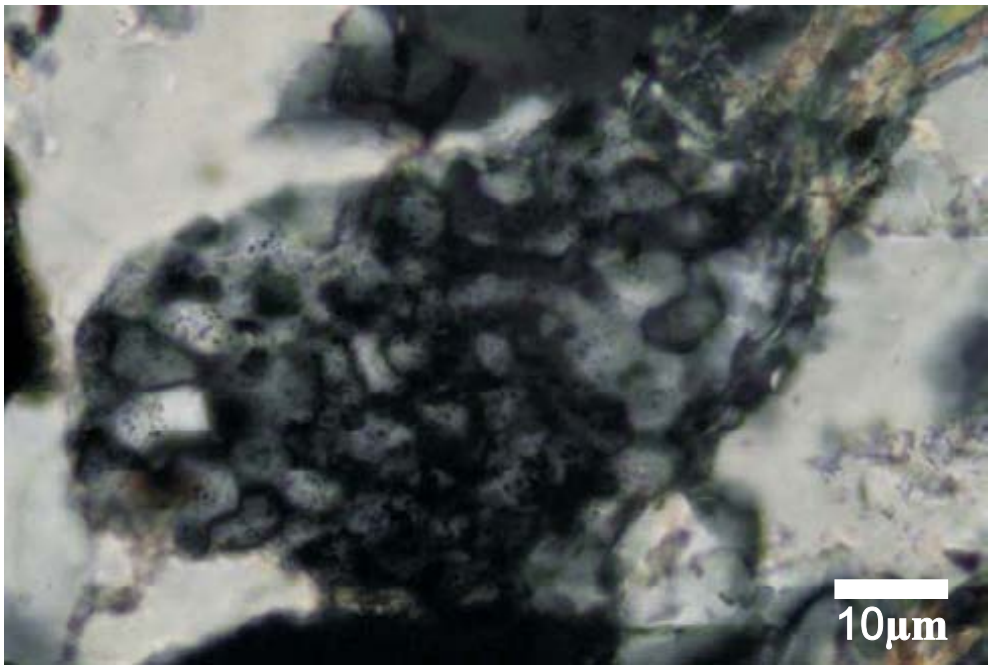

Figure 4: Rhyolitic lithic clast, composed mainly of quartz and K-feldspar, from Mohican 3692.42. 40x magnification, xpl.

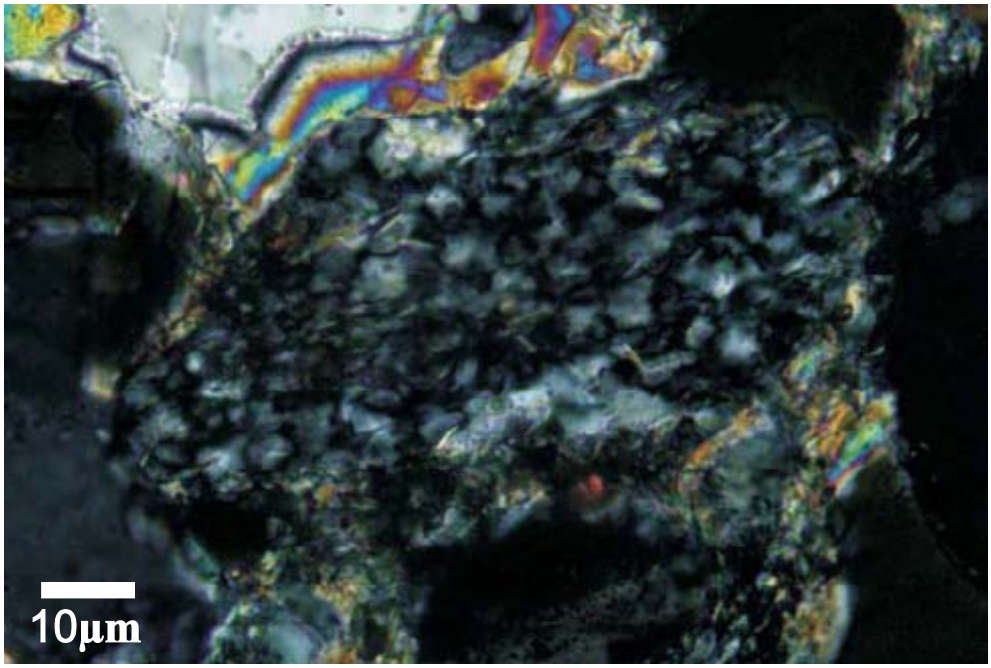

Figure 5: Greenschist lithic clast composed of quartz and chlorite banding, from Mohican I-100 3697.86. 40x magnification, xpl.